



**CSCE** | 31<sup>st</sup> August  
**2022**

# Proceedings Book

**Editor-in-Chief**  
Dr. Majid Ali

**Editor**  
Engr. Minhas Shah

ISBN 978-969-23344-3-3

Capital University of Science and Technology, Islamabad  
Department of Civil Engineering

# Publication Note

This book has been produced from files received electronically by the individual authors. The publisher makes no representation, express or implied, with regard to accuracy of the information contained in this book and cannot accept any legal responsibility or liability for any errors or omissions that may have been made. All titles published by 4<sup>th</sup> Conference on Sustainability in Civil Engineering and Capital University of Science and Technology (CUST) Islamabad Pakistan publishers are under copyright protection said copyrights being the property of their respective holders. All Rights Reserved. No part of this book may be reproduced or transmitted in any form or by any means, graphic, electronic or mechanical, including photocopying, recording, taping or by any information storage or retrieval system, without the permission in writing from the publisher.

**August 31<sup>st</sup>, 2022**

**Published By**

Department of Civil Engineering

Capital University of Science and Technology, Islamabad, Pakistan

**ISBN: 978-969-23344-3-3**

[www.csce.cust.edu.pk](http://www.csce.cust.edu.pk)

[www.cust.edu.pk](http://www.cust.edu.pk)

# Foreward

Welcome to the CSCE 2022, 4<sup>th</sup> Conference on Sustainability in Civil Engineering (CSCE'22) was held by Department of Civil Engineering, Capital University of Science and Technology, Islamabad, Pakistan. The main focus of CSCE'22 was to highlight sustainability related to the field of civil engineering. It aimed to provide a platform for civil engineers from academia as well as industry to share their practical experience and different research findings in their relevant specializations. We hope all the participants experienced a remarkable opportunity for the academic and industrial communities to address new challenges, share solutions and discuss future research directions. The conference accommodated several parallel sessions of different specialties, where the researchers and engineers interacted and enhanced their understanding of sustainability in the civil engineering dynamics.

This year, we had six wonderful and renowned keynote speakers for this edition of CSCE. We had received 225 manuscripts from different countries around the world including UK, Ireland, Cyprus, China, Egypt, Malaysia, KSA, and Pakistan. All papers have undergone a comprehensive and critical double-blind review process. The review committee was comprised of 51 PhDs serving in industry and academia of UK, USA, Australia, New Zealand, Hong Kong, Poland, Italy, Thailand, Chile, Malaysia, China, Turkey, Oman, KSA, and Pakistan. After the screening and review process, 66 papers are compiled in this proceeding book.

We are grateful to all the reviewers and keynote speakers who have dedicated their precious time to share their expertise and experience. With this opportunity, we would also like to express our gratitude to everyone, especially all the faculty and staff at the Capital University of Science and Technology for their great support and participation. In this regard, the participation and cooperation of all authors, presenters and participants are also acknowledged, without whom this conference would not have been possible. Last but not least, an appreciation to our advising and organizing committees whose hard work and dedication has made this day possible.

*Conference Chair of CSCE,22*

*Dr. Majid Ali*

*Capital University of Science and Technology,  
Islamabad, Pakistan*

# Technical Committee

Dr. Rabee Shamass	London South Bank University, UK
Dr. Robert Evans	Nottingham Trent University, UK
Dr. Irshad Qureshi	Washington State University, USA
Dr. Hasan Tariq	Thornton Tomasetti, USA
Dr. Mizan Ahmed	Monash University, Australia
Dr. Wajiha Mohsin Shahzad	Massey University, New Zealand
Dr. Mehran Khan	The Hong Kong Polytechnic Uni, Hong Kong
Dr. Jincheng Liu	The University of Hong Kong
Dr. Arslan Akbar	City University of Hong Kong
Dr. Khursheed Ahmed	University of Hong Kong
Dr. Piotr Smarzewski	Lublin University of Technology, Poland
Dr. Nicola Fontana	Universita Degli Studi del Sannio, Italy
Dr. Muhammad Shakeel	The Hong Kong University of Sci. and Tech. Thailand
Dr. Krit Saowiang	Asian Institute of Technology, Thailand
Dr. Claudio Oyarzo Vera	UCSC, Chile
Dr. Khairunisa Binti Mthusamy	Pahang, Malaysia
Dr. Noor Aina	Universiti Pertahanan Nasional Malaysia
Dr. Cao Mingli	DUT, China
Dr. Li Li	Northwest A&F University, China
Dr. Teoman Ozer	ITU Academy, Turkey
Dr. Mohsin Usman Qureshi	Sohar University, Oman
Dr. Munir Ahmed	DAR, KSA
Dr. Umar Farooq	Islamic University Madina, KSA
Dr. Shunde Qin	Jacobs Sutton Coldfield, UK
Dr. Furqan Qamar	WSP, UK
Dr. Hamid Mahmood	Dept of Transportation, Victoria, Australia
Dr. Mohsin Shehzad	Mott MacDonald, New Zealand
Dr. Irfan Yousuf	NEPRA, Pakistan

Dr. M Zia ur Rehman Hashmi	Global Change Impact Studies Center, Pakistan
Dr. Rao Arsalan Khushnood	NUST, Islamabad
Dr. Hammad Anis Khan	NUST, Islamabad
Dr. Habib Ur Rehman	UET, Lahore
Dr. Ammad Hassan	UET, Lahore
Dr. Khurram Rashid	UET, Lahore
Dr. Naeem Ejaz	UET, Taxila
Dr. Faisal Shabbir	UET, Taxila
Dr. Usman Ali Naeem	UET, Taxila
Dr. Naveed Ahmad (Transportation)	UET, Taxila
Dr. Jawad Hussain	UET, Taxila
Dr. Muhammad Usman Arshid	UET, Taxila
Dr. Afaq Ahmed	UET, Taxila
Dr. Naveed Ahmad	UET, Taxila
Dr. Mudasser Muneer Khan	BZU, Multan
Dr. Rashid Farooq	IIU, Islamabad
Dr. Zeeshan Alam	IIU, Islamabad
Dr. Anwar Khitab	MUST, Pakistan
Dr. Adnan Nawaz	COMSATS, Abbottabad
Dr. Faisal Javed	COMSATS, Abbottabad
Dr. Shaukat Ali Khan	Muslim Youth University, Islamabad
Dr. Shaukat Ali Khan	Abasyn, Peshawar
Dr. Sabahat Hassan	HITEC University, Taxila

---

## **Advisory Committee**

---

**Dr. Muhammad Mansoor Ahmed**

*(Vice-Chancellor CUST Islamabad)*

Patron

**Dr. Imtiaz Ahmed Taj**

*(Dean Faculty of Engineering)*

General Advisor

**Dr. Ishtiaq Hassan**

*(Head of Civil Engineering Department)*

Principle Advisor

---

---

## **Organizing Committee**

---

**Dr. Majid Ali**

Chair

**Dr. Muhammad Usman Farooqi**

Co – Chair

**Engr. Sohail Afzal**

Conference Secretary – I

**Engr. Minhas Shah**

Conference Secretary –II

---

# Keynote Speakers

---

**Dr. Syed Abid Ali Shah**

*Ex-Vice Chancellor  
University of Science and Technology,  
Bannu, Pakistan*

*Sustainable health monitoring with non-linear wave propagation in cement-based materials*

---

**Dr. Ayub Elahi**

*Project Director (Development Works)  
University of Engineering and  
Technology, Taxila, Pakistan*

*Self-Compacting Concrete- an innovative and sustainable material*

---

**Dr. Naveed Anwar**

*Vice President for Knowledge Transfer  
Asian Institute of Technology, Thailand*

*IT applications in construction*

---

**Dr. Anas bin Ibrahim**

*Head of Centre for CE Studies  
UiTM Caw. Pulau Pinang, Malaysia*

*Assessment of railway's ground track degradation and subgrade-induced mud pumping*

---

**Dr. Naveed Ahmad**

*Stanford University, California, USA*

*Methodology for developing seismic fragility functions to support risk assessment at national level*

---

**Dr. Tariq Umar**

*University of the West England Bristol,  
England*

*Improving safety performance in construction*

---

# Table of Contents

<b>PAPER ID</b>	<b>TITLE</b>	<b>PAGE NO.</b>
PAPER ID.22-101	PHYSICAL, MECHANICAL, AND, NON-DESTRUCTIVE EVALUATION OF GRIT IRON SCALE HEAVY-DENSITY CONCRETE	1
PAPER ID.22-130	EFFECT OF STEEL SLAG ON CONCRETE HAVING VARYING AMOUNT OF CEMENT	6
PAPER ID. 22-131	COMPARATIVE ANALYSIS OF CEMENT-SAND MORTAR AND GEO-POLYMER MORTAR UNDER FIRE	17
PAPER ID.22-132	EFFECT OF HUMAN HAIR FIBER ON MECHANICAL PROPERTIES OF CONCRETE	24
PAPER ID.22-134	REDUCING THE WATER ABSORPTION OF MORTAR BY USING ECO-FRIENDLY WASTEPAPER SLUDGE ASH	37
PAPER ID.22-135	INFLUENCE OF SILICA FUME, STEEL, AND POLYPROPYLENE FIBERS ON MECHANICAL PROPERTIES OF PLASTIC CONCRETE	44
PAPER ID.22-139	THE EFFECT OF POLYPROPYLENE FIBERS ON TENSILE STRENGTH OF SELF COMPACTING CONCRETE	51
PAPER ID.22-141	MECHANICAL BEHAVIOR OF MORTAR USING POZZOLANA AS PARTIAL REPLACEMENT OF CEMENT	56
PAPER ID.22-142	MECHANICAL PROPERTIES OF BAMBOO CORE SANDWICH PANELS	62
PAPER ID.22-144	AN EXPERIMENTAL STUDY ON PARTIAL REPLACEMENT OF BITUMEN USING WASTE ENGINE OIL & CRUMB RUBBER	69
PAPER ID.22-145	MICROSTRUCTURAL STUDY OF COCONUT SHELL CONCRETE	77
PAPER ID.22-146	FRESH AND MECHANICAL PROPERTIES OF HIGH STRENGTH SELF-COMPACTING CONCRETE MODIFIED WITH FLY ASH AND SILICA FUME	84
PAPER ID.22-148	STRENGTHENING OF A FLAT PLATE SLAB -CASE STUDY	93
PAPER ID.22-149	CHARACTERIZATION OF ASPHALT USING NEURAL NETWORK AND IMAGE ANALYSIS TECHNIQUE	99



<b>PAPER ID</b>	<b>TITLE</b>	<b>PAGE NO</b>
PAPER ID.22-150	INFLUENCE OF AGING ON THE PENETRATION PERFORMANCE OF WASTE POLYMER MODIFIED ASPHALT BINDER	111
PAPER ID.22-153	EFFECT OF AGGREGATE REPLACEMENT WITH WASTE TIRE RUBBER ON PROPERTIES OF CONCRETE – AN OVERVIEW	117
PAPER ID.22-155	EXPERIMENTAL STUDY OF FIBRE SYNERGY TO INVESTIGATE THE TENSILE & COMPRESSIVE STRENGTH OF FIBRE REINFORCED CONCRETE	123
PAPER ID.22-156	PERFORMANCE EVALUATION OF A PARTIALLY SYNTHETIC BITUMEN COMPOSED OF INDUSTRIAL WASTE	134
PAPER ID.22-160	A REVIEW ON REPAIRING FIRE-DAMAGE GYPSUM BOARD	141
PAPER ID.22-161	A REVIEW ON THE USAGE OF MODERN TECHNIQUES TO OVERCOME THE ISSUES IN RAPID SETTING CONCRETE FOR EXTREME TEMPERATURE ZONES	147
PAPER ID.22-201	COMPARISON OF EXPERIMENTAL SHEAR CENTRE OF VARIOUS SECTIONS WITH THEORETICAL ANALYSIS THROUGH RESPONSE SURFACE METHODOLOGY	152
PAPER ID.22-202	MASS DISTRIBUTION EFFECT ON THE FINITE MODEL UPDATING USING OPERATIONAL MODEL ANALYSIS TECHNIQUE	158
PAPER ID.22-203	NUMERICAL SIMULATION OF FRACTURE IN CONCRETE USING PHASE FIELD MODEL	163
PAPER ID.22-204	OUT-OF-PLANE RESPONSE OF ENGINEERED CEMENTITIOUS COMPOSITE FACED BLOCK MASONRY	171
PAPER ID.22-205	NUMERICAL STUDY OF SHAPE MEMORY ALLOY (SMA) REINFORCED BEAM SUBJECTED TO SEISMIC LOADING	177
PAPER ID.22-206	NUMERICAL INVESTIGATION OF CFRP RETROFITTED QUARRY ROCK DUST, FLY ASH, AND SLAG BASED GEO-POLYMER CONCRETE BEAMS	184
PAPER ID.22-207	COMPUTATIONAL MODELING OF DAMAGES IN BRIDGE PIERS	191
PAPER ID.22-208	INVESTIGATION OF PUNCHING SHEAR RESPONSE OF GFRP REINFORCED CONCRETE FLAT PLATE SLAB USING CDP MODEL IN ABAQUS	198
PAPER ID.22-209	OPTIMUM DESIGN OF PRESTRESSED CONCRETE GIRDER USING JAYA ALGORITHM	205
PAPER ID.22-210	3D FINITE ELEMENT ANALYSIS OF REINFORCED CONCRETE BEAMS UNDER FIRE	211

<b>PAPER ID</b>	<b>TITLE</b>	<b>PAGE NO</b>
PAPER ID.22-211	REVIEW OF INFILL WALL MODELLING TECHNIQUES: MACRO AND MICRO MODELS	220
PAPER ID.22-212	STRUCTURAL SYSTEMS IDENTIFICATION USING WEIGHTED TRANSMISSIBILITY OPERATOR UNDER FORCED VIBRATIONS	228
PAPER ID.22-213	STRENGTH PREDICTING OF FLY ASH-BASED CONCRETE VIA MACHINE LEARNING ALGORITHMS	234
PAPER ID.22-214	INVESTIGATION OF STRESSES IN A CONCRETE GRAVITY DAM UNDER COMBINED LOADINGS OF SEISMIC AND FLOOD WAVES	242
PAPER ID.22-301	COST OVERRUNS AND DELAYS IN CONSTRUCTION: A STUDY ON CAUSES AND CONTROL MECHANISMS	249
PAPER ID.22-335	CONSTRUCTION COST ESTIMATION OPTIMIZATION USING BUILDING INFORMATION MODELLING (BIM).	256
PAPER ID.22-336	BARRIERS TO IMPLEMENT BIM IN PAKISTAN	261
PAPER ID.22-337	FIBERGLASS AS AN INSULATION LAYER IN ROOF GARDENINGS	267
PAPER ID.22-338	AN OVERVIEW ON THE 3D PRINTING TECHNOLOGY IN CONSTRUCTION INDUSTRY	273
PAPER ID.22-340	APPRAISAL OF DESERT SAND AS A SOURCE OF SUSTAINABLE DEVELOPMENT	280
PAPER ID.22-341	CONCEPTUAL DESIGN OF RESIDENTIAL BUILDINGS FOR DAYLIGHT EMPLOYING CONTEMPORARY BEST PRACTICES	286
PAPER ID.22-342	OPERATIONAL ENERGY LIFE CYCLE ASSESSMENT OF RESIDENTIAL HOUSES – ANALYTICAL STUDY OF AN URBAN DISTRICT OF PAKISTAN	292
PAPER ID.22-343	APPLICATION OF CONSTRUCTION AND DEMOLITION WASTE FOR SUSTAINABLE PAVEMENT CONSTRUCTION-A REVIEW	298
PAPER ID.22-344	CHALLENGES FOR INCORPORATING BIM BASED LCA IN A NEW COMMERCIAL BUILDING PROJECT & CONSTRUCTION FIRM IN PAKISTAN: A REVIEW	304
PAPER ID.22-401	EXPERIMENTAL STUDY OF SCOURING AROUND ELLIPTICAL PILE-CAP BY USING THE SUBMERGED BROAD CRESTED TRAPEZOIDAL WEIR AT DOWNSTREAMS	312

<b>PAPER ID</b>	<b>TITLE</b>	<b>PAGE NO</b>
PAPER ID.22-403	EXPERIMENTAL ANALYSIS OF SCOURING AROUND THE ROUND NOSE BRIDGE PIER USING DIFFERENT BED MATERIAL CONDITIONS	318
PAPER ID.22-404	DESIGN OF CIVIL COMPONENTS OF MICRO HYDRO POWER PLANT: A CASE STUDY	325
PAPER ID.22-405	ANALYZING THE LAND-USE IMPACT ON FLOOD REGIME IN SOAN BASIN	332
PAPER ID.22-406	EXPERIMENTAL STUDY OF BRIDGE PIERS OF DIFFERENT SHAPE SURROUNDED BY MESH WIRE TO MINIMIZE THE LOCAL SCOUR.	339
PAPER ID.22-407	TO STUDY THE IMPACT OF FLOATING DEBRIS ON BRIDGE PIER	345
PAPER ID.22-408	FEM-BASED APPROACH TO STUDY THE IMPACT OF DRAINAGE ON HYDRAULIC BEHAVIOUR OF EARTH DAMS	351
PAPER ID.22-410	TO CALCULATE THE DISCHARGE COEFFICIENT FOR A BROAD CRESTED WEIR WITH NON-SUBMERGED FLEXIBLE VEGETATION	357
PAPER ID.22-411	EXPERIMENTAL STUDY OF T-SHAPED SPUR DIKE WITH DIFFERENT INCLINATION TO MINIMIZE THE LOCAL SCOUR	363
PAPER ID.22-540	AN OVERVIEW OF SUSTAINABLE REPAIR STRATEGIES FOR POTHOLES IN FLEXIBLE PAVEMENTS DURING REHABILITATION PHASE	368
PAPER ID.22-544	RUTTING-DENSIFICATION MITIGATION MEASURES FOR PAVEMENTS OF PAKISTAN-SUSTAINABLE WAY FORWARD	374
PAPER ID.22-546	SMART AND SUSTAINABLE BRIDGE ABUTMENTS - A CASE STUDY	385
PAPER ID.22-547	USE OF MARBLE DUST AS A FILLER MATERIAL IN FLEXIBLE PAVEMENTS	393
PAPER ID.22-549	TO EVALUATE THE SELF-HEALING OF ASPHALT MATERIALS AT DIFFERENT TEMPERATURES	400
PAPER ID.22-601	EFFECT OF RAINFALL INTENSITY AND DURATION ON STABILITY OF NATURAL SLOPES OF UNSATURATED FINE SOILS	405

<b>PAPER ID</b>	<b>TITLE</b>	<b>PAGE NO</b>
PAPER ID.22-603	HELICAL PILE: AN INNOVATIVE AND SUSTAINABLE FOUNDATION TECHNIQUE	412
PAPER ID.22-605	EXPERIMENTAL STUDY ON LOAD CARRYING CAPACITY OF INDIVIDUAL PILES IN A PILED RAFT FOUNDATION SYSTEM	419
PAPER ID.22-606	AN EXPERIMENTAL STUDY ON LATERAL CONTRIBUTION OF RAFT AND PILE IN A PILED RAFT FOUNDATION SYSTEM	425
PAPER ID.22-607	EXPERIMENTAL STUDY OF INFLUENCE THE BEARING CAPACITY OF SANDY SOIL BY USING CEMENT GROUTING	431
PAPER ID.22-713	SPATIO-TEMPORAL ANALYSIS OF PRECIPITATION IN PUNJAB PROVINCE, PAKISTAN	436
PAPER ID.22-714	REMOVAL OF ARSENIC AND PHARMACEUTICAL COMPOUNDS FROM DRINKING WATER: A META-ANALYSIS	446
PAPER ID.22-716	IDENTIFICATION AND COUNTERMEASURES OF SPATIAL CONCENTRATION FACTORS FOR PARTICULATE MATTER 2.5	455



# PHYSICAL, MECHANICAL, AND NON-DESTRUCTIVE EVALUATION OF GRIT IRON SCALE HEAVY-DENSITY CONCRETE

*<sup>a</sup>M. Shoaib, <sup>a</sup>Aazib Sardar, <sup>a</sup>M. Abad qayyum, <sup>a</sup>M. Nasir Ayaz Khan\**

<sup>a</sup>: Civil Engineering Department, HITEC University

\* Corresponding author: Email ID: [nasir.ayaz@hitecuni.edu.pk](mailto:nasir.ayaz@hitecuni.edu.pk)

**Abstract-** In this study, heavy density grit iron scale aggregate is composed of concrete to assess its physical and mechanical properties. Grit iron scale aggregate was utilized in 25%, 50%, 75%, and 100% as coarse aggregate by replacing normal weight aggregate. Moreover, a control mix for comparison purposes was also developed. It was found that increasing the content of the grit scale tends to increase density and slump. The Compressive strength in rebound hammer was found maximum for concrete mix having a 50% grit scale. At the same time, ultra-sonic pulse velocity (UPV) tends to decrease by increasing the content of the grit scale. This study will help assess heavy-density concrete as a biological shield.

**Keywords-** Heavy density, grit scale, density, compressive strength.

## 1 Introduction

Concrete is primarily used as structural and protective material against harmful and ionizing radiation [1]. Concrete as a biological shield has been used from the very beginning due to its low cost, versatile nature, and ease of molding techniques [2]. Gamma rays, on the other hand, are used for food preservations, archeological sites, cancer therapy hospitals, and Nuclear Power Plants (NPP). These rays harm living cells due to their high penetration power and shorter wavelength. Therefore, the shielding of these harmful rays is evitable. For the same purpose, heavy-density concrete made from heavy-weight aggregates is primarily used as a biological shield against harmful gamma rays in NPP and related constructs such as nuclear waste storage compounds [3]. However, the radiation shield mainly and strongly depends upon materials' composition and density, especially aggregates. Therefore, heavy-density aggregates play a vital role as a biological shield in heavy-density concrete [4], [5].

Heavy Weight concrete is defined as a density greater than 2600 kg/m<sup>3</sup> [6]. To achieve this density, need's special aggregate called heavyweight aggregate. For instance, magnetite, barite, limonite, steel slag, steel punching, and steel shots were used to achieve high-density concrete. Using magnetite aggregate, a concrete density of more than 3500 kg/m<sup>3</sup> could be achieved [7]. In the contemporary study, barite, steel slag, and steel shots could yield concrete with densities of 3400 kg/m<sup>3</sup>, 5500 kg/m<sup>3</sup>, and 6500 kg/m<sup>3</sup>, respectively [8], [9]. ACI 304-3R91 (2004) and ASTM C637- 14(2019) describe the density and composition of aggregate for radiation shielding [10], [11].

A study recommends using magnetite aggregate to attenuate gamma rays more efficiently compared to normal weight aggregates [12]. Whereas Non-destructive testing (NTD) are widely used techniques to assess the quality of concrete, especially for post-construction. For example, the compressive strength and porosity of concrete have been assessed with a rebound hammer and ultrasonic pulse velocity (UPV) [13], [14].



In this experimental study, heavy density grit Iron scale aggregates are utilized in concrete to assess its physical and mechanical properties. This study will help study nuclear shields against gamma rays.

## 2 Research Methodology

ASTM Type-1 Ordinary Portland Cement (OPC) has been utilized in this study. Fine aggregate collected from a local vendor (Lawrancepur origin) with Fineness modulus 2.6 was used. Normal weight Coarse Aggregate (NCA) from Margalla has been collected and utilized. The Heavyweight Grit iron Scale (HWGS) density of 3912.26 kg/m<sup>3</sup> was collected from the foundry section of Heavy Mechanical Complex (HMC), Taxila, Pakistan. The physical and chemical properties of NCA and HWGS are given in table 1. The HWGS aggregate was a mix of both smooth and rough texture aggregates.

Table 1 Physical and chemical properties of HWGS and NCA

Aggregate Type	Physical properties		Chemical properties (%)		
	NCA	HWGS	NCA	HWGS	S
Density (kg/m <sup>3</sup> )	1550	3912.26	Fe	0.43	96
Hardness	7	9	Si	44.2	1.02
Color	Off white (limestone)	dark grey	Mn	0.03	1.2
Shape	angular	angular	C	-	1.2
Water absorption (%)	1.30	1.2	Cu	0.03	0.2
	-	-	Ni	0.06	0.15

For the compressive strength test, cubical molds of the control mix (having no Heavy Weight Grit iron Scale (HWGS) aggregates) and Heavy density Concrete were cast under controlled laboratory conditions. The Normal weight Coarse Aggregate (NCA) was replaced with 25%, 50%, 75%, and 100% HWGS designated as HDC1, HDC2, HDC3, and HDC4, respectively. After demolding, the concrete cubes were cured for 28 days in water under controlled laboratory conditions. After curing, the cubes were tested for compression in Compression Testing Machine (CTM) as per specifications laid by ASTM C 39/C 39M – 03. The workability of fresh concrete was also assessed in terms of Slump values ASTM as per the specification mentioned in C 143/C 143M – 03. The experimental program is shown in figure 1.



Figure 1: Experimental program



Chemrite SP303 superplasticizers were used to control the workability. For the HDC mixes, NCA was replaced with HWGS by volume method with constant water to cement ratio of 0.4. Moreover, for non-destructive evaluation, a rebound hammer and ultrasonic plus velocity tests were also carried out on concrete cubes. For each mix, the density at the 28 days of curing was also noted. The results of the density of concrete are shown in figure 2.

### 3 Results and discussion

#### 3.1 Slump

The variations of slump value concerning grit scale content are shown in figure 3. The slump value for the control mix was 50 mm, whereas HDC1, HDC2, HDC3, and HDC4 showed Slump of 53 mm, 62.5 mm, 70 mm, and 87.5 mm, respectively. The slump is decreasing by increasing the content of HWGS. The slump variations may be explained due to the irregular and angular structure of grit scale aggregates which offers more interlocking effect and intra-particle friction and results in a harsh mix. Irregular aggregates find it difficult to move smoothly in a mix.

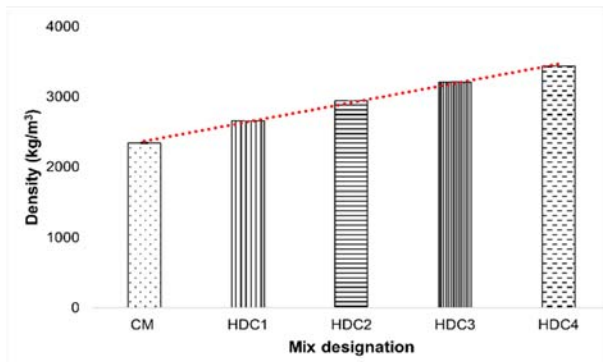


Figure 2: Density of concrete

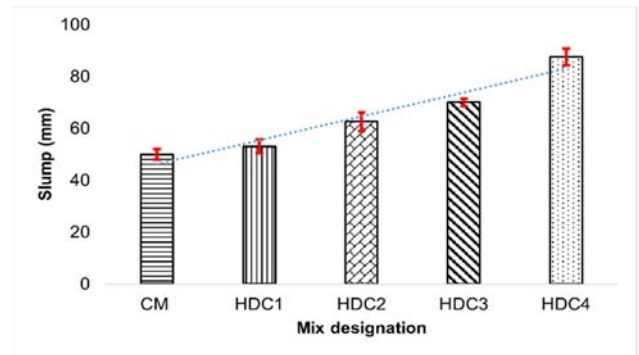


Figure 3: slump variations

#### 3.2 Compressive Strength

Figure 4 shows the variations of the compressive strength concerning the content of HWGS. The compressive strength observed for CM was found to be 20.5 MPa. Whereas HDC1, HDC2, HDC3, and HDC4, showed a maximum compressive strength of 20.8, 25.6, 22.5, and 19.7 MPa, respectively. The results show that up to 50% replacement of NCA with HWGS tends to increase the strength, whereas it decreases by increasing the HWGS content beyond this replacement. This is because the grit scale aggregate tends to make stronger bonds due to its irregular and angular texture. However, increasing the content of HWGS lacks an interlocking effect due to the abundance of aggregates, resulting in low strength.

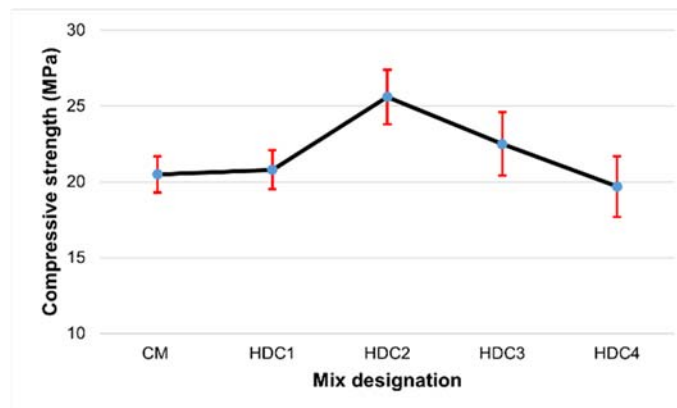


Figure 4: Compressive strength of concrete



### 3.3 Rebound hammer

The rebound hammer results indicate that the maximum value was obtained for HDC2 having 50% HWGS was found to be 33 and lies in the "Good Layer" of the concrete quality. The lowest was noted for HDC4, which was found to be 22 and lies in the "poor Concrete" category. The rebound hammer result is shown in figure 5. As mentioned in section 3.2, compressive strength was found maximum for HDC2 mix due to good interlocking effect and irregular aggregates shape. The same criteria and engineering knowledge could be applied to the rebound hammer. Due to its compact and dense structure, the mix showed good rebound values due to the hardness of the mix.

### 3.4 Ultra-sonic plus velocity (UPV)

The UPV test shows opposite results compare to the compressive strength and rebound hammer. The lowest UPV value was found for CM, and the largest was for HDC4. This is because grit scale aggregates are composed of heavy and dense structures with high atomic weight. The pulses of UPV are easily attenuated by the dense atomic structure of the concrete due to the inclusion of grit scale aggregate, resulting in more value. The grit scale has a density of more than 3.9 g/cm<sup>3</sup>, meaning the aggregates are densely packed with atoms. Therefore, UPV rays find it difficult to pass through such densely packed structures. Therefore, a linear trend in UPV increment could be observed for concrete by increasing the content of HWGS as shown in figure 6.

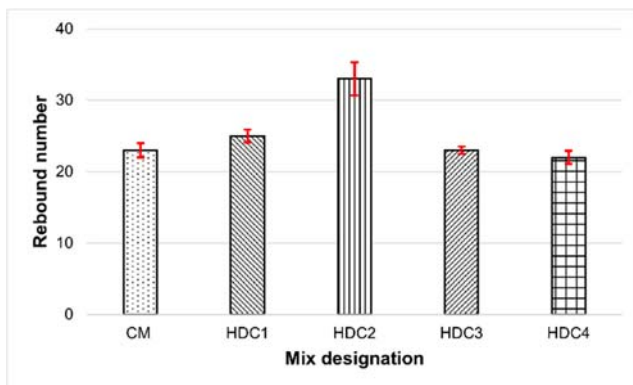


Figure 5: Rebound hammer results

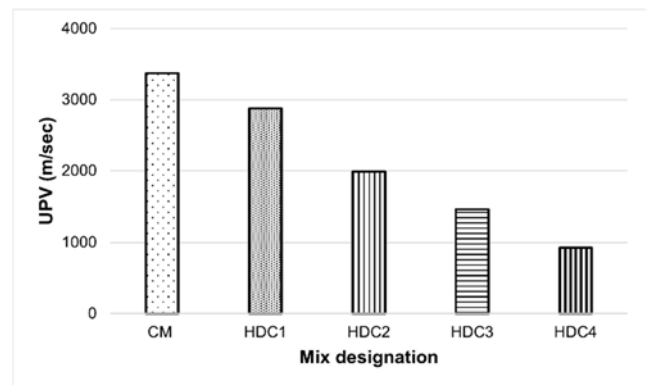


Figure 6: Ultrasonic Pulse Velocity test variations

## 4 Practical implementation

This study deals with developing heavy-density concrete by incorporating heavy-density grit iron scale aggregates. This study could be efficiently implemented in gamma irradiation facilities. The gamma irradiation facilities include nuclear power plants, cancer therapy rooms, nuclear waste storage facilities and research laboratories. Heavy-density concrete is made from aggregates that possess more atoms per unit area. Thus, such concrete can efficiently attenuate gamma rays compared to normal weight concrete. Moreover, heavy-weight concrete could also be utilized in underwater structures where more weight is required to sink the concrete at the bottom of a water body. Also, heavy-density concrete could also be used for counterweights such as overhead cranes working on site.

## 5 Conclusion

In this study, heavyweight grit iron scale aggregates were incorporated into the concrete to study its physical and mechanical properties. The following conclusion could be made:





- HDC1, HDC2, HDC3, and HDC4 showed slumps of 53 mm, 62.5 mm, 70 mm, and 87.5 mm, respectively. The slump decreased by increasing grit scale aggregates due to irregular and dense structure.
- HDC2 mix showed 25.6 MPa compressive strength as maximum among mixes. This is because an excellent interlocking effect was observed in grit scale, and compacted concrete structure was formed.
- Rebound hammer for HDC2 mix was found more due to the dense and compact structure of the mix.
- Ultrasonic pulse velocity was found to be minimum for the control mix (3400 m/sec) while the maximum for the HDC4 mix (980 m/sec). The UPV rays travel difficult in dense atomic structures; hence increasing the grit iron scale tends to show a good result for UPV.

## Acknowledgment

The authors would like to express their deep gratitude towards the concrete lab staff and HoD foundry section, HMC, Taxila, Pakistan. The careful review and constructive suggestions by the anonymous reviewers are gratefully acknowledged.

## References

- [1]. I. M Nikbin., S. Mehdipour., S. Dezhampanah., R. Mohammadi., R. Mohebbi., Sadrmomtazi. A., "Effect of high temperature on mechanical and gamma-ray shielding properties of concrete containing nano-TiO<sub>2</sub>". Rad. Phy and Chem, vol. 174, pp. 1-16, 2022, doi:10.1016/j.radphyschem.2020.10
- [2]. E. Zorla et al., "Radiation shielding properties of high performance concrete reinforced with basalt fibers infused with natural and enriched boron," Nucl. Eng. Des, vol. 313, pp. 306–318, 2017, doi: 10.1016/j.nucengdes.2016.12.029.
- [3]. I. Bashter, "Calculation of radiation attenuation coefficients for shielding concretes," Ann. Nucl. Energy, vol. 24, no. 17, pp. 1389–1401, 1997, doi: 10.1016/S0306-4549(97)00003-0.
- [4]. L. Lincheng., C. Zhenfu., T. Qiuwan., X. Liping., D. Du., "Effects of high temperatures on the splitting tensile strength and gamma ray shielding performance of radiation shielding concrete", Construction and Building Materials, Vol.343, pp. 127953, 2022, <https://doi.org/10.1016/j.conbuildmat.2022.127953>
- [5]. K.M. Nasir Ayaz., Y. Muhammad., M. Azhar H., "High density concrete incorporating grit scale aggregates for 4th generation nuclear power plants", Construction and Building Materials, Vol. 337, pp. 127-143, 2022, <https://doi.org/10.1016/j.conbuildmat.2022.127578>.
- [6]. E. S. A. Waly and M. A. Bourham, "Comparative study of different concrete composition as gamma-ray shielding materials," Ann. Nucl. Energy, vol. 85, pp. 306–310, 2015, doi: 10.1016/j.anucene.2015.05.011.
- [7]. H. S. Gökçe, B. C. Öztürk, N. F. Çam, and Ö. Andiç-Çakır, "Gamma-ray attenuation coefficients and transmission thickness of high consistency heavyweight concrete containing mineral admixture," Cem. Concr. Compos., vol. 92, pp. 56–69, 2018, doi: 10.1016/j.cemconcomp.2018.05.015.
- [8]. C. Sivathanu Pillai et al., "Evaluation of microstructural and microchemical aspects of high density concrete exposed to sustained elevated temperature," Constr. Build. Mater, vol. 126, pp. 453–465, 2016, doi: 10.1016/j.conbuildmat.2016.09.053.
- [9]. D. Jozwiak-Niedzwiedzka, K. Gibas, A. M. Brandt, M. A. Glinicki, M. Dąbrowski, and P. Denis, "Mineral Composition of Heavy Aggregates for Nuclear Shielding Concrete in Relation to Alkali-silica Reaction," Procedia Eng., vol. 108, pp. 162–169, 2015, doi: 10.1016/J.PROENG.2015.06.132
- [10]. ACI 304.3R-96, "Heavyweight Concrete : Measuring, Mixing, Transporting, and Placing Reported by ACI Committee 304", vol. 96, pp. 1–8, 2004.
- [11]. ASTM C637 Standard Specification for Aggregates for Radiation-Shielding Concrete 1", vol 04, pp. 1-4, 2019
- [12]. M. Nikbin et al., "Effect of high temperature on mechanical and gamma ray shielding properties of concrete containing nano-TiO<sub>2</sub>," Radiat. Phys. Chem., vol. 174, pp. 108967, 2020, doi: 10.1016/j.radphyschem.2020.108967.
- [13]. A. Jain., A. Kathuria., Y. Kumar., and K. Murari., "Combined use of non-destructive tests for assessment of strength of concrete in structure," Procedia Eng, vol. 54, pp. 241–251, 2013, doi: 10.1016/j.proeng.2013.03.0
- [14]. B. Baten., T. Manzur., "Formation Factor Concept for Non-Destructive Evaluation of Concrete's chloride diffusion coefficients", Cement and Concrete Composites, Vol.128, 2022, 104440, <https://doi.org/10.1016/j.cemconcomp.2022.104440>.



# EFFECT OF STEEL SLAG ON CONCRETE HAVING VARYING AMOUNT OF CEMENT

<sup>a</sup> *Qaiser Bashir*, <sup>b</sup> *Raja Bilal Nasar Khan*, <sup>c</sup> *Anwar Khitab*\*

a: Department of Civil Engineering, Mirpur University of Science and Technology (MUST) Mirpur-10250 (AJK) Pakistan,  
[qaiserbashir14@gmail.com](mailto:qaiserbashir14@gmail.com)

b: Department of Civil Engineering, Mirpur University of Science and Technology (MUST) Mirpur-10250 (AJK) Pakistan,  
[bilal.ce@must.edu.pk](mailto:bilal.ce@must.edu.pk)

c: Department of Civil Engineering, Mirpur University of Science and Technology (MUST) Mirpur-10250 (AJK) Pakistan,  
[anwar.ce@must.edu.pk](mailto:anwar.ce@must.edu.pk)

\* Corresponding author: Email ID: [anwar.ce@must.edu.pk](mailto:anwar.ce@must.edu.pk)

**Abstract-** Concrete with cement as main ingredient has a high demand in construction industry. Due to its increasing demand, new materials in combination with cement are used for improving its properties. A concrete needs higher paste volume when using cement alone, which may lead to greater heat of hydration with excessive shrinkage and increased cost. It is reported that cement is one of the largest source of CO<sub>2</sub> emission on the planet. Now-a-days serious efforts are being made for finding a suitable substitution of cement. In this research, cement was partially replaced by steel slag (steel slag). Preliminary tests like strength activity index and XRF indicated its chances to use as a partial substitute of OPC. Control specimens with varying cementitious contents of 220kg, 310kg and 400kg were prepared. In modified specimens, cement was replaced by steel slag (30% by mass of cement). The mechanical strengths (compressive, tensile and bending) were examined at 7 and 28 days. The outputs show an increase in strength with steel slag. It is also observed that the strength increment is more pronounced at higher binder content.

**Keywords-** Concrete, steel furnace slag, cement, sustainability, mechanical strength.

## 1 Introduction

In the construction industry concrete is being used plenteously. The demand of concrete is increasing with every passing day and so are the expectations from the concrete vis-a-vis its performance. New techniques and materials are being furnished to produce concrete having enhanced properties. In its composition, concrete chiefly consists of cement (binder), sand and coarse aggregate. Despite being the most important material in any concrete mix, the production of cement comes at a very high economic and environmental cost, depleting natural resources on the one hand and polluting the environment on the other. From the extraction and transportation of raw material from quarry site to the factories of cement, all this process involves the release of hazardous gases which are serious threat to our environment [1], [2]. The raw materials used for the cement production are limited. In addition to these, manufacturing cement requires a great amount of energy and labor that is also a serious health hazard. These factors call for finding a binder material that is both economic and eco-friendly, yet does not compromise on the properties that cement brings to the concrete. In this regard, the utilization of steel slag has emerged as a viable replacement for the cement because it reduces the demand of cement and make the otherwise appropriate disposal of this waste much easier without any compromise on the properties of concrete. Different researchers have explored the useful effects of steel slag using different cementitious materials.

Samad et al. investigated the effect of partial substitution of cement by steel slag. They used replacement levels as 30%, 40% and 50%. They have concluded that concrete having 50% substitution of cement with a water to binder ratio of 0.35



gains more strength than ordinary Portland cement [3]. Gholampour et al. utilized high early strength cement in combination with steel slag. They substituted cement in different percentages and found steel slag effective for imparting better workability and absorption. They indicated optimum percentage of steel slag as 50% by mass of cement [4]. El-Gamal et al. used slag for producing geo-polymer concrete in the presence of alkali activators. They also examined the impact of substituting slag with 5 and 10 percent of waste from clay-bricks. They concluded that 5 and 10% brick waste substitution efficiently improves compressive strength, enhances microstructural properties and creates dense geo-polymer structures [5]. Vinai et al. used pulverized fuel ash and steel slag for producing a cement free concrete. They used  $\text{Na}_2\text{SO}_3$  and  $\text{NaOH}$  solutions as activator. They investigated the compressive strengths at different ages and found that for the given composition, a water to binder ratio of more than 0.41 results in considerable strength reduction [6]. Nazari et al. focused on the use of steel slag as a partial replacement of cement in concrete. The substitution proportions were kept as 0%, 15%, 30% and 45%. Various hardened properties were evaluated. They found that concrete with slag up to 45% had enhanced properties of absorption and split tensile strength [7]. Dai et al. used et-grinding steel slag as partial replacement of cement in cement pastes. They have highlighted that 10% partial replacement results in the highest compressive strength under constraint conditions [8]. Lai et al. used steel slag aggregates as partial as well as full replacement of natural aggregates in concrete. They found that the slump of the mix decreases due to porous nature of the steel aggregates, however the compressive strength was enhanced. The slag also promoted denser packing, which reduced the chloride permeability in the concrete [9]. Low heat cement is highly desirable in mass concrete. Zhang et al. developed a novel low heat cement by using a combination of steel slag and nano silica. The results revealed that the novel mix met the standard requirements for low-heat cement and there was increase in the early strength as compared to the control specimens [10].

Pakistan has a vast steel industry, producing thousands of tons of waste, which is dumped in land spaces. There is need to convert this waste to wealth in accordance with the Sustainable Development Goals (SDGs). In this Research the main objective was to study the likelihood/feasibility of making good quality concrete by partially replacing varying amounts of cement with local steel slag, which is otherwise an important environmental burden. The control specimens with different cementitious contents of 220kg, 310kg and 400kg were prepared along with the specimens with 30% replacement of cement by steel slag. Different mechanical parameters evaluation techniques were performed and the results of control and modified specimen were compared.

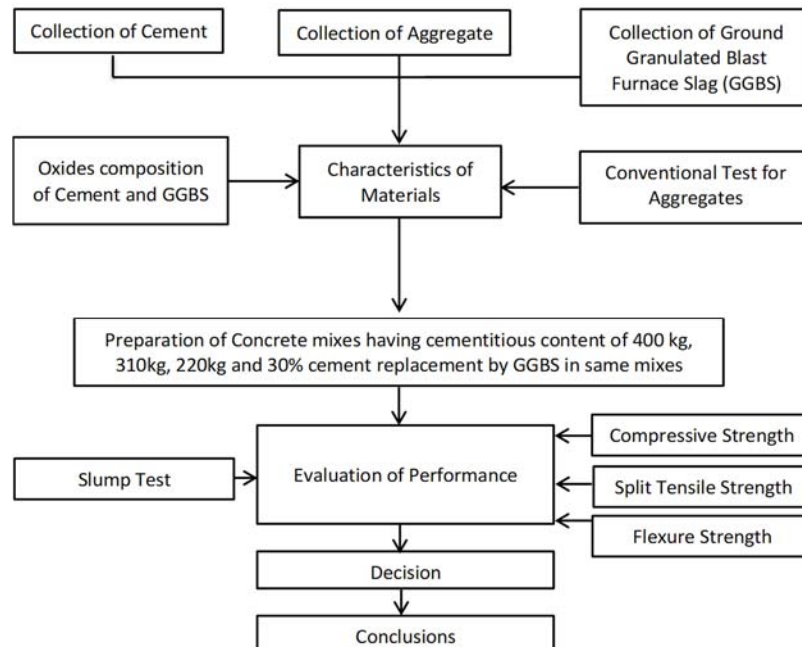


Figure 1. Research methodology



## 2 Materials and Methods

The cylindrical samples were prepared for evaluation of compressive and split tensile strength, whereas, beams were prepared for flexural strength test. Specimens were casted by replacing cement with 30% of steel slag and then results were compared with the set of controlled specimens. The cement content taken in this study relates to the minimum required cement content for conventional concrete mixes of 1:1.5:3, 1:2:4, 1:4:8 [11]. The research methodology is described in the flow chart given in Figure 1.

### 2.1 Raw materials.

The Ordinary Portland Cement (53 Grade) Type-I conforming ASTM C-150 is used in this research program [12]. Table 1 presents the oxides composition of the cement. Table 2 shows the physical characteristics of the cement. Lawrencepur sand and Margalla crush were applied as fine and coarse aggregates fractions. Their physical and mechanical properties are well-documented [1].

Table 1 Chemical composition of cement and steel slag (%)

Sr. No.	Oxides	Cement	steel slag
1.	CaO	64.19	40.04
2.	SiO <sub>2</sub>	21.45	34.88
3.	Al <sub>2</sub> O <sub>3</sub>	5.20	12.04
4.	Fe <sub>2</sub> O <sub>3</sub>	3.25	1.16
5.	SO <sub>3</sub>	2.70	0.59
6.	MgO	1.90	7.14
7.	K <sub>2</sub> O	1.0	0.544
8.	L.O.I	1.88	0.53
9.	Na <sub>2</sub> O	0.25	0.121

Table 2 Physical and mechanical properties of cement and steel slag

Sr. No.	Tests	Cement	steel slag
1	Compressive Strength (28 days)	63.84 MPa	-
2	Initial Setting Time	90 min	-
	Final Setting Time	247 min	-
3	Specific Surface Area	322 m <sup>2</sup> /kg	587 m <sup>2</sup> /kg
4	Specific Gravity	3.15	2.89
5	Soundness	1.00 mm	-
6	Passing	>90% (sieve #200)	>85% (sieve #325)

The pozzolanic activity of the steel slag was confirmed through strength activity index in accordance with the ASTM C618 [13]. The strength activity indices are mentioned in Table 3.

Table 3 Strength activity index

Sr No.	Tests	Result	Recommended
1	7 Days (Percentage of Control)	102.6 %	95%
2	28 Days (Percentage of Control)	118.3 %	115%



The chemical admixture (water reducer and super plasticizer) used was based on polycarboxylate ether at 1.2% by mass of cement in each mix designs [14]. It has a specific gravity of 1.180.

## 2.2 Casting of specimens.

The concrete mix design is shown in Table 4. For each test, a set of three samples was casted. Four sets of cylinders of control specimens for each mix design, while other four sets comprise of samples with 30% cement by mass replaced by steel slag. For performing flexural test, a set of three beams were casted. Two sets of beams for control and modified samples were prepared. Overall 72 cylindrical specimens and 36 beams were casted for this research. The casting and curing procedure was in accordance to ASTM C31 [15].

Table 4 Mix designs

Designation	Cement (Kg)	STEEL SLAG (Kg)	Sand (Kg)	Quantity per m <sup>3</sup>			
				Course Aggregate (Kg)	Water (l)	w/c	Superplasticizer (l)
A1	400	0	732	1083	169	0.42	4.80
A2	280	120	724	1083	169	0.42	4.80
A3	310	0	811	1083	169	0.54	3.72
A4	217	93	803	1083	169	0.54	3.72
A5	220	0	889	1083	169	0.77	2.64
A6	154	66	883	1083	169	0.77	2.64

## 2.3 Methods.

The samples were tested against slump, compressive strength, split tensile strength and flexural strength tests; The tests were performed in accordance with ASTM C143/143M [16], ASTM C-39/C39M [17], ASTM C-496/C-496M [18] and ASTM C-78 [19] standard methods respectively.

## 3 Results and discussion

### 3.1 Workability.

The workability was determined by slump test and the test setup is shown in Figure 2. The results are shown in Table 5.



Figure 2 Slump setup

The results given in Table 5 highlight that the workability increases if cement is replaced by steel slag (30% by mass of cement).



Table 5 Effect of steel slag on slump

S. No.	Mix Designation	Slump (mm)
1	A1	134
2	A2	142
3	A3	109
4	A4	115
5	A5	80
6	A6	83

The factors affecting the workability are water content, cement content, the properties of fine and coarse aggregate particles such as size, shape, grading, mix design and the admixture [20]. In all the samples, admixture was added @ 1.2 % by mass of binder. As such, the only difference was the cement replacement by steel slag. The steel slag particles have higher specific area than that of the cement; as such the concrete having steel slag should have lower workability values. Contrarily, there is increase in workability. There are two possible reasons. Firstly, the steel slag has lower bulk specific gravity. The specific gravity values depend upon the voids inside the material. More voids lead to higher workability and vice versa [21]. Secondly, steel slag has lesser lime content (40%) than cement (60%), and as such its primary hydration is lower than that of the cement during the very early age of the cementitious mix. Therefore, more water is available in fresh state for a material having steel slag as compared to the control specimen having 100% cement. This unreacted water in fresh state increases the workability of the concrete [22].

### 3.2 Compressive strength.

The cylinders having dimension of 150mm x 300mm were casted. The samples were test at loading rate of 4400N/s in the direction of depth of cylinder, as shown in Figure 3.



Figure 3 Compressive strength setup

The compressive strength results are the average of three tested specimens and are presented in Figure 4. While the 7 and 28 days' strength of the specimens are compared in Figure 5. Figure 4 shows that the compressive strength of concrete increases with replacement of cement by steel slag. The steel slag has much finer particles than those of cement. The pozzolanic activity strongly depends on the fineness of the particles. The presence of  $\text{SiO}_2$ ,  $\text{Al}_2\text{O}_3$ ,  $\text{Fe}_2\text{O}_3$  along with  $\text{CaO}$  imparts significant cementing and pozzolanic characteristics to the slag particles, that combined with a fine size ultimately enhances the compressive strength. When slag is added to the cementitious composites, it chemically reacts with portlandite (CH phase) and form additional Calcium Silicate Hydrate gel: This in turn provides additional



density and the strength is enhanced [23]. The higher cement content samples exhibit greater compressive strength development as compared to their control ones.

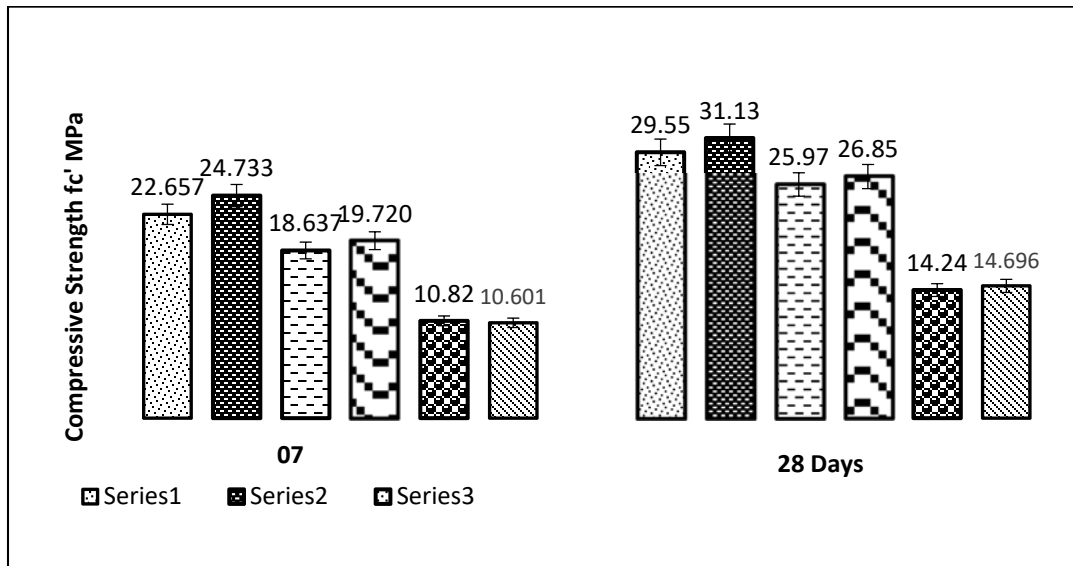


Figure 4 Effect of steel slag replacement on compressive strength

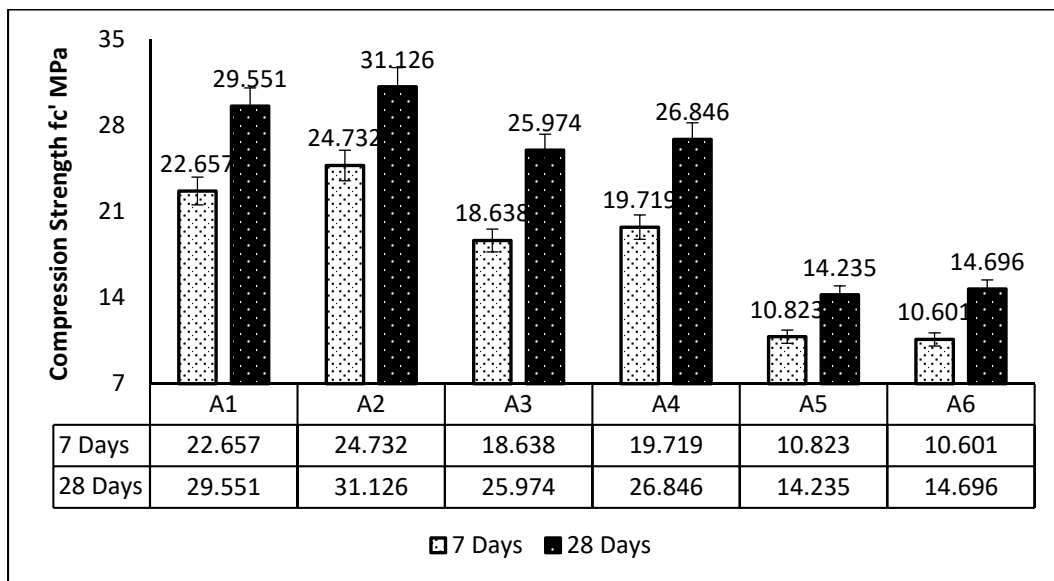


Figure 5 Comparison of 7 and 28 days compressive strength of all specimens

For sample A2, compressive strength increases by 5.33% of control sample A1, at 28 days. The strength increase for specimen A4 is 3.36% as compared to its control A3 on 28th day. While for sample A6, compressive strength increases by 3.24% of its control counterpart.

Normally, higher compressive strength is associated with a lower workability. Here, in this case, higher strength is accompanied with higher workability. Workability is associated with fresh state, whereas, strength is associated with hardened state. The unreacted water content is utilized while performing the pozzolanic activity, which ultimately enhances the strength.



### 3.3 Split tensile strength.

The split tensile strength was measured using the test setup presented in Figure 6. The test results (average of three) are shown in Figure 7. While the 7 and 28 days' strength of the specimens are compared in Figure 8.



Figure 6 Split tensile strength test setup

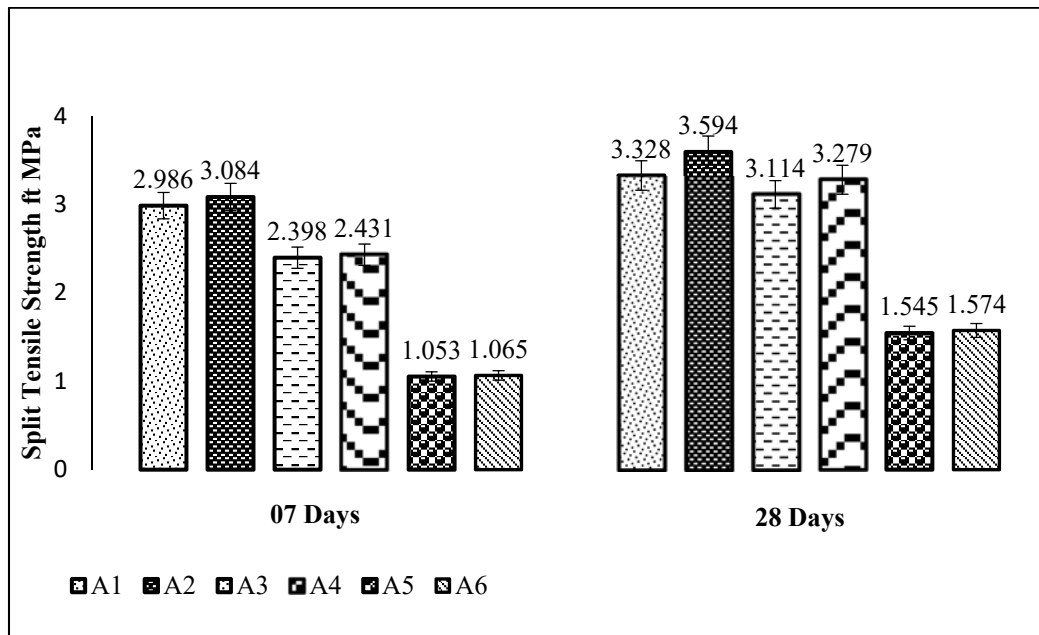


Figure 7 Effect of steel slag replacement on split tensile strength

Figure 7 and Figure 8 depict that split tensile strength of concrete increases with replacement of cement by steel slag. For higher binder content of 400 kg, specimen exhibit greater split tensile strength development as compared to their control specimen while for lower binder content of 220kg, sample exhibit lower increase in split tensile strength. For sample A2, split tensile strength increases by 7.99% of control sample A1 at 28 days.

The strength for specimen A4 increases by 5.30% as compared to its control specimen A3. While for sample A6, split tensile strength increases by 1.87% of its control sample. Increase in strength with steel slag confirms its pozzolanic and cementitious characteristics and the fine size of the steel slag adds to the strength of the material.



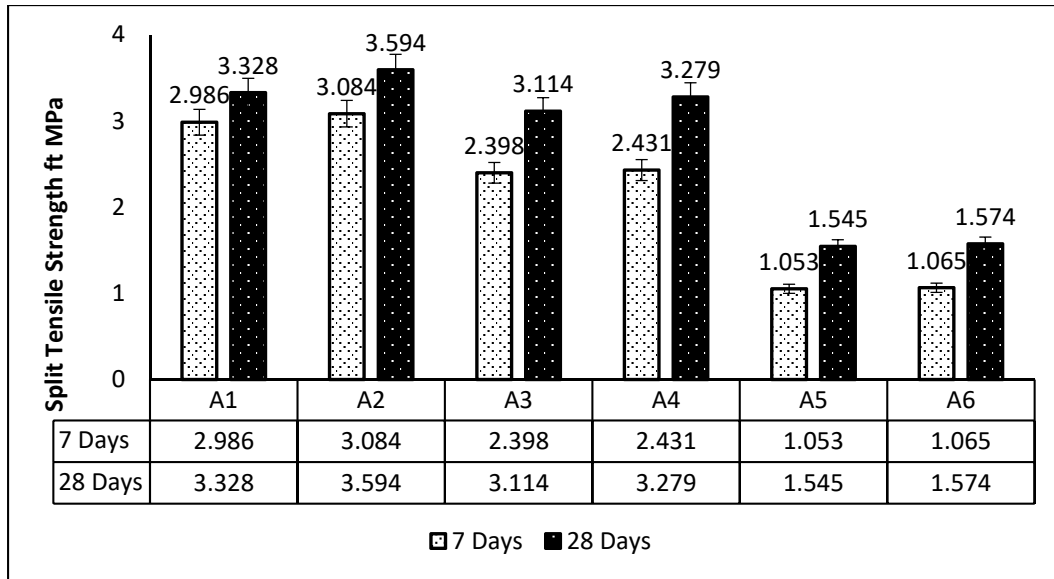


Figure 8 Comparison of 7 and 28 days split tensile strength of all specimens

### 3.4 Flexural strength.

The flexural strength test was performed using the setup shown in Figure 9. The results (average of three) are presented in Figure 10. While the 7 and 28 days' strength of the specimens are compared in Figure 11.



Figure 9 Flexural strength test setup

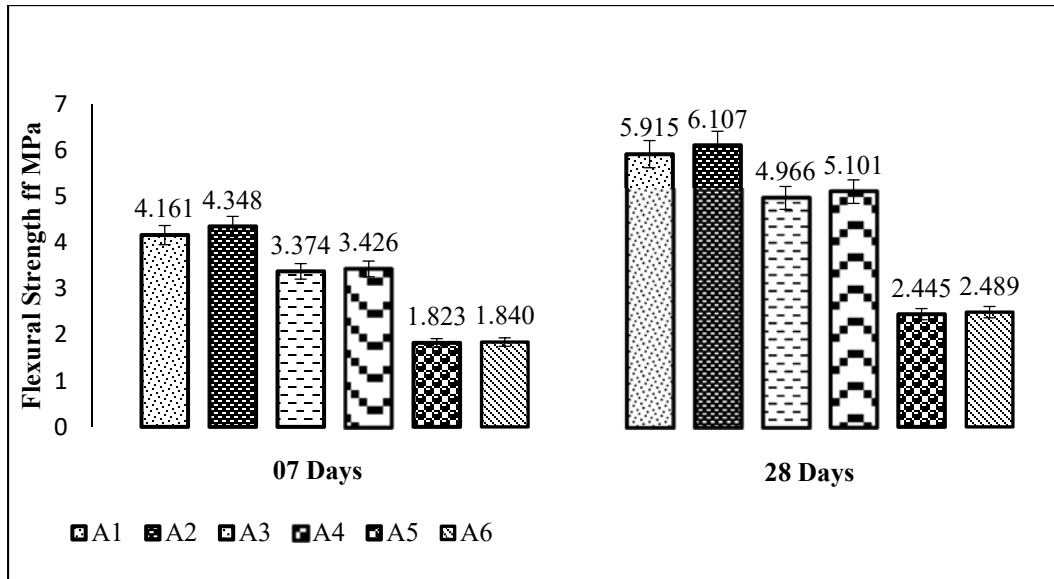


Figure 10 Effect of steel slag replacement on flexural strength

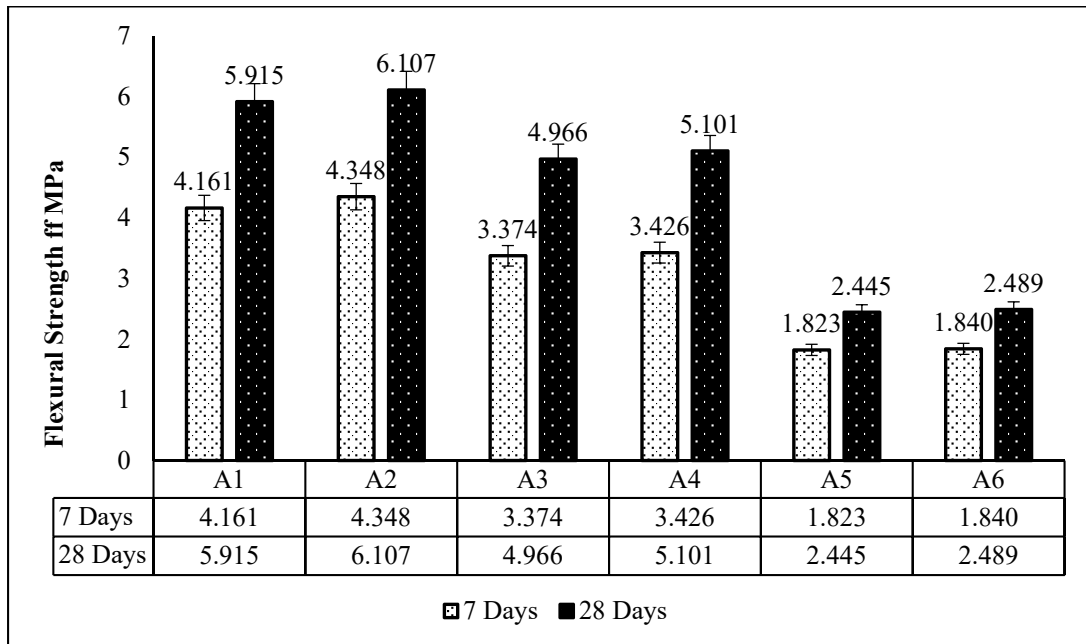


Figure 11 Comparison of 7 and 28 days flexural strength of all specimens

Figure 10 and Figure 11 highlight that the flexural strength of concrete increases with replacement of cement by steel slag. For sample A2, flexural strength increases by 3.25% to that of control sample A1, at 28 days. The flexural strength increases by 2.71% for specimen A4 as compared to its control A3. While for specimen A6, the strength increases by 1.80% of its control counterpart.

This happens because there is more volume occupation by steel slag in comparison to that of the OPC. So the paste volume also increases along with an increase in binding properties towards aggregates. According to Dai et al., the ultrafine slag particles, which initially do not participate in hydration reaction because of its pozzolanic property spread evenly in the pores and improve the pore structure and compactness of the samples [24].



### 3.5 Relationship between different strength results.

The relationship between different strength results of concrete is shown in Table 6.

Table 6 Ratio of split tensile and flexural strengths to compressive strength

	7 Days		28 Days	
	$\sigma_t/\sigma_c$	$\sigma_f/\sigma_c$	$\sigma_t/\sigma_c$	$\sigma_f/\sigma_c$
A1	0.131791	0.183651	0.112619	0.200162
A2	0.124697	0.175804	0.115466	0.196203
A3	0.128662	0.181028	0.119889	0.191191
A4	0.123282	0.173741	0.122141	0.19001
A5	0.097293	0.168437	0.108535	0.17176
A6	0.100462	0.173568	0.107104	0.169366

Table 6 demonstrates that the ratio of split tensile to compressive strength and that of flexural to compressive strength does not change appreciably if cement is partially replaced by 30% steel slag. Fapohunda et al. experimentally investigated the ratios of split tensile and flexural strength of the concrete containing different grades of cement [25]. As per their findings, the ratio of  $\sigma_t/\sigma_c$  at a water to cement ratio of 0.5 decreases from 0.126 at 7 days to 0.09 at 28 days. It has been reported that the split tensile strength is approximately 8-12% of the compressive strength for conventional concrete [26]. According to Lee et al., the ratio  $\sigma_f/\sigma_c$  varies from 10% to 20% for normal concrete [27]. Hence, the given results are in agreement with those of normal concrete.

The local steel slag used in this experiment is a pozzolanic material. Its pozzolanic activity enhances with increase in cement content. The use of steel slag offers many environmental and cost-effective benefits; It saves energy as regard lesser use of cement and, more performing products, being a partial cement replacement. Therefore, its substitution in concrete helps in sustainable development.

## 4 Conclusion

. Following conclusions can be drawn from the conducted study:

- 1 The workability of concrete increases as much water is available in fresh state for a material having steel slag as compared to the control specimen. This unreacted water in fresh state increases the workability of the concrete.
- 2 The 28 days' compressive strength increases from 3.24% to 5.79% of the control specimen for 220 kg to 400kg binder content with 30% replacement.
- 3 The 28 day split tensile strength of concrete increases for all mixes. This increase in strength is as much as 7.99% for higher binder content (400kg/m<sup>3</sup>) to that of its control specimen while 1.87% for lower binder content (220kg/m<sup>3</sup>) specimen.
- 4 The Flexural strength also increases for every concrete mix.
- 5 It is concluded that the steel slag can be utilized as a partial replacement material of cement, and 30% replacement of cement with steel slag gives better result in compression, tensile and flexural strength as compared to the normal concrete.

## Acknowledgment

The authors would like to thank every person at MUST, who helped thorough out the research work, particularly Civil Engineering department, ORIC and Engr. Muhammad Tausif Arshad.

## References

- [1] R. Arif, A. Khitab, M. Serkan, R. Bilal, and N. Khan, "Experimental analysis on partial replacement of cement with brick



- powder in concrete Case Studies in Construction Materials Experimental analysis on partial replacement of cement with brick powder in concrete,” *Case Stud. Constr. Mater.*, vol. 15, no. October, p. e00749, 2021.
- [2] A. Khitab, R. A. Khan, M. S. Riaz, K. Bashir, S. Tayyab, and R. B. N. Khan, “Utilization of Waste Brick Powder for Manufacturing Green Bricks and Cementitious Materials,” in *Ecological and Health Effects of Building Materials*, Cham: Springer International Publishing, 2022, pp. 361–370.
- [3] S. Samad, A. Shah, and M. C. Limbachiya, “Strength development characteristics of concrete produced with blended cement using ground granulated blast furnace slag (GGBS) under various curing conditions,” *Sādhanā*, vol. 42, no. 7, pp. 1203–1213, Jul. 2017.
- [4] A. Gholampour and T. Ozbakkaloglu, “Performance of sustainable concretes containing very high volume Class-F fly ash and ground granulated blast furnace slag,” *J. Clean. Prod.*, vol. 162, pp. 1407–1417, Sep. 2017.
- [5] S. M. A. El-Gamal and F. A. Selim, “Utilization of some industrial wastes for eco-friendly cement production,” *Sustain. Mater. Technol.*, vol. 12, pp. 9–17, Jul. 2017.
- [6] R. Vinai, A. Rafeet, M. Soutsos, and W. Sha, “The Role of Water Content and Paste Proportion on Physico-mechanical Properties of Alkali Activated Fly Ash–Ggbs Concrete,” *J. Sustain. Metall.*, vol. 2, no. 1, pp. 51–61, Mar. 2016.
- [7] A. Nazari and S. Riahi, “RETRACTED: Splitting tensile strength of concrete using ground granulated blast furnace slag and SiO<sub>2</sub> nanoparticles as binder,” *Energy Build.*, vol. 43, no. 4, pp. 864–872, Apr. 2011.
- [8] S. Dai, H. Zhu, D. Zhang, Z. Liu, S. Cheng, and J. Zhao, “Insights to compressive strength, impermeability and microstructure of micro-expansion steel slag cement under constraint conditions,” *Constr. Build. Mater.*, vol. 326, p. 126540, Apr. 2022.
- [9] M. H. Lai, Z. H. Chen, Y. H. Wang, and J. C. M. Ho, “Effect of fillers on the mechanical properties and durability of steel slag concrete,” *Constr. Build. Mater.*, vol. 335, p. 127495, Jun. 2022.
- [10] T. Zhang, B. Ma, S. Wu, Z. Jin, and J. Wang, “Mechanical properties and hydration process of steel slag-cement binder containing nano-SiO<sub>2</sub>,” *Constr. Build. Mater.*, vol. 314, p. 125660, Jan. 2022.
- [11] A. Khitab and W. Anwar, “Classical Building Materials,” in *Sustainable Infrastructure*, IGI Global, 2020, pp. 304–326.
- [12] ASTM C150/C150M, “Standard Specification for Portland Cement,” 2021.
- [13] A. Cheng, S. J. Chao, and W. T. Lin, “Effect of Calcination Temperature on Pozzolanic Reaction of Calcined Shale Mortar,” *Appl. Mech. Mater.*, vol. 174–177, pp. 843–846, May 2012.
- [14] A. Khitab and S. Mir, “Evaluation of polycarboxylate ether for use in locally manufactured cement composite materials,” in *International symposium vacuum science and technology (ISVST-2010)*, 2010.
- [15] ASTM C31 / C31M-12, “Standard Specification for Making and Curing Concrete Test Specimens in the Field,” *ASTM Int.*, pp. 1–6, 2012.
- [16] ASTM C143/C143M, “Standard Test Method for Slump of Hydraulic-Cement Concrete,” West Conshohocken, Pennsylvania UnitedStates, 2015.
- [17] A. C. 39/C39M, “Standard Test Method for Compressive Strength of Cylindrical Concrete Specimens,” pp. 3–9, 2014.
- [18] ASTM C496 / C496M-17, “Standard Test Method for Splitting Tensile Strength of Cylindrical Concrete Specimens,” West Conshohocken, PA, 2017.
- [19] ASTM C78/C78M, “Standard Test Method for Flexural Strength of Concrete (Using Simple Beam with Third-Point Loading),” West Conshohocken, Pennsylvania UnitedStates, 2018.
- [20] A. M. Neville, “Properties of concrete Fourth and Final Edition,” in *Perason-Prentice Hall*, 2004.
- [21] Vicky, “Workability of Concrete & Factors Affecting It,” *Civil Engineering Notes*, 2019. [Online]. Available: <https://civilengineeringnotes.com/workability-of-concrete/>.
- [22] K. Pazhani and R. Jeyaraj, “Study on durability of high performance concrete with industrial wastes,” *Appl. Technol. Innov.*, vol. 2, no. 2, pp. 19–28, Aug. 2010.
- [23] K. V. Schuldyakov, L. Y. Kramar, and B. Y. Trofimov, “The Properties of Slag Cement and its Influence on the Structure of the Hardened Cement Paste,” *Procedia Eng.*, vol. 150, pp. 1433–1439, 2016.
- [24] J. Dai, Q. Wang, C. Xie, Y. Xue, Y. Duan, and X. Cui, “The Effect of Fineness on the Hydration Activity Index of Ground Granulated Blast Furnace Slag,” *Materials (Basel)*, vol. 12, no. 18, p. 2984, Sep. 2019.
- [25] C. A. Fapohunda, B. A. Adigo, and B. I. Famodimu, “SPLITTING TENSILE STRENGTH AND COMPRESSIVE STRENGTH RATIOS AND RELATIONS FOR CONCRETE MADE WITH DIFFERENT GRADES OF NIGERIAN PORTLAND LIMESTONE CEMENT (PLC),” *FUW Trends Sci. Technol. J.*, vol. 5, no. 3, pp. 802–808, 2020.
- [26] S. H. Kosmatka, B. Kerkhoff, and W. C. Panarese, *Design and control of concrete mixtures*, 14th ed. USA: Portland Cement Association, 2002.
- [27] D. T. C. Lee and T. S. Lee, “The effect of aggregate condition during mixing on the mechanical properties of oil palm shell (OPS) concrete,” *MATEC Web Conf.*, vol. 87, p. 01019, Dec. 2017.



# COMPARATIVE ANALYSIS OF CEMENT-SAND MORTAR AND GEOPOLYMER MORTAR UNDER FIRE

<sup>a</sup> Muqadas Imran, <sup>b</sup> Khuram Rashid\*

a: Department of Architectural Engineering and Design, University of Engineering and Technology Lahore, [mqdsimran@gmail.com](mailto:mqdsimran@gmail.com)

b: Department of Architectural Engineering and Design, University of Engineering and Technology Lahore, [khuram\\_ac@uct.edu.pk](mailto:khuram_ac@uct.edu.pk)

\* Corresponding author: Email ID: [khuram\\_ac@uct.edu.pk](mailto:khuram_ac@uct.edu.pk)

**Abstract-** Fire hazard is the most common hazard and causes a significant reduction in physical and mechanical properties. Under high temperatures, the structural integrity of conventional cement mortar decreases drastically. Along with that, the dependency of the construction industry on cement should be reduced and alternatives must be considered as the production of cement requires a high rate of fuel consumption with excessive CO<sub>2</sub> emissions. Geopolymer is an emerging alternative binder to cement as it is more sustainable. In addition, it has superior fire resistive properties due to its in-organic polymeric nature. In this paper, cement-sand and geopolymer mortar was prepared and a comparative analysis was performed by observing the residual physio-mechanical properties after exposure at elevated temperatures. It was observed after performing various tests that the physical and mechanical strength of cement-sand mortar specimens were found to be extremely affected in contrast to geopolymer mortar. This study focused on the fire-resistive approach of geopolymer composite as compared to cement composites, in order to consider it as a surrogate to conventional cement in the future.

**Keywords-** Cement mortar, Fire hazard, Geopolymer mortar, Residual Strength.

## 1 Introduction

Fire incidents can be due to various reasons. It has an impact on human life and also damages the physical structure of the buildings. The intensity of the fire blazes affects the structure accordingly. In conventional cement structures, fire causes damage due to the difference in thermal characteristics between aggregate, cement, and steel, which results in the development of pore pressure and thermal stresses with the decomposition of cement hydration products as well. Cracking and spalling start at 300°C and 1200°C respectively. At sufficiently high temperatures, hydration products started to decompose and cause a reduction in materials' mechanical strength [1]. To increase the sustainability of our structure against fire, we need to integrate such materials that have significant fire-resistive properties and can enhance the residual strength of the structure as compared to cement composites. Secondly, there is also a need to reduce the dependency of our industry on cement composites because of its high fuel consumption for its production. Cement production contributes about 7% of total CO<sub>2</sub> production worldwide. One ton of cement produces almost one ton of CO<sub>2</sub> emission during its synthesis [2].

Precursors involved in the synthesis of geopolymer are mostly raw materials like calcinated clays, coal ashes, and slag. Fly ash (FA) is a waste or by-product of coal and in accordance with ASTM C618-19, a low calcium compound containing FA (Class F) can be used for the preparation of alkaline activated geopolymer. Recent studies have also shown that potassium hydroxide (KOH) containing composites have better fire-resisting properties than NaOH [4]. Alkaline activators are considered to be binders in geopolymer and will be the reason for the reaction between the precursors and activators resulting in achieving material strength. Alkaline-activated geopolymers have better fire resisting properties and are more stable than conventional ceramic composites. At high temperatures, the strength of the geopolymer increases because of the geopolymerization process i.e., the geopolymer matrix stabilizes due to a further increase in the temperature or heat



because it is accelerating the reaction [3]. Geopolymers are in-combustible because of their inorganic polymeric nature, and they have high endothermic properties because of the presence of physically and chemically bonded water. That is why they are capable of absorbing heat. Thermal conductivity varies between 0.1-0.3 W/m-K which is less compared to other materials hence it can work as a flux barrier. The thermal resistance value of geopolymer is comparable to fire-resistive materials [1].

Through this background, our goal is to introduce geopolymer mortar as a surrogate for conventional cement mortar because it possesses superior fire-resistive properties with high residual strength. This work is designed to observe the comparative performance of geopolymer mortar as compared to cement-sand mortar at elevated temperatures.

## 2 Experimental Procedures

Cube molds of dimension 70mm x 70mm x 70mm were taken and considered to be the desired shape for the given experiment. Molds were cleaned and oiled properly a day before the sample casting. Geopolymer and cement-sand mixtures were prepared according to the defined ratios and then samples were cast, by placing the mixtures in the oiled mold specimens. The detailed experimental procedure is explained below:

### 2.1 Material

Low calcium containing Class F FA, according to ASTM C618-19 is used as the main precursor for the preparation of geopolymer, as shown in Table 1. FA contains rich alumina-silica compounds, which play a role in achieving better strength because the more the alumina-silica compounds, the more the alkaline reaction takes place. Lawrencepur sand is used as a filler in geopolymer mortar preparation. Alkaline activators used are; 14 molar KOH solution and sodium silicate ( $\text{Na}_2\text{SiO}_3$ ) solution. Whereas DG cement and Lawrencepur sand were used for the preparation of conventional cement mortar.

Table 1: Specifications of Class F FA according to ASTM C618-19

Properties	FA Classes	
	Class F	Class C
Silicon Dioxide ( $\text{SiO}_2$ ) + Aluminum Oxide ( $\text{Al}_2\text{O}_3$ ) + Iron Oxide ( $\text{Fe}_2\text{O}_3$ ), min %	70.0	50.5
Sulphur Trioxide ( $\text{SO}_3$ ), min %	5.0	5.0
Moisture Content, min %	3.0	3.0
Loss on ignition	6.0	6.0

### 2.2 Mortar Synthesis

Geopolymer and cement-sand mortar were prepared according to the mix design ratios as described in Table 2. For the preparation of geopolymer mortar, alkaline activators were used in liquid form so, a solution of 14M KOH was prepared a day prior to the mortar synthesis. Firstly, FA and sand were taken according to given ratios and dry mixed together. After that, both liquids were mixed and added slowly into the dry mix. Gently mixed with an electrical mixer while adding liquids to the dry materials evenly, to form a uniform paste. Similarly, in the case of cement-sand mortar, the required amount of cement, sand, and water was taken according to the defined ratios (Table 2). Water was added to the dry mix to form a uniform paste. The mix design ratio for geopolymer and cement-sand mortar preparations is shown in Table 2.

Table 2: Mix design ratios for the preparation of mortars

Geopolymer Mortar	Ratios	Cement-sand Mortar	Ratios
Alkaline activator/Precursor	1:3	C/S	1:3
FA/Sand	1:1	W/C	1:2
KOH/ $\text{Na}_2\text{SiO}_3$	2.5		



### 2.3 Specimen Casting

Cube specimens (70 mm) were cast by placing the prepared mixtures of both geopolymer and cement-sand mortar in the oiled molds. Molds were cleaned and oiled properly a day before the sample casting. In the case of cement-sand mortar, the prepared mix was poured in three different layers into the cube mold. While pouring into the molds, each layer was tamped with a tamping rod 25 times each time to remove the voids. After that, molds were placed on a vibration table for further compaction. Similarly, in the case of geopolymer mortar, the prepared mix was immediately placed into the molds as the setting time of geopolymer is very quick.

Curing conditions play an important role to achieve the strength of the casted specimens. For cement-sand mortar, samples were cured at room temperature for 27 days while the geopolymer specimens were placed in an oven at 90 – 110°C for 24 hours as geopolymer mortar gains strength at high temperature because the rate of initial alkaline reaction increases at high temperature. After oven curing, samples were placed at room temperature to gain further strength.

### 2.4 Exposure conditions and testing

Mortar specimens were prepared and cured for 28 days, according to their condition. Cured specimens were then placed in a furnace over for 120 minutes at elevated temperatures (400°C, 600°C, and 800°C). A number of specimens of both mortars at each temperature are shown in Table 3. Experimental tests were then performed on cooled specimens, by placing them under different tests for the comparative analysis of fire-resistive properties. Both mechanical and physical tests including compressive strength, crack pattern, and crack width were performed, and observations were made in order to observe the damage or the effect of high temperature on residual strength properties of specimens.

Table 3: Exposure conditions for both geopolymer and cement-sand mortar

Sr #	Temperature (°C)	Time Duration (minutes)	Number of specimens
1	20	120	3
2	400	120	3
3	600	120	3
4	800	120	3

## 3 Research Methodology

In order to introduce a material having better fire-resisting properties and can be used as an alternative to cement, experimental research is important. In order to do the comparison, twelve cube specimens of both geopolymer and cement-sand mortar were cast according to the fixed ratios. Samples were then cured according to their required conditions in order to achieve full material strength.

When reached their 27-day strength, samples were then placed in an oven for thermal exposure, at elevated temperatures (400°C, 600°C, and 800°C) for two hours. After thermal treatment, cube specimens are allowed to cool down properly. Experimental tests were then performed on cooled specimens, by placing them under different tests for the comparative analysis of fire-resistive properties. Both mechanical and physical tests including compressive strength, crack pattern, and crack width were performed and observations were made in order to observe the damage or the effect of high temperature on residual strength properties of specimens.

## 4 Results

Mechanical and physical properties of both geopolymer and cement-sand mortar were observed by performing different experimental tests including residual compressive strength test, maximum crack width, and crack pattern as well. Samples were placed under observation when they properly cooled down after the thermal exposure in the furnace for the required time. Three specimens of both mortars were placed at each temperature for 120 minutes. Following is a detailed discussion on experimental observations.

#### 4.1 Compressive Strength

Average residual compressive strength of both geopolymer and cement-sand mortars were taken and then the representative graphs were made to show the comparison properties of the effect of thermal exposure on compressive strength. Figure 1 shows that cement specimens have maximum strength at room temperature and then show a decreasing trend from 24.3MPa to 2.7MPa, with the increase in temperature. But in the case of geopolymer mortar, there is a slight difference in compressive strength of geopolymer at room temperature and after thermal exposure at 400 °C. This shows that geopolymer mortar has maximum strength at 400 °C because with the increase in temperature, the rate of geopolymerization increases. After 400 °C, there is a bit decreases in compressive strength after the initial stability. At 800°C, compressive strength further decreases to 24.9MPa as shown in Figure 1.

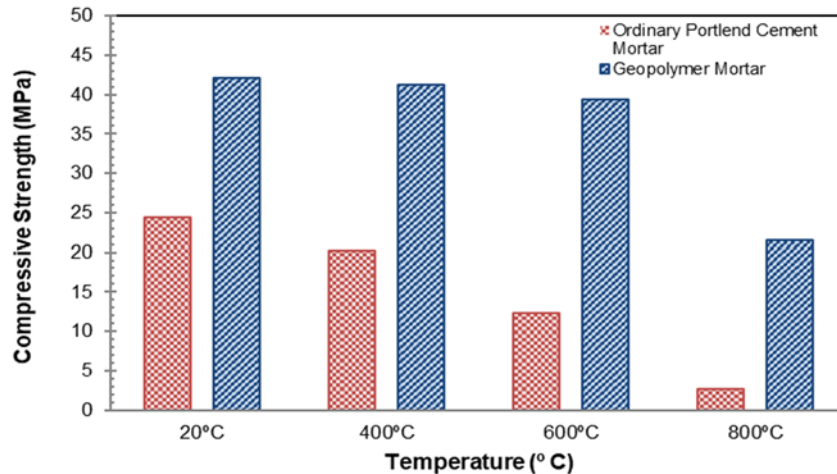


Figure 1: Influence of temperature on compressive strength of geopolymer and cement-sand mortar

#### 4.2 Cracking Pattern

The cracking pattern of each cube specimen was visually observed from the specimen after exposure to the conditions. To observe the effect of thermal treatment on the physical properties of OCM specimens, crack pattern of samples at each temperature was drawn simply by visualizing without using any equipment. To enhance the crack pattern, the J-image effect of every specimen oneach temperature was made. From the enhanced image, the crack pattern was drawn to create a schematic diagram by using Autodesk AutoCAD 2018.

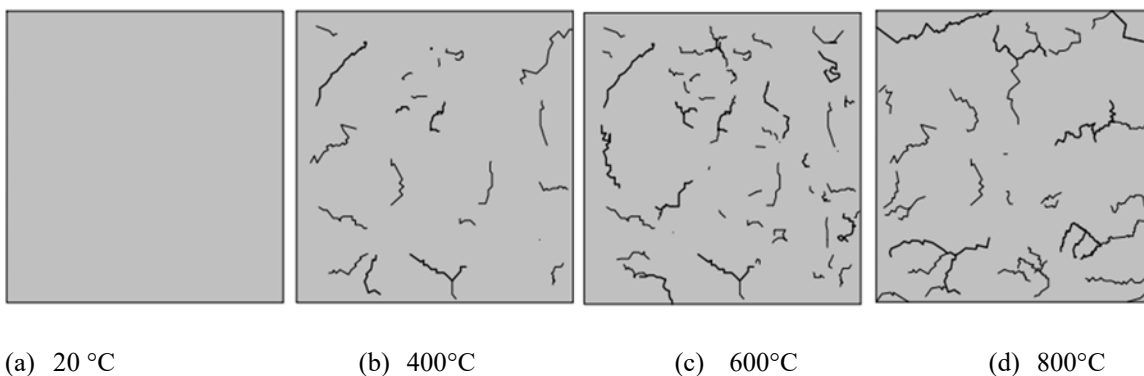


Figure 2: Schematic image representing influence of temperature on crack pattern of cement-sand mortar

Crack pattern of cement mortar specimens at each temperature are shown in Figure 2. Schematic diagram shows that with the increase in temperature, the number of cracks in cement mortar specimen increases. Cracks in cement mortar is mainly due to thermal expansion and pore pressure build-up. At 100°C, free water starts





evaporating causing weight loss, after 100°C up to 300 °C, dehydration of chemically bounded water occurs resulting into increase in number of cracks [1]. And further increase in temperature also damages the strength, as a result at 800 °C, the corners of cement specimens were also damaged (Figure 3). But in case of geopolymer specimens at 600 °C having less cracks as compared to specimens at 400 °C. This is because at 400 °C, excessive shrinkage occurred due to the evaporation of chemically and physically bounded water. And at 600 °C, the geopolymer gel started melting and filling the gaps [5, 6]. But further increase in temperature from 700 °C, crack pattern in geopolymer increases.

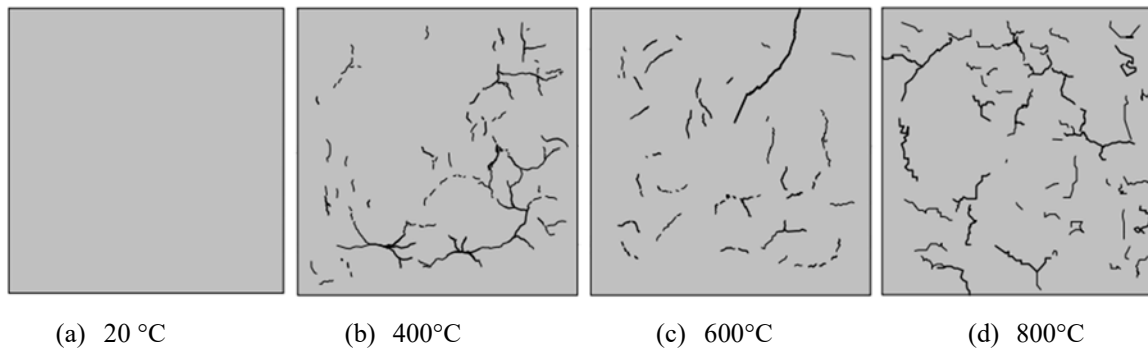
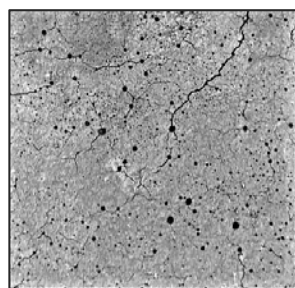


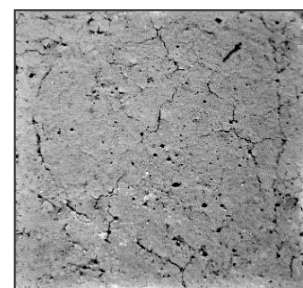
Figure. 3: Schematic image representing influence of temperature on crack pattern of geopolymer mortar

### 3.3 Maximum Crack Width

Cube specimens prepared from both mortars were placed under a microscope to observe the maximum crack width. Three samples at each temperature were taken and the lens was adjusted on the scale as well as on the crack of maximum width. The crack width of all the specimens was taken in mm. And graph was made by taking an average of two nearby values of maximum crack width as shown in Figure 4. No cracks were found in both mortars at room temperature but with the temperature increasing from 400°C to 800°C, the maximum crack width in cement-sand mortar also increased. Maximum crack width shows an increasing trend and the maximum crack width value in the case of cement-sand mortar is 800°C. But in geopolymer mortar, crack width even at 200°C was greater in comparison to cement-sand mortar. It is evident from the graph that its value shows a drastic increase at 600°C and the maximum value is recorded at 600°C which is 0.06mm because there is more drying shrinkage as more chemically bound and physically attached water with the hydroxyl group as well is present in geopolymer mortar as compared to cement mortar [1]. This value is greater than the maximum crack width at 800°C. It is shown in Figure 4 that the further increase in temperature from 600°C causes a decrease in maximum crack width. This is because, all water evaporates at 600°C, and after that geopolymer gel starts melting and filling the cracks [5, 6]. This is the reason at high temperatures or under fire, the maximum crack widths in the case of geopolymer are less as compared to cement-sand mortar.



(a) Geopolymer Mortar



(b) Cement-sand Mortar

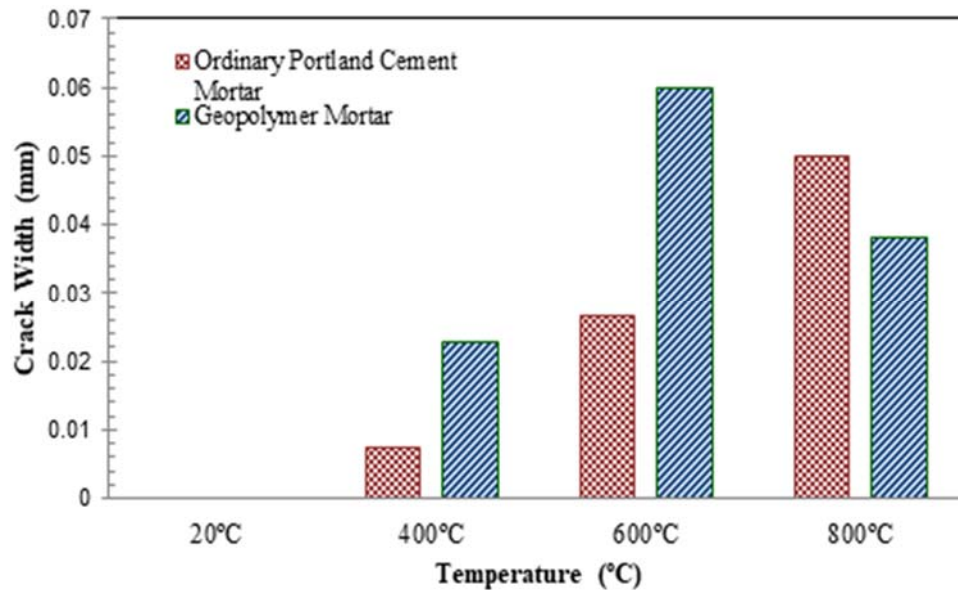


Figure 4: Influence of temperature on maximum crack width of geopolymer and cement mortar

## 5 Practical Implementation

As geopolymer mortar has better fire resistance and high residual thermal properties as compared to cement-sand mortar. To enhance the sustainability and lifespan of our structures, we should integrate geopolymer mortar in areas that are more sensitive to catching fire. Ceramic composites should be replaced with geopolymer mortar in those areas which are more vulnerable to fire hazards. In order to avoid direct damage to the structural integrity of buildings, geopolymer mortar lining should be applied in areas like (tunnels, basements parking, kitchen areas, compacted apartments, etc.) as passive protection.

## 6 Conclusion

Experimental analysis of this research concludes that the specimen prepared from geopolymer mortar has high residual compressive strength, less porosity, and crack width as compared to conventional cement-sand mortar even at elevated temperatures. The crack width of geopolymer mortar started to decrease with the increase in temperature, as the polymeric gel filled the gap and strengthen the mortar specimen. Edges of cement-sand cube specimens started to damage from 600°C while geopolymer specimens remain un-damaged even at 800°C.

## Acknowledgement

This paper and the research behind it would not have been possible without the careful suggestion and exceptional support of my supervisor. I am also very grateful and would like to thank the Department of Architectural Engineering and Design especially the Structural Engineering and Foundation Engineering Laboratory of the Department.

## Reference

- [1] F. Pacheco-Torgal, J. A. Labrincha, C. Leonelli, A. Palomo, and P. Chindapasirt, Handbook of alkali-activated cements, mortars and concretes. Cambridge: Woodhead Publishing, 2015.
- [2] Assi, L. N., Carter, K., Deaver, E., & Ziehl, P. (2020). Review of availability of source materials for geopolymer/sustainable concrete. *Journal of Cleaner Production*, 263, 121477.
- [3] Payakaniti, P., Chuewangkam, N., Yensano, R., Pinitsoontorn, S., & Chindapasirt, P. (2020). Changes in compressive strength, microstructure and magnetic properties of a high-calcium fly ash geopolymer subjected to high temperatures. *Construction and Building Materials*, 265,
- [4] Hager, I., Sitarz, M., & Mróz, K. (2021). Fly-ash based geopolymer mortar for high-temperature application – effect of slag addition. *Journal of Cleaner Production*, 316, 128168.



**4<sup>th</sup> Conference on Sustainability in Civil Engineering (CSCE'22)**  
Department of Civil Engineering  
Capital University of Science and Technology, Islamabad Pakistan



- [5] He, R., Dai, N., & Wang, Z. (2020). Thermal and mechanical properties of geopolymers exposed to high temperature: A literature review. *Advances in Civil Engineering*, 2020, 1–17.
- [6] Khalil, M. G., Elgabbas, F., El-Feky, M. S., & El-Shafie, H. (2020). Performance of geopolymer mortar cured under ambient temperature. *Construction and Building Materials*, 242, 118090.



# EFFECT OF HUMAN HAIR FIBER ON MECHANICAL PROPERTIES OF CONCRETE

*<sup>a</sup> Muhammad Waqas\*, <sup>b</sup> Ayub Elahi, <sup>c</sup> Rana Muhammad Waqas,*

a: Department of Civil Engineering, University of Engineering and Technology Taxila. [engrwaqas782@gmail.com](mailto:engrwaqas782@gmail.com)

b: Department of Civil Engineering, University of Engineering and Technology Taxila. [ayub.elahi@uettaxila.edu.pk](mailto:ayub.elahi@uettaxila.edu.pk)

c: Department of Civil Engineering, University of Engineering and Technology Taxila. [rana.waqas@uettaxila.edu.pk](mailto:rana.waqas@uettaxila.edu.pk)

\* Muhammad Waqas: Email ID: [engrwaqas782@gmail.com](mailto:engrwaqas782@gmail.com)

**Abstract-** In the whole world tons of hair are wasted annually, which creates many health problems by damaging our ecosystem. Thus, it is very fruitful for us to use concrete and increase its properties of concrete and save the environment from future crises. The construction industry needs a lot of natural assets like limestone, aggregate, sand etc. to make concrete. These resources are finite and have to consume/expand someday, so an alternative must be adopted to overcome the needs. This paper presents the mechanical properties of concrete when human hair fiber is used as a fiber. A detailed experiment was carried out on three types of concrete specimens i.e. cube, beam and cylinder having different percentages of human hair fiber such as 0%, 1%, 2% and 3 % by weight of cement. In addition in research different lengths of human hair fiber which varied from 20mm to 60mm were used. All the specimens were cast at two different concrete mix proportions i.e 1:2:4 and 1:1.5:3 with a 0.50 water-cement ratio. Furthermore, specimens were tested in Universal Testing Machine at 28 days curing period, for compressive strength, splitting tensile strength and UPV test and flexural strength of concrete. The conclusion from the experiments shows that there is a reduction in the workability of fresh concrete besides that there is an increment found in density and water absorption. Moreover, with increasing the percentage of the human hair fiber, mechanical properties were enhanced.

**Keywords-** Workability, human hair, compressive strength, ultrasonic pulse velocity, flexural and split tensile strength.

## 1 Introduction

Concrete is the most ubiquitous material used after water. Same as water, it is also the need of every person. Because of its high durability, ingredients are easily available, resistant to water and wind, it can be cast in any desired shape and is also economical material and has a low maintenance cost. Nevertheless, it possesses low tensile strength, less ductility and micro cracks. [1] For improving the strength and different properties, in this project, hair fiber is used as fiber in concrete. The purpose of using human hair fiber is to increase tensile strength and it increases the physical and mechanical properties of concrete. Concrete is a brittle material, it is weak in tension and after hardening, it has micro-cracks, which decrease the life span of the concrete structure. [2] Hair is non-degradable material, it causes environmental pollution, which directly affects humans and animals as well. Hence, sometimes using human hair as a fiber in the concrete can increase the properties of concrete. Human hair is used for increasing its strength in tension and reducing the micro-cracks helps, to increase the life period of the structure [3] It is defining characteristic of mammals. Human fiber has recently become eye-catching to researchers, scientists, and engineers as a replacement or with reinforcement in fiber-reinforced concrete composites Human hair is a non-degradable material and is present in a very amount. The cost of Human fiber is almost zero or very cheap cost. [4] Thus, most developing countries also face the same problems as poor countries regarding their disposal and handling. Recent research exposed that the growth speed of hair is 1.25 per month. In a year it is 15cm or 6 inches. By weighting, it is approximate 80 to 100gm per year (Shankar Lal Meghwar2016) [5]. Now consider that annually every Pakistani cuts 80gm hair and the population of Pakistan is 22 million's, its mean production of hair is 17600 tons



annually and annually the whole world produces  $6.4 \times 10^6$  tons and now think about those who already dumped in past years. And same as in past, in future the amount of hair will increase by enhancing in population for controlling this pollution, the researcher took initiative and did research about to how to control earl dangerous evil and then in 1963 human hair invented as a natural fiber and after 2012s it is the part of the construction industry on the specific area. Hair is added to concrete to increase its mechanical properties of concrete. [6] Recent research revealed that if the proportion of hair and concrete ingredients is correct as well as the method of distribution of hair fiber into concrete is correct then the mechanical and physical properties of concrete are easily enhanced. These properties of concrete are changed after adding hair to plain cement concrete [7]. Some countries are working on that used hair in medicine and agricultural industries but the amount of hair is too high. Thus, the remaining part affects our environment. Many types of fibers are used in concrete as fiber but the problem is, that they are all not renewable. Human hair is waste material in most of the world. Some countries are working on that used hair in medicine and agricultural industries. Therefore, it directly damages to people in future Therefore, it directly damages people in future. That's why the global wise now trend changed toward hair, as fiber in concrete. [8] This study was checked the effect of hair Fibers on the mechanical properties of concrete. Environmentally friendly, sustainable & economic concrete. For improving the strength and different properties, in this project, human hair is used as fiber in concrete. The purpose of using human hair fiber increases the mechanical properties of concrete. This study is found that by using human hair not just mechanical properties are increased same as physical properties. This study is of interest to clients, concrete manufacturers, concrete additive manufacturers and designers' specifiers who need to know what effect human hair as fiber additives have upon the final compressive strength, split tensile strength and flexural strength.

## 2 Experimental Procedures

The experimental work was performed in the laboratory. In this experimental work two categories of tests are performed by "ASTM" procedures. First for fresh concrete and second for hardened concrete. Moreover, the complete detail of each material used in the whole project is also explained. The concrete laboratory of UET TAXILA is used for all experiments work. [9] Ordinary Portland cement was used as the main binding material followed by ASTM C150 Properties of Ordinary Portland cement are shown in table 1 properties of inert material in table 2 and properties of human hair fiber in table 3.

Table 1 Properties of OPC

Chemicals	SiO <sub>2</sub>	TiO <sub>2</sub>	Al <sub>2</sub> O <sub>3</sub>	Fe <sub>2</sub> O <sub>3</sub>	MnO	MgO	CaO	Na <sub>2</sub> O	K <sub>2</sub> O	P <sub>2</sub> O <sub>3</sub>	LOI
Ordinary Portland cement	17.4	-	10.2	3.6	-	1.8	62.3	0.9	1.4		0.9

Table 2 Properties of inert materials

Properties	Fine aggregate (F.A)	Coarse aggregate (C.A)
Specific gravity	2.7	2.65
Water Absorption (% age)	1.2	0.54
Fineness modulus	2.99	-

Table 3 Properties of the human hair fiber

Properties	Ranges
Hair length	20mm to 60mm
Hair Diameter	80 to 150 $\mu$ m
Tensile Strength of human hair fiber	359 Mpa



### 3 Research Methodology

#### 3.1 Specimen preparation

In this extensive research work, all specimens are made and cured. The materials used during casting were also the same as ASTM standards. The purpose of this code is to cast the specimen's accurate control of the material and gain high strength. This standardized requirement provides the way how to prepare the sample, mixing of concrete and the curing of concrete test specimens under laboratory condition. All specification is done then the stipulated strength is achieved. The treatment of human hair is essential for gaining the required properties. [10] Most of the time hair is oily. This oil can be effective during bonding between materials of the concrete and not good for bonding. Besides, same as wastage and dust are also affected by it. Hair was collected from different barbershops and parlours. While collecting many wastages (tissue paper, blade and paper) were present [11] Thus, it is a very important step to clear all hair from these wastages and just used hair during mixing time as a filler in concrete. The sorting method is very important for concrete. Grouping is done on the base of the cooler, length and diameter of the hair. Color and diameter are checked randomly done by eyes but the length is checked according to the required length by scale. In this project, the required length is 20mm to 60mm. By giving a lot of time hair was categorized accurately in length. Scaling and grouping of human hair fiber are shown in Figure 1.

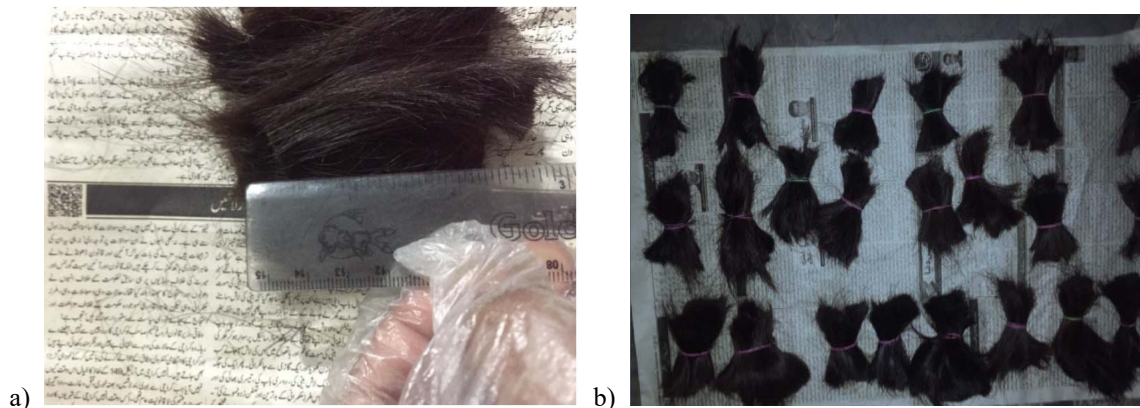


Figure 1: human hair treatment, a. Scaling of hair, and b. Grouping the human hair

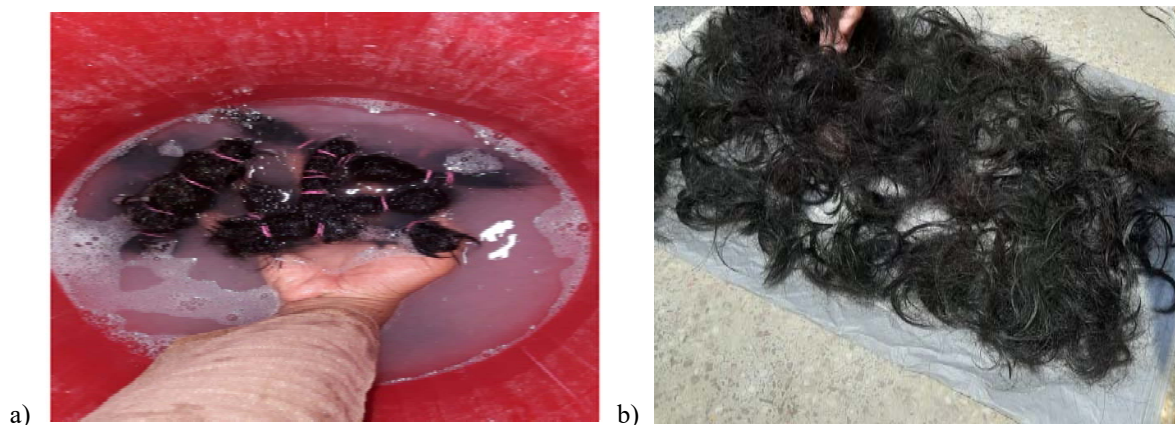


Figure 2: human hair treatment, a. washing of human hair, and b. drying the human hair

The third step of the hair treatment is washing. In which head & shoulder shampoo is used. The intention of using this chemical it gives very good results for hair to remove all types of impurities. After the washing hair is dry in the oven and sunlight. Washing of hair and drying of hair are shown in Figure 2.



Casting Procedure in this work, the casting of cylinders and beams and cubes was done. But it depends on proportion to proportion and conventional concrete samples and human hair fiber samples were cast for 28 days are the curing span. The different concrete mixes ratio 1:2:4 proportion and 1:1.5:3 proportion with the water /cement ratio is 0.50 with the percentage of human hair fiber was 1%, 2% and 3%. used. Casting and testing of beams are shown in Figure 3, Casting and testing of cylinders are shown in Figure 4, and Casting and testing of cubes are shown in Figure 5.

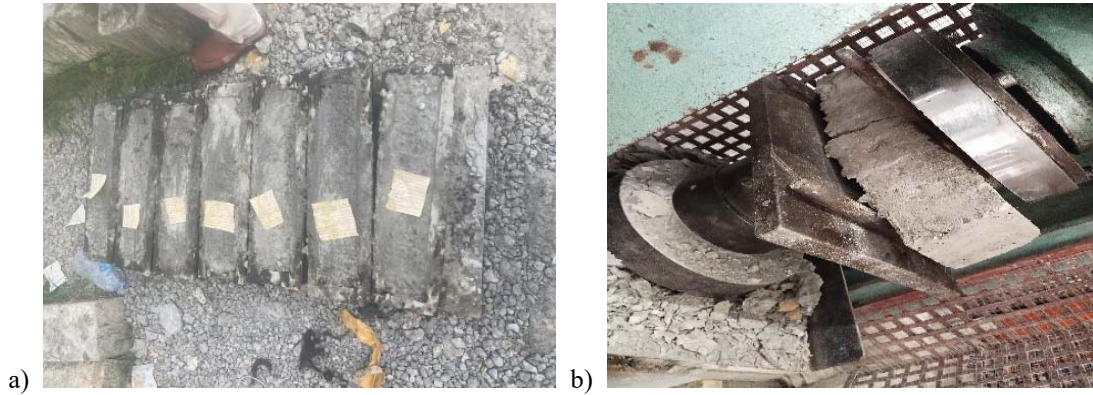


Figure 3: Beam, a. casting of the beam, and b. testing of beam

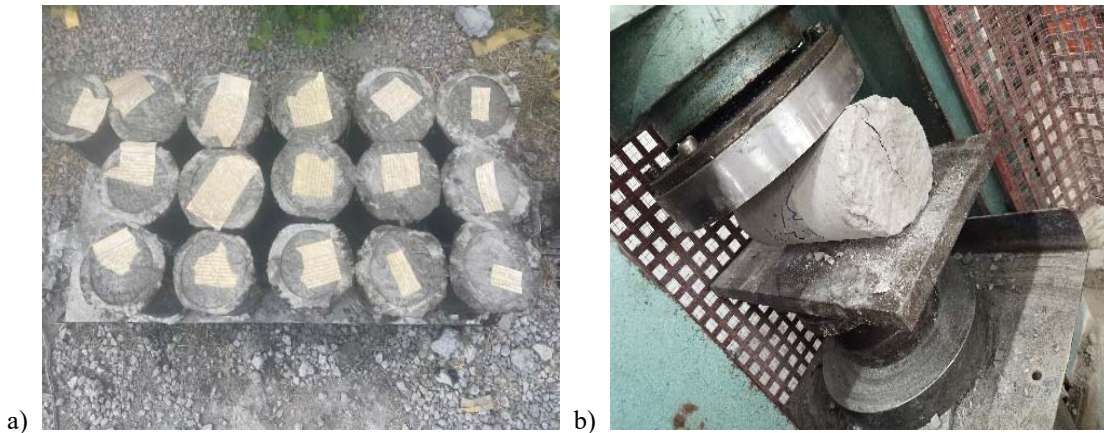


Figure 4: Cylinders, a. casting of Cylinders, and b. testing of cylinder



Figure 5: Cubes, a. casting of cubes, and b. testing of cube



## 4 Results

The practical work was done in the laboratory for checking the mechanical properties of the concrete. The experiment results show the strength of the concrete is increased. Not just the mechanical properties, but the physical is also enhanced. The results of all tests show, that the optimum value of hair is 2%. The maximum values of all tests are noted on the point of 2% hair. And all values are compared with conventional concrete and the value of human hair use in concrete is more as compared to normal concrete. The workability of the concrete is decreased by increasing the percentages of the hair. For workability slump test is conducted as the hair increase, workability decreases and the balling effect is also increased while mixing. During filling the cone of the slump, hair makes more voids than the hammer is used for good compaction. Different types of tests and properties investigate workability, density, Modulus of elasticity, compressive strength, splitting tensile strength and UPV test and flexural strength of concrete and the result is given below.

### 4.1 Workability

The workability of concrete in the terms of the slump test was investigated. Results showed a decrease in the slump values with an increase's percentage of the human hair fibre. The value of Slump is noted as higher and lower at 1:1.5:3 mix proportion of 90mm and 30mm than 1:2:4 mix proportion of 50mm and 9mm at 0% of human hair and 3% of human hair fiber respectively. Graph show comparison between both mix respectively increases the percentage of hair a), and reduction of slump value increases the percentage of hair b) are shown in figure 6.

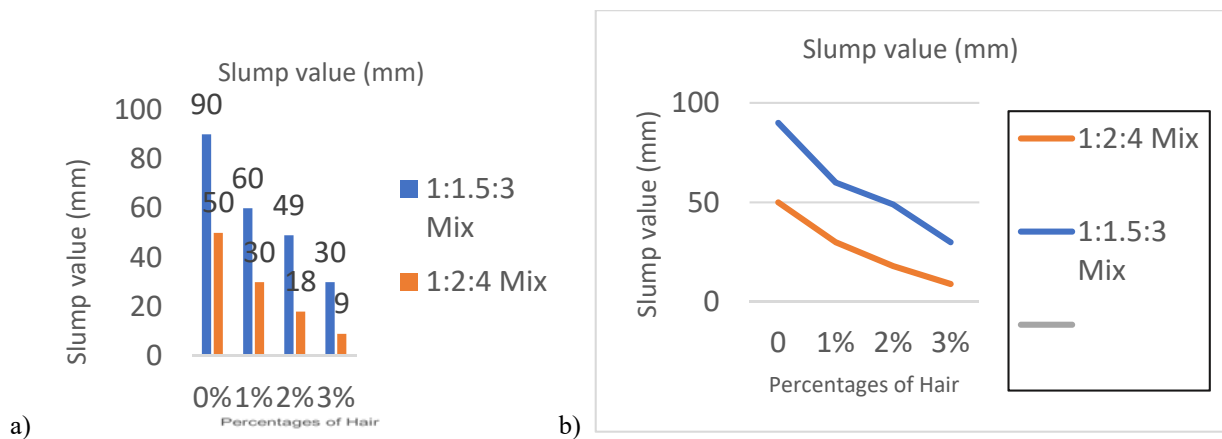


Figure 6: Slump value of concrete, a. graphically comparison between both mix, and b Reduction of slump value by increasing hair

This experiment results of both mixes proportions 1:2:4 mix proportion and 1:1.5:3 mix proportion respectively are shown in table 4.

Table 4 Result of Slump cone test

Mix percentage of hair	Slump value (mm) 1:2:4 Mix	Slump Value (mm) 1:1.5:3 Mix
0 % of hair	50	90
1 % of hair	30	60
2% of hair	18	49
3% of hair	9	30

### 4.2 Density of concrete

The density of the concrete is measured at each percentage of the human hair fiber to know the relationship between the strength and density of concrete. The maximum density is noted at 0% of the human hair fiber, while the minimum at 3% of human hair fiber both mix proportions 1:2:4 and 1:1.5:3 respectively. Results showed the decrease in the density values





with an increase's percentage of the human hair fiber. Graph show comparison between both mix respectively increases the percentage of hair a), and reduction of density value increases the percentage of hair b) are shown in figure 7.

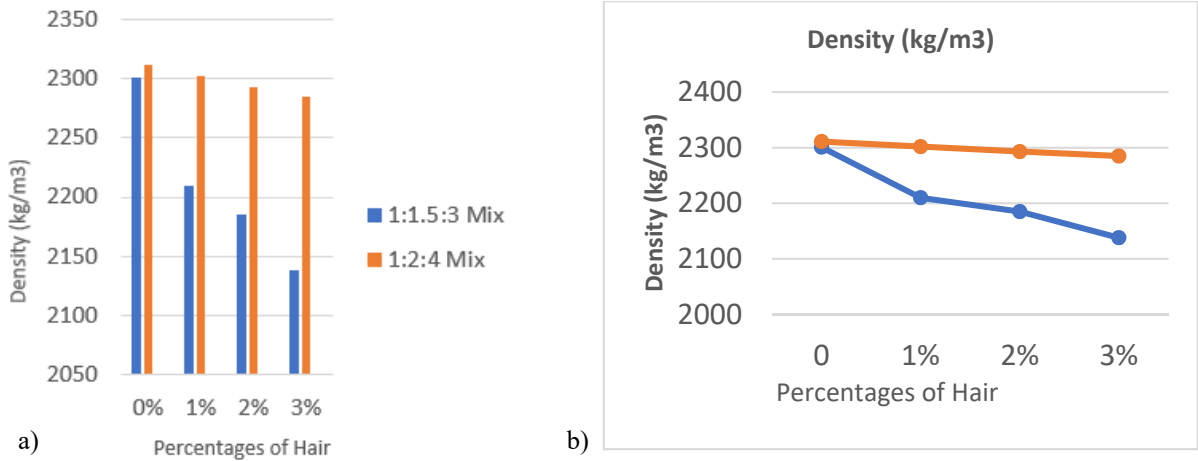


Figure 7: Density of concrete, a. graphically comparison between both mix, and b reduction of density value by increasing hair

This experiment results of both mixes proportions 1:2:4 mix proportion and 1:1.5:3 mix proportion respectively are shown in table 5.

Table 5 Result of density of concrete

Mix percentage of hair	Density (kg/m <sup>3</sup> ) 1:2:4 Mix	Density (kg/m <sup>3</sup> ) 1:1.5:3 Mix
0 % of hair	2311	2301
1 % of hair	2302	2210
2% of hair	2293	2185
3% of hair	2285	2138

### 4.3 Compressive strength of Concrete

The test was performed on cubes of size 150mmX150mmX150mm to check the compressive strength of concrete by using human hair fibre. The compressive strength of concrete is investigated during 28 days curing period. The compressive strength of concrete is determined by the following ASTM C39/C 39M – 03. The standard cube specimens were placed in the Universal Testing Machine and the load applied all specimens at each proportion of human hair fiber was tested and then the average is taken. The compressive strength increases gradually with an increase in the percentage of Human hair fiber in both concrete mix proportions as compared to plain concrete, till it increases the compressive strength by increasing the human hair fiber and maximum value achieved at 2% of human hair fiber in both Mix ratio 1:2:4 and 1:1.5:3 respectively. After that increasing the compressive strength to 5.84% at 1 % human hair fiber and 9.59 % at 2% human hair fiber and 3.13% at 3% human hair fiber by using a concrete proportion 1:2:4 mix and 5.96 % at 1% human hair fiber and 8.15% at 2 % human hair fiber and 3.58% at 3% human hair fiber by using 1:1.5:3 mix ratio respectively. Results showed an increase in the compressive strength with an increase's percentage of the human hair fibre. Graph show comparison between both mix respectively increases the percentage of hair a), and increment of compressive strength increases the percentage of hair b) are shown in figure 8.

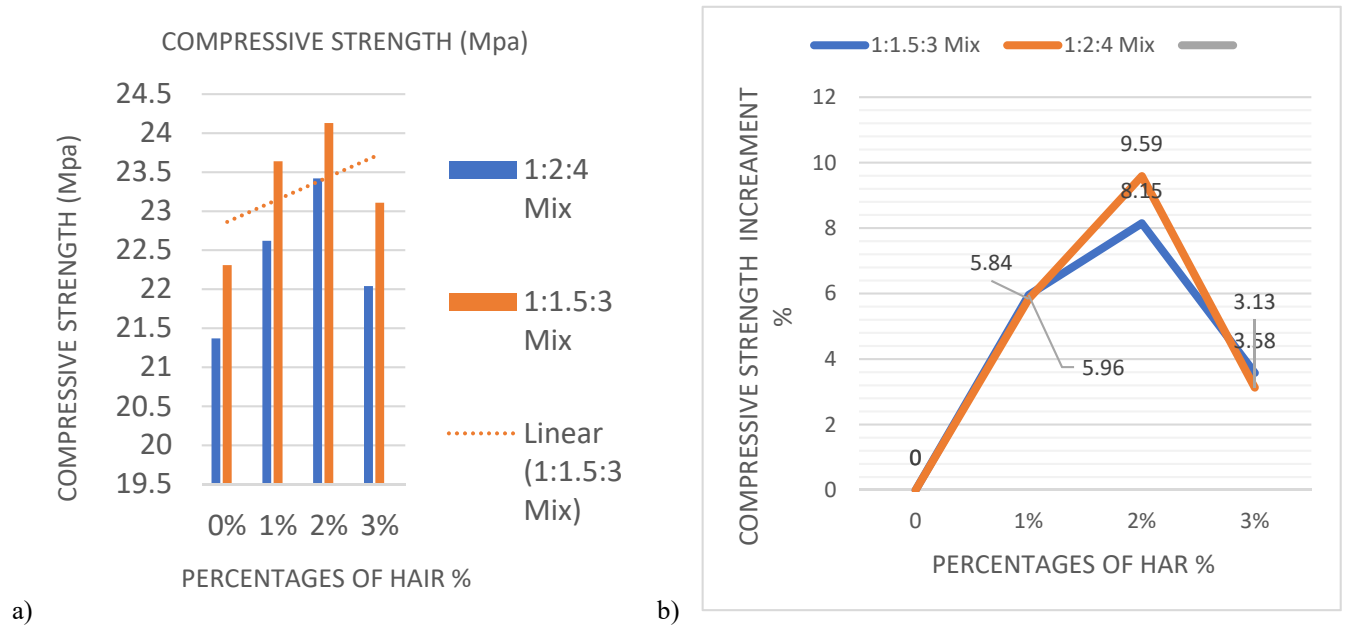


Figure 8: Compressive strength, a. graphically comparison between both mix, and b Increment of compressive strength by increasing hair

This experiment results of both mix proportion 1:2:4 mix proportion and 1:1.5:3 mix proportion respectively are shown in table 6.

Table 6 Result of compressive strength

Mix percentage of hair %	Compressive strength (Mpa) 1:2:4 Mix	Compressive strength (Mpa) 1:1.5:3 Mix
0 % of hair	21.37	22.31
1 % of hair	22.62	23.64
2% of hair	23.42	24.13
3% of hair	22.04	23.11

#### 4.4 Splitting tensile strength of Concrete

The Splitting tensile strength of the concrete is indirectly to tensile strength of concrete. This test was performed on the concrete cylinders. The maximum tensile strength value has been noted at 2% of hair and code by following the ASTM code C-496. After that increasing the Splitting tensile strength to 16.58 % at 1 % hair and 19.9 % at 2% hair and 9.95% at 3% hair by using a 1:2:4 mix ratio and 3.47 % at 1% hair and 6.56 % at 2 % hair and 1.58% at 3% hair by using 1:1.5:3 mix ratio respectively.

As compared to both mix ratios percentage of increase in Splitting tensile strength in mix ratio 1:2:4 is more than compared mix ratio 1:1.5:3 respectively. Results showed an increase in the Splitting tensile strength with an increase's percentage of the human hair fibre. Graph show comparison between both mix respectively increases the percentage of hair a), and increment of Splitting tensile strength increases the percentage of hair b) are shown in figure 9.

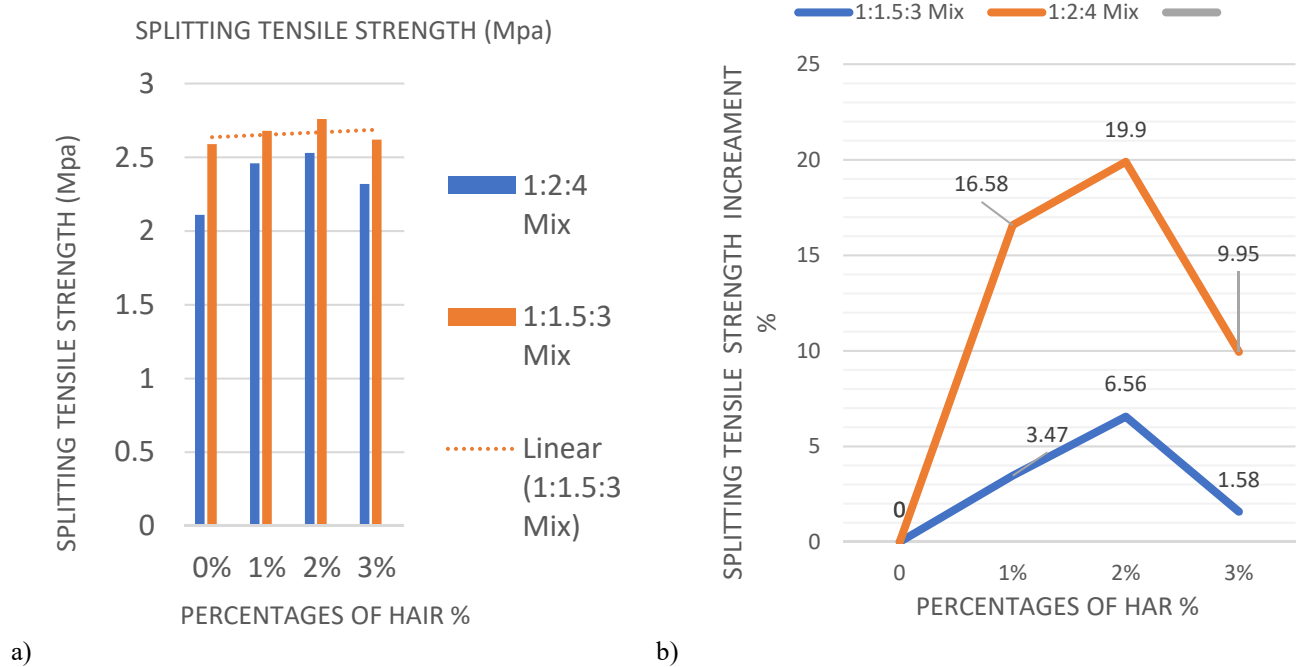


Figure 9: Splitting tensile strength, a. graphically comparison between both mix, and b Increment of Splitting tensile strength by increasing hair

This experiment results of both mixes proportions 1:2:4 mix proportion and 1:1.5:3 mix proportion respectively are shown in table 7.

Table 7 Result of Splitting tensile strength

Mix percentage of hair %	Splitting tensile strength (Mpa) 1:2:4 Mix	Splitting tensile strength (Mpa) 1:1.5:3 Mix
0 % of hair	2.11	2.59
1 % of hair	2.46	2.68
2% of hair	2.53	2.76
3% of hair	2.32	2.62

#### 4.5 Flexural Strength of Concrete

The flexural strength of the concrete test is performed on the beam. By using the center point loading method. This method also gives the indirectly tensile strength of the concrete. The ratios of hair were used 0%, 1%, 2% and 3% and the curing span were 28 days. After that increasing the flexural strength by 15.9% % at 1 % hair and 21.1 % at 2% hair and 10.3% at 3% hair by using a 1:1.5:3 mix ratio and 11.98 % at 1% hair and 17.8 % at 2 % hair and 9.93 % at 3% hair by using 1:2:4 mix ratio respectively. The optimum value is 2% of human hair. Results showed an increase in the flexural strength with an increase's percentage of the human hair fiber. Graph show comparison between both mix respectively increases the percentage of hair a), and increment of Flexural strength increases the percentage of hair b) are shown in figure 10.

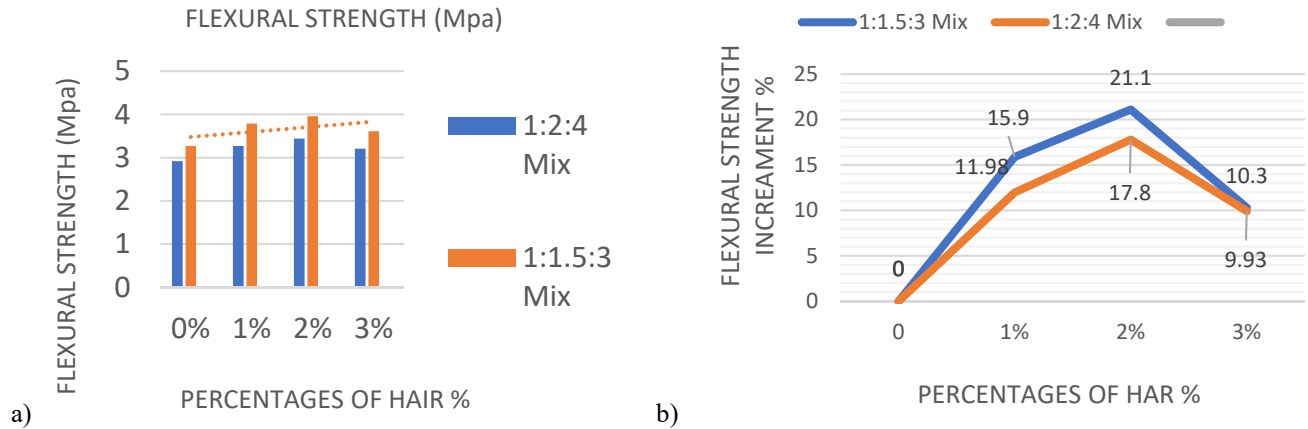


Figure 10: Flexural strength, a. graphically comparison between both mix, and b Increment of Flexural strength by increasing hair

This experiment results of both mixes proportions 1:2:4 mix proportion and 1:1.5:3 mix proportion respectively are shown in table 8.

Table 8 Result of Flexural strength

Mix percentage of hair %	Flexural strength (Mpa) 1:2:4 Mix	Flexural strength (Mpa) 1:1.5:3 Mix
0 % of hair	2.92	3.27
1 % of hair	3.27	3.79
2% of hair	3.44	3.96
3% of hair	3.21	3.61

#### 4.6 Ultrasonic Pulse Velocity (UPV) Test of Concrete

The quality of concrete was determined by a non-destructive UPV test by using directly the method. Results Shown an increase in the UPV value with an increase's percentage of the human hair fiber. Graph show comparison between both mix respectively increases the percentage of hair a), and increment of Ultrasonic Pulse Velocity increases the percentage of hair b) are shown in figure 11.

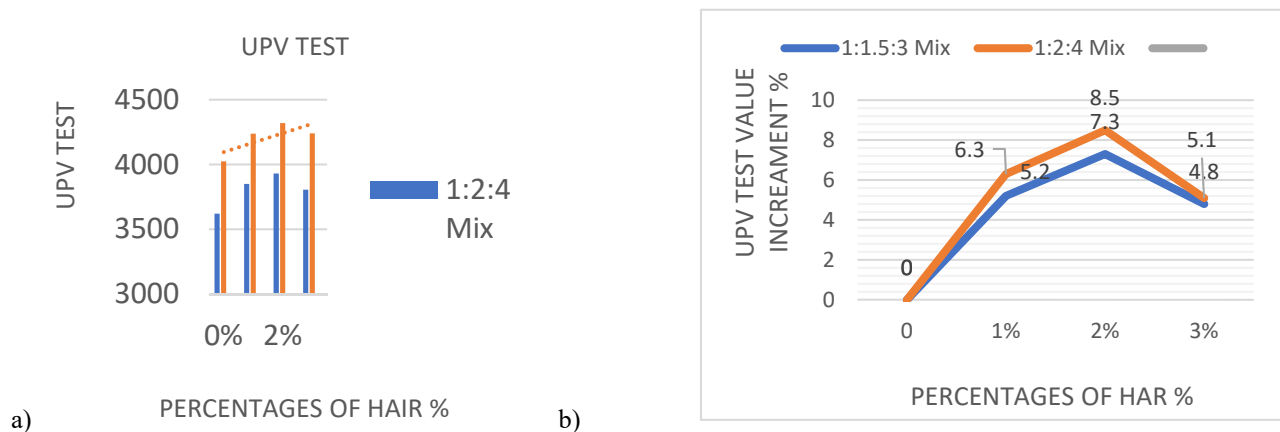


Figure 11: Ultrasonic Pulse Velocity, a. graphically comparison between both mix, and b Increment of Ultrasonic Pulse Velocity by increasing hair



This experiment results of both mixes proportion 1:2:4 mix proportion and 1:1.5:3 mix proportion respectively are shown in table 9.

Table 9 Result of Ultrasonic Pulse Velocity

Mix percentage of hair %	Ultrasonic Pulse Velocity 1:2:4 Mix	Ultrasonic Pulse Velocity 1:1.5:3 Mix
0 % of hair	3620	4024
1 % of hair	3850	4238
2% of hair	3930	4320
3% of hair	3805	4240

#### 4.7 Modulus of elasticity of Concrete

The Modulus of Elasticity is checked concrete resistance and elastic deformation and elasticity module defines stiffness higher elasticity modulus of the material, The optimum value at 2% of human hair. Results Showed the increase Modulus of elasticity with an increase's percentage of the human hair fiber. Graph show comparison between both mix respectively increases the percentage of hair a), and increment Modulus of elasticity increases the percentage of hair b) are shown in figure 12.

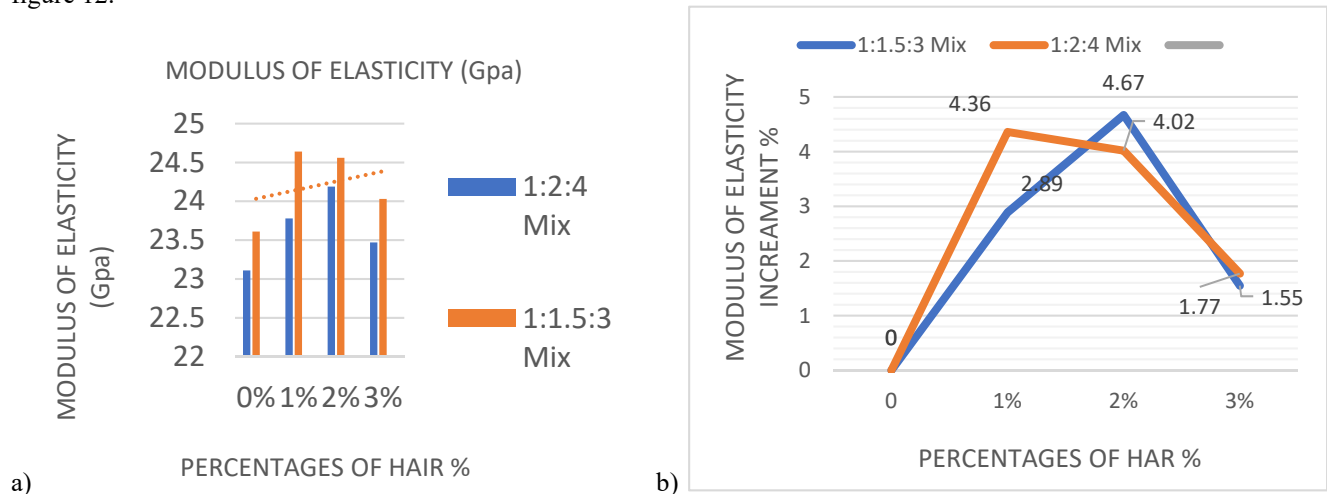


Figure 12: Modulus of elasticity, a. graphically comparison between both mix, and b Increment of Modulus of elasticity by increasing hair

This experiment results of both mixes proportion 1:2:4 mix proportion and 1:1.5:3 mix proportion respectively are shown in table 10.

Table 10 Result of Modulus of elasticity

Mix percentage of hair %	Modulus of elasticity 1:2:4 Mix	Modulus of elasticity 1:1.5:3 Mix
0 % of hair	23.11	23.61
1 % of hair	23.78	24.64
2% of hair	24.19	24.56
3% of hair	23.47	24.03



#### 4.8 Water Absorption of Concrete

The concrete samples were tested water absorption of concrete and water absorption property was increased with increasing the percentage of human hair, addition to the water absorption in concrete may be human hair absorbs more water as compared to the control mix of concrete. Graph show comparison between both mix respectively increases the percentage of hair a), and increment water Absorption increases the percentage of hair b) are shown in figure 13.

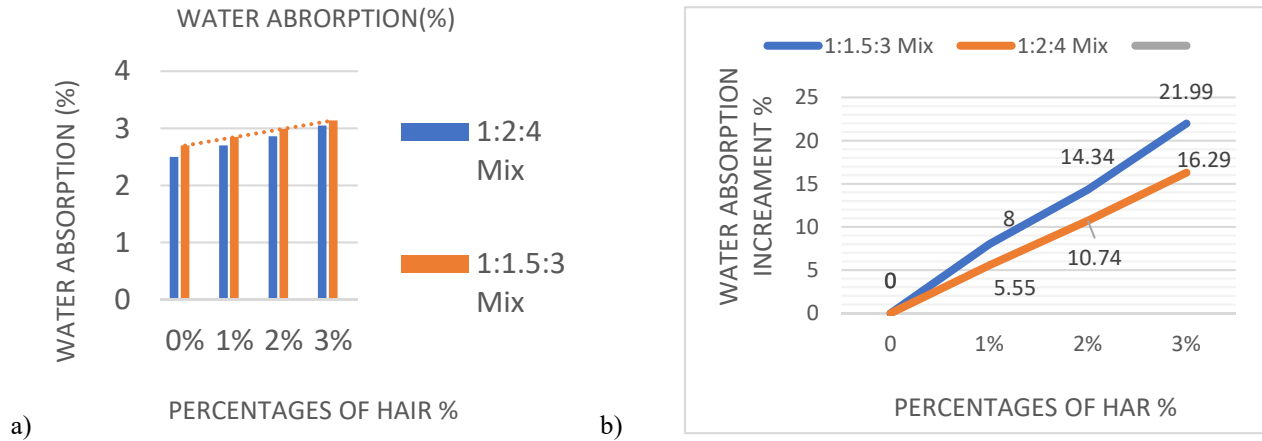


Figure 13: Water Absorption, a. graphically comparison between both mix, and b Increment of Water Absorption by increasing hair

This experiment results of both mixes proportion 1:2:4 mix proportion and 1:1.5:3 mix proportion respectively are shown in table 11.

Table 11 Result of compressive strength

Mix percentage of hair %	Water Absorption (%) 1:2:4 Mix	Water Absorption (%) 1:1.5:3 Mix
0 % of hair	2.50	2.70
1 % of hair	2.70	2.85
2% of hair	2.86	2.99
3% of hair	3.05	3.14

## 5 DISCUSSION

The practical work was done in the laboratory for checking the mechanical properties of the concrete. The experiment results show the strength of the concrete is increased. Not just the mechanical properties, but the physical is also enhanced. The results of all tests show, that the optimum value of hair is 2%. The maximum values of all tests are noted on the point of 2% hair. And all values are compared with conventional concrete and the value of human hair use in concrete is more as compared to normal concrete. The workability of the concrete is decreased by increasing the percentages of the hair. For workability slump test is conducted as the hair increase, workability decreases and the balling effect is also increased while mixing. During filling the cone of the slump, hair makes more voids than the hammer is used for good compaction.

## 6 Conclusion

These are the following conclusions are shown at the end of this comprehensive research work:

- 1 Workability in terms of slump value decreases with an increase in the percentage of human hair fiber a lower value is recorded at 3% of the human hair fiber. Comparatively, a higher slump value is noted at 1:1.5:3 mix proportion.



- 2 The density of concrete decreases as the percentage of human hair fibers increases. Reduction in density is 1.12% and 7.15% at 1:2:4 and 1:1.5:3 mix proportion respectively.
- 3 The compressive strength increases to 9.59 % and 8.15% in 1:2:4 and 1:1.5:3 mix proportion respectively at 2% addition of human hair fiber and it decreases at other percentages of hair fibers and the same as Modulus of Elasticity of concrete is maximum noted at 2 % addition of human hair fiber.
- 4 The splitting tensile strength of concrete increases to 19.9 % and 6.56% in 1:2:4 and 1:1.5:3 mix proportion respectively at 2% addition of human hair fiber and it decreases at other percentages of hair fibers.
- 5 The flexural strength of concrete by using human hair fiber in concrete increases to 17.8% and 21.1% in 1:2:4 and 1:1.5:3 mix proportion respectively at 2% addition of hair fibers. It decreases at other percentages of human hair fibers.
- 6 The UPV value of concrete by using human hair fiber in concrete increases to 8.5% and 7.3% in 1:2:4 and 1:1.5:3 mix proportion respectively at 2% addition of hair fibers.
- 7 The concrete samples were checked the water absorption of concrete and maximum water absorption was noted 16.29 % at 3% of hair mix ratio 1:1.5:3 and 21.99 % at 3% of hair mix ratio 1:2:4 respectively, and minimum water absorption was noted by at 0% of hair after 28 days. After that increasing the water absorption to 8 % at 1 % human hair fiber and 14.34 % at 2% human hair fiber and 21.99% at 3% human hair fiber by using a concrete proportion 1:2:4 mix and 5.55 % at 1% human hair fiber and 10.74% at 2 % human hair fiber and 16.29% at 3% human hair fiber by using 1:1.5:3 mix ratio respectively.
- 8 Comparatively, a higher value in both strengths was recorded at a 1:2:4 mix proportion rather than a 1:1.5:3 mix proportion at the same water/cement ratio.

## Acknowledgement

The authors especially thank the Director of Postgraduate Studies and the Civil Engineering department at the University of Engineering and Technology Taxila, Pakistan for their support to provide labs and accomplish this research of the M.Sc. thesis of the corresponding author.

## References

- [1] Achal, A., Abhishek, S., Siddharth, P., & Anant, B. (2016, May). A Concept of Improving Strength of Concrete using Human Hair as fiber Reinforcement. *International Journal of Innovative Research in Science*, Vol.5(Issue 5), 8624-8630. doi:10.15680/IJRSET.2016.0505257.
- [2] Akarsh , V., V, K. S., S, K. V., & Anshul , S. (2016, April 2). Human Hair: A Biodegradable Composite Fiber – A Review. *International Journal of Waste Resources*, Vol. 6(Issue:3). doi:10.4172/2252-5211.1000206.
- [3] ASTM. (1996, Jan 10). Standard Test Method for Splitting Tensile Strength of Cylindrical Concrete Specimens C 496. Retrieved from ASTM International.
- [4] ASTM. (2002, April). Standard Test Method for Flexural Strength of Concrete (Using Simple Beam With Center-Point Loading) C 293 – 02. Retrieved from ASTM International.
- [5] ASTM. (2007, October 9). Standard Method of Test for Slump of Hydraulic Cement Concrete C143/C. Retrieved from ASTM International.
- [6] ASTM International. (n.d.). Retrieved from <https://www.astm.org/>.
- [7] Batham, G. (2018, June). Recent innovations in Concrete Reinforced with Human Hair: A Review. *International Research Journal of Engineering and Technology*, Volume:5(Issue:6), 3128-3130. Retrieved from [www.irjet.net](http://www.irjet.net).
- [8] D., J., & A., K. (2012, januray 25). Hair Fiber Reinforcement Concrete. *Research journal of recent science*, 1(15 Jan 2012), 128-133. Retrieved 6 10, 2020, from [www.isca.in](http://www.isca.in).
- [9] ASTM. (2002, April). Standard Test Method for Flexural Strength of Concrete (Using Simple Beam With Center-Point G, S., & Smt, B. A. (2017, May). Human Hair as Fibre Reinforcement in Concrete. *International Journal of Engineering Science and Computing*, Volume 7(Issue No.5), 11358-11364. Retrieved from <http://ijesc.org/>.
- [10] Hummaira, K., Tayyaba, L. M., Muhammad, S. A., Muhammad Asim, & Reena, M. M. (2019, April 11). Human hair as a Fiber Reinforced Concrete for Enhancement of Tensile Strength of the Concrete. *Mehran University Research Journal of Engineering & Technology*, Vol. 39, No. 1, 63-70,(January 2020), 63-70. doi:10.22581/muet1982.2001.071] Achal, A., Abhishek, S., Siddharth, P., & Anant, B. (2016, May). A Concept of Improving Strength of Concrete using Human Hair as fiber Reinforcement. *International Journal of Innovative Research in Science*, Vol.5(Issue 5), 8624-8630. doi:10.15680/IJRSET.2016.0505257.
- [11] Khawar, A., Hikmatullah , J., Muhammad Waqas, M., Arslan , S., & Faiza , K. (2019, August 01). Development of Structural Concrete Via Waste Hair Fibers. Capital University of Science and Technology.



**4<sup>th</sup> Conference on Sustainability in Civil Engineering (CSCE'22)**  
Department of Civil Engineering  
Capital University of Science and Technology, Islamabad Pakistan



- [12] Mohammad , O., & Gagan , D. S. (2019, May 5). An Experimental Investigation on Hair Fibre as Fibre Reinforcement in Concrete. *Asian Journal of Current Engineering and Maths*, 8, 1-8.
- [13] Mridula , D., & Dr, R. D. (2017, October). Study on Concrete Reinforced With Human Hair as Fiber. *International Journal of Innovative Research in Science*,, Vol. 6(Issue 10), 19366-19373. doi:10.15680/IJRSET.2017.0610008.
- [14] Ramya, T., & Tamilamuthan, B. (2017, Nov). Human Hair Fiber Reinforced Cement Concrete. *INTERNATIONAL JOURNAL FOR RESEARCH IN EMERGING SCIENCE AND TECHNOLOGY*,, VOLUME-4(Issue-11), 1-6.
- [15] Sakshi , G., & Aakash , S. (2018, March 7). HUMAN HAIR AS FIBRE MATERIAL IN REINFORCED CONCRETE. *Advances in Construction Materials and Structures*. Retrieved from <https://www.researchgate.net/publication/324248622>
- [16] Shanker , L. M., G , B. K., Aneel, K., & R, B. M. (2018, August 31). Recycling of Human Scalp Hair as Environment-Friendly Material in Cement Concrete. *Energy, Environment and Sustainable Development*. Retrieved from <https://www.researchgate.net/publication/313470130>.
- [17] S, M., S, N. K., S, P., & S, A. K. (2017, April). EXPERIMENTAL STUDY ON HUMAN HAIR FIBER REINFORCED CONCRETE WITH PARTIAL REPLACEMENT OF CEMENT BY GGBFS. (editor@iaeme.com, Ed.) *International Journal of Civil Engineering and Technology*, Volume 8(Issue 4), PP 1145-1155. Retrieved from <http://www.iaeme.com/IJCIET/issues.asp?JType=IJCIET&VType=8&IType=4>.
- [18] Narain, D. B., Sohail, A. A., Shanker, L. M., & Fahad, A. S. (2017, November 25). Effect of Human Hair as Fibers in Cement Concrete. *Sustainable Development in Civil Engineering*.





# REDUCING THE WATER ABSORPTION OF MORTAR BY USING ECO-FRIENDLY WASTEPAPER SLUDGE ASH

<sup>a</sup>Ahsin Ihsan\*, <sup>b</sup>Asad Shafique, <sup>c</sup>Muhammad Faisal Javed, <sup>d</sup>Sardar Kashif-ur-Rehman

a: Department of Civil Engineering, Comsats University Islamabad (Abbottabad Campus), [500ahsin@gmail.com](mailto:500ahsin@gmail.com)

b: Department of Civil Engineering, Comsats University Islamabad (Abbottabad campus), [asadshafiquekhan1@gmail.com](mailto:asadshafiquekhan1@gmail.com)

c: Department of Civil Engineering, Comsats University Islamabad (Abbottabad Campus), [arbabfaisal@cuiatd.edu.pk](mailto:arbabfaisal@cuiatd.edu.pk)

d: Department of Civil Engineering, Comsats University Islamabad (Abbottabad Campus), [skashif@cuiatd.edu.pk](mailto:skashif@cuiatd.edu.pk)

\* Corresponding author: Email ID: [500ahsin@gmail.com](mailto:500ahsin@gmail.com)

**Abstract-** The aim of this research is to utilize the paper waste in mortar mixtures as a cement replacement in form of Wastepaper Sludge Ash (WPSA) to make them more efficient and enhance their required properties such as water resistance, permeability, sorptivity. Mixture was then investigated to understand its chemical, mechanical and physical properties. Depletion of natural resource can be reduced by using WPSA as cement replacement. Carbon dioxide (CO<sub>2</sub>) and Sulphur dioxide (SO<sub>2</sub>) emissions can be reduced as well because of less usage of cement proportions. The physical and chemical properties of WPSA was compared with the cement. As the result of testing, WPSA showed similar cementitious properties and at 25% cement replacement by weight with the WPSA, it showed favorable ultimate strength of 19.05 MPa. Also by using WPSA, water absorption was reduced approximately up to 60% hence it increases water resistivity and decreases permeability and sorptivity thus making the structure more durable.

**Keywords-** Ecofriendly, mortar, wastepaper sludge ash, water absorption.

## 1 Introduction

The Global Population massively increases with time which puts increased pressure on urban construction including residential, commercial, and industrial buildings. This led to increase in the need for cement use worldwide [1,2]. Cement is a basic construction material that has many applications [3,4]. Nevertheless, the cement industry is identified by a high energy consumption [5,6] and high greenhouse gases emissions [7–9]. Cement industries emits about 7% of Carbon dioxide (CO<sub>2</sub>) worldwide. [9,10]. Hence, there is an urgent need to explore a feasible replacement for cement to reduce this environmental impact [11]. The reutilization of waste products rather than disposal in landfills is an economical and viable solution to these issues [12,13]. A huge amount of paper waste is produced at daily basis in Pakistan. It is produced in every part of the country and it constitutes a huge proportion of total wastes produced. Waste paper sludge is produced in paper production industries and especially newspaper printing industries which is then incinerated and then disposed of to landfills which have harmful effects on soil properties. During the production of Paper and Pulp/Paper sludge, chlorine based bleaches are used. These are toxic materials or additives so when the paper waste is dumped in soil or released in the water (rivers, seas or oceans) it causes hazardous pollution. Also when the paper rots it emits methane gas which is 25 times more toxic than CO<sub>2</sub> emission.

These current disposal methods are not environmentally helpful rather causes more pollution. Increasing rate of population is increasing the rate of production of paper waste, it is also increasing because paper is taking place of plastic products worldwide such as paper bags and cardboards. Apart from all that use of cement is increasing day by day as well which is decreasing the natural resources for its production. Also it requires a huge portion of budget to treat these wastes that is ultimately effecting the economy of the country. In order to overcome all of these problems



a proper solution is needed to reduce the depletion of natural resources and reutilizing the waste materials that will be beneficial for both environment and economy. Therefore, a search for alternative methods to efficiently reuse WPSA is initiated and the most appropriate way to recycle the wastepaper sludge is in mortars, concrete or bricks manufacturing. This will alleviate the costs needed to dispose the WPSA and it will preserve the soil properties as well. Also by partially replacing WPSA with cement it will shrink the cement production rate and will eventually decrease the depletion of natural resources that will help the environment. By fulfilling the 3R concept, reuse, recycling and recovery of WPSA as an alternate method in construction, it is helping the environment and ecosystem in a positive manner. Replacement of cement with other ashes has been done and investigated by many researchers within last few decades. [14-16]. The research on WPSA is very limited. As per Scopus website data, only few documents were found related to WPSA in different fields like Veterinary, decision sciences, mathematics etc. however more research is carried out in engineering fields as given in Fig 1.

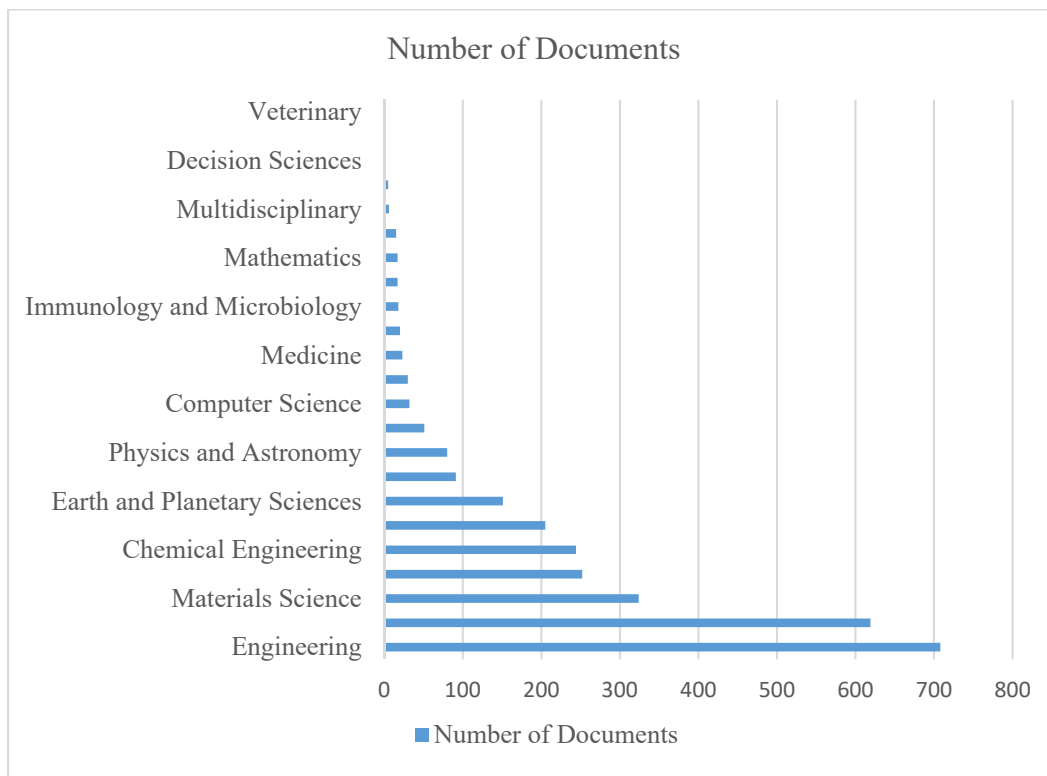


Figure 1: Publications of WPSA in different study fields.

In this research work WPSA is used as a partial replacement of Cement in the Mortar mix of 1:2.75 (binder/sand ratio). WPSA binds the Sand particles together similar to Cement. To produce waste paper sludge ash, paper sludge is combusted at 700-750 °C. As it contains a high proportion of organic matter, in form of cellulose and some inorganic compounds such as clays and calcium carbonate [17]. At 700 °C temperature, combustion of paper sludge transforms the clay minerals such as kaolinite into metakaolinite [17] and thus WPSA will behave as pozzolanic material [18,19]. Although composition of WPSA varies, it commonly contains a sufficient amount of Lime (CaO), Silica (SiO<sub>2</sub>) and Alumina (Al<sub>2</sub>O<sub>3</sub>) and because of this reason it is being used as a supplementary cementitious material (SCM) [18,19]. The main objective of this research is to make green technology material. Also physical and chemical properties are not effected at a larger scale of material.

Thus durability of a structure is not compromised. It also does not affect the compressive strength and water absorption is decreased. Researches have been done by replacing Cement with WPSA in concrete and bricks but our aim is to make mortar usage ecofriendly and efficient because it is a key material used for grey structure finishing and for other masonry purposes during the construction of projects. Mortar is also used to repair joints and cracks. By replacing 25% of cement by WPSA in mortar mix we can obtain such efficient mortar [17].



## 2 Materials and Methodology

### 2.1 Materials.

In this test Ordinary Portland cement (OPC) and waste paper sludge ash (WPSA) was used as a cementitious material. Waste paper sludge was collected from Private schools and universities of Abbottabad. It was then sun dried for 10 to 15 days and then burnt in electric furnace at 700°C for 2 hours. WPSA used in this test is shown in Fig 2.



Figure 2: Wastepaper sludge Ash (125g).

The Conventional chemical composition of OPC and WPSA is similar as given in the Table 1. [20,21]. Concentration of SiO<sub>2</sub>, Al<sub>2</sub>O<sub>3</sub> and CaO is greater in both of Cementitious materials. These oxides are present in similar quantities in both Cement and WPSA. Table 1 is showing detailed comparison of oxides present in Ordinary Portland Cement and WPSA. Sand used in this test was passed through 3.35mm IS sieve for better gradation as used in [9]. Ground water was used for mixing of materials.

Table 1 Chemical composition of OPC and WPSA

Empirical formula	OPC (% w/w)	WPSA (% w/w)
SiO <sub>2</sub>	21.3	23.3
Al <sub>2</sub> O <sub>3</sub>	5.6	5.3
Fe <sub>2</sub> O <sub>3</sub>	3.4	0.8
TiO <sub>2</sub>	0.1	0.5
MgO	2.1	2.5
CaO	64.6	62.4
Na <sub>2</sub> O	0.1	0.4
K <sub>2</sub> O	0.2	0.4
P <sub>2</sub> O	0.1	0.5
MnO	0.1	0.5
SO <sub>3</sub>	2.1	0.6

### 2.2 Mix Proportion.

Mortar samples were prepared with 25% replacement with WPSA. Mixing proportion details are given in the Table 2 where M0 denotes samples with zero percent WPSA and M25 is named for samples having 25 percent WPSA as a cement replacement. Sand to binder ratio was taken as 1:2.75 and water to cement ratio used for mixing was restricted to 0.48.



Table 2 Mix proportion of WPSA and OPC.

Mix ID	Ordinary Portland cement (OPC)	Waste paper sludge Ash (WPSA)	Sand	Water
M0	500 g	0 g	1375 g	242 g
M25	375 g	125 g	1375 g	242 g

### 2.3 Preparation of Samples.

Specimens were prepared according to ASTM C109/C109M. Materials (OPC, PSA and sand) in dry form were firstly mixed in an Automatic Programmable Mortar mixer UTCM-0085 for 2 min. Water is added to the mixture and then blended for 5 more min in a mixture machine. Then wet mix was casted in (50x50x50) mm cube moulds shown in Fig 3. Samples were taken out of moulds after 24h and then placed in water container for curing at room temperature (20°C to 25°C). Samples were ready for testing after ultimate strength was achieved as shown in Fig 4.



Figure 3: Mortar mix Casted in Moulds.



Figure 4: WPSA (25%) Mortar Samples.

### 2.4 Water Absorption.

Mixes with 0% and 25% WPSA were tested for water absorption using ASTM C642-97. Samples were firstly dried in oven for 24h at 100°C to 110°C temperature and then allowed to cool down in air at room temperature. Saturated mass was then determined after immersion of samples for 48h in a water container. Specimens were then boiled for



5h and after boiling, their saturated mass was determined. After that immersed apparent weights of specimens were examined. Water absorption percentage was then calculated using these weights.

### 3 Results and Discussion

#### 3.1 Compressive strength.

The impact of curing period and replacement of Ordinary Portland Cement (OPC) with 25% Waste Paper Sludge Ash (WPSA) is tested. Increase in curing time increased the compressive strength of mortar mix while an addition of WPSA has decreased the compressive strength. At early ages of curing both samples were having same compressive strength. Similar results were obtained by other researchers [9,22]. Mortar cubes with 0% WPSA showed Compressive strength of 16.47 and 24.17 MPa after 7 and 28 days of curing and cubes with 25% WPSA gave compressive strength of 14.9 and 19.05 MPa as mentioned in Table 3. Therefore, at 25% cement replacement by weight with WPSA showed favourable ultimate strength of 19.05 MPa, thus it can be adopted for environmental friendly and economical construction.

Table 3 Compressive strength at 7, 14, 21, 28 days.

Curing days	Compressive strength (MPa)	
	0 % WPSA	25% WPSA
7	16.47	14.9
14	21.73	17.21
21	23.1	18.95
28	24.173	19.05

#### 3.2 Water Absorption.

Addition of 25% WPSA reduced water absorption up to 55%, 57%, 60% after 7, 14 and 28 days of curing respectively as given in Table 4. Mortar samples with 0% WPSA has water absorption of 10.49 and 9.79 percent after 7 and 28 days of curing while samples having 25% WPSA has water absorption of 4.8 and 3.9 percent as shown in Table 4. Replacement of 100% cement with WPSA increases water absorption as mentioned in [23]. However, using 25% WPSA with cement increased water resistivity, reduced pores, decreased permeability and water absorption. Hence using WPSA can make structure more durable.

Table 4 Water Absorption at 7, 14, 28 days.

Curing days	Water Absorption (%)	
	0 % WPSA	25% WPSA
7	10.49	4.8
14	10.20	4.4
28	9.79	3.9

As waste paper sludge ash is lighter in weight as compared to cement particles, it occupies more volume when we replace 25% of it by weight. By excessive volume it decreases internal voids that decreases the water absorption. And also WPSA provides an adequate amount of compressive strength by binding the aggregate.

### 4 Conclusion

By obtaining all the favourable results we can conclude many significances and can predict the usages of WPSA mortar. From experimental data following conclusions are made:

1. Chemical and physical properties of WPSA showed similar behaviour as that of cement.
2. WPSA reduces the emission of CO<sub>2</sub> and SO<sub>2</sub> causing less environmental damages and is ecofriendly.
3. Replacement of 25% WPSA with cement showed favourable ultimate compressive strength of 19.05 MPa.



4. By usage of WPSA, water absorption reduced to approximately 60% which indicated less permeability.
5. The technique developed in this study can be used in runoff structures, sewage pipes, canal surfaces and wall plastering.

## Acknowledgment

The authors would like to express an acknowledgement to the Department of Civil Engineering, Comsats University Islamabad Abbottabad Campus, for providing the facilities especially Material Lab and also their support to accomplish this study.

## References

- [1] Leong Sing Wong, Sujendran Nair Chandran, Raghu Ram Rajasekar and Sih Ying Kong, Pozzolanic characterization of waste newspaper ash as a supplementary cementing material of concrete cylinders, *Case Studies in Construction Materials*, 2022, doi: 10.1016/j.cscm.2022.e01342.
- [2] A. A. F. Influence et al., "LJMU Research Online Influence of Using High Volume Fraction of Silica Fume on Mechanical and," 2020.
- [3] A. R. G. Azevedo et al., "Analysis of the compactness and properties of the hardened state of mortars with recycling of construction and demolition waste (CDW)," *J. Mater. Res. Technol.*, vol. 9, no. 3, pp. 5942–5952, 2020, doi: 10.1016/j.jmrt.2020.03.122.
- [4] M. T. Marvila, A. R. G. Azevedo, and S. N. Monteiro, "Verification of the application potential of the mathematical models of lyse, abrams and molinari in mortars based on cement and lime," *J. Mater. Res. Technol.*, vol. 9, no. 4, pp. 7327–7334, 2020, doi: 10.1016/j.jmrt.2020.04.077.
- [5] Mavroulidou, M., Feruku, B. & Boulouki, G. Properties of structural concrete with high-strength cement mixes containing waste paper sludge ash. *J Mater Cycles Waste Manag* 24, 1317–1332, 2022, doi: 10.1007/s10163-022-01402-z
- [6] L. F. Amaral et al., "Eco-friendly mortars with addition of ornamental stone waste - A mathematical model approach for granulometric optimization," *J. Clean. Prod.*, vol. 248, no. xxxx, p. 119283, 2020, doi: 10.1016/j.jclepro.2019.119283.
- [7] F. Pacheco-Torgal and S. Jalali, "Compressive strength and durability properties of ceramic wastes based concrete," *Mater. Struct. Constr.*, vol. 44, no. 1, pp. 155–167, 2011, doi: 10.1617/s11527-010-9616-6.
- [8] A. R. G. de Azevedo, J. Alexandre, G. de C. Xavier, and L. G. Pedroti, "Recycling paper industry effluent sludge for use in mortars: A sustainability perspective," *J. Clean. Prod.*, vol. 192, pp. 335–346, 2018, doi: 10.1016/j.jclepro.2018.05.011.
- [9] A. Duarte Alonso, Kok, SK, and S. O Brien, "LJMU Research Online m," *Tour. Recreat. Res.*, p. 19, 2018, [Online]. Available: <http://researchonline.ljmu.ac.uk/id/eprint/8705/>.
- [10] M. Abed, M. Nasr, and Z. Hasan, "Effect of silica fume/binder ratio on compressive strength development of reactive powder concrete under two curing systems," *MATEC Web Conf.*, vol. 162, pp. 10–13, 2018, doi: 10.1051/mateconf/201816202022.
- [11] A. A. Shubbar, D. Al-Jumeily, A. J. Aljaaf, M. Alyafei, M. Sadique, and J. Mustafina, "Investigating the mechanical and durability performance of cement mortar incorporated modified fly ash and ground granulated blast furnace slag as cement replacement materials," *Proc. - Int. Conf. Dev. eSystems Eng. DeSE*, vol. October-20, pp. 434–439, 2019, doi: 10.1109/DeSE.2019.00086.
- [12] H. seok Jang, Y. T. Lim, J. H. Kang, S. young So, and H. seok So, "Influence of calcination and cooling conditions on pozzolanic reactivity of paper mill sludge," *Constr. Build. Mater.*, vol. 166, pp. 257–270, 2018, doi: 10.1016/j.conbuildmat.2018.01.119.
- [13] A. R. G. de Azevedo, J. Alexandre, L. S. P. Pessanha, R. da S. T. Manhães, J. de Brito, and M. T. Marvila, "Characterizing the paper industry sludge for environmentally-safe disposal," *Waste Manag.*, vol. 95, pp. 43–52, 2019, doi: 10.1016/j.wasman.2019.06.001.
- [14] A. Ergün, "Effects of the usage of diatomite and waste marble powder as partial replacement of cement on the mechanical properties of concrete," *Constr. Build. Mater.*, vol. 25, no. 2, pp. 806–812, 2011, doi: 10.1016/j.conbuildmat.2010.07.002.
- [15] A. U. Elinwa and Y. A. Mahmood, "Ash from timber waste as cement replacement material," *Cem. Concr. Compos.*, vol. 24, no. 2, pp. 219–222, 2002, doi: 10.1016/S0958-9465(01)00039-7.
- [16] E. M. R. Fairbairn, B. B. Americano, G. C. Cordeiro, T. P. Paula, R. D. Toledo Filho, and M. M. Silvano, "Cement replacement by sugar cane bagasse ash: CO2 emissions reduction and potential for carbon credits," *J. Environ. Manage.*, vol. 91, no. 9, pp. 1864–1871, 2010, doi: 10.1016/j.jenvman.2010.04.008.
- [17] J. Pera and A. Amrouz, "Development of highly reactive metakaolin from paper sludge," *Adv. Cem. Based Mater.*, vol. 7, no. 2, pp. 49–56, 1998, doi: 10.1016/S1065-7355(97)00016-3.
- [18] R. García, R. Vigil de la Villa, I. Vegas, M. Frías, and M. I. Sánchez de Rojas, "The pozzolanic properties of paper sludge waste," *Constr. Build. Mater.*, vol. 22, no. 7, pp. 1484–1490, 2008, doi: 10.1016/j.conbuildmat.2007.03.033.
- [19] I. Vegas, M. Frías, J. Urreta, and J. T. S. José, "Obtención de una adición puzolánica a partir de la calcinación controlada de lodos de destintado de papel : estudio de prestaciones en matrices de cemento Obtaining a pozzolanic addition from the controlled calcination of paper mill sludge . Performance i," *Mater. Construcción*, vol. 56, no. July, pp. 49–60, 2006.



**4<sup>th</sup> Conference on Sustainability in Civil Engineering (CSCE'22)**  
Department of Civil Engineering  
Capital University of Science and Technology, Islamabad Pakistan



- [20] M. A. Fauzi, H. Sulaiman, A. R. M. Ridzuan, and A. N. Azmi, "The effect of recycled aggregate concrete incorporating waste paper sludge ash as partial replacement of cement," *AIP Conf. Proc.*, vol. 1774, no. October 2016, 2016, doi: 10.1063/1.4965063.
- [21] V. Logeswaran and G. Ramakrishna, "Waste Paper Sludge Ash - State of art," *Int. J. Innov. Technol. Explor. Eng.*, vol. 8, no. 9, pp. 2333–2338, 2019, doi: 10.35940/ijitee.i8572.078919.
- [22] H. S. Wong, R. Barakat, A. Alhilali, M. Saleh, and C. R. Cheeseman, "Hydrophobic concrete using waste paper sludge ash," *Cem. Concr. Res.*, vol. 70, no. February 2018, pp. 9–20, 2015, doi: 10.1016/j.cemconres.2015.01.005.
- [23] M. S. H. Bin Mohd Sani, F. Bt Muftah, and M. Ab Rahman, "Properties of Waste Paper Sludge Ash (WPSA) as cement replacement in mortar to support green technology material," *3rd ISESEE 2011 - Int. Symp. Exhib. Sustain. Energy Environ.*, no. June, pp. 94–99, 2011, doi: 10.1109/ISESEE.2011.5977117.



# INFLUENCE OF SILICA FUME, STEEL, AND POLYPROPYLENE FIBERS ON MECHANICAL PROPERTIES OF PLASTIC CONCRETE

<sup>a</sup> Amna Nasir\*, <sup>b</sup> Faheem Butt

a: Department of Civil Engineering, University of Engineering and Technology Taxila, Pakistan, [aminahnasir96@gmail.com](mailto:aminahnasir96@gmail.com)

b: Department of Civil Engineering, University of Engineering and Technology Taxila, Pakistan, [faheem.butt@uettaxila.edu.com](mailto:faheem.butt@uettaxila.edu.com)

\* Corresponding author: Email ID: [aminahnasir96@gmail.com](mailto:aminahnasir96@gmail.com)

**Abstract.** Recently many researchers have introduced the concept of using waste plastic in concrete to save natural resources and control environmental pollution. Because the strength of concrete decreases when plastic is used to partially substitute coarse aggregates, such concrete cannot be used for structural purposes. The goal of this research is to see how silica fume, stainless steel fibers, and polypropylene fibers affect the mechanical properties of plastic waste concrete to improve its strength and durability. Normal control mix was prepared for the comparison of results with plastic waste concrete. In plastic concrete, the proportion of coarse aggregates replaced by plastic aggregates was kept constant (20 %). Cement was replaced with silica fume by weight and fibers (steel and polypropylene) were added by volume of concrete. The addition of silica fume and fibers in mixes was optimum based on the literature review. When compared to the control mix, the split tensile, compressive, and flexural strength of plastic concrete with 20% replacement decreased by 50%, 16.29 %, and 33.25 %, respectively. By incorporating silica fume and steel fibers split tensile, compressive, and flexural strength of plastic concrete was reduced only by 4.72%, 4.56 %, and 1.376 %, respectively. Polypropylene fibers and silica fume improved the tensile, compressive, and flexural strength of plastic concrete by 86.18%, 69.75%, and 97.93% respectively. The mechanical properties were enhanced with the inclusion of steel fibers, polypropylene fibers, and silica fume. Hence, it is concluded that plastic concrete can be used for structural elements by adding some additional constituents to it.

**Keywords-** Mechanical properties, Plastic concrete, Polypropylene, Steel fiber

## 1 Introduction

The use of various types of plastics is a challenge to protect the environment. Currently, different types of plastic are used worldwide. However, the advantages of using plastic are outweighed by its negative environmental impact. In developing countries, improper disposal of plastic waste can be a chief cause of health problems and pollution. The reuse of plastic waste in concrete manufacturing is a feasible way to control its bad impacts on the environment. Many researchers have utilized plastic waste in their studies as a replacement material for coarse aggregate. Zeeshan Ullah [1] has researched concrete containing plastic waste up to replacement ratios of 15% and 20% with conventional aggregate concrete. The results revealed that with the inclusion of plastic waste aggregates in concrete there is a significant decrease in mechanical properties due to poor interlocking. The tensile and compressive strength was reduced by 32.4% – 23.5% at a 20% replacement ratio. Prasanna et al [2] has investigated the effect of using broken E-waste as a coarse aggregate substitute on concrete strength. It was determined that using more than a 20% replacement ratio of E-waste as coarse aggregate would be unsuitable because it would reduce the compressive strength of concrete by 33.7 %. Khawar Ali [3] has evaluated the mechanical properties of plastic waste concrete containing





silica fume and observed the thermal behavior against elevated temperatures. The Optimum result was obtained with 20% sand replacement and cement with plastic fine aggregate (PFA) and silica fume respectively. The compressive and tensile strengths were improved by incorporating silica fume in PFA concrete. Manjunath [4] has replaced both coarse and fine aggregates with waste particles.

At 20% replacement of coarse and fine aggregates split tensile, compressive, and flexural strength decreased by 22.44%, 52.98%, and 42.52% respectively. Zeeshan Ahmad [5] has utilized shredded electronic waste along with micro-synthetic fibers with a 30 % replacement ratio of coarse aggregates in concrete. The inclusion of 0.75 % fibrous material raised the compressive and tensile strengths by 30% and 75%, respectively.

Adewumi John [6] reviewed the engineering properties of recycled plastic waste. There was a reduction in strength by using plastic waste in concrete but still can be used in many engineering applications like temporary structures, concrete pavements, etc., Ramadevi [7] prepared concrete by using grounded PET bottle flakes for fine aggregates with the replacement of 1%, 2%, 4%, and 6%. The compressive and tensile strengths were increased and it was concluded that PET bottle fibers can be used to substitute fine aggregates up to an extent of 2%. Liliana Ávila Córdoba [8] casted concrete specimens containing PET particles.

The PET bottles were recycled to obtain PET flakes and were used in the ratio of 1, 2.5, and, 5% by volume and in three different sizes 0.5, 1.5, and 3mm. It was observed that with the increase in the size of PET particles, Young's modulus decreases whereas the smaller size of PET particles and lower concentration improve compressive strength and strain.

According to the above literature review, the use of plastic waste aggregates in concrete results in a decrease in strength properties. As a result, additives may be required to achieve good strength properties when using plastic concrete. The current study aims to improve the mechanical properties of plastic-containing concrete by using silica fume as a partial substitute for cement and different types of fibers

## **2 Methodology**

The current study's goal is to enhance the mechanical strengths of concrete that contains waste plastic using silica fume, steel, and polypropylene fibers. For this purpose, four types of mixes are prepared with mix IDs M1, M2, M3, and M4. The M1 mix represents natural coarse aggregate (NCA) concrete which acts as a control mix for comparison of results. The M2 mix represents plastic concrete in which natural coarse aggregates are partially replaced by plastic coarse aggregates (PCA).

The M3 represents a plastic concrete mix in which cement and NCA are partially replaced by silica fume (SF) and PCA respectively along with the inclusion of stainless-steel fibers (SSF). M4 mix contains polypropylene fiber (PPF) by volume, SF, and PCA as a partial replacement of cement and NCA respectively. A total of 24 cylindrical specimens (150 mm x 300 mm) six for each mix type are prepared for split tensile and compressive strength determination. Similarly, for modulus of rupture, 12 beam specimens (100mmx100mmx400mm) are prepared, three for each mix. All the samples are tested in a compression testing machine having a capacity of 3000KN.

## **3 Experimental program**

### **3.1 Constituents**

As adhesives in this study, silica fume and Portland cement (OPC) are used. The coarse aggregates are taken from Margallah quarries. The river bed sand from Lawrancepur having a maximum size of 4.75mm is used as fine aggregates. The plastic aggregates are mainly prepared from a scrap of TV, LCD, computer monitors, computer keyboards, etc. For the present study, plastic waste was obtained from the local market in processed form with a maximum size of 20 mm. The maximum size of natural coarse aggregate is kept as 20mm.

Gradation curves for both fine and coarse aggregates are shown in Figure 1. Potable water is used to mix all ingredients. The steel and polypropylene fibers are used to enhance strength properties. The properties of natural coarse aggregates (NCA), Plastic coarse aggregates (PCA), and fine aggregates are enlisted in Table 1. Figure 2 shows plastic aggregates, silica fume, and fiber types.

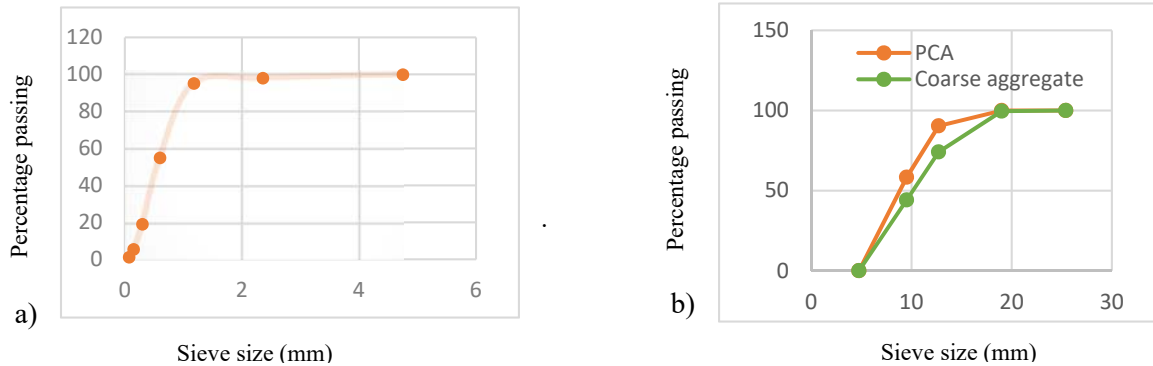


Figure 1: a) Gradation curve for sand b) Gradation curve for NCA and PCA

Table 1: Aggregate properties

Properties	NCA	PCA	SAND
Max aggregate size(mm)	20	19	4.75
Min aggregate size(mm)	4.75	4.75	-
Specific gravity	2.68	1.06	2.64



a) Silica fume and Plastic aggregate

b) Steel and polypropylene fibers

Figure 2: a) Plastic aggregate and silica fume b) Steel and polypropylene fibers

### 3.2 Mix design

The concrete mix is designed in a 1:1.68:3.20 ratio. The four mix types are prepared. Table 2 depicts the details of ingredients for mixes. The optimum values of PCA, silica fume, and steel and polypropylene fibers are taken from the previous studies. Therefore, the coarse aggregates were replaced with plastic aggregates at 20% [4, 9, 10], silica fume (SF) was replaced at 20% with OPC [3]; while steel and polypropylene fibers are used in the ranges of 0.75% and 0.5% respectively [11-13][12, 14, 15] by volume of concrete to enhance strength properties.



Table 2: Details of mix types and their proportions

Mix ID	Fiber type	PCA (%)	Fiber (%)	Silica Fume (%)	OPC kg/m <sup>3</sup>	Sand kg/m <sup>3</sup>	NCA kg/m <sup>3</sup>	PCA kg/m <sup>3</sup>	Silica Fume kg/m <sup>3</sup>	Fiber kg/m <sup>3</sup>	Water kg/m <sup>3</sup>	Plasticizer kg/m <sup>3</sup>
M1	-	-	-	-	392	661	1256	0	0	0	176	4.6
M2	-	20%	-	-	392	661	1004.8	62.88	0	0	176	4.1
M3	SSF	20%	0.75%	20%	313.6	661	1004.8	62.88	55.25	58.95	176	4.9
M4	PPF	20%	0.5%	20%	313.6	661	1004.8	62.88	55.25	4.55	176	4.9

### 3.3 Mix preparation and casting

A concrete mixer of capacity 0.15m<sup>3</sup> is used to prepare all mixes. In the first step, all dry concrete ingredients (sand, cement, NCA, PCA, and SF) are placed in a mixer and half of the required water is added to mix it for 3 to 4 minutes to produce a homogeneous mixture. After that, fibers are added to the addition of remaining water and allowed to mix for another five minutes. Super plasticizer is added to achieve slump within 100-120 mm range mm. After concrete preparation, following proper compaction, cylinders (150 mm x 300 mm) and beams (100mmx100mmx400mm) were casted for compressive, tensile, and flexural strengths.

### 3.4 Curing and testing

After 24 hours of casting, all samples are de-molded and placed in a water tank to cure for 28 days at room temperature. When the testing age is reached, the samples are air-dried and prepared for testing. The compressive and tensile strengths of cylindrical concrete specimens are determined using a compression testing machine for each mix type conforming to ASTM C39 [16] and ASTM C496 [17] respectively. For flexural strength/modulus of rupture, beams are tested by central point loading conforming to ASTM C293 [18]. See Figure 3 failure modes in compression, flexural and tension for all mixes.

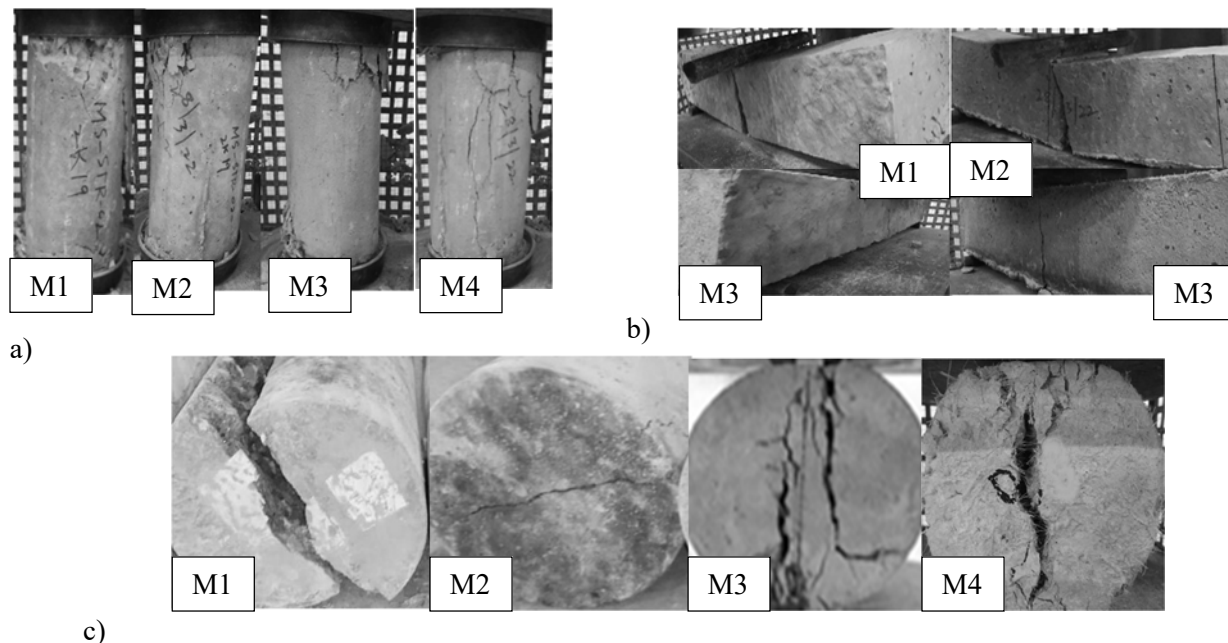


Figure 3: a) Failure modes in compression b) Failure modes in flexural c) Failure modes in tension



## 4 Results and Discussions

### 4.1 Compressive strength

Three cylindrical samples for each mix type were tested for average compressive strength determination. Figure 4 shows the variation of compressive strength for each mix type (M1, M2, M3, and M4). For controlled mix M1, compressive strength of 2715 psi is obtained. With the partial substitution of coarse aggregates with plastic waste aggregates in mix type M2, the compressive strength was reduced by 16.293%. Plastic aggregate's smooth texture causes poor adhesion with cement paste, resulting in a decrease in strength. For mix type M3 in which cement is partially replaced by silica fume and steel fibers are added by volume along with the incorporation of plastic aggregates, the compressive strength was decreased by 4.56% as compared to the control mix. Similarly for mix M4 in which polypropylene fibers are induced instead of steel fibers, the compressive strength was decreased by 4.9% to the control mix. The packing and pozzolanic action of silica fume, as well as the bridging and interlocking effect of steel and polypropylene fibers, are the primary causes of the increase in compressive strength.

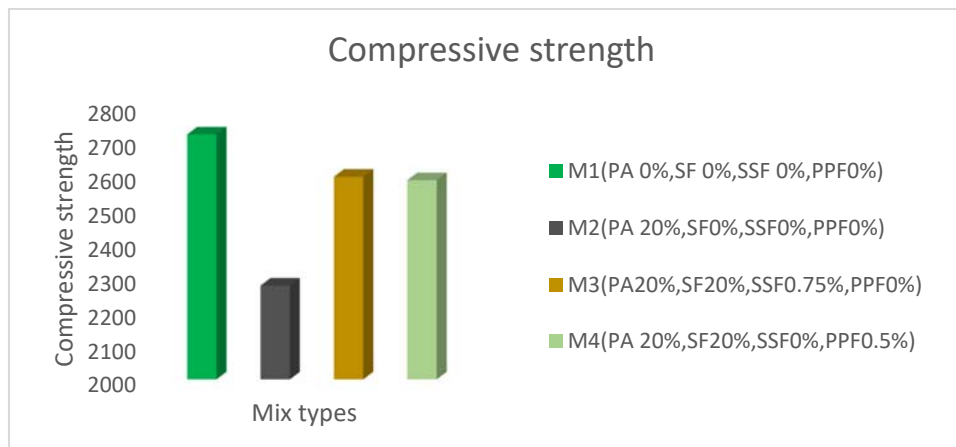


Figure 4: The Comparison of compressive strength results

### 4.2 Splitting tensile strength

Twelve cylindrical specimens, three for each mix type, were tested in a compression testing machine to determine the average splitting tensile strength. For the control mix, the tensile strength comes out to be 275psi. Tensile strength for Mix type M2 is 50% less as compared to control mix M1. This decrease in tensile strength is brought on by the flimsy adhesiveness or bond among cementitious material and plastic aggregates. With the inclusion of silica fume and steel fibers, the strength of plastic concrete improves by 90.54% (i.e. M3 mix). However, it was increased by 86.18% with the incorporation of, silica fume, and polypropylene fibers (i.e. M4 mix). Figure 5 shows the tensile strengths of all mixes. The ability of fibers to reduce small cracks in the concrete matrix accounts for the majority of the increase in tensile strength. When the splitting occurred and continued, the load was gradually supported by the fibers by acting as a conduit for stress transfer from the matrix to the fibers. The stress transfer caused the tensile capacity to rise.

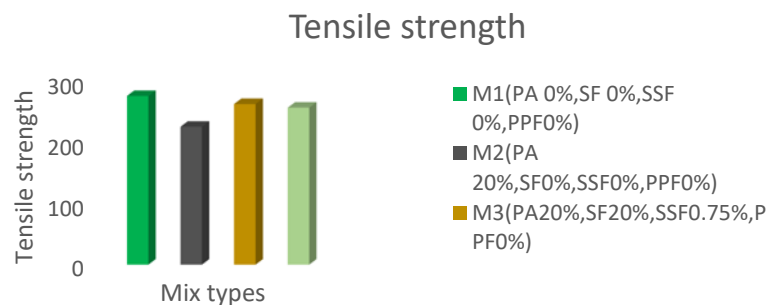


Figure 5: The comparison of split tensile strength results



### 4.3 Modulus of rupture

The casted prisms were subjected to central point loading for each mix type. The flexural strength was decreased with the addition of plastic waste (M2 mix) due to PCA's smooth surface texture and the cement paste's poor interfacial binding, or adhesiveness; however, it improved with the incorporation of silica fume, steel, and polypropylene fibers (i.e. M3 and M4 mixes). For control mix M1, the flexural strength is 436psi. For mix M2 it decreased by 33.25%. Mix M3 and M4 improved the flexural strength of plastic concrete by 95.86% and 97.93% respectively. Figure 6 shows flexural strength results. The improved fiber-matrix bond may be responsible for the increase in flexural strength. The main reason for the increase could be the fibers that cross the crack in the tension half of the reinforced beam.

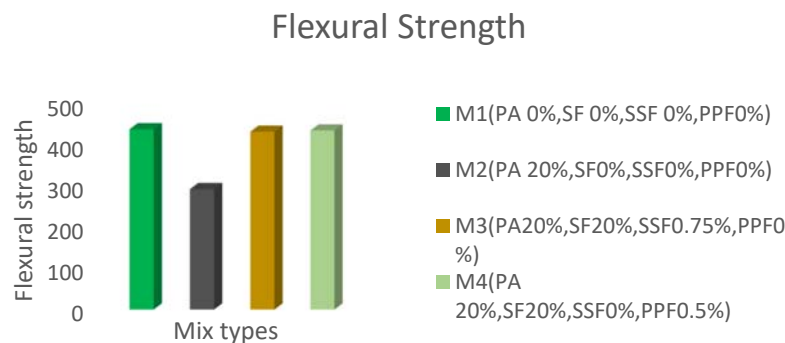


Figure 6: The comparison of flexural strength test results

## 5 Conclusions

The current study leads to the following conclusions:

- 1 When plastic waste is mixed into concrete, the compressive, tensile, and flexural strength decrease by 16.29 %, 50 %, and 33.25 %, respectively because of the hydrophobic nature of plastic aggregates and poor bonding between cement matrix and PCA.
- 2 By adding silica fume the compactness of the matrix increased due to the pozzolanic and filling effects of SF as a result the mechanical properties of plastic concrete increased significantly.
- 3 The SSF and PPF fibers significantly enhanced the tensile and flexural strength due to crack arrest ability and the crack bridging mechanism.

## References

1. Ullah, Z., et al., *An experimental study on the mechanical and durability properties assessment of E-waste concrete*. Journal of Building Engineering, 2021. **38**: p. 102177.
2. Prasanna, P.K. and M.K. Rao, *Strength variations in concrete by using E-waste as coarse aggregate*. International Journal of Education applied research 2014. **4**(2).
3. Ali, K., et al., *Effect of waste electronic plastic and silica fume on mechanical properties and thermal performance of concrete*. Construction Building Materials 2021. **285**: p. 122952.
4. Manjunath, B.A., *Partial replacement of E-plastic waste as coarse-aggregate in concrete*. Procedia Environmental Sciences, 2016. **35**: p. 731-739.
5. Ahmed, Z. and M.I. Qureshi, *Influential assessment of macro synthetic fibers on mechanical properties of concrete containing e-waste coarse aggregates*. in *Proceedings of the 3rd Conference on Sustainability in Civil Engineering (CSCE'21), Islamabad, Pakistan*. 2020.
6. Babafemi, A.J., et al., *Engineering properties of concrete with waste recycled plastic: a review*. Sustainability, 2018. **10**(11): p. 3875.
7. Ramadevi, K. and R. Manju, *Experimental investigation on the properties of concrete with plastic PET (bottle) fibres as fine aggregates*. International journal of emerging technology advanced engineering 2012. **2**(6): p. 42-46.
8. Ávila Córdoba, L., et al., *Effects on mechanical properties of recycled PET in cement-based composites*. International Journal of Polymer Science, 2013. **2013**.



**4<sup>th</sup> Conference on Sustainability in Civil Engineering (CSCE'22)**  
Department of Civil Engineering  
Capital University of Science and Technology, Islamabad Pakistan



9. Lakshmi, R. and S. Nagan, *Studies on concrete containing E plastic waste*. International journal of environmental sciences, 2010. **1**(3): p. 270.
10. Shinu, N.M.T. and S. Needhidasan, *An experimental study of replacing conventional coarse aggregate with E-waste plastic for M40 grade concrete using river sand*. Materials Today: Proceedings, 2020. **22**: p. 633-638.
11. Shaikh, F.U.A. and A. Hosan, *Mechanical properties of steel fiber reinforced geopolymer concretes at elevated temperatures*. Construction building materials, 2016. **114**: p. 15-28.
12. Zhang, P., et al., *Mechanical properties and durability of polypropylene and steel fiber-reinforced recycled aggregates Concrete (FRRAC): A Review*. Sustainability, 2020. **12**(22): p. 9509.
13. Afroughsabet, V., L. Biolzi, and T. Ozbakkaloglu, *Influence of double hooked-end steel fibers and slag on mechanical and durability properties of high performance recycled aggregate concrete*. %J Composite Structures, 2017. **181**: p. 273-284.
14. Das, C.S., et al., *Performance evaluation of polypropylene fiber reinforced recycled aggregate concrete*. Construction Building Materials, 2018. **189**: p. 649-659.
15. Ahmed, T.W., A.A.M. Ali, and R.S. Zidan, *Properties of high strength polypropylene fiber concrete containing recycled aggregate*. Construction Building Materials, 2020. **241**: p. 118010.
16. International, A., *ASTM C39: Standard Test Method for Compressive Strength of Cylindrical Concrete Specimens*. 2014, American Society for Testing and Materials (ASTM).
17. International, A., *C496/C496M-11: Standard test method for splitting tensile strength of cylindrical concrete specimens*. 2011.
18. International, A., *ASTM, C293/C293M-16 :Standard Test Method for Flexural Strength of Concrete*. 2016.



# THE EFFECT OF POLYPROPYLENE FIBERS ON TENSILE STRENGTH OF SELF COMPACTING CONCRETE

<sup>a</sup> Muhammad Tariq\*, <sup>b</sup> Moazam Sattar, <sup>c</sup> Muhammad Aleem

a: Department of Civil Engineering, University of Engineering and Technology Taxila, tariqdaud2@gmail.com

b: Department of Civil Engineering, University of Engineering and Technology Taxila, moazam.malik59@gmail.com

c: Department of Civil Engineering, University of Engineering and Technology Taxila, engrm.aleem@gmail.com

\* Corresponding author: Email ID: tariqdaud2@gmail.com

**Abstract-** The mechanical characteristics of fiber reinforced self compacting concrete in the hardened condition are investigated in this study. The goal of this experiment is to see what impact polypropylene fibers (PPF) have at different doses, such as 0%, 0.50%, 1%, and 1.50% and to estimate the maximum amount of polypropylene fibers (PPF) that can be added safely. Furthermore, Silica fume was used to displace up to 10% of the cement, which was consistent across all blends. The replacement of fine aggregate was carried out with 10% fly ash for blends (M1, M2, M3 and M4). Then percentage increased up to 20% for mixtures (M5, M6, M7 and M8). The purpose of the experimental study programme was to look at split tensile strength after 14 and 28 days of curing. The mix containing varied amounts of polypropylene fibers was then compared to conventional concrete. Tensile strength was improved by adding polypropylene fibers to the mix. At 1% polypropylene fiber insertion, the tensile strength reaches its maximum.

**Keywords-** Polypropylene fibers (PPF), split tensile strength, self-compacting concrete (SSC)

## 1 Introduction

Self-consolidating concrete is another name for self-compacting concrete. By its own weight, this form of concrete can be placed or modified in any location. It may be conveniently installed in busy reinforcing areas. There is no need to use mechanical vibrators to compact the SCC during installation.

In this experiment, seven PPF-containing mixtures and one control blend were used to test SCC tensile strength. All mixtures had a predetermined substitution of cement with silica fume and fine aggregate with fly ash. Fibers were gradually added to all combinations at a rate of 0.5 percent. The percentages of replacement were 0 percent, 0.5 percent, 1 percent, and 1.5 percent. All mixtures used a fixed 0.33 water-cement ratio, and using super plasticizer increased the workability of SCC while maintaining the water content. The goal of this research effort was to determine the mechanical characteristics of concrete, including compression, split tensile and flexural strength. All of the polypropylene fiber mixtures were compared to the control mix. It was discovered that adding fibers to SCC increased tensile strength of concrete [1]. Four different amounts of polypropylene fibers were used in the concrete mixes to determine the tensile strength. The amounts of fibers were 0.10, 0.20, 0.30, and 0.40 percent by the weight of cement. Four different blends were created for this purpose. At 28 days, the tensile strength was assessed. Polypropylene fibers were found to enhance the tensile strength of self-compacting concrete. [2]. The properties of SCC in fresh and hardened states were assessed using an experimental method. Polypropylene fibers were added in various amounts of 0 percent, 0.50, 0.75 and 1 percent, together with steel fibers, for this purpose. The greatest tensile strength was reached with the addition of 1% PPF [3]. Polypropylene fibers in the numbers of 1, 2, and 3 kg/m<sup>3</sup> were used in this study. High-performance PPF was used in this study. At temperatures of 250 °C, 1000 °C, 2000 °C, and 3000 °C, mechanical properties such as tensile, compressive, and flexural strengths were investigated. When 1 kg of fibers were added to concrete, the compression strength enhanced by 14.0 percent, the split tensile strength improved by 17.0 percent, and the flexural strength increased by 8.50 percent [4].



The damage evolution rule, compressive strength, and damage performance of PPF concrete were all tested experimentally. The ordinary concrete was used as a comparison for the results. The results showed that adding PPF to concrete increased its split tensile strength [5]. The 28-day mechanical properties of PP fibers increases at low values, but decreases by 3% - 5% at higher concentrations [6]. The split tensile strength of fibers reinforced concrete was related to the fibers length used. With longer fibers, the split tensile increases [7]. Flexural, split tensile, and modulus of rupture were all significantly increased when compared to conventional concrete [8]. The purpose of this experimental program was to study the effect of PPF on SCC modified with fly ash. Moreover, to find the optimum content of PPF for SCC modified with fly ash for mechanical property like tensile strength of SCC.

## 2 Experimental Procedures

The first of all the selection of materials used in the mixes was carried out. The selection of aggregate quarries was influenced by the petrography of the rock resources. The Margalla, Rohi, Sargodha, and Gari Habib Ullah quarries, for example, yield calcium carbonate, dolomite, limestone, and granite minerals. At this point, the project's ingredients included cementitious materials, fly ash, Portland cement, and polypropylene fibers. Then typical mix designs were created in the. The ACI-211 requirements were followed with a one-to-one mix ratio (1:1.4:1.6).

PPF was used at the following concentrations: 0%, 0.50%, 1%, and 1.5. The mixes were made with 0.33 w/c ratio to investigate the impact of PPF on concrete properties. The researcher used PPF dosages of 0, 0.5, 1, and 1.5 percent. Figure 1 shows the quantities and identities of cement (C), fine aggregate, coarse aggregate, silica fume (SF), fly ash (FA), admixture, and polypropylene fibres (PPF) in self compacting concrete mixtures. First and foremost, all aggregates were combined in a drum type concrete mixer for about one minute in a dry state. After that, PPF was applied, and the missing was completed for another minute in a dry environment. At the beginning, 2/3 of the water was utilised, and the mixture was mixed for another minute. The last 1/3 of the water and the super plasticizer were added at this point. The fresh properties like slump flow, flow ability and passing ability were determined. The mix proportions used for experimental program are given below. Sample 1:1.4:1.6 mix was used for all the batches. It was because, in Pakistan most commonly used concrete mix as shown in Figure 1.

Mix No	Mixture ID	W/B	Water	C	SF	FA	Fine Agg	Coarse Agg	PPF Fraction	Admixture		
			Kg/m <sup>3</sup>	Kg/m <sup>3</sup>	%	Kg/m <sup>3</sup>	%	Kg/m <sup>3</sup>	Kg/m <sup>3</sup>	%	Kg/m <sup>3</sup>	Kg/m <sup>3</sup>
1	Control	0.32	142	444	-	-	-	690	769	0	0.0	5.3
2	M1	0.32	128	400	10	44	10	69	621	769	0	4.8
3	M2	0.32	127	397	10	44	10	69	621	769	0.5	4.8
4	M3	0.32	126	395	10	44	10	69	621	769	1	4.7
5	M4	0.32	126	393	10	44	10	69	621	769	1.5	4.7
6	M5	0.32	128	400	10	44	20	138	552	769	0	4.8
7	M6	0.32	127	397	10	44	20	138	552	769	0.5	4.8
8	M7	0.32	126	395	10	44	20	138	552	769	1	4.7
9	M8	0.32	126	393	10	44	20	138	552	769	1.5	4.7

Figure 1: Polypropylene fibers

### 1.1 Materials

The Naturally available sand of Lawrence pur quarry was used as a fine aggregate (FA) & coarse aggregate (CA) of crushed Margalla Hills was used. The addition of silica fume & polypropylene fiber (PPF) reduces the workability of concrete, to get desirable slump value superplasticizer was used. In this research, an Ultra high range water reducing admixture viscrete 3110 was used.

### 1.2 Polypropylene fibre

The monomer C3H6 is used to make polypropylene fibres. These fibres are chemically resistant. Figure 2 shows the white polypropylene fibres with a diameter of 12 mm that were employed in the research for the experimental programme.





Figure 2: Polypropylene fibers

## 2 Research Methodology

Splitting tests on cemented concrete may be used to assess tensile strength. Moreover, direct tension test and the flexural test can be used to find the tensile strength of concrete. Crack size and depth in constructed settings are directly related to the tensile strength of concrete. Because of this, concrete is very brittle and hence extremely weak under strain. Furthermore, the concrete is extremely weak under tension due to its brittle character. As a result, direct tension is unlikely to be tolerated. Cracks emerge when tensile forces exceed the concrete's tensile strength. The maximum load bearing capacity of concrete components was determined by determining its strength. It's also possible to assess the tensile strength of concrete by breaking it in half. According to ASTM C496 standards. As a last step, we'll go through the various aspects of the split cylinder's test for concrete samples. The tensile strength of SCC in the hardened condition was tested at 14 and 28 days after curing to see how PPF affected its performance.

The tensile strength of SCC was determined by applying stress to cylindrical samples having 150 mm diameter and 300 mm height. According to ASTM C39, compression testing machine was used to determine the split tensile strength. For this purpose, the specimen was placed on a flat surface with the vertical and centered lines drawn on the ends. Laid another plywood strip over the specimen and lowered it until it touched the plywood strip. Determined the breaking load. By using that load, tensile strength was determined. The calculated tensile strength is shown in Figure 3. The average of three samples were used as a final result.



Figure 3: Polypropylene fibers

## 3 Results

*The split tensile strength was determined according to ASTM C496. The tensile strength of SCC with different proportions of PPF and proposed contents of silica fume and fly ash are shown in the Figure 4.*

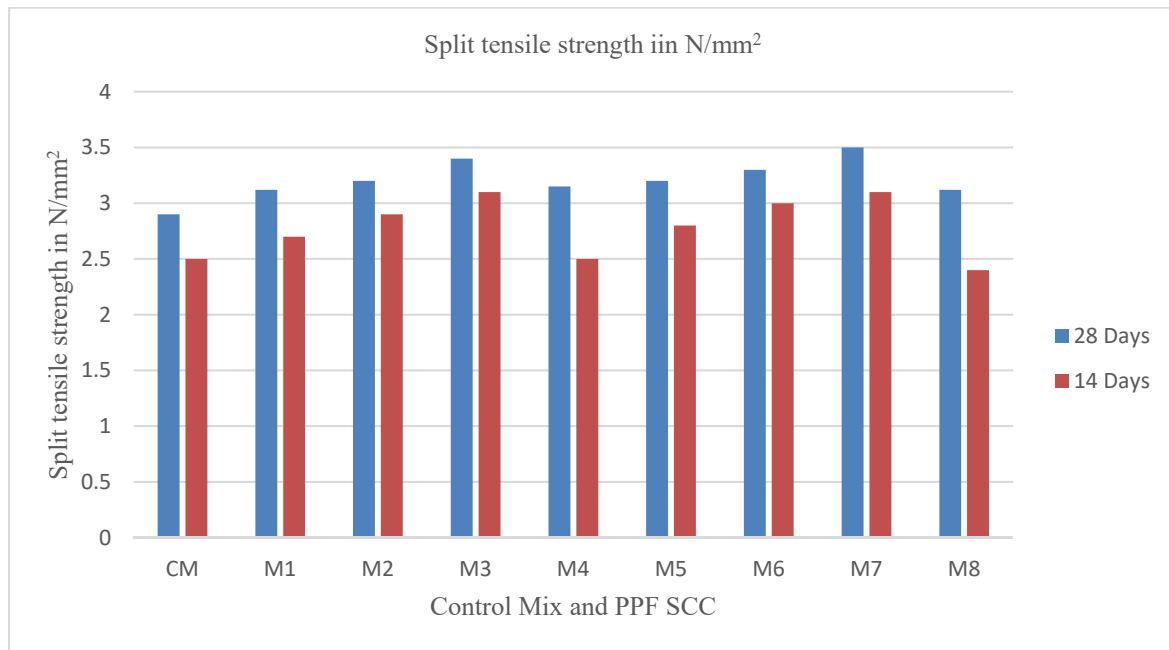


Figure 4: Polypropylene fibers

Figure 3 shows the tensile strength of SCC with various PPF percent and proposed silica fume and fly ash contents. The improvement in mixes containing 10% fly ash for M1 to M4 and 20% for M5 to M8, 10% silica fume for mixes and proposed contents of PPF are shown in the graph. The effect of PPF in increasing split tensile strength was more than that of compression test & get the improvement in the results up to 1% PPF. The mix containing 0%, 0.5%, 1% and 1.5% PPF increased the strength by 8%, 10%, 17% and 7% respectively at 28 days for M1 to M4 for mixes M5 to M8 the strength improved by 10%, 14%, 21% and 8% respectively at 28 days of curing. Since PPF and cement paste were interlocked during testing, this failure pattern differed from that of plain concrete mixtures, the failure pattern was unique as shown in Figure 5.



Figure 5: Polypropylene fibers

## 4 Conclusion

The main purpose of the study was to evaluate the beneficial effect of polypropylene fibers in contents like 0%, 0.5%, 1% and 1.5% on self compacting. SCC behavior was also studied under the influence of fly ash and silica fume. From the research, the following findings can be drawn:

- 1 In case of tensile strength, the addition of PPF increased the tensile strength of SCC. The addition of PPF reduced the brittleness nature of concrete. As a result tensile strength increased.



- 2 The maximum strength was obtained at 1% addition of PPF. The failure pattern was different than the plain concrete mixes, after testing the two parts were not separated from each other due to the interlocking of PPF in the cement paste.
- 3 As a result of the entire experimental study, it is possible to use polypropylene fibers in the creation of SCC up to a maximum of 1%. Further addition of PPF causes the reduction of tensile strength of SCC.

## References

- [1] Rani, B.S. and N. Priyanka, "Self compacting concrete using polypropylene fibre, " *International Journal of Research Studies in Science, Engineering and Technology*, vol. 4, pp. 16-19,2020.
- [2] Kurian, S.V and A. Sarah, "Influence of polypropylene fibre in self compacting concrete," *International Research Journal of Engineering and Technology*, vol. 5, pp. 1102-1104,2021.
- [3] Abaeian, R., et al., "Effects of high temperatures on mechanical behavior of high strength concrete reinforced with high performance synthetic macro polypropylene (HPP) fibres," *Construction and Building Materials*, vol. 165, pp. 631–638,2018
- [4] Liu, X, et al., "Properties of self-compacting lightweight concrete reinforced with steel and polypropylene fibers," *Construction and Building Materials*, vol. 226, pp. 388–398,2022.
- [5] Qin, Y.,et al., "Experimental study of compressive behaviour of polypropylene-fibre-reinforced and polypropylene-fibre-fabric-reinforced concrete," *Construction and Building Materials*, vol. 194, pp. 216–225,2022.
- [6] Priti A. Patel, Dr. Atul K. Desai and Dr. Jatin A. Desai, "Evaluation of Engineering Properties for PP Fiber Reinforced Concrete," *International Journal of Advanced Engineering Technology*, Vol.3,pp. 42-45,2022.
- [7] Miss Komal Bedi, "Experimental Study For Flexure Strength on PP Fiber Reinforced Concrete," *IOSR Journal of Mechanical and Civil Engineering (IOSR-JMCE)*, vol.3, pp. 16-22,2022.
- [8] Mounir M. Kamal, Mohamed A. Safan, Zeinab A. Etman,, Bsma M. Kasem,"Mechanical Properties of Self Compacted Fiber Mixes," *Housing and Building National Research Center Journal (HBRC)*, Vol.10,pp. 25–34,2022



# MECHANICAL BEHAVIOUR OF MORTAR USING POZZOLANA AS PARTIAL REPLACEMENT OF CEMENT

*<sup>a</sup> Adil Khan\*, <sup>b</sup> Muhammad Shakeel, <sup>c</sup> Irfan Ullah, <sup>d</sup> Yasir Khan*

a: Department of Civil Engineering, University of Engineering and Technology Peshawar, [18pwciv5027@uetpeshawar.edu.pk](mailto:18pwciv5027@uetpeshawar.edu.pk)

b: Department of Civil Engineering, University of Engineering and Technology Peshawar, [18pwciv5186@uetpeshawar.edu.pk](mailto:18pwciv5186@uetpeshawar.edu.pk)

c: Department of Civil Engineering, University of Engineering and Technology Peshawar, [irfanullah20120@gmail.com](mailto:irfanullah20120@gmail.com)

d: Department of Civil Engineering, University of Engineering and Technology Peshawar, [yasirkhancivileng@gmail.com](mailto:yasirkhancivileng@gmail.com)

\* Corresponding author: Email ID: [18pwciv5027@uetpeshawar.edu.pk](mailto:18pwciv5027@uetpeshawar.edu.pk)

**Abstract-** Lightweight concrete structures are being built by human beings since ancient time for shelter and other purposes. These structures are composed of different materials like concrete, wood, glass, steel, stones and mud. But in the modern world, the use of lightweight concrete is increasing. After water, concrete is the most widely used material on our planet. Due to its relatively low cost, it is commonly used building material. The major binding material of concrete is cement. This leads to the production of cement in very large amount. The excess use and production of cement leads to environmental problems and concrete structure disintegration. We can reduce the production of cement by adding different types of pozzolanic materials as partial replacement of cement which will also decrease the dead load of the building. In this study we will evaluate the results of adding different proportions of Pozzolana as partial replacement of cement. The type of pozzolanic material used in this study is pumice. Pumice is available naturally in the form of stones. The pumice stone is always easily available everywhere and having low density than all the other aggregates used in the concrete mortar. The light weight mortar cubes are prepared by partially replacing the cement with powdered pumice aggregate by 12, 24, and 36%. The mix design and all the respective percentages are prepared by mixing it with water. After proper curing the mechanical and the durability properties of conventional control mix and the partially replaced mortar cubes are compared by conducting compressive strength and porosity tests for specific replacement of the

**Keywords-** Lightweight concrete, Admixtures, Durability, control mix.

## 1 Introduction

Construction is a very old human practice. Human beings are involved in construction since ancient times. With time the structures become more durable and stronger. For more than 2000 years LWC has been used as a building material [1]. In this study, the main focus is on concrete. As cement is the major constituent of concrete, there are many side effects of excess cement production such as environmental degradation [2]. Chromium in it that can cause allergy. Crystalline silica is not good for lungs and skin, lime and other alkaline compounds are highly corrosive to human tissues [3]. The solution is to use as minimum cement as possible. One of the ways is to replace this with another material that needs to have the same properties or even better properties than cement. We have to reduce the use of cement in concrete by replacing it with another material that is pozzolanic or simply known as pozzolan [4]. Pumice stone being embossed volcanic rock, comes into form when lava with a very high content of gases and water is squeezed out of volcanic action. Pumice is a lightweight stone that floats on the surface of the water [5]. The main objective of this study is to find a combination of cement and pumice that should not affect the properties of concrete.

Nowadays we need a type of concrete that will be LWC to decrease the weight of the building, which leads to economical and safe building construction. The novelty of this research is that pumice stone being lightweight when used as a partial







replacement for cement will decrease the weight of the concrete, which decreases the weight of the structure and hence will lead to less cement production and economical building construction. In this study, different percentages of pumice were used to obtain such a percentage of pumice as a replacement for cement to improve its properties.

## 2 Research Methodology

### 2.1 Material Collection

The following is the material collected for the research as shown in Table 1.

Table 1: Material collection

S. NO	Material	Description	Image
1	Pumice Stone	In this study, the pumice stone was collected from Lahore and then brought to Peshawar. Pumice stones were then ground at 100 °C and 700 °C temperatures in PCSIR Laboratory located on Nasir Bagh Road, Peshawar. Then it was passed through sieve no 200, in this way the desired fine form of pumice stone was obtained.	
2	Sand	In this study, different samples of sand were collected from different locations, in search of sand having a modulus of about 2.5. The fineness modulus of all the collected samples was evaluated and the sand with a fineness modulus of 2.5 was selected for the study. The selected sample was obtained from Uzair Material Stock Forest Bazar Peshawar.	
3	Cement	The type of cement used in this study was ordinary Portland cement conforming to ASTM C204-18e1., from a company called Kohat Cement. An admixture of Sika-viscocrete was also added to reduce shrinkage and creep in the concrete.	
4	Water	Looking into different parameters such as alkalinity, turbidity, oxygen saturation, temperature, conductivity, and freshwater conforms IS 456-2000 were used for the preparation of concrete.	

### 2.2 Percentage of Pumice Stone as Partial Cement Replacement

Different percentages of pumice stone were used as a replacement for cement to find out the required percentage of a pumice stone to achieve high-performance quality. In this study 12, 24, 36% of pumice stone was used as a partial replacement for cement, and properties were evaluated.



### 2.3 Quantity of Specimens

The number of specimens prepared and tested in this study is given in Table 2.

Table 2: Calculation for Number of Samples

Percentages	Ages	No. of cubes for Compression test	No. of cubes for Porosity test	Sum
P-12	7	9	6	15
	28	9	6	15
P-24	7	9	6	15
	28	9	6	15
P-36	7	9	6	15
	28	9	6	15

### 2.4 Mixing Procedure

The mixing procedure of cement mortar was followed by ASTM C-305 to get a uniform mix, having plastic consistency and adequate workability to be placed easily in the mould.



### 2.4 Specimen Preparation

In this study, the standard cubes of size (25.4 x 25.4 x 25.4) mm were prepared in the cube moulds. For compression, the 9 specimens will be cast for each age and each percentage. The casting of partially replace pumice mortar is similar to that of conventional control mix design, before grinding the pumice it should be uniformly pre-wet to get its total saturation, then allow to sit until the whole of the water drains out from it [8]. After the casting of concrete, the specimens were kept for 24 hours and then de-mould. After the demolding, all these will have immersed in the curing tank for curing, and then they should be extracted at their specific testing time.

### 2.5 Laboratory Tests

The following are the tests performed in this research as shown in Table 3.

Table 3: Laboratory Tests

S. No	Test	Standard	Description	Image of Assembly
1	Compressive strength	ASTM C109	It gives the determination behavior of the material under a load and the maximum stress that a material can sustain over a period under applied load.	
2	Porosity	ASTM C1754	Porosity is the percentage of void spaces in mortar or concrete. It is the measure of the volume of voids in concrete.	



### 3 Results and Discussion

#### 3.1 Compressive Strength

The following are the results of compressive strength as shown in Table 4.

Table 5: Compressive strength

S. No	Compositions	Compressive strength (Ksi)			
		P-700		P-100	
		7-days	28-days	7-days	28-days
1	Control	2.342	3.290	2.342	3.290
2	P-12	2.623	3.417	2.299	3.053
3	P-24	2.105	3.797	2.502	3.373
4	P-36	2.194	4.321	2.001	3.549

##### 3.1.1 Compressive Strength Comparison

It is clearly shown in Figure 1 below that P-36-700 at 28 days curing gives us maximum strength i.e 4.321 ksi. And P-36-100 at 7 days curing gives us minimum strength i.e 2.105 ksi.

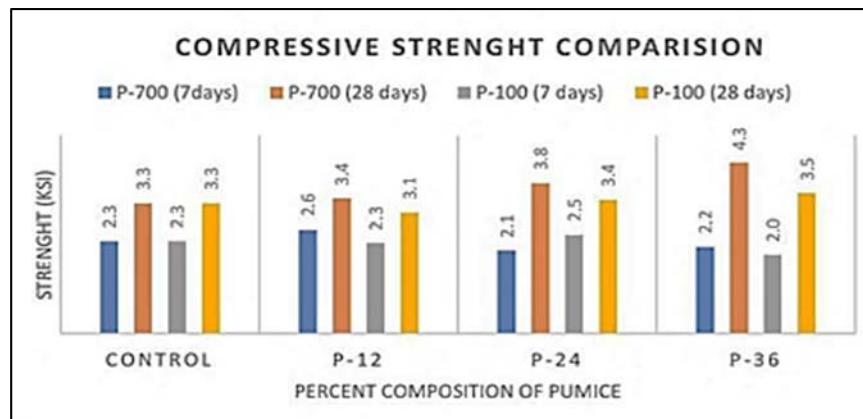


Figure 1: Compressive strength comparison chart

#### 3.2 Porosity

To find porosity, we need the oven-dried weight (W<sub>d</sub>), surface saturated weight (W<sub>ssD</sub>), and submerge in water weight (W<sub>w</sub>). The soaked and dry weights were founded for all the specimens of all ages and the average was taken for each set. Table 5 below shows the porosity of samples.

Table 6: Porosity of samples

S. No.	Compositions	P-700						P-100					
		7 days			28 days			7 days			28 days		
		W <sub>w</sub>	W <sub>ssD</sub>	W <sub>d</sub>	W <sub>w</sub>	W <sub>ssD</sub>	W <sub>d</sub>	W <sub>w</sub>	W <sub>ssD</sub>	W <sub>d</sub>	W <sub>w</sub>	W <sub>ssD</sub>	W <sub>d</sub>
1	Control	167	294.2	277	164	292	274	167	294.2	277	164	292	274
2	P-12	162	293.3	267	160	290	263	161	296.3	276	159	289.5	268
3	P-24	163	297.5	270	162	294	268	159	296.7	275	162	300	282
4	P-36	164	299.7	289	165	296.7	280	160	292.5	270	162	300	282



### 3.2.1 Porosity Comparison

The following column chart as shown in Figure 2 below is showing the comparison of porosity for different pumice compositions for 7- and 28-days curing. It is clear from the chart that P-24-700 7 days curing has maximum porosity of 20.497% while P-36-700 7 days have a minimum porosity of 7.721%.

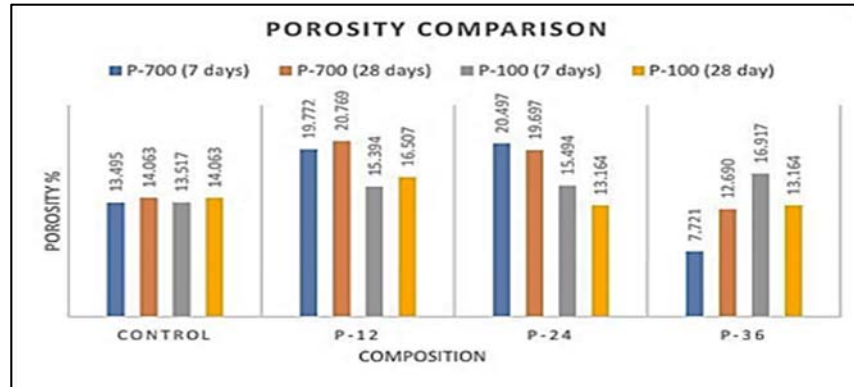


Figure 2: Porosity comparison chart

From the results, it is clear that compressive strength increases with the increasing percent of pumice and curing period as shown in Figure 3. Generally, porosity is going to decrease when pumice stone percentage is going to increases as shown in Figure 3.

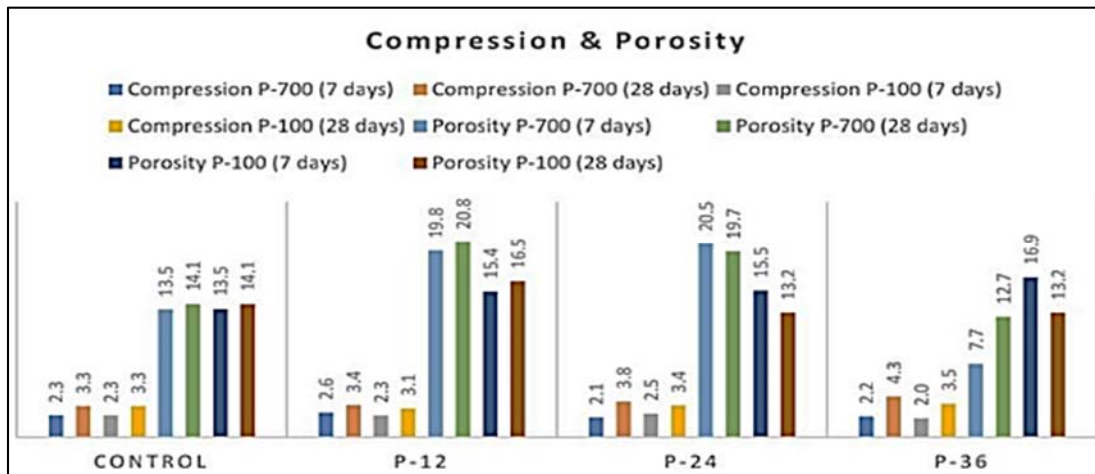


Figure 3: Compression & Porosity

### 3.3 Discussion

From our research being lightweight, when pumice is used as a partial replacement for cement it will form LWC having the following benefits:

1. It will decrease the production of cement and hence environmental degradation will decrease.
2. It will decrease the health risks associated with cement.
3. It will decrease the dead load of the building.
4. It will reduce transportation costs.





## Conclusion

From the conducted study the following conclusions can be drawn:

1. P-36-700 at 28 days curing give us maximum strength i.e 4.321 ksi. And 36-100 at 7 days curing gives us minimum strength i.e 2.105 ksi.
2. P-24-700 7 days curing has maximum porosity of 20.497% while P-36-700 7 days have a minimum porosity of 7.721%.
3. The best combination is P-36-700 (28 days) which gives compressive strength of 4.3 ksi and 12.7% porosity.

## References

- [1] (ACI 211.2-98) - Standard Practice for Selecting Proportions for Structural Lightweight Concrete.
- [2] K.Syamala Devi, V.Vijaya Lakshmi, and A.Alakanandana. (2017, November). IMPACTS OF CEMENT INDUSTRY ON ENVIRONMENT – AN OVERVIEW. *Asia Pacific Journal of Research*, 1, 7.
- [3] Hinson AV, Lawin H, Mikponhoué R, Adjobimey M, Ayélo P, & Péreira R. (2020, July 28). Environmental & Health Impacts of Cement Production Activity in Benin. *Austin Environmental Sciences*, 4.
- [4] Dr. Ghassan K. Al-Chaar, & Dr. Mouin Alkadi. (2013, July). Natural Pozzolan as a Partial Substitute for Cement in Concrete. *The Open Construction and Building Technology Journal*, 11. doi:10.2174/1874836801307010033
- [5] Pietro Lura Technical University of Mineral Information Institute, Pumice Aggregates For Internal Water Curing, [Http://Www.Mii.Org](http://www.Mii.Org) (Accessed On 6th May 2009)



# MECHANICAL PROPERTIES OF BAMBOO CORE SANDWICH PANELS

<sup>a</sup> Vireen Limbachiya\*, <sup>b</sup> Jayawardena Perera, <sup>c</sup> Rabee Shamass

a: Civil and Building Services Engineering, London South Bank University [limbachv@lsbu.ac.uk](mailto:limbachv@lsbu.ac.uk)

b: Civil and Building Services Engineering, London South Bank University [pereraj@lsbu.ac.uk](mailto:pereraj@lsbu.ac.uk)

c: Civil and Building Services Engineering, London South Bank University [shamassr@lsbu.ac.uk](mailto:shamassr@lsbu.ac.uk)

\* Corresponding author: Email ID: [limbachv@lsbu.ac.uk](mailto:limbachv@lsbu.ac.uk)

**Abstract-** Bamboo is a material that has been used in construction for generations. One of the biggest disadvantages to this material is the natural variability, however, there is the potential for it to be used as core material in sandwich panels. Therefore, to maximise bamboo's potential for usage as a structural material and limit the impact of natural variability, bamboo core sandwich panels were developed. The experimental procedure was broken down into 3 stages. The first stage reviewed the impact of different core configurations on the modulus of rupture and compressive strength of sandwich panels produced with plywood as the outer skin and bamboo rings as the core. The second stage took the best configuration from stage 1 and produced a 2m beam to review the mechanical properties and was thereafter compared to a control beam with no bamboo rings. The final stage of the experimental procedure reviewed the compressive strength of the bamboo rings both parallel and perpendicular to the grain to validate the results obtained in stage 1 and 2. Results showed that the core configuration has a big impact on the modulus of ruptures and that there was a clear relationship between density and modulus of rupture. Stiffness of the beams and cubes tested increased as the cross-sectional area of rings increased and allowed for a greater contact area. Finally, the testing of the bamboo rings aligned with results that were expected when testing parallel and perpendicular to the samples, with split bamboo rings producing good strengths in comparison to good rings.

**Keywords-** Bamboo, Sandwich Panels, Mechanical properties.

## 1 Introduction

There are around 1000 different subspecies of bamboo in the world, and many of them are common in temperate, tropical, and subtropical climate zones. Bamboo has been a dependable building material for both temporary and permanent structures for generations, among its many other uses. One of the reasons that bamboo has been used for construction is because of its strength to weight ratio, mechanical properties, rate of growth and seismic performance [1]. Although, there have been comparisons to materials such as steel, studies have showed that the strength properties are similar to that of lumber, with certain species approaching strengths of high grade (D40) [2]. The allowable stresses for most species are found to be between 10 and 20 N/mm<sup>2</sup> [3].

Sandwich panels have been extensively employed in construction because of its inherent thermal, acoustic, and fire insulation capacities and where weight is a major consideration [4][5]. Currently, many of the available sandwich panels employ less dense materials as their core material, but this method is not the most effective when flexural pressures are involved. The core's function in flexural resistance is essential because it must transfer shear forces between the encasing skins. Therefore, the core must provide a stability in resisting shear deformations. A study evaluated how the bamboos core diameter and the type of adhesive used to connect the skin to the core affected the panels' equivalent density, flexural strength, and shear strength with a brand-new sandwich panel made of prepreg flax skins [6]. It was concluded that both the density and diameter of the bamboo rings had an impact on the characteristics of sandwich panels [6]. Both diameter and density were found to have an impact on the mechanical properties. As the diameter of the bamboo cores increased,



there was greater flexural strengths and as the diameter decreased there was an improvement in the core transverse shear modulus [6]. A separate study conducted a numerical analysis on the flexural behaviour of how the height of bamboo rings and the thickness of plywood skins affected the bending stiffness in comparison to cross-laminated timber (CLT) sections [7]. It was concluded that that the bending stiffnesses of the sandwich panels constructed from bamboo rings were similar to that of the CLT. Therefore, showed that there is potential for more slender areas and much lighter components [7]. A similar review with bamboo cores with multiplex plywood skins was conducted to understand the impact of both core and skin thickness on the mechanical properties of sandwich panels [8]. With the use of a two-way ANOVA statistical analysis, it was concluded that individually altering the thickness of both elements impacted the results. However, increasing the thickness of both elements together, tended to not impact the bending strength of the panels [8]. It has also been reported that bamboo rings in a honeycomb configuration can improve flexural strength and impact resistance [9]. As well as configuration of bamboo rings, the adhesive plays a crucial role, as bamboo in comparison to wood has a higher density and starch, wax and silica content which impacts its bonding ability [10]. Overall, studies have shown the potential for bamboo to be used as a core in sandwich panels for structural application. The sustainable benefits could prove popular with the strategies that have been placed by many governments across the world. Therefore, the aim of the paper is to determine the structural capability of using bamboo cores in timber sandwich panels. With the purpose of determining if the mechanical properties bamboo sandwich panels have the potential to be used for structural application.

## 2 Experimental Procedures

To review the impact of bamboo sandwich panels, the experimental procedure was broken down into 3 stages.

### 2.1 Stage 1

In this stage, there were four beams (500mm x 165mm x 120mm) and two cubes (100\*100\*100) with different core configurations produced and one beam was produced with no cores as a control sample. Beams were tested for their flexural strength and the cubes were tested in compression. Table 1 provides the details of the specimen number, core configuration and number of cores used for the beam samples. For the cube samples, there were 3 and 4 cores in the two different samples produced. The cores used were 100mm in length and the plywood used for the outer casing had a thickness of 9mm. Figure 1 provides an image of a cube sample that was prepared. The beams were tested under 4-point bending, with loading at a rate of 3kN/sec and two-point loads were applied at 300mm.

Table 1. Details of beam samples

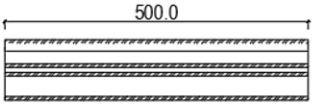

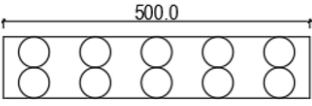
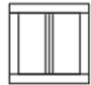
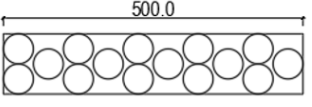
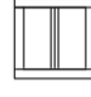
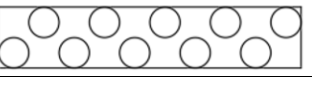

Specimen Number	Core Configuration		Number of Cores
	Plan View	Elevation	
S1-01	Control specimen with no bamboo 	N/A 	None Longitudinal core configuration, with equivalent length of bamboo as S1-04
S1-02			10
S1-03			15
S1-04			10



Figure 1. Compression samples

### 2.2 Stage 2

The second stage of the experimental procedure involved producing 2m sandwich panels and investigating the structural behaviour. A 2m control beam (S2-01-P) was compared to the 2m sandwich panel using the configuration of S1-03 (S2-01-BP) in phase 1, as this has the greatest strength to weight ratio of any samples tested. The beams were tested under 4-point bending, had dimensions of 2000 x 120 x 165 mm and an effective span of 1800mm. Figure 2 provides the setup of the 4-point bending tests and the location of the linear variable displacement transducer (LVDT) which was used to measure the deflection at mid span. The loading rate for the test was 0.15 mm/s

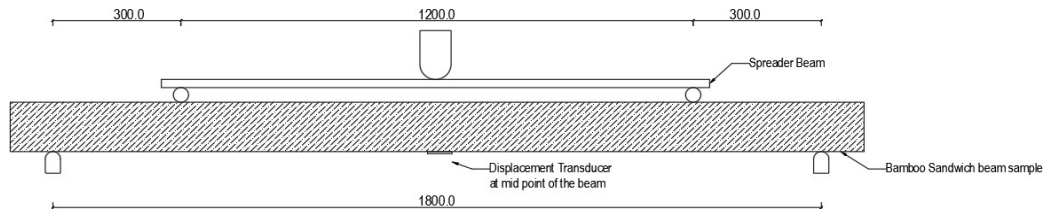


Figure 2: Test setup for four-point loading on 2m beam

### 2.3 Stage 3

The final stage of the experimental procedure reviewed the compressive strength of the bamboo ring both parallel and perpendicular to the grain. Furthermore, in addition to testing the good quality bamboo rings, bamboo with defects and those rings that had failed in the sandwich panels were also investigated for their compressive strength in both directions. Table 2 provides details of the samples that were tested.

Table 2: Compression test specimen details

Specimencode	Description
PD-1	Parallel to grain of damaged beams
PD-2	
PPD1	Perpendicular to grain of damaged beams
PPD2	
PS-1	Parallel to grain of split bamboo
PPS-2	Perpendicular to grain of split bamboo
PP-1	Perpendicular to grain off good bamboo
PP-2	
P-1	Parallel to grains of good bamboo
P-2	



### 3 Results

#### 3.1 Mechanical properties of the bamboo sandwich panel

Figure 3 provides the Modulus of Rupture (MOR) vs density of the 5 beams produced in stage 1. Results show that there is a direct link between density and MOR, as density increases so does the MOR. The beam that produced the greatest MOR was S1-02 which had rings arranged longitudinally along the longitudinal axis of the beam. It assumed that this produced the greatest strength as the arrangement allowed for the loads to be distributed parallel to the grain, which has been stated to be its strongest direction [11]. S1-04 failed due bamboo rings being compressed. It is assumed that the higher shear stresses located around the support caused the rings to fail in compression in those areas. From the results it can be noted that S1-04 which has a similar density to that of S1-05 and S1-03 produced a higher MOR value. The reason for this is due to the increase in bamboo rings that were used in S1-04. S1-04 had 33% more rings in comparison to S1-05 and S1-03, which is assumed to have provided greater rigidity due to an increase in the contact area. Similar studies concluded that an increase in the number of rings will increase the MOR due to the rings having a greater contact area with the outer skins and therefore, increasing the rigidity and providing greater resistance [8]. Figure 4 provides an image of the failure mode of one of the beams and it was noted that all beams had similar modes of failure. It was noted that initially the top skin of beam failed and thereafter there was delamination from the core. Similar trends had been noted in other studies where it was observed that failure of top skin occurred in the initial phase of loading, followed by the complete separation of the specimen in the mid-span at failure [12].

Table 3 provides the results of the cube samples that were tested for its compressive strength. Testing showed that S1-C1 failed due to vertical cracks running along the longitudinal axis while S1-C2 failed due the punching of plywood skins. Although S1-C2 had more bamboo rings, the results show that there is a direct link between the cross-sectional area of the rings and the compressive strength. As the cross-section area increased, so did the compressive strength. S1-C1 is assumed to have produced greater strengths as its cross-sectional area was 43% greater than that of S1-C2.

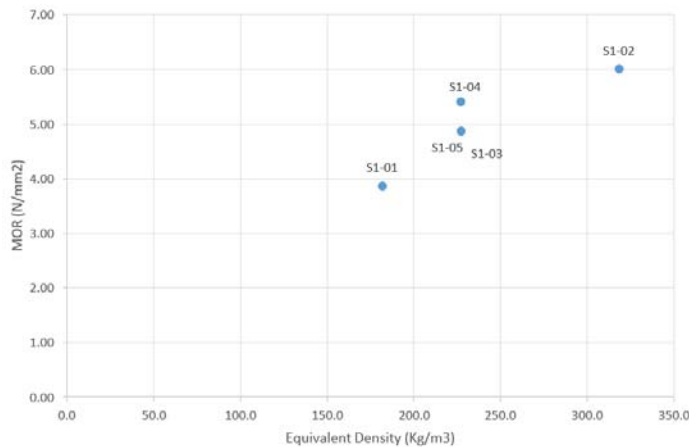


Figure 3: MOR vs Density

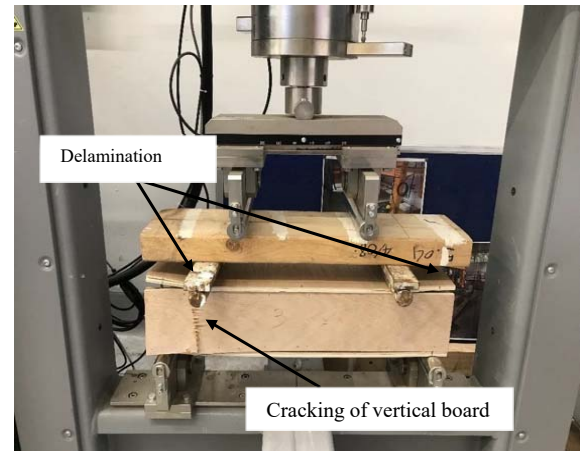


Figure 4: Failure mode of beam

Table 3: Test results and calculations of compressive specimens

Specimen	Number of bamboo cores	Mass (Kg)	Total cross-sectional area of bamboo culms (mm <sup>2</sup> )	Load at failure (kN)
S1-C1	3	0.35	2490	124
S1-C2	4	0.27	1740	92



### 3.2 Structural behaviour of the bamboo sandwich panel

Figure 5 provides the load vs deflection of the 2m sandwich panels that were produced in stage 2. Figures 6 and 7 show the failure of S2-01-P and S2-01-BP, respectively. The trends for both control sample (S2-01-P) and sample with bamboo rings (S2-01-BP) are initially similar. However, S2-01-BP produces a slightly greater maximum load and withstands load for a greater period after the initial linear trend. At about 27mm of mid-span deflection, which corresponds to the vertical board of the beams cracking, the initial failure of both beams was visible. Following the initial failure, S2-01-P failed, however S2-01-BP had better capacity resistance by 0.2kN. The nonlinear behaviour that can be noted in S2-01-BP is assumed to be due to the incorporation of the bamboo rings, which is increasing the flexural stiffness of the panel. This in turn could be related to the hogging that was observed near the supports. When reviewing the Modulus of Elasticity (MOE), S2-01-BP had an MOE of 3.97 GPa. These results seem reasonable as they are similar to trends which were noted in other studies where the MOE ranged from 2.2 GPa to 4.2 GPa depending on the diameter and the type of adhesive used [4]. Although the range is similar, it must be noted that different materials were used for the outer skins of the sandwich panels, which would then have an impact on the mechanical properties of the panels. Overall, it may be seen that S2-01-BP gains more strength from the bamboo core as the weight is increased. Even though the beam's midspan has a consistent bending force during the four-point bending test, S2-01-BP fails under the right-side load point. This might be because the bamboo core's properties vary widely, distributing the load unevenly.

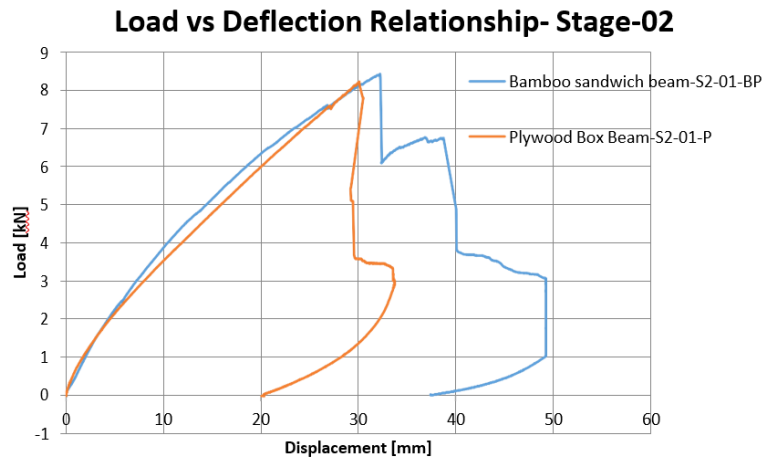


Figure 5: Load-deflection relationship of the beams

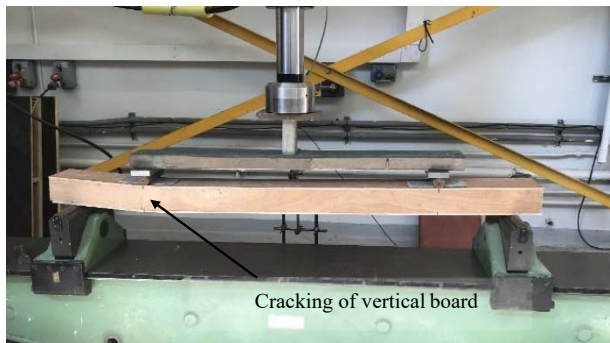


Figure 6: Failure of S2-01-P

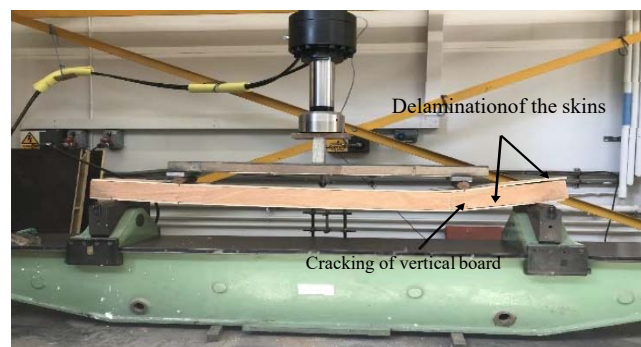


Figure 7: Failure of S2-01-BP



### 3.3 Compressive strength of bamboo culms

Table 4 provides the results of all sample tested in stage 3 of the experimental procedure. The stress at failure was only able to be determined for those samples tested parallel to the grain as those tested perpendicular to the grain were insignificant.

Table 4: Compression test results of bamboo cores

Specimenn Code	Max. Load (kN)	Avg. Dia (mm)	Thickness(mm)	Stress at failure(N/mm <sup>2</sup> )
PD-1	34.4	43.7	4.7	60.2
PD-2	45.1	45.2	4.4	80.5
PPD1	5.7	45.6	6.4	-
PPD2	7.6	39.7	3.9	-
PS-1	65.7	43.8	6.4	87.4
PPS-2	0.0	45.0	5.8	-
PP-1	0.0	47.0	4.7	-
PP-2	0.0	42.3	7.2	-
P-1	71.9	40.3	7.6	91.9
P-2	44.7	43.0	4.0	90.6

The cross-sectional area has a significant impact on bamboo's compressive strength. The test findings show that the impact of a split bamboo ring on the final compressive strength is negligible. Every sample of bamboo examined perpendicular to grain failed with no discernible failure. The two specimens that were removed from the damaged beams were the only exceptions. It can be inferred that the only reason these samples could support some loads was because they included nodes, which served as a strong point to withstand the tensile strains created within the sample. Bamboo ring failure in the direction of the grains can be characterised by longitudinal splitting and bulging, with compressive stresses achieving the expected values. These findings support the longitudinal configuration's failure mechanism that was put to the test in stage 1. Even though the longitudinal direction of the bending stresses was aligned, the beam broke because of the compressive force perpendicular to the grain, which caused the ring to fracture.

When reviewing all results, the flexural strength values were high enough to consider using bamboo sandwich panels for a floor application. The use of bamboo core sandwich panels increases the depth of the structure compared to wood floors, but the increased joist spacing can reduce the overall weight of the floor. Apart from that, services may also accompany within structural zones, mitigating the effects of increasing structural depth. Overall, bamboo core sandwich panels have excellent mechanical properties and have been shown to somewhat minimize practical problems caused by bamboo's natural variability, making it a good candidate for secondary structural applications.

## 4 Conclusion

The following conclusions can be drawn from the conducted study:

1. S1-04 provided the greatest strength to weight ratio due to the increase in contact area which increased the rigidity and strength.
2. Although S1-C2 contained a lower number of rings, the cross-sectional area of rings used allowed for a greater contact area which in turn increased the compressive strength.
3. the incorporation of bamboo rings in 2m sandwich panels increased the maximum load and stiffness.



4. testing of the bamboo rings aligned with results that were expected when testing parallel and perpendicular to the samples.

The aim of the paper was to determine the structural capability of using bamboo cores in timber sandwich panels. From the results obtained in the stages of this study, it can be concluded that bamboo core sandwich panels have the potential to be used in construction due to the mechanical properties and minimised impact of variability that is expected due to it being a natural product.

## Acknowledgment

The authors would like to thank every person/department who helped thorough out the research work, particularly the laboratory staff at London South Bank University. The special thank you also goes to the Jayawardena Perera who conducted this work as part of his MSc dissertation and London South Bank University.

## References

- [1] Y. Li, Q. Shan, M. Mao, and J. Zhang, "Study on the bond performance of bamboo-steel interface after cyclic loading," *Structures*, Vol 37, pp 807-818, 2022.
- [2] S. Kaminski, L. Lawrence, and D. Trujillo, "Structural Use of bamboo-Part 1 Introduction," *The Structural Engineer*, pp. 1-3, 2016.
- [3] S. Kaminski, L. Lawrence, and D. Trujillo, "Structural use of bamboo-Part 03-Durability and preservation," *The Structural Engineer*, pp. 1-6, 2016.
- [4] F. McCann, " Analysis and design of recycled glass bead sandwich panels in bending," *Composite Structures*, vol.265, 113730, 2021
- [5] L. Oliveira, M. Tonatto, G. Coura, T. Freire, T. Panzera, and F. Scarpa, "Experimental and numerical assessment of sustainable bamboo core sandwich panels under low-velocity impact," *Construction and Building Materials*, Vol 292, 123437, 2021
- [6] L. Oliveira, G. Coura, M. Tonatto, T. Panzera, V. Placet, and F. Scarpa, "A novel sandwich panel made of prepreg flax skins and bamboo core," *Composites Part C: Open Access*, Vol 3, 100048, 2020.
- [7] H. Karampour, S. Darzi, B. Gilbert, and H. Bailer, "Flexural behaviour of a novel bamboo-plywood sandwich composite panel," *WCTE2018 Conference*, 2018.
- [8] J. Hartoni, B. Fajrin, Anshari, and A. Catur, " Effect of core and skin thicknesses of bamboo sandwich composite on bending strength," *International Journal of Mechanical Engineering and Technology*, Vol 8, pp.551-560, 2017.
- [9] P. Oliveira, M. May, T. Panzera, and S. Hiermaier, "Bio-based/green sandwich structures: A review," *Thin-Walled Structures*, Vol 177, 109426, 2022.
- [10] W. Nkeuwaa, J. Zhang, K. Semple, M. Chen, Y. Xia, and C. Dai, "Bamboo-based composites: A review on fundamentals and processes of bamboo bonding," *Composites Part B: Engineering*, Vol 235, 109776, 2022.
- [11] D. Trujillo, "Bamboo structures in Colombia," *The Structural Engineer*, Vol 65, pp 25-30, 2007
- [12] L. Oliveira, J. Orth, R. Freire, T. Panzera, A. Christoford and F. Scarpa, " Sustainable Sandwich Panels Made of Aluminium Skins and Bamboo Rings," *Materials Research*, Vol 24, 2021.





# AN EXPERIMENTAL STUDY ON PARTIAL REPLACEMENT OF BITUMEN USING WASTE ENGINE OIL & CRUMB RUBBER

*<sup>a</sup> Muhammad Sarmad Kazmi\* & <sup>b</sup> Imran Hafeez.*

a: Civil Engineering Department, University of Engineering and Technology Taxila, [msarmadkazmi@gmail.com](mailto:msarmadkazmi@gmail.com)  
b: Civil Engineering Department, University of Engineering and Technology Taxila, [imran.hafeez@uettaxila.edu.pk](mailto:imran.hafeez@uettaxila.edu.pk)  
\* Sarmad Kazmi: Email ID: [msarmadkazmi@gmail.com](mailto:msarmadkazmi@gmail.com)

**Abstract-** Bitumen is a strong hydrocarbon that is often used as a binding material in flexible pavement and is produced as a by-product of petroleum refineries. Bitumen is non-toxic at room temperature, although when heated between 165–200 C to cover all the aggregates, it generates a poisonous smoke which is extremely damaging to someone's health also environmental destruction, depletion of petroleum resources, and rising prices were among the consequences. Other binder sources for pavement structure will be investigated by researchers. This experiment will examine the impact of using wasted crumb rubber and engine oil to reduce emissions. The amount of bitumen used was a combination of crumbs rubber and wasted engine oil. Both Modifiers are manufactured from waste products, are easily accessible, and are low-cost. This technique of recycling these waste items reduces clutter and helps to keep the environment clean. AASHTO and ASTM standards were used to examine the rheological and physical properties of modified binders in the laboratory. To determine if the unique mixture might be utilized on an industrial level, the results will be compared to a sample group of neat bitumen. To determine the relationship between factors such as shear modulus and phase angle at different frequencies, master curves were produced. According to the study findings, bitumen could be replaced up to 12.5 percent as a sample of W5CR7.5, resulting in comparable or better performance based on rutting resistance, stability, and flow. This work directly makes a unique contribution to highway and transportation developments in the establishment of alternate materials for pavement structure by providing improved binder composition from waste resources.

**Keywords-** Bitumen, Waste materials, Modified binder, Pavement material.

## 1 Introduction

At the end of its life, the asphaltic pavement has a significant amount of value [1]. Overlays of fresh concrete mixture layers can be used to repair degraded parts in which situation the underneath old asphalt can still provide significant structural strength. In places at which modifications in ending pavement level can impair storms water draining and bridge clearance, all or a section of the affected pavement is shaved away from the sections such that the overlay's elevation conforms to the pavement surface [2]. Pavement grinding is now so common that massive amounts of Recycled Asphalt Pavements (RAP) are produced each year.

RAP would either be landfilled or preserved for use in future construction projects. To conserve natural resources and to save finances, the use of RAP in asphalt binders is becoming more popular as a rehabilitation alternative. RAP substance also has been commonly used as a granular base course content in Portland and asphalt cement concrete construction, while also integrated back into asphalt mixtures for innovative pavement construction [3].



With the advancement of the Superpave efficiency grading scale, a necessity for the formation of Superpave recommendations for using RAP in asphalt pavement has recently arisen [4]. Superpave is a key product of the Strategic Highway Research Program (SHRP), which is a framework of specified requirements, testing procedures, and engineering practices that allow for the adequate selection of material as well as mixture layout of hot mix asphalt to fulfill the atmospheric and traffic patterns of road surface pavement projects. Highway engineers and builders can utilize this methodology to produce pavement that lasts longer, needs less maintenance, and has a shorter life expense than pavement planned to use earlier engineering techniques [5]. Realizing the importance of flexibility of asphalt pavement recycling as well as its potential application in Pakistan, there is an urgent need to design and establish Superpave guidance to use RAP in asphalt pavement recycling and rehabilitative operations under severe climate and loading conditions. These standards must be founded on rigorous testing of materials to assess the predicted performance of various ingredients and their quantities in asphalt binder [6].

This study examines the performance qualities of several mixes for existing grades 60-70 virgin and recovered asphalt binders from two tasks on N-5 (i.e., Mandra & Nowshera). To characterize the binder mixes according to the Superpave function graded system, extensive laboratory testing is performed (PG grades). This study only considers the low and high-temperature characteristics of Rolling Thin Film Oven (RTFO) residues as evaluated by Dynamic Shear Rheometer (DSR) and Bending Beam Rheometer (BBR). Furthermore, the mixing charts and master curves are produced as guidelines for PG grade determination and prospective asphalt pavement recycling and rehabilitation operations in Pakistan.

## 2 Experimental Procedures

Bitumen Pen 60/70 was chosen to determine the physical properties of both the modified asphalt binder and make a comparison to the properties of the pure bitumen binder. Different types of physical tests such as the ductility test (ASTM D113), softening point test (ASTM D36-06), penetration test (IS:1203-1978), and viscosity test was carried out (IS 1206-PART-2). The procedure of Preparation of some experimental samples is shown in **Figure 1**. The purpose of this study was to compare the effects of crumb rubber and waste motor oil on the rheological performance of asphalt binders. The AASHTO T315 Dynamic Shear Dynamometer test was carried out.



Figure 1: Preparation of Sample

The phase angle, viscous and elastic components termed loss modulus and storage modulus were all determined using a dynamic shear rheometer. The rheometer test is carried out to study the effect of bitumen aging at different temperatures on its performance at different frequencies in terms of Phase Angle versus Complex Modulus.



As shown in **Table 1**, test samples of various bitumen ratios were prepared with the replacement of waste engine oil and crumb rubber.

Table 1 Mix Design Ratio of samples

Sample ID	Bitumen Type	Binder %	Waste Engine Oil %	Crumb Rubber%
Virgin (W0CR0)	Pen 60/70	100	0	0
W5CR5	Pen 60/70	90	5	5
W5CR7.5	Pen 60/70	87.5	5	7.5
W5CR10	Pen 60/70	85	5	10
W7.5CR5	Pen 60/70	87.5	7.5	5
W7.5CR7.5	Pen 60/70	85	7.5	7.5
W7.5CR10	Pen 60/70	82.5	7.5	10

### 3 Research Methodology

Before the start of experimental work detail, literature studies were performed. Experimental work involved sample preparation with two different materials including waste engine oil and crumb rubber. The raw material including waste engine oil and crumb rubber was collected from local workshops, Bitumen material of Pen 60/70 was also procured. After that test doses of 0.5%, 7.5%, and 10% of waste engine oil and crumb rubber were given in replacement of neat bitumen as shown in **Table 1**.

#### 3.1 Selection of materials

The most important aspect of developing a customized alternatives binder is material selection. Materials were chosen based on their availability and cost-effectiveness. The following materials were used to make samples.

- i. Bitumen 60/70 (Penetration grade)
- ii. Waste Engine oil.
- iii. Crumb Rubber.

#### 3.2 Laboratory evaluation

Laboratory tests were separated into two categories to assess the qualities of modified binder samples and compared them to the behavior and properties of neat sample bitumen 60/70.

- i. Physical test

The viscosity test, penetration, and softness point elasticity were used to determine physical attributes. Physical testing results supported the research by determining allowable combining ratios of crumb rubber and waste engine oil. Results of the physical test are shown in **Figures 2,3,4 and 5**.

- ii. Rheological test

In this study, a dynamic shear rheometer test was used to analyze the rheological properties of the sample to identify rutting requirements and fatigue. The viscoelastic properties of bitumen were determined using a Dynamic Shear Rheometer (DSR). DSR can measure the sample's phase angle ( $\delta$ ) and complex shear modulus ( $G^*$ ).



## 4 Results

### 4.1 Physical test

Physical test revealed that by replacing the Waste Oil and Crumb Rubber Content in greater content samples softening points were found decreasing and Penetration depth found in an increasing trend as shown in **Figure 4** and **Figure 2** respectively. Also, by increasing cooking oil waste the sample becomes less viscous and increasing the content of crumb rubber results in more viscous as shown in **Figure 3** but overall, these additives enhance the working abilities of the binder. **Figure 5** shows that the sample's ductility may vary with a change in the composition of both additives as by increasing the percentage of crumb rubber due to its elastic nature, the sample shows more ductile behavior but by increasing the percentage of waste engine oil the sample's elastic limit may decrease up to certain limit.

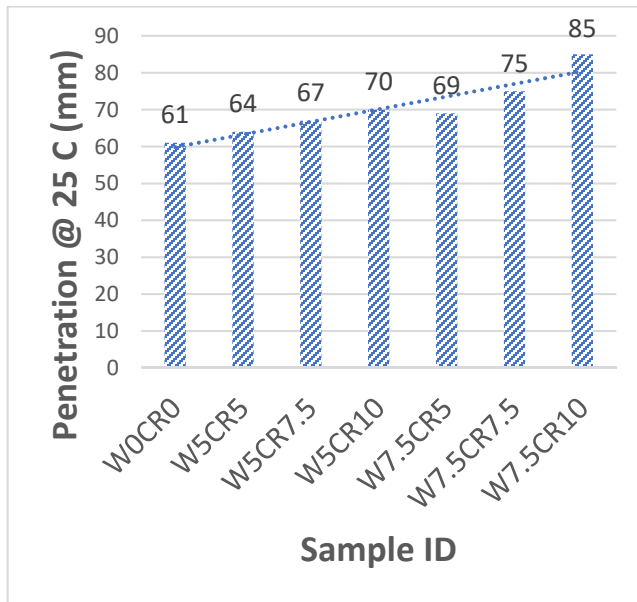


Figure 2: Penetration Test results

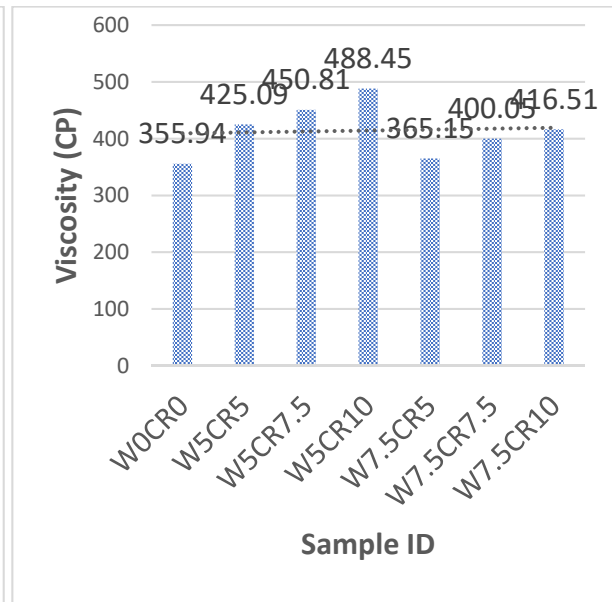


Figure 3: Viscosity Test results

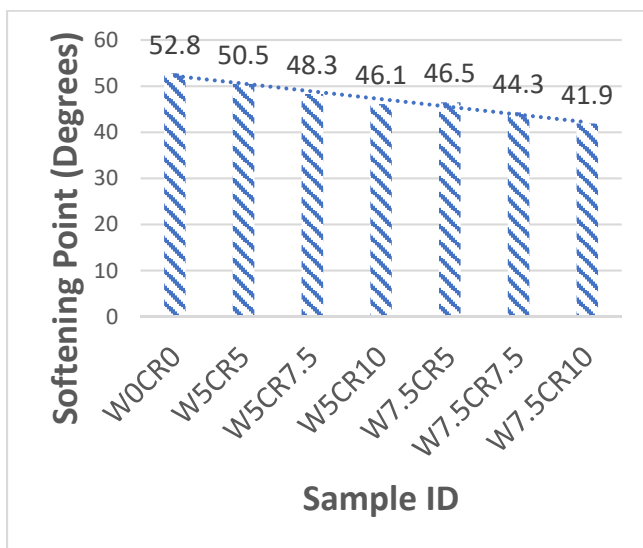


Figure 4: Softening Point Test results

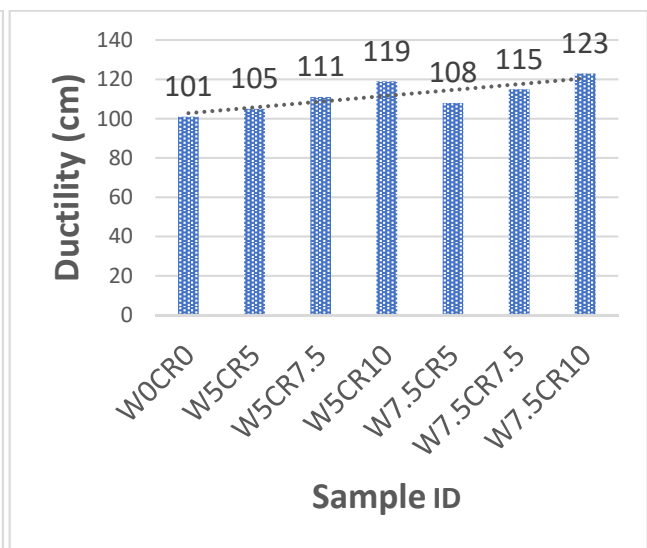


Figure 5: Ductility Test results



#### 4.2 Rheological test

Results shown in **Figure 6** indicated that under a specific loading frequency, the complex modulus decreases with an increase in temperature. In contrast, at a given temperature, it increases with an increase in frequency. This demonstrates that the viscoelastic properties of the elastic component decrease over the temperature range from 22°C to 74°C. The phase angle values of the binders were primarily in the 39° to 87° range.

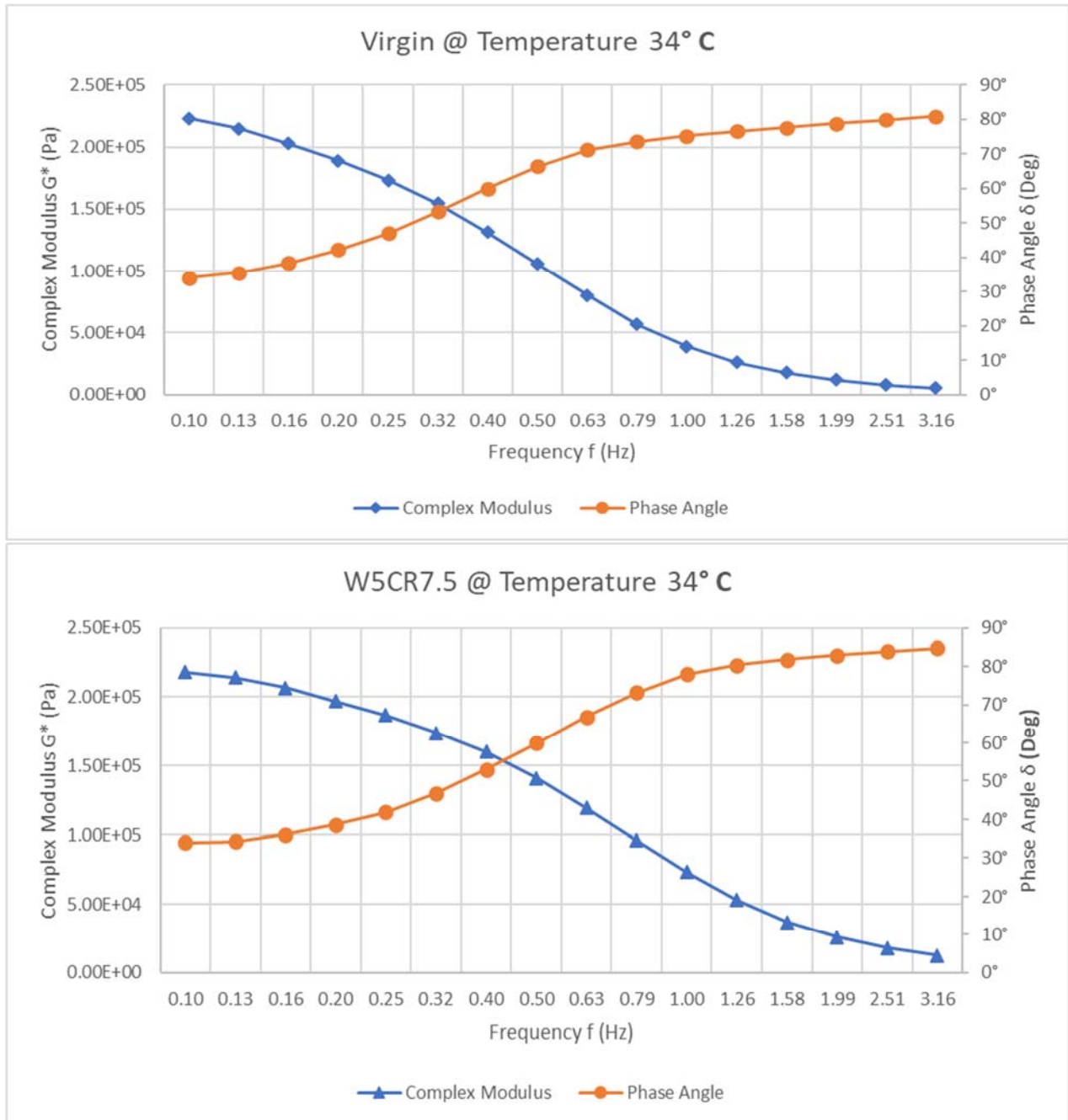


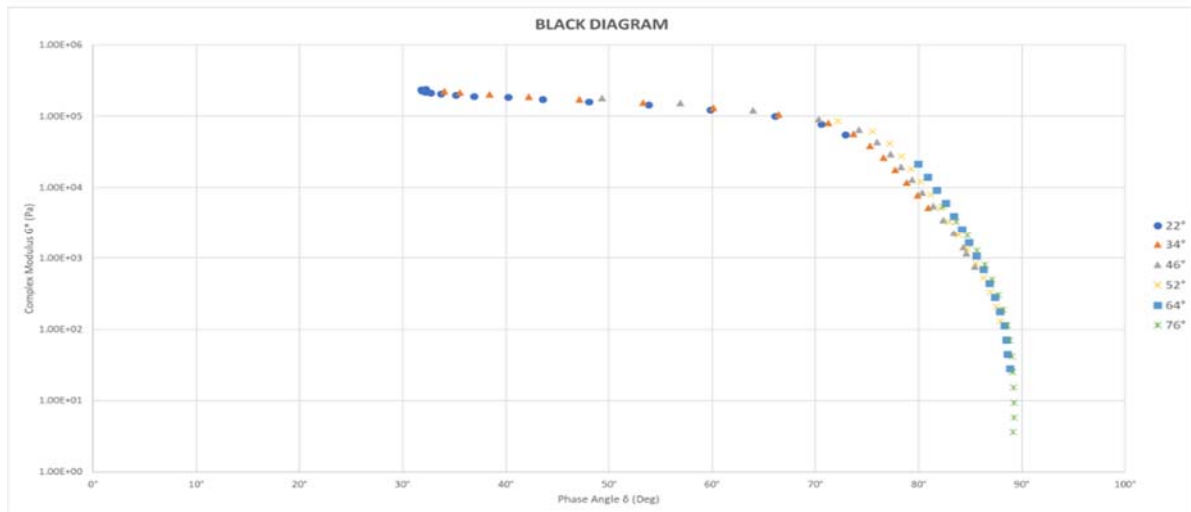
Figure 6a & 6b: comparison of virgin sample @ 34° and W5CR7.5 @ 34°C

These values of phase angles for both asphalt binders and mixtures confirm the results of previous research and are in accordance with their limits.



The black diagram in Figure 7 of the Virgin sample vs W5CR7.5 indicates linear trends in results. We can see from this comparison shown in Figure 7 that by adding W5CR7.5 with bitumen, the value of complex modulus rises from a high value that indicates the improved performance of the binder sample.

### Black Diagram of Virgin Sample



### W5CR7.5 Black Diagram

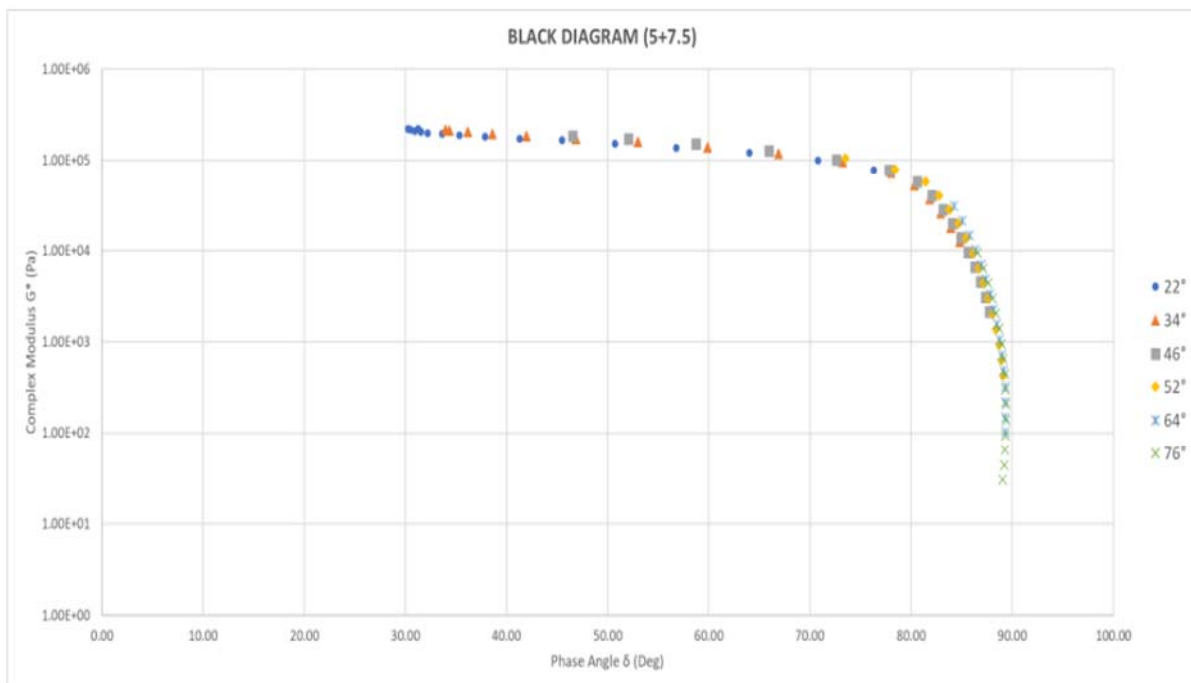


Figure 7a & 7b: comparison of black diagram of virgin sample and W5CR7.5 @ temperature ranges from 22°-76°

Master curves were created for the examination of the relationship between complex modulus and phase angle at different frequency levels using neat bitumen with engine oil and crumb rubber under various time and temperature circumstances



as shown in **Figure 8**. Results indicated that temperature and loading frequency had a significant impact on asphalt's physical behavior.

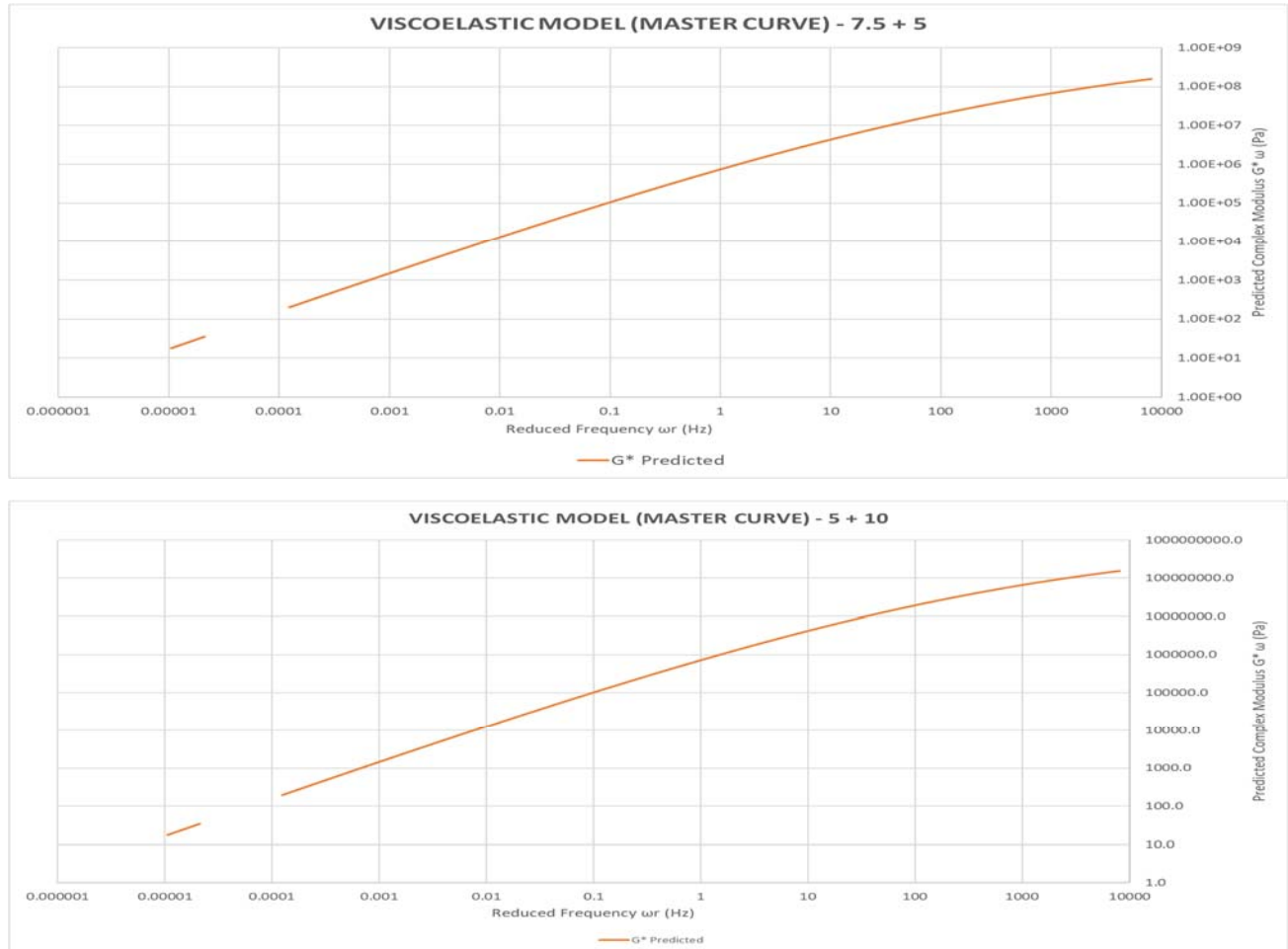


Figure 8a & 8b: comparison of Master Curve of virgin sample and W5CR7.5 to find Predicted Complex Modulus  $G^*$

## 5 Conclusion

The research has led to the following conclusions:

1. From a detailed study of the physical properties of the modified sample of engine oil and crumb rubber with neat bitumen, it is revealed that by increasing cooking oil waste the sample becomes less viscous and increasing the content of crumb rubber results in more viscose but overall, they enhance the abilities of the sample if added up to some limit.
2. It is also concluded that by replacing the Waste oil and Crumb Rubber Content in greater content samples Softening points were found decreasing and Penetration depth was found in increasing trend.
3. From the rheological properties study, it is also observed that the Complex Modulus which is resistant to deformation for a mix of Waste Engine oil and crumb rubber has shown greater value up to  $34^\circ$  resulting in better performance as compared to the virgin sample.
4. It is concluded from the black diagrams that by increasing additive as in the case of W5CR7.5 up to certain limits black diagram has shown a linear trend indicating consistent behavior of binder which results in a good performance.



Finally, it is concluded that the replacement of engine oil and recycled crumb rubber with bitumen is a very useful technique to meet the industry requirement and utilizing this waste material will help a more significant cause to protect the environment.

## Acknowledgment

This research work owes its existence to help, support, and inspiration to several people. Firstly, I would like to express my sincere appreciation and gratitude to Dr. Imran Hafeez (Professor Civil Engineering Department U.E.T. Taxila) for his guidance and cordially supervision during this research work. His support and inspiring suggestions have been precious for the development of this content. This study would not have been possible without the guidance and help of several individuals who are gratefully acknowledged.

## References

- [1] W. Rafiq et al., "Life Cycle Cost Analysis Comparison of Hot Mix Asphalt and Reclaimed Asphalt Pavement: A Case Study," *Sustainability*, vol. 13, no. 8, p. 4411, Apr. 2021.
- [2] Hend Ali Omar, Nur Izzi Md. Yusoff, Muhammad Mubarak, Halil Ceylan, Effects of moisture damage on asphalt mixtures, *Journal of Traffic and Transportation Engineering (English Edition)*, Volume 7, Issue 5, 2020.
- [3] Thakur, J.K., Han, J. Recent Development of Recycled Asphalt Pavement (RAP) Bases Treated for Roadway Applications. *Transp. Infrastruct. Geotech.* 2, 68–86 (2015).
- [4] Ahmad, Juraidah & Md Yusoff, Nur Izzi & Hainin, Mohd Rosli & Rahman, M.Y. & Hossain, M. Evaluation on performance characteristics of superpave asphalt mix design under tropical climatic conditions. *International Journal of Pavement Research and Technology.* 7. 331-342. 10.6135/ijprt.org.tw/2014.7(5).331 (2014).
- [5] Jitsangiam, Peerapong & Chindapasirt, Prinya & Nikraz, Hamid. An evaluation of the suitability of SUPERPAVE and Marshall asphalt mix designs as they relate to Thailand's climatic conditions. *Construction and Building Materials.* 40. 961-970. 10.1016/j.conbuildmat.2012.11.011. (2013).
- [6] Hasnain, Syed. Use of Reclaimed Asphalt Pavement (RAP) in Cement Concrete under Different Environmental Conditions for Rigid Pavement Application. *International Journal for Research in Applied Science and Engineering Technology.* 8. 404-406. 10.22214/ijraset.2020.32429, (2020).
- [7] M. Shakirullah, I. Ahmad, M. Saeed et al., "Environmentally friendly recovery and characterization of oil from used engine lubricants," *Journal of the Chinese Chemical Society*, vol. 53, no. 2, pp. 335–342, 2006.
- [8] Colbert B. and Zhanping, "The properties of asphalt binder blended with variable quantities of recycled Asphalt using short term and long term aging simulations" *Journal of Construction and Building Materials*, volume 26, pp. 552–557, 2012.
- [9] J. L. A. Filho, L. G. M. Moura, and A. C. S. Ramos, "Liquid-liquid extraction and adsorption on solid surfaces applied to used lubricant oils recovery," *Brazilian Journal of Chemical Engineering*, vol. 27, no. 4, pp. 687–697, 2010.
- [10] Md Maniruzzaman A. Aziz, Md Tareq Rahman, Mohd. Rosli Hainin, Wan Azelee Wan Abu Bakar. An overview on alternative binders for flexible pavement; 2014.





# MICROSTRUCTURAL STUDY OF COCONUT SHELL CONCRETE

<sup>a</sup> Ahmad Rusydie Ramli, <sup>b</sup> Noor Aina Mison\*, <sup>c</sup> Faridah Hanim Khairuddin, <sup>d</sup> Muhammad Syaquir  
Sha'rani

a: Faculty of Engineering, National Defence University of Malaysia, Kuala Lumpur, [ahmadod98@gmail.com](mailto:ahmadod98@gmail.com)

b: Faculty of Engineering, National Defence University of Malaysia, Kuala Lumpur, [nooraina@upnm.edu.my](mailto:nooraina@upnm.edu.my)

c: Faculty of Engineering, National Defence University of Malaysia, Kuala Lumpur, [hanim@upnm.edu.my](mailto:hanim@upnm.edu.my)

d: Faculty of Engineering, National Defence University of Malaysia, Kuala Lumpur, [nyaqirshaq@gmail.com](mailto:nyaqirshaq@gmail.com)

\* Corresponding author: Email ID: [nooraina@upnm.edu.my](mailto:nooraina@upnm.edu.my)

**Abstract-** Rapid growth of the construction industry results in high demand for the aggregate. However, the aggressive consumption of aggregate significantly affects the environment when mining and quarry activities need to be carried out to supply the aggregate. This study was conducted to use agricultural waste, i.e., crushed coconut shells as an alternative to coarse aggregate in the concrete mix known as coconut shell concrete (CSC). A series of experiments were carried out to determine the compressive strength of CSC and to study the micro-morphologies of the CSC at 1, 7 and 28 days. The strength development of the CSC was observed and validated with the compressive strength of the samples at different ages. The use of crushed coconut shells as aggregates replacement does not change the micro-morphologies of normal concrete mix.

**Keywords-** Agricultural wastes, Coconut Shell Concrete, Lightweight Aggregate Concrete, Sustainability.

## 1 Introduction

Concrete is widely used in building construction due to its properties and strength. The main constituents of the concrete are cement, sand, and aggregate which are mixed with water. Concrete production requires a significant number of natural resources such as rocks and sand since approximately three-quarters of the concrete volume is occupied by aggregate. The aggregates have a significant effect on the structural performance and durability of the concrete [1]. The high demand for concrete due to the rapid growth of the construction industry and aggressive consumption of non-renewable sources caused a shortage of the aggregate [2]. Recent studies have been carried out to develop alternative materials to substitute the use of aggregate in the concrete mixture including the utilization of agricultural wastes such as palm kernel shells (PKS) and coconut shells (CS) [3]–[9].

The CS has great abrasion, high strength and toughness [10]. It is also can be classified as lightweight aggregate [11]. The physical characteristics of CS with smooth surface, angular shape and varies in size offer a good bond and workability for the concrete mix [12]. Table 1 shows physical properties of coconut shell and coarse aggregate [13]. Previous studies reported that the use of crushed coconut shells as aggregate replacement in conventional concrete reduced the density in the range of 1750 kg/m<sup>3</sup> to 1900 kg/m<sup>3</sup> [5], [14]. Comprehensive studies reported the potential of CSC as the alternative to aggregate substitution in the concrete mix with reliable mechanical properties and performance of the CSC as structural and non-structural application [5], [10], [15], [16]. Incorporation of pozzolana and fibres in the CSC also showed improvement in the ultimate moment capacity and flexural toughness up to 14% and 45% respectively [17]. However less reported on the micro-morphologies of the CSC.

Strength development and micro-morphology of concrete is studied by observing the interior microstructure characteristics of the concrete. It provides understanding on the interaction between the CSC constituents since the microstructure of concrete changes with time due to ongoing hydration and environmental factors. Various methods are used to investigate the microstructure such as Scanning Electron Microscope (SEM) and X-Ray Diffraction (XRD). The SEM is used to reveal vast cross-sectional regions while XRD is common to determine the quantity of components of the samples in different



phases [18]. This study was carried out to examine the micro-morphologies of CSC at different ages of curing days. A comparison was made with the interior characteristics of normal concrete.

Table 1 Physical properties of coconut shell and coarse aggregate [13]

Properties	Coarse aggregate	Crushed coconut shell
Fineness modulus	4.2	6.5
Specific gravity	2.7	1.3
Loose bulk density (kg/m <sup>3</sup> )	1480	510
Dense bulk density (kg/m <sup>3</sup> )	1610	600
Water absorption (%)	1	6
Aggregate crushing value (%)	16.6	2.5
Aggregate impact value (%)	11.0	4.2

## 2 Experimental Procedures

### 2.1 Sample preparation

A total of 18 samples were prepared which consist of control samples (NC) and coconut shell concrete (CSC) with a design mix ratio of 1: 1.6: 0.7 (cement: sand: aggregate/CS). The cement contents and water-cement ratio were 480 kg/m<sup>3</sup> and 0.42 respectively. The design mix for 1 m<sup>3</sup> samples is shown in Table 2.

Table 2 Concrete mix design for 1 m<sup>3</sup> sample

Sample	Cement	Sand	Water	Coarse aggregate	Crushed coconut shell
NC	480	770	200	340	-
CSC	480	770	200	-	340

\* All units in kg

The concrete mix batches were mixed using a concrete mixer approximately for 3 minutes to ensure the constituents were mixed well. The CS was purchased from the wider of east coast of Malaysia and available in a crush form. The range size of CS (see Figure 1a) and coarse aggregate approximately 10 mm – 13 mm. Prior to the CSC mixing, the crushed coconut shells were immersed in the water for 24 hours to confirm that the condition of the crushed coconut shells was in a saturated surface dry (SSD) state. In the SSD state, all the pores in the CS are full and the water absorption during concrete mixing can be controlled. All the 18 samples were cast in cube moulds with dimensions of 150 mm x 150 mm x 150 mm and demoulded after 24 hours. The samples were covered with plastic sheet for curing purposes (Figure 1b). The plastic cover was used to keep the moisture of the samples for the cement hydration process.

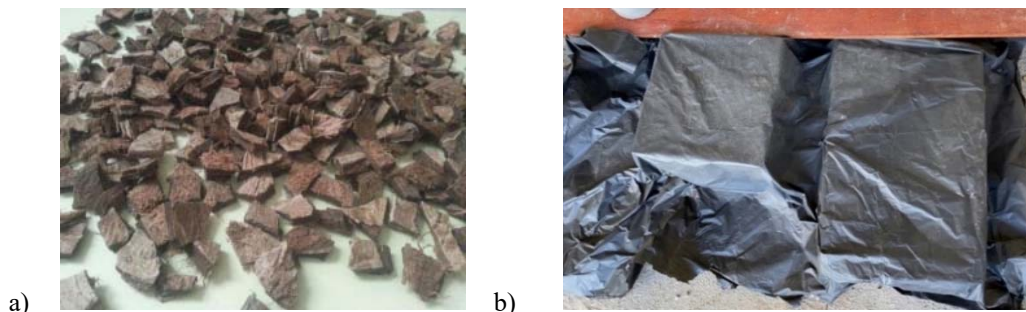


Figure 1: (a) Crushed coconut shell (b) curing with plastic cover



## 2.2 Compression test setup

A compression test was conducted to determine the compressive strength of samples in accordance with [19]. The compressive strength of the cube samples was measured at ages 1, 7 and 28 days of the samples using the Universal Testing Machine (UTM) as shown in Figure 2a. Figure 2b shows the compression test setup of the cube samples. The compressive strength of the samples was calculated using equation (1) [19].

$$f_c = \frac{F}{A_c} \quad (1)$$

where  $f_c$  is the compressive strength (N/mm<sup>2</sup>),  $F$  is the maximum load at failure (N) and  $A_c$  is the cross-sectional area of the specimen on which the compressive force acts (mm<sup>2</sup>).

## 2.3 Scanning electron microscope (SEM) and energy-dispersive X-ray spectroscopy (EDS) analysis

In this study, the surface morphology observations of samples were performed using a ZEISS Gemini SEM 500 (Figure 3) and EDS was used to determine composition of the samples which was measured in terms of weight percentage (wt. %). Prior to the SEM and EDS analysis, the samples from post compression test at age 1-, 7- and 28 days were taken at the middle of the broken samples.

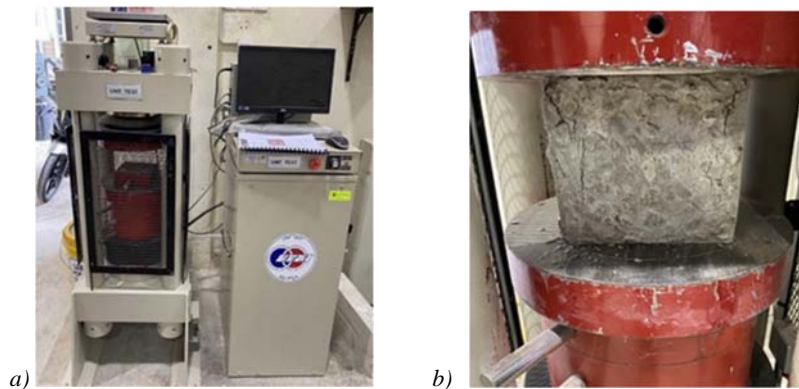


Figure 2: (a) Universal testing machine (b) compression test setup



Figure 3: Gemini SEM 500 instrument

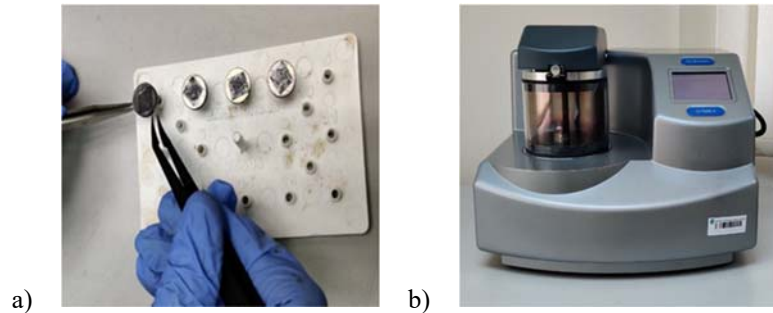


Figure 4: (a) Sample powder on aluminium stub (b) Sample coating with platinum

### 3 Results and Discussion

#### 3.1 Compressive strength, $f_c$

Crushed coconut replacement with aggregate slightly reduced the compressive strength approximately 3.7% when compared to the NC. The compressive strength both type of the concrete samples increased with the increment of the curing age (see Figure 5). With the presence of water, the cement hydration process began when the silicates and luminates in cement produce hard mass called hardened cement paste [1]. Strength development of both concrete samples showed significant increment at the early age with the strength rate up to 180% when measured from day-1 to day-7 of the samples. However, at the later age, the increment rate showed slight reduction when the strength increment of the samples was only about 30% at the age of 28 days. At this phase the cement hydration process was almost complete, and the hard mass also occupied the concrete volume. The aggregate replacement with crushed coconut shell did not change the cement hydration process of the samples since the CSC also showed similar pattern with NC on the strength development from day-1 to day-28. Similar finding also reported by [10], [20]. Concrete samples with coconut shell coarse aggregate showed compressive strength up to  $19.84 \text{ N/mm}^2$ , which satisfies the use of the CSC mix for structural lightweight concrete [21].

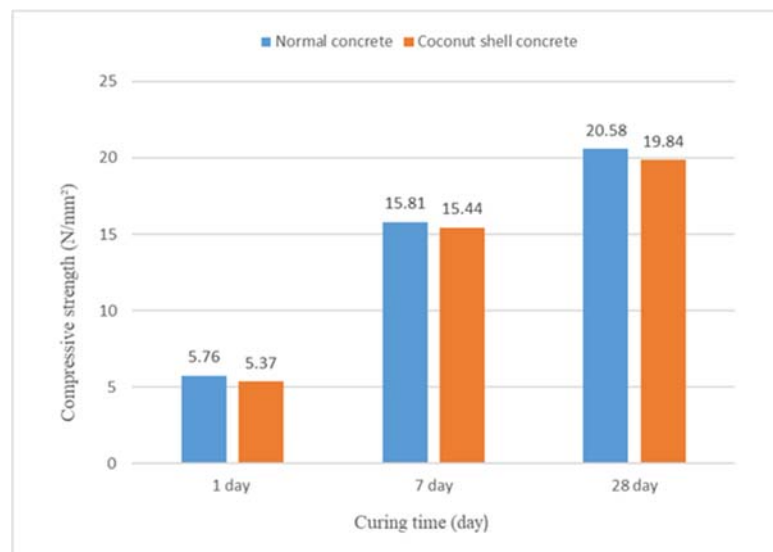


Figure 5: Compressive strength of the samples for 1-, 7-, and 28 days of curing

#### 3.2 SEM observations

The micro-morphologies of the normal concrete and CSC for 1, 7 and 28 days are shown in Figure 6, Figure 7 and Figure 8, respectively. At early age of the samples, multiple ettringite fiber bundles were observed as the most hydration products occupied the samples. This agreed with the final product of cement hydration process where the first product to form in the process is ettringite [1]. The ettringite distribution was varied for both types of concrete samples. From the observation,

the CSC sample showed high amount of ettringite at the age day -1 when compared to normal concrete (see Figure 6). The amount of ettringite started to decrease when the important product for the concrete strength (C-S-H) began to dominate the concrete volume at day-7 (see Figure 7) and significantly increased at the age 28 days (see Figure 8) for both normal concrete and CSC samples.

At this age, the matrix became more denser [22], and the C-H was incorporated in the concrete samples and the strength of the samples already achieved up to 99% of the targeted strength [23]. The normal concrete sample showed C-S-H products filled the concrete volume with less pores were observed while CSC sample showed porous characteristics where larger and darker area was spotted (Figure 8 (b)). The SEM observations agreed with the finding of compressive strength where the CSC samples showed lower strength when compared to the NC samples as explained in section 3.1.

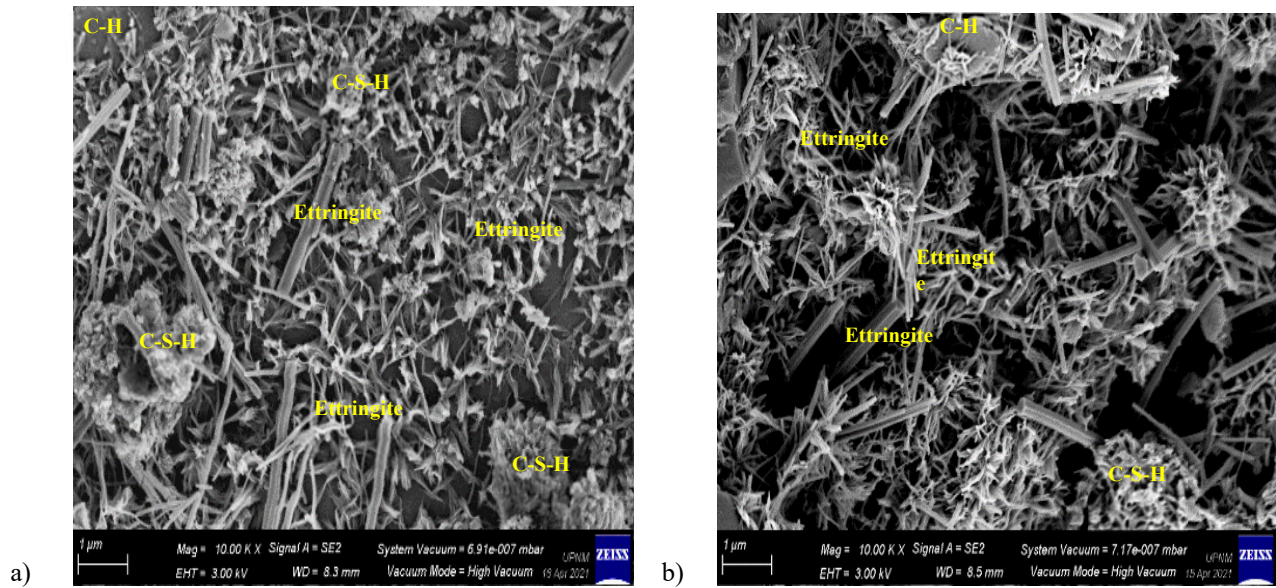


Figure 6: SEM images of (a) normal concrete (b) coconut shell concrete at age 1 day

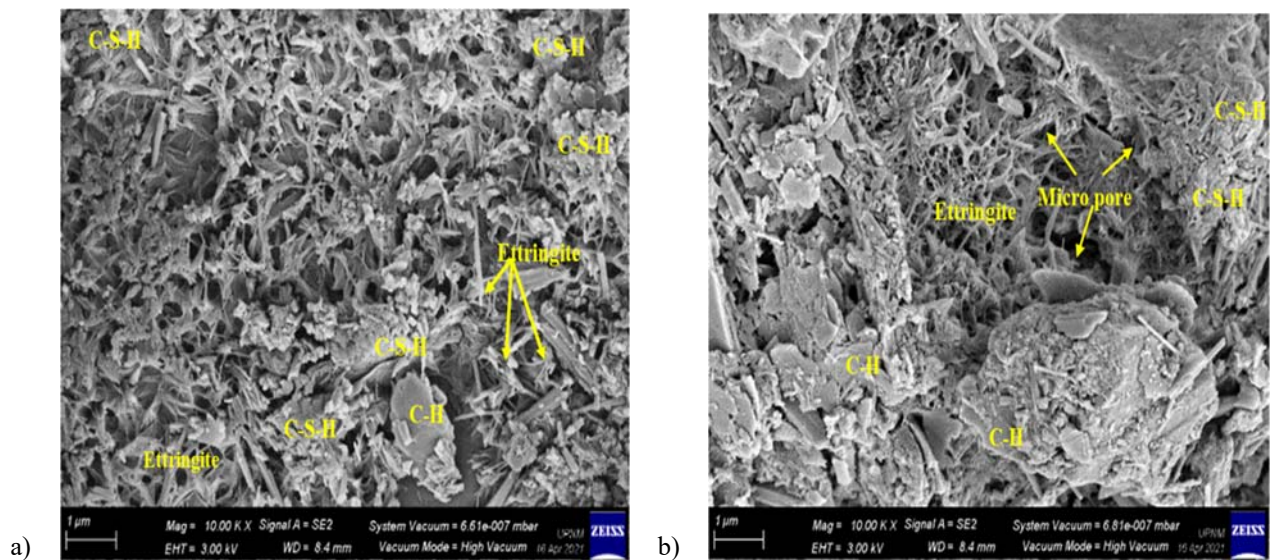


Figure 7: SEM images of (a) normal concrete (b) coconut shell concrete at age 7 days

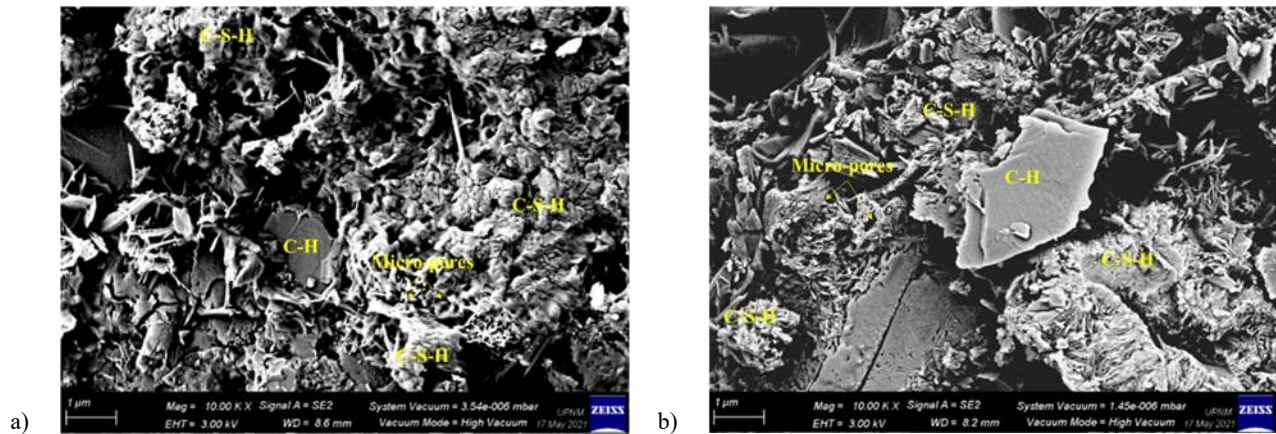


Figure 8: SEM images of (a) normal concrete (b) coconut shell concrete at age 28 days

## 4 Conclusion

The utilization of crushed coconut shells as aggregate replacement in concrete production promotes sustainability development goals. The development of CSC as lightweight concrete is encouraging yet the strength development of the CSC is less reported. This study was carried out to investigate the micro-morphologies of the CSC using SEM method. It can be concluded that:

- The rate of strength increment between CSC and NC are similar where the early-age strength rates (180%) were higher than the later age strength rate (30%) of the concrete samples. The compressive strength of the CSC is slightly lower than NC approximately -3.6%.
- The crushed coconut shell replacement in the concrete mix does not change the micro-morphologies of the concrete with C-S-H products occupied the volume of the matrix. However, the CSC samples showed porous characteristics when compared with the NC.

## Acknowledgement

This project was funded by Universiti Pertahanan Nasional Malaysia (UPNM) under grant number PS0018-UPNM/2021/GPPP/TK/10. The team members gratefully acknowledge the assistance of technical staff of heavy structural and material laboratory in UPNM. The careful review and constructive suggestions by the anonymous reviewers are gratefully acknowledged.

## References

- [1] A. Neville, *Properties of concrete*. Pearson Education Limited, 1995.
- [2] S. Ismail, K. W. Hoe, and M. Ramli, "Sustainable Aggregates: The Potential and Challenge for Natural Resources Conservation," *Procedia - Soc. Behav. Sci.*, vol. 101, no. November, pp. 100–109, 2013, doi: 10.1016/j.sbspro.2013.07.183.
- [3] K. H. Mo, U. J. Alengaram, and M. Z. Jumaat, "A review on the use of agriculture waste material as lightweight aggregate for reinforced concrete structural members," *Adv. Mater. Sci. Eng.*, vol. 2014, no. December, 2014, doi: 10.1155/2014/365197.
- [4] W. Aziz *et al.*, "Mechanical properties, drying shrinkage and structural performance of coconut shell lightweight concrete," *Structures*, vol. 35, pp. 26–35, Jan. 2022, doi: 10.1016/J.ISTRUC.2021.10.092.
- [5] S. Anandh and K. Gunasekaran, "Mechanical characterisation of coconut shell concrete with quarry dust and saw dust as fine aggregate using coconut fibre," *Int. J. Eng. Technol.*, vol. 7, no. 3.34 Special Issue 34, pp. 867–871, 2018.
- [6] S. A. Tukiman and S. Mohd, "Investigate the Combination of Coconut Shell and Grained Palm Kernel to Replace Aggregate in Concrete: A Technical Review," in *National Conference on Postgraduate Research (NCON-PGR) 2009*, 2009, no. October, pp. 49–58.
- [7] K. H. Mo, S. P. Yap, U. J. Alengaram, M. Z. Jumaat, and C. H. Bu, "Impact resistance of hybrid fibre-reinforced oil palm shell concrete," *Constr. Build. Mater.*, vol. 50, pp. 499–507, Jan. 2014, doi: 10.1016/j.conbuildmat.2013.10.016.
- [8] S. Janani, P. Kulanthaivel, G. Sowndarya, H. Srivishnu, and P. G. Shanjayvel, "Study of coconut shell as coarse aggregate in light weight concrete- a review," *Mater. Today Proc.*, May 2022, doi: 10.1016/J.MATPR.2022.05.329.
- [9] S. Zubaidah *et al.*, "Palm Kernel Shell as Partial Coarse Aggregate Replacement in Asphalt Mixture : Optimum Binder Content and Volumetric Properties Investigation," vol. 1047, pp. 179–185, 2021.



- [10] K. Gunasekaran, R. Annadurai, and P. S. Kumar, "Long term study on compressive and bond strength of coconut shell aggregate concrete," *Constr. Build. Mater.*, vol. 28, no. 1, pp. 208–215, Mar. 2012, doi: 10.1016/j.conbuildmat.2011.08.072.
- [11] ASTM C330, "Standard Specification for Lightweight Aggregates for Structural Concrete," 2009. doi: 10.1520/C0330.
- [12] A. S. Leman, S. Shahidan, M. Y. Yusuf, S. S. Mohd Zuki, and N. A. Misnon, "Workability and Compressive Strength for Concrete With Coconut Shell Aggregate 3 Behaviour Of Concrete With Coconut," *MATEC Web Conf.*, vol. 87, no. 01017, pp. 1–6, 2017, doi: 10.1051/mateconf/20178701017.
- [13] K. Rajasekhar and K. Spandana, "Strength Properties of Partial Replacement of Coconut Shells As," vol. 1, no. 04, pp. 172–177, 2016.
- [14] N. A. Misnon, S. Shahidan, F. H. Khairuddin, N. L. Rahim, S. K. Che Osmi, and H. Husen, "Effect of Coconut Fibre on Coconut Shell Concrete," in *Advances in Civil Engineering Materials*, M. M. F. Meor Razali, M. Awang, and S. S. Emamian, Eds. Springer, 2021, pp. 239–247.
- [15] S. U. Azunna, "Mechanical properties of concrete with coconut shell as partial replacement of aggregates," *IOP Conf. Ser. Mater. Sci. Eng.*, vol. 431, no. 3, pp. 0–7, 2018, doi: 10.1088/1757-899X/431/3/032001.
- [16] K. Gunasekaran, R. Annadurai, and P. S. Kumar, "Plastic shrinkage and deflection characteristics of coconut shell concrete slab," *Constr. Build. Mater.*, vol. 43, pp. 203–207, Jun. 2013, doi: 10.1016/j.conbuildmat.2013.02.019.
- [17] R. Prakash *et al.*, "Effect of Steel Fiber on the Strength and Flexural Characteristics of Coconut Shell Concrete Partially Blended with Fly Ash," *Materials (Basel)*, vol. 15, no. 12, p. 4272, 2022, doi: 10.3390/ma15124272.
- [18] R. Theenathayalan, S. N. Thirisha, and R. Suganya, "Impact of different concrete ingredients on the microstructure of lightweight concrete – A comprehensive review," *Mater. Today Proc.*, no. xxxx, 2022, doi: 10.1016/j.matpr.2022.04.886.
- [19] BS EN 12390-3, "Testing hardened concrete Part 3: Compressive strength of test specimens," 2009.
- [20] K. V. Rao, A. H. L. Swaroop, P. K. R. Rao, and N. Bharath, "Engineering Study on Strength Properties of Coconut," *Int. J. Civ. Eng. Technol.*, vol. 6, no. 3, pp. 42–61, 2015.
- [21] J. P. Ries *et al.*, "Guide for Structural Lightweight-Aggregate Concrete Reported by ACI Committee 213," pp. 1–38, 2010.
- [22] M. Rao, J. Wei, Z. Gao, W. Zhou, Q. Li, and S. Liu, "Study on Strength and Microstructure of Cement-Based Materials Containing Combination Mineral Admixtures," *Adv. Mater. Sci. Eng.*, vol. 2016, 2016, doi: 10.1155/2016/7243670.
- [23] G. Fahim Huseien, Z. Hussein Joudah, R. Pervez Memon, and A. Rahman Mohd Sam, "Compressive strength and microstructure properties of modified concrete incorporated effective microorganism and fly ash," *Mater. Today Proc.*, vol. 2020, no. xxxx, 2021, doi: 10.1016/j.matpr.2021.03.054.



# FRESH AND MECHANICAL PROPERTIES OF HIGH STRENGTH SELF-COMPACTING CONCRETE MODIFIED WITH FLY ASH AND SILICA FUME

<sup>a</sup> Iftikhar Younis, <sup>b</sup> Mehwish Asad, <sup>c</sup> Ayub Elahi

a: Department of Civil Engineering, University of Engineering and Technology Taxila. [chiftikhar.younis@gmail.com](mailto:chiftikhar.younis@gmail.com)  
b: Department of Civil Engineering, University of Engineering and Technology Taxila. [mehwish.asad@uettaxila.edu.pk](mailto:mehwish.asad@uettaxila.edu.pk)  
c: Department of Civil Engineering, University of Engineering and Technology Taxila. [ayub.elahi@uettaxila.edu.pk](mailto:ayub.elahi@uettaxila.edu.pk)

**Abstract-** The effects of Fly Ash (FA) and Silica Fume (SF) on the fresh and mechanical properties of high-strength self-compacting concrete (HSSCC) are examined in this research. Slump, J-ring, and L-box tests are used to study fresh properties, while compressive strength, split tensile test, and flexural test are used to investigate mechanical properties. This research is based on the previously published research and selected the optimum percentages of supplementary cementing material (SCMs) for FA and SF. The concrete mixture consists of total of seven mixes: control mix (CC), M1 (5%SF and 0%FA), M2 (5%SF and 10%FA), M3 (5%SF and 20%FA), M4 (5%SF and 30%FA), M5 (5%SF and 40%FA) and M6 (5%SF and 50%FA). The study indicates that adding up to 5% SF and 20% FA to HSSCC mixes improves the fresh qualities of the mixtures. On all ages, the mechanical parameters of HSSCC, such as compressive strength, flexural strength, and split tensile strength, are shown to be higher than the control. In comparison to control mixtures at the appropriate ages, the addition of SF and FA at the optimum dose (5% SF and 20% FA) results in a rise in compressive strength, flexural strength, and split tensile strength. It is concluded that 5% SF and up to 20% FA mixes show improvement in the fresh properties as well as mechanical properties of HSSCC while further increment of FA decreases the fresh and mechanical properties of HSSCC.

**Keywords-** Workability, Supplementary Cementing Material, Compressive Strength, Flexural Strength, Split Tensile

## 1 Introduction

The amount of CO<sub>2</sub> produced into the atmosphere by the cement production industry can be reduced by including SCMs and efficiently using cement clinker [1]. Silica Fume (SF), Ground Granulated Blast Furnace (GGBF), Bentonite (BE), Fly Ash (FA), and other SCMs with pozzolanic properties can partially substitute cement to lessen the cement's harmful effects on the environment while still meeting industrial demands [2]- [6]. Many studies have employed SCMs to produce more sustainable, effective, and durable concrete because most SCMs tend to increase concrete's durability by thinned the interfacial transition zone (ITZ) [7]. The use of natural pozzolans in concrete has gotten special attention due to their unique properties which include low heat of hydration, low permeability, higher content of SiO<sub>2</sub>, and enhancement in the ultimate strength of concrete [8].

Supplementary cementing material (SCMs) is one of the solutions to minimize the consumption of natural raw material for cement, energy consumption reduces the negative impacts on the environment. Different researchers use SCMs to investigate fresh properties and harden properties to study the fresh and mechanical performance of concrete [9]. The pozzolanic material can also be added during the manufacturing process of cement at different proportions. L.T.B Uzal studies the manufacturing of laboratory-based blend Portland cement with the addition of natural volcanic pozzolanic





material. An experimental study is limited to material from two volcanic sources by 55% replacement at the different grinding times. The blend cement improves compressive strength and reduces the ability of alkali-silica expansion [11].

Fly ash is a byproduct which is obtained in the form of fine powder when pulverized coal is burned in power plants. FA is a pozzolanic material, which is a mixture of aluminous and silicious materials that forms cement when mixes with water. When fly ash is mixed with lime and water, it forms a material that resembles Portland cement. Fly ash is therefore suited for usage as a primary component in several construction materials, such as mixed cement, hollow blocks, and mosaic tiles. When added to the concrete mix, fly ash increases the strength and improves segregation of the concrete and makes it easier to pump [8]. Fly ash is divided into two categories: Class F and Class C. Class F is more typically used for structural concrete since it has a low calcium percentage and, in most circumstances, a carbon content of less than 5% [10]. Class C fly ash is primarily composing of high-calcium fly ashes containing less than 2% carbon. To enhance the mechanical and durability properties of cement, silica fume is employed in a predetermined proportion as a partial replacement. Through pozzolanic reaction, the addition of the right amount of SF (up to 12%) greatly reduced the strength loss of lightweight concrete (LWC) mixtures and increased compressive strength [11]. The results reveal that the mechanical strength of rich fly ash rubberized SCC is marginally improved by the addition of SF [12][13]. Using scanning electron microscopy found that employing SF and FA in concrete reduced porosity and produced dense concrete, which decreased permeability [14]. Another study discovered that the pozzolanic reaction's production of calcium silicate hydrate gel (C-S-H) increased the mechanical and durability of concrete [15].

The purpose of this study is to assess the fresh and hardened properties of HSSCC incorporating SF and FA. The novelty of this research program is that I have used different proportion of SF and FA that is I have used 5% SF throughout the mix and FA with the increment of 10% for each mix in order to evaluate the Fresh and mechanical properties then develop a comparison between control mix and the mixes with SF and FA and select the optimum percentages of SF and FA for HSSCC.

## 2 Experimental Work

### 2.1 Materials used

The major binding ingredient is ordinary Portland cement (OPC) type I, follow by ASTM C150. OPC has a specific gravity of 3.1, with starting and final setting times of 45 and 330 minutes, respectively [15]. FA and SF are used as SCMs. In Table 1, properties of OPC, FA and SF are shown.

Table 1 Properties of OPC, FA and SF

Chemicals	SiO <sub>2</sub>	TiO <sub>2</sub>	Al <sub>2</sub> O <sub>3</sub>	Fe <sub>2</sub> O <sub>3</sub>	MnO	MgO	CaO	Na <sub>2</sub> O	K <sub>2</sub> O	P <sub>2</sub> O <sub>3</sub>	LOI
OPC	17.9	-	10.7	3.60	-	1.8	62.8	0.9	1.4	-	0.9
Fly Ash	50.8	1.45	15.75	8.61	-	4.17	11.31	3.08	1.99	-	2.74
Silica fume	94.5	-	0.09	0.10	-	0.43	0.23	-	0.93	-	2.7

The concrete samples are mixed and cured with tap water. The addition of both SCMs cause a reduction in workability. The water-to-cement ratio is maintained constant for all mixtures. To get the require slump, the dosage of the superplasticizer is adjusted.

Table 2 Properties of fine Agg. and Coarse Agg.

	FA	CA
Sp. Gravity	2.70	2.65
Water Absorption (%age)	1.3	0.54
Loose Density (Kg/m <sup>3</sup> )	-	1412
Rodded Density (Kg/m <sup>3</sup> )	-	1550
Fineness Modulus	2.99	-

Fine aggregate (FA) is used from the Lawrencepur source in Pakistan. Coarse aggregate (CA) from Margalla hills source is used in concrete. The coarse aggregate size limit is 12 mm. Table 2 lists the characteristics of FA and CA.



## 2.2 Methodology and Mix Design

This research program has been divided into three phases. In first phase material has been chosen. In second phase mix design has been made. In third and last phase mixing and costing has been done, after mixing fresh properties has been measured, and for mechanical properties costing has been done.

To evaluate the fresh and mechanical qualities of concrete, seven different mix proportions are adopted. Mixes include Control Concrete (CC) mix, M1 (5%SF and 0%FA), M2 (5%SF and 10%FA), M3 (5%SF and 20%FA), M4 (5%SF and 30%FA), M5 (5%SF and 40%FA) and M6 (5% SF and 50%FA). The optimum percentage for partial replacement of SF and FA was selected based on previous research [16] [17].

HSSCC mix designs are created using EFNARC acceptance criteria and SF and FA as partial replacements of cement. Various mix proportions with constant water-to-binder ratio (W/B) 0.30, 5% constant SF and FA contents 10% increment other than control mix, sand content (743 kg/ m<sup>3</sup>) and coarse aggregate (878 kg/m<sup>3</sup>) as reported in Table 3, are used in this experimental plan. The binary mixes tagged as M1, M2, M3, M4, M5, and M6 contain same dosages of SF (i.e., 5%) along with different dosages of FA (i.e., 10%, 20%, 30%, 40%, and 50%) respectively. The dosage of super plasticizer is adjusted according to required slump.

Table 3 Mix Proportions

Mix No.	Mix ID	W/B Ratio	W kg/m <sup>3</sup>	C kg/m <sup>3</sup>	SF % kg/m <sup>3</sup>	FA % kg/m <sup>3</sup>	Fine Agg. kg/m <sup>3</sup>	Coarse Agg. kg/m <sup>3</sup>	Admixture % kg/m <sup>3</sup>
1	CC	0.30	142.2	474	-	-	743	878	1.4 6.636
2	M1	0.30	142.2	450	5 24	0 0	743	878	1.4 6.636
3	M2	0.30	142.2	402.6	5 24	10 47.4	743	878	1.4 6.636
4	M3	0.30	142.2	355.2	5 24	20 94.8	743	878	1.4 6.636
5	M4	0.30	142.2	307.8	5 24	30 142	743	878	1.5 7.10
6	M5	0.30	142.2	260.4	5 24	40 190	743	878	1.6 7.584
7	M6	0.30	142.2	213	5 24	50 237	743	878	1.6 7.584

## 2.3 Sample preparation

Yielding of all the batches of ingredients is done by weight. The ingredients are mixed in an electric concrete mixer and revolved at a rate of 30 rev/min. To get the desire workability, Viscocrete-3110 superplasticizer (SP) is used in the concrete mixes. Different samples are prepared for different tests. To get the average value of each testing result, three samples are prepared and tested. Hardened properties of concrete are investigated by performing mechanical and durability tests.

According to ASTM C39, a 150x300 mm cylinder is used to measure compressive strength, and tensile strength is tested using a split test according to ASTM C496/C496M, while flexural strength is tested using 150x150x700mm size beam samples according to ASTM C293 standard method [18] [19]. The slump test, J-ring test, and L-Box test are used to determine the fresh property, to accord with ASTM C1611, ASTM C1621, and ASTM C1611 standard method tests, respectively [20] [21].

## 3 Results and discussion

### 3.1. Fresh properties

The fresh properties testing is carried out for two main reasons. The first is to determine whether the concrete is self-compacting, and the second is to assess the deformability or consistency of the concrete to calculate the necessary mixture proportioning if the concrete lacks sufficient self-compatibility. There is no segregation or bleeding in any of the blends, according to the results. In table 4 there are the results of the fresh properties tests that were obtained in this study.



Table 4 Fresh properties of HSSCC

Type of Test	CC	M1	M2	M3	M4	M5	M6
Slump Flow Diameter (mm)	715	725	735	737	720	710	705
J-Ring Height H <sub>in</sub> -H <sub>out</sub> (mm)	12	11	10	10.5	12.5	13	13.5
J-Ring Flow Diameter (mm)	700	710	715	720	75	695	680
L-Box ratio	0.92	0.94	0.95	0.96	0.92	0.82	0.78

### 3.1.1. Slum flow test

The workability of each mix (with a constant water-binder ratio) is determined using the slump test according to ASTM C1611 [18]. Slump values for varying percentages of FA and SF are tried to keep constant. Dosage of SP (by %age weight of binder) reflected that workability is reduced by adding FA and SF. The results show that adding FA and SF greatly boosts workability up to the optimum limit, after which there is a decrease in workability. The require dosage of SP for the FA and SF mix is more as compared to that of the control mix, showing a comparatively severe effect of FA as compare with that of SF in reducing workability. However, FA and SF mix, being highest replacement value among un-strengthen mixes are use a combatively high dosage of SP. The workability results of all the mixes are discarded in figure 1. Because of the fine particle size of FA and SF are compared to cement particles, a reduce slump is value experienced after the optimum limit. The particle shape of FA and SF are spherical. Due to its spherical nature, FA and SF show better workability at lower percentages than higher percentages of FA and SF which is under other studies [22].

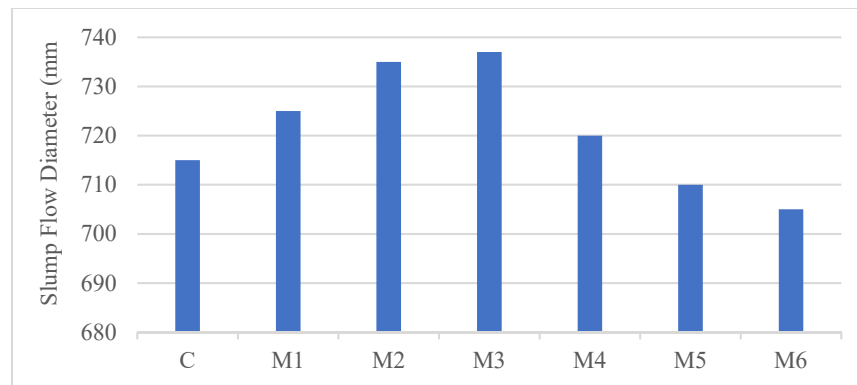


Figure 1: Slump Test Results

### 3.1.2. J-ring test

HSSCC's capacity to pass is determined by the J-ring test. The capacity of the HSSCC to pass through congest reinforcement and small holes without vibrating is referred to as passage ability [21].

During the J-ring test, the diameter of the concrete and the height difference between the concrete inside and outside of J-ring bars are measured. As shown in table 1, the height differences between the various blends vary over the ranges. Because of the reduce viscosity and share stress, M1, M2, and M3 have the lowest values (11 mm, 10 mm, and 10.5 mm, respectively), allowing the concrete to flow more easily.

Besides that, as shown in figure 2a, all mixes having lower percentages of FA and SF have lower values than those containing larger percentages of FA and SF, and all mixes containing SF and FA had lower values than the control mix. In addition, the concrete's diameter was measured. And, as demonstrated in figure 2b, a higher percentage of SCMs at optimum doses have a larger diameter than a higher percentage of SCMs in HSSCC. This could be because FA and SF have a lower specific gravity than cement-only concrete. J-ring flow diameter acceptability values range from 580 to 780 mm, and J-ring height H<sub>in</sub>-H<sub>out</sub> ranging between 0-15mm.

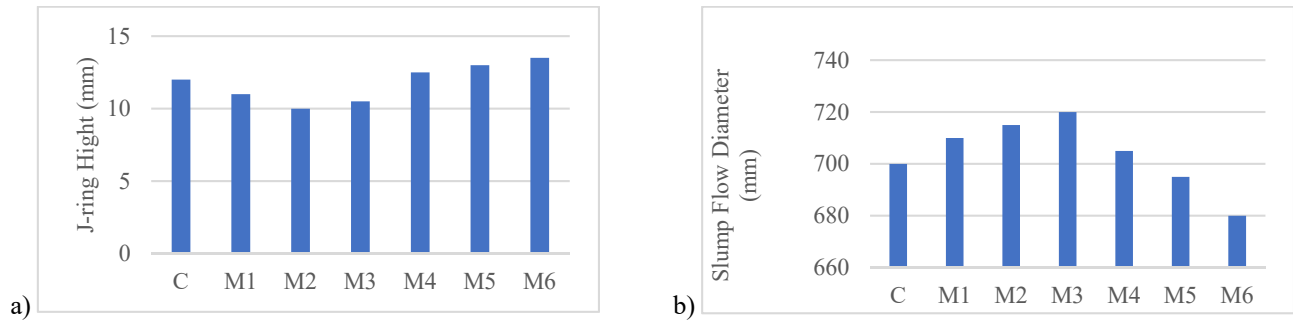


Figure 2: J-Ring Test, a. J-Ring Height Results, and b. J-Ring Flow Diameter Results

### 3.1.3. L-box test

To determine the concrete's capacity to fill, pass, and resist segregation this test is carried out. The L-box test is often used to measure the ability of HSSCC to pass reinforcement blocks when it is subjected to them. [21]. The L-box value grows as the FA and SF powder concentrations approach the optimum limit (5% SF and 20% FA), This can be related to lowering concrete viscosity and increasing yield value. Because of the high viscosity and shearing resistance, adding more powder reduces the L-box ratio compared to the control mix, as illustrated in figure 3. To determine L-box results, the heights of the concrete at both ends of the device (H1 and H2) are measured. The L-box has an acceptance ratio of 0.75 to 1.

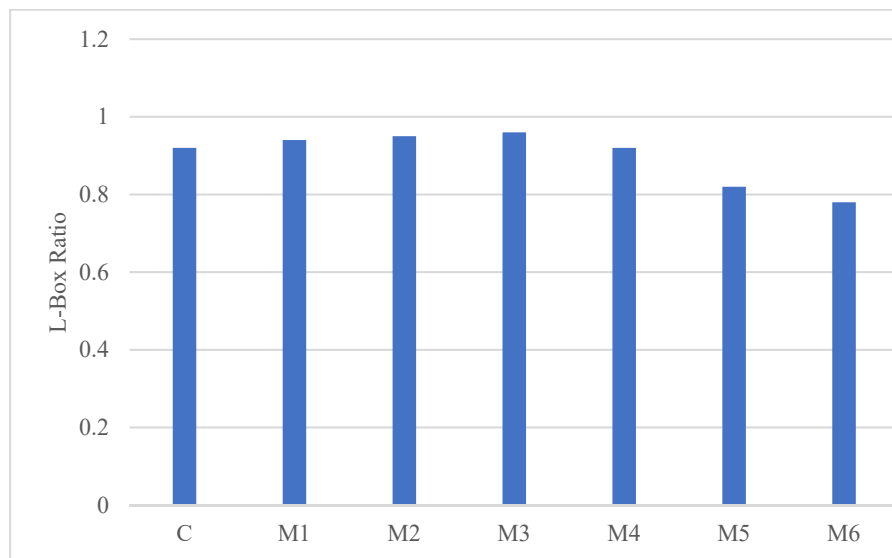


Figure 3: L-Box Ratio results

## 3.2. Mechanical Properties

### 3.2.1 Compressive strength

It's one of the most crucial parameters for determining concrete's uniaxial load-carrying capacity. It is determined using an ASTM C39 concrete cylinder [19]. The specimens are tested at 7, 14, and 28 days after curing in water. Table 5 and Figure 4 demonstrate the compressive strength results of HSSCC mixtures. The lowest compressive strength is 28.54 MPa for M6 mix with 5% SF and 50% FA after 7 days, while the highest compressive strength is 50.45 MPa for M3 mix with 5% SF and 20% FA after 28 days. FA and SF has a considerable impact on the HSSCC's strength and strength developed properties, as shown by the overall results.



Table 5 compressive strength values of HSSCC

Age (Days)	Compressive Strength (MPa)						
	CC	M1	M2	M3	M4	M5	M6
7	30.14	30.24	38.67	39.97	33.84	30.95	28.54
14	39.35	39.46	44.38	45.50	36.92	35.52	34.28
28	43.70	43.93	49.95	50.45	42.48	39.42	36.49

HSSCC mixtures containing 5% SF and 20% FA (M3) have better compressive strength than other mixes after 28 days of testing. Furthermore, the results show that when the percentage of FA and SF substitution rises, the compressive strength of HSSCC with FA and SF rises until it reaches specified limits, beyond which it begins to drop. As 5%SF and 20% FA are mixed, the compressive strength of concrete increase by 16% and 15%, respectively, at 14 and 28 days, when compared to the control mix. The increase in concrete compressive strength is due to the pozzolanic interaction of FA and SF with cement [20]. FA and SF may have bridged the matrix and aggregates by boosting interfacial properties and lowering stress concentrations in the cross-section [17] [22]. The research shows that mixing substantial doses of SF and FA mixes lower compressive strength when compared to an optimum mix, but that strength is improved when compared to a control mix.

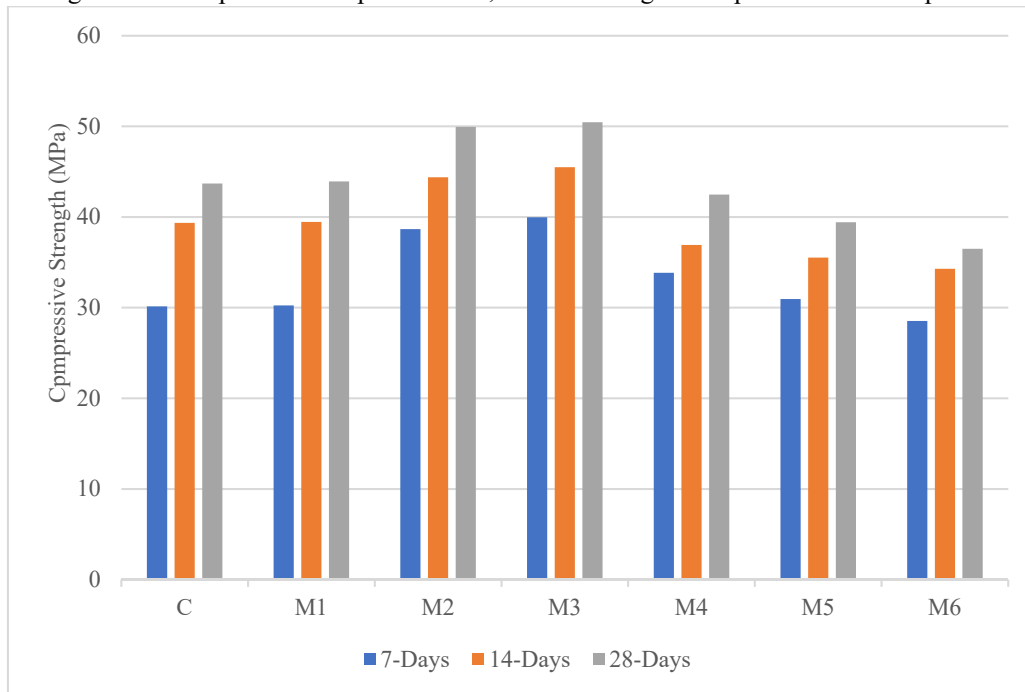


Figure 4: Compressive strength development of HSSCC mixture

### 3.2.2 Flexural Strength

Figure 5 presents the difference in flexural strength of concrete specimens. The study shows that concrete beams containing 10% and 20% dosages of FA in mixes somehow contribute toward flexural strength, however, the higher dosage of FA mixes exhibited low flexural strength. The increase flexural strength could be attributed to SF adherence to the matrix and improved bond quality, which is prevented crack propagation [23]. On the other hand, the percentage reduction in flexural strength of a concrete beam with the addition of FA after defined limits.

The results show that three mixes of HSSCC registered high flexural strength than the control mix (CC) by 5%, 7%, and 5.12% for M1, M2, and M3 respectively while the other three mixes with higher dosages of SCMs registered lower values by 14%, 16%, and 27% for M4, M5, and M6 respectively.



HSSCC with 5% SF and 10% FA (M2) register the higher flexural strength compared with all mixes.

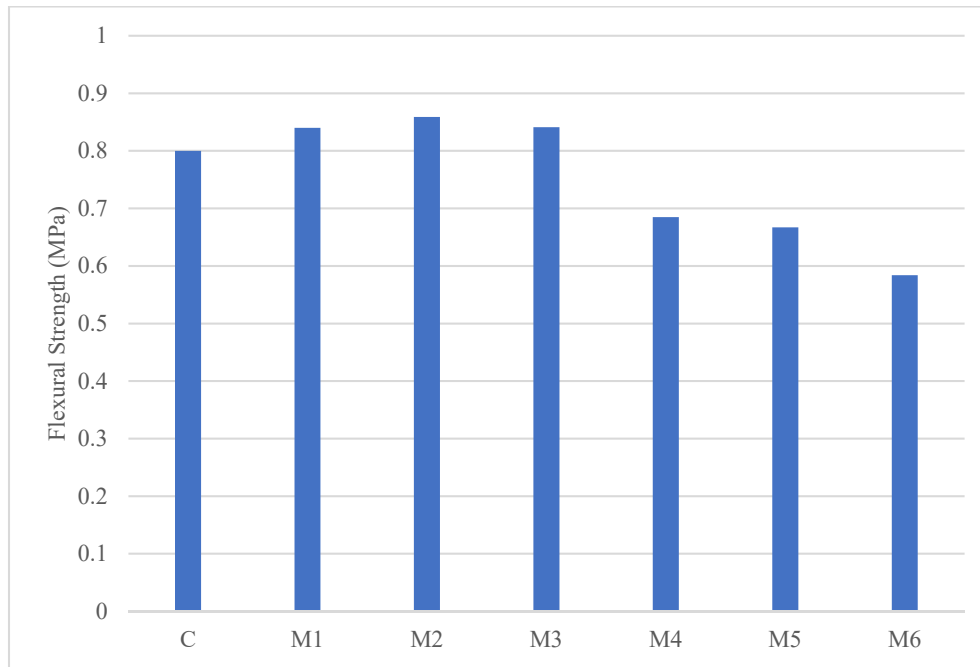


Figure 5: Flexural Strength HSSCC at 28 days

### 3.2.1 Split tensile test

The split tensile strength of concrete is measured using 150mm x 300mm concrete cylinders in accordance with ASTM C496/C496M-17 (ASTM C496/C496M 17 2011) specifications. The cylinder is placed horizontally inside the loading plates and two splitters are attached to these plates. The purpose of these splitters is to confine the load for splitting the concrete cylinder. The loading rate is adjusted to 1300 N/S. Study shows that mixing of FA and SF in concrete mixes adversely affects the split tensile strength of HSSCC concrete. In table 6 there are the results of the split tensile test that are obtained in this study.

Table 6 Split Tensile Strength Values

Age (Days)	Split Tensile Strength (MPa)						
	CC	M1	M2	M3	M4	M5	M6
14	13.01	13.14	13.89	14.10	10.82	10.05	7.65
28	15	15.06	15.62	16.86	12.19	11.09	9.04

It is observed that concrete specimens containing dosages of SF and FA up to optimum limits exhibited higher resistance to load which is 8% and 12.4% higher in M3 (5% SF and 20% FA) mix at 14 days and 28 days respectively as shown in figure 6. However, specimens with larger doses of SF and FA have lower tensile strength than control concrete, which are 41% and 39% lower at 14 and 28 days, respectively, in M6 (5% SF and 50% FA) mix.

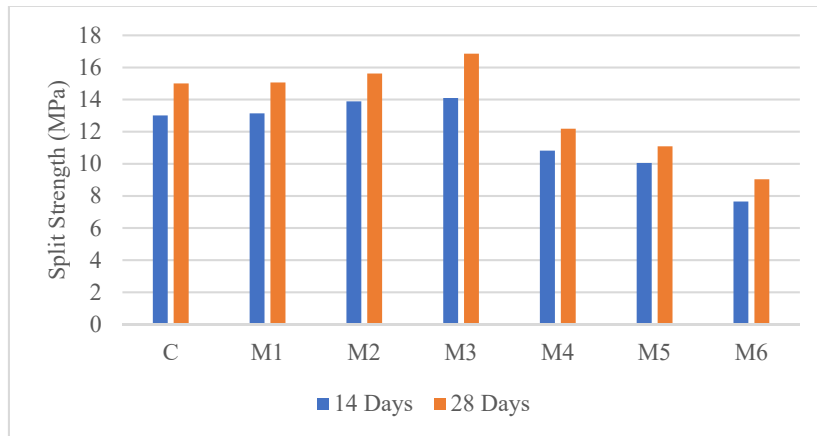


Figure 6: Split tensile strength development of HSSCC

## 4 Conclusion

SCMs (Silica Fume and Fly Ash) were used to partially substitute cement in concrete in this investigation. SCMs' impacts on concrete parameters like compressive strength, flexural strength, and the split tensile strength were investigated. From the experimental results, it was concluded that,

1. Adding SF and FA to high-strength self-compacting concrete increases its workability up to the optimal limit when the water-to-binder ratio is kept constant (5%SF and 20%FA). This is due to the FA content in the concrete mix. The greater surface area of the SF content causes a decrease in workability after the optimum limit.
2. Fresh characteristics of HSSCC which is indicated J-ring test and L-box test including FA and SF are better than the control mix. This is owing to the decreased viscosity and shear stress, which allow the concrete to flow more easily. This is because SF and FA particles have a lower specific gravity and are spherical in shape.
3. HSSCC mixes including SF and FA have better compressive strength than the control mix, but the compressive strength decreased as the SCMs replacement level increased, such HSSCC have 15% higher and 16% lower compressive strength of M3 and M6 mixes, respectively, at 28 days than control mix. Higher compressive strength of M3 mix is because of SF, it has more silica content which has cementitious properties and the lower compressive strength of M6 is due to low hydration of silica content.
4. Flexural strength of HSSCC including SCMs is 7.37% greater for M2 mix than the control mix. The increase flexural strength could be attributed to SF adherence to the matrix and improved bond quality, which is prevented crack propagation.
5. Split tensile strength of HSSCC containing SF and FA exhibited higher tensile strength which is 12.4% higher for M3 mix than control mix at 28 days. This is also pozzolanic effect of SF.

Thus, it is determined that the maximum SF and FA concentrations that can be employed to enhance the mechanical and fresh properties of HSSCC are 5% and 20%, respectively. The further increment of FA will decrease the mechanical and fresh properties of HSSCC.

## Acknowledgement

The authors are appreciative to the editor and all reviewers for suggesting improvements to the paper, and they are grateful for the attentive review and constructive suggestions by the anonymous reviewers.



## References

- [1] U. N. e. a. Environment, "Eco-efficient cements: Potential economically viable solutions for a low-CO<sub>2</sub> cement-based materials industry," *Cement and Concrete Research*, vol. 114, pp. 2-26, 2018.
- [2] R. M. e. a. Waqas, "Influence of Bentonite on Mechanical and Durability Properties of High-Calcium Fly Ash Geopolymer Concrete with Natural and Recycled Aggregates," *Materials*, vol. 14.24, p. 7790, 2021.
- [3] M. I. M. F. R. M. A. M. U. U. A. M. H. & L. Q. F. Ashraf, "Developing a sustainable concrete incorporating bentonite clay and silica fume: Mechanical and durability performance.," *Journal of Cleaner Production*, vol. 337, p. 130, 2022.
- [4] V. P. B. V. H. a. J. F. Nežerka, "Impact of silica fume, fly ash, and metakaolin on the thickness and strength of the ITZ in concrete.," *Cement and concrete composites*, vol. 130, pp. 252-262, 2019.
- [5] H. SüleymanGökçea, "Effect of fly ash and silica fume on hardened properties of foam concrete.," *Construction and building materials*, vol. 194, pp. 1-11, 2019.
- [6] M. M. e. a. Johari, "Influence of supplementary cementitious materials on engineering properties of high strength concrete.," *Construction and Building Materials*, vol. 25.5, pp. 2639-2648.
- [7] R. K. A. P. a. A. N. N. Majhi, "Performance of structural lightweight concrete produced by utilizing high volume of fly ash cenosphere and sintered fly ash aggregate with silica fume.," *Cleaner Engineering and Technology*, vol. 3, p. 10012, 2021.
- [8] B. U. R. A. K. & T. L. U. T. F. U. L. L. A. H. Uzal, "Studies on blended cements containing a high volume of natural pozzolans.," *Cement and Concrete Research*, vol. 33(11), pp. 1777-1781, 2018.
- [9] W. S. M. M. A. H. S. L. K. T. B. A. R. W. & A. S. Alaloul, "Mechanical properties of silica fume modified high-volume fly ash rubberized self-compacting concrete.," *Sustainability*, vol. 13(10), p. 5571, 2021.
- [10] J. e. a. Gražulytė, "Effect of silica fume on high-strength concrete performance.," *5th World Congress on Civil, Structural, and Environmental Engineering (CSEE'20)*, 2020.
- [11] A. C. /. C150M-20, "Standard Specification for Portland Cement.," ,," *ASTM International, West Conshohocken, PA*, , 2020.
- [12] S. S. B. W. a. I. A. Gull, "Exploring optimum percentage of fly-ash as a replacement of cement for enhancement of concrete properties.," pp. 16-25, 2020.
- [13] T. W. W. a. A. C. Nochaiya, "Utilization of fly ash with silica fume and properties of Portland cement–fly ash–silica fume concrete.," *Fuel*, vol. 89.3, pp. 768-774.
- [14] A. C496/C496M-11, "Standard Test Method for Splitting Tensile Strength of Cylindrical Concrete Specimens," *ASTM Standards*, 2017.
- [15] "A. C39, ""Standard Test Method for Compressive Strength of Cylindrical Concrete Specimens"".,".
- [16] A. C. 1611, "Standard Test Method for Slump Flow of Self-Consolidating Concrete."".".
- [17] A. C. 1. 1621M1, "Standard Test Method for Passing Ability of Self-Consolidating Concrete by J-Ring."".".
- [18] A. Chaipanich, "Utilization of fly ash with silica fume and properties of Portland cement–fly ash–silica fume concrete," *fuel*, vol. 189, pp. 768-774, 2014.
- [19] B. MohamedAbd Elrahmanab, "Combined effect of fine fly ash and packing density on the properties of high performance concrete.," *Construction and Building Materials*, vol. 14, pp. 225-233, 2014.
- [20] A. e. a. Habibi, "RSM-based evaluation of mechanical and durability properties of recycled aggregate concrete containing GGBFS and silica fume.," *Construction and Building Materials*, vol. 270, p. 121431, 2021.
- [21] L. A. A. J. a. U. M. Qureshi, "Effect of Cement Replacement by Silica Fume on Compressive Strength of Glass Fiber Reinforced Concrete.," *International Journal of Structural and Civil Engineering Research*, vol. 7.3, pp. 117-182, 2018.
- [22] A. e. a. Nawaz, "Effect and limitation of free lime content in cement-fly ash mixtures.," *Construction and Building Materials*, vol. 102, pp. 515-530, 2016.
- [23] A. C. C.-0. o. C. a. C. Aggregates, "Standard specification for coal fly ash and raw or calcined natural pozzolan for use in concrete.," *ASTM international*, 2013.





# STRENGTHENING OF A FLAT PLATE SLAB -CASE STUDY

<sup>a</sup> Naeem Ullah\*, <sup>b</sup> Muhammad Yaqub.

a: Department of Civil Engineering, University of Engineering and Technology, [Naeem.ullahkhadim@students.uettaxila.edu.pk](mailto:Naeem.ullahkhadim@students.uettaxila.edu.pk)

b: Department of Civil Engineering, University of Engineering and Technology, [muhhammad.yaqub@uettaxila.edu.pk](mailto:muhhammad.yaqub@uettaxila.edu.pk)

\* Corresponding author: Email ID:[naeemullahbajour@gmail.com](mailto:naeemullahbajour@gmail.com)

**Abstract-** Flat Plate Slab is a popular structural floor system. The popularity of this structural system is due to the speed of construction, which has become a critical consideration in many projects. The slab could be deficient because of under-design or lack of quality control. Strengthening of reinforced concrete slab for flexural is crucial to enhance the capacity of the deficient slab. This study describes the strengthening methodology for a badly designed-story building having Flat Plate slab flooring system. A visual and detailed inspection of the building was carried out, and the bottom and top cracks on the flooring system were inspected thoroughly. The deflection on each floor panel was observed in detail. The pattern of the cracks was noted in the soffit of each slab panel and at the top and in the middle and column strips. The cracks were measured using a digital vernier caliper. The deflections were measured using auto level and inverted staff rod. The whole building was modeled in ETABS software considering all the in-situ parameters. The design was reviewed and found that the slab was under-designed in flexural and shear reinforcement. This paper deals with the flexural strengthening of reinforced concrete (RC) slab which is deficient in flexural steel. This work conducted a detailed field investigation and modeling to control slab deflection and crack using several strategies such as column jacketing, drop panels, creation of beams. This study suggested the best economical and safer solution for a badly designed plate slab flooring system. The innovation of this case study is real big scale commercial building where in literature small scale structures have been discussed.

**Keywords-** Flat Plate slab, Strengthening, Flexural capacity, Column Jacketing, Drops panels

## 1 Introduction

Flat plate structures are flat slab constructions without drop panels. Flat Plate slab constructions are commonly found in commercial and residential structures. Flat plate buildings have several advantages, including simple formwork, lower construction costs, ease of installation, greater flexibility in interior arrangement, ease of future restoration, and more clear space. Increased architectural design freedom will also help to reduce maintenance and building costs[1]. Since this structural method was implemented, flat slab strengthening approaches have emerged. Depending on the breadth of the strengthening solution chosen, it could range from a simple extension of the column that supports the slab to more complex solutions involving composite materials[2]. Over several decades, external bonding (EB) technology has been widely employed in civil engineering to strengthen reinforced concrete (RC) structures[3]. EB-bonded steel plates can successfully raise the ultimate flexural capacity and stiffness of the reinforced structure, delay the emergence of the first crack, and lower the crack breadth of RC structures[4]. The major drawbacks of EB-steel plate technique are the corrosion of the steel plate and the premature failure due to plate end debonding of steel plate and shear, which prevent the strengthened member to obtain higher flexural capacities[5],[2]. The corrosion of the steel plate and premature failure owing to plate end debonding of steel plate and shear are the key downsides of the EB-steel plate technology, which prohibit the reinforced member from achieving larger flexural capabilities[6], [7]. The most frequent materials used to reinforce RC structures are steel and fiber-reinforced polymers (FRP). Although each material has its own set of benefits for EB applications, it also has its own set of drawbacks. Steel plates are heavy and have poor corrosion resistance, and their thickness is limited for strengthening RC structures due to a lack of shape flexibility[3], [8]. This research study uses steel and concrete to strengthen a Flat Plate Slab. Finding existing strength of selected structure & expected future life at present



condition. Strengthening of a plate slab. Safe and economical solutions for strengthening a flat slab have less reinforcement than required.

## 2 Methodology

### 2.1 Preliminary Data & structure details:

The building is in Rawalpindi Fifth road which occurs in seismic zone 2B according to building code of Pakistan . It' a commercial shopping mall consisting of eight story (three-story basement). The building is constructed in 2018. The slab type is Flat Plate. Span is 25'x25'.

### 2.2 Preliminary inspection of the building

This structure has been thoroughly inspected from top to bottom, detecting cracks, spells, crazing, seepage, and so forth. The key areas of inquiry and repair are highlighted on the building's plan. All these cracks are in the middle strip at the bottom of the slab in both x and y direction as shown in figure a and figure b. The pattern and width of the cracks measured digital vernier caliper. Figure F and G represent the cracks at the bottom of the slab, also these cracks and their pattern is noted on plan of the building for each story's slab as shown in figure D. Furthermore, the deflection of slab is found by detailed survey using Auto-level and inverted staff rod and written on building plan in inches as mentioned in figure C. These values of deflection are more than the allowable limit as specified by ACI-318-11 in 9.5(b) . Some cracks are also detected around the column at the top of the slab. these are shown in figure E. The experimentally measured widths of the cracks were found in the range of 0.2mm to 1.64mm at the bottom in the middle strip. The width of the cracks at the top of the slab varies from 0.25mm to 1.18mm. The middle strip at the bottom of the slab and in the column strip at top of the slab. Deflection and crack's width were measured .The similar pattern of cracks was specialized in middle strip tut the slabs.



Figure 1: A. and B. cracks pattern at the bottom of the slab

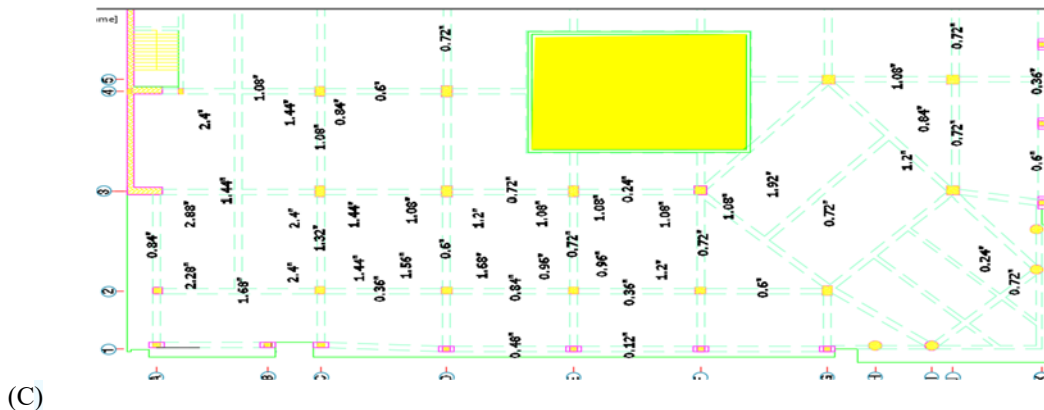
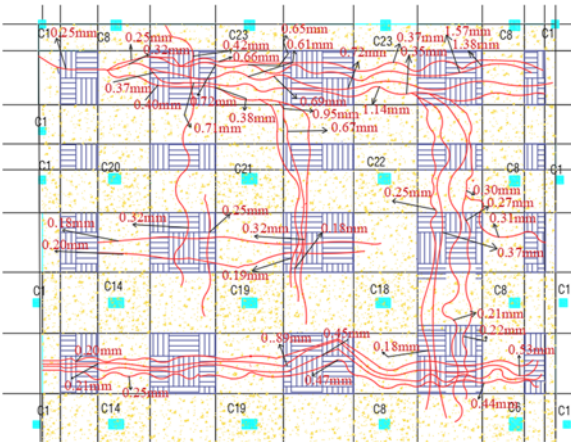
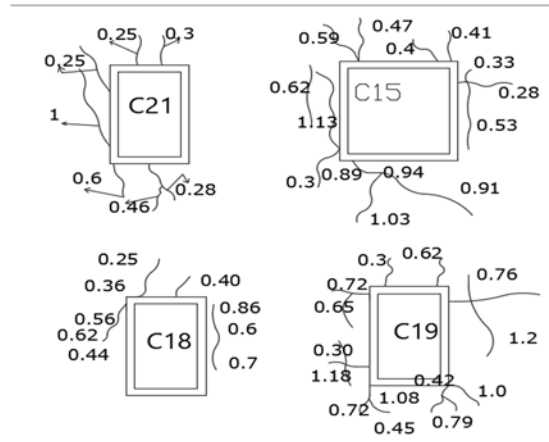


Figure 2: C. Deflection measured during Visual inspection using auto level and staff rod



(D)



(E)

Figure 3: D. cracks pattern and cracks width measured in millimeters of Ground Floor slab.

Figure 3:E. cracks in middle strip of columns at the top of slab



(F)



(G)

Figure 4: F. and G. width of the cracks measured by Digital Vernier Caliper

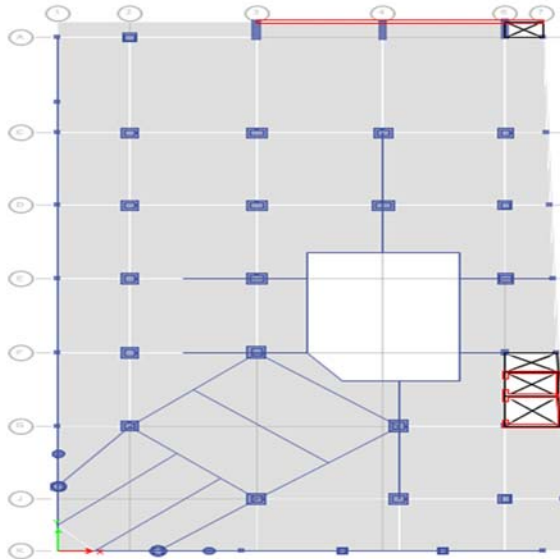
### 3 SOFTWARE MODELLING & ANALYSIS

This work conducted a detailed field investigation and modelling to control slab deflection and crack using several strategies such as column jacketing, drop panels, creation of beams. The flexural strengthening of RC slab-type elements with concrete and steel to control the deflection of the slab. The building is modeled in ETABS according to the drawings. Gravity and seismic loads are applied to the structure. The slab is exported to CSI-SAFE-16 with all defined loads combinations also a new load combination Long Term Deflection is defined, and deflection checked against this combination as shown in figure 9.

Materials are defined in software as Concrete of strength 4000psi and 5000psi and Steel of grade 60, then Frame sections are defined as Column of 18"x18", 24"x24", 30"x30", 30"x24", 36"x36" and beams are defined 12"x18", 12"x24", 12"x30", 15"x24", 18"x24", 18"x27", 18"x36" also is defined as slab 10" thick and shear wall 9" thick is defined. Load patterns are defined as live load <100, live >100, partition wall load (pw), flooring load (fcd) self-dead load, water load, HVAC and laterals loads EQX and EQY both negative and positive are defined. Seismic loads are defined according to UBC-97 code. Total 38 loads combinations are defined according to ACI-318 code. After defining the materials and frame sizes the model is analyzed and then one story is exported to CSI-SAFE, where long term deflection load combination is also defined.

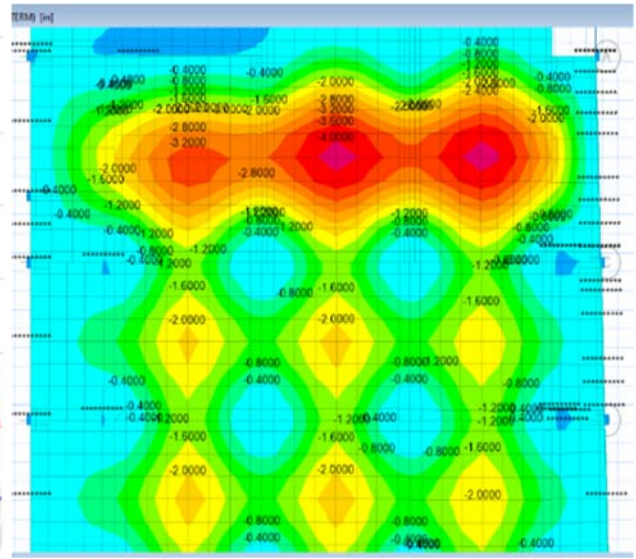


After checking the deflection against long-term load combination, the value of deflection was greater than the allowable limit as shown in figure. Figure 5 H shows the original structure modeled in ETABS-16. There are peripheral beams on the edges of the slab. The lines represent shear walls. The figure 5 I show the long-term deflection, values vary from 0.4 inches to 3.5 inches. These values are like Figure 2 C which were obtained from site survey. Figure 6 J describes long term deflection when beams were included whose values vary from 0.28 inches to 0.32 inches. Figure 6 k represents deflection of column Jacketed model slab whose values are varies from 0.4 inches to 3.20 inches..



(H)

Figure 5: H. plan view of ETABS Model



(I)

Figure 5: I. deflection of original slab in inches

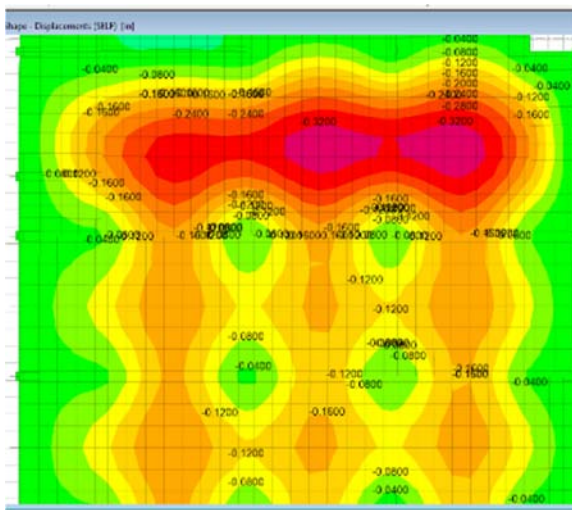


Figure 6: J. Deflection after beams were inserted

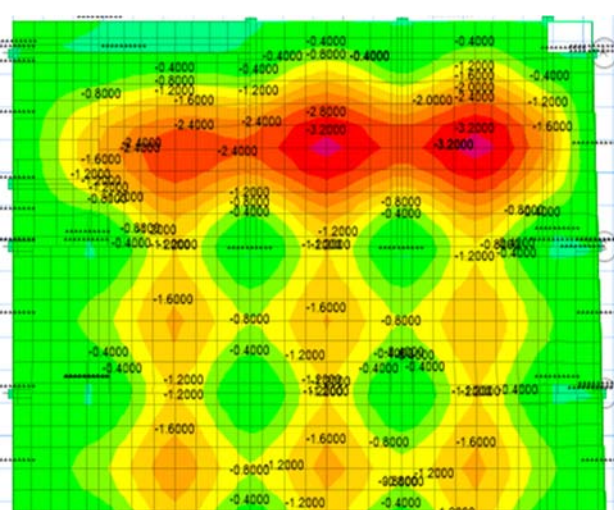
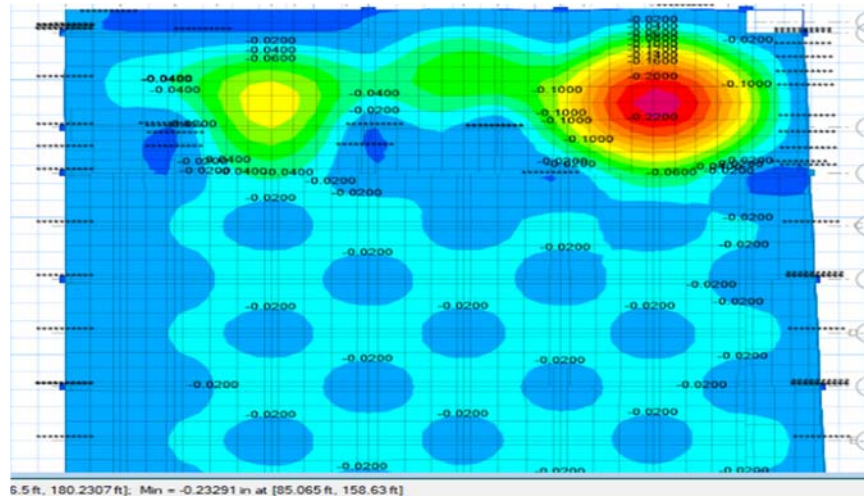


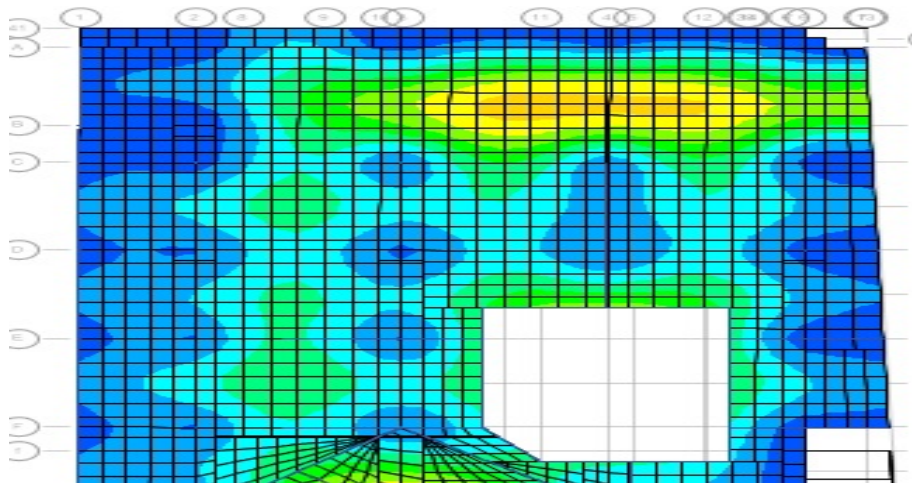
Figure 6: K. Deflection of column Jacketed model slab.



Figure 7 I show deflection of slab with Drop Panel values are up to 0.22 inches. Figure 8 H show long term deflection when a middle column is included and a few beams above the ramp region with maximum value of 0.16 inches.



(I) *Figure 7: l. Deflection of slab with Drop Panel*



(H) *Figure 8: h. Deflection of the slab when middle column and beams are applied*

## 4 Conclusion

- The collected data of the building was modeled and analyzed in software considering in-situ parameters and the following conclusions were made.
- The cracks and deflection that were present in the building were also confirmed by the software results under the same type of loading which means that the building was under designed.
- Jacketing was applied to the columns, and they were unable to control the deflection of the slab.
- Drops panels were applied to the columns which controlled the deflection.
- Extra Beams were introduced to the model that controlled the deflection of the slab but at the same time it imparts extra weight to the building due to which the building fails in soil bearing pressure.



- A middle column was added to the model and shows the best results for controlling the deflection of slab.
- The best economical is inclusion of the columns in the middle of each slabs' panel throughout the height of the buildings, also a few beams were added to the structure above the ramp region where columns cannot be added to the structure because of access of vehicles to the basements.
- If we apply only beams to all slab, they increase the weight of the building due to which the building fails in soil bearing pressure. The option of column jacketing cannot control the deflection and cracks of the slab. The method of inserted a middle column and a few beams above ramp area resulted better in term of controlling deflection which can be seen in Figure H and this method can be done easily because above the ramp there are walls where beams can be added. This method is economical because there is no high initial cost of steel and concrete. the span is 25 and 25 feet so middle columns can be added without the compromising the space. The sum up, this method neither creating problems of footing failing nor the issue of cost, so this technique is safer and economical.

## References

- [1] H. Daniel and P. Fernandes, "Strengthening of flat slabs with reinforced concrete overlay – Analysis and development of the solution," 2019.
- [2] F. R. P. Ebr and T. Group, *Externally bonded FRP reinforcement for RC structures*. .
- [3] *437R-19: Strength Evaluation of Existing Concrete Buildings*. 2019.
- [4] L. De Lorenzis and A. Nanni, "Ceg\_Jansze\_19971027[1].Pdf," *ACI structural Journal*. 2002, [Online]. Available: <http://www.concrete.org/Publications/InternationalConcreteAbstractsPortal.aspx?m=details&i=11534>.
- [5] "s50502119123-47986413.pdf." Pooja Nama , Ankush Jain and Rajat Srivastava.
- [6] Y. Sreevalli, "A Review on Progressive Collapse of Reinforced Concrete Flat Slab Structures," vol. 54, no. 1, pp. 181–194, 2021, doi: 10.22059/cej.2020.291570.1624.
- [7] X. Zheng, B. Wan, P. Huang, and J. Huang, "Experimental study of hybrid strengthening technique using carbon fiber laminates and steel plates for reinforced concrete slabs," *Constr. Build. Mater.*, vol. 210, pp. 324–337, 2019, doi: 10.1016/j.conbuildmat.2019.03.100.
- [8] N. Banu, DragosTaranu, "Traditional Solutions for Strengthening Reinforced Concrete Slabs," *Bul. Institutului Politeh. din Iasi. Sect. Constr. Arhit.*, vol. 56, no. 3, p. 53, 2010.



# CHARACTERIZATION OF ASPHALT USING NEURAL NETWORK AND IMAGE ANALYSIS TECHNIQUE

*<sup>a</sup> Samreen Sajjad\*, <sup>a</sup> Naveed Ahmad, <sup>a</sup> Afaq Ahmad*

a: Transportation Engineering department, University of Engineering and Technology Taxila, [samreensjidd@gmail.com](mailto:samreensjidd@gmail.com)

**Abstract-** Artificial neural networks (ANN) and image processing (IP) are significant computer science methodologies. These methods are employed to forecast the properties of asphalt binder. To evaluate the asphalt binder's parameters, i.e., homogeneity and volumetrics, by performing a job mix formula. Several tests were conducted in the laboratory with different types of aggregate, i.e., Margallah, Sargodha, Sakhi Sarwar, and Rohi with bitumen material. The IP and ANN approaches were used in this investigation are appropriately mixed and are used to forecast the volumetrics of asphalt, i.e., air voids (Va), percent voids filled with asphalt (VFA), and voids in mineral aggregate (VMA). For this specimen, bitumen and aggregate were cast with 3.5, 4.0, 4.5, 5.0, and 5.5 aggregate grading. Two sets of specimens were created from them: (i) to determine air voids (Va), percent voids filled with asphalt (VFA), and voids in mineral aggregate (VMA); and (ii) to create an image database. An image of the top view is needed for image capturing which is taken by a smart phone. Preprocessing is performed on the obtained data (converted to grayscale, cropped, and resized to 256 256 pixels), and using the ANN method, the statistical features are collected to evaluate the VA, VMA, and VFA. The actual values of the job mix formula were differentiated from the relative values evaluated by the given methods, i.e., IP and ANN. The data set has a massive effect on the reliability of the conclusions.

**Keywords-** Artificial neural network, Image processing, Job mix formula, Volumetrics.

## 1 Introduction

In civil engineering, HMA asphalt binder is the most important material for paving highways. As laboratory testing is used to forecast the features of HMA asphalt binder for its attainment of results, which is a very laborious, time-consuming and expensive method. To overcome this problem is the use of image processing..[1] The dataset obtained from the image computation are then correlated with laboratory computations. The results obtained by image computations were quite close to laboratory computations. Both IP and ANN are used as tools to calculate the information obtained through an image. Digital cameras are used for inspection and monitoring [2].

The use of image processing helps us to investigate the homogeneity of HMA asphalt binder. So, determining the homogeneity of HMA asphalt binder through images requires a smart phone and a computer. To achieve this, IP and ANN algorithms were generated to evaluate the attributes of asphalt binder. There are two machine learning techniques. These are ANN and ANFIS, which have a great ability to forecast. The Human brain process is similar to ANN and ANFIS as it follows the relationship between neurons[2].

The properties of HMA Asphalt binder depends on the homogeneity of the HMA asphalt concrete. There are a factors which play a key role in distribution of aggregate and asphalt binder i.e. Gradation of aggregate, temperature, and compaction of the asphalt mixture[3]. In the HMA pavement homogeneity Asphalt is due to the quality of distribution of aggregate. The performance of the pavement is stimulated by the homogeneity of HMA asphalt concrete. The pavement surface is used to estimate the homogeneity of HMA asphalt concrete. This homogeneity is not estimated from inside the pavement. The macroscopic indicators of HMA asphalt concrete are porosity; density and texture depth. These macroscopic indices reflect the homogeneity of the asphalt mixture [4].



The volumetric parameters of HMA asphalt concrete are air voids, percent voids filled with asphalt and voids filled with mineral aggregate. These parameters are established by numerous laboratory tests. Air voids in HMA Asphalt are directly related to moisture damage, rusting and fatigue life. A value of 3–5% for air voids in 2006 is recommended by NCHRP 567. This value has been used until now. A range of 7-9 micro meters for workability and rutting resistance, which was suggested by NCHRP 673 in 2011, has been used until now. A criterion for voids in mineral aggregate, which was proposed by NCHRP in 2006, is 1.5 % to 2.0 % above the minimum value. To predict whether the designed mix is workable or not, this can be done with the aid of volumetric parameter[5].

Li cong and jiachen shi[3] the images of paved asphalt mixtures were used to estimate the segregation of compacted asphalt mixture. An image processing method was used to classify the images of the paved asphalt mixture. Those images were captured during construction. There are 224 samples of HMA asphalt mixture. Images were captured from these samples for segregation detection. In this study, GLCM was used to estimate features like contrast, correlation, etc. A Naïve Bayesian classifier is used to classify the segregation of asphalt mixture images. The accuracy rate of naïve Bayesian classifier is 80% when compared to manually labelled results. The distribution of aggregates after paving can be used to characterise the distribution of aggregates in the finished pavement.

Cristine yohana ribas and Liseanepa dihlathives[6] There are three methods adopted for compaction ,i.e., impact, kneading and vibration. These three methods are then correlated with the compaction carried out in the field. It was studied whether compaction methods could be used for analysis, which is done with software. The Marshall and gyratory compactors was the most representative of the field compacted. The compactor was best approximated in the field. Results for the samples' macro-structural parameters that were acquired in the lab and those that were collected in the field were compared. There is a greater flexibility shown in results by Marshall Compactor. The results show that the super pave gyratory compactor is the most accurate method of compaction with a gyration angle of 1.25 under Brazilian conditions.

Muhammad A, Abed, zahir noori M.taki[7] In flexible pavement, tensile related cracking is a major defect. An artificial neural network (ANN) is designed to interpret the effects of nature. In this paper by the construction of the ANN model is used to predict the stiffness of asphalt. A good correlation was found between actual and estimated values. It has a coefficient of determination of 88.6%. The stiffness model's training relative error was 0.093. The discrepancy between observed and anticipated outputs is measured by this number. The relative errors for the models, nevertheless, show that there isn't much of a gap between actual values and predictions.

Vidhi vyas and ajit partap singh [8] For pavement rehabilitation and maintenance, models are developed by using the mechanisms of artificial intelligence. ANN for asphalt pavement structural condition models is developed. There are three parameters used in that network used as input data. These parameters are structural, functional, and environmental. The data is collected in the field. The accuracy of the correlations discovered in this research is predicted to raise greater perception of the significance of structural adequacy factors in asphalt M&R judgment. The use of neural network as it performs well in even case of limited data.

The aim of this research is to develop a protocol for the characterization of asphalt using image analysis techniques. The major objectives of the research work are (a) development of a setup for capturing images; (b) development of an algorithm for studying/analyzing homogeneity & volumetrics of different types of asphalt mixtures; (c) training of laboratory values (output) versus image processing results (input) in Matlab or Python; and (d) correlation of experimental and image processing results. The fundamental goal of this research work is create a model for forensic analysis of asphalt concrete. In this way, IP and ANN are used to estimate the features of HMA asphalt concrete through images. The purpose of this research work is to correlate the laboratory values (VA, VFA, and VMA) with the software values (results of images which are mean, mode, median, entropy, skewness, and third moment) and to create a model for this purpose.

In the present work, a job mix formula (ASTM D1559) which is based on IP, ANN, and ANFIS, is used to predict the properties of HMA asphalt concrete. With the use of aggregate gradation, 82 samples of varying VA, VMA, and VFA are prepared. With the use of each aggregate gradation, similar asphalt concrete samples are prepared. In a conventional test, one of the asphalt concrete samples was utilized. The second sample was used to evaluate features like mean mode etc, from the obtained HMA asphalt mixture images. To predict the properties of HMA asphalt concrete, the images were used to test and train the network.

## **2 Processing of Image and ANN**

Processing of images is done to collect fruitful information by the using computer algorithms. Various programs, such as Matlab and Python programming[9], have been effectively utilised to interpret photographs. Digitalization is a technique





in which photographs are converted into digit form by technique of image processing. A pixel from the digitally created image is represented by each element of the matrix. The fundamental logical building block of an image, a pixel, indicates the brightness of a gray scale image's unit area. Convergence with ANNs can be utilised to solve issues by using matrices produced through image processing[10]. An algorithm based on an artificial neural network uses concepts from the human brain to tackle difficult and time-consuming tasks. The first layer of an ANN is the input layer, the second is the hidden layer, and the third is the output layer. These layers are shown in Figure 1.

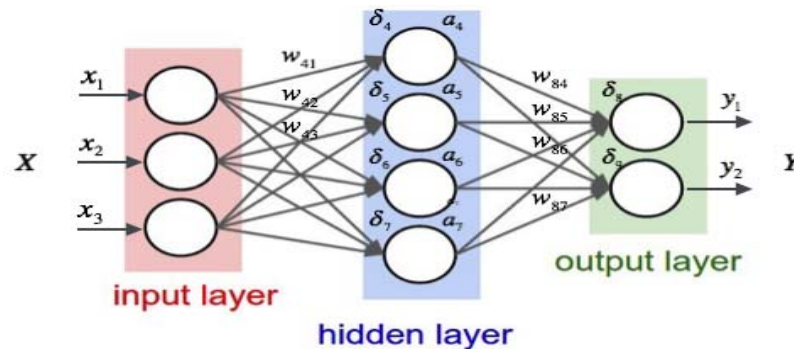


Figure 1: Connection of weight and bias to an input[2]

### 3 Sample Productions and Testing

It begins with material mixing and sample preparation, then moves on to image acquisition, and finally, specimen training.

#### 3.1 Sample Preparation.

In this section, we prepared 82 samples with a Diameter 102 mm and height of 64mm as shown in Figure2.1. Only hot mixtures employing penetration grades of asphalt cement and incorporating aggregates with a maximum size of 25 mm are eligible for JMF. The key goal is to come up with an affordable and practical mix that includes the right combination of materials and the right amount of asphalt. Under traffic loading, HMA should not rut or deform (shove). Achieving fatigue life, temperature conditions cracking resistance, durability, moisture damage resistance, skid resistance, and workability is JMF's top priority. The two main ingredients of HMA are aggregate and asphalt binder. The process of deciding which aggregate to use, which asphalt binder to utilise, and what the ideal ratio of these two components should be is known as HMA mix design.

Table 1: Asphalt concrete wearing course requirement

Mix Designation		Class A	Class B
Compacted Thickness		50-80 mm	35-60 mm
Combined Aggregate Grading Requirements			
Sieve Designation		Percent Passing by Weight	
Mm	Inch		
25	1	100	—
19	3/4	90-100	100
12.5	1/2	-	75-90
9.5	3/8	56-70	60-80
4.75	No. 4	35-50	40-60
2.38	No. 8	23-35	20-40
1.18	No. 16	5-12	5-15
0.075	No. 200	2-8	3-8
Asphalt Content by weight percent of total mix		3.5 (Min.)	3.5 (Min.)



Figure 2: Particle size distribution of aggregate

The aggregate is graded to measure its workability, permeability, fatigue resistance, friction resistance, stiffness, stability, durability, and resistance to moisture damage. In the JMF, the aggregate gradation is a crucial component. The prepared aggregate is sent through a sequence of progressively smaller sieves that are stacked on top of one another. The aggregate is shaken, and as it goes through each sieve, its nominal size is determined. Sieve analysis is frequently employed to assess gradation. A sample of dry aggregate with known weight is separated using a series of sieves with progressively smaller apertures in a sieve analysis.

Table 2: Aggregate gradation

Size	Percentage Passing	Percentage Retained						
mm	%	%	3.50%	4%	4.50%	5%	5.5%	
			Weight Retained (gm)					
25	100	0	0	0	0	0	0	
19	95	5	57.9	57.6	57.3	57	56.7	
9.5	63	32	370.56	368.64	366.72	364.8	362.88	
4.75	42.5	20.5	237.39	236.16	234.93	233.7	232.47	
2.36	29	13.5	156.33	155.52	154.71	153.9	153.09	
0.3	8.5	20.5	237.39	236.16	234.93	233.7	232.47	
0.075	5	3.5	40.53	40.32	40.11	39.9	39.69	
Pan	-	5	57.9	57.6	57.3	57	56.7	

Table 3 Mix design criteria

Total Weight of Sample = 1200 gms				
Maximum Aggregate Size = 19 mm				
Trial Mixes	Bitumen Content	Bitumen	Aggregate Content	Aggregates
	%	gm	%	gm
1	3.5	42	96.5	1158
2	4	48	96	1152
3	4.5	54	95.5	1146
4	5	60	95	1140
5	5.5	66	94.5	1134

Following separation, the weight of the particles retained on each sieve is determined and the weight of the entire sample is compared. The particle size distribution defined as a percent retained by weight on each filter size is shown in Table 1, Figure 2, Table 2, and Table 3. This approach uses numerous trial aggregate-asphalt binder mixes, each with a different asphalt binder content, to perform this experiment (roughly 5 blends with 3 sample each, for a total of 15 specimens). The best asphalt binder content can then be chosen after carefully examining the performance of each sample blend. The trial blends must have a range of asphalt content above and below the ideal asphalt content in order for this concept to be successful. Therefore, determining the ideal asphalt proportion is the first step in sample preparation.



Figure 2.1: Prepared samples

Trial blend asphalt content is then calculated from this appraisal. The link between asphalt mix density and voids is crucial to JMF design. To create a mix formula, two density values are used: theoretical maximum specific gravity (TMSG) and bulk specific gravity (G<sub>mb</sub>) (G<sub>mm</sub>). The volumetric parameters for the JMF can be computed from the G<sub>mm</sub> value once it has been determined using a standard process recognised by the industry. For density and void calculations, the following calculations are used: (I) Bulk Specific Gravity, G<sub>sb</sub>. (II) Effective Specific Gravity, G<sub>se</sub>. (III) Effective Asphalt, P<sub>be</sub>. V) Air Voids, V<sub>a</sub>. VI) Asphalt-filled Voids, VFA Their calculations and formulas are shown in Figure 2.2, Figure 2.3, Figure 2.4, Figure 2.5, Figure 2.6, and Figure 2.7.

$$G_{sb} = \frac{P_1 + P_2 + \dots + P_N}{\frac{P_1}{G_1} + \frac{P_2}{G_2} + \frac{P_N}{G_N}}$$

Where, G<sub>sb</sub> = Bulk specific gravity for the total aggregates  
 P<sub>1</sub>, P<sub>2</sub>, P<sub>N</sub> = Individual percentages by mass of aggregates  
 G<sub>1</sub>, G<sub>2</sub>, G<sub>N</sub> = Individual (e.g. coarse, fine) bulk specific gravity of aggregates.

Figure 2.2: Formula for bulk specific gravity

$$G_{se} = \frac{P_{mm} - P_b}{\frac{P_{mm}}{G_{mm}} - \frac{P_b}{G_b}}$$

G<sub>se</sub> = effective specific gravity of aggregates  
 G<sub>mm</sub> = maximum specific gravity of paving mixes.  
 P<sub>mm</sub> = percent by mass of total loose mixture=100  
 P<sub>b</sub> = asphalt content at which G<sub>mm</sub> test was performed, percent by total mass of mixture.  
 G<sub>b</sub> = specific gravity of asphalt.

Figure 2.3: Effective Specific Gravity

$$P_{be} = P_b - \frac{P_{ba}}{100} \times P_s$$

P<sub>be</sub> = Effective asphalt content, percent by total mass of mixture  
 P<sub>b</sub> = asphalt content, percent by total mass of mixture.  
 P<sub>ba</sub> = absorbed asphalt, percent by mass of aggregates

Figure 2.4: Effective Asphalt, P<sub>be</sub>

$$VMA = 100 - \frac{G_{mb} \times P_s}{G_{sb}}$$

VMA = voids in the mineral aggregates, percent of bulk volume.  
 G<sub>sb</sub> = bulk specific gravity of total aggregates  
 G<sub>mb</sub> = bulk specific gravity of compacted mixture  
 P<sub>s</sub> = aggregates content, percent by total mass of mixture.

Figure 2.5: Voids in mineral Aggregates

$$V_a = 100 \times \frac{G_{mm} - G_{mb}}{G_{mm}}$$

V<sub>a</sub> = air voids in compacted mixture, percent of total volume.  
 G<sub>mm</sub> = maximum specific gravity of paving mixture (as determined in previous article or as determined directly for a paving mixture by ASTM D2041/AASHTO T209)  
 G<sub>mb</sub> = bulk specific gravity of compacted mixture

Figure 2.6: Air Voids

$$VFA = 100 \times \frac{VMA - V_a}{VMA}$$

VFA = Voids filled with asphalt, percent of VMA  
 VMA = Voids in the mineral aggregates, percent of bulk volume  
 V<sub>a</sub> = air voids in compacted mixture, percent of total volume.

Figure 2.7: Voids filled with Asphalt



### 3.2 Image Acquisition

Images of prepared HMA Asphalt samples were captured by smart phone huawei y6p. Images were captured by a smart phone having 13 megapixels with triple camera. The images of top view were taken as HMA Asphalt samples were homogenous. In pavement homogeneity of HMA Asphalt is due to quality of distribution of aggregate and asphalt. There is no need to capture images of bottom view and side view due to homogeneity of HMA asphalt binder. So, only images of top view were taken to apply computer algorithms to obtain a matrix. The collected images had a 1600 × 720 pixels resolution. For example, there is a Matrix representation for an image as shown in Figure 2.8.

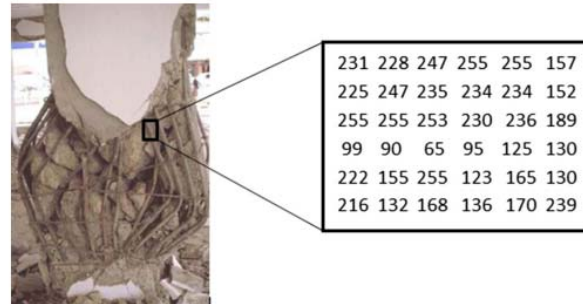


Table 2.8: Matrix representation of an image [11]

### 3.3 Job mix Formula

Furthermore, the distribution of aggregate, aggregate gradation, temperature, and compaction of the asphalt mixture all has an influence on the characteristics of asphalt binder. The Marshall Mix design method consists of six basic steps. (1) Aggregate selection (2) Asphalt binder selection (3) Sample preparation (including compaction) (4) Calculation of density and voids (5) Determining stability using the Marshall Stability and Flow Test. (6) Choosing the best asphalt binder content. The preparation Specimens of HMA asphalt concrete samples containing bitumen and aggregate were examined through density voids calculations, which are given as shown in Table 4, Table 5, Table 6, and Table 7.

Table 4: Binder content for Sakhi Sarwar at 4.4% air voids

Binder Contents (%)	Stability, Kgs	Flow (mm)	Unit Weight Kg/m <sup>3</sup>	Va	VMA	VFA
3.5	718.86	7.05	2302.617	8.09296	16.15	49.8887
4	818.31	7.85	2315.46	8.52705	16.1193	47.1003
4.5	941.16	8	2294.09	9.60295	17.3261	44.5388
5	958.71	8	2323.10	9.70744	16.7191	41.9363
5.5	958.71	7.7	2317.28	7.83236	17.3651	54.896

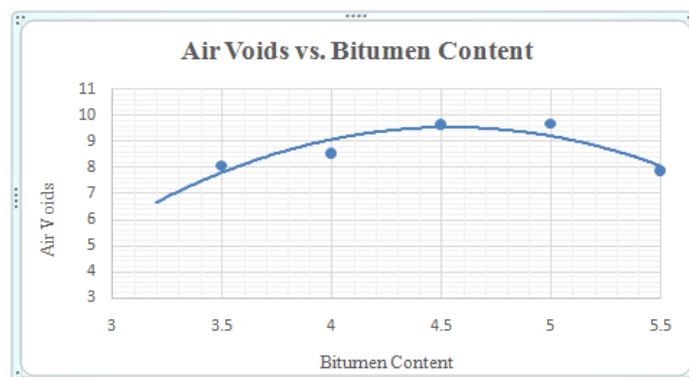




Table 5: Binder content for Sargodha at 4.0% air voids

Binder Contents (%)	Stability, Kgs	Unit Weight Kg/m <sup>3</sup>	Va	VMA	VFA
3.5	950.2	2367.395	5.22103	13.7911	62.142
4	1040.61	2392.84	4.694	13.361	64.7495
4.5	1114.31	2396.25	5.21577	13.644	61.7737
5	1073.37	2407.14	5.31275	13.7064	61.239
5.5	868.2	2396.04	4.98375	14.5564	65.7626

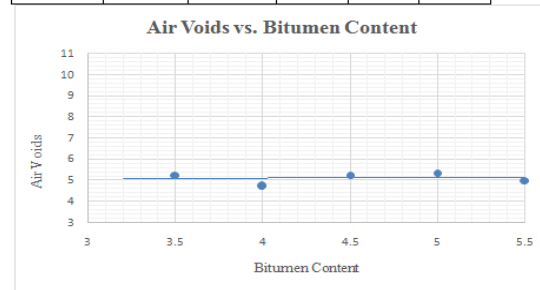


Table 6: Binder content for Rohi at 4.3% air voids

Binder Contents (%)	Stability, Kgs	Unit Weight Kg/m <sup>3</sup>	Va	VMA	VFA
3.5	1052.31	2308.61	6.1658	15.9266	61.2764
4	1166.97	2343.99	5.64762	15.0858	62.5693
4.5	1134.21	2368.63	5.29055	14.6399	63.8622
5	989.13	2346.32	5.97607	15.8868	62.3834
5.5	970.41	2327.36	6.5201	17.0055	61.6589

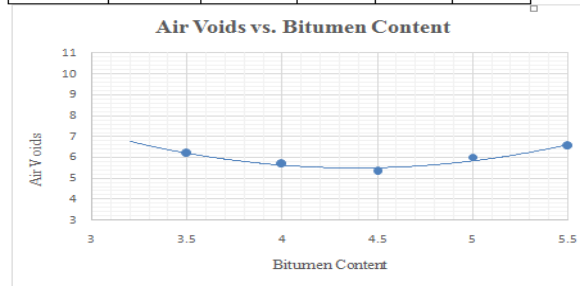
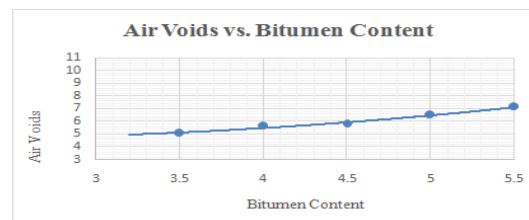


Table 7: Binder content for Margallah at 3.9% air voids

Binder Contents (%)	Stability, Kgs	Unit Weight Kg/m <sup>3</sup>	Va	VMA	VFA
3.5	1072.59	2307.99	5.04	15.95	68.37
4	1078.83	2315.45	5.6	16.11	65.23
4.5	1127.19	2347.36	5.79	15.4	62.35
5	1004.34	2333.28	6.49	16.35	60.15
5.5	970.41	2323.88	7.14	17.12	58.3





## 4 Proposed method (IPAN)

### 4.1 Image processing of samples

Matlab is an image visualization tool, and images were obtained through a smart phone. These images were converted to matrices by computer algorithms. The resolution for images is 720 x 1600 with a 13 megapixel triple camera. Photographs were cut off to confine only the HMA asphalt binder part. True color photographs made up the originals (RGB images). By using Eq(1) to create a weighted sum of the R (red), G (green), and B (blue) components, the RGB images were transformed to grayscale format.

$$GS = 0.298 R + 0.589 G + 0.113 B \quad (1)$$

Where GS is the estimated grayscale component and R, G, and B stand for the red, green, and blue color components of a pixel. The grayscale photographs were then scaled to 256 x 256 pixels in size. The portion of the HMA asphalt sample that was cropped, scaled, grey scaled, and further processed by the computer algorithm to produce the necessary matrix is indicated by the matrix's pixel values[2]. The arithmetic mean, standard deviation, median, third moment, skewness, and entropy were estimated statistical features using Matlab code. The Levenberg-Marquardt mode was used to calculate these statistical characteristics[10]. Figures 3.1 and 3.2 contain their mathematical calculations as well as descriptions of these qualities.

-----

Statistical features.

Feature	Expression	Description
Mean	<i>M</i>	Measure of average intensity
Median	<i>Me</i>	Middle value of pixel in an ordered column
Standard deviation	<i>Std</i>	Measure of average contrast
Third moment	<i>Mo</i>	Measure of the distribution skewness
Entropy	<i>E</i>	Measure of randomness in pixels
Skewness	<i>Sk</i>	Measure of asymmetry in matrix

Figure 3.1: Statistical features.

$$M = \frac{1}{k} \sum_{i=1}^k V_i$$

$$Me = \{(k + 1) \div 2\}^{th}$$

$$Std = \sqrt{\frac{1}{k} \sum_{i=1}^k (V_i - M)^2}$$

$$Mo = \frac{1}{k} \sum_{i=1}^k (V_i - M)^3$$

$$E = - \sum_i p_i \log_2(p_i)$$

$$Sk = \frac{\frac{1}{k} \sum_{i=1}^k (V_i - M)^3}{Std^3}$$

Figure 3.2: Formulas for statistical features

Where k is the total number of data values for the variable, V displays the variables in the digitalized matrix, Me represents the median value of the pixels in the digital images, Std stands for the standard deviation, Mo for the third moment, E is entropy, p represents the normalized histogram counts, and Sk represents the skewness value. As mentioned above, there are six features, which together make up six rows and twenty-four columns (6 x 256).

### 4.2 ANN Modelling

Image processing in Matlab gives a matrix of 256 columns, and that matrix is used as an input value for image processing. Input values have features like mean, mode, standard deviation, third moment, skewness, and entropy. That input value is used for training ANN by the Levenberg-Marquardt model. The output of ANN used for its training is VA, VFA, and VMA. The values for this output are obtained by experiment in laboratory. Data from both the input and the output were normalized to lie between 0 and 1.using Eq. (2).

$$N = (V - Vmin) / (Vmax - Vmin) \quad (2)$$

Where N denotes the normalized value of the variable V, while Vmin and Vmax are the lowest and highest values of the variable V, respectively.



### 4.3 Training and Testing of Data Set

After normalizing the data to a range of 0–1, then that data is used for ANN modelling by the Levenberg-Marquardt model. This program uses the ANN toolbox and we have to choose input and output variables. We will also choose the number of neurons and start training the data with a ratio of 75% training, 15% validation, and 15% testing. After the completion of the process, it will give us three plots. Tables 8 and 9 show regression plots, histogram plots, and error plots. Input is used as input data and output is used as target data.

### 4.4 Practical implementation of image processing

The detection of cracks in asphalt pavement using a convolution neural network [12], using random aggregate packing for computer simulation of the microstructure of asphalt concrete [1], determination of the internal asphalt structure change during the wheel tracking test [13], detection of bugholes on concrete surface [14], to evaluate segregation of compacted asphalt pavement [3] are practical image processing implementations. The practical implementation of this research work is to characterize the HMA asphalt concrete with the use of image processing.

## 5 Results and Discussions

In this study, amalgam of IP and ANN was used to evaluate the properties of the asphalt mixture. In the first step, IP was used to derive the matrix of images, and secondly, the matrix of this image is normalized to a range of 0-1 and thirdly. The data is trained in ANN by using the Levenberg-Marquardt model. Three sets of data are used, i.e., Training, Testing and validation of the data set. After the completion of the process, it will give us three plots. The first is the regression plot, which will give us the R value, the second is the histogram, which shows the precision of data, and the third is the error plot, which will give us the accuracy of data. The results of regression values at the overall stage obtained from the optimized (IP, ANN) model, with  $R = 1$ , are also depicted in Table 9. The regression value shows the accuracy of data being related to the accuracy of the model being developed. These plots are shown above in Table 8 and Table 9, Table 10, Table 11, Table 12, Table 13 and Table 14.

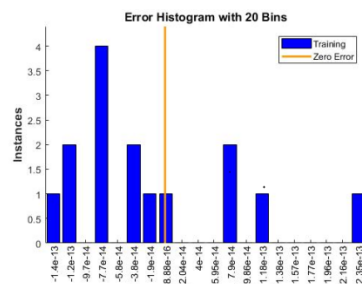


Table 8: Error histogram with 20 bins for Margallah

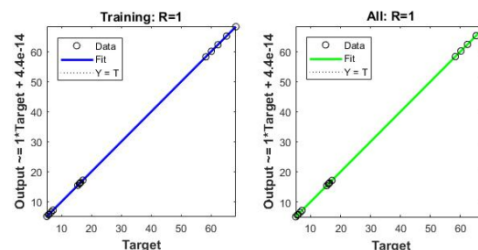


Table 9: Training and testing of data set

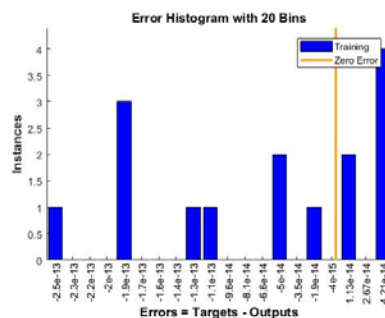


Table 10: Error histogram with 20 bins for Sargodha

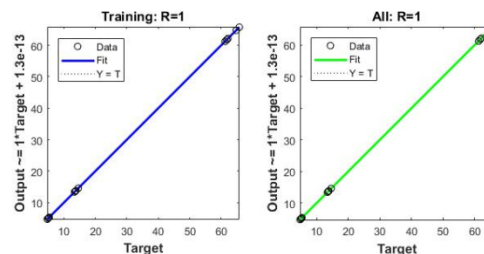


Table 11: Training and testing of data set

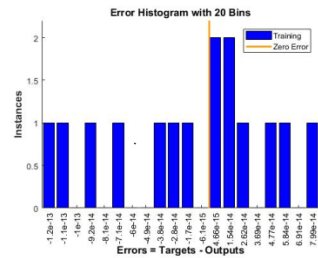


Table 11: Error histogram with 20 bins for Rohi

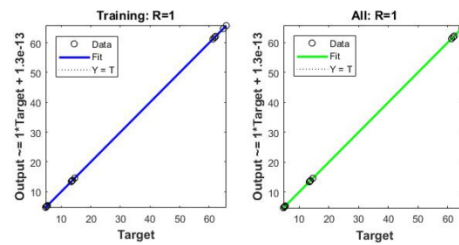


Table 12: Training and testing of data set

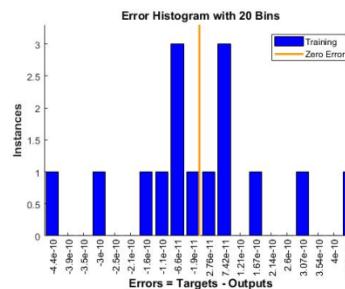


Table 13: Error histogram with 20 bins for Sakhi Sarwar

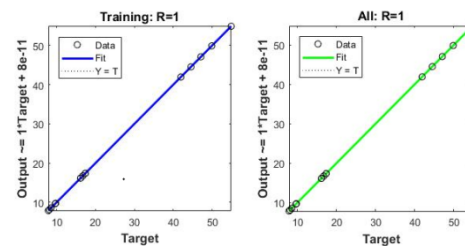


Table 14: Training and testing of data set

The error histogram is the histogram of the errors between the target values and forecasted values after a feed-forward neural network has been trained. These error values, which could be negative, demonstrate the discrepancy between the projected and goal values. Bins are how many vertical bars plotted on the graph. 20 smaller bins comprise the entire error range in this instance. In the case of Margallah, the Y-axis displays the number of instances in each bin of the dataset. For this reason, the height of the bin for the training dataset is greater than but near to 4, and it corresponds to an error of  $7.7 \times 10^{-14}$  in the left side of the plot. It implies that numerous samples from various datasets have an error that falls within the range given below. The error axis's zero error value is expressed by the zero error line (i.e., X-axis). The zero error point in this instance comes under the bin with a left of  $8.86 \times 10^{-14}$ .

The number of samples in a given bin on the dataset is shown on the Y-axis in case of Sargodha. For this purpose, in the right side of graph, there is a bin that corresponds to an error of  $4.21 \times 10^{-14}$ , and for the training dataset, that bin's height is greater than but not quite 4. It means that many samples from different datasets have an error lying in that following range. The zero error point in this instance is within the bin that has a right side of  $-4 \times 10^{-15}$ .

The number of samples in a given bin on the dataset is shown on the Y-axis in case of Rohi. For this purpose, in the right side of graph, there is a bin that corresponds to an error of  $4.66 \times 10^{-15}$ , and that bin's height for the training dataset is greater than but not quite 2. It means that many samples from different datasets have an error lying in that following range. The zero error point in this instance is within the bin having a right side of  $4.66 \times 10^{-15}$ .

The number of samples in a given bin on the dataset is shown on the Y-axis in case of Sakhi Sarwar. For this purpose, in the right or left side of graph, there is bin that corresponds to an error of  $1.9 \times 10^{-11}$ , and For the training dataset, that bin's height is greater than but not quite 3. It means that many samples from different datasets have an error lying in that following range. The zero error point in this instance occurs beneath the bin with a centre of  $4.0 \times 10^{-12}$ .

However, the majority of the error comes inside the range of x-values where you can see the high bars. In the instance of Margallah, all of the error was fairly modest and falls in the range of  $-1.4e0-13$  to  $2.5e0-13$ . Each bar's height represents the total number of tests, or "instances." Take note of how the orange "zero error" line divides the positive and negative ticks. You may establish the bias's direction by looking at the error's sign. On the x-axis label that specifies error as Targets-





Outputs, positive error implies the outputs were less than the targets, and negative error means the targets were greater than the outputs (assuming the targets are positive values). The bulk of outputs were slightly bigger than the targets because the majority of tests were negative.

In case of Sargodha all of the error was quite low and falls in the range of  $-2.5e0-13$  to  $4.2e0-14$  but most of the error falls within the range of x-values where you see the high bars. Take note of how the orange "zero error" line divides the positive and negative ticks. You may establish the bias's direction by looking at the error's sign. On the x-axis label that specifies error as Targets-Outputs, positive error implies the outputs were less than the targets, and negative error means the targets were greater than the outputs (assuming the targets are positive values). Since most tests were negative, most outputs were a little bit greater than the targets. The same is true for Sakhi and Rohi Sarwar. Using IP, these four forms of aggregate describe the asphalt. In tables 15 and 16, a combine model for these four categories of aggregate is displayed.

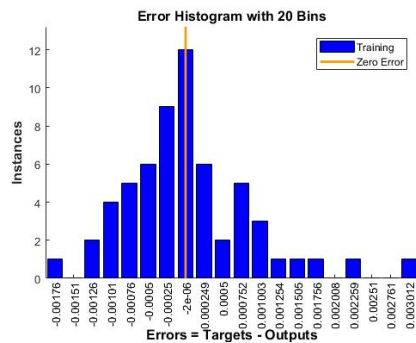


Table 15: A combine model of Data set

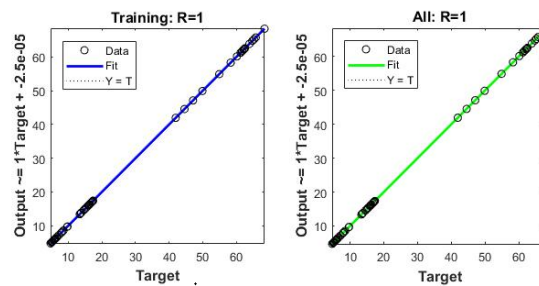


Table 16: A combine model of Regression values

## 6 Conclusion

This study has demonstrated the viability of employing an image processing technology and a smart phone to quantify the properties of HMA asphalt based on job mix formula. A number of image processing techniques are used to obtain data in the shape of a 256-column matrix. To compare the outcomes with those discovered by IP, manual lab tests were also carried out. IP characterization was demonstrated to be quicker and easier. Results from image analysis can be more accurate than those from lab tests. Average values are presented by laboratory testing, and statistical distributions for each parameter are shown by picture analysis. The data sets have a significant impact on the results' correctness. For further study, the proposed method can be used in the field. Images of pavements can be captured and then image processing procedures are adopted. This process helps to predict the properties of asphalt pavement for further study.

## Acknowledgment

The structural engineering department and Engr. Dr. Afaq Ahmed in particular deserve special thanks from the authors for their assistance throughout the research project. We sincerely thank the anonymous reviewers for their thorough analysis and helpful recommendations.

## References

- [1]. Salemi, M. and H. Wang, *Image-aided random aggregate packing for computational modeling of asphalt concrete microstructure*. Construction and Building Materials, 2018. 177: p. 467-476.
- [2]. Muhammad Imran Waris, V.P., Junaid Mir, Nida Chairman, Afaq Ahmad,, *An alternative approach for measuring the mechanical properties of hybrid concrete through image processing and machine learning*, Construction and Building Materials, april 2022. Volume 328, 2022,; p. 16.



- [3]. Cong, L., et al., *A method to evaluate the segregation of compacted asphalt pavement by processing the images of paved asphalt mixture*. Construction and Building Materials, 2019. 224: p. 622-629.
- [4]. Xuelian li, Y.z., Zhanping you, *Homogeneity evaluation of hot in place recycling asphalt mixture using digital image processing technique*. journal of cleaner production, 10 june 2020.
- [5]. Yining zhang, h.c.l., *Determination of volumetric criteria for designing hard asphalt mixture*. Construction and building material, 5 april 2021: p. 12.
- [6]. Ribas, C.Y. and L.P. Thives, *Evaluation of effect of compaction method on the macrostructure of asphalt mixtures through digital image processing under Brazilian conditions*. Construction and Building Materials, 2019. 228: p. 116821.
- [7]. Muhaamed a. abed, z.n.t., *Artificial neural network modeling of the modified hot mix asphalt stiffness using Bending Beam Rheometer*. materials today, 2021.
- [8]. vidhi vyas, a.p.s., *Modeling asphalt pavement condition using artificial neural networks*. materials today proceedings, 2022.
- [9]. masoomah mirrashid, h.n., *Computational intelligence-based models for estimating the fundamental period of infilled reinforced concrete frames*. journal of building engineering, april 2022.
- [10]. Seghier, M.E.A.B., et al., *On the modeling of the annual corrosion rate in main cables of suspension bridges using combined soft computing model and a novel nature-inspired algorithm*. Neural Comput. Appl., 2021. 33(23): p. 15969–15985.
- [11]. gamze dogan, M.h.a., *Concrete compressive strength detection using image processing based new test*. Concrete compressive strength detection using image processing based new test. 2017: p. 12.
- [12]. Nhat-Duc, H., Q.-L. Nguyen, and V.-D. Tran, *Automatic recognition of asphalt pavement cracks using metaheuristic optimized edge detection algorithms and convolution neural network*. Automation in Construction, 2018. 94: p. 203-213.
- [13]. Ni, J.J.F., *Investigation of the internal structure change of two-layer asphalt mixtures during the wheel tracking test based on 2D image analysis*. Construction and Building Materials, 10 june 2019.
- [14]. Baoju Liu, T.Y.a., *Image analysis for detection of bugholes on concrete surface*. Construction and Building Materials, 15 april 2017.



# INFLUENCE OF AGING ON THE PENETRATION PERFORMANCE OF WASTE POLYMER MODIFIED ASPHALT BINDER

<sup>a</sup> Zohra Jabeen\*, <sup>b</sup> Arshad Hussain, <sup>c</sup> Lubna Tabassum

a: School of Civil and Environmental Engineering (SCEE), National University of Science and Technology (NUST) Islamabad, Pakistan, [zaujarehan@gmail.com](mailto:zaujarehan@gmail.com)

b: School of Civil and Environmental Engineering (SCEE), National University of Science and Technology (NUST) Islamabad, Pakistan

c: Design Section, National Highway Authority (NHA) Islamabad, Pakistan

\* Corresponding author: Email ID: [zaujarehan@gmail.com](mailto:zaujarehan@gmail.com)

**Abstract-** A promising strategy that has been widely accepted for improving the pavement deficiencies, is the use of commercial polymers for asphalt binder modification. However, their high cost is the major hurdle in their use, especially in the developing countries. Instead of these commercial polymers researchers are using waste plastic polymers to attain the same benefits. Their cost effectiveness and environment friendly quality is making them the most popular asphalt binder modifier all over the world. The current study aimed at studying the impact of aging on the penetration performance of waste polymer modified asphalt binder. Two such polymers, waste PET (polyethylene terephthalate i.e., plastic bottles) and waste LDPE (low-density polyethylene i.e., plastic bags) were collected from the vicinity, then cleaned, uncapped and shredded to a size less than 0.5mm and blended separately with 60/70 penetration grade bitumen using 2%, 4%, 6% and 8% waste polymers by weight of bitumen. Penetration test was performed on the unaged modified binder samples, short term aged (using rolling thin film oven test (RTFO)) modified binder samples, and long term aged (using pressure aging vessel test (PAV)) modified binder samples. To sum up, it could be said that the use of these non-biodegradable waste polymers enhances the physical performance of the binder and save the cost of material and environment from pollution as well.

**Keywords-** Aging, Modified Asphalt Binder, Waste PET Polymer, Waste LDPE Polymer.

## 1 Introduction

In order to handle the dramatic increase in the traffic volume and the demand for high quality pavement, researchers have been trying hard to improve the comprehensive performance of the asphalt binder by adding different modifiers [1, 2]. The modifier that gained recognition worldwide in pavement industry is polymer. Polymer modification increases the resistance against permanent distresses and failures. It can provide with the improved performance as well as durability. The pavements service life increases and maintenance cost reduced significantly by increasing the viscosity of asphalt binder at higher temperatures and improving the ductility at lower temperatures [3, 4]. Incorporating polymers to asphalt binder could improve the aging resistance [5, 6].

The commercial polymers such as polyethylene and its by products, styrene-butadiene-styrene (SBS), and ethylene-vinyl-acetate (EVA), are being used successfully for flexible pavement quality improvement all over the world, but in developing countries it's use is still limited due to their high cost. Rather in most recent studies waste polymers are being used instead, as a bitumen modifier successfully. They are cost effective and environment friendly, along with the quality of enhancing asphalt binder properties [7, 8]. In other words, we can say that the use of waste polymers results in overall lower product costs as well as is a step towards resolving the non-biodegradable i.e. plastic waste disposal issues without compromising the properties of asphalt binder rather enhancing the flexible pavement quality [9].



In Pakistan one kilometer patch of road has been constructed in Islamabad at Ataturk Avenue as a trial section using different waste polymers. So, there is a dire need to dig into details related to the use of such polymers in our country efficiently. Present study focuses on the use of these locally available waste polymeric additives as a modifier, than thoroughly examining the aging phenomenon on the penetration performance of modified asphalt binder. The aging of waste polymer modified asphalt binder is observed with RTFO and PAV in laboratory. Penetration test was then conducted for different samples of aged and unaged WPMB.

## 2 Research Methodology

The methodology used in carrying out this detailed research is summed up in a hierarchical chart as shown in figure 1. First of all, material was selected and then conventional testing i.e., Penetration test, was carried out after modifying the bitumen with waste PET and waste LDPE respectively.

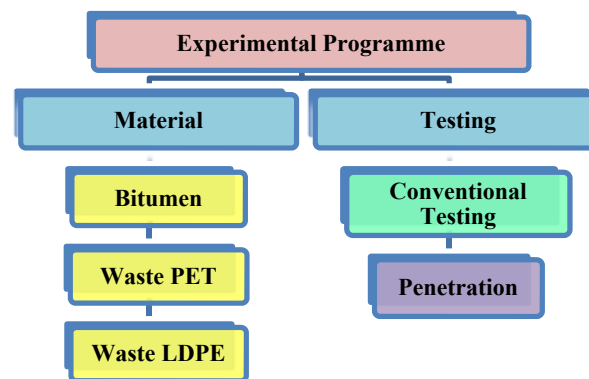


Figure 1: Hierarchical chart of Experimental Work

### 2.1 Material Selection

The selection of the materials was carried out by keeping in view their availability and cost efficiency. Researchers are using waste polymers like waste rubber and waste plastic successfully, instead of commercial polymers [10-14]. Keeping in view the facts and figures, following mixture of materials were used for preparation of modified binder samples.

- 60/70 Asphalt binder
- Waste polyethylene terephthalate (PET)
- Waste low density polyethylene (LDPE)

#### 2.1.1 Asphalt Binder

The Penetration grade of 60/70 bitumen was acquired by the Attock Refinery Limited (ARL) Rawalpindi, and used as a base binder. In Pakistan the above-mentioned grade is used mostly. It performs better in colder regions as well as intermediate temperature regions. Moreover, it was easily and abundantly available in our area.

#### 2.1.2 Waste Polyethylene Terephthalate (PET)

Polyethylene terephthalate a non-biodegradable waste, is a thermoplastic polymer. It is a clear and strong plastic that is commonly used for food packaging. Mineral water and soft drink bottles are mostly made by this PET plastic. In this research local waste plastic bottles as shown in figure 2a with PET code i.e., 1, were collected after proper identification. Then after removal of the stickers, caps, and cap rings the bottles were washed and dried. After that they were shredded to a size  $\leq 0.5\text{mm}$  as shown in figure 2b, with the help of shredding machine.

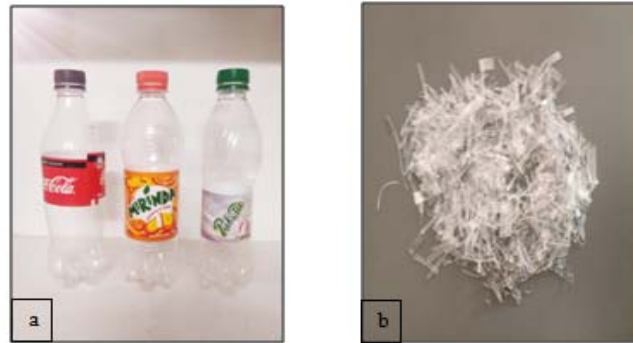


Figure 2:(a) Waste PET Plastic Bottles;(b) Waste Shredded PET Plastic

### 2.1.3 Waste Low-Density Polyethylene (LDPE)

Low-density polyethylene (LDPE) another non-biodegradable waste having chemical formula  $(C_2H_4)_n$ , is also a thermoplastic made from the monomer ethylene. Its most common use is in plastic bags. In this research local waste plastic bags with LDPE code were collected after proper identification, cleaned and shredded to a width  $\leq 1$ mm and length  $\leq 15$  mm. Figure 3 shows the waste plastic bags, code of LDPE plastic polymer and its shredding.



Figure 3: (a) Waste LDPE Plastic bags; (b) LDPE Plastic Code; (c) Shredded Waste LDPE Plastic

## 2.2 Preparation Of Waste Polymer Modified Asphalt Binders

Samples were prepared by adding waste polyethylene terephthalate (W-PET) into 60/70 penetration grade in different percentages i.e., 2%, 4%, 6% and 8% by weight of the base binder. A measured amount of neat binder for each percentage of modifier, was liquefied by heating till  $180^{\circ}C$  and then premeasured shredded waste PET was gradually added. High-rate shear mixer was used keeping the temperature  $180^{\circ}C$  at 2000 rpm, for about 60 minutes, to get homogeneous blend. In order to avoid segregation and maintain uniform distribution, waste modified asphalt binder was prepared in small quantity as needed and was used for sample preparation right after that.

Same procedure was adopted for the preparation of W-LDPE modified asphalt binder samples at four different percentages i.e., 2%, 4%, 6% and 8% by weight of the base binder. Mixing was done at  $170^{\circ}C$  and 2000 rpm, for about 40 minutes to get homogeneous blends.

## 2.3 Aging

Aging is the change in chemical composition of bitumen due to atmosphere and the high temperatures [15]. In laboratory, the effect of short-term aging was stimulated by Rolling Thin Film Oven (RTFO). The temperature in RTFO was  $163^{\circ}C$  and the samples were aged in the chamber for 80 minutes. To simulate the effect of in-service aging (long term aging) of asphalt binder Pressure Aging Vessel (PAV) was used. The samples were kept under high temperature i.e.  $100^{\circ}C$  and high pressure i.e. 2.1 MPa for 20 hours.



### 3 Material Testing

Conventional test was performed on virgin, aged, modified aged and modified unaged asphalt binder samples. Modified asphalt binder was obtained through extensive physical testing by determining an optimum content of waste PET and waste LDPE.

The test include penetration for determining consistency of bitumen at room temperature (AASHTO Specification T49). In this test, a standard loaded needle is vertically penetrated in the sample of asphalt binder under standard condition and its penetration depth is measure up to tenths of a millimeter. Penetration values are more for softer binder. According to AASHTO T49-03 temperature was maintained at 25°C, load was 100 grams, and the test time was 5 seconds. Using ARL 60/70 specimen, three values from each specimen were taken after performing penetration tests. The results of the test were shown on a screen attached with the penetrometer. All values obtained fulfilled the required criteria as per specification.

### 4 Results

In current research, the influence of aging on penetration performance of unaged and aged modified binder samples was analyzed using aging index. Aging index is basically the ratio of physical/performance property of aged binder to the same property of unaged binder. The aging index used in this research work includes penetration aging ratio (PAR). It is calculated by formula given below:

$$\text{Penetration Aging Ratio (PAR)} = \frac{\text{Aged Penetration Value}}{\text{Unaged Penetration Value}} \times 100$$

#### 4.1 Penetration Test

The penetration value is used to show the stiffness as well as hardness of the binder at 25°C. Lower penetration value indicates that binder has become stiff. From the results, it is observed that after increasing the waste polymer content from 2% to 8%, decrease in the penetration value of asphalt binder is considerable. This shows that the consistency of the modified asphalt binder increased at normal temperature. The results are based on the average of two readings as shown in table 1.

Table 1: Penetration results for W-PET modified Asphalt Binder

Additive rate	Penetration		
	Unaged	RTFO aged	PAV aged
0%	65	59	48
2%	57	48	40
4%	49	40	33
6%	41	31	26
8%	38	27	22

The decrease in the penetration value of 4% waste PET modified asphalt binder is 25% as shown in figure 4, whereas it is 21% in case of waste LDPE modified asphalt binder as compared to the unmodified binder as shown in figure 6. This decrease is the indication of the higher stiffness by the addition of polymers, that makes them perfect for warmer regions. Figure 5 and 7 represents the results of PAR for unmodified and waste polymer modified binder after the short term and long-term aging. It is observed that penetration values of unmodified and modified binder decreased after aging. Moreover, higher the waste content, lower the value of penetration aging ratio that shows reduction in the degree of aging. Therefore, waste polyethylene terephthalate and waste low density polyethylene addition improves the binder's resistance to oxidative aging.

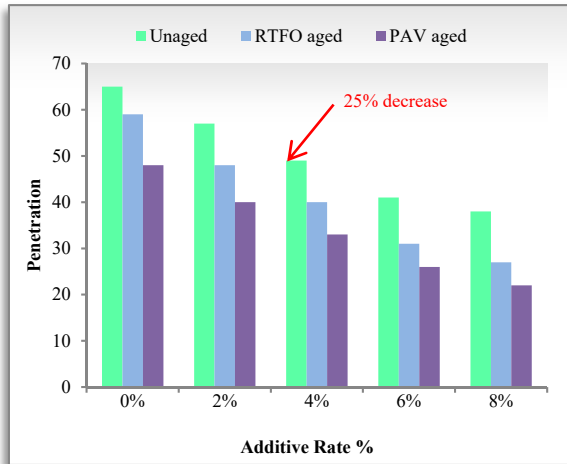


Figure 4: Penetration Values of W-PET Modified Binder



Figure 5: PAR Graph for W-PET Modified Binder

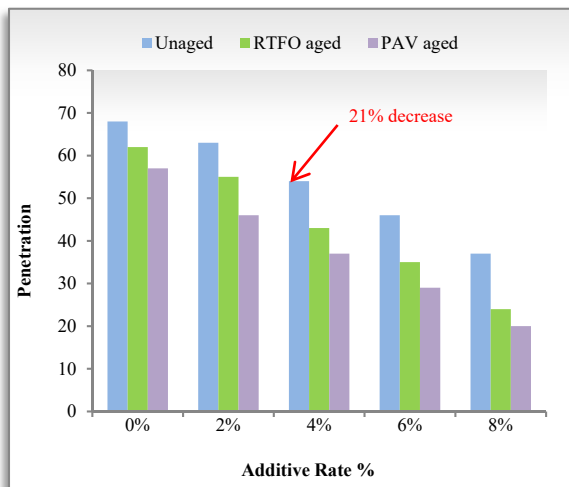


Figure 6: Penetration values of W-LDPE Modified binder

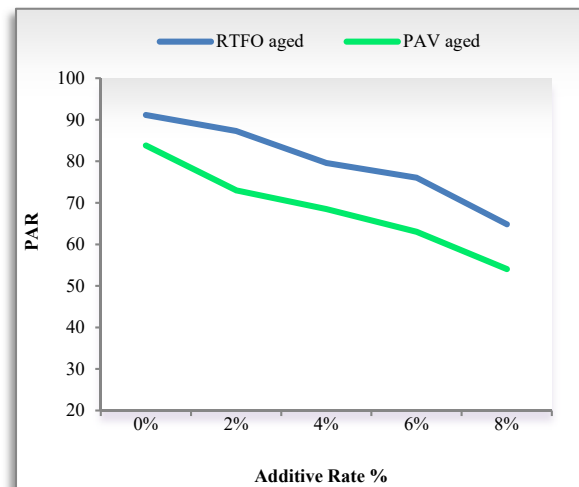


Figure 7: PAR Graph for W-LDPE Modified Binder

## 5 Conclusions

After successful completion of extensive lab testing, carried out in an effort to obtain the targeted objectives of this research work, the below mentioned conclusions could be derived.

- 1 Results indicate that the addition of W-PET and W-LDPE improved the penetration performance of the binder.
- 2 Penetration value of the W-PET modified and W-LDPE modified binder decreased by 25% and 21% respectively, which indicate high resistance of the modified binder against rutting due to improved stiffness.
- 3 Penetration aging ratio at 4% addition of the waste polymers decreased by 10% for W-PET and 12% for W-LDPE after the short-term aging which indicate binders improved resistance to oxidative aging.

## 6 Recommendations

- 1 Investigations should be done by using different combinations of plastic wastes as an asphalt binder modifier and evaluate their effects on physical and performance properties before and after aging.
- 2 Effect on the low temperature performance and effect on Fatigue properties of asphalt binder and asphalt should be studied before implementing W-PET and W-LDPE modified asphalt binders in cold areas.



## References

- [1] S. R. Karnati, D. Oldham, E. H. Fini, and L. Zhang, "Surface functionalization of silica nanoparticles to enhance aging resistance of asphalt binder," *Construction and Building Materials*, vol. 211, pp. 1065-1072, 2019.
- [2] C. Zhu, H. Zhang, D. Zhang, and Z. Chen, "Influence of base asphalt and SBS modifier on the weathering aging behaviors of SBS modified asphalt," *Journal of Materials in Civil Engineering*, vol. 30, no. 3, p. 04017306, 2018.
- [3] A. Behnood and M. M. Ghahreveran, "Morphology, rheology, and physical properties of polymer-modified asphalt binders," *European Polymer Journal*, vol. 112, pp. 766-791, 2019.
- [4] L. Zani, F. Giustozzi, and J. Harvey, "Effect of storage stability on chemical and rheological properties of polymer-modified asphalt binders for road pavement construction," *Construction and building materials*, vol. 145, pp. 326-335, 2017.
- [5] A. Diab, M. Enieb, and D. Singh, "Influence of aging on properties of polymer-modified asphalt," *Construction and Building Materials*, vol. 196, pp. 54-65, 2019.
- [6] P. Lin, W. Huang, X. Liu, P. Apostolids, H. Wang, and C. Yan, "Laboratory evaluation of the effects of long-term aging on high-content polymer-modified asphalt binder," *Journal of Materials in Civil Engineering*, vol. 32, no. 7, p. 04020157, 2020.
- [7] I. B. Joohari and F. Giustozzi, "Waste tyres crumb rubber as a sustainability enhancer for polymer-modified and hybrid polymer-modified bitumen," *International Journal of Pavement Engineering*, pp. 1-15, 2021.
- [8] S. Nizamuddin, Y. J. Boom, and F. Giustozzi, "Sustainable polymers from recycled waste plastics and their virgin counterparts as bitumen modifiers: A comprehensive review," *Polymers*, vol. 13, no. 19, p. 3242, 2021.
- [9] Z. N. Kalantar, M. R. Karim, and A. Mahrez, "A review of using waste and virgin polymer in pavement," *Construction and Building Materials*, vol. 33, pp. 55-62, 2012.
- [10] C. Brovelli, M. Crispino, J. Pais, and P. Pereira, "Using polymers to improve the rutting resistance of asphalt concrete," *Construction and Building Materials*, vol. 77, pp. 117-123, 2015.
- [11] A. Cuadri, M. García-Morales, F. Navarro, and P. Partal, "Isocyanate-functionalized castor oil as a novel bitumen modifier," *Chemical Engineering Science*, vol. 97, pp. 320-327, 2013.
- [12] C. Fang, R. Yu, Y. Zhang, J. Hu, M. Zhang, and X. Mi, "Combined modification of asphalt with polyethylene packaging waste and organophilic montmorillonite," *Polymer Testing*, vol. 31, no. 2, pp. 276-281, 2012.
- [13] C. Fuentes-Audén *et al.*, "Evaluation of thermal and mechanical properties of recycled polyethylene modified bitumen," *Polymer Testing*, vol. 27, no. 8, pp. 1005-1012, 2008.
- [14] E. González, L. M. Costa, H. M. Silva, and L. Hilliou, "Rheological characterization of EVA and HDPE polymer modified bitumens under large deformation at 20 C," *Construction and Building Materials*, vol. 112, pp. 756-764, 2016.
- [15] O. Sirin, D. K. Paul, and E. Kassem, "State of the art study on aging of asphalt mixtures and use of antioxidant additives," *Advances in Civil Engineering*, vol. 2018, 2018.





# EFFECT OF AGGREGATE REPLACEMENT WITH WASTE TIRE RUBBER ON PROPERTIES OF CONCRETE – AN OVERVIEW

*<sup>a</sup> Syed Bilal Hussain Shah, <sup>b</sup> Shehryar Ahmed\**

a: Department of Civil Engineering, Abasyn University Islamabad, [bilal.shah20151@gmail.com](mailto:bilal.shah20151@gmail.com)

b: Department of Civil Engineering, Abasyn University Islamabad, [enr.shehryar@outlook.com](mailto:enr.shehryar@outlook.com)

\* Corresponding author: Email ID: [enr.shehryar@outlook.com](mailto:enr.shehryar@outlook.com)

**Abstract-** Tire rubber never decomposes, hence it's a waste product. When tires are piled up at landfills, harmful chemicals are released into the air, ground, and water. Toxic black smoke may be emitted into the air when rubber tires catch fire. Many of the dangerous compounds typically utilized in tire manufacture may be found in this smoke. There are chemical substances in this Fire that are wiped away when water is sprayed. These pollutants then permeate the soil and contaminate lakes and ponds. In this situation, it is preferable to repurpose rubber. This paper focuses on the strategies adopted by researchers to utilize waste rubber as an additive in concrete. Studies have been conducted for the replacement of coarse and fine aggregate ranging from 0-100% and investigation of mechanical properties including flexural strength, tensile strength, compressive strength and physical properties including ductility, unit weight density, etc. have been part of the studies. Dynamic properties like impact resistance and energy absorption have been investigated at different ages and results were compared with normal concrete (NC). It has been discovered, as a result, that rubberized concrete (RC) is better in durability, ductility, lightweight, and has greater crack resistance but reduced mechanical properties. However, RC's capacity of energy absorption and impact resistance is higher than NC. The mechanical properties of RC can be enhanced by adding different types of admixtures.

**Keywords-** Rubberized Concrete, Mechanical Properties, Dynamic Properties, Physical Properties, Energy Absorption.

## 1 Introduction

One of the causes of environmental pollution includes the decomposition of waste tire rubber. It is observed that a large amount of waste rubber requires a large area or site for deposition. Waste rubber produces harmful chemicals which are dangerous to the environment and soil. The world is facing a challenging problem because rubber is nondegradable. Rubber waste recycling is a considered option. Concrete is one of the most commonly used building materials in the world today. A portion of sand or coarse aggregate may be replaced with recycled rubber in concrete. The sustainability of natural resources, primarily aggregate, is a primary issue because concrete is the most widely used man-made construction material. Utilizing waste tires in the manufacturing of concrete efficiently addresses the issues related to waste tire disposal and a sustainable approach toward natural resources [1]. The RC's thermal insulation, electrical resistance, freezing resistance, ductility strain capacity, energy absorption, and impact energy can all be enhanced by the addition of rubber [2]. According to [3], 37 million truck tires are thrown away in the UK each year, and this number is expected to rise in the future. Rubber waste is a very long-lasting product [4]. Thus, the removal of non-usable tires is the main issue. The concrete mix in which rubber is added is known as rubber-treated concrete. Partial substitution of coarse or fine aggregates in concrete further enhances its characteristics like unit weight, high impact resistance, and impact resistance ability. Also, the addition of rubber shows high durability. RC shows better results where the above-mentioned properties are required.



Three aspects, including slump, air void, and density, are examined in the physical characteristics of rubberized concrete. In a study, it was found that adding rubber crumbs to freshly laid concrete has a severe impact on the slump values [5]. In almost every type of structure, reinforced concrete and steel are the essential elements. These elements provide structural integrity to building structures. The lifecycle of concrete is affected by different factors which include: extreme weather conditions, higher temperatures, and climate change. These factors sometimes lead to premature deterioration. As the world is progressing towards sustainable energy and technology, the efforts for sustainable technologies can contribute greatly to the maintenance of infrastructures.



Figure 1: Crumb rubber particles

Figure 1 shows the crumb rubber generated from waste rubber tires. The findings demonstrate that using rubberized concrete will sustainably reuse waste material to assist in protecting the environment and save natural aggregates [6]. This paper reports a comprehensive comparison of mechanical, physical and dynamic properties of rubberized concrete with normal concrete. Role of rubber addition in modifying concrete's properties has been highlighted. Key parameters have been identified and recommendations are made for future research directions.

## 2 Mechanical Properties of RC

[4] evaluated the compressive load-bearing capacity of RC columns and found that the inclusion of rubber in the columns lowered their load-carrying capacity. This is due to the specific gravity of rubber which is much lower than fine aggregate [5] Used split Hopkinson pressure bar (SHPB) set up to find the compressive strength and the results showed a decrease in compressive strength from 50.12 MPa NC to 17.91 MPa RC at 50% replacement. Split tensile strength decreased from 4.60 MPa to 2.21 MPa at 50% replacement. [8] investigated compressive strength using the SHPB system, findings suggest that increasing rubber particles reduces compressive strength and flexural strength of rubber-treated concrete. Research also stated it is advised that replacement should not exceed 30%. Although, the compressive strength of RC starts decreasing after 7 and 28 days. The findings reveal that 0%, 1.75%, 3.25%, and 7.0% addition are equivalent to NC in terms of split tensile strength, which ranges from 4.46MPa to 4.48MPa [9]. When rubber is added to concrete, the tensile strength is somewhat improved [10]. The compressive and tensile strength of rubber-treated concrete was estimated at 7 and 28 days. The results show 10%, 20%, 30%, 40%, and 50% rubber content reduces the compressive strength by 17.7%, 39.9%, 54.1%, 62.0% and 72.2% at 7 days and 21.3%, 37.9%, 54.3%, 62.5% and 66.4% at 28 days, respectively [11]. RC's compressive strength can be enhanced by the addition of silica fume. Strength increased from 1.52MPa to 1.79MPa at 7 days and 1.66MPa to 1.93 MPa at 28 days when 5% silica and 40% rubber were added. These improvements result from pozzolanic reactions between silica fume and free calcium hydroxide in the paste, as well as mechanical improvements brought on by the addition of a very fine powder to the cement paste mixture [12]. When crumb rubber and steel fibers are added in various amounts of 5%, 15%, and 25% by volume of fine aggregate, compressive strength decreases by 12%, 24%, and 43% after 90 days [13]. Compressive strength decreased with increasing rubber concentration, whereas rubber particles containing ground granulated blast furnace slag (GGBFS) showed relatively less decrement in strength [14]. Pretreatment of rubber has positive impacts on compressive and split tensile properties of RC. The addition of rubber particles produces a negative impact on compressive strength [15]. Strength decrement in RC is caused due to poor bonding between rubber particles and concrete matrix [16,17].



Table 1: Mechanical properties of RC

References	Specimens	Properties Investigated	Output (RC Vs NC)
[9]	Cylinder 100×200 mm 50×300 mm	Compressive strength Split tensile strength	-37% Decreased -8.7% Decreased
[10]	Cylinder 150×300 mm 63.5×150 mm	Compressive strength Split tensile strength	-63% Decreased -56.48% Unchanged
[12]	Cubes 100×100×100 mm 150×150×150 mm	Compressive strength Split tensile strength.	-70% Decreased 38.55% Increased
[15]	Cylinder Beams 150×300 mm 150×150×600 mm	Compressive strength split tensile strength	-59.22% Decreased -31.93% Decreased
[24]	Cylinder 150×300 mm	Compressive strength Split tensile strength	-51.12% Decreased -21.61% Decreased

A Series of tests were conducted and obtained results show that compressive strength was reduced by 10%, 18%, and 20% for 5%, 10%, and 15% replacement, and flexural strength decreased up to 14% for 15% replacement [18]. [19] found that the mechanical properties of RC decreased as rubber content increased, much as the split and flexural strength inflection points between 40% and 60% rubber substitution. Untreated RC has shown lower compressive strength than treated RC, according to a study in [20]. The compressive strength of treated RC is 24% more than NC. Also, pretreated RC has a greater split tensile strength than untreated RC however, this only increases by 20% in the case of a 20% replacement. The compressive strength of pretreated RC was found to be 92.62% less than NC, however, flexural strength was found to be 130% greater in treated RC when 5% of the treated rubber was substituted for the NC [21].

In comparison to NC, the tensile strength of treated RC is 2.67 times greater. Rubber particles have low specific gravity, which reduces the compressive strength of concrete when they are substituted with coarse aggregate [22]. Concrete's compressive strength decreases with increasing rubber content. Replacement of rubber by 10% to 50% resulted in a 20% to 85% decrease in compressive strength [23]. When epoxy resins were added to RC as an additive, the compressive strength of the concrete increased for 28 days. The reason reported was that the epoxy is an adhesive material that facilitates the enhancement of bonding between cement matrix and rubber particles despite a progressive decline in the concrete's compressive strength over time. At 28 days, epoxy resin admixture improves the split tensile strength. flexural and compressive strength of RC with and without 1% superplasticizer addition as rubber content was increased, compressive strength decreased. However, mixing admixtures increased compressive strength a little. The RC's flexural strength improved, while the addition of mixing admixtures increased strength even more [25]. Compressive and split-tensile characteristics of RC have been studied, the findings showed that rubber inclusion lowered the strength of concrete, but a 25% substitution yielded substantial results [26].

### 3 Physical Properties of RC

[14] found that the slump and unit weight of RC was reduced as the percentage of rubber particles increased, with a decrease in a slump from 220 mm to 185 mm and an increase in air content. Rubber in concrete reduces concrete's workability owing to rubber's high-water absorption, hence as rubber percentage increases, so decrease RC's unit weight. As a result of its lower unit weight, RC contains a larger percentage of air. Due to rubber's elastic characteristics, RC has a greater modulus of elasticity than NC [17]. When rubber content was increased in RC, the unit weight decreased. With a 15% substitution of rubber aggregate, water absorption of RC increased by 8% during 28 days [18]. The low binding strength of the cement paste to the rubber reduces the workability of both treated and untreated RC [21]. RC's dry unit weight decreased as the rubber content increased, resulting in a 33% decrease in 25-mm aggregate density and a 46% decrease in 12.5-mm aggregate density with 50% replacement. Rubber content has a direct correlation to porosity in RC. The permeability of RC varies from 0.25 to 0.61 cm/s depending on the proportion of rubber in the concrete. There is no change in unit weight when 10% rubber, is added to concrete [11]. The water absorption of rubber-treated concrete increases with the addition of more rubber particles. Whereas the modulus of elasticity decreases when rubber content is raised by 10%, 20%, 30%, and 50%. Water absorption is not significantly altered by a 10% replacement.



Table 2: Physical properties of RC

References	Specimens	Properties	Replacement	Output (RC Vs NC)		
[17]	Column Specimens	240×1500 mm 400×400×1200 mm 350×350×350 mm	Unit weight Air content	25-100% -12% +172%	Decreased Increased	
[18]	Cylinder Beams	150×300 mm 150×150×762 mm	Unit weight. Water absorption	0-15%	-7% +8.6%	Decreased Increased
[22]	Cubes	150×150×150 mm	Unit weight	0-15%	-14.33%	Decreased
[23]	Cubes	150×150×150 mm	Porosity Permeability	0-50%	59%	Increased Increased
[29]	Cubes	150×150×150 mm	Density	5-20%	-92.213%	Decreased

## 4 Dynamic Properties and Impact Resistance of RC

Table 3: Dynamic properties and energy absorption of RC

References	Specimens	Properties Investigated	Output (RC Vs NC)		
[13]	Cube Beam	100×100×100 mm 100×100×500 mm	Impact energy absorption	+171% Increased	
[12]	Cubes	100×100×100 mm 150×150×150 mm	Impact resistance Energy absorption	+239% +9.46%	Increased Increased
[14]	Cube Prism	150×150×150 mm 70×70×100 mm	Energy absorption	+24%	Increased
[27]	Cylinder	150×300 mm	Impact resistance	+2%	Increased
[32]	Railway sleeper	63×250 mm	Impact resistance Impact strength	+50% +40-60%	Increased Increased

RC absorbs more energy than NC, as shown by a 0.5 kg steel ball drop test from a standard height of 1 m [14]. The higher the rubber content, the greater the energy absorption capacity. A 5%, 15%, and 25% rubber replacement yields 3.682, 4.083, and 4.586 kgm<sup>2</sup>/sn<sup>2</sup> respectively. According to [27], a 65 kg mass was dropped from 650 mm height and the impact resistance of RC was better than that of NC, making it suitable for highway barriers. Using both computational and experimental data, [28] demonstrated that RC with steel reinforcement resists blast loading. [29] calculated the damping ratio of RC, results show that crumb RC dissipated energy about 2.6 times the energy dissipated by NC. Slightly reduction in crumb RC decreased energy dissipation by 1.8% compared to NC.

The impact resistance of RC is higher than NC, this is because of the elastic nature of rubber [18]. It was noted that RC has a high dynamic compressive strength. RC has been studied for its dynamic properties, and the results reveal that it has stronger impact resistance and energy absorption than NC. RC offers a higher impact strength than NC [32]. Concrete's impact energy was improved by the addition of steel fibers to crumb rubber. Replacement of 5%, 15%, and 25% increased impact energy by 30.6%, 66.6%, and 70.6%, respectively [13].

## 5 Practical Application of Rubberized Concrete

Significant increment in dynamic properties makes rubberized concrete an efficient material for energy absorption and toughness relied applications. Structures, where strength requirement is not the primary objective and dissipation of stresses through energy absorption is desired, rubberized can play a vital role instead of normal concrete. In addition, structures subject to impulsive loading like bridge piers and roadside barriers can have enhanced toughness through utilization of rubberized concrete.



## 6 Conclusions

The following conclusions can be drawn from this study:

- 1 Greater rubber content results in decreased mechanical properties but increased dynamic and impact resistive properties of rubberized concrete. However, both positive and negative aspects have been discovered in response to physical properties.
- 2 The negative results have an obvious reason of poor bonding between rubber particles and cement paste but pretreatment of rubber enhances the mechanical properties of concrete.
- 3 Crumb rubber replacement with fine aggregates shows better results instead of coarse aggregate.

Admixtures like silica fume, epoxy resins, superplasticizer, etc. can be utilized for better mechanical properties by improving the bond strength of rubber particles and cement paste. A thorough study needs to be conducted to identify the most suitable admixture that could result be used for enhancement of mechanical properties. In addition, comparison of strength properties through different pretreatment techniques of rubber should be investigated.

## Acknowledgment

The primary author would like to acknowledge the sincere efforts of the supervisor in providing continuous guidance. The careful review and constructive suggestions by the anonymous reviewers are gratefully acknowledged.

## References

1. M. Adamu, S. I. Haruna, Y. E. Ibrahim, and H. Alanazi, "Investigating the properties of roller-compacted rubberized concrete modified with nano silica using response surface methodology," *Innovative Infrastructure Solutions*, vol. 7, pp. 1--13, 2022.
2. T. . M. Pham , . N. Renaud , V.-L. Pang, . F. Shi , H. Hao and . W. Chen, "Effect of rubber aggregate size on static and dynamic compressive properties of rubberized concrete," *Structural Concrete*, 2021.
3. K. B and R. Kigali, "A review on construction technologies that enable environmental protection: RC," *Am. J. Eng. Appl. Sci.*, vol. 1, pp. 40-44, 2008.
4. S. Ki Sang, I. Hajirasouliha and K. Pilakoutas, "Strength and deformability of waste tire rubber-filled reinforced concrete columns.," *Construction and building materials*, vol. 25.1, pp. 218-226, 2011.
5. H. Hasani, S. M. Mosavi Nezhad, A. Soleymani, F. S. Aval and H. Jahangir, "The Influence of Treated and Untreated Crumb Rubber on," pp. 0-9, 2022.
6. E. A. Alwesabi, B. A. Bakar, I. M. Alshaikh, A. M. Zeyadc, and H. Alghamdid , "Experimental investigation on fracture characteristics of plain and rubberized concrete containing hybrid steel-polypropylene fiber," *Structures* , vol. 37, pp. 379--388, 2021.
7. F. Wanhui, F. Liu, F. Yang, L. Li and L. Jing, "Experimental study on dynamic split tensile properties of RC," *Construction and Building Materials*, vol. 165, pp. 675-687, 2018.
8. F. Wanhui, F. Liu, F. Yang, L. Li, L. Jing, B. Chen and B. Yuan, "Experimental study on the effect of strain rates on the dynamic flexural properties of RC," *Construction and Building Materials*, vol. 224, pp. 408-419, 2019.
9. Y. Osama, M. A. ElGawady, J. E. Mills and X. Ma, "An experimental investigation of crumb RC confined by fibre reinforced polymer tubes," *Construction and Building Materials*, vol. 53, pp. 522-532, 2014.
10. G. Nagib N, C. A. Issa and S. Fawaz, "Effect of construction joints on the splitting tensile strength of concrete," *Case Studies in Construction Materials*, pp. 83-91, 2015.
11. Y. Osama, R. Hassanli and J. E. Mills, "Mechanical performance of FRP-confined and unconfined crumb RC containing high rubber content," *Journal of Building Engineering*, vol. 11, pp. 115-126, 2017.
12. L. Hai-long, Y. Xu, P.-y. Chen, J.-j. Ge and F. Wu, "Impact energy consumption of high-volume RC with silica fume," *Advances in Civil Engineering*, 2019.
13. N. A. Tareq, B. H. Abu Bakar and H. Md Aki, "Influence of crumb rubber on impact energy of steel fiber concrete beams," *Applied Mechanics and Materials*, vol. 802, pp. 196-201, 2015.
14. O. Erdogan, M. Lachemi and U. K. Sevim, "Compressive strength, abrasion resistance and energy absorption capacity of RCs with and without slag," *Materials and structures*, vol. 44(7), pp. 1297-1307, 2011.
15. D. Michelle, E. Cano and J. Pena, "Use of recycled tires as partial replacement of coarse aggregate in the production of concrete," *Purdue University Calumet*, 2006.



16. K. Zaher K and F. M. Bayomy, "Rubberized Portland cement concrete," *Journal of materials in civil engineering*, vol. 3, pp. 206-213, 1999.
17. B. Chen and L. Ning, "Experimental research on properties of fresh and hardened RC," *Journal of Materials in Civil Engineering*, vol. 8, p. 04014040, 2014.
18. S. S. F. A, A. Naseer, A. A. Shah and M. Ashraf, "Evaluation of thermal and structural behavior of concrete containing rubber aggregate," *Arabian Journal for Science and Engineering*, vol. 39, pp. 6919-6926, 2014.
19. N. M. Miller and F. M. Tehrani, "Mechanical properties of rubberized lightweight aggregate concrete," *Construction and Building Materials*, Vols. 264-271, pp. 264-271, 2017.
20. S. Dhiman, R. Garg and S. Singla, "Experimental investigation on the strength of chipped rubber-based concrete," *IOP Conference Series: Materials Science and Engineering*, vol. 961, p. 012002, 2020.
21. T. Shahid Rasool, "Effect of partial replacement of coarse aggregates in concrete by untreated and treated tire rubber aggregates," *International Journal of Advanced Science and Research*, vol. 1, pp. 65-69, 2018.
22. C. A, "Partial Replacement Of Coarse Aggregate In Concrete By Waste Rubber Tire," *International Journal of Engineering and Techniques*, vol. 5, pp. 88-95, 2017.
23. J. A. T and Z. H. Abdulabbas, "Production of sustainable pervious concrete by using waste tires rubber as partial replacement of coarse aggregate," *In AIP Conference Proceedings*, vol. 2213, p. 020221, 2020.
24. A. Khitab, S. Ahmed, I. Arif, F. A. Awan, A. Anwar, A. Mugha and H. A. Awan, "EVALUATION OF CONCRETE WITH PARTIAL REPLACEMENT OF COARSE AGGREGATES BY WASTE RUBBER PARTICLES," *International journal for innovative research in multidisciplinary field*, vol. 3, p. 12, 2017.
25. T. Abhishek, B. L. Panigrahi and R. Sahu, "Study of the behaviour of concrete after partial replacement of coarse aggregates by waste tire rubber fibres and addition of admixtures," *Int. J. Civ. Eng. Tech*, vol. 9, pp. 203-213, 2018.
26. K. G. Senthil, M. Lakshmipathy and N. Mushule, "An investigation on the behaviour of concrete with waste tire rubber fibres as a partial replacement of coarse aggregate," *Advanced Materials Research*, vol. 367, pp. 49-54, 2012.
27. T. I. BEKIR and N. Avcular, "Collision behaviours of RC," *Cement and concrete research*, vol. 12, pp. 1893-1898, 1997.
28. Y. Guo, X. Chen, W. Xuan and Y. Chen, "Dynamic compressive and splitting tensile properties of concrete containing recycled tire rubber under high strain rates," *Sādhanā*, vol. 11, pp. 1-13, 2018.
29. Y. Osama, M. A. ElGawady, J. E. Mills, X. Ma and T. Benn, "Behaviour of crumb RC columns under seismic loading," *In Proceedings of the 27th Biennial National Conference of the Concrete Institute of Australia/the 69th RILEM Week Conference. Concrete Institute of Australia, Melbourne*, 2015.
30. Y. Guo, X. Chen, W. Xuan and Y. Chen, "Dynamic compressive and splitting tensile properties of concrete containing recycled tire rubber under high strain rates," *Sādhanā* 43, vol. 11, pp. 1-13, 2018.
31. L. F, L.-Y. Meng, G.-X. Chen and L.-J. Li, "Dynamic mechanical behaviour of recycled crumb RC materials subjected to repeated impact," *Materials Research Innovations*, vol. 19, pp. S8-496, 2015.
32. H. Afia S and A. P. Shashikala, "Suitability of RC for railway sleepers," *Perspectives in Science*, vol. 8, pp. 32-35, 2016.
33. A. Priyanka,, S. B. Shinde and R. Patel, "Study on the behaviour of rubber aggregates concrete beams using analytical approach," *Engineering Science and Technology, an International Journal* , vol. 20, pp. 151-159, 2017.



# EXPERIMENTAL STUDY OF FIBRE SYNERGY TO INVESTIGATE THE TENSILE & COMPRESSIVE STRENGTH OF FIBRE REINFORCED CONCRETE

<sup>a</sup> Talha Rashid, <sup>b</sup> Muhammad Usman Rashid\*, <sup>c</sup> Irshad Qureshi, <sup>d</sup> Mohammad Zulqarnain

a: Department of Civil Engineering, University of Engineering & Technology Taxila, [engrtalharashid12@gmail.com](mailto:engrtalharashid12@gmail.com)

b: Department of Civil Engineering, University of Engineering & Technology Taxila, [m.usman@uettaxila.edu.pk](mailto:m.usman@uettaxila.edu.pk)

c: Department of Civil Engineering, University of Engineering & Technology Taxila, [irshad.qureshi@uettaxila.edu.pk](mailto:irshad.qureshi@uettaxila.edu.pk)

d: Department of Civil Engineering, University of Engineering & Technology Taxila, [zuuki786@gmail.com](mailto:zuuki786@gmail.com)

\* Corresponding author: Email ID: [m.usman@uettaxila.edu.pk](mailto:m.usman@uettaxila.edu.pk)

**Abstract-** The goal of this experimental research was to analyze the addition of carbon and glass fibers on the split-tensile and compressive strength of concrete cylinders. An approach to increase the strength of structures was carried out using fiber synergy. In this investigation, an effort was made by testing hybridized and mono fiber reinforced concrete (FRC) cylinders. Eighteen concrete cylinders were cast including six cylinders with different percentages of carbon fibers, six cylinders with different percentages of glass fibers, three control cylinders, and three hybridized cylinders were tested up to failure point. Eighteen samples each for split-tensile and compressive strength were tested in this experimental research. It was observed that the split-tensile and compressive strength of fiber reinforced concrete cylinders was improved using fiber synergy.

**Keywords-** carbon fibers, compressive strength, energy absorption glass fibers, hybrid fibres, split tensile strength

## 1 Introduction

Fibre reinforced concrete (FRC) is described as a composite material made with Portland cement, aggregate, and adding fibres that are discontinuous. FRC is super resistant against cracks formation and propagation. As a result of this ability to arrest cracks, fibre composites possess increased extensibility and tensile strength.

The strength of ordinary cement concrete is compromised by its least tensile resistance and very restricted ductility along with least resistance to cracking which makes it a brittle material leading to limited serviceability. Internal micro cracks lead to the brittle failure of concrete. The project specification led it to the durability requirements and being with the specific intended use it becomes necessary to modify the properties of concrete for broader use and durability limitations. Although, concrete has wide range of applications but it has some deficiencies too like low tensile strength, cracking capacity and brittleness.

The application of short and randomly distributed fibres to improve the properties of building materials is not a new concept and indeed its application is recorded in scriptures. Developing the concrete characteristics by strengthening fibre has its advantages including strength against cracks developing by contract drying and plastic, strength against moisture and thermal tension and increased formability.

Shabbir et al. [1] experimented the effect of carbon and steel fibres addition in concrete and analysed the cracking patterns. They concluded that the addition of carbon and steel fibres in concrete played a vital role in controlling the concrete cracks. Riyad et al. [2] investigated the load carrying capacity of glass fibre reinforced concrete and concluded that the load carrying capacity of GFRC increased as compared to ordinary concrete. Rashid [3] investigated durability characteristics of steel and polypropylene FRC exposed to natural weathering action and concluded that the durability is improved by natural weathering-exposure of polypropylene fibres. Anthony et al. [4] investigated optimum percentage of polypropylene



fibres contents for enhancement of strength of concrete in compression and concluded that the strength of concrete is improved by 0.5% when low percentage fraction of fibres was added. Ali et al. [5] studied the effect of glass-fibres on properties of concrete with recycled aggregates and concluded optimum dosage of glass fibres to be 0.25% for natural coarse aggregates, and 0.5% for recycled coarse aggregate concrete respectively. Sohail et al. [6] studied the comparison of confined glass and carbon FRC and concluded that both glass and carbon FRC have more strength as compared to high strength concrete. Rashid et al. [7] experimented the strength of FRC girders in flexural containing steel and polypropylene fibres and concluded that flexural strength is increased by 47% and split-tensile strength is increased by 123% by the use of steel and polypropylene fibre. They also concluded that steel FRC girders improve the strength by 47% in flexural and energy absorption by 69%. Patil and Sangle [8] concluded that almost 30-50% load carrying capacity of FRC having steel fibres was greater than that of plain concrete. They also concluded that the use of fibres enhanced the resistance against cracking. Shakor and Pimplikar [9] investigated the difference in compressive strength of FRC specimens with and without glass fibres and concluded glass FRC to have higher potential in construction industry. Chen and Chung [10] used carbon fibres inside concrete mix design and concluded minimum 0.1% by volume of carbon fibres inside concrete mix design for increase in flexural strength. Song and Yin [11] evaluated compressive toughness of steel and carbon FRC and concluded increase in crack resistance property of concrete specimens by the addition of steel and carbon fibres. Chandramouli and Srinivasa [12] carried out experimental investigation on alkali resistance glass FRC and observed 20-25% increase in strength in comparison of controlled concrete specimens with zero percent fibres.

There is not much research on strengthening of reinforced concrete using hybridized fibres (carbon and glass fibres). This gap is covered after testing hybrid and mono FRC cylinders. This experimental program provides evaluation of compressive & tensile strength, stress & strain curves, load & deflection curves and cracking patterns.

## 2 Research Methodology

The effect of the carbon & glass fibres on the strength of concrete was studied by varying the percentages of carbon and glass fibres in the concrete for which others parameters were remained constant. The compressive strength (ASTM C39-19) [13] and split-tensile strength (ASTM C496-12) [14] was tested by casting the concrete cylinders in casting yard of commercial suppliers working in Pakistan.

### 2.1 Materials

The concrete mix design of 1:1:2 was used for this experimental research consist of ordinary Portland cement (ASTM C 150-14) [15], coarse aggregates from Margalla crush with 70% (by 9.5mm sieve passing) and 30% (by 20mm sieve passing) (ASTM C-33) [16], fine aggregates from Lawrencepur sand having 2.12 Fineness Modulus, simple tap water and 0.7% superplasticizer (ASTM C 494-14) [17].

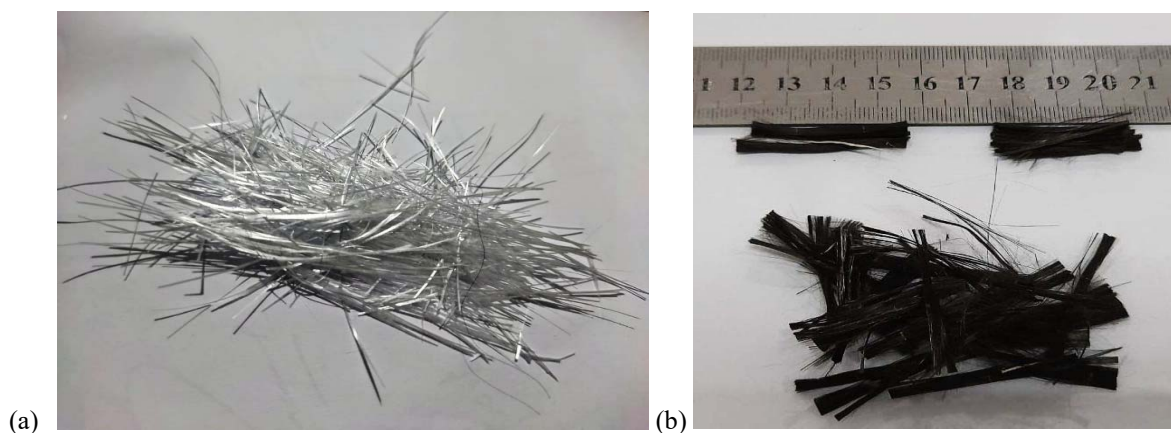


Figure- 1: Different fibers used in this research (a) Glass Fibers (b) Carbon Fibers

Chopped Glass and Carbon fibers are shown in Figure 1. were also used with varying percentages





The materials for 1m<sup>3</sup> of concrete are estimated as shown in Table 1.

Table 1: Concrete mix design and material calculations

Sr.#	Specimen	Cement Content (kg/m <sup>3</sup> )	Water Content (L)	Sand Content (kg / m <sup>3</sup> )	Coarse Aggregates Content (by 9.5mm passing) (kg / m <sup>3</sup> )	Coarse Aggregates Content (by 20mm passing) (kg / m <sup>3</sup> )	Admixture Content (kg / m <sup>3</sup> )	Carbon Fibers Content (kg / m <sup>3</sup> )	Glass Fibers Content (kg / m <sup>3</sup> )
1	S1-CM							0	0
2	S2-CFRC-1							2.9	0
3	S3-CFRC-2	132.3	66.2	132.3	185.27	79.4	0.7	3.7	0
4	S4-GFRC-1							0	1.8
5	S5-GFRC-2							0	2.6
6	S6-HyFRC							3.3	2.2

## 2.2 Casting of Specimens

A total 36 number of concrete cylinders were casted in Banu Mukhtar Plant located in KPK as shown in Figure- 2a. For all concrete specimens, the concrete mix ratio was kept same. The compaction of concrete carried out via an external vibrator After 24 hours, the moulds were removed and cylinders were placed in curing tanks as shown in Figure- 2b in accordance with ASTM C-31 [18].

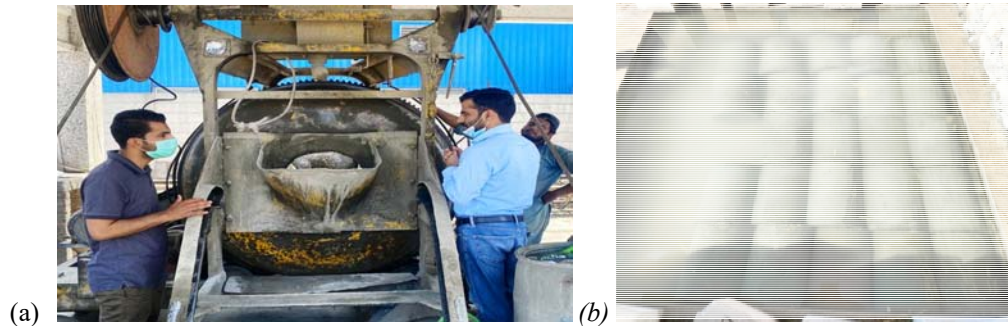


Figure- 2: Casting and Curing of Specimens (a) Preparation of Concrete mixing in Plant (b): Placement of concrete cylinders inside curing tanks for 28 days

The ratios of various types of fibres used inside all concrete cylinders is shown in Table 2.

Table 2: Percentages of fibres in concrete specimens

Sr. No.	Specimen	Fiber Content (by % of weight of concrete)	
		Carbon Fibers	Glass Fibers
1	S1-CM	-	-
2	S2-CFRC-1	0.65%	-
3	S3-CFRC-2	0.85%	-
4	S4-GFRC-1	-	0.40%
5	S5-GFRC-2	-	0.60%
6	S6-HyFRC	0.75%	0.50%



### 2.3 Testing of Specimens

The determination of compressive strength and split-tensile strength of concrete specimens was carried out at each 25kN load interval. Load was applied via compression testing machine with capacity of 3000kN at the centre of cylinders, and deflection of the cylinder was measured using linear displacement sensors (LDS) at each respective load interval. The strains were recorded by using P3-strain indicator and data recording device (Figure 4) connected to LDS. The complete setup installation is shown in Figure- 3(a) along with complete setup schematic diagram in Figure- 3(b).

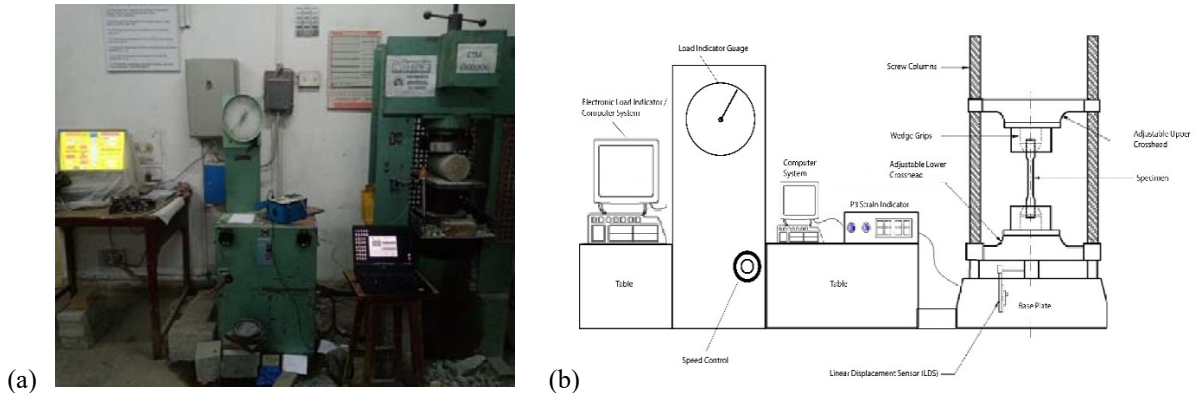


Figure- 3: Complete Testing Setup (a): Compression Testing Machine (3000 kN), Computer Setup, P3 Strain Indicator and Linear Displacement Sensor; (b): Schematic Diagram of Complete Setup

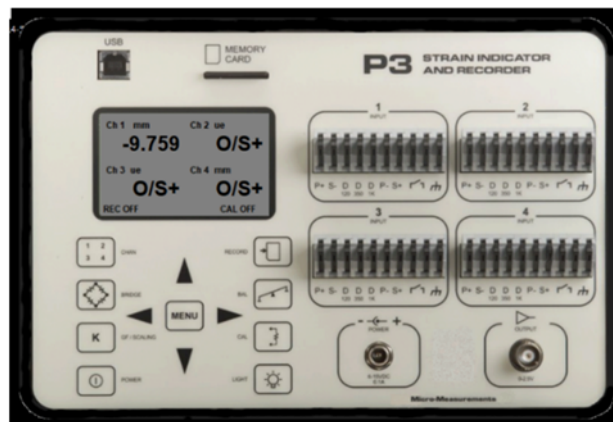


Figure- 4: P3 Strain Indicator and Recorder

## 3 Results

### 3.1 Compressive Strength of Concrete Mixes

Three number of cylinders were tested for each type of concrete mix and average of three is reported in this section. Load-Deflection and Stress-Strain graphs are shown in Figure--5 and Figure--6 respectively. The average maximum compressive strength of all specimens are shown in Figure- 7.

The compressive strength of S6-HyFRC concrete specimens was achieved up to 33.90MPa which was maximum as compared to other concrete mix specimens. The concrete mixes with mono-fibers i.e. (i.e., mixes of S2-CFRC-1, S3-CFRC-2, S4-GFRC-1, S5-GFRC-2) didn't showed much difference in compressive strength as compared to that of control specimen. The fiber synergy (hybridization of carbon and glass fibers) played a vital role in increasing the compressive strength of S6-HyFRC concrete specimens.

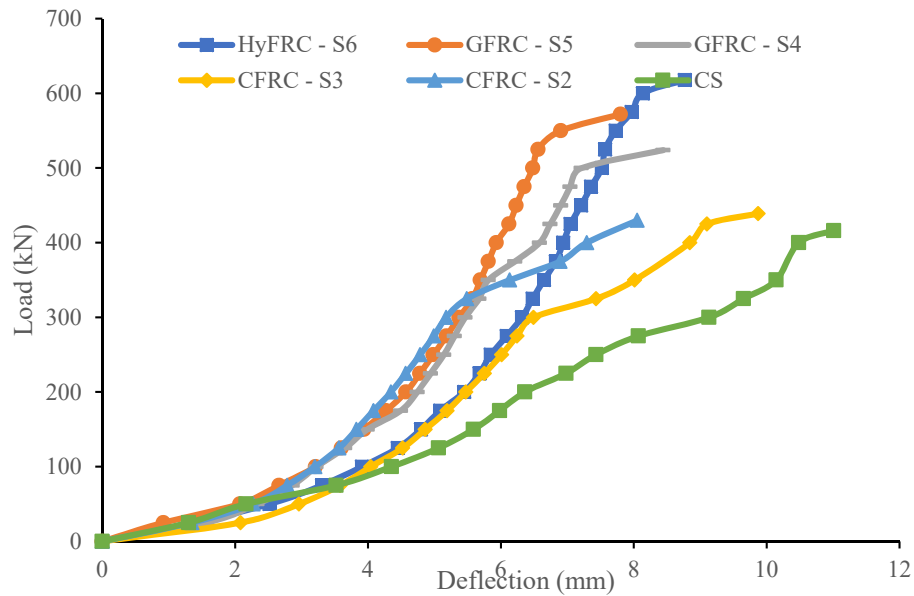


Figure- 5: Load-Deflection curves against compressive strength testing of all concrete specimens

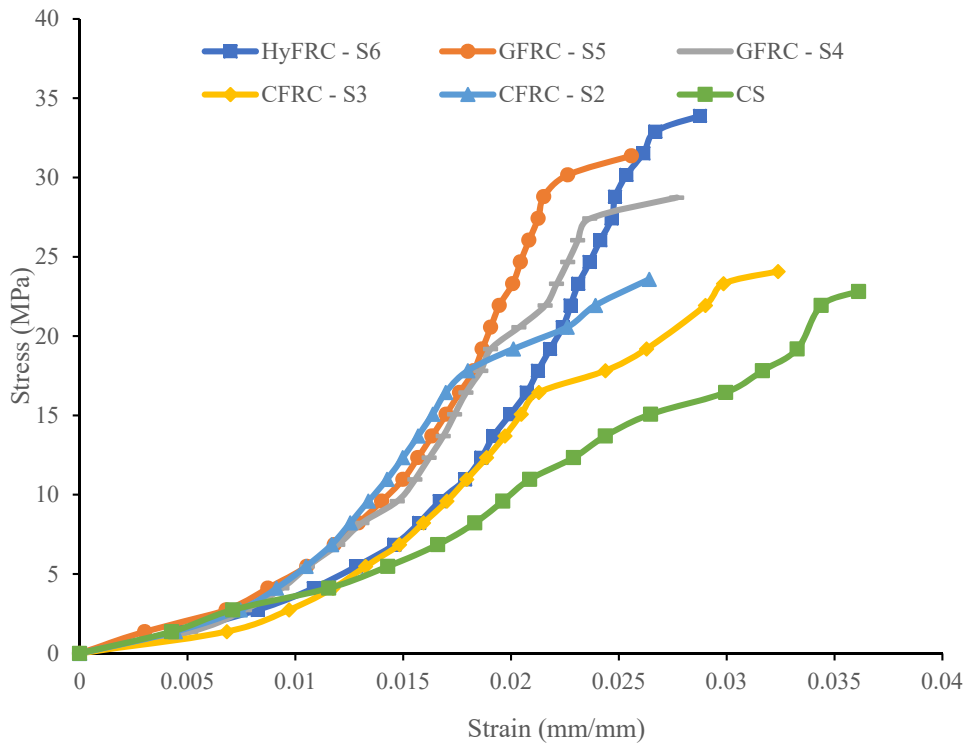


Figure- 6: Stress-Strain curves against compressive strength testing of all concrete specimens

### 3.2 Split-tensile Strength of Concrete Mixes

The concrete cylinders were tested for split-tensile strength as per ASTM C496-12 [14]. Load-Deflection and Stress-Strain graphs are shown in Figure- 8 and Figure- 9 respectively. Maximum load carrying capacity and average maximum compressive strength of all specimens are shown in Figure- 10.

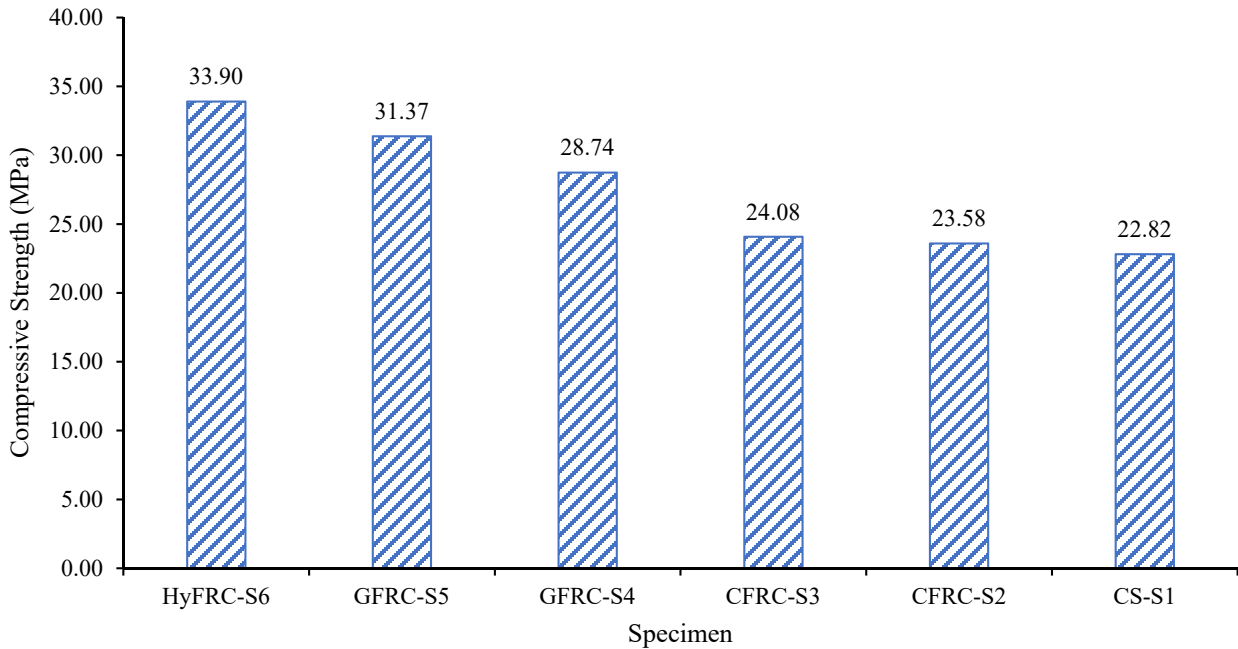


Figure- 7: Average Max. Compressive strength of all concrete specimens

S6-HyFRC concrete specimens have shown maximum tensile strength due to their composition containing hybridized fibres that improved the capability of both fibres' types inside the concrete matrix. The tensile-strength of 12.5 MPa was observed for mix of concrete cylinder S6-HyFRC. The use of carbon and glass fibres (S2-CFRC-1, S3-CFRC-2, S4-GFRC-1 and S5-GFRC-2) improved the tensile-strength of concrete, but negligible in comparison to that of S6-HyFRC concrete specimens.

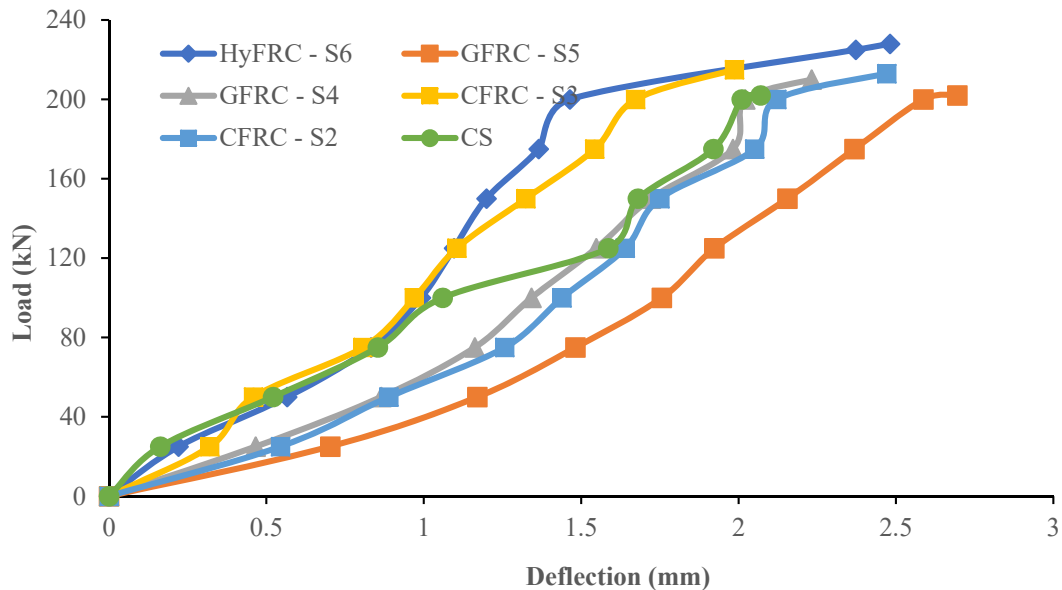


Figure- 8: Load-Deflection curves of split-tensile strength testing of all concrete specimens

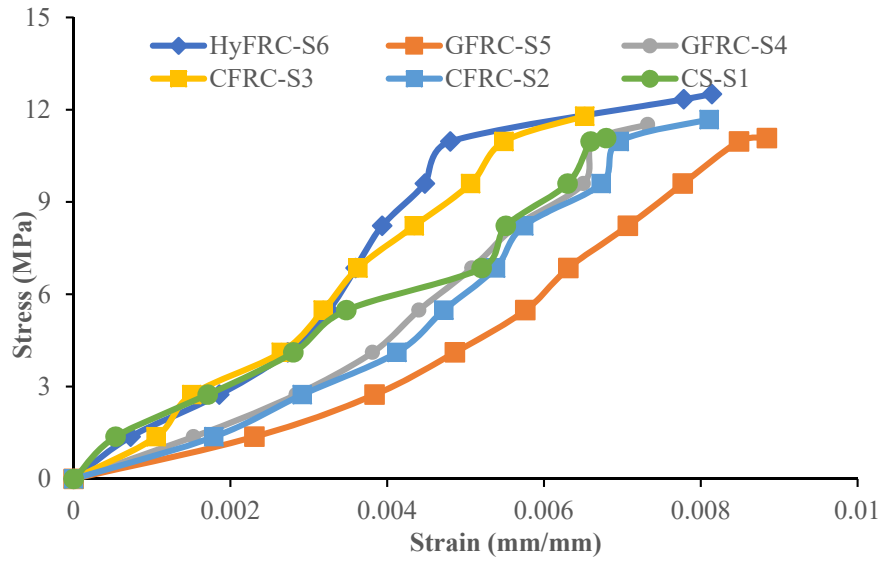


Figure- 9: Stress-Strain Curves of split-tensile strength testing of all concrete specimen

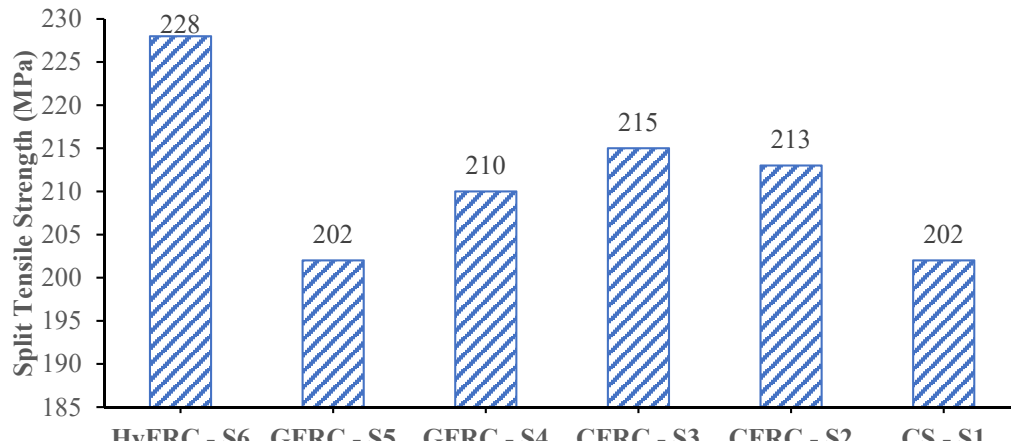


Figure- 10: Average split-tensile strength of concrete specimens

### 3.3 Slump of Different Concrete Mixes

The slump test for every concrete batch was performed according to ASTM C-143 [19] as shown in Figure 11.



Figure- 11: Slump Cone Test for concrete specimens

The results of slump test are elaborated as shown in Table 3:



Table 3: Average Slump values for each concrete specimen

Sr. No.	Specimen	Mix Design Ratio	Slump (mm)
1	S1-CM		50
2	S2-CFRC-1		38
3	S3-CFRC-2	1:1:2	40
4	S4-GFRC-1		42
5	S5-GFRC-2		45
6	S6-HyFRC		47

### 3.4 Energy Absorption of Concrete Mixes

Toughness of concrete cylinders is indicated by the amount of energy being absorbed [20]. The area under Load-Deflection curves is calculated and depends on both ultimate load and maximum deflection achieved at failure point. S6-HyFRC concrete cylinders absorbed 82% more energy as compared to S1-CS as shown in Figure- 12.

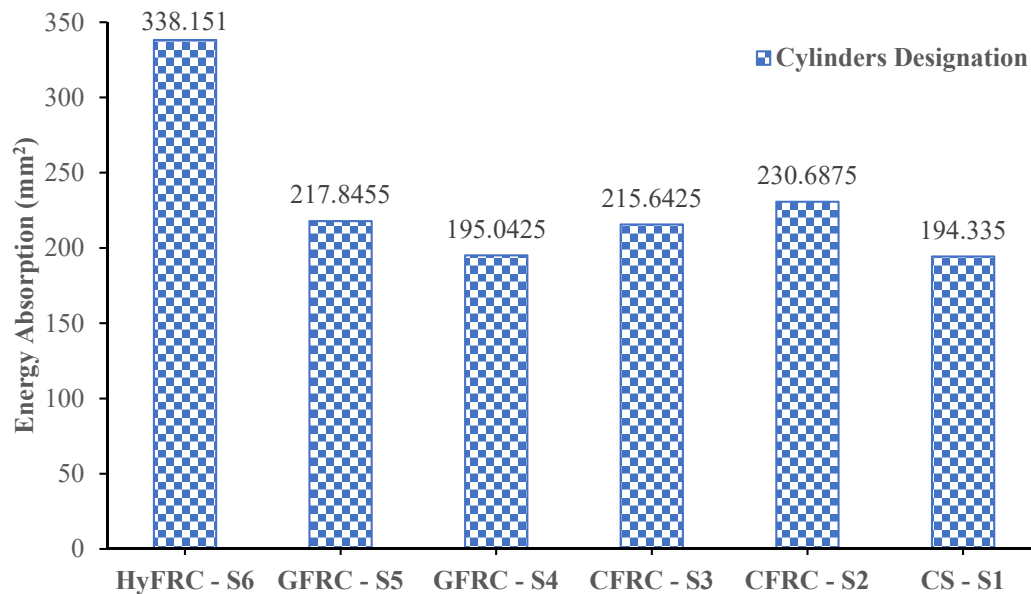


Figure- 12: Average Energy Absorption Capacity for each Concrete Specimen

### 3.5 Crack Patterns

The propagation of the cracks was observed before and after testing each specimen of concrete during experimental work. The cracks were vertical in majority and inclined along the height of cylinder and they differ with various fibre contents inside the specimens. The cracking patterns under compression testing along with their development can be observed in Figure- 16, 17 and 18.

The specimens were also tested under split-tensile strength test. The concrete specimens were put horizontally to get the tensile strength after splitting them apart. The initiation of tensile cracks from the top and propagation to the bottom of cylinder was observed. All the concrete specimens have resulted in horizontal under split-tensile strength testing and can be observed in Figure- 19, 20 and 21.



Figure- 13: HyFRC-S6 Cylinder after compressive strength test

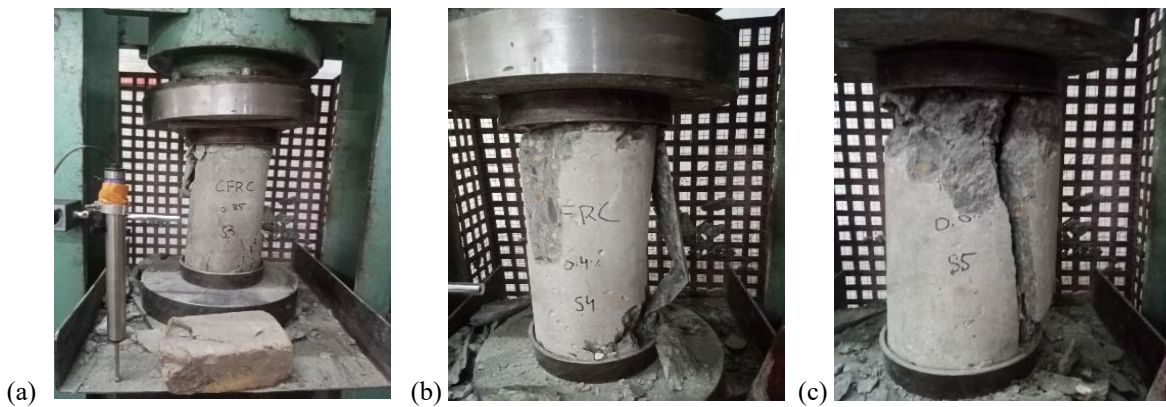


Figure- 14: CFRC and GFRC mixed Cylinders after compressive strength test (a) S3-CFRC (b) S4-GFRC (c) S5-GFRC



Figure- 15: Control Concrete Cylinder (CS) after compressive strength test

#### 4 Practical Implementation

Fiber reinforced concretes play important role to arrest cracks and due crack resisting nature of FRC it will considerably improve the mechanical strength of structural members. This research focuses on practical implementation of fiber reinforced concrete in structural members to enhanced compressive and split-tensile strength along with better crack resistance. Furthermore, this approach is also very beneficial from economical perspective as it will reduce the cross section of members which will greatly reduce the project cost.



Figure- 16: HyFRC-S6 Cylinder after split-tensile strength test

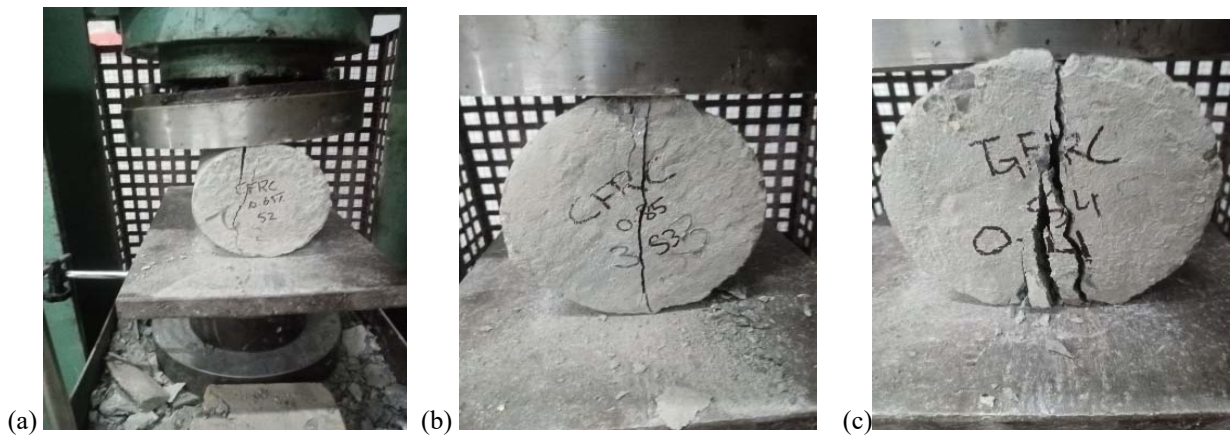


Figure- 17: CFRC and GFRC mixed Cylinders after split-tensile strength test (a) S3-CFRC (b) S3-CFRC (c) S4-GFRC



Figure- 18: Controlled Concrete Cylinders after split-tensile strength test





## 5 Conclusion

The experimental research, after performing compressive strength and split-tensile strength tests on all concrete specimens, concludes following points:

1. The use of hybridized fibre reinforced concrete (HyFRC) has increased the compressive strength by 49% and the split-tensile strength by 12.5% as compared to control specimen.
2. The crack resistance property of HyFRC was increased as compared to control specimen.
3. HyFRC specimens has absorbed 345% higher energy as compared to control specimens.

## Acknowledgment

The authors are thankful to Banu Mukhtar Pvt. Ltd who assisted during this experimental work. The suggestions by the reviewers are gracefully be taken into consideration. The careful review and constructive suggestions by the anonymous reviewers are highly acknowledged.

## References

- [1] F Shabbir, MU Rashid, A Muslim and A Raza, "The Efficiency of Hybrid Fibers (Steel and Carbon Fibers) in Controlling Micro Cracking of Concrete Beams," *Iranian Journal of Science and Technology, Transactions of Civil Engineering*, pp. 1-21, 2022.
- [2] Y RIYAD, B KISSI and I MRANI, "Reinforcement of concrete using Glass Fiber Reinforced Polymer," *Journal of Materials and Engineering Structures*, vol. 9, pp. 141-152, 2022.
- [3] MU Rashid, "Experimental investigation on durability characteristics of steel and polypropylene fiber reinforced concrete exposed to natural weathering action," *Construction and Building Materials*, vol. 250, p. 118910, 2020.
- [4] A. N. Ede and A. OluwabambiIge, "Optimal polypropylene fibre content for improved compressive and flexural strength of concrete," *IOSR Journal of Mechanical and Civil Engineering (IOSR-JMCE)*, vol. 11, pp. 129-135, 2014.
- [5] B Ali, LA Qureshi, A Raza, MA Nawaz and SU Rehman, "An investigation on shear behavior of prestressed concrete beams cast by fiber reinforced concrete," *Arabian Journal for Science and Engineering*, vol. 43, no. 10, pp. 5605-5613, 2018.
- [6] MR Sohail, N Ahmad, MU Rashid, R Waqas and U Muhammad, "Comparison of GFRP and CFRP confinement of normal and high strength concrete," *Gradevinar*, vol. 72, no. 06, pp. 475-484, 2020.
- [7] MU Rashid, LA Qureshi and MF Tahir, "Investigating flexural behaviour of prestressed concrete girders cast by fibre-reinforced concrete," *Advances in Civil Engineering*, vol. 2019, 2019.
- [8] S. P. Patil and K. K. Sangle, "Shear and flexural behaviour of prestressed and non-prestressed plain and SFRC concrete beams," *Journal of King Saud University-Engineering Sciences*, vol. 29, pp. 321-328, 2017.
- [9] PN Shakor and SS Pimplikar, "Glass Fibre Reinforced Concrete Use in Construction," *International Journal of Technology And Engineering System (IJTES)*, vol. 2, 2011.
- [10] PW Chen and DDL Chung, "Concrete reinforced with up to 0.2 vol% of short carbon fibres," *Composites*, vol. 24, no. 1, pp. 33-52, 1993.
- [11] W Song and J Yin, "Hybrid effect evaluation of steel fiber and carbon fiber on the performance of the fiber reinforced concrete," *Materials*, vol. 9, p. 704, 2016.
- [12] K Chandramouli and RP Srinivasa, "Strength properties of glass fiber concrete," *ARPN Journal of Engineering and Applied Sciences*, vol. 5, pp. 1-6, 2010.
- [13] A. C39/C39M-11, "Standard test method for compressive," *Annual Book of ASTM Standards*, 2011.
- [14] A. C496/C496M-11, "Standard test method for splitting tensile strength of cylindrical concrete specimens," *Annual Book of ASTM Standards*, 2011.
- [15] A. C150-14, "Standard Specification for Portland Cement," *Annual Book of ASTM Standards*, 2011.
- [16] A. C33, "Standard specification for concrete aggregates," *Annual Book of ASTM Standards*, vol. 4, 1994.
- [17] A. C494-14, "Standard Specification for Chemical Admixtures for Concrete," *Annual Book of ASTM Standards*, 2011.
- [18] A. C31/C31M-19, "Standard Practice for Making and Curing Concrete Test Specimens in the Field," *Annual Book of ASTM Standards*, 2019.
- [19] A. C143, "Slump of Hydraulic Cement Concrete," *Annual Book of ASTM Standards*, 2011.
- [20] KT Soe, YX Zhang and L Zhang, "Advances in Engineered Cementitious Composites," *Woodhead Publishing Series in Civil and Structural Engineering*, pp. 77-120, 2022.



# PERFORMANCE EVALUATION OF A PARTIALLY SYNTHETIC BITUMEN COMPOSED OF INDUSTRIAL WASTE

*<sup>a</sup> Hamza Javed\*, <sup>b</sup> Syed Bilal Ahmed Zaidi*

a: Department of Civil Engineering, University of Engineering and Technology Taxila, Hamzaj463@gmail.com  
b: Department of Civil Engineering University of Engineering and Technology Taxila, bilal.zaidi@uettaxila.edu.pk

**Abstract-** Bitumen is produced from non-renewable natural resources. Depletion of non-renewable resources intrigued researchers to look for alternative binders. Bitumen has been modified with many additives to enhance its properties and performance. The improper disposal of waste materials such as crumb rubber and use engine oil poses a significant threat to the environment. The addition of these industrial waste products to asphalt not only provides a safe and cost-effective way to dispose of them, but also improves the asphalt binder's performance. In this study, various combinations of waste engine oil and crumb rubber have been used with 60-70 penetration grade bitumen to produce a partially synthetic bitumen. Adhesion being one of the key characteristics of the bituminous binder has been assessed by using bitumen bond strength test along with penetration and softening point. The experimental results revealed that partially synthetic bitumen with 35% waste and 40% percent waste improves the adhesion along with conventional properties. Furthermore, the results of partially synthetic bitumen demonstrate that this bitumen is more suitable for cold regions of the country. A detailed and extensive testing program is needed to reach authentic findings but based on the results authors are hopeful that a handsome percentage of waste can replace the virgin binder giving a cost effective and environmentally friendly solution.

**Keywords:** - Synthetic Bitumen, Adhesion, Waste Engine Oil, Crumb Rubber

## 1 Introduction

Bitumen is a binding agent used in flexible pavements. Increased road transport volume, environmental and external factors, and construction-phase failures can reduce asphalt pavements' useful life and increase the probability of permanent faults [1]. Mohammad Gohar et al., investigated that the 15% addition of crumb rubber increases the stiffness, viscosity and high softening point and improves the rutting resistance of conventional bitumen [2]. Ahmed Eltwati et al, investigated that, the addition of the WEO-CR rejuvenator improved the overall performance of the mixture by improving the physical and chemical properties of the asphalt binder and the mechanical performance of hot-mixed asphalt (HMA) [3].

Christopher Daniel et al., investigated the use of waste engine oil mixed with reclaimed asphalt. He noticed that asphalt binders blended with Reclaimed asphalt binder (RAB) might have less stiffness and better low temperature qualities due to waste engine oil. Asphalt pavements can also be made softer by used engine oil without harming the pavements' susceptibility to moisture. [4]. Touqeer Shaukat et al., studied the Rheological evaluation of asphalt modified with automobile engine waste oil. He concluded that the increased cohesion of asphalt molecule chains is due to the increased viscosity of asphalt modified with 2.5% filtered waste engine oil. Comparison of master curves shows that binder modified with waste engine oil can better perform at low temperatures to resist fatigue cracking [5]. Jia, X. et al. conclude that waste engine oil residues have a significant impact on the reduction of asphalt binder's low-temperature stiffness and improvement of its low-temperature performance [6]. Birendra Kumar Singh et al. investigated that by lowering the size



of the crumb rubber, the resistance to rutting has been enhanced and can improve high temperature performance of bitumen.[7]. Herda Yati Katman et al. conclude that crumb rubber modifications of bitumen enhance bituminous binder properties such as Viscosity, softening point, loss modulus, and storage modulus. Consequently, this enhances the rutting resistance, resilience, and fatigue cracking resistance of asphaltic mixtures. [8]. M. F. Ahmad et al. evaluate the Bitumen is a petroleum product obtained from the fractional distillation of crude oil, a natural resource. Natural resources are depleting continuously, significantly impacting its price hike and environmental pollution. Asphalt binder has been modified with many modifiers to counter the problem of waste material management, depletion of natural resources, and improving the performance of conventional binder. The use of modified or alternative binders is both cost-effective and environmentally friendly [9]. Feng, Zhao et al. evaluated the waste engine oil-modified bitumen and concluded that WEO reduces the softening point and viscosity of binder while increasing its penetration. He also concluded that an excess WEO adversely affects the binder properties [10]. Liu et al. evaluated the rheological behavior of waste engine oil-modified bitumen and concluded that fatigue resistance and low-temperature performance are improved, but the binder's rutting resistance and high-temperature performance are impaired. They concluded that from chemical tests, there is no evidence of a chemical reaction between bitumen and WEO. They recommended the range of 4-8% WEO modification [11].Liu et al. studied the rheological behaviour of WEO-modified bitumen and determined that the addition of waste engine oil reduces the asphalt binder's elasticity. it shows lower values of complex modulus and higher values of phase angles. WEO improves the fatigue performance but impairs the rutting resistance of bitumen [12].

The objectives of this research are as follows:

1. To examine the combined impact of WEO and CR on bitumen's conventional properties.
2. To examine the impact of WEO and CR on the adhesion properties of asphalt mixture.
3. Determination of the optimum combination dosage of various constituents for manufacturing of cost effective and environmental friendly partially synthetic bitumen.

## 2 Experimental Procedures

### 2.1 Material Preparation and its Mixing Proportion:

The 60/70 pen grade bitumen was collected from PARCO refinery. Waste engine oil was collected from local motor vehicle repairing plants and markets. Using filter paper of grade Whatman 1002-150, waste engine oil was filtered out. CR was extracted from used tire scrape and grind them in shredder plants.

Table1: Mixing proportions of WEO and CR

Sr. No	Dosage
1	B+5% WEO+20% CB
2	B+5% WEO+25% CB
3	B+5% WEO+30% CB
4	B+10% WEO+20% CB
5	B+10% WEO+25% CB
6	B+10% WEO+30% CB
7	B+15% WEO+20% CB
8	B+15% WEO+25% CB
9	B+15% WEO+30% CB

After being crushed, the material passes through sieve No. 50/300 microns/0.2997 mm Then, various proportions of used motor oil and crumb rubber were mixed with bitumen.

Prior to adding waste engine oil and CR into bitumen, the bitumen is heated to 150°C on a hot plate, where the temperature is kept constant and then mixed using a shear mixer.



### 2.3 Testing Methodology:

The penetration and softening point tests, which were performed in accordance with ASTM D5 [13] and D36 [14], were used to characterize the impact of WEO and CR. PATTI was used as per ASTM D 4541 to evaluate the bond strength of bitumen under dry and wet conditions [15]. Then used the burst pressure values in equation 1 to calculate the Pull-off tensile strength (POTS).

$$POTS = \frac{(BP * Ag) - C}{Aps} \quad 1$$

Burst Pressure (BP), the contact area (Ag), which has a value of 2620 mm<sup>2</sup>, and C which has a value of 0.286, is the piston constant. Aps has a value of 127 mm<sup>2</sup>.

## 3 Research Methodology

This project's research methodology is shown in Figure 1.

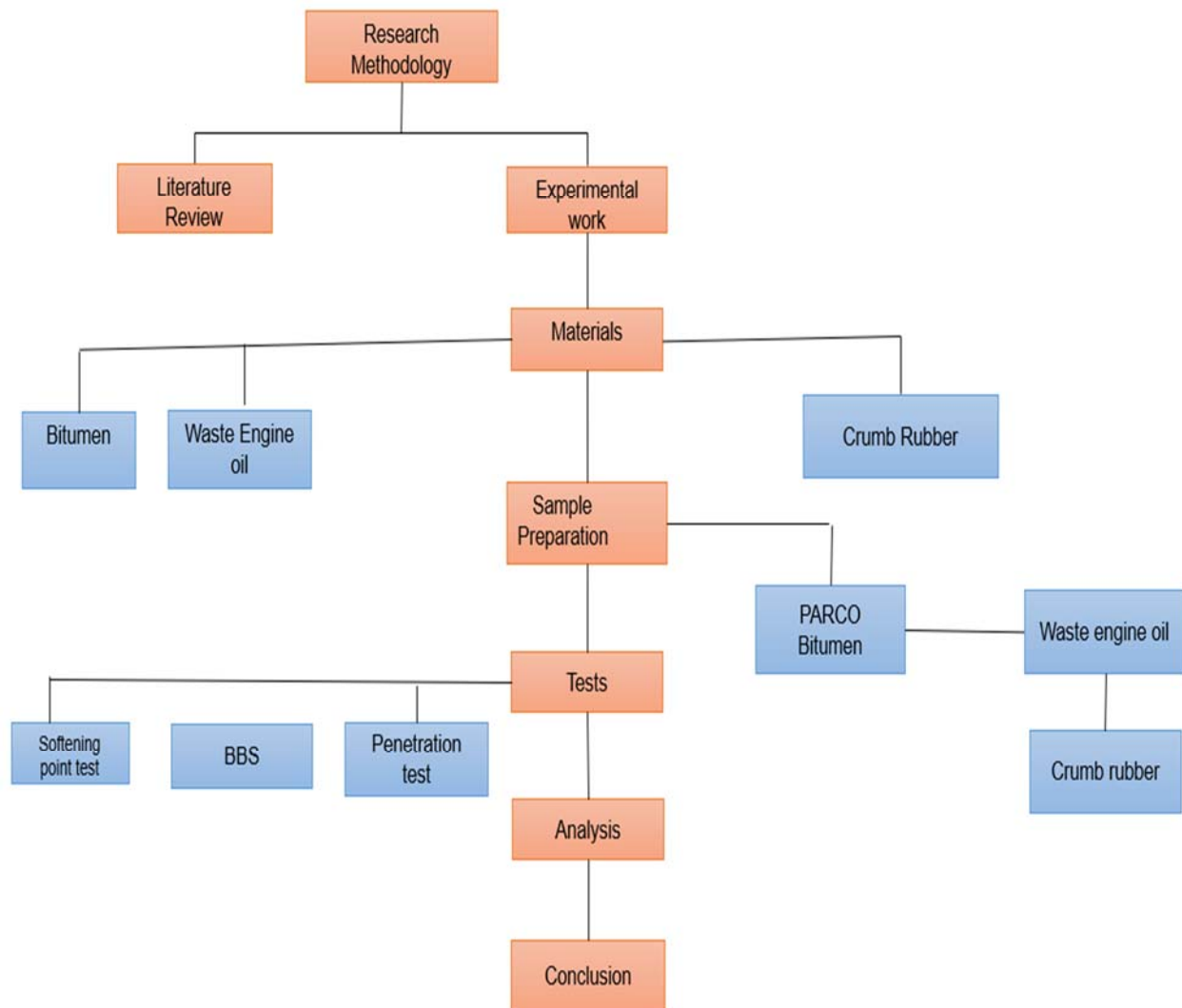


Figure 1: Research Methodology



## 4 Results

### 4.1 Conventional Testing:

In this method, for investigating the impact of modifiers on bitumen, conventional testing was conducted. The penetration and softening point test are performed to determine whether modified bitumen becomes soft or hard. Figure 2 depicts the experimental results of conventional testing.

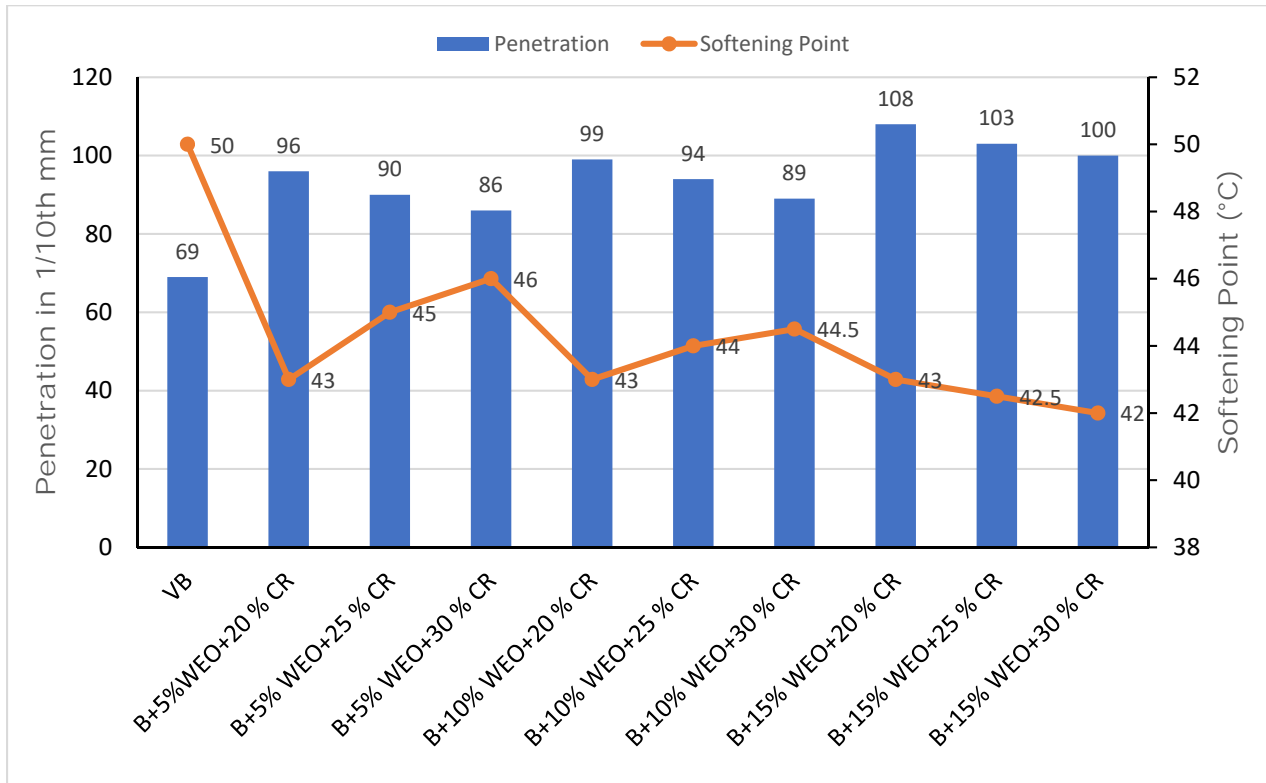


Figure 2: Effect of penetration and softening on partially synthetic bitumen

In Figure 2, The addition of 5% WEO with 20%, 25%, and 30% CR by total binder content increases the penetration value by 28%, 23%, and 20%, respectively, while the softening point decreases by 14%, 10%, and 8%. In 10% WEO with 20%, 25%, and 30% CR, a 30%, 26%, and 22% increase in penetration value and an 8%, 14%, and 12% decrease in softening point value were observed. Similarly, the addition of 20%, 25%, and 30% CR with 15% WEO resulted in a 36%, 33%, and 31% increase in penetration value and a 16%, 15%, and 14% decrease in softening point, respectively. Its mean that increasing the dosage of WEO results in higher penetration values and a lower softening point, whereas increasing the dosage of CR results in lower penetration values and a higher softening point. The addition of WEO softens the binder, whereas the addition of crumb rubber hardens and stiffens it, thereby enhancing its conventional properties.

### 4.2. Evaluation of Adhesion by using BBS Test:

The effect of WEO and CR on adhesion were experimentally evaluated by using PATTI. To determine the bonding strength of the binder to the aggregate surface, a Bitumen Bond Strength (BBS) test was performed for both dry and wet conditions. For dry conditioning, in figure 3, the addition of 5% WEO with the inclusion of 20%,25% and 30% CR by total binder content, after 24 hours of dry conditioning, POTS values decrease by 38 %,27% and 13%, In 10 % WEO with the inclusion of 20%,25% and 30% CR, a decrease of 67%,50% and 38% in value of POTS was observed at dry condition. Similarly, when 15% WEO was mixed with 20%, 25%, and 30% CR, the POTS value of the dry sample decreased by 72%, 58%, and 50%, respectively, when compared to the virgin binder

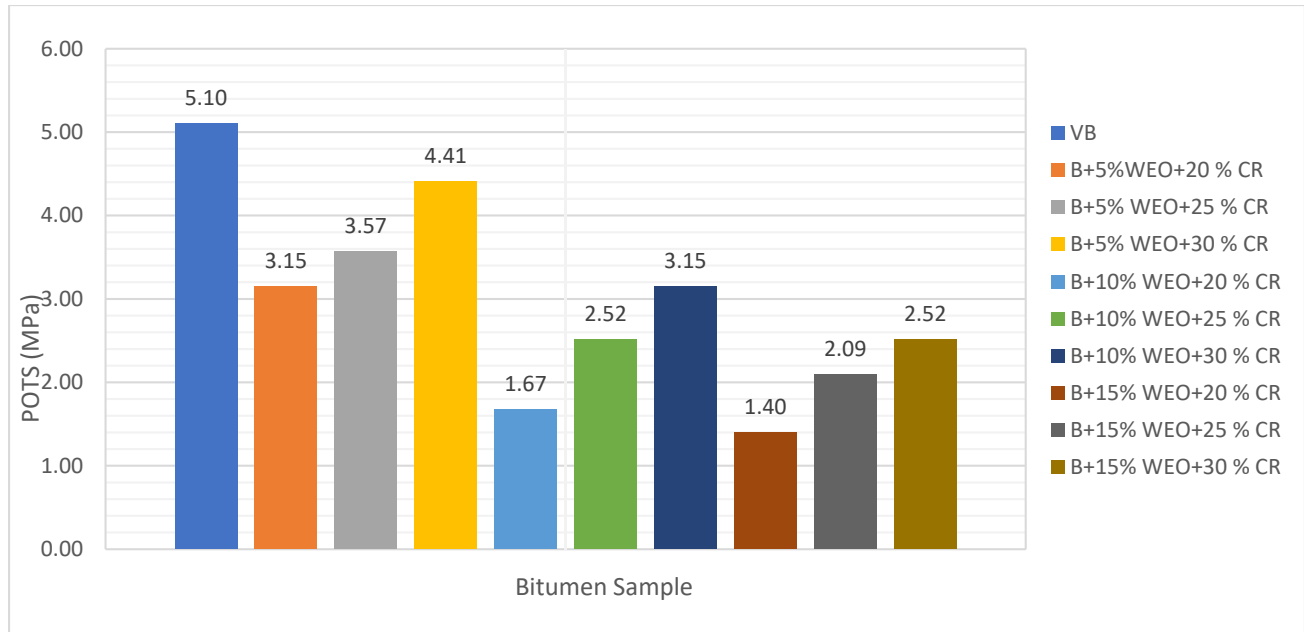


Figure 3: Effect of POTS at dry condition

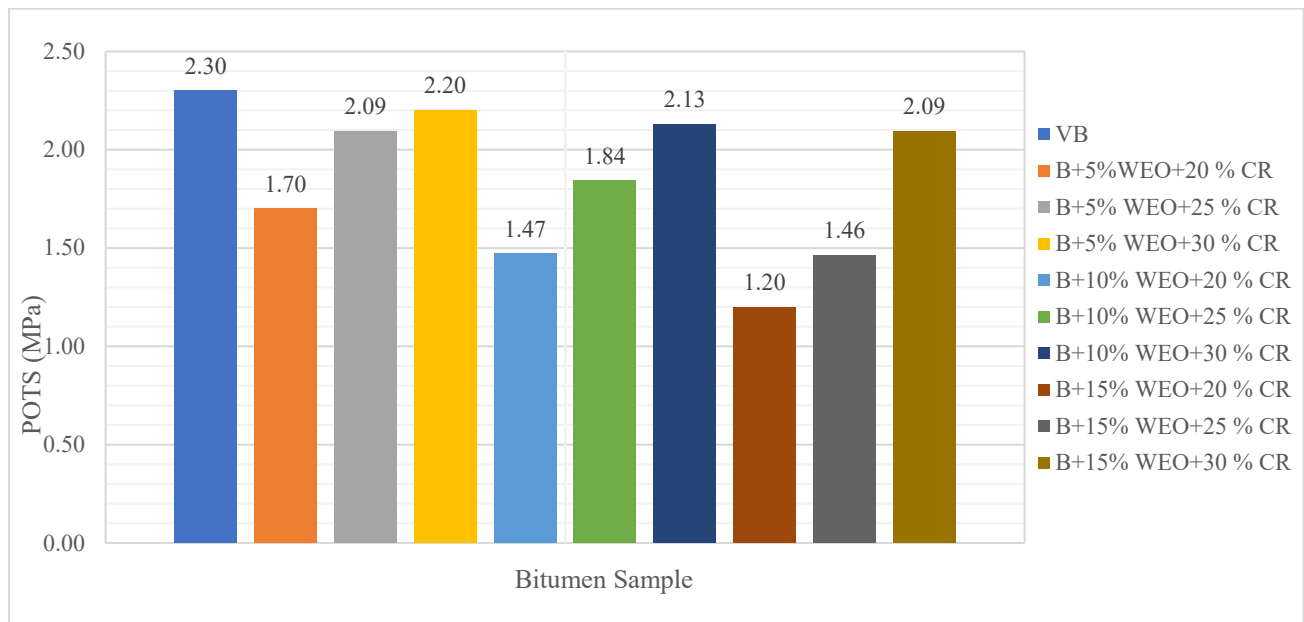


Figure 4: Effect of POTS at Wet condition

In Figure 4, The addition of 5% WEO with the inclusion of 20%,25% and 30% CR, by the total binder content, POTS values decrease by 26 %,11% and 4% at wet condition. In 10 % WEO with the inclusion of 20%,25% and 30% CR, a decrease of 36%,19% and 7% in POTS values was observed. Like that, in 15 % WEO with the inclusion of 20%,25% and 30% CR, a decrease of 47% ,36% and 17% in POTS value of wet sample was observed. However, compared to dry condition, the partially synthetic bitumen showed lower values after water conditioning, because, Water permeates the bitumen-bitumen interface as well as the bitumen-aggregate interface, thereby weakening the bond. It means that due to the incorporation of crumb rubber, an increase in the value of POTS authenticates a stronger association between aggregates and binder specimen and a decrease in the value of POTS indicates a weaker bond between aggregates and binder specimens as a result of the incorporation of waste engine oil. Increased WEO dosage results in a lower POTS value, whereas increased CR dosage results in a higher POTS value, and vice versa.



## 5 Conclusion

In the light of results attained, the results of partially synthetic bitumen demonstrate that this bitumen is more suitable for cold regions of the country, conclusions are summarized as:

1. From conventional testing, i.e., Penetration Test, Softening Point Test, it has been observed that of WEO in the binder increases its penetration values, decreases its softening point, and decreases the consistency of bitumen because waste engine oil softens the bitumen but with the addition of crumb rubber, improved the properties of partially synthetic bitumen.
2. When compared to virgin binder, the addition of 35% waste by total binder content, decreases the POTS value of dry sample by 13%, and the value of POTS dropped by 38% when 40% waste was added. For the wet sample, the addition of 40% waste by weight of binder, decreases the POTS value of wet sample by 4%, and the addition of 40% waste, a decrease of 7% in value of POTS was observed. Wet strength and dry strength decrease with increase in WEO which depicts that WEO induces moisture damage. However, addition of crumb rubber resulted in improvement in the resistance against moisture providing better adhesion.
3. The optimum percentage of industrial waste which can be used for the production of partially synthetic bitumen lies between 35% and 40% contributing to a significant saving in non-renewable resources.
4. This scope of this study was very limited so a detailed and extensive testing program is needed to reach authentic findings but based on the results authors are hopeful that a handsome percentage of waste can replace the virgin binder giving a cost effective and environmentally friendly solution.

## Acknowledgment

I attribute my success to "Allah," the Almighty, who bestowed upon me the strength and capacity to conduct this study. My supervisor, Associate Professor Dr. Syed Bilal Ahmed Zaidi, deserves a huge debt of appreciation for giving me the chance to work on this project and for offering advice and support throughout the research process. Throughout each and every meeting, his technical and spiritual assistance has been invaluable. I consider it a privilege to have studied with him and feel that I've grown as a person and as a student because of it. The time I spent learning under his guidance is something I will always appreciate.

## References

- [1] Ricardo S. Souza, Leila L. Y. Visconte, Ana L. N. da Silva, Aléria G. Costa, "Thermal and Rheological Formulation and Evaluation of Synthetic Bitumen from Reprocessed Polypropylene and Oil", *International Journal of Polymer science*, AUG, 2018.
- [2] Mohammad Gohar, Naveed Ahmad, Waqas Haroon, "Effect of Addition of Crumb Rubber on Bitumen Performance Grade (PG) and Rutting Resistance", 1st International Conference on Advances in Civil & Environmental Engineering, University of Engineering & Technology Taxila, FEB, 2022.
- [3] Ahmed ELTWATI, Mahmoud ENIEB, Saleh AHMEED, Zaid AL-SAFFAR, Azman MOHAMED, Effects of waste engine oil and crumb rubber rejuvenator on the performance of 100% RAP binder, *Journal of Innovative Transportation*, July, 2022.
- [4] Christopher Daniel DeDene, "Investigation of Using Waste Engine Oil Blended with Reclaimed Asphalt Materials to Improve Pavement Recyclability", Jan, 2011.
- [5] Touqeer Shoukat and Yoo, Pyeong Jun, "Rheological evaluation of asphalt modified with automobile waste engine oil", 18th International Conference Road Safety on Five Continents (RS5C 2018), Jeju Island, South Korea, May 16-18, 2018.
- [6] Jia, Xiaoyang, Huang, Baoshan, Bowers, Benjamin F, Zhao, Sheng %J Construction, & Materials, Building. (2014). "Infrared spectra and rheological properties of asphalt cement containing waste engine oil residues". 50, 683-691.
- [7] Birendra Kumar Singh, Martand Siroliya, "Application of Crumb Rubber as Modifier in Bitumen" *International Journal for Scientific Research & Development* | Vol. 4, Issue 07, 2016.
- [8] Mohd Rasdan Ibrahim, Herda Yati Katman, Mohamed Rehan Karim, Suhana Koting, and Nuha S. Mashaan, A Review on the Effect of Crumb Rubber Addition to the Rheology of Crumb Rubber Modified Bitumen, OCT, 2013.



- [9] Ahmad, Malik Farooq, Ahmed Zaidi, Syed Bilal, Fareed, Ayyaz, Ahmad, Naveed, & Hafeez, Imran %J "International Journal of Pavement Engineering. (2021). "Assessment of sugar cane bagasse bio-oil as an environmental friendly alternative for pavement engineering applications." 1-12.
- [10] Feng, Zhengang, Zhao, Peixin, Yao, Dongdong, & Li, Xinjun. (2020)."Performance Evaluation of Waste Engine Oil Regenerated SBS Modified Bitumen".In *CICTP 2020* (pp. 1150-1162).
- [11] Liu, Shengjie, Peng, Aihong, Zhou, Shengbo, Wu, Jiantao, Xuan, Weian, Liu, Wu %J Construction, & Materials, Building. (2019). "Evaluation of the ageing behaviour of waste engine oil-modified asphalt binders".223, 394-408.
- [12] Liu, Shengjie, Meng, Hankuo, Xu, Yinshan, Zhou, Shengbo %%J Petroleum Science, &Technology. (2018).“Evaluation of rheological characteristics of asphalt modified with waste engine oil (WEO)" 36(6), 475-480.
- [13] D. ASTM, “Standard test method for penetration of bituminous materials,” USA, ASTM Int., 2013
- [14] ASTM, “Astm D 36,” “Standard Test Method Softening Point Bitumen”, ASTM Int. West Conshohocken, PA, USA., vol. 1,no. d,pp. 3–6, 2006.
- [15] BSI Standards Publication Bituminous mixtures — Test methods for hot mix asphalt:“Determination of theaffinity between aggregate and bitumen,”2012.





# A REVIEW ON REPAIRING FIRE-DAMAGE GYPSUM BOARD

*Muhammad Rizwan Ul Haq*

Sarhad University of Science & Information Technology, Peshawar,  
[mrizwanulhaq89@gmail.com](mailto:mrizwanulhaq89@gmail.com)

**Abstract-** Recently, different types of gypsum board composition are being used in buildings due to their excellent thermal properties. Thus, the requirement for fire safety concerns rose. As a result, the goals of these studies are to first reduce the fire risk of gypsum board at normal temperatures, and then to increase the maximum failure time of gypsum-based boards when exposed to fire. Finally, maintenance or repair of fire-damaged gypsum-based material. Fire-resistant plasterboards were used because of their thermal, physical, and heat transfer properties. Various types of gypsum board were manufactured around the globe and studied for their chemical composition and thermal effects at high temperatures. By executing fire tests on gypsum-based boards, the results showed that gypsum board slows the process of extinguishing fire, and it performed well up to 400 °C. When the temperature was raised to 600 °C, cracking and volume shrinkage were observed. When the temperature rises by up to 1000 °C, the gypsum board crumbles. According to the findings of this study, increasing the thickness of the board, decreasing the density of the main element pure gypsum, the initial mass friction dehydration process, then hemi-deration process, air cavity filled with insulation material, and the addition of mixed proportions of PCM with gypsum all help to improve the failure time.

**Keywords** - Gypsum board, High Temperature, Fire Test, Shrinkage, Cracking, Falling off.

## 1 Introduction

Kong et al. (2022) reported that, due to its exceptional fire resistance, gypsum board (GB) is used as a fire-resistant component of walls. However, cracking and separation lead to partition failure because water leaks out at high temperatures [1]. As Feng and Jihong (2022) reported, a key factor in the accuracy of the thermal response simulation for cold-formed steel (CFS) composite buildings is the specific heat capacity at high temperatures of fire-resistant gypsum boards. However, the current standard does not provide complete and precise values for the test parameters (such as heating rate, sample quality, and sample size) that were used to determine the specific heat capacity of gypsum boards [2]. D.Norsk et al. (2022) studied that partition walls composed of gypsum plasterboard are commonly used in construction, and they provide passive fire protection as separating elements due to their significant role in determining the wall's fire resistance Thermo-mechanical characteristics [3]. In 1888, Augustine Sackett, combined layers of paper with plaster of Paris, and moulded a sample of the first gypsum board, which became "Sacket Board". In the 1950s, technology for gypsum board was developed, allowing for the invention and modification of designs of fire-rated gypsum board on peak and the manufacture of different types of gypsum board including partitions in curves, curved edges, partitions without stud and runner, special types of nails, low density plaster board, and sound-controlling systems. Gypsum board materials in that period were at their peak in commercial and residential buildings due to inventions and experimental studies [4]. Gypsum board is used in approximately 50% of new houses that were constructed in 1955. Lightweight steel-framed buildings were most compatible with lightweight gypsum assemblies,



which encouraged the design of high-rise commercial and residential building construction in the 1960 to 1970 eras [4]. Nowadays, different types of gypsum products are used in interior designing, ceiling decoration, wall partitions, duct closing of HVAC, wet areas of kitchens and toilets, fire rated partitions, stairwells and lift shafts. Because of the cost-saving and fire-resistance properties of gypsum assemblies, Gypsum minerals are sedimentary rocks in crystalline form called "calcium sulphate dehydrate". Chemically combined water was found in 21 pounds of raw material. Rock is taken from mines, then big-sized rocks are turned to small aggregates by crushing. After crushing, the material is ground into powder and dried at 350 °C. Drying off 3/4 of the chemically combined water is known as calcining. This calcined powder is used in gypsum plaster and in other products [5].

Gypsum board manufacturing, additives and calcined powder mixed with water will become a paste, then using a machine put on a layer of paper. The conveyor machine moves down, then the gypsum board rehydrates and turns into its original shape. The chemical and mechanical bonds cause the paper layer to harden. Then the board moves toward and cuts into the stander length to clean the surface or remove the dampness on the surface [6]. Gypsum board is the best fire-resistant material in the construction industry. It is used in interior decoration and where fire resistance requirements as per stander are met. Because its core has chemically combined water when exposed to fire, it evaporated slowly in a form of steam, which helps to slow the heat transfer rate. Even after releasing all the water steam, it becomes a heat insulation barrier. Furthermore, tests conducted according to ASTM Standard (E 84) show that gypsum board has a low flame and smoke spreading index. Gypsum-based material is used with other materials to protect the building element effectively from fire at specified times [7]. The study's goal, it is quite difficult to simulate the fire behavior of plasterboard's cracking, falling off, and water transport caused by gypsum. The effectiveness of the wall's fire resistance is determined by carrying out fire tests. The aim of the study is to assess the fire resistance of walls lined with gypsum plasterboard and steel studs. On the gypsum plasterboard walls, a number of large, medium, and small-scale fire tests are carried out. The goal of these studies is to identify the risk of fire with gypsum board assemblies in commercial and residential buildings so that humans can be evacuated before the gypsum board assemblies fail during fire exposure.

## **2 Fire Risk for Gypsum Board Assemblies**

The fire risk in residential and commercial buildings can vary depending on the building's specific use. In residential buildings garage areas where flammable materials or vehicles were parked, kitchen areas, hearths, and electrical main boards on or inside partition walls and behind the ceiling where shortcutting chases. Commercial buildings have a higher fire risk than residential buildings because they are used more frequently than residential buildings. For those reasons, specific uses of gypsum boards, which include Type X Gypsum Board for fire-resistance-rated building systems, roof systems, interior walls, exterior walls, soffits and ceilings, vertical openings, stairs, and HVAC duct enclosure, By keeping in mind fire risk aspects, failure in gypsum-based material could be in the form of a collapsed structure due to losing thermal properties. Research restricted the focus only on the thermal failure of non-load-bearing elements, and when the temperature of the backside of the unexposed surface of a board increases beyond 700 C, it is known as the thermal failure time [8]. During the furnace test, the temperature in the beginning gradually increased until it reached a critical temperature. After that, a sudden increase in temperature was noticed and reported as failure time [9]. Furthermore, failure time analysis by considering different characteristics of gypsum components When gypsum is heated, two dehydration processes happen in the range of 80 °C to 250 °C [3]. First, it was converted to di-hydrated gypsum, then to hemi-hydrate gypsum, and finally to anhydrous gypsum. During this process, first water turns into steam and evaporates from gypsum, and then a slow reaction happens until all water evaporates from gypsum. At that stage, gypsum board loses all resistance against thermal protection. At this stage, when gypsum loses thermal resistance, it is known as failure time [10].

One of the oldest materials is gypsum board. Around the globe, use of gypsum board began around 7000 years B.C. Use of gypsum board was noticed. Nowadays, more use of gypsum-based products in building construction is due to the availability of raw materials for their manufacturing. They are easy to fabricate, environmentally friendly, and have excellent thermal insulation and fire protection qualities. Fire resistant qualities depend on the dehydration process and the low thermal conductivity of gypsum products. These properties demonstrated the ability to effectively delay or retard temperature in a fire situation environment. However, the volume shrinkage and cracks due to high temperatures lead to the gypsum product collapsing, which brings challenges to fire-resistant gypsum board members [11]. Current studies show different admixtures were used with gypsum material for different purposes, such as metakaolin, latex, expanded



polystyrene, glass fiber, fly ash, furnace slag, silica fume, lime, cement, vermiculite, and perlite. In the same period, considerable attention was gained by the fire resistance requirements of buildings. Studying the behaviour of fire and understanding the philosophy of gypsum material exposed to elevated temperatures are flattering principles for safety and business motive. Studies mainly focused on the most commonly used pure gypsum board products compared with fire resistance behavior. For example, Thomas et al. studied the chemistry behind the dehydration process while increasing the temperature. Ghazi et al. and Park et al. explored the thermal properties of gypsum material exposed to fire. Nevertheless, the impact of admixtures on gypsum material properties at elevated temperatures has been investigated until now [12].

### 3 Post Fire Assessment

According to laboratory fire test evidence from US gypsum companies, fire resistance characteristics may vary from company to company manufacturing. Gypsum board is well known due to its characteristics of fire resistance. Yanqiu Chen's research found that gypsum board structure performing well to resist heat, flame, and smoke due to slow dehydration process, evacuation time will increase if escape ways are available and clear, and gypsum board thickness is greater than fire resistance time will also increase. These were the board thickness, the di-hydration process of gypsum, and the hemi-hydration process of gypsum. When those were increased to 5%, the increase in failure time was noticed from 8 % to 12% [13]. Zhong Taoa performed tests for pure gypsum board with formable phase change material [table 01]. For economic analysis, a ceiling model for FSPCM-gypsum board was created and tested in normal environmental conditions. Results discussed 16% cooling load saved while using FSPCM with a gypsum board ceiling [14] [Table 1]. Lenka Scheinherrová investigated the changes in properties of different gypsum materials at elevated temperatures. Three gypsum board samples, one pure gypsum, one gypsum-lime binder, and one gypsum-lime-silica fume binder, were prepared and exposed to 1000 C temperature. Only the gypsum-lime binder did not perform well at 400 C temperatures. Pure gypsum binder performed best at high temperatures [15]. C.N. Ang and Y.C. Wang concluded that additional specific heat value is affected by the heating rate of natural fires and the permeability of gypsum plasterboard [16].

Table 1- Gypsum Board and PCM GB Mix Design proportions

Specimen	Pure gypsum (g)	PCM (g)	Gauge water	Foam water	Potassium sulphate	Glass fibres	Polyacrylic acid	Alkyl sulphate oligomers
GB	715		257	358	1.61	4.6	0.11	0.46
PCM GB	511	204	184	256	1.15	3.3	0.08	0.33

Xianyong Li conducted fire resistance tests, preparing a steel column covered by gypsum board and then analysing it at various temperatures. SAFIR standard was compared with test results, steel temperature histories were used to obtain fire exposed results, and fire results were used to develop a formula for predicting test model critical temperature less than 1,000 °F (538 °C) [17]. Rene Prieler and companions performed fire resistance tests to determine the heat transfer rate and water vapour transformation. The results show that at 65 °C, thermal heat conduction was the primary cause of heating in thin gypsum assemblies up to 2.5 cm thick.

When the temperature was raised to 100 °C, more water vapour condensed. Furthermore, during fire exposure, a sudden decrease of water vapours recorded in mineral wool from 33.3 mm<sup>2</sup>/s to 26.7 mm<sup>2</sup>/s was determined. Finally, the result shows that the water vapour mean velocity was determined to be between 1 and 3 mm/s [18]. Jae D and companions investigated the characteristics of functional gypsum board (FGB) with expanded vermiculite (EV), expanded perlite (EP), nano carbon material (C300), and noctadecane (PCM) were analysed by Fourier transform infrared (FTIR) spectroscopy for structural stability. As a result, FGB's thermal conductivities decreased by 15% when compared to conventional gypsum board. In the case of moisture properties, the water vapour resistance and water content of FGB were increased, compared with the conventional gypsum board (SR). However, the simulation results showed that there were no moisture problems, such as condensation, mould growth, or structural damage [19].



Ahmed Allam investigated: mathematical equations were developed to predict the behaviour of gypsum board during fires, which were calibrated during fire tests. A gypsum board wall test was built with C-section studs and gypsum fixed on both sides of the studs. Rockwool insulation was used to fill the cavity between the two layers of gypsum board. The sample was subjected to a standard fire test. During exposure to fire, the wall was found damaged and changed in physical, thermal, and chemical behaviour. The prediction of the equation for maximum thermal bowing of walls was quite close to the maximum values collected during the fire test. He proposed adopting the equation for structural fire engineers and fire laboratories as tools to solve the exercise [20]. She investigated the deformation, mechanical, and thermal properties of foamed gypsum at high temperatures. Two samples were prepared; one was pure gypsum (800 kg/m<sup>3</sup>), the second was foamed gypsum (650 kg/m<sup>3</sup>), and the third was fibre glass or vermiculite with foamed gypsum. They were tested under temperatures from 25 °C to 800 °C. Test results showed the first sample had more cracks than the second sample when exposed to high temperatures. Furthermore, adding fibre glass could increase thermal cracks and shrinkage of gypsum board when fibre glass melts during fire exposure, but use of vermiculite enhanced the properties of shrinkage, reducing the cracking in gypsum board and reducing the loss of strength while exposed to fire [21].

#### 4 Repairing of Gypsum Board Assemblies

Raffaele Landolfo investigated the fire side of gypsum board, which lost strength due to dehydration, loss of physical properties, and also in vertical direction, bowing is found during fire tests [22]. Sajith Wijesuriya investigated many factors effecting the failure time while exposed to fire. One was the density of board; the second was the thickness of board; the third was the mass fraction in the initial phase of di-hydrate of gypsum content; the fourth was the di-hydration process; and the fifth was the hemi-hydration process. Sixth, the time of failure could be increased if highly reflective paper were used. The seventh was that failure time was extended when the air cavity of gypsum board could be filled with insulation, and also that melting of insulation and heat transfer ratio were impacting the failure time. In the thickness of board, di-hydration and hemi-hydration were increased by 5%. Then, the extension of failure time increased from 8% to 12% [23]. Gypsum board assemblies can be repaired if the fire exposure temperature is not more than 400 °C. Otherwise, when exposed to high temperatures, gypsum-based assemblies fully fall off or partially fall off. In this condition, fire damaged gypsum board residual material is used in its initial processing phase to make new gypsum board. According to studies, there is no evidence for fire damaged gypsum board repair. Damaged portions could be identified by physical appearance and replaced with new gypsum board [24].



(a)



(b)

Figure 1. (a) Bowing in test wall (one hour exposure) (b) Post fire inspection of test wall



## 5 Conclusion

Gypsum board is the best fire-resistant material in the construction industry. It is used in interior decoration and where fire resistance requirements as per standard are met. Because its core has chemically combined water when exposed to fire, it evaporated slowly in a form of steam, which helps to slow the heat transfer rate. Even after releasing all the water steam, it becomes a heat insulation barrier. It is quite difficult to simulate the fire behaviour of plasterboard's cracking, falling off, and water transport caused by gypsum. The effectiveness of the wall's fire resistance is determined by carrying out fire tests. The aim of the study is to assess the fire resistance of walls lined with gypsum plasterboard and steel studs. On the gypsum plasterboard walls, a number of large, medium, and small-scale fire tests are carried out. The below outcome is favourable indicating the fire damaged gypsum board at safe fire temperature could be repaired but if exposed to high temperature gypsum board shrinks, cracked and fall of due to chemically and physically change in gypsum board. Fire damaged gypsum board residual material could be used with raw material to gypsum board to make new gypsum boards. Following conclusions can be drawn from the conducted study:

- The fire resistance ratings of single layer loadbearing assemblies were enhanced by the addition of glass fibre to standard lightweight gypsum board cores.
- Gypsum board type X, Type C could be used for fire resistance because they have contain shrinkage-compensating additive
- Gypsum board slows the process of fire expanding due to Gypsum dehydration processes cause water vapour to be produced and then dispersed in the fire compartment when gypsum plasterboard wall assemblies are subjected to a high temperature environment. These phenomena are frequently disregarded in pertinent Computational Fluid Dynamics (CFD) simulation.
- Thermal variation causes volume shrinkage, crack formation, and strength loss. As a result, high-temperature fire-exposed gypsum board was damaged partially or fully. It will then need to replace the affected area of gypsum board with new GB.

## Recommendations

- Future research requirements are defined in the context of current performance-based fire safety engineering ideas.
- The essay ends with a list of important study areas that will increase our understanding of how gypsum boards perform on wood during a fire.
- Future experiments and numerical studies will focus on combined heat and mass transmission in multilayered buildings.
- This work unequivocally shows that it is crucial to include gypsum board contraction and crack formation in future models in order to model the failure of partition assemblies.
- Gypsum boards tend to disintegrate after being exposed to moisture. It needs potential research on water resistance as well

## Acknowledgment

The authors would like to express their gratitude to everyone who assisted with the research particularly CE department, Dr. M Ali. The anonymous reviewers' thorough examination and constructive suggestions are gratefully acknowledged.

## References

- [1] Kong Yue, Bing Liang, , "Fire resistance of light wood frame walls sheathed with innovative gypsum-particle composite: Experimental investigations", *Journal of Building Engineering*, 2022
- [1] D.Norsk, A.Sauca, "Fire resistance evaluation of gypsum plasterboard walls using machine learning method", *Fire Safety Journal*, 2022



- [3] Yu Feng, “Standardization of high-temperature specific heat capacity test parameters of fire-resistant gypsum board”, *Fire and Materials*, 2021
- [4] Bronwyn Chorlton, John Gales, “Fire performance of heritage and contemporary timber encapsulation materials”, *Journal of Building Engineering*, 2022
- [5] McLaggan, R. M. Hadden, M. Gillie, “Fire Performance of Phase Change Material Enhanced Plasterboard”, *Fire Technology*, 2021.
- [6] Yanqiu Chen, Naveen Punati, Suman Sinha Ray, Lizhong Yang, Kuldeep Prasad, “Thermal failure time of non-loadbearing gypsum board assemblies in standard furnace tests”, *Applied Thermal Engineering*, 2020.
- [7] Md Jaynul Abdena, Zhong Taoa, Zhu Pana, Laurel Georgeb, Richard Wuhreb, “Inclusion of methyl stearate /diatomite composite in gypsum board ceiling for building energy conservation” *Applied Energy*, 2022.
- [8] Magdaléna Doležalová, Lenka Scheinherrová, Jitka Krejssová, Alena Vimmrová, “Effect of high temperature on gypsum-based composites”, *Construction and Building Materials*, 2021.
- [9] C.N. Ang, Y.C. Wang, “The effect of water movement on specific heat of gypsum plasterboard in heat transfer analysis under natural fire exposure”, *Construction and Building Materials*, 2004.
- [10] Wei Chen, Jihong Ye, Xianyong Li, “Thermal behavior of gypsum-sheathed cold-formed steel composite assemblies under fire conditions”, *Journal of Constructional Steel Research*, 2021.
- [11] Rene Prieler, Peter Kitzmüller, Stefan Thumser, Günther Schwabegger, Erhard Kaschnitz, Christoph Hochenauer, “Experimental analysis of moisture transfer and phase change in porous insulation exposed to fire and its effect on heat transfer”, *International Journal of Heat and Mass Transfer*, 2022.
- [12] Ji Hun Park, Yujin Kang, Jongki Lee, Seunghwan Wi, Jae D. Chang, Sumin Kim, “Analysis of walls of functional gypsum board added with porous material and phase change material to improve hygrothermal performance”, *Energy & Buildings*, 2019.
- [13] Ayman Y. Nassif, Isamu Yoshitake, Ahmed Allam, “Full-scale fire testing and numerical modelling of the transient Thermo-mechanical behaviour of steel-stud gypsum board partition Walls”, *Construction and Building Materials*, 2014.
- [14] Zhenxing Du, Wei She, Wenqiang Zuo, Jinxiang Hong, Yunsheng Zhang, Changwen Miao, “Foamed gypsum composite with heat-resistant admixture under high temperature: Mechanical, thermal and deformation performances”, *Cement and Concrete Composites*, 2022.
- [15] Naser P. Sharifi, Ahsan Aadil Nizam Shaikh, Aaron R. Sakulich, “Application of Phase Change Materials in Gypsum Boards to Meet Building Energy Conservation Goals”, *Energy and Buildings*, 2020.
- [16] Fabio Iucolano, Barbara Liguori, Paolo Aprea, Domenico Caputo, “Thermo-mechanical behaviour of hemp fibers-reinforced gypsum Plasters”, *Construction and Building Materials*, 2021.
- [17] Luigi Fiorino, Bianca Bucciero, Raffaele Landolfo, “Evaluation of seismic dynamic behaviour of drywall partitions, façades and ceilings through shake table testing”, *Engineering Structures*, 2019.
- [18] Sajith Wijesuriya, Matthew Brandt, Paulo Cesar Tabares-Velasco, “Parametric analysis of a residential building with phase change material (PCM)-enhanced drywall, precooling, and variable electric rates in a hot and dry climate”, *Applied Energy*, 2018.
- [19] Zheng Peng, Hossein Mostafaei, “Fire Resistance of Gypsum Board Protected Steel Columns with High Load Ratios”, *Journal of Structural Engineering*, 2021.
- [20] Anthony Deloge Ariyanayagam, Mahen Mahendran, “Fire tests of non-load bearing light gauge steel frame walls lined with calcium silicate boards and gypsum plasterboards”, *Thin-Walled Structures*, 2020.
- [21] Harikrishnan Magarabooshanam, Anthony Ariyanayagam, Mahen Mahendran, “Fire resistance of non-load bearing LSF walls with varying cavity depth”, *Thin-Walled Structures*, 2022.
- [22] Wei Chen, Jihong Ye, Qingyang Zhao, Jian Jiang, “Full-scale experiments of gypsum-sheathed cavity-insulated coldformed Steel walls under different fire conditions” *Journal of Constructional Steel Research*, 2022.
- [23] Samuel L. Manzello, Richard G. Gann, Scott R. Kukuck and David B. Lenhart, “Influence of gypsum board type (X or C) on real fire performance of partition assemblies”, *Fire and Materials*, 2006.
- [24] Andrea Frangi, Vanessa Schleifer and Mario Fontana, Erich Hugi, Empa, “Experimental and Numerical Analysis of Gypsum Plasterboards in Fire”, *Fire Technology*, 2009.



# A REVIEW ON THE USAGE OF MODERN TECHNIQUES TO OVERCOME THE ISSUES IN RAPID SETTING CONCRETE FOR EXTREME TEMPERATURE ZONES

<sup>a</sup> Ayesha Aziz, <sup>b</sup> Minhas Shah\*

a: Bahria Business school, Bahria University, Islamabad, [ayeshaaziz744@gmail.com](mailto:ayeshaaziz744@gmail.com)

b: Department of Civil Engineering, CUST [shahminhas96@yahoo.com](mailto:shahminhas96@yahoo.com)

\* Corresponding author: Email ID: [shahminhas96@yahoo.com](mailto:shahminhas96@yahoo.com)

**Abstract-** Rapid setting concrete has a wide range of use in the construction industry which has helped it gain significance. Conventionally admixtures are used to reduce the setting time of concrete for extreme temperature sites, underwater construction, and pavements where the waiting time is a crucial issue. Therefore, extensive research is being carried out around the globe to find solutions that can help, overcome the issues arising in the conventional rapid setting concrete. The objective of this study is to discuss all the major flaws and propose remedies based on the literature. A comprehensive review of the literature, mostly from articles published in the last decade, was carried out to find the issues observed in the conventional rapid setting concrete, the governing properties, and finally, solutions have been given based upon the conclusive remarks of the authors of the reviewed articles. After a careful study of the literature, it was deduced that using Polyurethane in fresh concrete along with some kind of natural fiber can result in effective outcomes. The study will help in exploring modern ways that can be of great significance for the construction industry.

**Keywords-** Fiber Reinforced Concrete, Hydration, Polyurethane Elastic Concrete, Rapid setting concrete.

## 1 Introduction

Rapid setting concrete is a type of concrete formed when an admixture, specifically an accelerator, is mixed with conventional cement concrete. Due to its property of achieving strength and setting in a very short time, it has been used for a long time in situations where exposing fresh concrete to the surrounding environment is not favorable for example in heavy volume roads and bridge decks where maintenance time could result in inconvenience for the road users, underwater construction where fresh concrete would lose its properties due to interference of water surrounding it, construction sites at high and low-temperature zones where the early setting is necessary as the hydration process is hindered by the environment. In addition to the required strength, concrete used for laying pavements needs to be rapid-setting concrete with good workability and durability [1]. Expansion joints of concrete bridge decks are vulnerable entities that require high and quick maintenance for proper functioning in order to facilitate the users [2]. Due to cold weather in the northern areas, the construction season is very limited. Due to the use of conventional rapid hardening concrete, there are detrimental effects on the reactivity and mechanical performance of concrete [26]. Using the conventional method for rapid hardening is not effective as it has drawbacks that compromise the performance of the concrete.

In hot temperature zones, the water evaporates quickly resulting in the insufficient curing of concrete, and in low-temperature zones the hydration process doesn't happen efficiently which leads to shrinkage cracks in the concrete. The current practice all around the globe to cater to shrinkage cracking is the usage of fibers, this includes natural, synthetic and even hybrid form of fibers. This method does not only give good results but is a sustainable way of catering to this challenge. Wu et al. [3] performed a study on waste concrete using fibers are different quantities. It was found that using



the optimum quantity of fibers in concrete showed that the addition of fibers is very useful in incorporating shrinkage cracks. Salvador et al. [4] studied the effect of accelerator type and dosage and the results showed that the use of accelerators deteriorates the concrete due to the sulfate action. Rapid hardening concrete containing phosphate has a short setting time but it cannot meet the requirements of rapid hardening concrete [25]. Hence, the alternates for conventional hardening concrete which include inorganic chemicals cannot help to meet the standard properties.

This study is aimed at finding the major issues that arise in the conventional rapid setting concrete that has been mentioned in the literature and then assessing the governing parameters that become the cause of these issues and finally, on the basis of available studies, proposing different modern solutions that would help the industry avoid the issues faced in the conventional rapid setting concrete. With the availability of literature that contains different solutions for this particular problem can help in choosing the best solution based on the resources and the ease of construction and the properties required.

## 2 Issues in usage of rapid setting concrete

From the very start of usage of rapid setting concrete there have been issues with it which range from shrinkage cracks due to improper dissipation of heat during the hydration process, that cause the shrinkage cracks to develop, to Sulfate action due to the aluminum sulfate in the form of accelerator. Moreover, the high cost of this accelerator and its handling is also an issue that needs to be addressed in a more sustainable manner. Rapid setting time can help in achieving early strength but at the same time decreases the workability and interlayer adherence [5].

### 2.1 Chemical attack.

The rapid hardening of concrete is achieved by the addition of a chemical to the ordinary Portland cement, this imposes that the accelerator will react to form other chemicals that would be not in favour of the concrete. Zhang et al. [6] performed an experimental investigation in which OPC was mixed with Calcium Sulfoaluminate cement (CSA) which acted as a rapid-setting cement. It was observed that mixing CSA and OPC increases the PH value of the matrix hence compromising the morphology of CSA. Briendl et al. [7] performed a comparative study on the fast-setting spray binder and OPC with aluminium sulphate and it was concluded that the strength of OPC concrete is compromised by the availability of aluminium sulphate due to the formation of Calcium-Aluminium-Silicate hydrates.

### 2.2 Formation of Shrinkage Cracks.

Shrinkage cracks is a common phenomenon that occurs due to incomplete hydration during the curing of cement concrete. Ziari et al. [8], using a digital monitoring approach, observed the effects of temperature and humidity on freshly poured concrete pavements, the results indicated that temperature has a significant hand in the formation of shrinkage cracks. Moelich et al. [9] proposed in their study that solar radiations increase the temperature of the concrete hence increasing the pore water loss ultimately causing shrinkage cracking. As shown in figure 1 that for samples containing blast furnace slag, the area of crack is more as compared to the samples containing limestone and overall the crack area is more for samples that were placed in sun.

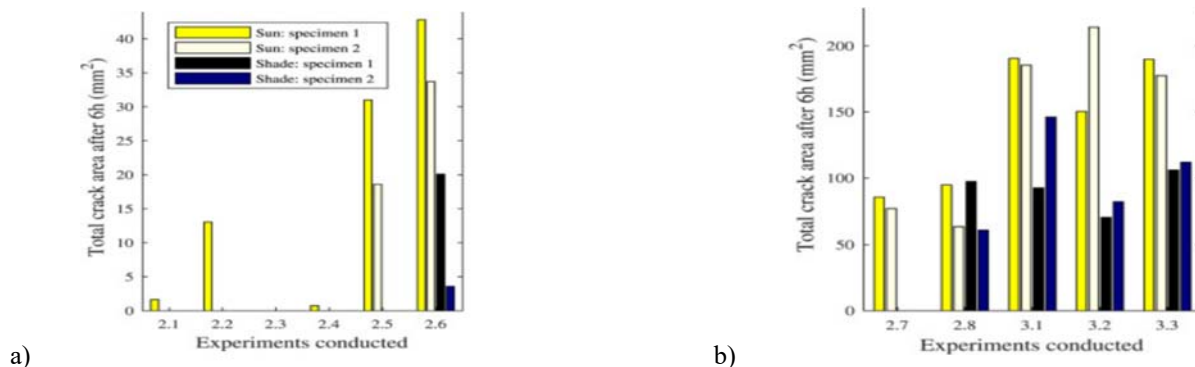


Figure 1: Specimen total crack area (a) for samples containing limestone (b) for samples containing blast furnace slag [9]





Sayahi et al. [10] in their study, about plastic shrinkage due to accelerated hydration, have discussed that accelerators usually increase the rate of hydration and this increase in hydration increases the amount and rate of autogenous shrinkage that further increases the width of initial shrinkage cracks. Once the cracks are generated freeze and thaw action or crack propagation for any other reason can take place hence increasing the crack width and compromising the performance of the concrete element

### **3 Governing parameters**

The issues that arise in conventional rapid-setting concrete are controlled by some parameters. These parameters include the existence of additive itself in the rapid setting concrete, surrounding temperature and humidity and the fineness of the cement particles which are responsible for shrinkage. Use of Alkaline based accelerator reduced the strength in later stage after casting of concrete also resulting in shrinkage cracking and alkali deterioration [11]. The final hydration degree of concrete is reduced by alkaline accelerators as hydration products of alkaline accelerators are composed of Calcium Silicate Hydrates and Calcium Aluminate Hydrates [12]. Fine cement particles tend to have more surface area which means more water will be required for the hydration process, hence when the water content is not taken into account against the fineness of cement shrinkage and cracks start to appear [13]. Alaskar et al. [14] performed an investigative study on cements having different fineness values and it was observed that higher fineness resulted in higher shrinkage whereas lower fineness resulted in lower shrinkage. Maruyama et al. [15] performed a study to find the relation between fineness and shrinkage. However, the relation was not established on the other hand it was found that Calcium Silicate Hydrate undergoes volumetric expansion resulting in shrinkage cracks. Sulfate attack due to the use of conventional Aluminum Sulfate as an accelerator leads to formation of crystalline structures like gypsum and ettringite which produce high crystallization pressure hence affecting the life of the concrete [16]

### **4 Modern remedies**

The modern methods include using composites to cater different issues at the same time. Sika Rapid 3 accelerator was used along with steel fibers and mechanical tests were performed, the results were then compared with samples without Sika Rapid 3 accelerators. It was seen that the shrinkage cracking was reduced and the flexural and compressive strength values were substantial [17]. Liquid accelerator when used with Sulfoaluminate expansive agent for shotcrete for rapid setting, showed that the shrinkage cracking can be controlled and setting time can be enhanced [18]. Reduction of paste content by increasing the size of aggregate not only resulted in more durability but also helped in mitigating shrinkage cracks [19].

#### **4.1 Fibre Reinforced concrete for shrinkage cracks.**

It is a fact that fibers cannot completely stop shrinkage cracking from taking place but they are very significant as they contribute by stopping the propagation of these cracks [20]. Using different types of fibers with different distribution patterns have resulted in good resistance against shrinkage cracking along with improving the mechanical properties of concrete [21]. Statkauskas et al. [22] performed an investigative study which involved the addition of Polypropylene fiber and Hemp fiber to concrete in addition to quick lime and shrinkage reducing agent. The results were impressive as the highest shrinkage reduction value was obtained.

#### **4.2 Polyurethane Elastic Concrete**

PE Concrete is a modern composite material that comprises quartz sand as the filler material and polyurethane as the binder. The polyurethane used in the manufacturing of this concrete is done by adding two chemicals i.e. polyol and Isocyanate. As compared to conventional concrete this concrete has a rapid setting property with a gain of mechanical strength at an early age. The use of fibers along with Polyurethane is also under study. The incorporation of fiber leads to the reduction in shrinkage cracks. Incorporation of steel fiber in polyurethane concrete with different proportions and their optimization using modern methods and then their mechanical tests revealed that steel fiber helps in increasing the toughness whereas the overall flexural and compressive strength increases with the usage of Fiber Reinforced Polyurethane Elastic Concrete (FRPEC) [23]. It can be seen in table 1 that steel fibers having a tensile strength of more than 2500MPa and 13mm in length were used for the investigation of FRPEC.



The incorporation of steel fiber helps in resisting crack formation and propagation due to the anchoring it provides to the concrete matrix. The tensile strength increases due to the bridging effect that steel fibers provide as the fibers are anchored in the concrete. Polyurethane concrete has good UV aging resistance along with good wear, frost and fatigue resistance but the polyurethane concrete has fast setting time that makes it difficult for long distance transportation however addition of retarder like phosphate ester can solve the issue [26].

Table 1 Properties of steel fibers for optimum results [23]

Material	Density (g/cm <sup>3</sup> )	Length (mm)	Tensile strength (MPa)
Steel fibers	7.8	13	>2500

### 4.3 Calcium Sulfoaluminate-OPC blend with nano-silica

Limited research is available on the use of the blend of Ordinary Portland Cement and Calcium Sulfoaluminate, which transforms the setting time of concrete. Different strategies have been applied to overcome the issues that arise in early setting concrete. Li et al. [24] studied the mechanical properties of the blend of CSA-OPC along with Nano-silica and during the SEM analysis, it was observed that the addition of Nano-silica gives a more viable result in terms of early setting time as compared to conventional methods. The use of Nano-silica enhances the properties because of its pozzolanic reactivity and the ability to fill pores due to the small size of particles.

## 5 Practical Implementation

Concrete has been used for a very long period because of its durability, strength, and ease of pouring. However, using concrete in extreme temperatures has always been an issue. Mostly in cold climate areas construction is seized during extremely low temperatures and hence reducing the speed of development. Rapid hardening concrete was then introduced to overcome this issue but due to the sulfate action that occurs in the rapid hardening concrete and insufficient hydration of the concrete, there arise problems that can affect the performance of concrete. For this reason, it is important to find new developments that can help cater to the above-mentioned problems.

The mentioned techniques have a wide range of use based on the results that have been obtained by different researchers. The increased compressive strength and resistance to sulfate action make the modern methods adaptable for compression members like columns and piers. Moreover, the increased flexural strength and rapid hardening without any, currently known, drawbacks these modern methods are best suited for rigid pavement construction. These techniques, especially Polyurethane concrete are best suited for the repair of concrete bridge joints.

## 6 Conclusion

Following conclusions can be drawn from the conducted study:

- 1 Using conventional rapid setting concrete has some setbacks which include loss of workability, shrinkage cracking and sulfate attack which leads to concrete deterioration.
- 2 Rapid hydration process without enough dissipation of heat leads to shrinkage and the accelerator, containing sulfate ions, is responsible for the sulfate attack at a later stage.
- 3 Different Remedies have been proposed to substitute sulfate accelerators which include using Nano-silica with OPC-CSA blend and Polyurethane concrete with are viable solutions to avoid sulfate attack.
- 4 To avoid shrinkage cracks and sulfate attack at the same time fibers can be used and using natural fibers can be a good strategy and a sustainable solution.

The above outcome is favorable indication that using Polyurethane with natural fibers could reduce the cost of this concrete and it is hence required to study the use of natural waste fibers in this modern concrete that has not yet been studied in depth.



## Acknowledgment

The authors would like to thank every person/department who helped thorough out the research work, particularly Engr. Dr. Majid Ali. The careful review and constructive suggestions by the anonymous reviewers are gratefully acknowledged.

## References

- [1] Tahir, M. F. M., Abdullah, M. M. A. B., Abd Rahim, S. Z., Hasan, M. R. M., Saafi, M., Jaya, R. P., & Mohamed, R. Potential of industrial By-Products based geopolymer for rigid concrete pavement application. *Construction and Building Materials*, 344, 128190, 2022.
- [2] P. Lu, C. Zhou, S. Huang, Y. Shen, Y. Pan, Experimental study on mix ratio design and road performance of medium and small deformation seamless expansion joints of bridges, *Transp. Res. Rec.* 0361198120984741, 2021.
- [3] Wu, X., Zhou, J., Kang, T., Wang, F., Ding, X., & Wang, S. (2019). Laboratory investigation on the shrinkage cracking of waste fiber-reinforced recycled aggregate concrete. *Materials*, 12(8), 1196, 2019.
- [4] Salvador, R. P., Rambo, D. A., Bueno, R. M., Lima, S. R., & Figueiredo, A. D. Influence of accelerator type and dosage on the durability of wet-mixed sprayed concrete against external sulfate attack. *Construction and Building Materials*, 239, 117883, 2020.
- [5] Şahin, H. G., & Mardani-Aghabaglou, A. Assessment of materials, design parameters and some properties of 3D printing concrete mixtures; a state-of-the-art review. *Construction and Building Materials*, 316, 125865, 2022.
- [6] Zhang, J., Li, G., Ye, W., Chang, Y., Liu, Q., & Song, Z. Effects of ordinary Portland cement on the early properties and hydration of calcium sulfoaluminate cement. *Construction and Building Materials*, 186, 1144-1153. 2018.
- [7] Briendl, L. G., Mittermayr, F., Röck, R., Steindl, F. R., Sakoparnig, M., Juhart, J., ... & Galan, I. The hydration of fast setting spray binder versus (aluminum sulfate) accelerated OPC. *Materials and Structures*, 55(2), 1-27, 2022.
- [8] Ziari, H., Fazaeli, H., Vaziri Kang Olyaei, S. J., & Ziari, M. A.. Evaluation of effects of temperature, relative humidity, and wind speed on practical characteristics of plastic shrinkage cracking distress in concrete pavement using a digital monitoring approach. *International Journal of Pavement Research and Technology*, 15(1), 138-158, 2022.
- [9] Moelich, G. M., Van Zyl, J. E., Rabie, N., & Combrinck, R. The influence of solar radiation on plastic shrinkage cracking in concrete. *Cement and Concrete Composites*, 123, 104182, 2021.
- [10] Sayahi, F., Emborg, M., Hedlund, H., & Ghasemi, Y. Experimental validation of a novel method for estimating the severity of plastic shrinkage cracking in concrete. *Construction and Building Materials*, 339, 127794, 2022.
- [11] Zhang, L., Ma, R., Lai, J., Ruan, S., Qian, X., Yan, D., ... & Wang, S. Performance buildup of concrete cured under low-temperatures: Use of a new nanocomposite accelerator and its application. *Construction and Building Materials*, 335, 127529.
- [12] Wang, J., Xie, Y., Zhong, X., & Li, L. Test and simulation of cement hydration degree for shotcrete with alkaline and alkali-free accelerators. *Cement and Concrete Composites*, 112, 103684, 2022.
- [13] Šmilauer, V., Reiterman, P., Šulc, R., & Schořik, P. Crack-Resistant Cements under Drying: Results from Ring Shrinkage Tests and Multi-Physical Modeling. *Materials*, 15(12), 4040, 2022.
- [14] Alaskar, A., & Hooton, R. D. Effect of binder fineness and composition on length change of high-performance concrete. *Construction and Building Materials*, 237, 117537, 2020.
- [15] Maruyama, I., Sugimoto, H., Umeki, S., & Kurihara, R. Effect of Fineness of Cement on Drying Shrinkage. Available at SSRN 4036222.
- [16] Kaufmann, J., Loser, R., Winnefeld, F., & Leemann, A. Sulfate resistance testing of shotcrete—Sample preparation in the field and under laboratory conditions. *Construction and Building Materials*, 276, 122233, 2021.
- [17] Kos, Ž., Krovčakov, S., Kryzhanovskiy, V., & Grynyova, I. Research of Strength, Frost Resistance, Abrasion Resistance and Shrinkage of Steel Fiber Concrete for Rigid Highways and Airfields Pavement Repair. *Applied Sciences*, 12(3), 1174, 2022.
- [18] Zeng, L., Zhao, S., Wang, W., Qiao, M., Hong, J., Ran, Q., & Wang, Y. Accelerated Early Age Hydration of Cement Pastes Blended with Sulphoaluminate Expansive Agent. *Journal of Advanced Concrete Technology*, 19(6), 655-667, 2021.
- [19] Flatt, R. J., & Wangler, T. On sustainability and digital fabrication with concrete. *Cement and Concrete Research*, 106837.
- [20] Aghaee, K., & Khayat, K. H Effect of shrinkage-mitigating materials on performance of fiber-reinforced concrete—An overview. *Construction and Building Materials*, 305, 124586, 2021.
- [21] Bertelsen, I. M. G., Ottosen, L. M., & Fischer, G. Influence of fibre characteristics on plastic shrinkage cracking in cement-based materials: A review. *Construction and Building Materials*, 230, 116769, 2020.
- [22] Statkauskas, M., Grinys, A., & Vaičiukynienė, D. Investigation of Concrete Shrinkage Reducing Additives. *Materials*, 15(9), 3407, 2022.
- [23] Yahye, M. A., Liu, L., Honglin, W. U., Sun, Y., Sun, H., Ma, J., & Zhang, L. Experimental research on mechanical properties of Fiber-Reinforced Polyurethane Elastic Concrete (FRPEC). *Construction and Building Materials*, 328, 126929, 2022.
- [24] Li, G., Liu, Q., Niu, M., Cao, L., Nan, B., & Shi, C. Characteristic of silica nanoparticles on mechanical performance and microstructure of sulphoaluminate cement/ordinary Portland cement binary blends. *Construction and Building Materials*, 242, 118158, 2020.
- [25] Yu, R., Zhang, X., Hu, Y., Li, J., Zhou, F., Liu, K., ... & Shui, Z. Development of a rapid hardening ultra-high performance concrete (R-UHPC): From macro properties to micro structure. *Construction and Building Materials*, 329, 127188, 2022.
- [26] Li, L., & Yu, T. Curing comparison and performance investigation of polyurethane concrete with retarders. *Construction and Building Materials*, 326, 126883, 2022.



# COMPARISON OF EXPERIMENTAL SHEAR CENTRE OF VARIOUS SECTIONS WITH THEORETICAL ANALYSIS THROUGH RESPONSE SURFACE METHODOLOGY

<sup>a</sup> *Hassan bin Tariq*, <sup>a</sup> *S.M. Hassan Kazmi*, <sup>a</sup> *Muhammad Arslan*, <sup>a</sup> *M. Nasir Ayaz Khan*\*

a: Department of Civil Engineering, HITEC University Taxila, [19-Civil-027@Student.Hitecuni.Edu.Pk](mailto:19-Civil-027@Student.Hitecuni.Edu.Pk)

\*: [nasir.ayaz@hitecuni.edu.pk](mailto:nasir.ayaz@hitecuni.edu.pk)

**Abstract-** In this experimental study, three cross-sections of mild steel were studied to locate their shear center concerning the rotation of the load. Z-cross section was symmetrical, whereas L-section and semicircular section were symmetrical on one axis and unsymmetrical on another. The shear center's location is vital to designers in structural analysis. For the symmetrical section, the shear center was found to be zero in experimental as well as in Response Surface Methodology (RSM). The location of the shear center for the L-section was 43 mm, and for semicircular, the shear center was 28.5 mm. At the same time, the difference in error for L-section and semicircular section was found to be 45% and 0.77%. This study shows that an excellent theoretical and experimental relation has been established through RSM.

**Keywords-** shear center, symmetrical, unsymmetrical, Response Surface Methodology

## 1 Introduction

Thin-walled sections are produced through fabrication or extrusion method, are getting popularity, and become increasingly important due to the cost and manufacturing techniques of the materials. Although the level of shear stresses is small and sometimes negligible, however, the location of the shear center is of vital importance among the designers due to the twisting of the section [1]. Moreover, in structural analysis, the determination of the geometrical properties of cross-sections is necessary for the true depiction of the material. The shear center is defined as the point where the resultant of the shear stresses acts on it or the torsional rise due to axial force on a point in a flexural-torsional problem [2]. In the beam theory, several assumptions are made such as the beam is a thin structure, long as well as the cross-sectional dimension is very small compared to the rest of the dimensions. Hedgehog is a technique that could be effectively used in thin-walled sections to counter the horizontal effects on structure [3]. In recent research, optimization and algorithms has been successfully implemented to locate the shear point of complex thin-walled section [4]. There are several beam sections for which the shear center is determined. For instance, [5] studied the shear center and centroid of composite beam box cross-section. In the parallel study, [6] determine the properties of laminated composite tubes, and [7] studies the shear center of arbitrary sections through mathematical analysis by developing matrices for finding shearing and torsional rigidity. Response Surface Methodology is an optimization tool that could be efficiently implemented in many research studies to determine the best relation of experimental with theoretical study [8], [9].

In this research, various cross-sections of mild steel including semi-circular, Z-section, and L-sections are studied to find the shear center location. Moreover, the results were compared with statistical and mathematical modeling through Response Surface Methodology (RSM). This research will be helpful in assessing thin-walled sections position of load and point of rotation. When thin walled are subjected to lateral forces such as seismic or wind, torsional effect may encounter and twist the section. Moreover, RSM is an optimization tool which could be used to locate the point of zero shear which will benefit designers with economic and time constraints.



## 2 Research Methodology

In this study, 3 cross-sections of mild steel are studied for the location of the shear center. The cross-section section includes the Z-cross-section which is unsymmetrical, and L-section as well as semi-circular cross-sections are symmetrical on one axis and unsymmetrical on another axis. The materials, thickness, and length of all the cross-sections are constant so that only the shear location is focused. The dimensions of all cross-sections were carefully examined including the diameter and cross-section. Each beam was also visually observed for any dents or flaws. The sections were fixed in shear center apparatus and made sure no other movements/motions is influencing. The load was applied at an equal angle at various positions marked on sections. The front and back dial gauge reading was noted for every load position. The dial gauge reading was later converted to displacements by applying the least count. The rotations were calculated for every marked position on the section. The results were plotted for the position of load against the rotation. The experimental results were analyzed and modeled in Design-Expert software for Response Surface Methodology (RSM).

### 2.1 Materials.

The properties of sections are given in table 1. All sections were created with the same material (mild steel) having the same modulus of elasticity 210 (GPa) and the thickness of the flange is approximately 2.52 (mm). All the cross-sections were made through the fabrication method from M/S Smart Tech Multan through proper machining and tools after providing them dimensions. The cross-sections of different sections are shown in figure 1.

Table 1 Material properties of cross-sections

Material	Modulus of elasticity (GPa)	Flange thickness (mm)	Material thickness (mm)	Maximum constant load (N)
Mild steel	210	$2.52 \pm 2$	$1.7 \pm 2$	6.86

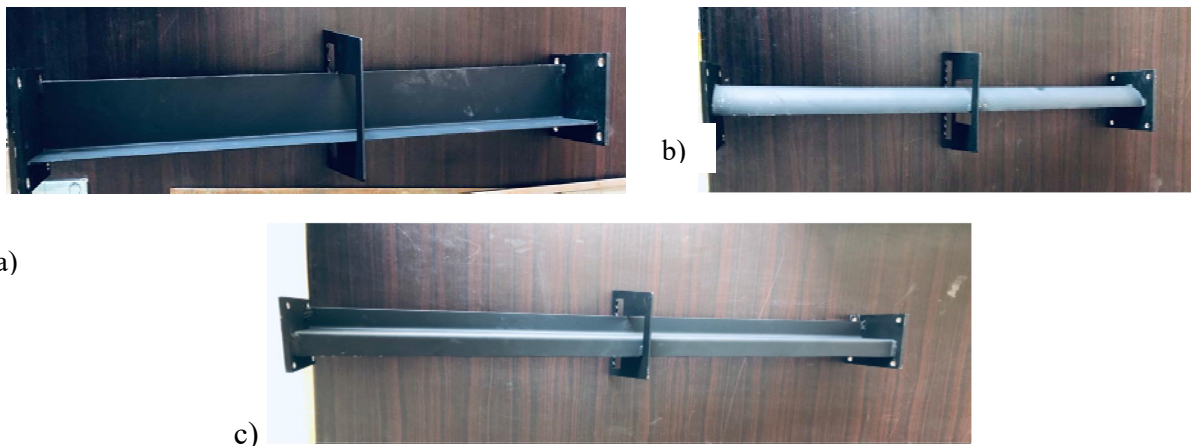


Figure 1: cross sections used in experiment, a. L-cross section, b. semi-circular cross section, and c. Z-cross section

## 3 Results

### 3.1 Experimental calculations

The plots between the position of load at the x-axis and rotation on the Y-axis were plotted after the necessary correction of dial gauges. The point where the graph crosses the zero notation is the exact point of the shear center. For instance, for all the load positions, the shear center for the Z-cross section was found to be zero as shown in figure 2.



The cumulative interpretation of the shear center for all three sections is shown in figure 4. It shows that the z-section is symmetric on all axis as the shear center lies at zero however, the L-section and semicircular section is symmetrical on one axis and unsymmetrical on another axis. The response surface methodology was carried out for all three sections. The experimental data load of position and rotation were input parameters in RSM. The output parameters rotation in mm were fixed for all three cross-sections. The ANOVA analysis and contours graphs are shown in figure 5.

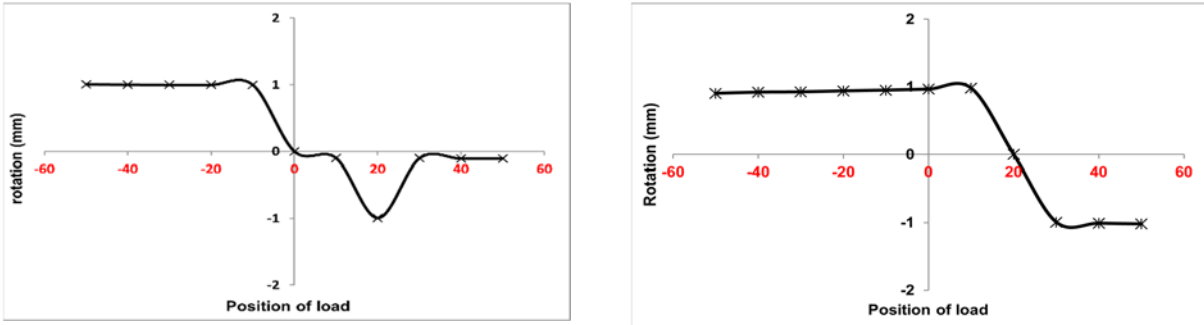


Figure 2: Z-cross section (left) and semi-cross section (right)

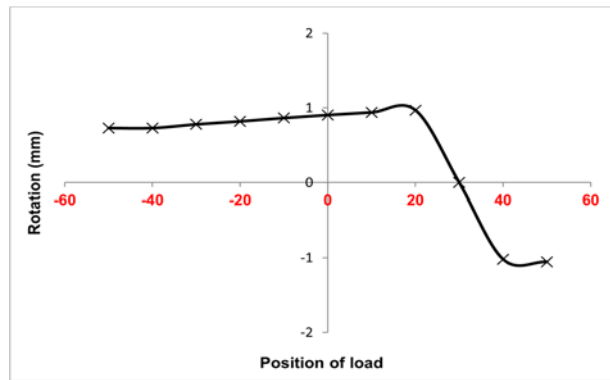


Figure 3: shear center of L-section

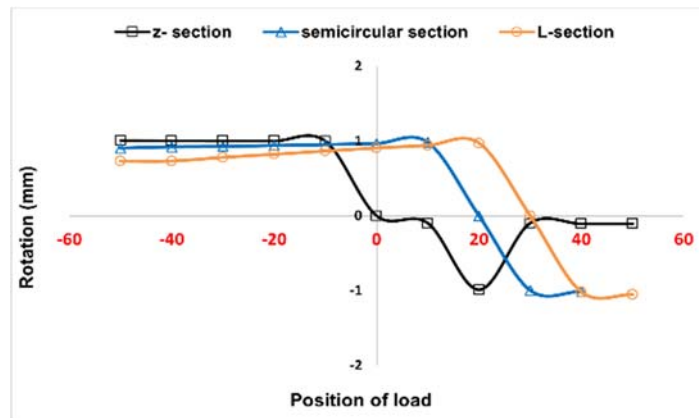


Figure 4: Cumulative representation of shear center for all sections

The position of load is mapped against various cross-sections. The means and standard deviations are also shown in the table. The value of rotation is plotted against the position of load. For instance, at zero position of load, the value of rotation noted for Z-section, Semi-circular and L-section were 0, 0.965 and 0.905 respectively.

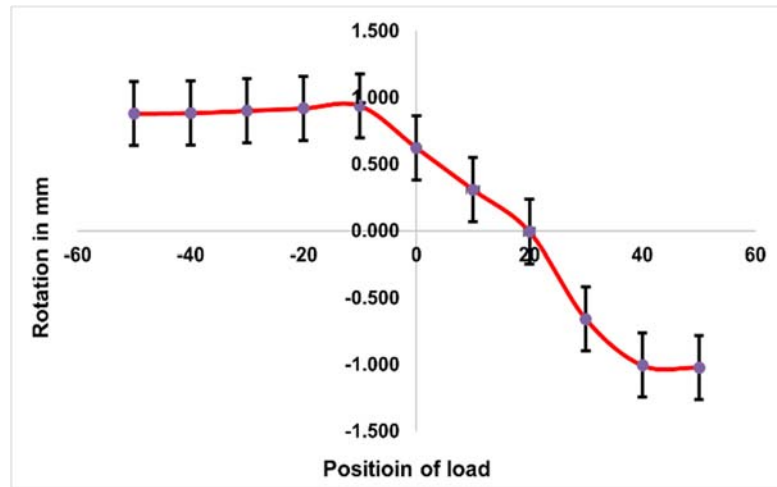


Figure 5: Mean and standard deviation of combined shear center.

### 3.2 Theoretical calculations

#### 3.2.1 Z-section

Compared to the experimental value of the Z-section, which was zero rotation at zero position of load, the RSM predicted the values of 0.01 mm rotation at zero position of load. The ANOVA analysis predicted that there is a 3.18% chance that a value greater than this could occur. The ANOVA result of the Z-section is shown in figure 6.

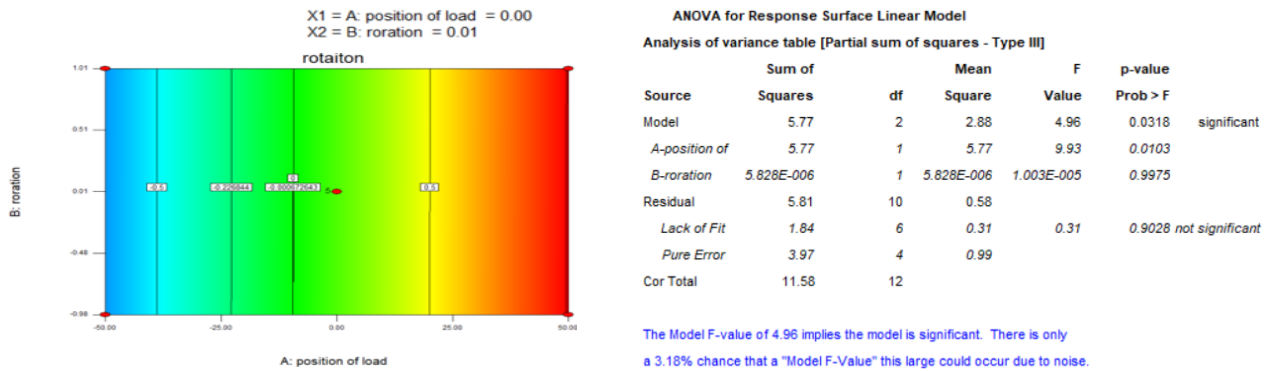


Figure 6: ANOVA results and 3D graphs of Z-section

#### 3.2.2 Semi Circular

For the Semi-circular section, the results from the ANOVA analysis were found to be “no significant” due to error variation. Out of the 13 runs, the error probability was found to be 43% which is above the recommended value. Hence, the experimental results could not be compared with theoretical results in this case. The contour and ANOVA results of semi-circular are shown in figure 7.

#### 3.2.3 Standard error of rotation

The standard error for the position of load against the rotation of the section is shown in figure 9. The std error of design showed good agreement between theoretical and experimental values. For instance, at load position -50, the rotation is 0.94 mm, showing an error of 0.472. In the same way, at position load 0,0, the rotation of the section is 0.73 showing an error of 0.361.

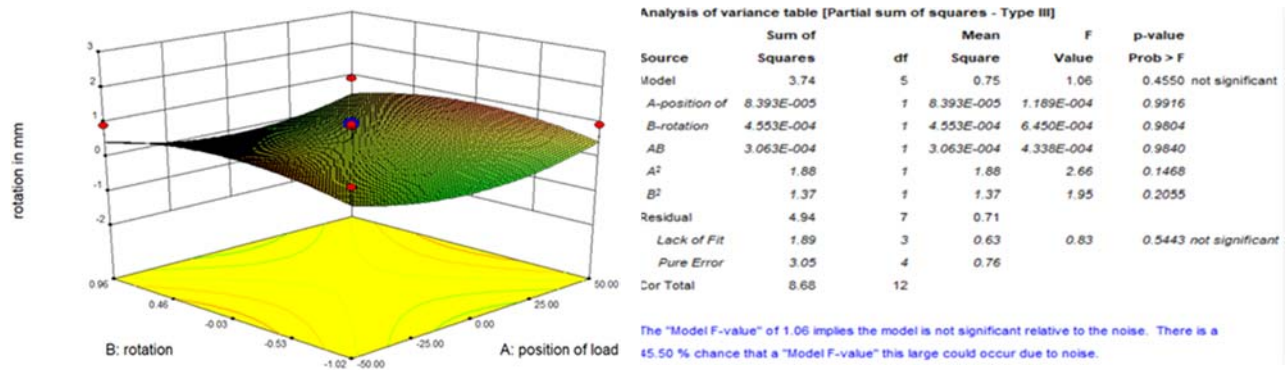


Figure 7: ANOVA results and 3D graphs of semicircular section

### 3.2.4 L-section

The optimization and ANOVA analysis of RSM of the L-section is shown in figures 8 and 9. In this analysis, as shown, the predicted value for the analysis is 0.89, which establishes a good relationship between the actual experimentation and the predicted value. The predicted value for the rotation is 0.82 mm when the positioning load is 0.0, whereas the actual value observed was 0.86 when the positioning load is 0.0. the difference in error between the actual and predicted value is 4.6%. This difference shows that optimized and actual results have established a good relationship. This also suggests that the experiment was conducted in a controlled way following the codes. However, the difference could be attributed to laboratory conditions and human error.

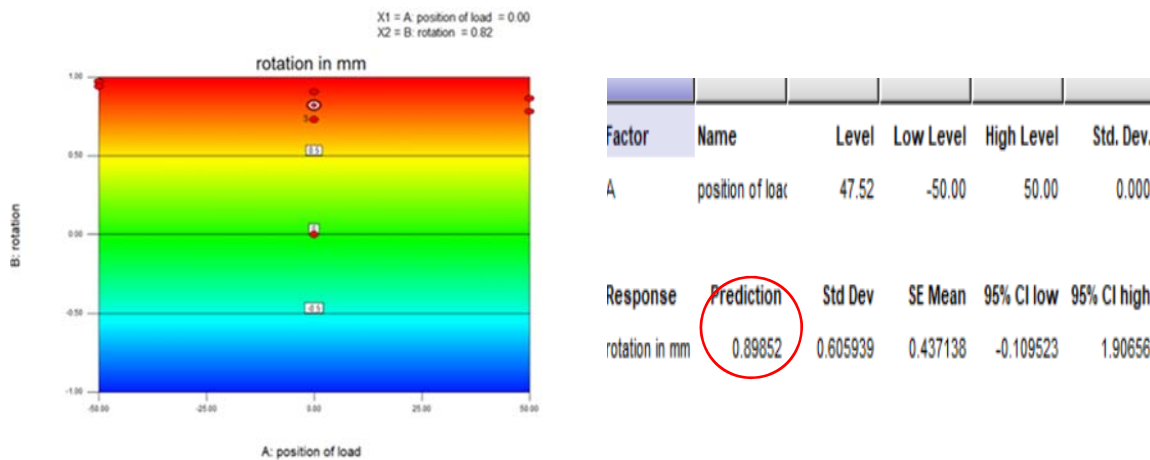


Figure 8: ANOVA results and 3D graphs of L-section

## 4 Practical implementation

The shear center is the point of a cross-section, where loads can be applied without causing torsion over the longitudinal axis (normal to the cross-sectional plane). Theoretical and experimental procedures may enhance calculations and save time by improving analytic methodologies to obtain correct results for various specimens. The point of no torsion can be determined without lengthy and hectic calculations; however, Shear Centre is particularly useful in designing thin-walled open steel sections as they are weak in resisting torsion and can be implemented in the construction sector to enhance the performance capabilities and utilize the resources effectively. However, if a seismic force acts on a structure. In non-scientific words, it is a collection of horizontal forces operating at each level's center of mass (gravity). However, depending on the stiffness of the lateral resisting system, the Centre of mass may differ from the Centre of rigidity (comparable to the shear Centre of a cross-section). If this occurs, twisting will occur and must be accommodated in the design.



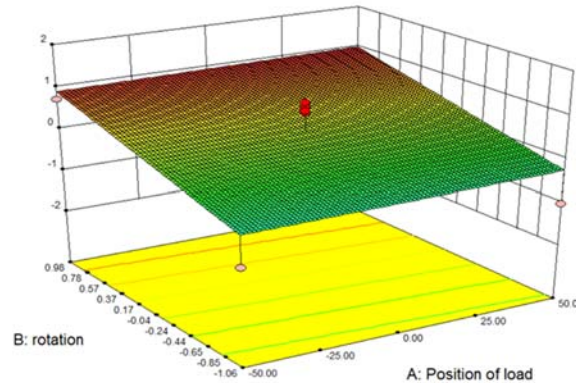


Figure 9: Std error of rotation of L-section against the position of load

## 5 Conclusion

Following conclusions are drawn from this experimental as well as theoretical study:

- Experimental calculations show that the Z-Section is symmetrical along both axes. At the same time, L-section and semi-circular section are symmetrical on one axis and unsymmetrical on the other.
- In comparison to the experimental Z-section value of zero rotation at zero position of load, the RSM predicted 0.01 mm rotation at zero position of load.
- The experimental and theoretical values for the semi-circular section were 0.965 and 0.455, respectively, indicating a 45.5 percent error.
- At load position -50, the rotation is 0.94 mm, indicating an error of 0.472. Similarly, at position load 0,0), the rotation of the section is 0.73, with a 0.361 error.
- The experimental rotational value of the L-section has been 0.905, and the RSM value has been 0.898, with a 0.77 percent error.

## Acknowledgment

The authors would like to express their deep gratitude toward the lab engineer Hamza Munir and lab assistant Muhammad Waqas for helping us in this experimental study.

## References

- [1]. C. Grant, "Shear center of thin-walled sections," The Journal of Strain Analysis for Engineering Design, vol. 27 (3) , pp.151–155, 1992. doi:10.1243/03093247v273151.
- [2]. H. Katori, "Consideration of the Problem of Shearing and Torsion of Thin-Walled Beams with Arbitrary Cross- Section." Thin-Walled Structures, vol. 36, pp.671-68, 2001. [http://dx.doi.org/10.1016/S0263-8231\(01\)00029-5](http://dx.doi.org/10.1016/S0263-8231(01)00029-5).
- [3]. W. Zhiquan., X. Xianghong., "Numerical study on impact resistance of novel multilevel bionic thin-walled structures," Journal of Materials Research and Technology, vol.16,2022, pp.1770-1780, 2022, <https://doi.org/10.1016/j.jmrt.2021.12.105>.
- [4]. X. Xiang., X. Gaoxiang., C.Jiawei., L. Zhe., C.Xinbo., "Multi-objective design optimization using hybrid search algorithms with interval uncertainty for thin-walled structures," Thin-Walled Structures, Vol.175, PP.109218, 2022, <https://doi.org/10.1016/j.tws.2022.109218>.
- [5]. W. S. Chan and K.A.Syed, "Determination of Centroid and Shear Center Locations of Composite Box Beams.", ICCM International Conferences on Composite Materials, 2009.
- [6]. W. S. Chan and Demirhan K. C, "A Simple Closed-Form Solution of Bending Stiffness for Laminated Composite Tubes. J.", of Reinforced Plastic & Composites, vol.19(4), p p. 278-291, 2000.
- [7]. H. Katori,(2016),"Determination of Shear Centre of Arbitrary Cross-Section.", World Journal of Mechanics, vol 6, pp.249-256, 2001. <http://dx.doi.org/10.4236/wjm.2016.68020>.
- [8]. L.Junru., W.Zhenyu., C. Jiankang., "An advanced Bayesian parameter estimation methodology for concrete dams combining an improved extraction technique of hydrostatic component and hybrid response surface method",Engineering Structures,Vol. 267,pp. 114687, 2022, <https://doi.org/10.1016/j.engstruct.2022.114687>
- [9]. K. K. Senthil., L. Lufan., L.Tung-Chai Ling., "Response surface methodology for the optimization of CO2 uptake using waste concrete powder", Construction and Building Materials, Vol. 340, 2022,<https://doi.org/10.1016/j.conbuildmat.2022.127758>



# MASS DISTRIBUTION EFFECT ON THE FINITE MODEL UPDATING USING OPERATIONAL MODEL ANALYSIS TECHNIQUE

<sup>a</sup> *Khizar Hayat*, <sup>b</sup> *Syed Saqib Mehboob*\*

a: Department of Civil Engineering, University of Engineering and Technology Taxila, [khizar.hayat@students.ucttaxila.edu.pk](mailto:khizar.hayat@students.ucttaxila.edu.pk)

b: Department of Civil Engineering, University of Engineering and Technology Taxila, [syed.saqib@ucttaxila.edu.pk](mailto:syed.saqib@ucttaxila.edu.pk)

\* Corresponding author: Email ID: [syed.saqib@ucttaxila.edu.pk](mailto:syed.saqib@ucttaxila.edu.pk)

**Abstract-** The findings of a model update investigation on a planar steel shear frame modal are presented in this paper. The operational modal analysis from the modal ambient vibration data were utilized to update the finite element model of the structure. The model of the structure was created using information from the model design paperwork. To increase the connection between observed and estimated modal parameters, several model parameters were adjusted using an automated approach. The parameters to be adjusted by the updating program were chosen with care to guarantee that the model modifications were meaningful, physically reliable, and realistic. The model update procedure is highlighted in the study.

**Keywords-** Ambient vibration, Finite Element model, Model parameters, Operational modal analysis.

## 1 Introduction

Ambient vibration testing is the most cost-effective non-destructive testing approach for obtaining vibration data from big civil engineering structures among the various methods for obtaining vibration data for Output Only Modal Identification [1]. The fundamental advantage of this approach is that no artificial sort of stimulation is required to ascertain the dynamic features of the structure of interest. Human activity, traffic, wind, and micro-tremors continuously excite a civil engineering structure, and with the right equipment and data analysis system, one may use these natural building excitations to evaluate the structure's dynamic qualities.

From the standpoint of structural engineering design practice, there are various reasons for doing vibration measurements in an existing building. For example, the client of a building in a seismically prone zone could be curious about whether the construction follows contemporary practice of seismic engineering design. If the structure is discovered to be vulnerable during a major disaster, structural adjustments in various portions of the structure may be required. The structural engineer who is in charge of this structural upgrade would attempt to offer a design that meets the local building code's safety and serviceability standards in the most cost-effective manner. Not only would a good assessment be required by the structural engineer, but it would also necessitate the creation of a computer model with realistic finite elements, which could be used to evaluate alternative scenarios of a retrofit. Based on the factual state of the structure, including its dynamic properties, a computer-based analysis should be done to validate the structural properties and its response to various static and dynamic loads. In these cases, not only is it good to have, but it is also an economical method for determining the features of civil engineering structures in terms of dynamic behavior experimentally. But also, to have economical methods for gaining complete confidence that the structure's finite element model is a true representation of the physical structure [2].

In order to accurately simulate civil engineering structures using finite element techniques, it is necessary to model the structural geometry, material properties, member fixities, connection types, and underlying assumptions in great detail.



However, the results of the finite element model are only approximations and may not accurately reflect the structural behavior. To confirm the finite element model outputs, structures are dynamically tested under operational conditions. The accuracy between the expected and measured OMA (Operational Modal Analysis) outcomes can always be improved with the finite element model upgrades [3]. For structural engineers, particularly in regions with high seismic risk, understanding the behavior of ancient buildings that have undergone structural alterations, restorations, and damage over time remains a significant problem. Due to the many uncertainties that exist in historic structures, the study of constructed heritage for its protection and conservation is an important research area. Finite element modelling has emerged as the most popular and practical technique to analyze the behavior of complex masonry buildings. Yet, the discrepancy between numerical and experimental analysis could result in inaccurate findings. Techniques for model updating can minimize the disparity between the behavior of the numerical models and the testing findings [4].

The density of the load and its magnitude have increased, and the regulations' criteria have also been stricter, all of which have affected the design of structures nowadays. The numerical modelling of the structure is completed in accordance with current regulations to ensure the basic requirements, notably the mechanical resistance and stability. Because of several assumptions, conceptions, discretization, and parameterization that are included during numerical modelling, the results may not always accurately represent the actual structural response. In order to reduce the differences between the actual and expected structural responses, experimental investigations (static as well as dynamic tests) and finite element model updating approaches can be used to determine the hidden resistance of these structures [5].

The analytical finite element (FE) model of any structure can be enhanced using the finite element model updating (FEMU) method from its experimental modal test data. To remove any uncertainties or errors in the analytical FE model, FEMU is still mostly applied to structures. A variety of FEMU approaches can be used to reduce uncertainties in the FE model of real engineering structures [6]. The purpose of this research is to demonstrate how Output-Only Modal Identification approaches can be used in combination with Model Updating tools to construct trustworthy models of civil engineering structures.

Since 1998, researchers from many universities and industry have conducted a series of ambient vibration experiments to determine the modal properties of civil engineering structures and structural models [7]. The dynamic property of interest in this study is the initial natural frequencies of the primary deflection axis. This paper uses a mass distribution effect on finite model updating using an operational model analysis technique to justify different parameters involved in modal updating, which are involved in changing different modal properties. Although these changes are so minute that their effect may be neglected, The modal description, experimental procedure, modal updating, and conclusion of this research work are discussed one by one in detail.

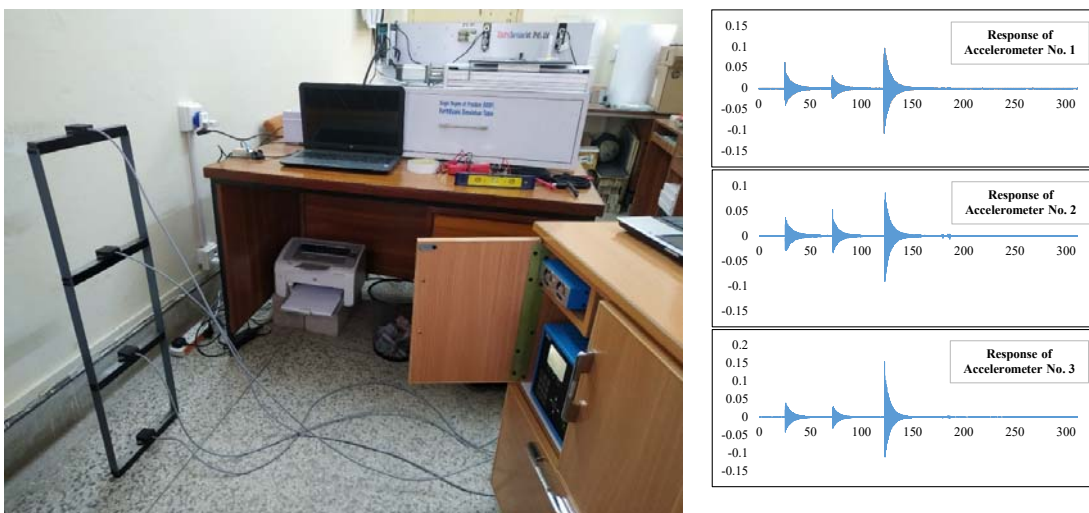


Figure 1. Experimental setup and structural response accelerograms excluding fixed base



## 2 Model Description

The model considered in this study was the steel shear frame model. It's a 3-story shear frame, two-dimensional and quite regular. The model is rectangular in plan with no projections or setbacks. The dimensions that are typical of the upper, middle, and lower floor beams are all the same, which is about 25.33 mm by 25.33 mm, while the dimensions of the columns are 28.43 mm by 2.10 mm. All three stories of the frame are equal, which is about 300 mm in height. The width of the frame model is the same throughout its height, which is about 274 mm. The total height of the frame model is about 900 mm. The frame model structure was fixed on the concrete bed with the help of steel screws. An overview and typical cross-sectional dimensions of the model are presented in Figure 1.

## 3 Experimental Procedure

A Vishay System7000 with 128-channels (supported with MEMS accelerometers having a sensitivity of 1000 mV/g) was used to conduct the vibration measurements. Every story, starting from the top down to the last one, has accelerometers installed on the top and middle of every beam. The model was simplified to a rectangle with nodes arranged vertically. By assuming rigid body motion of the floor beams, the modal characteristics of the shear type building model were determined using the OMA technique under ambient vibrations. Table 1 lists the first three natural frequencies of vibration. The OMA results are compared with the time domain approach, stochastic subspace identification (SSI), and the analytical calculations. The choice of SSI was mainly due to the fact that the stimulus is unknown in the case study of this research work. Therefore, this specialized algorithm of stochastic subspace identification (SSI) has been applicable that only requires knowledge of the response and does not require knowledge of the stimulus.

Table 1: Eigenvalues for model frame building

Mode	OMA Results (Hz)	SSI Results (Hz)	Analytical (Hz)
1	3.64	3.67	3.28
2	10.16	10.15	10.05
3	14.78	14.78	14.51

## 4 FEM Updating

Using a manual updating procedure, the reference presents [8] an attempt to link experimental and analytical modal features of model building. That research clearly demonstrates the challenges and limitations of attempting for a civil engineering structure to get a satisfactory general combination between operational and analytical modal characteristics. As a result, it was decided to update the structure's initial FE model using a more efficient platform. The CivilFEM tool [9] was chosen for this project, which includes different tools for integrating test and Finite Element analysis data quickly and effectively. An analytical study included correlating the OMA and FEM models' inherent frequencies until an acceptable connection was found. The provided information on the FE model utilized in this research as well as the parameters chosen for model updating are presented in the below sections [10].

### 4.1 FE model of shear frame

To generate an "initial" model of the structure, FE modelling and analysis capabilities were used. The geometry and material attributes of the model were developed using information already known. The ground level/base was considered "fixed" based on the testing data. The model comprised the key structural elements (columns and header beams). 3D beam-column components were used to model the beams and columns. All the properties of the model are the same throughout the height of the model. The design specifications given in the general material properties were used to determine the steel material properties. The model had 9 beam-column elements and 8 nodes, single material characteristics, and 2 possible element geometries in total. As a result, a three-degree-of-freedom Finite Element model was built.



#### 4.2 Parameters for model updating.

Model updating parameters are listed below:

- The beams, columns Modulus of elasticity,  $E$ .
- Mass density of the same elements mentioned previously.

The mass density of each element can be varied to see how sensitive the model is to the mass distribution of model elements coupled to the structural system of the model. The moment of inertia and, as a result, the lateral stiffness of the columns are two tough features for model frame constructions. The value of  $I$  is largely dependent on the type of material used and how the composite action of the construction materials is accounted for in the model. Furthermore, because a column's stiffness varies greatly as a function of the column's effective length, changes in the values of  $I$  can be understood as needed model adjustments to significantly depict the column's effective length.

#### 4.3 Results of model updating

Table 2 shows the resulting modal frequencies after various iterations of parameter updating. The table indicates the operational frequencies (OMA) and FEM frequencies after and before updating. This table shows that some of the revised model's frequencies are, for all intents and purposes, identical to the operational ones. The third mode has the highest difference, roughly 1.3%, although this is still suitable for practical applications.

FEM tools made changes to the FE model to achieve the compared values shown in the previous table. The entries in the table are assumed to be in meters, kilograms, and newtons. Furthermore, a sensitivity study of the frame model to modifications in different parameters revealed that their overall impact isn't significant, which shows the negligible differences in the model parameters as shown in the table above.

Table 2: Eigenvalues after FE model updating

Mode	OMA Freq.	FEM Before	FEM updated (Hz)	
			Freq.	Diff. (%)
1	3.64	3.49	3.62	-0.6
2	10.16	9.70	10.23	0.7
3	14.78	13.88	14.97	1.3

## 5 Conclusion

Experimentation and analysis were used to establish the natural frequencies of the steel shear frame modal. This case study demonstrates that using the results of an operational model analysis, it is possible to update the model effectively. The automatic model-updating makes it much easier to figure out which model parameters can be changed to improve the comparison between operational and analytical results. In this regard, the finite element model update-based updating techniques can be applied to correct the simulated FE model and remove the difference between the FE model outputs and measured data. Reviewing and effectively implementing the automatic model-updating method on the shear frame modal is the primary accomplishment of this work. Updates can be made to the simulated FE model quickly and easily without taking a lot of time, The effective use of updating methods is important. The analyst must, however, decide whether to accept the changes or not and to show how useful the suggested changes.

## Acknowledgements

The work presented is the initial phase of a research project being conducted in the UET Taxila Civil Engineering Department. The authors are thankful to the laboratory staff for their technical support and to all those who are helping



on this project. The development of the robust algorithm and its application to civil structures are the next steps of the project. The careful review and constructive suggestions by the anonymous reviewers are gratefully acknowledged.

## References

- [1] R. Brincker and P. Andersen, "Ambient response analysis of the Heritage Court Tower Building structure," *Proceedings of the International Modal Analysis Conference - IMAC*, vol. 2, pp. 1081–1087, 2000.
- [2] A. K. Chopra, *Accidental And Natural Torsion In Earthquake Response And by*, no. June. 1994.
- [3] O. Avci, K. Alkhamis, O. Abdeljaber, A. Alsharo, and M. Hussein, "Operational modal analysis and finite element model updating of a 230 m tall tower," *Structures*, vol. 37, pp. 154–167, Mar. 2022, doi: 10.1016/j.istruc.2021.12.078.
- [4] C. Baggio, V. Sabbatini, S. Santini, and C. Sebastiani, "Comparison of different finite element model updates based on experimental onsite testing: the case study of San Giovanni in Macerata," *Journal of Civil Structural Health Monitoring*, vol. 11, no. 3, pp. 767–790, 2021, doi: 10.1007/s13349-021-00480-1.
- [5] S. Ereiz, I. Duvnjak, and J. Fernando Jiménez-Alonso, "Review of finite element model updating methods for structural applications," *Structures*, vol. 41, no. April, pp. 684–723, 2022, doi: 10.1016/j.istruc.2022.05.041.
- [6] A. Sharma, A. K. Bagha, D. K. Shukla, and S. Bahl, "Finite element model updating of metallic and composite structures—A state of the art review," *AIMS Materials Science*, vol. 8, no. 3, pp. 390–415, 2021, doi: 10.3934/mat.2021025.
- [7] W. X. Ren and Z. H. Zong, "Output-only modal parameter identification of civil engineering structures," *Structural Engineering and Mechanics*, vol. 17, no. 3–4, pp. 429–444, 2004, doi: 10.12989/sem.2004.17.3\_4.429.
- [8] H. Court and T. In, "Measured and calculated modal characteristics," pp. 44–47.
- [9] A. Toivonen, P. Aaltonen, P. Nenonen, U. Ehrnsten, A. Käki, and O. Hietanen, "Properties and IASCC susceptibility of austenitic stainless steel 08X18H10T," *VTT Symposium (Valtion Teknillinen Tutkimuskeskus)*, no. 227, pp. 277–308, 2003.
- [10] A. Barontini, "Bio-inspired algorithms for Structural Health Monitoring of Civil Engineering Systems," no. March, 2021.



# NUMERICAL SIMULATION OF FRACTURE IN CONCRETE USING PHASE FIELD MODEL

<sup>a</sup> Ghufuranullah khan Khattak, <sup>b</sup> Awais Ahmed

a: Department of Civil Engineering, University of Engineering and Technology Peshawar, [ghufuranullahkhattak@gmail.com](mailto:ghufuranullahkhattak@gmail.com)  
b: Department of Civil Engineering, University of Engineering and Technology Peshawar, [awais.ahmed@uetpeshawar.edu.pk.com](mailto:awais.ahmed@uetpeshawar.edu.pk.com)

**Abstract-** In this paper, a phase field-based numerical model has been presented to study fracture in concrete. All nonlinearities in the fracture process zone are modeled using cohesive zone approach with traction-separation constitutive law for concrete. A localized band of finite width is used to regularize the crack path using scalar phase-field. The phase-field discriminates between intact and broken surface using numeric values of 1 and 0. The critical fracture energy is modeled as the algebraic sum of the critical fracture energy of mode I and mode II. A finite element method is used to implement the proposed model. Numerical simulation for mode I fracture is performed on a three-point notched concrete beam. The concrete response under applied loading is represented using load-displacement curve. A study related to effect of mesh size and length scale parameter on the output results is carried out. The results indicated that the length scale parameter and finite element size has little effect on the model. It is concluded that the phase-field model has the ability to simulate crack growth in concrete under the given loading condition.

**Keywords-** Mode I fracture, Mixed mode fracture, Phase-field, Fracture energy, Length scale parameter.

## 1 Introduction

Concrete is composite material and is widely used in construction industry as a building material. When subjected to normal and shear stresses, the crack tends to propagate along an inclined path, indicating the mixed mode fracture in concrete. The mixed mode fracture in concrete is one which occurs as result of the combination of mode I (tensile failure) and mode II (shear failure). Various experimental tests have shown that concrete generally fails in mixed mode (I-II) when subjected to environmental loading [1]. Understanding the fracture phenomena in concrete is vital for the accurate analysis and design of concrete structure. This is because the cracking reduces the stiffness of concrete, thereby effecting its serviceability, durability and may lead to complete failure. A numerical model generally needs two ingredients to model crack growth problem in concrete: the first one is the crack initiation criterion and the second one is the damage criterion. The crack initiation criterion is generally based on maximum principle tensile stress or strain. Other crack initiation criterion can also be used. The damage criterion has to be based on mode I and mode II fracture energies if one wants to study the crack growth under mixed mode condition. Developing these criteria for mixed mode fracture is challenging [2]. Although, most of the numerical model, which are proposed earlier [3], [4], can simulate the crack initiation and crack propagation, they are unable to simulate some aspects of crack related to fracture process, for example crack kinking, coalescence, branching and nucleation. The phase field model presented in this paper has the ability to predict the crack initiation, propagation, nucleation, branching and kinking during crack growth.

The macro model behaviors of concrete structure can be determined from the meso or micro model if mechanical properties of the two matches [5]. In addition, performing experiments on macro structures is time consuming and uneconomical. For



this reason, meso and micro scale model of the actual physical structures are generally used for simulation. To achieve better results, greater degree of mechanical, geometrical and compositional similarity between the prototypes and actual system is required [6]. Two approaches are generally used to model the fracture in concrete: discontinuous and continuous approach. The discontinuous approach is largely based on the work presented in [7], [8] and Cohesive Zone Model (CZM) [9], [10]. In this approach the crack is modeled as a strong discontinuity embedded in the finite element mesh. In contrast, the continuous approach models the crack by distributing the damage in a band of finite width using a scalar phase field.

The Cohesive Zoned Model and Extended Finite Element Method (XFEM) are the two prominent methods which are based on the discontinuous approach. In CZM, the cohesive elements are distributed along the boundary of the element in finite element mesh. A mechanical behavior of cohesive element is controlled by traction separation law, that also account for all nonlinearities at the crack tip. Many researchers [11]–[13] have used this approach to simulate the fracture phenomena in concrete and other material. This approach requires the crack path to be known in advance. In addition, this method is mesh sensitive [14]. The complicated stress distribution in the fracture process zone cannot be accounted for in this method [15]. This method requires advance software and packages for implementation. As opposed to CZM, the XFEM is free from mesh sensitivity problems and can easily handle the displacement discontinuity due to sharp crack [16]. This method is based on partition of unity [17]. The discontinuity is included in the finite element mesh by enriching specific node using special function without altering the original mesh. XFEM has the ability to simulate complex phenomena and more powerful as compare to CZM. Numerous researcher have used this method for simulating and numerical modeling of complex problems like fracture in concrete, see for example [18]–[22]. Although, XFEM is a powerful numerical method, it too like CZM suffer in cases of complex crack topologies including crack branching, intersecting and kinking. It is also not suitable to simulate problem involving friction action and high degree of material nonlinearities. The continuous approach, as opposed to discontinuous approach, does not model the crack as a strong discontinuity rather smears it in a localized band. The phase field model (PFM) falls in this category. In this model, the damage is distributed in a localized band and a scalar phase field  $\phi$  is used to indicate the degree of damage in the material. The width of the damage is controlled by a length scale parameter  $l_c$ . The phase field take value of 0 and 1 for completely intact and damage state of the material. The PFM gives the displacement and phase field as output of the model by solving multivariable problem. It do so by fusing the Griffith criterion and phase field in the total potential of the system and extremizing it using the variational principle [23]. The phase field, surface density and damage equation used in the PFM can vary and thus results in different phase field models. Feng and Wu [24] used a phase field model to investigate the boundary and size effect on fracture in concrete. The cohesive zone model approach was used to model the strain softening behavior of concrete. In [25], the phase field model was used to study fracture in cement-based material. A modified constitutive law inclusive of the early-age processes including shrinkage, thermal expansion and creep was used to simulate fracture. In addition, many other researcher [26]–[30] have used phase field model to simulate the fracture process in solids.

In this paper, phase field model proposed in [30] has been used to simulate mode I fracture in simply supported notched concrete beam. The load is applied at mid-point of the beam to ensure that the crack grow in mode I. The aim of the study is to investigate the suitability of phase field model in simulating fracture in concrete. In addition, the effect of length scale parameter on the crack growth has been undertaken. The concrete mass is assumed to be homogenous in composition. All nonlinearities are included in the model using an exponential traction-separation law. No viscous parameter is included in the model. The simulations are performed using the elastic mechanical properties of the material. The crack and damage visualization in the model during simulating is assisted by the scalar phase field discriminating between intact and damage state of the material using numerical value of 0 and 1.

## 2 Phase Field Model

In this section, the formulation of phase field model based on the variation approach has been presented. For a solid body with domain  $\Omega$ , the external potential energy can be written as:





$$P(\mathbf{u}) = \int_{\Omega} b \cdot \mathbf{u} dV + \int_{\partial\Omega} t \cdot \mathbf{u} dA \quad (1)$$

Here  $b$  is the body force,  $t$  is the traction applied on  $\partial\Omega$ , and  $\mathbf{u}$  is the displacement applied at the boundary.

For a crack set  $\Gamma$  in the solid domain  $\Omega$ , the expression for the surface energy is given by:

$$\Psi(\Gamma) = \int_{\Gamma} G_c dA \quad (2)$$

The  $G_c$  is the critical energy release rate of the material. it can be obtained from tensile test on the material.

The internal strain energy stored in the solid body can be represented as following:

$$\Psi_0(u) = \frac{1}{2} \lambda tr^2[\varepsilon] + \mu tr[\varepsilon^2] \quad (3)$$

Where  $\lambda$  and  $\mu$  are the lame constant and  $\varepsilon$  is the strain tensor.

After having equations for the external potential energy, surface energy and strain energy density function, the total potential energy of system, ignoring the body forces, can be written as:

$$\Pi(\mathbf{u}, \phi) = \int_{\Omega} \Psi(\varepsilon(\mathbf{u})) dV + \int_{\Gamma} G_c dA - \int_{\partial\Omega} t \cdot \mathbf{u} dA \quad (4)$$

The numerical implementation of the equation (4) is a challenge because of the discontinuous displacement field and unknow nature of the crack set. These limitation are addressed by regularizing the total potential of the system using variation approach presented in [26], [27], [31]. The regularized total potential is given by:

$$\Pi(\mathbf{u}, \phi) = \Psi_s(\mathbf{u}, \phi) + \Psi_c(\Gamma) - P(\mathbf{u}) \quad (5)$$

Where

$$\Psi_s(\mathbf{u}, \phi) = \int_{\Omega} g(\phi) \psi_0(\dot{\mathbf{u}}) dV \quad (6)$$

$$\Psi_c(\Gamma) = \int_{\Omega} G_c \gamma(\phi; \nabla \phi) dA \quad (7)$$

Here  $\Psi_s(\mathbf{u}, \phi)$ ,  $\Psi_c(\Gamma)$  is the regularized strain energy density functional and regularized surface energy functional.

$\gamma(\phi; \nabla \phi)$  is the crack surface density functional characterizing the growth of phase field in the solid domain.  $P(\mathbf{u})$  is the external potential energy due to body forces and traction.

The crack surface density,  $\gamma(\phi; \nabla \phi)$  function is given by, [26], [32]:

$$\gamma(\phi; \nabla \phi) = \frac{1}{2} \left[ \frac{1}{l_0} \phi^2 + l_0 (\nabla \phi \cdot \nabla \phi) \right] \quad (8)$$

After putting Equation (6), (7) and (8) in Equation (5), the total potential can be rewritten as, [30]:

$$\Pi(\mathbf{u}, \phi) = \int_{\Omega} g(\phi) \psi_0(\dot{\mathbf{u}}) dV + \int_{\Omega} G_c \frac{1}{2} \left[ \frac{1}{l_0} \phi^2 + l_0 (\nabla \phi \cdot \nabla \phi) \right] dV - \int_{\Omega} b \cdot \mathbf{u} dV - \int_{\partial\Omega} t \cdot \mathbf{u} dA \quad (9)$$

In equation (9)  $\psi_0(\dot{\mathbf{u}})$  is the elastic free energy functional and  $g(\phi)$  is the damage function. The damage function is bound to the following conditions, [26]:

$$g(0) = 0, \quad g(1) = 1 \quad \text{and} \quad \dot{g}(1) = 0 \quad (10)$$



After expressing the total potential of the solid body in term of phase field model, the problem comes down to finding the variation of Equation (9) w.r.t phase field  $\phi$  and displacement  $u$  given by:

$$\delta\Pi(\mathbf{u}, \phi) = \int_{\Omega} \sigma : \delta\epsilon dV + \int_{\Omega} \frac{\partial\psi}{\partial\phi} \delta\phi dV + \int_{\Omega} G_c \left( \frac{\partial\gamma}{\partial\phi} + \frac{\partial\gamma}{\partial\nabla\phi} \cdot \delta\nabla\phi \right) dV - \int_{\Omega} b \cdot \delta u dV - \int_{\partial\Omega_t} t \cdot \delta u dA \quad (11)$$

It yields the following equations and boundary conditions, [30]:

$$\nabla \cdot \sigma + b = 0 \quad \text{in } \Omega \quad (12)$$

$$\sigma \cdot n = t \quad \text{on } \partial\Omega_t \quad (13)$$

$$Y - G_c \partial_{\phi} \gamma = 0 \quad \dot{\phi} > 0 \quad \text{on } \Omega \quad (14)$$

$$Y - G_c \partial_{\phi} \gamma = 0 \quad \dot{\phi} = 0 \quad \text{on } \Omega \quad (15)$$

Where

$$Y := -\frac{\partial\psi}{\partial\phi}$$

$$\partial_{\phi} \gamma := \frac{\partial\gamma}{\partial\phi} - \nabla \cdot \left( \frac{\partial\gamma}{\partial\nabla\phi} \right) \quad (16)$$

$$\frac{\partial\gamma}{\partial\nabla\phi} \cdot n_B = 0 \quad \text{on } \partial B \quad (17)$$

Equation (12) is called the equilibrium equation while Equation (14) and (15) are the phase field evolution equation. In addition, equation (13) and (17) are the boundary condition.

In order to simulate the mixed mode fracture and avoid the crack growth under compression, the initial strain energy is decomposed into tensile, shear and compression part as following, [30]:

$$\psi_0 = g_I(\phi) \psi_{0I}^+ + g_{II}(\phi) \psi_{0II}^+ + \psi_0^- \quad (18)$$

$$\psi_0^- = \psi_0 - \psi_{0I}^+ - \psi_{0II}^+ \quad (19)$$

The mixed mode phase field evolution equation becomes:

$$g_I'(\phi) \frac{\psi_{0I}^+}{G_{cI}} + g_{II}'(\phi) \frac{\psi_{0II}^+}{G_{cII}} \geq \frac{2l_0^2 \nabla^2 \phi - \alpha'(\phi)}{c_0 l_0} \quad (20)$$

Where  $g_I'$  and  $g_{II}'$  are the degradation function for mode I and mode II. Similarly,  $G_{cI}$  and  $G_{cII}$  are the fracture energies for the two modes.

The weak form of the governing differential equation is given by:

$$\int_{\Omega} B_u^T \hat{D} B_u \partial\Omega u = \int_{\partial\Omega} \Phi_u^T t d\partial\Omega \quad (21)$$

$$\int_{\Omega} \frac{2l_0}{c_0} B_s^T B_s d\Omega \hat{\phi} + \int_{\Omega} \frac{1}{c_0 l_0} \alpha(\phi) \Phi_{\phi}^T d\Omega + \int_{\Omega} \left[ \frac{g_I'(\phi)}{b_I} h_I \right] + \left[ \frac{g_{II}'(\phi)}{b_{II}} h_{II} \right] \Phi_{\phi}^T d\Omega = 0 \quad (22)$$

Where  $\hat{u}$  and  $\hat{\phi}$  are the known displacement and phase field values at nodes.  $\hat{D}$  is the modified constitutive matrix.  $\Phi_u$  and  $\Phi_{\phi}$  are shape functions for displacement and phase field. The  $b_I$  and  $b_{II}$  are constants that can affect fracture



angles during crack growth. The phase field evolution equation and equilibrium equation are solved for displacement and phase field and the crack path is obtain as part of the solution. The propose scheme is implemented in a finite element code using C++ Jem and Jive libraries

### 3 Methodology

The methodology used for simulating fracture in concrete using the proposed phase field model is discussed in the following sections.

#### 3.1 Specimen Selection

The concrete beam specimen used in [33] has been selected for numerical simulation of mode I fracture in concrete using the proposed phase field model. The dimensions of the beam are: length,  $L = 36$  in, Depth,  $D = 9$  in and thickness,  $t = 3.375$  in. However, to reduce the computational cost, the dimensions are taken in millimeter (mm). The beam has a notch of depth 3 mm in the middle on the lower face as shown in the Figure 1.

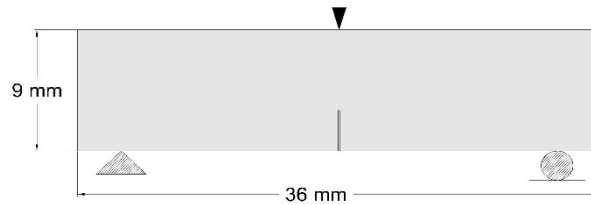


Figure 1. Geometry of notched concrete beam with boundary condition

#### 3.2 Numerical Simulation of Three-Point Beam

The material properties required in the model include modulus of elasticity  $E$ , the Poisson's ratio  $\nu$ , critical fracture energy  $G_f$ , the ultimate tensile strength  $f_t$ . For the given beam, the fracture energies of mode I and mode II are taken to be equal. Such assumption can be made because the scope of the study conducted in this paper is limited only to simulating the fracture process. More specifically, the ability of the model to produce the generic load-displacement curve of concrete is the center of focus. There is no validation work to be carried out. The problem is considered as a plane strain problem and exponential cohesive law has been used. The initial notched is modelled as a discrete crack in the beam.

The beam has length of 36 mm and depth of 9 mm. The notch has depth of 3 mm and is located in the center of beam. The material properties of the beam are taken from [13] and include modulus of elasticity  $E = 142000 \text{ N/mm}^2$ , Poisson's ratio  $\nu = 0.35$ , fracture energy  $G_f = 0.344 \text{ N/mm}$ , tensile strength  $f_t = 3.4 \text{ N/mm}^2$  and shear strength  $f_s = 3.4 \text{ N/mm}^2$ . The fracture energy of mode I has deliberately been taken equal to mode II fracture energy i.e.,  $G_I = G_{II} = G_f$ .

The simulation is performed under displacement scheme with load scale of  $1.0 e^{-3}$  in 900 iterations. The beam domain is discretized using 6037 quadrilateral elements as shown in Figure 2. In order to reduce the computation time, the Dirichlet boundary condition  $\phi = 0$  has been assign to the elements close to the support.

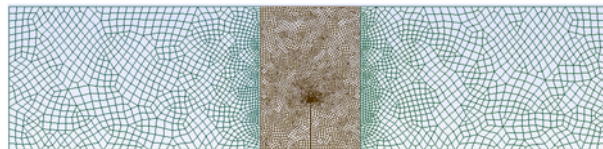


Figure 2. Descretized geometry of the notched concrete beam



## 4 Results and Discussion

The first trial of simulation is performed using mesh size of 0.3 mm in the region close to the crack and 0.5 mm in the remaining region. It can be observed that during the initial iteration the stress at the crack tip increases. As a result, the phase field values increase and upon reaching 1, the element damages completely and the crack progress further. The crack path, as shown in the Figure 3, propagates vertically indicating the mode I fracture. This can be attributed to the fact that

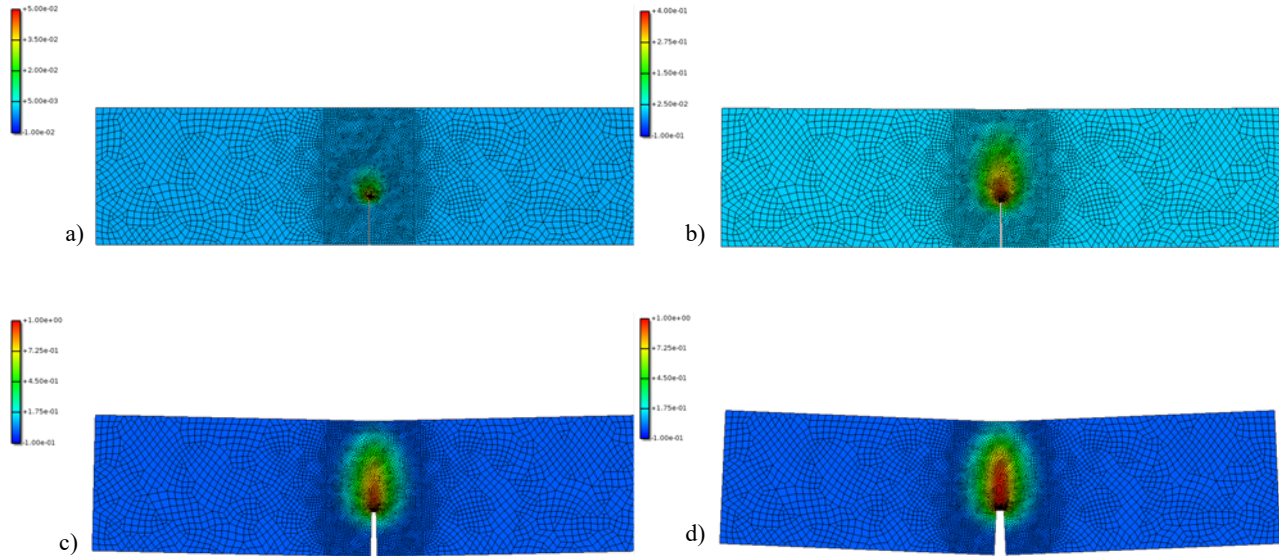


Figure 3. Crack propagation in notched concrete beam under three-point bending, a. crack initiation, b, c, d. crack propagates as loads increases

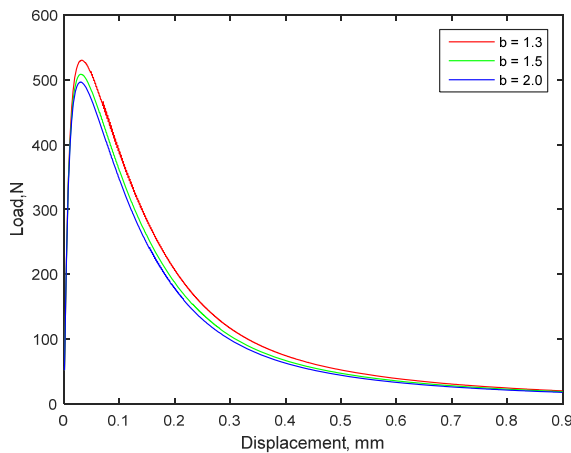


Figure 4. Load-Displacement curve for length scale parameter of  $b = 1.3$  mm,  $b = 1.5$  mm and  $b = 2.0$  mm

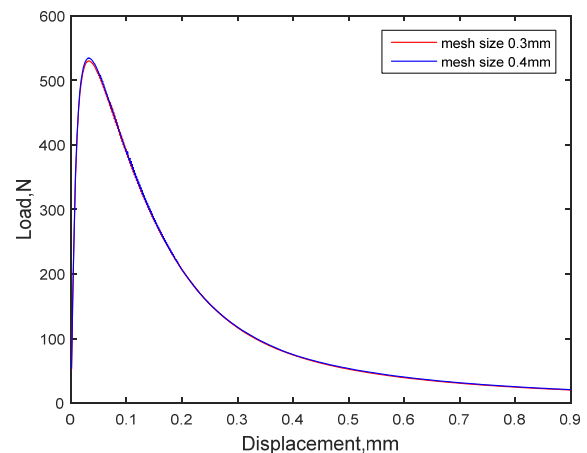


Figure 5. Load-Displacement curve for mesh size of 0.3 mm and 0.4 mm with constant  $b = 2$  mm

the boundary condition (loading and supports) is such that mode I fracture is favored. As a result, the crack growth is in mode I and mode II contribution are negligible. The pattern of crack growth and load-displacement curve obtained are similar to the one obtained experimentally during mode I fracture test on three-point notched concrete beam. The load-displacement curve has been plotted for different length scale parameter in order to study its effect as shown in the Figure 4.

The Load-displacement plot shows that for the fixed value of material properties, the length scale parameter has negligible effect on the load-displacement curve. The length scale parameter in a sense controls the damage area. A higher value of  $b$  would mean that more area will get damage and so the corresponding peak load will slightly increase. In order to study



the effect of mesh size on the load-displacement curve, simulations are performed at mesh size of 0.3 mm and 0.4 mm at a constant length scale parameter of 2.0 mm. The results shows that the proposed model is almost independent of the mesh size as evident in Figure 5. The mesh independency is one of the attributes of phase field model. The numerical result generally converges when a relative fine mesh is used. In this case the converging mesh size seems to be 0.4 mm.

## 5 Conclusion

After simulating mode I fracture in concrete, it is concluded that the phase field model can simulate the fracture in concrete. It can also produce the post-peak strain softening behavior if proper cohesive law is used. In addition, the model is mesh independent and the length scale parameter has very little effect on the peak load. The model can be used for simulating mixed mode fracture in concrete if relevant parameter related to mixed mode are taken into account.

## References:

- [1] Z.-M. Wu, R. C. Yu, C.-Y. Sun, Y.-J. Wang, X.-X. Zhang, and X.-D. Fei, "A new test method for the complete load-displacement curve of concrete under mixed mode I-II fracture," *Theor. Appl. Fract. Mech.*, vol. 108, p. 102629, Aug. 2020, doi: 10.1016/j.tafmec.2020.102629.
- [2] M. T. Kazemi and F. V. Shahvari, "Mixed Mode Fracture of Concrete: An Experimental Investigation," p. 9.
- [3] A. Hillerborg, M. Mod er, and P.-E. Petersson, "Analysis of crack formation and crack growth in concrete by means of fracture mechanics and finite elements," *Cem. Concr. Res.*, vol. 6, no. 6, pp. 773–781, 1976.
- [4] T. Belytschko and T. Black, "Elastic crack growth in finite elements with minimal remeshing," *Int. J. Numer. Methods Eng.*, vol. 45, no. 5, pp. 601–620, 1999.
- [5] F. Wittmann, "Structure of concrete with respect to crack formation," *Fract. Mech. Concr.*, vol. 43, no. 5, p. 6, 1983.
- [6] P. Dawson, A. Needleman, and S. Suresh, "Issues in the finite element modeling of polyphase plasticity," *Mater. Sci. Eng. A*, vol. 175, no. 1–2, pp. 43–48, 1994.
- [7] A. A. Griffith, "VI. The phenomena of rupture and flow in solids," *Philos. Trans. R. Soc. Lond. Ser. Contain. Pap. Math. Phys. Character*, vol. 221, no. 582–593, pp. 163–198, 1921.
- [8] G. R. Irwin, "Analysis of stresses and strains near the end of a crack traversing a plate," 1957.
- [9] D. S. Dugdale, "Yielding of steel sheets containing slits," *J. Mech. Phys. Solids*, vol. 8, no. 2, pp. 100–104, 1960.
- [10] G. I. Barenblatt, "The mathematical theory of equilibrium cracks in brittle fracture," in *Advances in applied mechanics*, vol. 7, Elsevier, 1962, pp. 55–129.
- [11] R. Graffe and D. Linero, "Simulaci n num rica del proceso de fractura en modo I de vigas de concreto con trayectoria de fisuraci n conocida mediante un modelo discreto de fisura cohesiva Numerical modeling of the fracture process in mode I of concrete beams with known cracking path by means of a discrete model of cohesive crack," vol. 25, p. 20, 2010.
- [12] J. M. Sancho, J. Planas, J. C. G lvez, E. Reyes, and D. A. Cend n, "An embedded cohesive crack model for finite element analysis of mixed mode fracture of concrete," *Fatigue Fract. Eng. Mater. Struct.*, vol. 29, no. 12, pp. 1056–1065, Dec. 2006, doi: 10.1111/j.1460-2695.2006.01076.x.
- [13] S. H. Song, G. H. Paulino, and W. G. Buttlar, "Simulation of Crack Propagation in Asphalt Concrete Using an Intrinsic Cohesive Zone Model," *J. Eng. Mech.*, vol. 132, no. 11, pp. 1215–1223, Nov. 2006, doi: 10.1061/(ASCE)0733-9399(2006)132:11(1215).
- [14] F. Zhou and J.-F. Molinari, "Dynamic crack propagation with cohesive elements: a methodology to address mesh dependency," *Int. J. Numer. Methods Eng.*, vol. 59, no. 1, pp. 1–24, 2004.
- [15] Z. P. Ba ant and M. Jir sek, "Nonlocal integral formulations of plasticity and damage: survey of progress," *J. Eng. Mech.*, vol. 128, no. 11, pp. 1119–1149, 2002.
- [16] N. Moos, J. Dolbow, and T. Belytschko, "A finite element method for crack growth without remeshing," *Int. J. Numer. Methods Eng.*, vol. 46, no. 1, pp. 131–150, Sep. 1999, doi: 10.1002/(SICI)1097-0207(19990910)46:1<131::AID-NME726>3.0.CO;2-J.
- [17] J. M. Melenk and I. Babuška, "The partition of unity finite element method: Basic theory and applications," *Comput. Methods Appl. Mech. Eng.*, vol. 139, no. 1–4, pp. 289–314, Dec. 1996, doi: 10.1016/S0045-7825(96)01087-0.
- [18] R. M. de O. Pereira, E. C. M. Sanchez, and D. Roehl, "A PARAMETRIC STUDY OF MIXED-MODE FRACTURE PROPAGATION IN CONCRETE USING XFEM," Florianopolis, Brazil, 2017. doi: 10.20906/CPS/CILAMCE2017-0345.
- [19] J. F. Mougard, P. N. Poulsen, and L. O. Nielsen, "Modelling concrete structures applying XFEM with a mixed mode constitutive model," p. 6, 2010.
- [20] I. Lancaster, H. Khalid, and I. Kougoumtzoglou, "Extended FEM modelling of crack propagation using the semi-circular bending test," *Constr. Build. Mater.*, vol. 48, pp. 270–277, 2013.
- [21] E. Mahmoud, S. Saadeh, H. Hakimelahi, and J. Harvey, "Extended finite-element modelling of asphalt mixtures fracture properties using the semi-circular bending test," *Road Mater. Pavement Des.*, vol. 15, no. 1, pp. 153–166, 2014.
- [22] T. Xiaoge, R. Zhang, Z. Yang, Y. Chu, S. Zhen, and Y. Xv, "Simulation of bending fracture process of asphalt mixture semicircular specimen with extended finite element method," *Adv. Mater. Sci. Eng.*, vol. 2018, 2018.
- [23] G. A. Francfort and J.-J. Marigo, "Revisiting brittle fracture as an energy minimization problem," *J. Mech. Phys. Solids*, vol. 46, no. 8, pp. 1319–1342, Aug. 1998, doi: 10.1016/S0022-5096(98)00034-9.



- [24] D.-C. Feng and J.-Y. Wu, "Phase-field regularized cohesive zone model (CZM) and size effect of concrete," *Eng. Fract. Mech.*, vol. 197, pp. 66–79, Jun. 2018, doi: 10.1016/j.engfracmech.2018.04.038.
- [25] T.-T. Nguyen, D. Waldmann, and T. Q. Bui, "Phase field simulation of early-age fracture in cement-based materials," *Int. J. Solids Struct.*, vol. 191–192, pp. 157–172, May 2020, doi: 10.1016/j.ijsolstr.2019.12.003.
- [26] C. Miehe, M. Hofacker, and F. Welschinger, "A phase field model for rate-independent crack propagation: Robust algorithmic implementation based on operator splits," *Comput. Methods Appl. Mech. Eng.*, vol. 199, no. 45, pp. 2765–2778, Nov. 2010, doi: 10.1016/j.cma.2010.04.011.
- [27] C. Miehe, F. Welschinger, and M. Hofacker, "Thermodynamically consistent phase-field models of fracture: Variational principles and multi-field FE implementations," *Int. J. Numer. Methods Eng.*, vol. 83, no. 10, pp. 1273–1311, Sep. 2010, doi: 10.1002/nme.2861.
- [28] Y. Hou, P. Yue, Q. Xin, T. Pauli, W. Sun, and L. Wang, "Fracture failure of asphalt binder in mixed mode (Modes I and II) by using phase-field model," *Road Mater. Pavement Des.*, vol. 15, no. 1, pp. 167–181, Jan. 2014, doi: 10.1080/14680629.2013.866155.
- [29] X. Zhang, S. W. Sloan, C. Vignes, and D. Sheng, "A modification of the phase-field model for mixed mode crack propagation in rock-like materials," *Comput. Methods Appl. Mech. Eng.*, vol. 322, pp. 123–136, Aug. 2017, doi: 10.1016/j.cma.2017.04.028.
- [30] Q. Wang, Y. T. Feng, W. Zhou, Y. Cheng, and G. Ma, "A phase-field model for mixed-mode fracture based on a unified tensile fracture criterion," *Comput. Methods Appl. Mech. Eng.*, vol. 370, p. 113270, Oct. 2020, doi: 10.1016/j.cma.2020.113270.
- [31] B. Bourdin, G. A. Francfort, and J.-J. Marigo, "The Variational Approach to Fracture," *J. Elast.*, vol. 91, no. 1, pp. 5–148, Apr. 2008, doi: 10.1007/s10659-007-9107-3.
- [32] J.-Y. Wu, "A unified phase-field theory for the mechanics of damage and quasi-brittle failure," *J. Mech. Phys. Solids*, vol. 103, pp. 72–99, Jun. 2017, doi: 10.1016/j.jmps.2017.03.015.
- [33] Y. S. Jenq and S. P. Shah, "NONLINEAR FRACTURE PARAMETERS FOR CEMENT BASED COMPOSITES: THEORY AND EXPERIMENTS," p. 41.



# OUT-OF-PLANE RESPONSE OF ENGINEERED CEMENTITIOUS COMPOSITE FACED BLOCK MASONRY

*<sup>a</sup> Muhammad Imran, <sup>b</sup> Faisal Shabbir\*, <sup>c</sup> Saeed Pourfalah, <sup>d</sup> Afaq Ahmad*

a: Civil Engineering, University of Engineering and Technology Taxila, [enr.imranahmad96@gmail.com](mailto:enr.imranahmad96@gmail.com)

b: Civil Engineering, University of Engineering and Technology Taxila, [faisal.shabbir@uettaxila.edu.pk](mailto:faisal.shabbir@uettaxila.edu.pk)

c: Civil Engineering, Head of Technical Department, Max Frank Limited, [s.pourfalah@maxfrank.co.uk](mailto:s.pourfalah@maxfrank.co.uk)

d: Civil Engineering, UET Taxila, [afaq.ahmad@uettaxila.edu.pk](mailto:afaq.ahmad@uettaxila.edu.pk)

\* Faisal Shabbir: Email ID: [faisal.shabbir@uettaxila.edu.com](mailto:faisal.shabbir@uettaxila.edu.com)

**Abstract-** The purpose of this study is to propose and demonstrate the effectiveness of engineered cementitious composite (ECC) for strengthening block masonry. Two cases have been studied: ECC only on the tension face and ECC on both tension and compression faces. Out-of-plane response of tension reinforced beam, and both tension and compression reinforced beam has been experimentally investigated under four-point loading systems. The findings of this study show that both the strength and ductility of masonry beams enhance using ECC, which advocates the use of ECC as a block masonry reinforcing material.

**Keywords-** Block masonry, bending response, ECC, four-point loading.

## 1 Introduction

Block masonry structures are distinct from other types of structures in terms of construction techniques. Concrete blocks have been widely used because of their low cost, easy availability, and high compressive strength. However, because block and cement mortar are fragile materials, failure occurs suddenly, without warning. During the life of a building, block masonry walls are subjected to various out-of-plane loadings i.e. static and seismic loads. Therefore, it is important to design block masonry walls resilient to out-of-plane loads [1]. For the purpose of reinforcing masonry constructions, much research has been conducted in the previous decades. The majority of research studies have indicated that intact masonry walls can be strengthened in an out-of-plane direction [2].

Concrete, one of the most extensively utilized composite materials in the construction sector, is a fragile material. Numerous studies on fiber-reinforced concrete/composites have been conducted in the past, but the ECC material and technique were developed in the early 1990s [3]. Many researchers found that analytical and empirical findings for concrete block walls loaded in the lateral direction are still inadequate, and numerous retrofitting solutions have been developed to increase masonry building efficiency.

The masonry walls must be built in a way that they can easily bear the external loads to ensure public safety, structural integrity, and resilience [4], [5]. The out-of-plane efficiency can be improved when ECC layers are added to the masonry walls [6]. A fully coated layer of ECC applied to the face of block masonry is predicted to improve out-of-plane efficiency, including load-bearing capabilities and ductility [7].

Thus, the objective of this research is to investigate the out-of-plane response of block masonry beams that have been externally reinforced with ECC on the tension face and on both compression/tension faces. Tests were conducted to determine the behaviors of beam-like specimens (essentially a bundle of blocks joined with mortar joints in between) under bending load [8]. The objective of the bending load test is to demonstrate the ability of the reinforcing technique to improve block masonry structural behavior. This study helps out to understand the behavior of ECC-retrofitted masonry walls against out-of-plane loads by using the proposed strengthening method.



## 2 Experimental Procedures

The experimental examination was divided into four distinct phases. First, the ECC was prepared. three masonry beams were cast, each with eight blocks in a row, and 1:3 cement mortar was used in between blocks. Beams were strengthened by ECC on the tension face and both on compression/tension (namely, sandwich). Bending tests were performed on masonry beams to determine the behavior of ECC. An overview of the experiments performed is presented in Table 1.

Table 1: Summary of bending tests performed on beam-like specimens.

Type of tests	Specimens tested	ID
Bending Tests	Controlled masonry beam-like specimens (non-retrofitted).	A
	A beam-like specimen retrofitted with ECC layer on tension face.	B
	A beam-like specimen retrofitted with ECC layer on tension/compression faces (sandwich).	C

### 2.1 Constituents of ECC

In this study, ECC contains Polypropylene (PP) fibres of 12 mm in length, cement, fly-ash, sand, and water. High-range superplasticizers (SP) are used to enrich the fresh properties of the mixture. The dosage rate of Polycarboxylate SP was 1% by weight of cement used, and the filler used was fine silica sand. The fly ash/cement ratio was 1.8 (by mass), whereas the water/cement ratio was 0.28 (by volume). The sand/cement ratio was taken as 0.6 (by mass). The sand and cement are blended and dried for 30–60 seconds till the mixture is homogenous in the creation of ECC. Then fly ash and SP are added sequentially. SP was added as per requirement. To make a cake, fibres are added at the end.

## 3 Research Methodology

### 3.1 Testing of beam-like specimens

Three beam-like specimens were manufactured and were subjected to a 4-point bending test. Each specimen has eight blocks with seven mortar joints in between, as shown in Fig. 1. 10mm thick layer of mortar joint was used internally. Out of three specimens, one benchmark specimen was un-strengthened (A series), one specimen had a 15mm ECC layer (B series) on the tension face, and one specimen was retrofitted with the ECC layer on both tension and compression faces. The length of the beam-like specimen was  $835 \pm 25$  mm with a 400 mm width. The thickness of specimens is: 200 mm in the A-series (see Fig. 1(a)),  $215 \pm 5$  mm in thickness for the B series (see Fig. 1(b)), and  $230 \pm 5$  mm in thickness for the C series (see Fig. 1(c)).

## 4 Results and analysis

### 4.1 Unstrengthened specimen response (A series):

Fig. 2(a) explains the behavior of the un-strengthened specimens (A series). As a result, these un-strengthened specimens broke suddenly (brittle), which resulted in immediate failure of the load holding capacity. The failure occurred shortly after a fracture developed along with one of the block/mortar contacts near the specimen's middle span (inside the two areas where the load was employed). The findings demonstrate the vulnerability of un-strengthened block masonry beams to out-of-plane loading. Fig. 3(a) shows the condition of the specimens after failure.



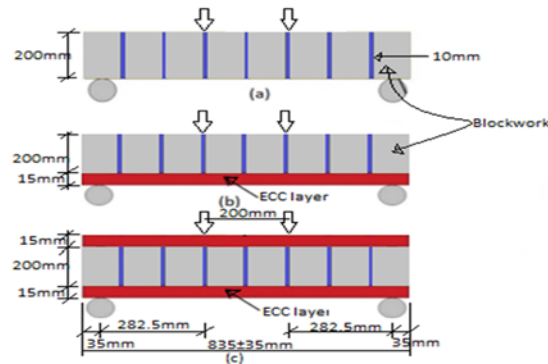


Figure 1: Schematic illustration of four-point flexure testing (a) unstrengthen specimens (A series) (b) Tension face strengthening (B series) (c) Sandwich bonded (C series)

#### 4.2 ECC strengthen specimen response (B and C series):

Fig. 6 depicts the crack pattern of the beam retrofitted with ECC on the tension face (B series) after failure. It has been noted that small fractures are formed initially. These small fractures coalesce to produce a bigger fracture that finally causes the ECC layer to fail. Furthermore, specimens strengthened with an ECC layer on the tension face (B Series) have a crack pattern that is localized at the joints in between the blocks. The micro-cracks converge to form wider cracks, which eventually fail the ECC layer, causing the beam specimens to collapse. Whereas in the case of sandwich beam (C series) specimens, a big crack is produced across the ECC layers and shows brittle failure. Contrasting the crack pattern of B series and C series beams, it is evident that the specimen retrofitted on the tension face permits the ECC to acquire a more homogenous (dispersed) cracked pattern than the sandwich beam.

Table 2 displays the load at first crack, load-carrying ability, and the accompanying mid-span deflection at failure. Fig. 3 shows the relationship between out-of-plane deflection and applied loading, which shows that the load-carrying capacity of sandwich beam is more than that of beam bonded with ECC on tension face (B series) and unstrengthened beam (A series). The average load due to the first fracture was determined to be 1.15 kN, 11.80 kN, and 17.95 kN for the A, B, and C series correspondingly. The average mid-span deflection at failure for A, B, and C series was 0.07 mm, 2.21 mm, and 1.34 mm, respectively. As seen in Table 2, the load-bearing capability of the sandwich beam is greater than that of the beam bonded on the tension side. In an un-strengthened beam, failure occurs after the peak load and causes flexure failure, as shown in Fig. 3(a). B and C specimens were retrofitted with ECC, a tension face and a sandwich bonded beam. The load-carrying capacity of B and C was 10.45 and 18.36 times greater than that of the controlled block masonry beams (A), respectively. The out-of-plane deformation of B and C series specimens was 31.57 and 19.14 times greater than that of the un-strengthened specimens (A series), respectively.

Table 2: Summary of four-point bending test.

ID	ECC layer thickness (mm)	Loading at first crack (kN)	Loading at failure (kN)	Deflection at failure (mm)
A	---	1.15	1.15	0.07
B	15.30	11.8	12.75	2.21
C	14.95	17.95	22.40	1.34

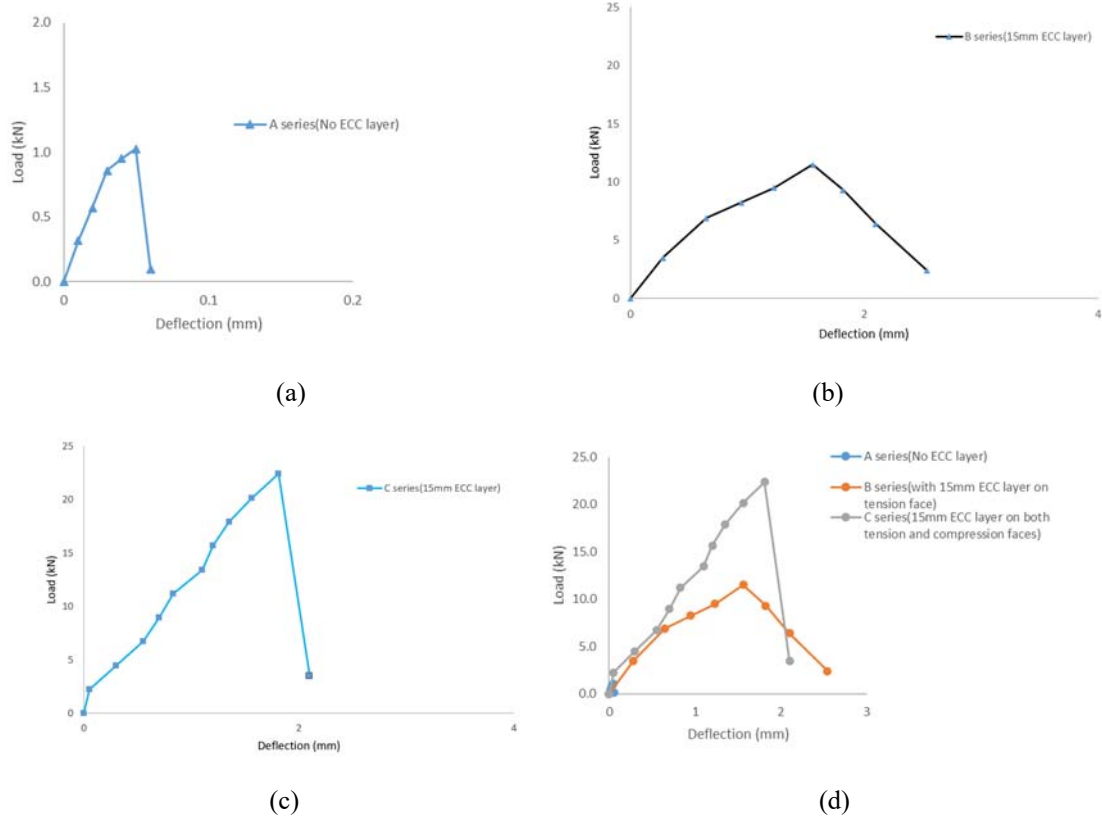


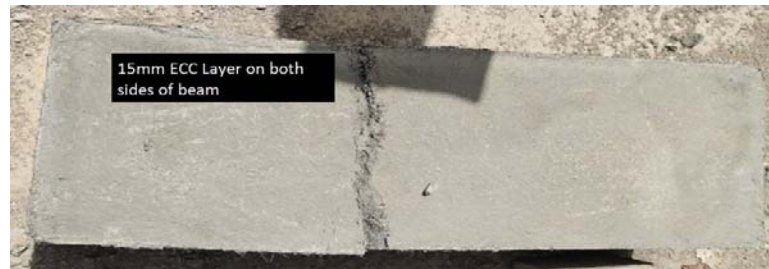
Figure 2 Load deflection responses of four-point bending test of (a) Non retrofitted specimens (A series) (b) Tension retrofitted specimens (B series) (c) Sandwich (C series) (d) comparison of A, B and C series



(a)



(b)



(c)

Figure 3: Failure crack pattern of (a) Non retrofitted specimen (A series), (b) Bottom retrofitted specimen (B series), (c) Sandwich specimen (C series)

## 5 Conclusions

The flexural response of block masonry walls retrofitted with the ECC layer was explored in this experimental research. The following are conclusions derived from the test results:

1. Unstrengthen specimens (A series) were more vulnerable to out-of-plane loading and produced sudden failure with a maximum load-carrying capacity of 1.15kN, and mid-span deflection was 0.07mm.
2. Specimens retrofitted with ECC on tension face show enhanced load carrying capacity of 12.75kN, which is about 10.45 times of unstrengthen specimens. Mid-span deflection of tension faced (B series) retrofitted specimen increased up to 31.57 times the unstrengthen specimens.
3. Specimens retrofitted with ECC both on tension and compression sides (C series, sandwich) show the load-carrying capacity is 18.36 times greater than that of unstrengthen specimens, and mid-span deflection was about 19.14 times of unstrengthen specimens.
4. The load-bearing capability of the sandwich beam is 1.76 times higher than that of a beam retrofitted on tension face only and 18.36 times the un-strengthen beam-like specimen. The tension faced ECC retrofitted specimens show more deflection than that of the sandwich and unstrengthen specimens and show more uniform cracks.

## Acknowledgement

Words cannot express my gratitude to Dr. Faisal Shabbir, Dr. Afaq Ahmad and Dr. Saeed Pourfalah for their invaluable patience and feedback. Additionally, BSc students Muhammad Abdullah and Adnan Ashraf are acknowledged for their help in the experimental program. I am also grateful to my classmates Uzma Bibi, Wajahat Zahoor and Fahim Abbas for their help in editing, late-night feedback sessions, and moral support.

## References

- [1] Z. Al-Jaberi, J. J. Myers, and M. A. ElGawady, "Experimental and Analytical Approach for Prediction of Out-of-Plane Capacity of Reinforced Masonry Walls Strengthened with Externally Bonded FRP Laminate," *Journal of Composites for Construction*, vol. 23, no. 4, p. 04019026, May 2019, doi: 10.1061/(ASCE)CC.1943-5614.0000947.
- [2] S. A. Hamoush, M. W. McGinley, P. Mlakar, D. Scott, and K. Murray, "Out-of-Plane Strengthening of Masonry Walls with Reinforced Composites," *Journal of Composites for Construction*, vol. 5, no. 3, pp. 139–145, Aug. 2001, doi: 10.1061/(asce)1090-0268(2001)5:3(139).
- [3] R. Sistani Nezhad and M. Z. Kabir, "Experimental investigation on out-of-plane behavior of GFRP retrofitted masonry panels," *Construction and Building Materials*, vol. 131, pp. 630–640, Jan. 2017, doi: 10.1016/j.conbuildmat.2016.11.118.
- [4] Chourasia A, Singhal S, Parashar J. Experimental investigation of seismic strengthening technique for confined masonry buildings. *Journal of Building Engineering*. 2019 Sep 1;25:100834, <https://doi.org/10.1016/j.job.2019.100834>
- [5] T. T. Bui and A. Limam, "Out-of-plane behaviour of hollow concrete block masonry walls unstrengthened and strengthened with CFRP composite," *Composites Part B: Engineering*, vol. 67, pp. 527–542, 2014, doi: 10.1016/j.compositesb.2014.08.006.
- [6] S. Pourfalah, B. Suryanto, and D. M. Cotsovos, "Enhancing the out-of-plane performance of masonry walls using engineered cementitious composite," *Composites Part B: Engineering*, vol. 140, pp. 108–122, May 2018, doi: 10.1016/j.compositesb.2017.12.030.



**4<sup>th</sup> Conference on Sustainability in Civil Engineering (CSCE'22)**  
Department of Civil Engineering  
Capital University of Science and Technology, Islamabad Pakistan



- [7] S. Türkmen, S. N. M. Wijte, B. T. de Vries, and J. M. Ingham, "Out-of-plane behavior of clay brick masonry walls retrofitted with flexible deep mounted CFRP strips," *Engineering Structures*, vol. 228, p. 111448, Feb. 2021, doi: 10.1016/J.ENGSTRUCT.2020.111448.
- [8] S. B. Singh, R. Patil, and P. Munjal, "Study of flexural response of engineered cementitious composite faced masonry structures," *Engineering Structures*, vol. 150, pp. 786–802, Nov. 2017, doi: 10.1016/j.engstruct.2017.07.089.



# NUMERICAL STUDY OF SHAPE MEMORY ALLOY (SMA) REINFORCED BEAM SUBJECTED TO SEISMIC LOADING

<sup>a</sup> Juna Bloy, <sup>b</sup> Rabee Shamass\*, <sup>c</sup> Vireen Limbachiya, <sup>d,e</sup> Mohammed El-desoqi

- a: Civil and Building Services Engineering, London South Bank University, [junabloy23@gmail.com](mailto:junabloy23@gmail.com)  
b: Civil and Building Services Engineering, London South Bank University, [shamassr@lsbu.ac.uk](mailto:shamassr@lsbu.ac.uk)  
c: Civil and Building Services Engineering, London South Bank University, [limbachv@lsbu.ac.uk](mailto:limbachv@lsbu.ac.uk)  
d: Civil Engineering Department, Faculty of Engineering, The British University in Egypt (BUE), El-Sherouk, Cairo, Egypt, [mohammed.eldesoqi@bue.edu.eg](mailto:mohammed.eldesoqi@bue.edu.eg)  
e: Civil and Building Services Engineering, London South Bank University, [eldesoqm@lsbu.ac.uk](mailto:eldesoqm@lsbu.ac.uk)  
\* Corresponding author: Email ID: [shamassr@lsbu.ac.uk](mailto:shamassr@lsbu.ac.uk)

**Abstract-** To safeguard against the loss of life and to maintain integrity, reinforced concrete structures are designed and constructed to withstand severe damage, impact and permanent displacement during a strong earthquake. Due to the dissipation of energy after a major earthquake, steel reinforcement undergoes large strains which lead to damage in the plastic hinge zone. Furthermore, the structure will be unserviceable due to the large residual deformations caused by the permanent strain in steel. Implementation and development of smart materials in structures will help to achieve these qualities. Shape Memory Alloy (SMA) is an example of a smart material, the use of such super elastic material in reinforced structures helps to recover the strain upon unloading which leads to improved recovery, without significant degradation or permanent deformation through repeated cycling. This ability gives a promise in civil engineering infrastructure applications specifically in seismic design. The primary objective of this study is to review the use of SMA in reinforced concrete at the plastic hinge region and to review the behavior of the hybrid beam using finite element software. After validation of the finite element model with the experimental results gathered from past literature, a parametrical study is conducted to understand the behavior of the hybrid beam with a change in parameters.

**Keywords-** Numerical study, RC beam, Shape Memory Alloy (SMAs), VecTor2

## 1. Introduction

When exposed to major earthquakes, ductile structures are built to respond inelastically. This is usually accomplished by placing plastic hinges at strategic spots throughout a building. The plastic hinges are engineered to provide flexure while avoiding nonductile failure mechanisms. While this prevents the structure from collapsing and ensures that the earthquake's energy is released effectively, residual deformations are to be expected. As the reaction continues into the inelastic region, residual deformation is mostly caused by the accumulation of residual strains in the reinforcement. After a seismic event, significant residual deformations can render structures unusable. It may also make repair and retrofitting impossible. However, a comparatively new class of alloys called as Shape Memory Alloys (SMAs) has just developed and piqued researchers' interest. Shape memory alloys are one-of-a-kind materials that change the crystalline phase when exposed to temperature or stress changes, and they come in two varieties: Austenite and Martensite. Due to their capacity to recover inelastic displacements, these alloys are appealing in seismic applications. Furthermore, at significant stresses, SMAs yield under load and strain hardening and have the same strength capacity as traditional deformed reinforcing bars. The high initial cost of SMAs is one of their key disadvantages; as a result, they should only be employed in vital areas. Another drawback is the reduced capacity to disperse energy due to its re-centering tendencies. The higher crack widths and crack spacing that should be expected in concrete members reinforced with SMAs because of their smooth surface are envisaged to a lesser extent. SMAs, on the other hand, are corrosion resistant and can tolerate higher crack widths than typical deformed bars.

Various research studies have been worked upon to improve the seismic resistance of concrete structures by using SMAs in critical regions to reduce residual deformation [1]. To allow the dissipation of energy in the critical region and to allow

yielding, and to recover deformation, SMAs were used in various RC structures such as beam-column joints [2], in beams [3], in shear walls [4, 5], and in reinforced concrete (RC) columns [6]. They found that in the event of an earthquake, SMA enables the structure to recover its residual deformation after yielding. However, there have been few numerical investigations of hybrid steel-SMAs reinforced concrete beams. Therefore, the main purpose of the paper is to build a numerical model for hybrid steel-SMAs reinforced concrete beams and conduct a validation against the experimental results conducted by Abdulridha et al. [3] in terms of ultimate capacity and hysteresis behaviour. Finally, a parametric study is conducted to investigate the effect of various reinforcement ratios as well as the concrete compressive strength on the seismic behaviour of hybrid steel-SMAs reinforced beams.

## 2. Review of Experimental Results

Abdulridha et al. [3] tested seven simply supported concrete beams subjected to monotonic, cyclic, and reverse cyclic loading. Nickel-Titanium SMA (Nitinol) alloy is used in the experiment. The goal of this experimental program was to look at the structural behaviour of SMA-reinforced beams and assess their applicability to be used as an alternative to steel in seismic applications. In the numerical modelling conducted in this paper, only two beam tests, Beams B3-SR and B6-NR will be explored in depth, both were subjected to reverse cyclic loading. B3-SR and B6-NR are reinforced with conventional steel and hybrid steel-SMA rebars, respectively. For B3-SR, 10M (11.3mm diameter) steel bars were used. centre of B6-NR was reinforced with 12.5 mm diameter Superelastic SMA smooth bars and coupled to 15M steel rebars (16 mm) (Fig. 2). The beams were 2800 x 125 x 250 mm (2400 mm from centre to centre of supports). Two central point loads, typically spaced at 125 mm apart, were used to maintain a consistent flexural zone (critical section). The SMA bars were utilized for a total length of 600 mm, centred at the beams' midspan. The SMA bars were threaded at the ends and threaded mechanical couplers were used to link them to the steel rebars. To enhance yielding at the midspan and away from the threaded sections at the ends of the bars, the SMA bars were reshaped to a diameter of 9.5 mm over a 300 mm length. The couplers had a diameter of 12.6 mm and a length of 50 mm. The shear reinforcement, which consisted of closed stirrups with a diameter of 6.35 mm, was everywhere spaced at 100 mm along the length of the beam. A typical test specimen installed in the testing apparatus is seen in Figure 1. To prevent the concrete from being crushed, a steel plate (75x150x25mm) was installed below each point stress. A hydraulic jack with displacement control was used to apply the load. Load cells were employed to measure the applied forces, and displacement cable transducers were used to continually record deflection values at the midspan (DCTs). ATC-24 [7], was used to apply reverse cyclic stress. Single repetitions at each displacement level were the sole change. One cycle of loading was performed at 0.33y, 0.66y, and 1.0y, where y is the yield displacement. Then, until failure, the following cycles were based on multiples of y. The yield displacement of the SMA and conventional reinforced beams was approximately 6.4 mm and 5.7 mm, respectively.

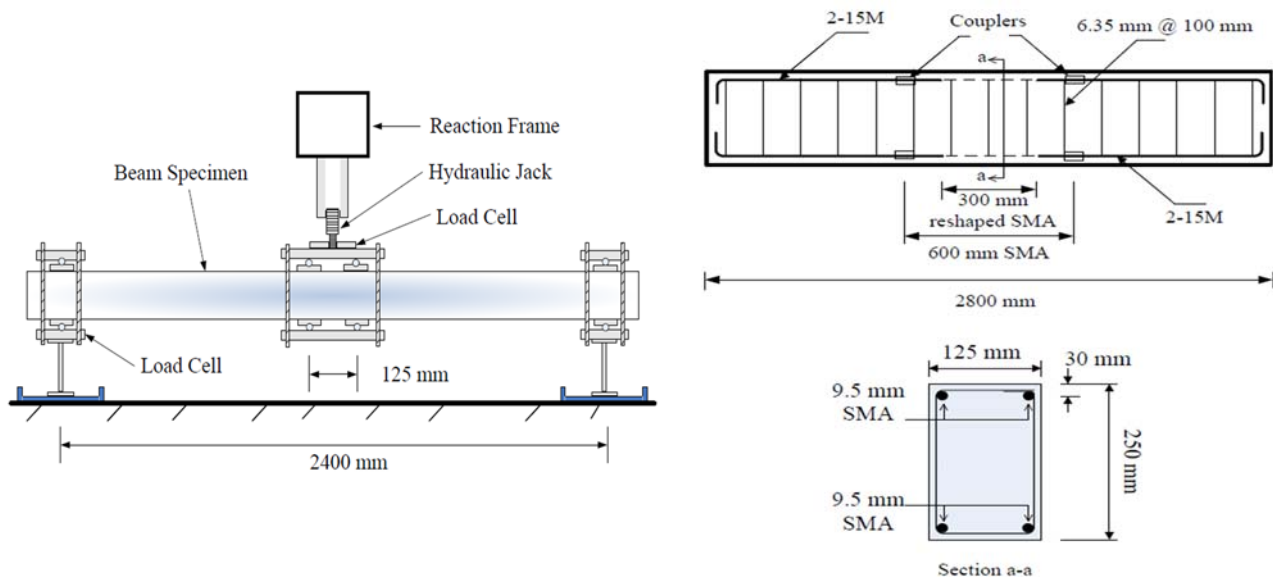


Figure 1. Typical test specimen and beam cross section

The SMA bars had a modulus of elasticity of around 60 GPa, whereas the 10M distorted bars had a modulus of elasticity of roughly 205 GPa.



The approximate yield stress for the SMA was determined to be 415 MPa, somewhat lower than the 425 MPa and 440 MPa yield stresses for the 10M and 15M conventional steel, respectively, based on a 0.2% offset. At around 1.5% strain, the ordinary steel experienced strain hardening. Hardening of the SMA bar occurred at a strain of around 5%. The ultimate strength for 10M, 15M and SMA rebars was 615 MPa, 650 MPa and 800 MPa, respectively. Concrete of conventional strength with 10 mm aggregates size was used to build the beams. On the day of testing, the SMA and conventional reinforced beams had average compressive strengths of 32.7 MPa and 34.6 MPa, respectively.

### 3. Numerical modelling and validation

A preliminary model was created and implemented in the nonlinear two-dimensional finite element software VecTor2 (Ver.4.4) [8], which is suitable for membrane structures. Based on the Modified Compression Field Theory and the Disturbed Stress Field Model, VecTor2 utilizes a smeared, rotating-crack formulation [9]. Both conventional and SMA beams were modelled, and the results were compared with the test results. All beams were modelled with rectangular plane stress concrete elements. The longitudinal flexural reinforcement bars were modelled with discrete truss bar elements and the transverse shear reinforcement was modelled with smeared within the concrete elements. For modelling conventional steel reinforcement, the truss bars were assumed perfectly bonded to the surrounding concrete while the SMA bars were partially bonded given the smooth surface of the bars leading to lower bond stresses. The applied load followed the same loading protocol in the test. The finite element model for the beams B3-SR and B6-NR are as shown in Figure 2. To coincide with the node of the concrete rectangular elements, the length of each truss element was 25 mm. Bond-slip elements were used to represent the bond between the SMA bars and the concrete, and it was assumed that the typical deformed reinforcement and couplers in SMA beams were perfectly connected to the surrounding concrete. Prior to the slippage, the bond-slip components were specified by paired nodes with the same coordinate. A concrete element was attached to one of the nodes, while a discrete reinforcement element was added to the other. At one end of the beam, pins were used to represent the supports, which were simulated with vertical and horizontal restraints, while at the other end, rollers were used to represent the supports, which were only provided with vertical restraints. The restraints were only attached at one end throughout the analysis, which was sufficient to simulate the behaviour of the supports.

Using two loading plates, two vertical loads spaced 125 mm apart were applied uniformly at mid-span in the experimental setup. In the Finite Element Model, each applied load at the top of the beam were represented by four nodes. That means four nodes were assigned at the top of the beam to apply the loads. To prevent the local crushing of the concrete the distributed load was intended to represent the spreading of the load due to the loading plate.

The reinforcement, concrete and bond constative models are illustrated in Table 1. The detailed descriptions of each model were described in the Vector2 Manual. Typically, the default models are chosen unless an alternative model better captures the behavioural response.

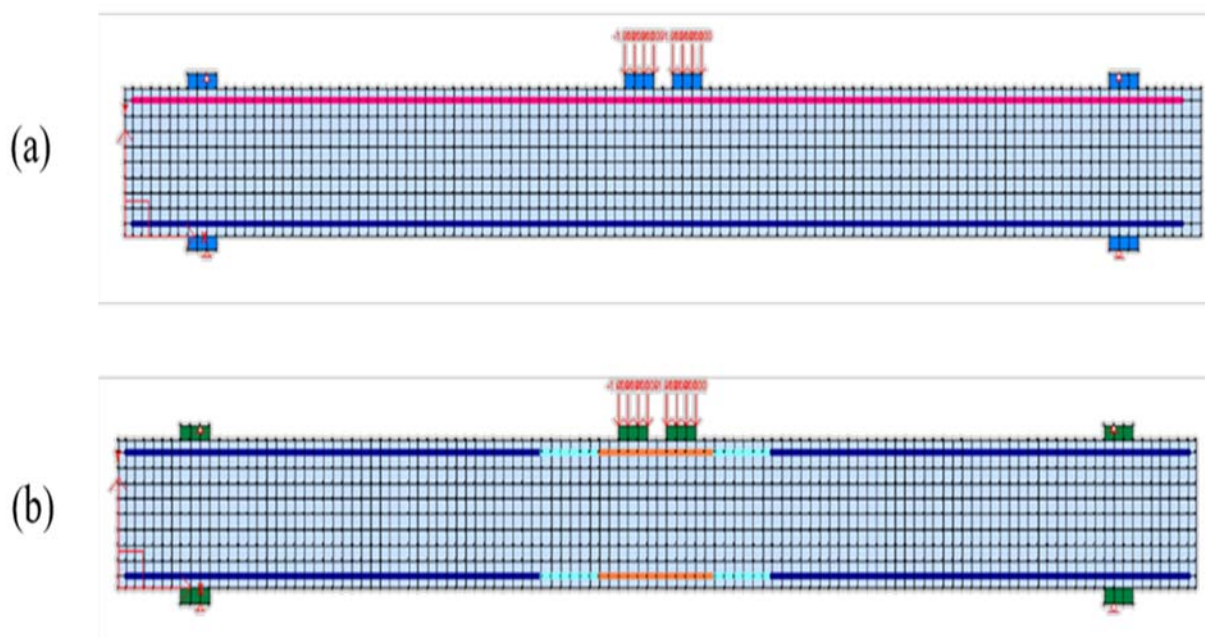


Figure 2: Finite element model of beam (a) B3-SR and (b) B6-NR



Table 1 Material and Behavioural models

Material Property	Material Model
Concrete Compression Base Curve	Popovics (NSC)*
Compression Post-Peak	Base Curve*
Concrete Compression Softening	Vecchio 1992-A
Concrete Tension Stiffening	Modified Bentz
Concrete Tension Softening	Linear
Concrete Tension Splitting	Not Considered
Concrete Confinement Strength	Kupfer I Richart
Concrete Dilatation	Variable - Kupfer
Concrete Cracking Criterion	Mohr-Coulomb (Stress)
Concrete Crack Width	Agg/5 Max Crack Width
Concrete Hysteresis	Non-Linear with Plastic Offset
Slip Distortion	Vecchio-Lai
Reinforcement Hysteretic Response	Seckin Model (Bauschinger)
Reinforcement Dowel Action	Tassios Model (Crack Slip)
Reinforcement Buckling	Asatsu Model
Concrete Bond	Eligehausen Model

#### 4. Numerical validation

The responses of the conventional reinforced and SMA reinforced beams are shown in Figures 3 (a) and (b), respectively. The strength capacities are often effectively replicated and match the experimental tests. The nonlinear unloading response of the SMA reinforced beam found during testing suggests that the recovery is significantly overstated, and the unloading curves do not represent the nonlinear unloading response of the SMA reinforced beam. The analytical response of a conventional reinforced beam is shown in Figure 3 (b) for comparison. The behaviour seen during testing, including strength and ductility capabilities, was successfully represented by the numerical model. Unloading and reloading curves were accurately modelled. The pinching is a noteworthy difference; slightly more was noted during testing. With a modified constitutive model for SMA bars that reflect nonlinear unloading and minor residual stresses accumulated as the ductility needs grow, better results for the SMA beam may be produced. Because reverse cyclic loading involves loading and unloading the beam in one cycle, the unloading and reloading curves following reverse cyclic loading were accurately modelled. In the analysis of the conventional beam, the analysis predicted slightly lower strength and higher initial stiffness than the experimental results. The measured displacement at failure following the numerical test was 57.125mm, however, the expected displacement was 59 mm. There were also differences that were noted around the yield strength. The observed value was 29 kN for the experimental test, however, the analysis revealed a value of 26.19 kN which is less than the experimental value of almost 9.7%. Both beams failed by concrete crushing after significant yielding of the longitudinal reinforcement but at slightly different displacements. In general, though, the numerical response of the conventional reinforced beam demonstrates the applicability of the finite element model and VecTor2 adopted for this study.

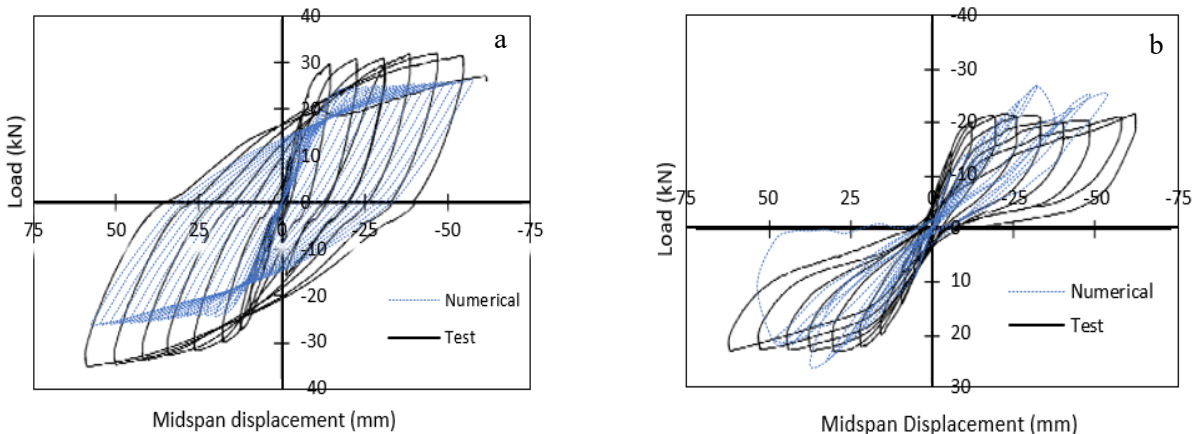


Figure 3: Analytical load-displacement response of beam (a) B3-SR and (b) B6-NR





The calculated response of the SMA reinforced beams indicates that the analysis reasonably predicted the behavior observed during testing. Comparing the observed results to the predicted numerical results, the predicted ultimate strength of B6-NR was 24.5 kN, however, the observed and recorded values for the experimental load capacity was 21.94 kN which is less than the predicted value of 10.45%. The difference in the value of ultimate load capacity is due to a large fracture outside the critical zone that occurred during the test procedure on this SMA beam. The midspan displacement at failure measured by the experiment was 60 mm, while the numerical analysis yielded a value of 53.29 mm. Permanent displacements were satisfactorily captured during the analysis; however, more pinching was observed in the experimental hysteretic response. Figure 3 (b) demonstrates the hysteretic behavior was well simulated, including peak strength, ductility, residual displacements, and unloading response. The discrepancy in the ultimate load capacity can be attributed to the fact that the SMA beam experienced a major crack outside the critical region during the test which resulted in a reduction in strength.

By comparing the computed and actual cracking patterns, the numerical models were further evaluated. As demonstrated in Figure 4, the model predicted closely spaced cracks in the conventional reinforced beam and much wider cracks in the SMA reinforced beam. These patterns matched observations made during testing, indicating that the finite element model was correct. These trends were consistent with observations noted during testing. Generally, the finite element results provided good predictions of the sequence and locations of the first flexural and shear cracks. For comparison purposes, the first numerical crack was defined by a crack width of 0.10 mm, which corresponds to the visible crack width during testing. Experimentally, flexural cracking at midspan was observed first followed by inclined shear cracks near the supports. Numerically, the sequence of cracking was similar to that observed in the conventional and SMA beams where local effects from the presence of the couplers governed the location of critical damage. This resulted in the first flexural crack initiating at the coupler location where failure was observed. All beams were designed as flexural members that experience significant reinforcement yielding prior to concrete crushing. This type of failure was predicted in the finite element analysis for both conventional and SMA beams. Experimentally, the tested beams had similar failure modes except for SMA beam which experienced failure by rupturing of the SMA at the transition point where the SMA changed diameter.

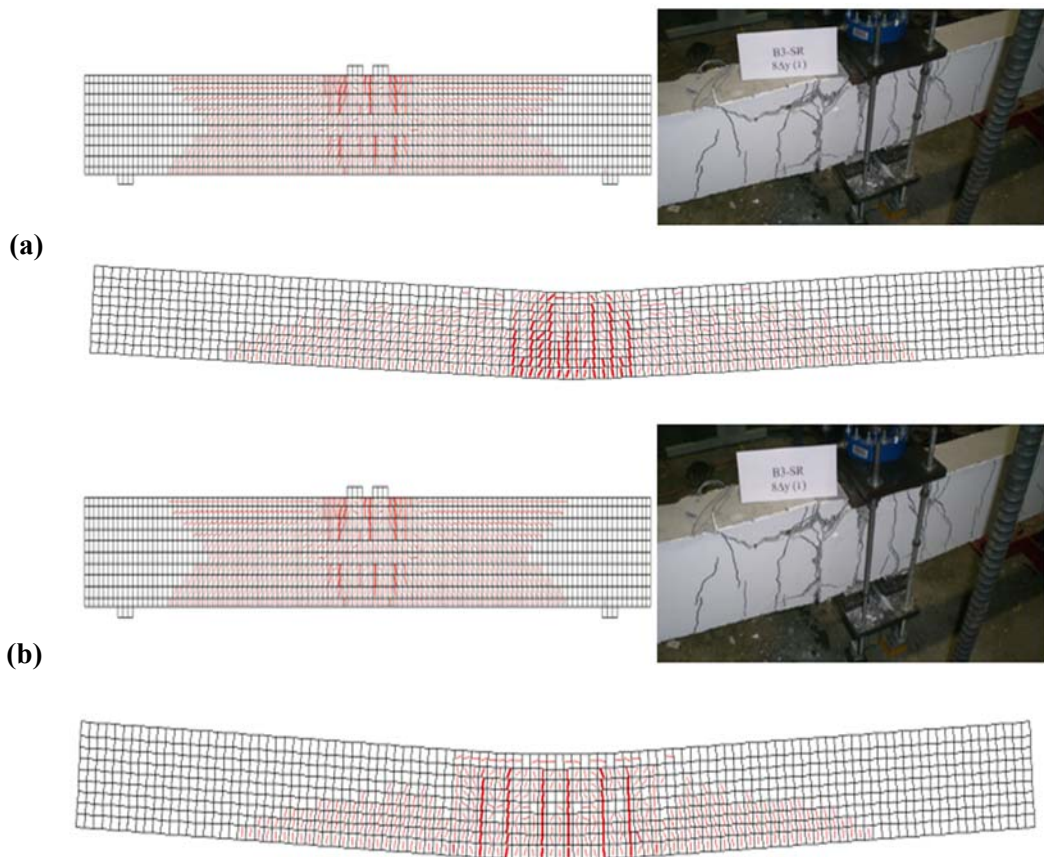


Figure 4: Crack Patterns of beam (a) B3-SR and (b) B6-NR



## 5. Parametric study

This part includes the changes in the seismic behaviour of Superelastic SMAs caused by varying the concrete strength and SMA reinforcement ratio of the beam B6-NR validated in the previous section. By using different SMA rebar diameter, SMA reinforcement ratio has been modified to get the reinforcement ratios of 0.20 %, 0.50 %, 0.80 %, and 1.07 %. In the second parametric study, the compressive strength of concrete is varied such as 30, 40, 50, and 60 MPa. Figure 5(a) and (b) show the effect of the reinforcement ration of the SMA on the envelop load-deflection curves and cumulative energy dissipation curves, respectively. It can be noted that as the reinforcement ratio increase, the ultimate load-carrying capacity slightly increases which allow the beam to sustain the more applied load. For instance, as the reinforcement ratio increases from 0.2% to 0.8%, the ultimate load capacity increases by 26% this is due to the beam becoming more ductile to sustain the extra applied load. Furthermore, an increase in the reinforcement ratio results in improvements in energy dissipation due to an increase in the overall ductility of the wall which leads to an increase in the area under the response curve. As the reinforcement ratio increases, the load-carrying capacity and the strength of the beam also increase so that the amount of energy dissipated will also increase.

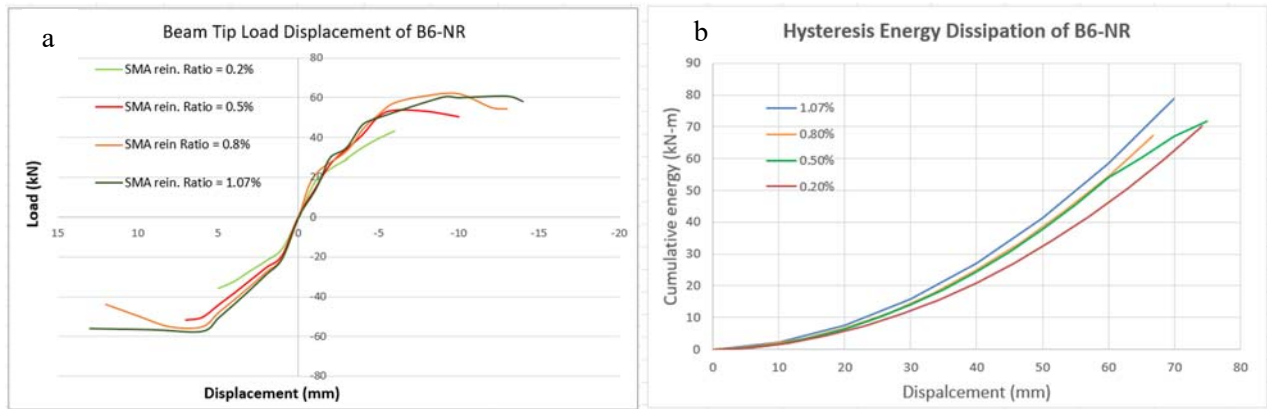


Figure 5:(a) Comparison of envelopes of load-displacement curves for SMA reinforcement ratio (b) Comparison of cumulative energy dissipation curves for SMA reinforcement ratio

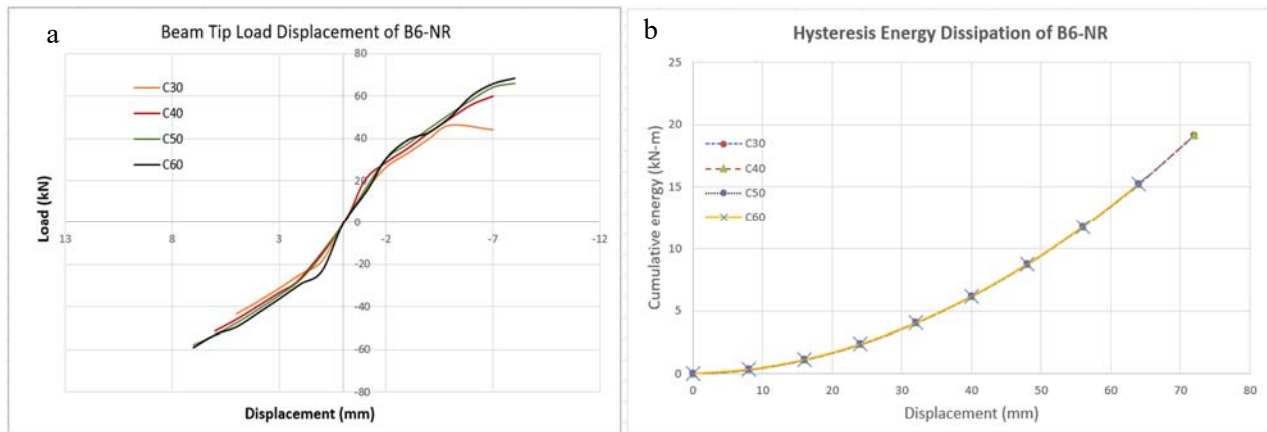


Figure 6:(a) Comparison of envelopes of load-displacement curves for concrete grades (b) Comparison of cumulative energy dissipation curves for concrete grades

When comparing the impact of concrete grades (C30, C40, C50 and C60), the ultimate load carrying capacity is increasing with an increase in the concrete grade, but all models failed in the last cycle. For example, as the compressive strength increase from 30MPa to 60MPa, the ultimate load capacity increase by 55%. There is only a marginal increase that can be found in the energy dissipation graph. Figure 9 shows the comparison results of load-displacement curves of various concrete grades.



## 6. Research significance

Long-term reverse cycle loads can cause fatigue failure in concrete flexural components reinforced with conventional steel, even at loads below their ultimate capacity. The goal of the current study project was to analyse the behaviour of concrete beams reinforced with a mix of conventional steel and SMA to reduce the risk of fatigue failure. Due to their superelasticity and high yield strength characteristics, SMAs may dissipate strain energy and recover deflection when used as reinforcement in RC flexural components. The findings of this study will help scientists and engineers better understand how concrete flexural components behave when reinforced with SMA and steel.

## 7. Conclusion

Based on the results, the following conclusions can be drawn:

- Nitinol SMA outperformed conventional beams in terms of minimizing residual movement in concrete beams and SMA reinforced beams have lower stiffness than conventional beams.
- The proposed numerical model using Vector2 provides accurate predictions in comparison with the test results for both conventional and hybrid steel-SMA rebars.
- In the case of parametric analysis with changing reinforcement ratios and concrete grade, the stress-strain behaviour and energy dissipation improve dramatically as the value of the parameters increases.
- The bigger diameter of Nitinol bars will assist in dissipating more energy and perform better in seismically active areas, but it is much more expensive than the smaller diameter, making it practically unfeasible in some circumstances.
- Finally, the ability to recover inelastic deformations, display strain hardening, and exhibit yielding while maintaining significant displacement ductility make Super-elastic SMA a promising alternative reinforcement in seismic design.
- However, because of the high initial cost, SMA may only be used in RC structures to a limited extent. As a result, in the design of reinforced members, optimization is essential.

## References

- [1] Saiidi, M.S. and Wang, H., 2006. Exploratory study of seismic response of concrete columns with shape memory alloys reinforcement. *ACI Materials Journal*, 103(3), p.436.
- [2] Youssef, M., M. Alam, and M. Nehdi, 2008. Experimental investigation on the seismic behaviour of beam-column joints reinforced with superelastic shape memory alloys,” *Journal of Earthquake Engineering*, 12, 1205-1222.
- [3] Abdulridha, A., Palermo, D., Foo, S. and Vecchio, F. J. (2013) Behavior and modeling of superelastic shape memory alloy reinforced concrete beams, *Engineering Structures*, 49, pp. 893–904. DOI: 10.1016/j.engstruct.2012.12.041.
- [4] Abdulridha, A. and Palermo, D., 2017. Behaviour and modelling of hybrid SMA-steel reinforced concrete slender shear wall. *Engineering Structures*, 147, pp.77-89.
- [5] Hault, R.D. and de Almeida, J.P., 2022. Residual displacements of reinforced concrete walls detailed with conventional steel and shape memory alloy rebars. *Engineering Structures*, 256, p.114002.
- [6] Lee, C.S., Choi, E. and Jeon, J.S., 2022. Estimating the plastic hinge length of rectangular concrete columns reinforced with NiTi superelastic shape memory alloys. *Engineering Structures*, 252, p.113641.
- [7] ATC-24, 1992. Guidelines for Cyclic Seismic Testing of Components of Steel Structures, Applied Technology Council, Redwood City, CA.
- [8] Wong, P.S., and F. J., Vecchio, 2002. *VecTor2 & Formworks user’s manual*, University of Toronto, Toronto, Canada.
- [9] Vecchio, F. J., 2000. Disturbed stress field model for reinforced concrete: formulation, *Journal of Structural Engineering*, ASCE, 126(9), 1070-1077.



# NUMERICAL INVESTIGATION OF CFRP RETROFITTED, QUARRY ROCK DUST, FLY ASH, AND SLAG BASED GEO POLYMER CONCRETE BEAMS

<sup>a</sup> Maaz Ahmad\*, <sup>b</sup> Faheem Butt,

a: Department of Civil Engineering, University of Engineering and Technology, Taxila [maaz4775@gmail.com](mailto:maaz4775@gmail.com)

b: Department of Civil Engineering, University of Engineering and Technology, Taxila [Faheem.butt@uettaxila.edu.pk](mailto:Faheem.butt@uettaxila.edu.pk)

\* Corresponding author: Email ID: [maaz.ahmad@students.uettaxila.edu.pk](mailto:maaz.ahmad@students.uettaxila.edu.pk)

**Abstract-** Geopolymers concrete (GPC) has gained popularity in the construction industry as a low-carbon, cement-free composite material with strong mechanical qualities that may be employed in various structural applications. In this paper, the behavior of simply supported geopolymer concrete beams employing symmetrical conditions is simulated using Abaqus (Finite Element Analysis) tool. A simplified version of the Concrete Damage Plasticity Model (CDP) is used as a nonlinear constitutive model. Using Abaqus (CAE), four geopolymer concrete beams were modeled with varying parameters depending on their compressive strength, and the experimental force-deflection curve. These beams were shear deficient and failed along the shear path experimentally, while the model followed the identical shear trajectory path in simulation. The same damaged beams were then strengthened by wrapping CFRP sheets around them and simulating the retrofitted beams using the ACI perfect bond condition method to validate the experimental force-deflection curve. The model has been validated against experimental load-deflection curves and shear trajectory failure paths for both controlled and CFRP-wrapped beams. The comparison of results from the experimental and numerical study suggests that the FEM is a good technique for the simulation and prediction of the elemental behavior under different loading conditions and restraints.

**Keywords-** Geopolymer, Concrete damage plasticity (CDP), Abaqus, sisal fibres, steel fibres, CFRP strips.

## 1 Introduction

In comparison to Ordinary Portland Cement (OPC) based construction materials, geopolymer concrete (GPC) has gained popularity in recent years due to its exceptional capacity to replace cement concrete and possessing improved mechanical and serviceability criteria. In terms of global warming, the GPC might reduce the CO<sub>2</sub> released into the atmosphere by the cement industry. Fly-ash (FA) and ground-granulated blast furnace slag (GGBS) are the industrial waste/by-products which are supplementary binding materials widely used for partial replacement of OPC due to their low cost and good binding or pozzolanic properties.

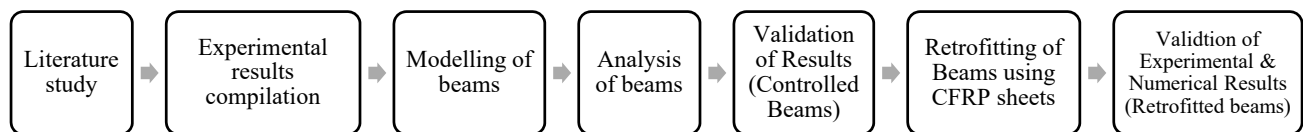
Develop a robust and efficient analytical/Numerical tools, such as the finite element method, by reducing the cost and time. The finite element approach can better simulate experimental conditions, including loads and deformation, as well as the support conditions of the actual test. Finite element analysis (FEA) is a significant tool in the study of fracture mechanics in elements. Linear elastic fracture mechanics (LEFM) has been well-studied, utilizing methods such as Damage for Traction Separation Laws (TSL) and Concrete Damaged Plasticity Model (CDP) [1]. Abaqus/CAE, or "Complete Abaqus Environment", is a three-dimensional finite element (FE) array with extensive modelling abilities that is mainly used as a research tool [2]. It offers a lot of commands for making different elements and a lot of material constitutive models for simulating the behavior of most common materials. Simulation with such models helps reduce the number of experimental tests required to determine an exact reaction of the materials.



As a result, any simulation research will save time, money, and exertion in the long run, especially when the material under consideration or the testing machine necessary is unavailable or demands a big budget. Because numerous tests have already been performed, the tradition is shifting toward concentrating solely on the numerical model and avoiding any experimental testing. Only a few tests are required to identify constitutive model parameters in new materials [3]. To predict their behavior, it is necessary to have a detailed knowledge of the flexural behavior of building materials. The four-point or centre-point loading method can be used to examine this property. As the test progresses, it's hard to identify the crack spreading and load distribution [4]. Abaqus is a Finite Element Analysis (FEA) tool that helps in computer drawing, mechanical component analysis, and visualization of FEA results. Modelling features, processing options, and post-processing animation display options are all included in Abaqus, allowing users to simulate, and forecast the behavior of their complex product. This feature helps determine load-deflection behavior, cracking patterns, and stress-strain curves. In this research work, a numerical investigation on geopolymer concrete beams has been carried out under four-point loading considering symmetrical conditions to minimize the analysis time and reduce the complexities in the model to make it easy to run [5-6]. The load deflection curve and shear failure trajectory results have been validated very well against the experimental test for both the controlled and retrofitted (wrapped by CFRP sheets) beams.

## 2 Methodology

The methodology for this study includes the modelling and analysis of the geopolymer concrete beams by using the finite element tool ABAQUS to perform. By using FEA Technique to reduce the analysis time and complexities of the model during analysis, Quarter symmetrical beams were modelled to run the analysis fast and smoothly. The Model beams then analyzed and validated the results with the experimental load-deformation curves. In total, eight beams were modeled (Table 1) in which four were analyzed under displacement-based loading, then these beams were retrofitted with CFRP sheets and analyzed again, simulated the beams, and validated with the experimental results. Different equations were used as per literature for the properties of these beams to input for the analysis as mentioned below.



## 3 Modelling and Analysis

### 3.1 Geometry modelling (Undamaged Beams)

Experimentally the dimensions of the beam were 1000 mm length x 150 mm depth x 150 mm width, while the beams for simulation were modelled as quarter symmetrical beams (dimensions 500 mm length x 150 mm depth x 75 mm width) & conditions to reduce the analysis time and minimize the complexities. Concrete is modelled as a 3D 8-Node solid brick homogenous element with reduced integration (C3D8R), while the steel bars (compression, tension & stirrups) have been modelled as a 2D truss element (T3D2) as shown in (Figure 1a, b). In the assembly part, the rebars are combined and embedded in the concrete beam by using the embedded region property. The beam has been restrained at the bottom by applying the support conditions, while at the sides of the beams symmetrical boundary condition has been applied. Displacement-based analysis was performed by applying the displacement to the experimental tests (load vs displacement) for all four beams. Meshing for the concrete beam and steel rebars was assigned in 25 mm and 15 mm, respectively. Four beams were modelled with the same geometry, but different compressive strength and different material properties input analyzed under displacement.

### 3.2 Geometry Modelling Retrofitted beams (wrapped by CFRP sheets)

The beams were modeled and analyzed under displacement control by obtaining the force-deflection curve, the beams failed in the shear path. These beams were then strengthened by wrapping the CFRP sheets. The CFRP sheets were modeled by deformable solid homogenous element as shown in (Figure 1c, d) having properties shown in (Table 2). Tie constraints were used between the beam and CFRP sheets & wrapping by considering perfect bonding between the sheet



and concrete beam by following ACI perfect bond condition [7]. No debonding was considered between the CFRP and concrete beams.

Table 1 Modeled Beams Ids

Controlled Modeled Beams Ids	Retrofitted (CFRP) Modeled Beams Ids
GPC beam	Retrofitted (CFRP) GPC beam
0.75SF-R-GPC Beam	Retrofitted (CFRP) 0.75SF-R-GPC Beam
0.5SF+1SsF-GPC beam	Retrofitted (CFRP) 0.5SF+1SsF-GPC beam
2.4SsF-GPC Beam	Retrofitted (CFRP) 2.4SsF-GPC Beam

### 3.3 Beam properties

As for the geopolymer concrete (elemental study), some of the researchers [1], [2] suggest equations for the constitutive model for the CPD input parameters, the elasticity of the beam, density, and Poisson's ratio. These properties are a little bit different from the ordinary Portland cement concrete.

### 3.4 Constitutive model

The concrete damage parameters are used by default [10-11]

$$\sigma c = fcm \left( \frac{\epsilon c}{\epsilon p} \right)^{\frac{n}{n-1 + (\epsilon c / \epsilon p)^{n_k}}} \text{ (MPa) [8-9]} \quad (1)$$

Where,

$f_c'$  = Peak / Maximum stress;  $\epsilon_{cp}$  = Strain at peak / maximum stress,  $n = 0.8 + (f_c'/17)$ ;  $k = 0.67 + (f_{cm} / 62)$  when  $\epsilon_c / \epsilon_{cp} > 1 = 1.0$  when  $\epsilon_c / \epsilon_{cp} \leq 1$ .

For Steel Fiber Reinforced Concrete [5]:  $n = \beta = 1.093 + 7.4818(3V_f \frac{l_f}{d_f})^{-1.387}$ ;  $V_f$  = Steel fibre fraction in Volume;  $l_f$  and  $d_f$  = length and diameter of the fibre, respectively; and  $\eta$  = Orientation factor of fibre which is taken as 0.5.

Modulus of Elasticity,  $E_c C_{GPC} = 4907.5 \sqrt{f_c'}$  [1]; Peak strain  $\epsilon = 1.65 \times 10^{-5} f_{cm} + 0.00168$ ; Tensile Strength =  $0.7 \sqrt{f_c'}$  [7]; Cracking Strain,  $\epsilon_{cr} = 0.000065 f_{ct}^{0.54}$  [7]

For Steel Fiber Reinforced-GPC beams:  $E_{cf(GPC)} = 21500 \times (\frac{f_c'}{10})^{1/3}$  [8]; Tensile Strength  $f_t' = 0.6 \eta (f_c')^{2/3} V_f \frac{l_f}{d_f}$  [9]

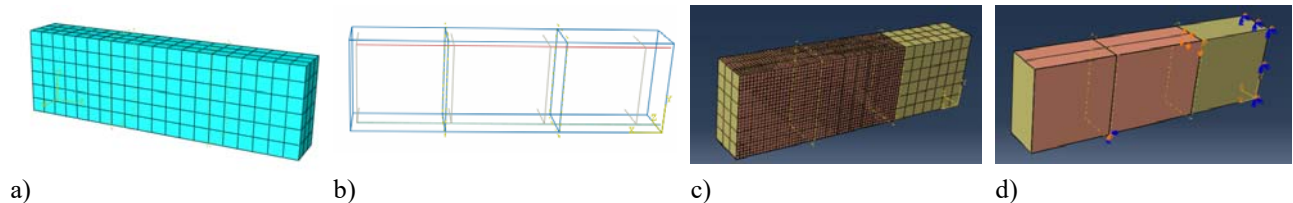
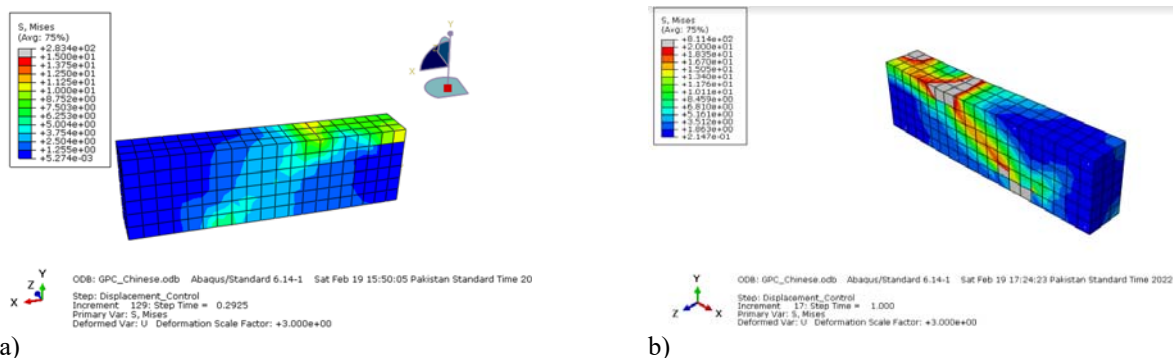
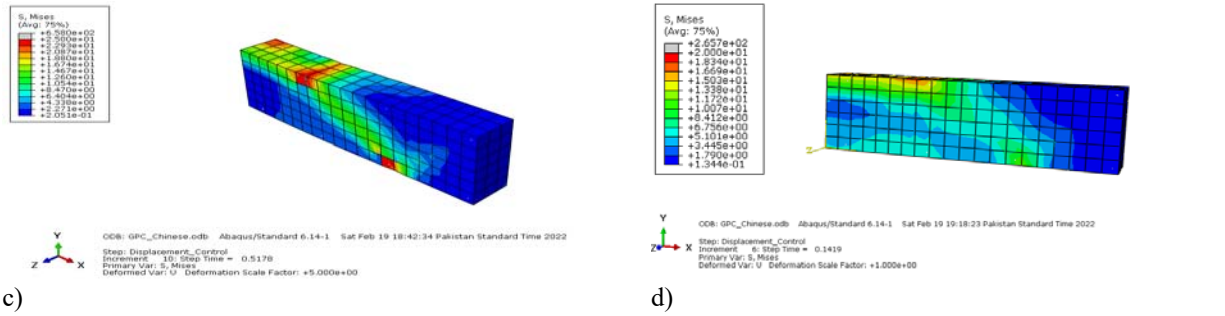


Figure 1: a. Quarter Beam Meshed, b. Quarter beam reinforcement, c. Meshing CFRP & Beam, d. CFRP wrapping & loading





c) Figure 2: a. GPC Beam stresses, b. 0.75SF-GPC Beam Stresses, c. 0.5SF+1SsF-GPC Stresses, d. 2.4SsF-GPC beam Stresses

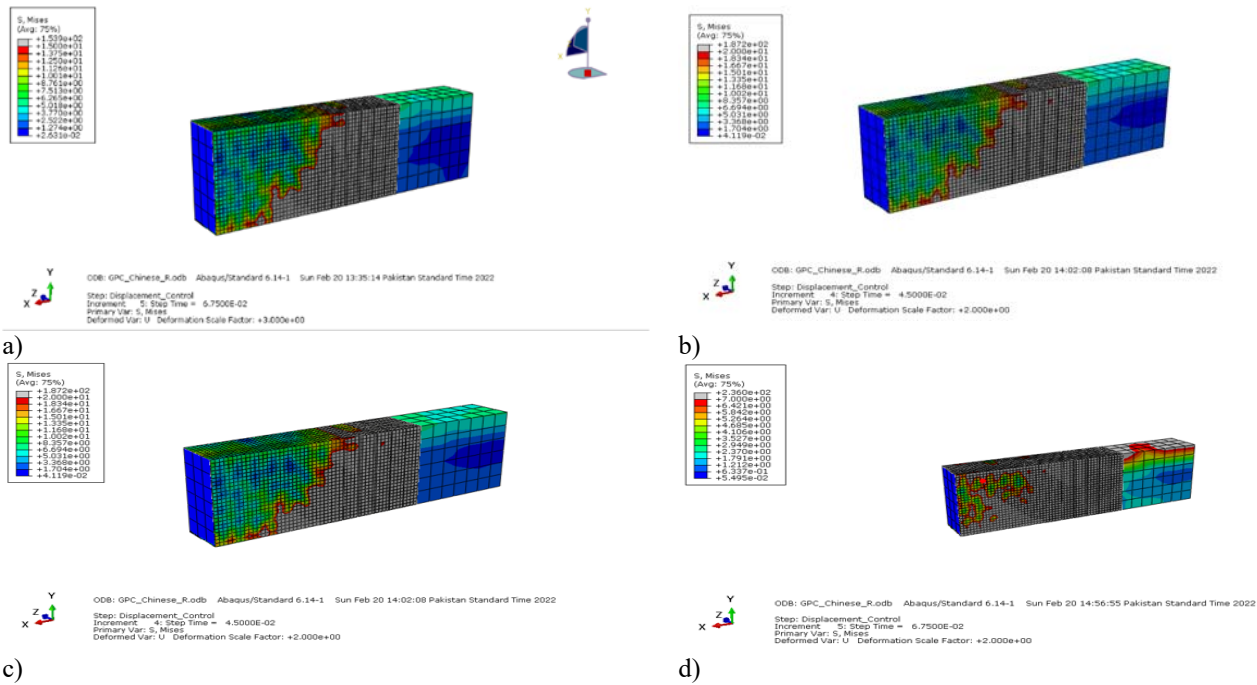


Figure 3: a. Retrofitted GPC Beam stresses, b. 0.75SF-GPC Retrofitted Beam Stresses, c. 0.5SF+1SsF-Retrofitted-GPC Stresses, d. 2.4SsF-Retrofitted-GPC beam Stresses

Table 2 CFRP Properties

Material	Width (mm)	Thickness (mm)	Elastic Modulus (GPA)	Tensile Strength (MPa)	Elongation at break %
CFRP Strip (S812)	80	1.2	165	3100	1.69
CFRP wrap (230C)	300	0.129	225	3500	1.59

## 4 Results and Discussion

The shear deficient beams were analyzed as a displacement-based & validate the numerical results with the experimental results for the four controlled & Retrofitted beams as the results shown in (Figure 4). The peak load and displacement were found to differ by less than 10 % as shown in (Table 3) when comparing experimental and numerical results, indicating a good agreement and validated results at the bottom of the beam and simulated for results. The predicted deflections were adequately close to the experimental results as by percentage difference less than 10% as observed by other researchers [10]. All the beams failed by the formation of diagonal cracks. Most stresses were produced near to the supports



and no tensile splitting was noticed along with the main reinforcement. The shear failure occurred in the concrete due to its brittle nature. The load carrying capacity reached to the ultimate limits after which sudden failure was occurred. As in the (Figure 2, Figure 3 ) it can be noted that most of the stresses are in the shear path, which also indicates that the beams were shear deficient as simulated numerically.

The plain GPC beam exhibit a displacement of 3.16 mm at a load of 40.4 kN. 0.75SF-R-GPC exhibit more displacement of 5.15 mm at a load of 73.3 kN because of the inclusion of steel fibers in the beam, which interlocks the bond between the concrete and itself and gives more strength to the beam in the flexural behavior. The beam with the addition of Sisal fiber (SsF) and steel fiber (SF), gives a displacement of 4.9 mm at a load of 58.1 kN, and the beam having only Sisal fiber which exhibits a displacement of 3.75 mm at a load of 47.1 kN.

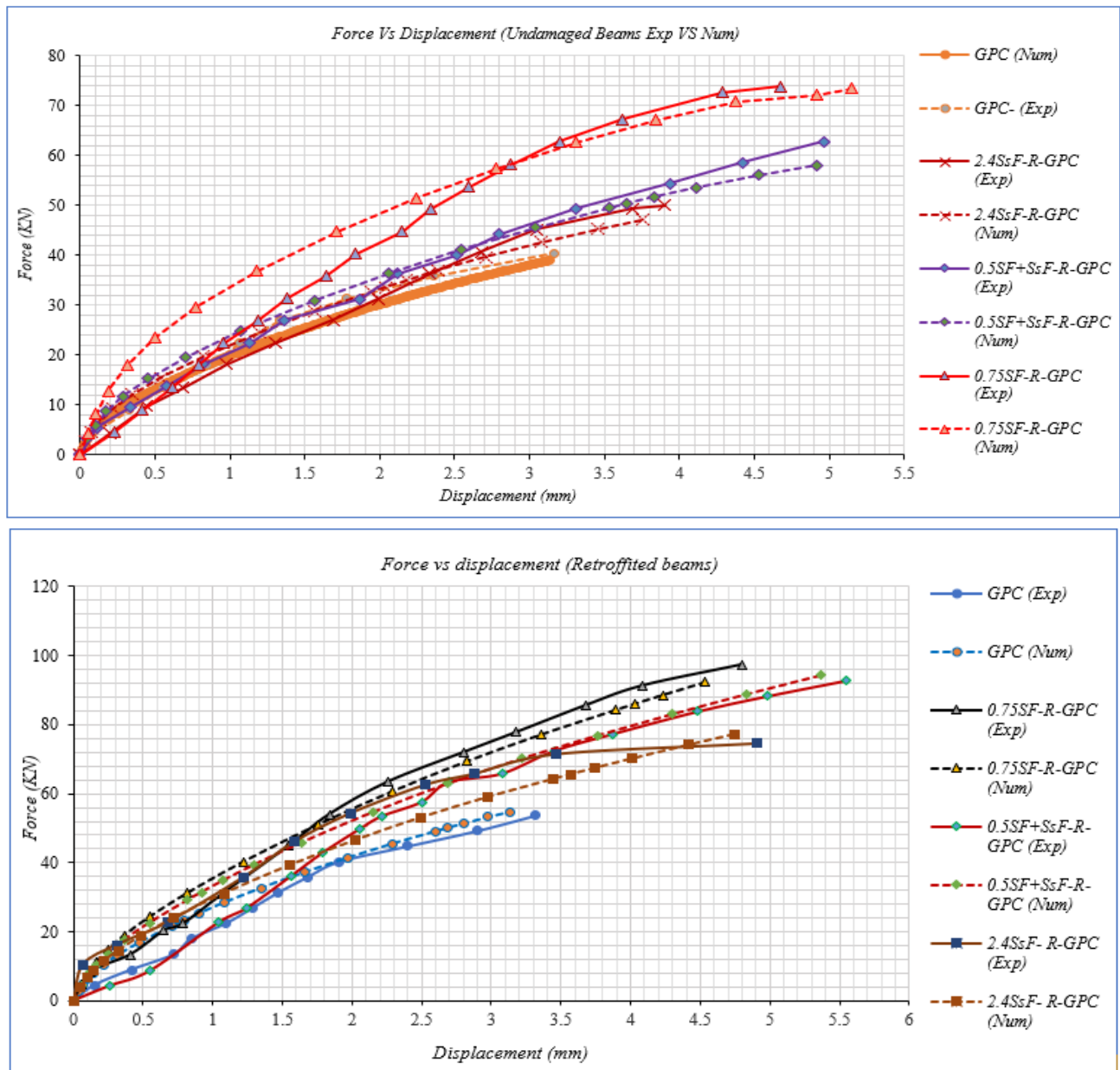


Figure 4: Load Vs Displacement (Controlled & Retrofitted Beams)





The shear failed beams were wrapped by CFRP sheet at the shear failure location and CFRP strips were adhered at the bottom to strengthen and check the displacement of the numerical model against the experimental results. The damaged beams CAE stresses and the damaged conditions were imported for the CFRP lamination analysis. The damaged beams were strengthened by wrapping CFRP sheets at the shear failure zone which enhanced the load-carrying capacity of the beams. CFRP sheets were modelled using linear elastic behavior by considering a perfect bond between concrete beams and CFRP sheets. CFRP sheets were modelled in such a way that no debonding occurs as per ACI 440.1R-15[11]–[13]. The strengthened beams have a steeper load-deflection curve and higher load-bearing capacity due to enhanced stiffness provided by the CFRP strengthening system. The CFRP sheets enhanced the load-carrying capacity of beams by 28.8 %, 20.40 %, 38.4 % & 39.0 % in the numerical model compared to the non-retrofitted model as observed by[14] Abdelrahman Mabrouk.

Table 3 Comparison between Experimental & Numerical results

Exp / Num	Specimen	Controlled Beams		Retrofitted Beams	
		Load (KN)	Displacement (mm)	Load (KN)	Displacement (mm)
Exp	GPC	40.465	3.17	53.76	3.32
Num		39.032	3.14	54.821	3.13
% Difference		3.67 %	0.98 %	1.94 %	5.91 %
Exp	0.75SF-R-GPC	73.872	4.678	97.429	4.797
Num		73.444	5.152	92.262	4.532
% Difference		0.58 %	9.20 %	5.60 %	5.83 %
Exp	0.5SF+SsF-R-GPC	62.791	4.96	92.779	5.545
Num		58.106	4.9164	94.408	5.364
% Difference		7.46 %	0.88 %	1.76 %	3.26 %
Exp	2.4SsF- R-GPC	50.023	3.900	74.679	4.903
Num		47.115	3.752	77.253	4.748
% Difference		5.81 %	3.788 %	3.45 %	3.17 %

## 5 Conclusion

1. The peak load and displacement were found to differ by less than 10 % as shown in when comparing experimental and numerical results, indicating a good agreement and validated results.
2. The CFRP sheets enhanced the load-carrying capacity of beams by 28.8 %, 20.40 %, 38.4 % & 39.0 % in the numerical model compared to the non-retrofitted model.
3. As the load increases on the beam, more stresses are generated in the concrete beams, which are transferred to the CFRP sheets that delay the beams' failure.
4. The comparison of results from the experimental and numerical study suggests that the FEM is a good technique for the simulation and prediction of the elemental behavior under different loading conditions and restraints.
5. The simulated results for all the beams are in good agreement to the experimental results. In some of the experimental curves, like in the retrofitted beam, there noted some humps in the curve; this may be due to the experimental errors, while in simulation, smooth curves are obtained.
6. As the beam 0.75SF-R-GPC beam shows a higher load capacity similar to in experimental, the inclusion of the steel fiber up to some extent increases their load-carrying capacity and does not let the crack propagate easily.
7. As in this study the numerical approach shows a good validation with experimental results also the finite element model is a time and money saving as compared to experimental testing/casting of concrete elements.
8. The Finite element model can be further used for more parametric studies and the shear deficiency in the beams may be excluded by confining the shear reinforcement at both end of beams.

## Acknowledgment

I would like to extend my gratitude to my supervisor Dr. Faheem Butt and to my mentor Muhammad Noman for guiding me and helping me in my research endeavors.



## References

- [1] S. Chitrala, G. J. Jadaprolu, and S. Chundupalli, "Study and predicting the stress-strain characteristics of geopolymer concrete under compression," *Case Studies in Construction Materials*, vol. 8, pp. 172–192, Jun. 2018.
- [2] S. Popovics, "A numerical approach to the complete stress-strain curve of concrete," *Cement and Concrete Research*, vol. 3, no. 5, pp. 583–599, Sep. 1973.
- [3] S. Michał and W. Andrzej, "Calibration of the CDP model parameters in Abaqus," 2015.
- [4] "Abaqus/CAE User's Manual Abaqus 6.11 Abaqus/CAE User's Manual."
- [5] S. Chitrala, G. J. Jadaprolu, and S. Chundupalli, "Study and predicting the stress-strain characteristics of geopolymer concrete under compression," *Case Studies in Construction Materials*, vol. 8, pp. 172–192, Jun. 2018.
- [6] S. Popovics, "A numerical approach to the complete stress-strain curve of concrete," *Concrete Research*, vol. 3, no. 5, pp. 583-599, 1973., 2013.
- [7] S. W. D. S. and B. R. D. Hardjito, "The stress-strain behaviour of fly ash-based geopolymer concrete," *Development in Mechanics of Structures and Materials*, 2004.
- [8] Comite Euro-International Du Beton, "CEB-FIP MODEL CODE 1990: DESIGN CODE," 1993".
- [9] A. K. M. D. M. S. M. A. and B. Y. M. Elchalakani, "Experiments and Finite Element Analysis of GFRP Reinforced Geopolymer Concrete Rectangular Columns Subjected to Concentric and Eccentric Axial Loading," *Structures*, vol. 17, pp. 273-289, 2018., 2018.
- [10] M. M. A. Chithambar Ganesh, "Finite Element Analysis over Geopolymer Concrete using Abaqus," *International Journal of Engineering and Advanced Technology (IJEAT)*, 2019.
- [11] ACI Committee 440, "Guide for the design and construction of externally bonded FRP systems for strengthening concrete structures (ACI 440.2R- 08). Farmington Hills, MI: American Concrete Institute".
- [12] U. Basappa and A. Rajagopal, "Modeling of CFRP strengthened RCC beam using the nonlinear finite element method Multiscale modeling of Damage in Composites View project," *Journal of Structural Engineering Vol. 40, No2, June- July 2013*, 2013, [Online]. Available: <https://www.researchgate.net/publication/263651524>
- [13] O. Ramadan, A. G. Mabrouk, and O. M. Ramadan, "Finite Element Modeling Of Rc Beams Shear-Strengthened With Side Bonded CFRP Sheets Apfis2017-6 Th Asia-Pacific Conference On FRP In Structures Finite Element Modeling Of Rc Beams Shear-Strengthened With Side Bonded CFRP Sheets," 2017.



# COMPUTATIONAL MODELLING OF DAMAGES IN BRIDGE PIERS

<sup>a</sup> Aizaz Ahmad, <sup>b</sup> Awais Ahmed

a: Department of Civil Engineering, University of Engineering and Technology, Peshawar. [aizazahmad815@gmail.com](mailto:aizazahmad815@gmail.com)

b: Department of Civil Engineering, University of Engineering and Technology, Peshawar. [awais.ahmed@uetpeshawar.edu.pk](mailto:awais.ahmed@uetpeshawar.edu.pk)

**Abstract-** Bridges are one of the most vulnerable structures to an earthquake damage. Due to an obsolete code for bridge design and poor construction practices in Pakistan, most of the bridges are seismically deficient. Experimental tests are helpful in assessment of bridge piers but requires considerable resources. In that account, numerical tools are also used for the assessment of bridge piers and various numerical techniques are available which can be utilized in this regard. This work focuses on non-linear modeling of bridge piers and validation of proposed computational scheme with experimental data using a Finite element based software–Abaqus. A single circular bridge pier subjected to a monotonic lateral load is modeled in the finite element software. For this purpose, a plasticity based damage model Concrete Damage Plasticity (CDP) is used for modeling damages in Abaqus. CDP considers concrete crushing and tensile cracking as the main failure mechanism. A constitutive model for concrete compression–Modified Kent and Park model–and tensile cracking–exponential relation for the tension stiffening–to obtain the CDP parameters are used. Mesh sensitivity analysis is performed to select a suitable mesh size as well as configuration for the numerical modeling. Additionally, the effect of step size on percentage of kinetic energy produced during the analysis is studied. Computational analysis demonstrates that the proposed scheme predicts damages in accord with the experimental results.

**Keywords-** Abaqus, Bridge Piers, Concrete Damage Plasticity (CDP), Explicit analysis, Finite Element Method.

## 1 Introduction

Bridge is an integral component of the transportation network of any country. Complete structural failure or malfunctioning due to non-suitable structural condition can have serious economic and life consequences. Among all the natural disasters earthquakes are most severe due to their unpredictability in magnitude and time. More than 40 deaths and \$1.8 billion loss occurred due to bridge damages in the Loma Prieta earthquake [1]. Pakistan lies in one of the most seismically active regions of the world. It is located at the junction of Indian, Eurasian and Arabian tectonic plate. The Himalayan region is alone capable of generating a magnitude 8.0 or above earthquake [2]. But, unfortunately due to an obsolete code for design of bridges and poor construction practices, the existing bridge stock of Pakistan is seismically deficient [3]. In the 2005 Kashmir earthquake many bridges experienced damages beyond repair due to improper seismic design and low quality concrete [3] [4].

Among the different structural elements of a bridge, bridge piers are most vulnerable to earthquake damages. They form the main lateral load resisting system of the bridge. Single column bridges are most vulnerable to earthquake because of a single load path and lack of redundancy in the system. Bridge piers vary in shapes and dimensions. Mostly, bridges having solid circular type of piers ranging in diameter from 3 feet to 5 feet are common in the northern areas of Pakistan – which is the most seismically active region [5]. The average loads on these piers were 760 kips [5].

Bridge piers behavior under the lateral demands can be studied by performing experimental studies. Multiple studies have been conducted in this regard [5]–[8]. However, experimental tests are mostly performed on scaled down models due to



lack of space and resources. Furthermore, it is also not feasible to perform experimental tests frequently to study bridge piers under lateral demand for case study research, design and retrofit purposes. Finite element method (FEM) based approaches are better alternative to experimental studies. Developing a finite element model that can predict the behavior of the bridges during an earthquake requires a proper definition of finite element model and material parameters. Different researchers utilize different FEM based tools and material models for both the concrete and steel for computational modelling [8], [9]. One of the models that can be easily employed in this regard is the Concrete Damage Plasticity (CDP) in Abaqus. This model is frequently used to study the nonlinear behavior of concrete structures in static, quasi-static and reverse cyclic condition. CDP is a continuum plasticity based model. It was presented by Lubliner [10] and modified by Lee and Fenves [11]. Quasi-brittle material like concrete, rocks, ceramics and mortar can be modeled with CDP. Compressive and tensile damages are considered by the CDP along with the stiffness recovery under cyclic loading in compression [12]. In the elastic range, the model uses elastic relations for the mechanical properties of the concrete. In the plastic region, the model utilizes the degraded elastic stiffness.

This study focus on non-linear modeling of bridge piers under lateral loading. The main objective of this research is to develop computational scheme that can easily be employed for the prediction of damage in bridge piers without the need for rigorous experimental work. Practically, such a computational scheme can be used for case study research, design or retrofit purposes. An experimental test [5] has been used for the validation of the proposed computational scheme using Abaqus. In the proposed numerical scheme, CDP is used to model damages related to concrete in a bridge pier under monotonic lateral load. Additionally, rebars are modeled using a simple elastoplastic model. Continuum 3-D elements and linear 1-D elements are used to model the concrete and rebars, respectively. Furthermore, fracture-energy based material model is utilized for the tension stiffening of concrete to avoid mesh sensitivity. In addition to this, mesh sensitivity analysis is also performed to select a suitable mesh size for the analysis. The effect of loading time on the kinetic energy of the model is also explored in this study.

## 2 Methodology

### 2.1 Numerical model geometry

Experimental test performed by Ali [5] was used for the validation of the proposed numerical technique. The model and test setup is shown below (Figure 1). The model is a scaled down version of a real bridge pier. The model is a single pier

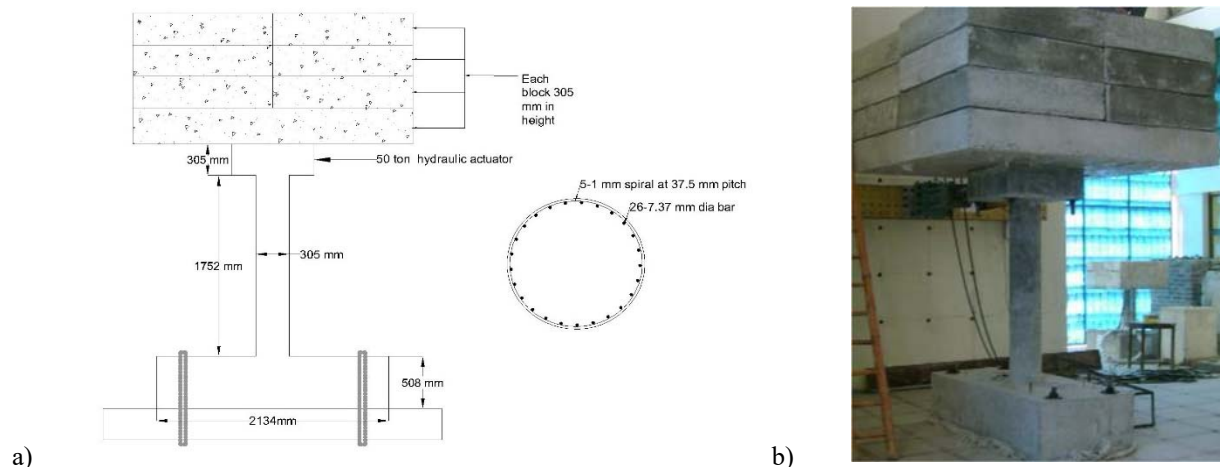


Figure 1: a. Geometry and b. Experimental test setup of the numerical model

having 305 mm diameter and 1750 mm clear height. At the top of the column, a 742 mm square pedestal having depth of 305 mm is provided for the placement of blocks. Furthermore, the column is erected from a base having 2133 mm length, 914 mm width and 505 mm depth—which is rigidly connected to the strong floor. The loads from the superstructure were modeled through concrete blocks, placed above the top of the column. Lateral loads in the form of drift were applied to the model in reverse cyclic manner during the experiment. Numerically lateral loads were applied monotonically in a single



direction. Both the experimental and numerical models were subjected to 4% drift. The material properties as determined during experiment are given in the Table 1.

Table 1: Material properties

Material Property	Compressive Strength	Modulus of Rupture	Modulus of Elasticity	Rebar yield Strength
value	2400 psi	674 psi	2798 ksi	60 ksi

## 2.2 CDP

CDP is a continuum-plasticity based model. The main failures that are considered by the CDP are compressive crushing and tensile cracking. The essential parts of any plasticity based model are yield criterion, flow rule and hardening rule. The yield function adopted by CDP is drucker-pruger hyperbolic function [13] shown in (1) with (2) (3) and (4) defining the dimensionless parameters.

$$F = \frac{1}{1-a} (\bar{q} - 3\alpha\bar{p} + \beta(\varepsilon^{pl}) \langle \hat{\sigma}_{max} \rangle - \gamma \langle \hat{\sigma}_{max} \rangle) - \sigma_c(\varepsilon^{pl}) = 0 \quad (1)$$

$$\alpha = \frac{\left(\frac{\sigma_{b0}}{\sigma_{c0}}\right)^{-1}}{2\left(\frac{\sigma_{b0}}{\sigma_{c0}}\right)^{-1} - 1}; 0 \leq \alpha \leq 0.5 \quad (2)$$

$$\beta = \frac{\bar{\sigma}_c(\varepsilon_c^{-pl})}{\bar{\sigma}_t(\varepsilon_t^{-pl})} (1 - a) - (1 + a) \quad (3)$$

$$\gamma = \frac{3(1-K_C)}{2.K_C - 1} \quad (4)$$

The flow rule considered by CDP is non-associated potential plastic flow. The plastic potential flow  $G$  is defined as

$$G = \sqrt{(\varepsilon \cdot \sigma_{t0} \cdot \tan\psi) + \bar{q}^2} - \bar{p} \cdot \tan\psi, \quad (5)$$

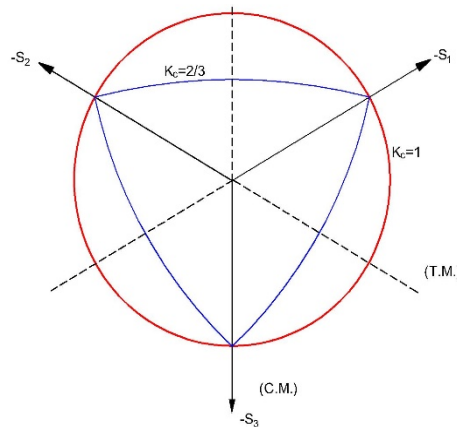


Figure 2: Yield Surface in deviatoric plane

The definition of CDP requires certain parameters. These parameters include: dilation angle  $\psi$ , eccentricity  $\epsilon$ , the ratio of biaxial to uniaxial yield compressive strength  $\left(\frac{\sigma_b}{\sigma_c}\right)$ , the ratio of the second stress invariant on the tensile meridian to the compressive meridian  $K_C$ , and viscosity  $\mu$ . The yield surface in deviatoric plane with the effect of  $K_C$  on the shape of



yield surface is shown (Figure 2). There has been no consensus in literature regarding the selection of a specific value [13], however, the values of these parameters used in this study are given in the Table 2.

Table 2: CDP model parameters

CDP Parameters	$\psi(^{\circ})$	$\epsilon$	$\left(\frac{\sigma_b}{\sigma_c}\right)$	$K_c$	$\mu$
value	40	0.1	1.16	0.667	0

### 2.3 Concrete material models

CDP data inputs requires the Inelastic strain  $\epsilon_c^{in}$  where subscript c and t are for tension and compression, and stiffness degradation variable  $d_c$ . The calculation of plastic strain and degradation variable are shown in (6) and (7).

$$\epsilon_c^{pl} = \epsilon_c^{in} - \frac{d_c}{(1-d_c)} \frac{\sigma_c}{E_0} \text{ (compression) , } \epsilon_t^{pl} = \epsilon_t^{ck} - \frac{d_t}{(1-d_t)} \frac{\sigma_t}{E_0} \text{ (tension)} \quad (6)$$

$$d_c = 1 - \frac{\sigma_i}{\sigma_{cu}} \text{ (compression) , } d_t = 1 - \frac{\sigma_i}{\sigma_{tu}} \text{ (tension)} \quad (7)$$

Where  $\epsilon_c^{in}$  and  $\epsilon_t^{ck}$  show strain hardening and tension stiffening in compression and tension, respectively.

Complete compressive and tensile stress-strain data is required to calculate the values of these parameters. The modified Kent and Park model [14] is used in this study to define the concrete compressive behavior (Figure 3). Stress-strain material models for tensile behavior of concrete encounters mesh-sensitivity issues, therefore, it is recommended [12] to use models based on crack opening displacement and stress for the definition of strain-softening in tension .

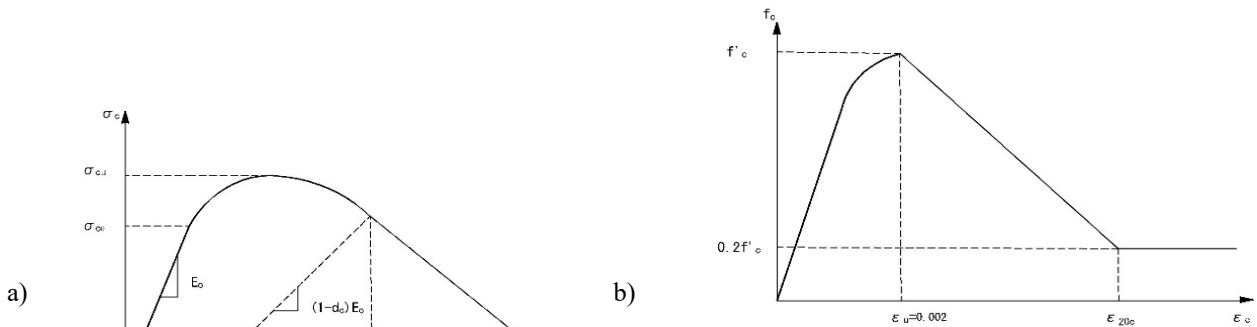


Figure 3: a. Typical compressive uniaxial stress-strain curve, and b. Modified Kent and Park model

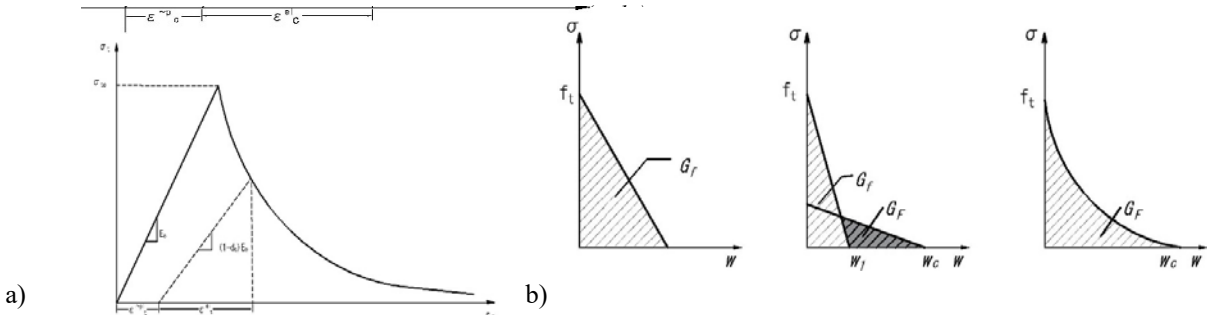


Figure 4: a. Typical uniaxial tensile stress-strain curve and, b. linear, bi-linear and exponential relations for tension stiffening.

These are fracture energy based material models and which relates the crack opening displacement with the stress. Linear, bilinear and exponential relations are available in literature (Figure 4) . Any of these relations can be used unless the areas under the curve are equal.



## 2.4 Rebar

A simple bi-linear (Figure 5) relation is used to model the rebars. The rebars are modelled using 1-D beam element.

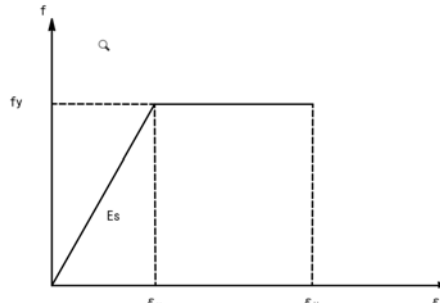


Figure 5: Bi-linear relation for rebar modeling

## 3 Results

As material degradation in the form of damages is modeled using CDP, therefore, an explicit dynamic analysis is performed to avoid the convergence error–encountered in the implicit analysis. The main failure that the CDP depicts is the concrete crushing in compression and cracking in tension. Since CDP is a smeared crack model, therefore, the damages are not depicted as a separate entity. Mesh sensitivity studies were carried out to check the suitable mesh size and arrangement, since modeling the whole model with same mesh element size will increase the computational time. Three types of mesh arrangements were used: a complete instance mesh with the same mesh size, a 1.5 mesh ratio between column and the foundation, and a localized mesh in the vicinity of the column. The complete instance mesh shows damages in the column as well as in the footing due to the connectivity of the meshed elements, which are in contrast to the real behavior observed during the experimental test. In the 1.5 mesh ratio, due to contact issues, an uplift was observed at the base of the column. The localized mesh comes out to be the most suitable arrangement. The damage patterns observed during the localized mesh are in good agreement with the experimental results (Figure 8) as shown in (Figure 7).

The localized mesh configuration which is the most suitable configuration for the proposed numerical scheme is used for the selection of suitable mesh size. Mesh size of 1-inch, 2-inch, 2.5-inch and 3-inch is used to study the effect of mesh size on damage pattern the results are shown below (Figure 7). Dispersed damage patterns, which are not in agreement with the experimental results, are observed with coarser mesh. Finer mesh shows clustered damages but with higher computational time. Hence, 2-inch mesh is the most optimum mesh which produces good results with a comparatively smaller computational time. The actual test was a quasi-static and the total time of the test was 3600 seconds, however, modeling lateral load with a time step of 3600 seconds requires high computational cost and time. Therefore, the step-time for the lateral load should be such that no dynamic effects are produced in the model with reasonable results. Two step-times are used, 40 seconds and 60 seconds, with both producing high kinetic energy which are not desirable in quasi-static analysis. The high kinetic energy is due to the dynamic effect caused by the high rate of loading in the explicit dynamic analysis. The recommended value of kinetic energy to total energy is 5 to 10 percent. The ratio of kinetic energy to total energy for 40 and 60 time steps was varying between 50% to 0.03%. Therefore, such analysis should be performed either with a higher time step. Contrarily, the analysis should be done through a combination of modified time-step with either mass-scaling or damping or both.

## 4 Conclusion

The material model for concrete by the name of CDP is used, to model the damages in bridge piers using Abaqus. In this study, a proposed scheme for the damage modeling was used on a single bridge pier to study the effect of mesh size and step-time. The following are the conclusions:

- 1 Mesh size has a significant influence on the damage pattern and the time required for analysis.



- 2 Coarser mesh shows a dispersed damage pattern which is not in agreement with the experimental results.
- 3 Finer mesh shows clustered damages but with higher computational time.
- 4 Step-time should be selected based on the recommended ratio of kinetic energy to potential energy.
- 5 In case of smaller step size, mass-scaling should be used to avoid excessive kinetic energy content.
- 6 Compressive crushing, tensile cracking and rebar yielding (Figure 7)— smeared over the finite elements— were observed during the numerical analysis which are in good agreement with the experimental results (Figure 8).

The above conclusion represents a number of variables that affect the damage in bridge piers when modeled with CDP. Further trials are required to study the effect of model parameter, concrete strength, and column geometry on the damages.

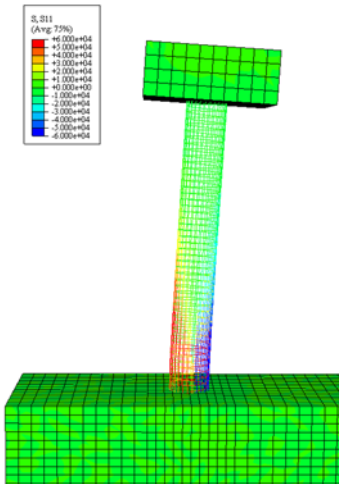


Figure 6: Rebar yielding

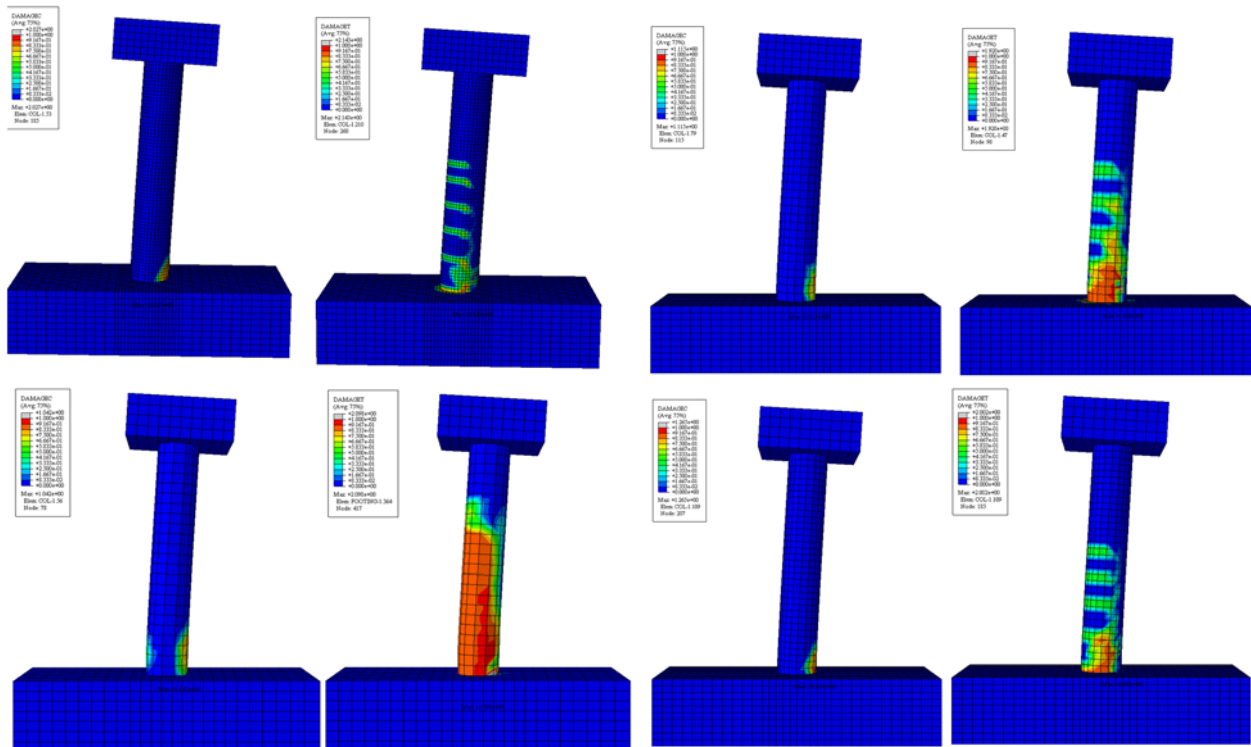


Figure 7: From top left to bottom right : 1 inch, 2.5 inch, 3 inch, and 2 inch meshed model with compressive and tensile damage patterns



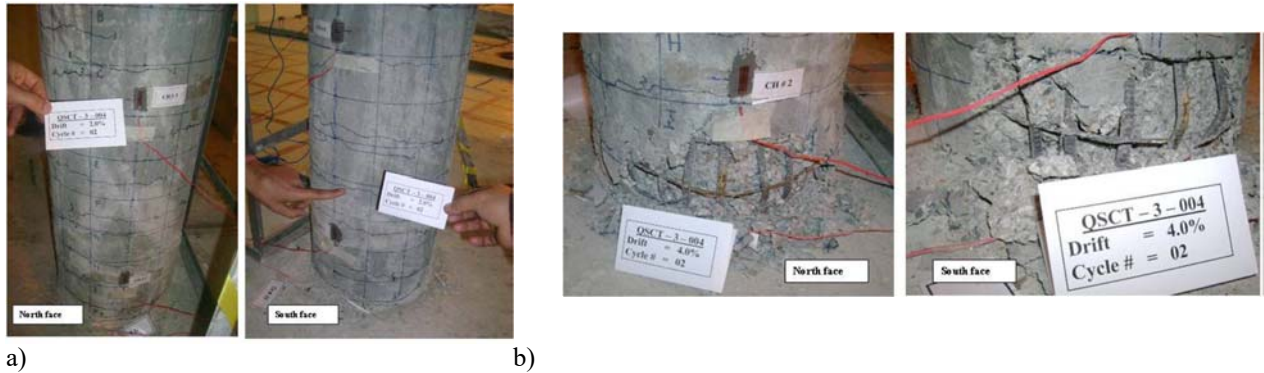


Figure 8: Failures observed in the experimental test a) Tensile cracking, b) Compressive crushing of concrete and rebar yielding

## 5 Acknowledgment

The authors would like to thank Prof. Dr. Muhammad Ashraf of Civil Engineering Department UET Peshawar, for providing computational facility for this research.

## References

- [1] S. Stefanidou and A. Kappos, "Optimum selection of retrofit measures for R/C bridges using fragility curves," presented at the 4th ECCOMAS Thematic Conference on Computational Methods in Structural Dynamics and Earthquake Engineering. Athens Greece: COMPDYN, 2013.
- [2] R. Bilham, "Earthquakes in India and the Himalaya: tectonics, geodesy and history," *Ann. Geophys.*, 2004.
- [3] Ali, S.M., Javed, M., and Alam, B., "Experimental Seismic Performance Evaluation of Bridge Piers Constructed In Low Grade Concrete," 2012.
- [4] S. M. Ali, A. N. Khan, S. Rahman, and A. M. Reinhorn, "A survey of damages to bridges in Pakistan after the major earthquake of 8 October 2005," *Earthq. Spectra*, vol. 27, no. 4, pp. 947–970, 2011.
- [5] S. M. Ali, "Study of energy dissipation capacity of RC bridge columns under seismic demand," 2009.
- [6] J. Sakai and S. Unjoh, "Earthquake simulation test of reinforced concrete bridge column under multidirectional loading," presented at the Fourth International Workshop on Seismic Design and Retrofit of Transportation Facilities Multidisciplinary Center for Earthquake Engineering Research Federal Highway Administration, 2006.
- [7] M. Schoettler, J. Restrepo, G. Guerrini, and D. E. Duck, "A full-scale, single-column bridge bent tested by shake-table excitation," 2012.
- [8] J. Deng, Z. John Ma, A. Liu, S. Cao, and B. Zhang, "Seismic performance of reinforced concrete bridge columns subjected to combined stresses of compression, bending, shear, and torsion," *J. Bridge Eng.*, vol. 22, no. 11, p. 04017099, 2017.
- [9] M. Moharrami and I. Koutromanos, "Finite element analysis of damage and failure of reinforced concrete members under earthquake loading," *Earthq. Eng. Struct. Dyn.*, vol. 46, no. 15, pp. 2811–2829, 2017.
- [10] J. Lubliner, J. Oliver, S. Oller, and E. Oñate, "A plastic-damage model for concrete," *Int. J. Solids Struct.*, vol. 25, no. 3, pp. 299–326, 1989.
- [11] J. Lee and G. L. Fenves, "Plastic-damage model for cyclic loading of concrete structures," *J. Eng. Mech.*, vol. 124, no. 8, pp. 892–900, 1998.
- [12] D. Systèmes, "Abaqus 6.12 Analysis User's Manual, Volume III: Materials," *Prov. Dassault Systèmes Simulia Corp Provid.*, 2012.
- [13] A. L. Christoforo and R. C. Carvalho, "Calibration of Concrete Damaged Plasticity Model parameters for shear walls," *Matér. Rio Jan.*, vol. 26, 2021.
- [14] D. C. Kent and R. Park, "Flexural members with confined concrete," *J. Struct. Div.*, vol. 97, no. 7, pp. 1969–1990, 1971.



# INVESTIGATION OF PUNCHING SHEAR RESPONSE OF GFRP REINFORCED CONCRETE FLAT PLATE SLAB USING CDP MODEL IN ABAQUS

<sup>a</sup> Hafiz Muhammad Aubaid Asaad\*, <sup>b</sup> Qaiser uz Zaman Khan, <sup>c</sup> Afaq Ahmad, <sup>d</sup> Ali Raza

<sup>(a,b,c,d)</sup>Department of Civil Engineering, University of Engineering and Technology, Taxila, 47080, Pakistan

\* Corresponding author: Email ID: [aubaid.asaad@uettaxila.edu.pk](mailto:aubaid.asaad@uettaxila.edu.pk)

**Abstract-** In this paper, the punching shear of glass fiber reinforced polymer (GFRP)-reinforced concrete two-way square flat slabs was investigated using the non-linear finite element analysis (NLFEA) and its comparison with experimental results from 2500 mm x 2500 mm x 200 mm including top and bottom square column stubs. The size of stubs was 300 mm reinforced with GFRP bars along with conventionally steel bars being tested under the monotonic loading. A commercial software ABAQUS Standard 6.14-1 was used for the NLFEA model of the concrete flat slab's specimens. The numerical results were calibrated by using the varying material strengths along with different geometric properties likely dilation angle, element types, mesh sizes, and viscosity parameters which are based on the earlier experimental test results. Furthermore, Concrete Damaged Plasticity (CDP) model is used for the reinforced concrete behavior, while linear elastic behavior for GFRP and steel bars is used in ABAQUS. Calibration of these 3D slab model analyses is completely done by simulating the slabs without shear reinforcement. Failure of punching shear and cracking patterns are examined by using these test prototypes. Finite Element Analysis (FEA) of these prototypes using GFRP bars also showed identical shear failure and the patterns of cracking at failure. The numerical modeling of flat plate slabs in Abaqus presented the load-deflection curves with a close relation with experimental results.

**Keywords-** Punching Shear, Flat plate slabs, Non-Linear Finite Element Analysis (NLFEA), Failure Behavior

## 1 Introduction

Slabs (Flat Slabs / Flat Plate Slabs) are a major constituent / flexural element of concrete structures which are frequently used in the construction of high-rise commercial buildings. Punching shear behavior in these buildings with flat or flat plate slabs and footings is a major damaging issue that is produced due to high shear stresses. Shear distribution in these slabs and foundations also impacts the performance along with failure mode. Although when Punching shear failure occurs in flat slabs, it shows no warning signs earlier due to slight deflection capabilities with internal and external cracks invisible at the top surface of the slab. These slabs/footings are cast with and without column capitals to safe design for punching shear failure. Failure of punching shear is produced due to larger shear stresses at the slab column junctions in reinforced concrete flat and flat plate slabs. Researchers observed different approaches for FRP flat slabs/footings structural behavior using analytical models, numerical models, and finite element analysis [1].

In ASIA, Pakistan is an arid area in which some of the areas are humid / semi-humid due to heavy or sudden rains and snowfalls throughout the year due to which corrosion is a major problem on construction sites. To overcome this phenomenon, de-icing salts or other products are used. Specifically, Glass Fiber Reinforced Polymer (GFRP) bars are also used for such projects as mentioned above. GFRP bars are more valuable here due to their uniqueness and this material is flimsy (lightweight), has a lesser modulus of elasticity, is non-magnetic, environment-friendly, electrically insulating (especially for Electric substations) and corrosion free has low thermal conducting as one-half of steel, very high tensile strength and cost-effectively [2].



Several Reinforced Concrete Slabs with and without shear transverse reinforcement used to envisage load-deformation response was conducted at the (ETH) in Zurich, Switzerland. The experiments demonstrate the impact of shear strength and deformation capacity of RC slabs [3]. Polak et al. also examined the response of punching shear in different steel reinforced slabs with column connections at the center and edges without shear reinforcement. They have analyzed parametric investigations using material properties in ABAQUS affected FEA of concrete structures and predict good agreement. Also, it gives enough results for cracking propagation along with load-displacement response using ABAQUS standard and Explicit.

Evaluation of the literature comes to know that limited work related to the numerical behavior of GFRP-reinforced flat slabs using the ABAQUS standard is demarcated. Also, there are limited geometrical and numerical parametric investigations on punching shear failure in GFRP reinforced slabs without shear reinforcement that have been conducted using Non-Linear FEA in ABAQUS with ACI codes. The critical parameters needed to examine the experimental/numerical parametric investigation which influences the punching shear behavior of these slabs. An innovative goal of the author in current research of flat slabs without shear reinforcement is to investigate the numerous parametric behavior of GFRP and steel-reinforced flat slabs with proposed Non-Linear FEA models of slabs specimen in software (ABAQUS Standard 6.14) to validate accurately against load-deflection curves of preceding experimental test results from Christian Dulude and Brahim Benmokrane [4]. Subsequently, a numerical study of different parameters from a controlled specimen of steel and GFRP has been done.

## 2 Experimental Procedures

A total of 03 full-scale rectangular RC flat plate slab prototypes (Notation 'S' is for Steel slabs and notation 'G' is used for GFRP slabs) were modelled using ABAQUS. Modeling of 2500 mm x 2500 mm x 200 mm including square column stubs of 300 mm without shear reinforcement along with GFRP and steel bars were used [4]. All the bars of GFRP reinforcement were kept free (in X, Y, and Z directions) when the slab was loaded with the applied axial load. A static monotonic Axial Load has been applied on the top of the square column stub central surface of two-way slabs for a load-deflection response till the punching shear failure occurred by using the displacement control technique at an equal rate of 25 mm at the center of square column stub in ABAQUS. For tie constraint, the load has been applied on the central surface of column stubs whose purpose was to monitor actual load distribution on slab through column stubs.

### 2.1 Geometric Model, Loadings, and Boundary Conditions

In this research, the different material proportions of concrete and size of loading with loading increments including controlled model properties and sizes of the ABAQUS Standard step module are discussed below in Table 1. In current modelling research, a concept of master and slave surface is used. This concept defines the properties of the interaction between the two-way concrete slab and column stubs. The bottom external surface of the top column stub and the lower bottom external surface of the two-way concrete slab was presented as master surfaces in Abaqus. Top external surface of the concrete slab and the top external surface of the bottom column stub were considered and monitored as slave surfaces. The whole analysis worked when load is transfer from master surfaces to slave surface. Figure 01 presenting the geometry configuration including FE modelling of GFRP reinforced concrete slabs.

Table 01: Different Parameters of Concrete properties including FEA model loads

Parameter	Value
Density of concrete in ton/mm <sup>3</sup>	2.4 X 10 <sup>-9</sup>
Young's modulus, E <sub>c</sub> (N/mm <sup>2</sup> )	31842
Poisson's ratio, $\nu$	0.2
Increment in size of loading (Initial and Maximum)	0.01
Number of increments	1000
Minimum increment size	10 <sup>-10</sup>

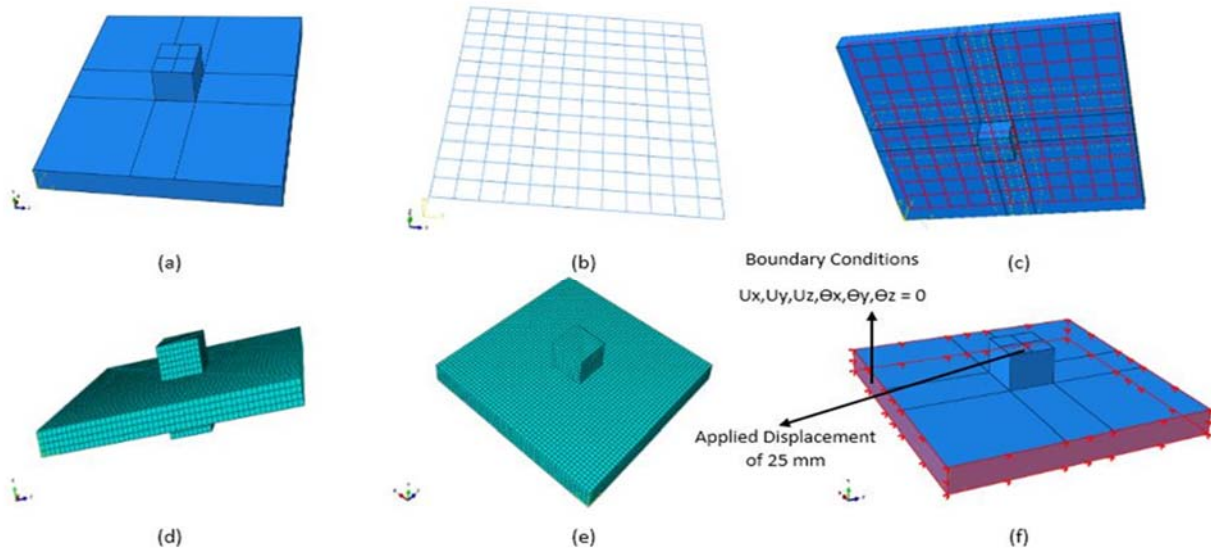


Figure 1. Flat Plate Slabs with Column Stub reinforced with GFRP (a) geometry configuration, (b) GFRP mesh, (c) slab with GFRP model, (d) FE meshing, (e) FE meshing top, (f) boundary conditions.

These prototypes were utilized from the paper [4] under different loading conditions. Only one prototype (S<sub>1.7</sub>30/20) was reinforced by steel bars longitudinally and transversely and the remaining specimens were included with GFRP reinforced bars. Different types of reinforcement ratios (6%), miscellaneous bar numbers (15mm, 18mm, and 20mm), and various compressive strengths (34.3 MPa, 44.9 MPa, and 45.4 MPa) based on cylindrical testing of 150 x 300 mm including square column stub has been used to study their impact on load-deflection behavior. Material characteristics of these all specimen are given in Table 2.

Table 2. Appropriate Geometric along with material aspects of two-way Concrete Slab specimens

Prototype Sample	Reinforcement type	Compressive strength of concrete (MPa)	Reinforcement		Concrete Cover (mm)	Reinforcement Ratio(%)	Column Stub Dimension Top/Bottom (mm(in))
			Bars No.	Spacing (mm)			
S <sub>(1.7)</sub> 30/20	Steel	45.4	ϕ18~20 M	160	50	6.35	300 (11.8)
G <sub>(0.7)</sub> 30/20	GFRP	34.3	ϕ15 mm	160	50	6	300 (11.8)
G <sub>(1.6)</sub> 30/20	GFRP	44.9	ϕ20 mm	160	50	6.35	300 (11.8)

## 2.2 Concrete Damaged Plasticity (CDP) Model.

In ABAQUS concrete inelastic behavior has been defined by three constitutive models which are as defined by Concrete Damaged Plasticity (CDP) model, Concrete Smeared Cracking model (CSCM), and another Brittle Cracking Concrete (BCC) model. In this research, only CDP model is discussed which deals with plastic as well as compressive and tensile behavior. CDP Model gives two types of concrete failure compressive crushing along with tensile cracking. In the current study, the Nonlinear behavior of RC concrete is commonly used by the CDP model as presented in Figure 2. CDP model in this study illustrates the correlation of concrete strain between plastic strain, inelastic strain, and compression stress [5].

## 2.3 Plastic Behavior of Concrete

The concrete plasticity model is precisely discussed by using concrete elastic potential eccentricity ( $\epsilon$ ), dilation angle ( $\psi$ ), the biaxial compressive strength factors in the shape of compressive stress ratio in the biaxial state to the uniaxial state ( $\sigma_{b0}/\sigma_{c0}$ ) including viscosity parameter and ( $K_c$ ) which is defined as the shape factor of yielding surface in the deviatoric plane. After calibration, different values of viscosity and dilation angle parameters were attained. It is also worth mentioning that this stress ratio is also quantified by Papanikolaou and Kappos [6] as projected in Eq. (1).



$$\frac{\sigma_{b0}}{\sigma_{c0}} = 1.5(f'_c)^{-0.075} \quad (1)$$

The CDP model recommended Also, different values of  $K_c$ , eccentricity ( $\epsilon$ ), and yield shape surface are 0.1 and 2/3, respectively. As per the ABAQUS manual, the specified value of  $(\sigma_{b0}/\sigma_{c0})$  is 1.16 [7].

## 2.4 Compressive and Tensile Performance of Concrete

To express the compressive and tensile performance/response of concrete during CDP model simulations, the behavior of compression failure can be obtained by increasing strain and ultimate elastic stress of concrete. Also, it is worth mentioning that the compression failure occurred due to an increased degree of inelastic strain  $\epsilon^{in}$ . In this research, concrete modulus of elasticity ( $E_c$ ) was considered through ACI code using Eq. (2) as mentioned below:

$$E_c = 4700\sqrt{f'_c} \quad (2)$$

Furthermore, Fig 3 expressed the concrete compressive stress-strain diagram according to Eurocode 2, in which the linear elastic behavior has been used  $0.4f_{cm}$  as mentioned in P. Kmiecik et al. [8]. Majewski [9] also proposed the experimental relationships of strain  $\epsilon_{c1}$  at the average concrete compressive strength and ultimate strain  $\epsilon_{cu1}$  given by Eq. (3) and (4).

$$\epsilon_{cu1} = 0.004 - 0.0011[1 - e^{-0.0215f_{cm}}] \quad (3)$$

$$\epsilon_{c1} = 0.0014[2 - e^{-0.024f_{cm}} - e^{-0.140f_{cm}}] \quad (4)$$

In current research structural nonlinear behavior is defined by Eq. (5) given by Euro Code [10] for a stress-strain relationship of concrete.

$$\sigma_c = f_{cm} \frac{k\eta - \eta^2}{1 + (k-2)\eta} \quad (5)$$

Desayi and Krishnan [11] have given the stress-strain relationship given by Eq. (6) where compressive strain at peak loads is denoted by  $\epsilon_{c0}$  and according to Mander et al. [12], its value is 0.002.

$$\sigma_c = \frac{E_0 \epsilon}{1 + (\frac{\epsilon}{\epsilon_{c0}})^2} \quad (6)$$

Simulation of FEA using stress-strain relationship and tensile behavior of concrete used at the condition of post-failure. Fig 4 shows the modified tension stiffening model used in current research where the stress-strain curve in tensile behavior at critical strain  $\epsilon_{cr}$  is used from ultimate stress  $\sigma_{t0}$  to  $0.77\sigma_{t0}$ . Using Eq. (8) proposed by Wang and Vecchio [13] and Genikomsou and Polak [14] was used for concrete ultimate tensile strength.

$$f'_t = 0.33\sqrt{f'_c} \text{ (MPa)} \quad (8)$$

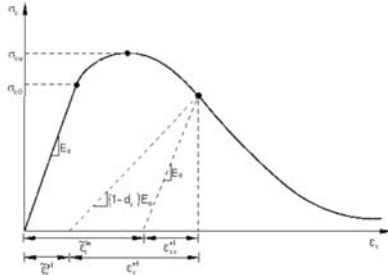


Figure 2. The CDP (Concrete Damaged Plasticity) model

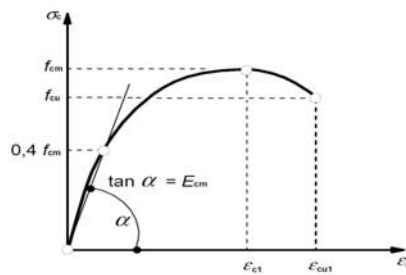


Figure 3. Eurocode 2 of Stress-strain diagram for structure (Under Compression)

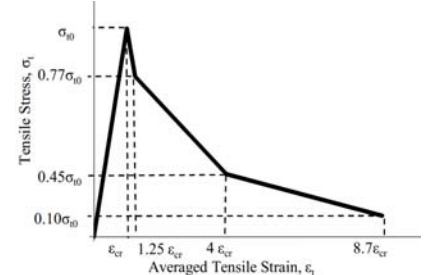


Figure 4. Eurocode 2 of Stress-strain diagram for structures (Under Tension)

## 3 Research Methodology

The foremost purpose of this research was to investigate and monitor the behavior of the two-way flat plate slabs which are reinforced with GFRP barriers facing increasing loading and compare their behavior with that of an iron rod. All the results have been obtained by numerical simulation on different Two Ways Glass fiber reinforced polymer concrete slabs samples using a commercial-based software Abaqus. All the simulations have been done on the specimens using CDP modeling. Samples were calibrated using various dilation angle parameters, different element types, varying mesh sizes, and different viscosity parameters along with boundary conditions and embedded regions/area constraints. The concrete and GFRP material properties were also discussed during these simulations process to achieve better results of punching shear response through the Computer.



## 4 Results

Various types of tests have been performed in Abaqus Simulia software for the prototype samples to monitor the action of punching shear in two-way flat plate slabs using GFRP bars. Different types of Two-noded element types GFRP & Steel (T3D2, T3D3, T3D2H, and T3D3H), Dilation angle parameter, mesh sizes, and viscosity parameters deformed truss elements which have three DOF at each node of reinforced bars were utilized in Abaqus for the simulations. Parameters needed for reinforcing bars modeling were discussed deliberately which are Poisson's ratio ( $\nu$ ) which has a value of 0.2 and the Modulus of elasticity including yield strength and zero plastic strain. GFRP and Steel bar physical properties utilized in this research as Young's Modulus (48.1 GPa, 48.2 GPa, and 200 GPa), Yield Strength (673 MPa, 699 MPa, and 470 MPa) respectively.

### 4.1 Discussions of Load Deflection Curves

Investigation of dilation angle parameter in Abaqus Simulia provided the response of load-deflection curves at an angle of  $30^\circ$  accurately and maximum load applied 367 kN in comparison with experimental results as 360 kN at 25 mm displacement as given in Fig 5. Similarly, Concrete Element types give better results at the C3D8R element type in line with experimental results as shown in Fig 6. Fig 7 shows excellent results with a slight difference of 6 kN only at T3D2, T3D3H, and T3D3H of GFRP element type. 50 mm mesh size (A finer mesh size) gives excellent results of load-deflection curves at 361 kN axial load-deformation in comparison with experimental value as shown in Fig 8. The exact Graphical value of the viscosity parameter of 0.003 also showed greater results for the experimental result as shown in Fig 9. It has been observed from the peak load curves that GFRP concrete progresses positively for the post-elastic effect of structures.

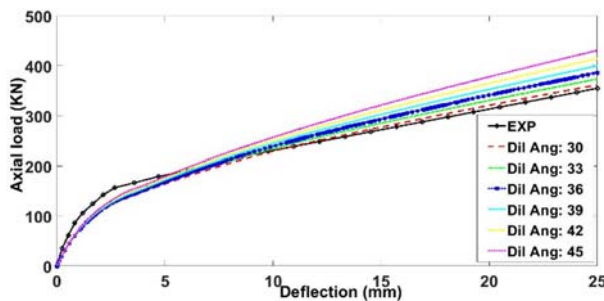


Figure 5. Dilation Angle Parameter

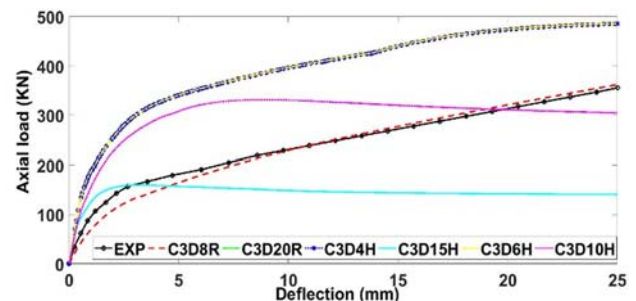


Figure 6. Concrete Element Types

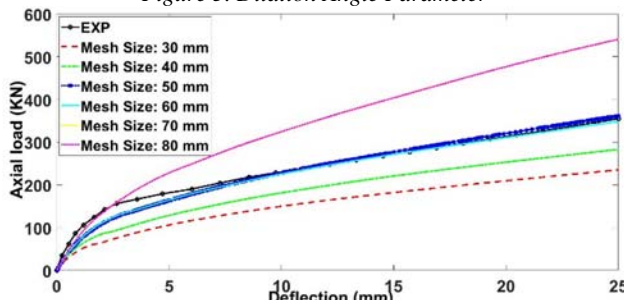


Figure 8. Mesh Sizes

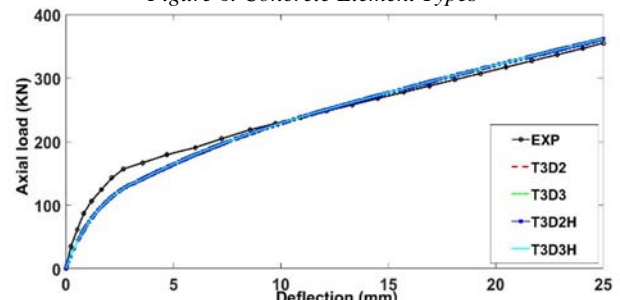


Figure 7. GFRP Element Types

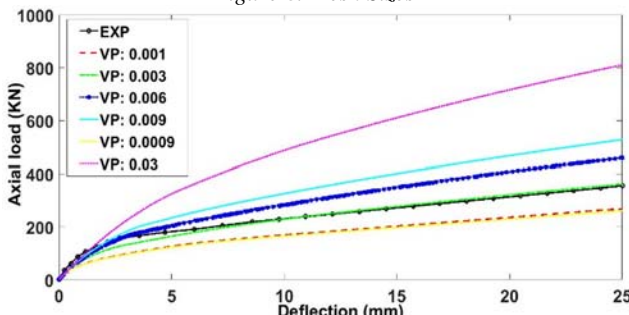


Figure 9. Viscosity Parameter

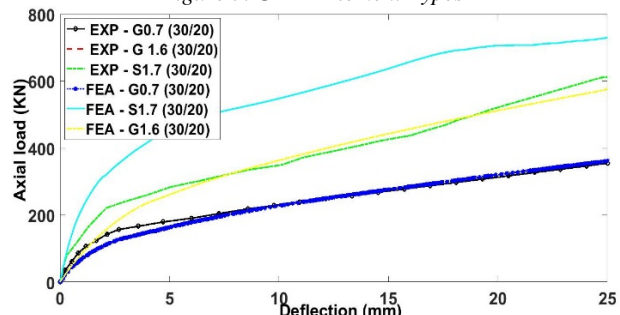


Figure 10. Experimental and FEA Results

## 4.2 Crack Patterns Discussion

As per experimental results, the cracks produced on the tension side of concrete slabs due to loading phenomena. Many software can predict the process and produce the FEA results. In current study, cracks propagation and punching shear response of GFRP reinforced concrete two-way flat plate slabs has been monitored by Abaqus Simulia software. FEA of these slabs are shown in Fig 11 (a, b, c & d) after loading increments of 1000 at a rate of  $10^{-10}$  on top of square column stub resulting maximum optimistic principal plastic strains. A good agreement was achieved between FEA and experimental results to check Punching shear behavior of two-way flat plate slabs.

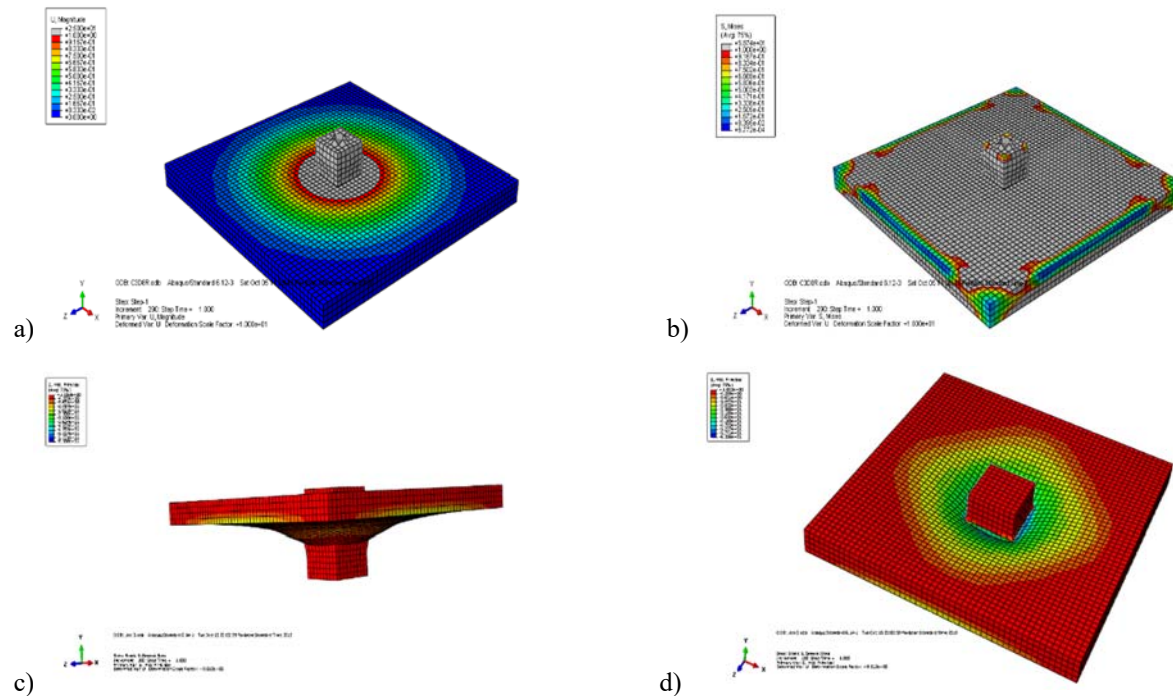


Figure 11: Punching Shear Results in ABAQUS (a) Load Increments (b) Deformed shape of 2 Way Slab (c) Deformation of Slab after load increments (d) Top View of Deflection Patterns during load increments

## 5 Conclusion

The planned FEA model of 3D solid homogeneous sections also presented a better relationship of parametric & geometric results. The following are the key findings obtained from the conducted simulation-based on NLFEA:

1. Two-way GFRP-reinforced flat plate slabs with top/bottom column stubs gave the most accurate results predicted by using the viscosity parameter 0.003, dilation angle  $30^\circ$ , concrete element type at C3D8R, GFRP element type T3D2, and 50 mm mesh sizes.
2. When the reinforcement ratio of prototype  $G_{0.730/20}$  increased from 0.71% to ratio 1.56%, and average punching shear stress improved by 39%. This increment in ratios enhanced the depth of the concrete contribution which describes as punching shear capacity that can be increased with the increase of reinforcement ratio. Similarly, when a higher effective reinforcement ratio was used (Ratio 0.17% to ratio 1.66%), the punching shear stress was enhanced.
3. The samples reinforced with steel bars yielded higher deflection at an equivalent load and demonstrated lesser punching shear stress compared with GFRP reinforced samples when the failure occurred. Exact value of  $E_f/E_s = 0.25$  approx. which shows lower modulus of elasticity of GFRP reinforcing bars.
4. All the two-way flat plate slab samples along with column stub displayed the same punching shear failure and parallel crack patterns irrespective of the reinforcement ratio and type. Although, the thickness of the slab affects the punching shear measurements.
5. Punching shear behavior is slightly affected by the axial stiffness of the reinforcement. Also, punching shear capacity increased with the increase of reinforcement axial stiffness which results in the decrease in crack width,



reinforcement strains, and deflections. The deflection of the two-way slabs was not reduced with a higher ratio of reinforcement, which shows the flexural cracks were fewer, and their widths were smaller.

## Acknowledgment

The author would like to acknowledge everyone who worked/helped throughout the research work, especially my whole family and Civil Engineering Department and Building and Works Section UET Taxila. The careful review and constructive suggestions by the anonymous reviewers are gratefully acknowledged.

## References

- [1] Aikaterini S. Genikomsou, Maria Anna Polak, "Finite Element Analysis of Punching Shear of Concrete Slabs using damaged plasticity model in ABAQUS" *Engineering Structures* 98 (2015): 38-48.
- [2] Ali Raza, Qaiser uz Zaman Khan, Afaq Ahmad, "Numerical Investigation of Load-Carrying Capacity of GFRP-Reinforced Rectangular Concrete Members Using CDP Model in ABAQUS", *Advances in Civil Engineering*. Volume 2019, Article ID 1745341.
- [3] Thomas Jaeger, Peter Marti, "Reinforced Concrete Slab shear Prediction Competition: Entries and Discussions", *ACI Structural Journal*/May-June 2009: 309-318.
- [4] Christian Dulude, Mohamed Hassan, Ehab A. Ahmed, and Brahim Benmokrane, "Punching shear behavior of flat slabs reinforced with glass fiber-reinforced polymer bars" *ACI Structural Journal*, 2013. 110(5): p. 723.
- [5] Liu W, X.M., Chen Z. , Parameters calibration and verification of concrete damage plasticity model of Abaqus. *Ind Constr* 2014. 44: p. 167-71.213.
- [6] Papanikolaou, V.K. and A.J. Kappos, Confinement-sensitive plasticity constitutive model for concrete in triaxial compression. *International Journal of Solids and Structures*, 2007. 44(21): p. 7021-7048.
- [7] ABAQUS Analysis user's manual 6.10-EF, Dassault Systems Simulia Corp., Providence, RI, USA; 2010.
- [8] Kmiecik, P. and M. Kamiński, Modelling of reinforced concrete structures and composite structures with concrete strength degradation taken into consideration. *Archives of civil and mechanical engineering*, 2011. 11(3): p. 623-636.
- [9] Majewski, S., *The mechanics of structural concrete in terms of elasto-plasticity*. Publishing House of Silesian University of Technology, Gliwice, 2003.
- [10] De Normalisation, C.E., *Eurocode 2: Design of concrete structures—Part 1-1: General rules and rules for buildings*. Brussels, Belgium, 2004.
- [11] Desayi, P. and S. Krishnan. Equation for the stress-strain curve of concrete. in *Journal Proceedings*. 1964.
- [12] Mander, J.B., M.J. Priestley, and R. Park, Theoretical stress-strain model for confined concrete. *Journal of structural engineering*, 1988. 114(8): p. 1804-1826.
- [13] Wong, P., F. Vecchio, and H. Tammlehner, *VecTor2 and FormWorks user's manual*. Civil Engineering, University of Toronto, Toronto, Ont, 2002.
- [14] Genikomsou, A.S. and M.A. Polak, Finite element analysis of punching shear of concrete slabs using damaged plasticity model in ABAQUS. *Engineering Structures*, 2015. 98: p. 38-48.
- [15] Elchalakani, M., Dong, M., Karrech, A., Mohamed A., Mohamed S. Huo, JS. "Circular Concrete Columns and Beams Reinforced with GFRP Bars and Spirals under Axial, Eccentric, and Flexural Loading", *Journal of Composites for Construction*, 24(3), 04020008, 2020. [https://doi.org/10.1061/\(asce\)cc.1943-5614.0001008](https://doi.org/10.1061/(asce)cc.1943-5614.0001008).
- [16] Abdel Wahab El-Ghandour, Kypros Pilakoutas, and Peter Waldron, "Punching Shear Behavior of Fiber Reinforced Polymers Reinforced Concrete Flat Slabs: Experimental Study" *Journal of Composites for Construction*, 2003, 7(3): 258-265, doi 10.1061/~ASCE:1090-0268~2003:7:3~258.





# OPTIMUM DESIGN OF PRESTRESSED CONCRETE GIRDER USING JAYA ALGORITHM

<sup>a</sup> Imran Shabbir, <sup>b</sup> Qaisar-uz-Zaman Khan

a: University of Engineering and Technology, Taxila, Civil Engineering Department, [imran.shabbir2@students.uettaxila.edu.pk](mailto:imran.shabbir2@students.uettaxila.edu.pk)  
b: University of Engineering and Technology, Taxila, Civil Engineering Department, [drqaiser@uettaxila.edu.pk](mailto:drqaiser@uettaxila.edu.pk)

**Abstract-** In the past few decades, there has been a significant rise in utilization of meta-heuristic algorithms, such as Genetic algorithm (GA), Ant colony optimization (ACO), Particle Swarm Optimization (PSO), Harmony Search (HS), Big Bang-Big Crunch (BB-BC), Artificial Bee Colony Algorithm (ABC) and Whale Optimization (WO), etc., for design and analysis of concrete structures. The objective of this paper is to apply one such algorithm, known as Jaya Algorithm, to optimize the design of Prestressed Concrete I Girder. Jaya Algorithm has been successfully applied in the field of structural engineering in the past. However, its robustness and efficacy for optimal design of prestressed girder is yet to be tested. For this study, a program was created on MATLAB, following the design guidelines of American Association of State Highway and Transportation Officials (AASHTO) LRFD Bridge Design Specifications for prestressed I girder design. Cross sectional dimensions and number of strands per tendon were used as variables. Flexural stress, shear stress, deflections limitations, and minimum geometric dimensions were used as constraints. To demonstrate the effectiveness of this technique, design optimization for a 40m long prestressed I Girder was successfully carried out in this study. The favorable results of this study indicate that Jaya Algorithm is highly effective and can be recommended for use in the industry.

**Keywords-** Jaya Algorithm, Optimization, Prestressed Post-tensioned I Girder, Meta-heuristic techniques.

## 1 Introduction

Prestressed Concrete Girders are used quite frequently in the highway construction for small-to-medium span bridges. Prestressing of girder reduces the overall impact of external forces by induction of internal stresses. According to National Highway Authority Pakistan (Project Completion Report BMS, 2018), almost one-third of more than four thousand bridges make use of Prestressed Concrete (PSC) Girders in their design. Of those, the most used PSC girder is the I-Girder. Typically, an iterative approach of trial and error is used for the design of structures. This iterative approach, depending upon experience of the designer, might result in high cost, time, and human effort and even then, the optimal design cannot be guaranteed. This is due to involvement of multiple variables such as cross-sectional dimensions, number of prestressing tendons, and number of strands per tendon, impacting the total cost. Thus, it is very difficult to find the desired optimal design using traditional methods due to large number of feasible solutions. In highway construction projects, standardization of cross-sectional dimensions of girders is done for different span lengths. This is done to minimize cost of form work. However, hardly any effort is done on overall cross section size to reduce the cost.

Optimization techniques such as utilization of Meta-heuristic algorithms change this trial-and-error process to a systematic, computer-based procedure that leads to an optimal or sub-optimal design solution without compromising structure's integrity. The success of the metaheuristic algorithm relies on imitation of biological phenomenon. As the nature tends to evolve towards favorable conditions, so does the metaheuristic algorithms with each iteration. The use of GA, inspired by Darwin's Theory, for optimization of prestressed girder bridge have been reported many times in literature. Aydin and Ayvaz [1] used GA for overall cost optimization of multiple bridges, taking number of spans, cross-sectional dimensions



of prestressed girders, and the area of Prestressing Steel (PS) as design variables. The solution turned out to be 12.6% more economical than the actual project. Kaveh et al. [2] presented that Modified Colliding Bodies optimization (MCBO) algorithm performs better than CBO and PSO for cost-optimum design of post-tensioned box girder bridges by 0.4% to 2.2% for various span lengths and cross-sectional widths. Nour et al. [3] demonstrated the optimization of fully and partially prestressed girder, with the help of methodology based on GA. A sensitivity analysis was also performed on numerical problems. Depth of beam was reduced by 39% by increasing concrete strength from 30MPa to 60MPa. Optimal design of cantilever retaining walls under seismic loads was done by Temur [4] using a hybrid TLBO algorithm. The solution was applied on three numerical problems and the results were compared with nine other, commonly used algorithms. For a population size of 50 and 100 runs, Hybrid TLBO yielded better results than its competitors. Munoz et al. [5] successfully employed a novel, hybrid meta-heuristic approach to reduce CO<sub>2</sub> emission of a box girder steel-concrete composite bridge.

Ozturk et al. [6] used Jaya Algorithm and TLBO for cost optimization of counterfort retaining wall. A total of seventeen variables and forty-six constraints were used. It was concluded in the research that TLBO performs better than Jaya Algorithm by almost 4%, however the latter converged more quickly towards the desired solution. Degertekin et al. [7] employed a novel, parameter-free Jaya Algorithm for sizing and layout optimization of truss structure. Efficiency was demonstrated by applying algorithm to eight benchmark truss problems with largest subject truss having fifty-nine discrete variables and was found to yield better solutions than other methods. Standard deviation in optimized weight was very small after just twenty independent runs. Sami et al. [8] developed a software program, employing Jaya Algorithm and ETABS. The software successfully optimized real life building structures comprising of shear walls and RC frames. Aydin et al. [9] employed Jaya Algorithm for design optimization of steel truss, wherein prestressing steel and layout of truss beams were considered variables. It was concluded that shape variables (profile of prestressing steel and layout of truss beams) results in significant cost savings compared to size variables. As prestressed concrete I girder has not yet been designed by this algorithm, its efficiency for this specific problem is yet to be tested.

## 2 Problem Formulation

### 2.1 Design Variables and Constants.

Material properties of concrete and reinforcing steel, number of tendons, and tendon profile were considered as constant design parameters. Design variables included cross sectional geometry and number of strands per tendon. Design parameters and their ranges used in the optimization are given in the following Table 1.

Table 1: Design Parameters Ranges

Design Parameter	Variable	Units	Range
Top flange Width	b <sub>1</sub>	mm	500 ≤ b <sub>1</sub> ≤ 2000
Bottom Flange Width	b <sub>2</sub>	mm	300 ≤ b <sub>2</sub> ≤ 1000
Web Thickness	b <sub>3</sub>	mm	100 ≤ b <sub>3</sub> ≤ 500
Total Depth of Girder	d <sub>1</sub>	mm	1500 ≤ d <sub>1</sub> ≤ 3500
Top Flange Thickness	d <sub>2</sub>	mm	100 ≤ d <sub>2</sub> ≤ 400
Top Flange Transition Thickness	d <sub>3</sub>	mm	100 ≤ d <sub>3</sub> ≤ 400
Bottom Flange Transition Thickness	d <sub>4</sub>	mm	50 ≤ d <sub>4</sub> ≤ 400
Bottom Flange Thickness	d <sub>5</sub>	mm	50 ≤ d <sub>5</sub> ≤ 700
Strands per Tendon	s	No	5 ≤ s ≤ 15

### 2.2 Objective Function.

Material cost was taken as an objective function to minimize the cost of girder. The cost of formwork and construction were incorporated in the cost of concrete. The objective function is defined in the following Equation (2.1).

$$\text{Minimize } C_T = (C_C \times V_C) + (C_{PS} \times W_{PS}) + \text{Penalty} \quad (2.1)$$



Where the variables  $C_C$ ,  $V_C$ ,  $C_{PS}$ , and  $W_{PS}$  are defined as concrete cost, concrete volume, prestressing steel cost, and weight of the prestressing steel, respectively. A massive penalty of  $10^8$  was applied if any of the constraints were violated.

### 2.3 Design Constraints.

General design procedure and limitations followed in this study were according to the guidelines of AASHTO LRFD design manual (2017). Total number of constraints considered were 30.

The allowable stress in girder at top and bottom was defined as follows:

$$\sigma_C \leq \sigma_W \leq \sigma_T \quad (2.2)$$

$$\sigma_W = \frac{P_e}{A} \pm \frac{P_e e}{S} \pm \frac{M}{S} \quad (2.3)$$

Where  $\sigma_C$  is stress in compression,  $\sigma_W$  is allowable working stress, and  $\sigma_T$  is stress in tension. This constraint was satisfied for various loading stages of prestressed girder.  $P_e$ ,  $e$ ,  $A$ ,  $S$  and  $M$  are Prestressing force, eccentricity, concrete area, section modulus, and working moments at a particular section, respectively. Allowable stresses were checked at three stages for two load combinations.

The ultimate flexural strength constraint was defined as

$$M_u \leq \phi M_n \quad (2.4)$$

where  $M_u$  is factored moment and  $\phi M_n$  is flexural strength of section. Flexural strength was calculated using AASHTO LRFD guidelines.

Also, enough reinforcement and prestressing should be provided to develop ultimate moment at least 1.2 times the critical moment.

$$1.2M_{cr} \leq \phi M_n \quad (2.5)$$

The ultimate shear stress constraint is governed by following equation:

$$V_u = \phi(V_c + V_s + V_p) \quad (2.6)$$

where  $V_u$  is factored shear at a particular section, whereas  $V_c$ ,  $V_s$ , and  $V_p$  are shear strength provided by concrete, shear reinforcement, and prestressing, respectively. Here,  $V_p$  was taken as zero as per Method 3 of AASHTO LRFD for calculation of shear capacity of the section.

The long-term deflection of the girder was also calculated and was limited by following expression:

$$\Delta \leq L/800 \quad (2.7)$$

where  $\Delta$  is long term deflection and  $L$  is span length.

Geometrical constraints were also observed where minimum dimensions were governed by: i) clear cover, ii) clear spacing between tendons and reinforcements, iii) dimensions for bearing plate for jack for bottom flange and end block, and iv) span to top flange ratio to avoid failure of lateral bending at prestressing transfer stage.

## 3 Research Methodology

Most of evolutionary and swarm intelligence meta-heuristic algorithms require algorithm-specific parameters such as GA uses mutation, cross-over and selection operator, PSO uses social and cognitive parameters etc. The desired outcome of results is highly dependent on fine tuning of these parameters. Jaya Algorithm proposed by Rao [10] is single phase algorithm-specific-parameter-less algorithm. The user only chooses population size and number of iterations, hence, it is easy to operate than others.



Jaya Algorithm simply converges towards a desired solution while diverging away from undesired solutions. After definition of design variables ( $j$ ), design constants, design constraints, population size ( $k$ ), and number of iterations ( $i$ ), initial set of design variables is generated randomly while obeying lower and upper bounds. Value of each variable is then updated stochastically using Eq. (3.1)

$$y_{j,k}^{i+1} = y_{j,k}^i + r_{j,1}^i (y_{j,kbest}^i - |y_{j,k}^i|) - r_{j,2}^i (y_{j,kworst}^i - |y_{j,k}^i|) \quad (3.1)$$

where  $i=1$  to  $n$  and  $k=1$  to  $m$ .  $y_{j,k}^i$  is  $j^{\text{th}}$  variable of  $k^{\text{th}}$  solution at  $i^{\text{th}}$  iteration.  $r_{j,1}^i$  and  $r_{j,2}^i$  are random numbers in the range of  $(0,1)$ . Their purpose is to ensure good diversification.  $y_{j,kbest}^i$  and  $y_{j,kworst}^i$  are the best and worst variables corresponding to  $k^{\text{th}}$  solution at any iteration “ $i$ ”. After updating the variables using Eq. (3.1), the values of variables are considered for next iteration only if the updated solution is better than the corresponding old solution. As the design of structures is bounded by constraints such as deflection and stress limitations, a heavy penalty of  $10^8$  is assigned to the solution upon the violation of constraints. A typical iterative cycle of Jaya algorithm is demonstrated in Figure 1.

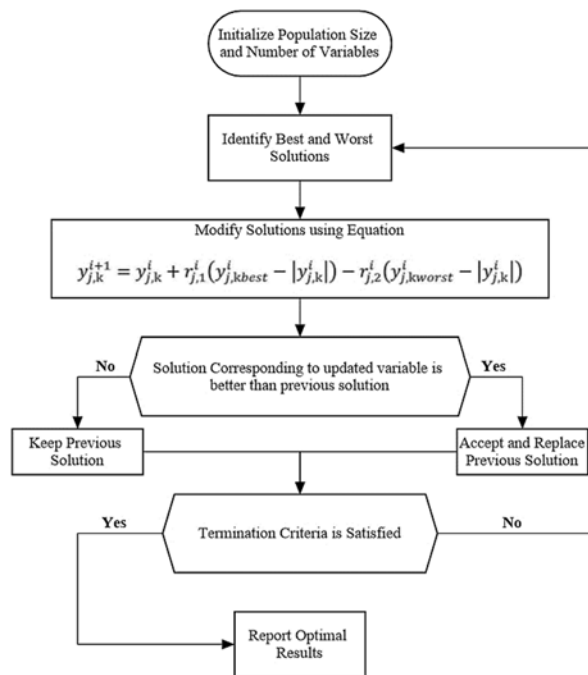


Figure 1: Flowchart of Optimization Process

## 4 Results and Discussion

A comparison of optimized girder section using Jaya Algorithm and numerical problem under similar design conditions was made to evaluate the algorithm's applicability. The optimization problem considered a forty meters long prestressed, post-tensioned interior “I” girder of bridge superstructure. The girder consisted of two (02) layers of six (06) tendons (03 in each layer) with an ultimate strength of 1862 MPa. The diameter of stress relieved strands used in this example was 12.7mm. Concrete flexural strength was kept constant at 41 MPa with a density of 24 kN/m<sup>3</sup>. Unit weight of prestressing steel was kept at 0.775 kg/m. The cost of prestressing steel was taken as 224657.89 Rs/Ton, whereas the cost of concrete was kept at 15255.49 Rs/m<sup>3</sup> based on Composite Schedule Rate of National Highway Authority. Live loads were applied according to AASHTO LRFD and West Pakistan Code of Practice for Highway Bridges-1967. The applied dead loads and super imposed dead loads were computed within the program developed in MATLAB.

Program was run for 300 iterations 30 times for a population size of 50 and the result converged to almost the same solution after 200<sup>th</sup> iteration. The computational effort is minimum as 300 iterations were completed in few seconds each time. Comparison of total cost against number of iterations for first five trails are shown in the following Figure 2.

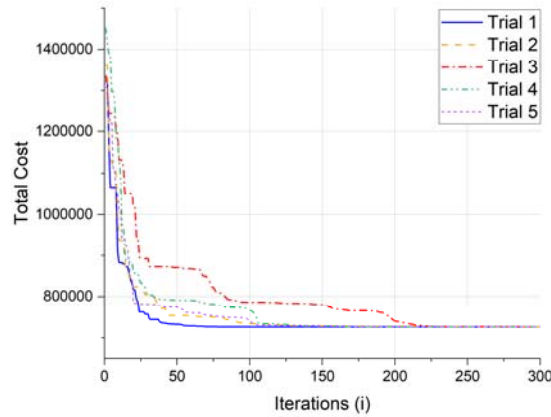


Figure 2: Convergence vs Iteration of Jaya Algorithm

The summarized results and comparison of sample and optimized section is provided in Table 2. The results consistently showed reduction of 29.81% in total cost of girder.

Table 2: Comparison of Result

Design Parameter	Numerical Problem	Optimized Section
Top flange Width ( $b_1$ ) (mm)	1100	887
Bottom Flange Width ( $b_2$ ) (mm)	750	615
Web Thickness ( $b_3$ ) (mm)	190	163
Total Depth of Girder ( $d_1$ ) (mm)	2500	3034
Top Flange Thickness ( $d_2$ ) (mm)	170	100
Top Flange Transition Thickness ( $d_3$ ) (mm)	225	100
Bottom Flange Thickness ( $d_5$ ) (mm)	280	101
Bottom Flange Transition Thickness ( $d_4$ ) (mm)	300	200
Strands per Tendon (s)	12	8
Cost	1,108,311 PKR	777,862 PKR

Mid-section of post-tensioned I girder designed by a typical hit-and-trial method and Jaya algorithm is shown in Figure 3a and Figure 3b, respectively. It can clearly be seen that prestressing contributes much more to the capacity of the section. Use of more tendons or strands per tendon will increase the capacity of section but it will be a costly solution.

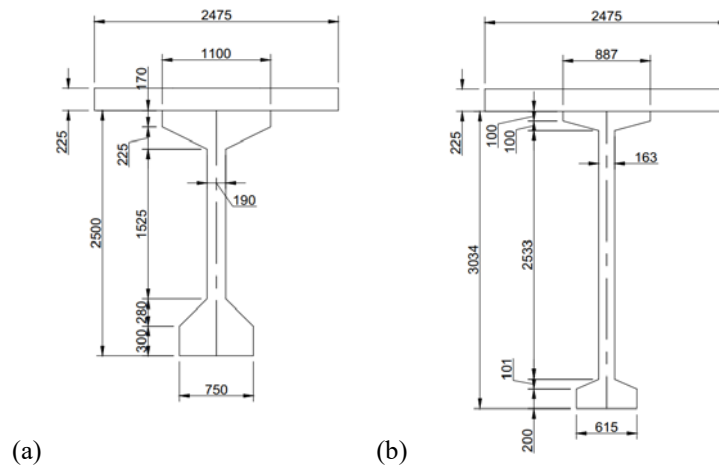


Figure 3: a. Section Designed by hit-and-trial method, b. Optimized Section



## 5 Practical Implementation

The program created using MATLAB is as easy to understand as other techniques in the industry such as finite element modeling software and excel sheets. The program can be improved to incorporate other features such as deck design, tendon profiling, and substructure design. It can also incorporate geometric features such as skew and curves of geometry to design more complex structures easily. For example, deciding between deck thickness and number of girders on curved geometry sometimes becomes a painfully tedious process. By providing few inputs to the software, it'll take less time to find the optimal option.

## 6 Conclusion

Following conclusions can be drawn from this study:

- 1 29.81% reduction in cost of girder mainly due to decrease in number of tendons.
- 2 Optimal design always results in a section with higher height to width ratio. A decrease in the number of tendons reduces the capacity of section which is accommodated by an increase in depth.
- 3 High convergence rate of Algorithm as it converged after approximately 200 iterations every time.
- 4 Time and computational efforts were minimum.

Use of similar algorithms in construction industry can help reduce the material and construction cost, and therefore, net embodied carbon. Since design stage of structural components are based on trial and error, simple yet robust working of Jaya Algorithm will result in saving time, computational efforts, and construction costs.

## References

- [1] Z. Aydın and Y. Ayvaz, "Optimum topology and shape design of prestressed concrete bridge girders using a genetic algorithm," *Struct. Multidiscip. Optim.*, vol. 41, no. 1, pp. 151–162, 2010.
- [2] A. Kaveh, M. Maniat, and M. Arab Naeini, "Cost optimum design of post-tensioned concrete bridges using a modified colliding bodies optimization algorithm," *Adv. Eng. Softw.*, vol. 98, pp. 12–22, 2016.
- [3] N. Abdel Nour, D. Vić, A. Chateaneuf, S. Amziane, and A. Kallassy, "Dimensioning of partially prestressed concrete beams, optimization of T-shaped section with heels," *Eng. Struct.*, vol. 235, p. 112054, 2021.
- [4] R. Temur, "Optimum design of cantilever retaining walls under seismic loads using a hybrid TLBO algorithm," *Geomech. Eng.*, vol. 24, no. 3, pp. 237–251, 2021.
- [5] D. Martínez-Muñoz, J. García, J. V. Martí, and V. Yepes, "Discrete swarm intelligence optimization algorithms applied to steel–concrete composite bridges," *Eng. Struct.*, vol. 266, p. 114607, 2022.
- [6] H. Tahsin Öztürk, T. Dede, and E. Türker, "Optimum design of reinforced concrete counterfort retaining walls using TLBO, Jaya algorithm," *Structures*, vol. 25, pp. 285–296, 2020.
- [7] S. O. Degertekin, G. Yalcin Bayar, and L. Lamberti, "Parameter free Jaya algorithm for truss sizing-layout optimization under natural frequency constraints," *Comput. Struct.*, vol. 245, p. 106461, 2021.
- [8] Semi Emrah Aslaya and T. Dede, "3D cost optimization of 3 story RC constructional building using Jaya algorithm," *Structures*, vol. 40, pp. 803–811, 2022.
- [9] Z. Aydın, "Size, layout and tendon profile optimization of prestressed steel trusses using Jaya algorithm," *Structures*, vol. 40, pp. 284–294, 2022.
- [10] R. V. Rao, "Jaya : A simple and new optimization algorithm for solving constrained and unconstrained optimization problems," *Int. J. Ind. Eng. Comput.*, vol. 7, pp. 19–34, 2016.



# 3D FINITE ELEMENT ANALYSIS OF REINFORCED CONCRETE BEAMS UNDER FIRE

<sup>a</sup> Javaria Mehwish\*, <sup>b</sup> Katherine Cashell, <sup>c</sup> Rabee Shamass

a: Civil & Environmental Engineering, Brunel University London, [javaria.mehwish@brunel.ac.uk](mailto:javaria.mehwish@brunel.ac.uk)

b: Civil & Environmental Engineering, Brunel University London, [Katherine.cashell@brunel.ac.uk](mailto:Katherine.cashell@brunel.ac.uk)

c: Civil & Environmental Engineering, London South Bank University, [shamassR@lsbu.ac.uk](mailto:shamassR@lsbu.ac.uk)

\* Brunel University London Email ID [javaria.mehwish@brunel.ac.uk](mailto:javaria.mehwish@brunel.ac.uk)

**Abstract-** This paper presents a numerical investigation of the fire behaviour of reinforced concrete beams reinforced with carbon steel. The main aim of this paper is to propose and validate a detailed finite-element model that considers the nonlinear behaviour of the materials and the heat transfer parameters that affect the fire performance of steel reinforced concrete beams using commercial FE software ABAQUS. The analysis was performed using sequentially coupled thermal stress analysis, for which the thermal analysis was firstly performed, and the structural analysis was then conducted. The EC2 constitutive material models for concrete in tension and compression at elevated temperature were simulated while the steel was modelled using either elastic-perfectly plastic or with strain hardening suggested in the EC2. Regarding the heat transfer, models with and without radiation heat transfer were conducted. The numerical results were compared with three tested beams. It was found that numerical models without radiation heat transfer provided results in good agreement with the test results. The elastic-perfect plastic material model for steel rebar at elevated temperatures can be utilized in FEA to reduce the computational time. However, the steel model with strain hardening provided more accurate predictions.

**Keywords-** Abaqus, fire analysis, material modelling and reinforced concrete.

## 1. Introduction

This paper is concerned with the elevated temperature behaviour of reinforced concrete beams. Reinforced concrete (RC) is one of the most commonly used structural materials and is regularly employed for various structures, including office blocks, hospitals, schools, and bridges. In addition to efficiently using the constituent materials, it behaves well in extreme conditions such as fire and offers excellent structural resistance. The fire resistance of a building or structural element is defined as the time in which the structural element retains sufficient structural integrity and stability. When a structural member is exposed to fire, it loses strength as the material properties deteriorate, increasing internal stress in the element. This may lead to the redistribution of stresses in the structure, loss of key elements and even possible collapse of the overall structure. Studies by Beitel and Iwankiw [1] and Lue Taerwe [2] assessed several reinforced concrete structures that suffered full or partial collapse due to fire, such as the warehouse building in Ghent, Belgium collapsed following a fire in 1974. According to statistics by N.N Brushlinsky [3], the average number of deaths caused by fire is 43,200 per year in 3.7 million fire incidents in 39 countries. The United Kingdom, on the other hand, faced 367 deaths per year [3] due to fire. In 2017, the recent fire incident in London Grenfell highlighted that this type of extreme event, although rare, is still a real threat to both structural integrity and human life.

Under a real fire scenario, the heat is transferred through convection, radiation and conduction. Radiation heat transfer mode should be considered when conduction and convection are small, or the-time scale is small for which conduction and convection effects are too slow, and radiation becomes the predominant transfer mode [4]. Conventionally heat



analysis in RC members is performed through all three modes of heat transfer [5-7]. This subject is still not addressed in most research [15-16]. Therefore, in the current study finite element analysis (FEA) of RC beam is performed using conduction and convection mode of heat transfer only. Thermo-structural analysis of the RC beam shows that this hypothesis produces very excellent results.

## 2. Finite element analysis

This section discusses the development of a three-dimensional finite element model that can simulate the nonlinear thermal and structural response of an RC beam under different fire conditions and employs a sequentially coupled analysis approach, including a thermal analysis to simulate the spread of elevated temperature through the section, followed by a Thermal stress analysis. Thermal stress analysis is performed in two models: (i) the heat transfer analysis model, and (ii) the structural model. The results of the first analysis model are used as a thermal load for the structural analysis model.

### 2.1. Thermal Analysis

A nonlinear transient heat transfer analysis (as the heat flow rate keeps changing with time and produces varying rates of heat transfer) is simulated in the first step to determine the thermal response of the RC beam and nodal temperature histories. In this analysis, the temperature field is calculated without consideration of the stress/deformation field. The result is then used as a thermal load for the structural analysis. Heat flux is the thermal energy flow inside the material per unit area per unit time is computed by Abaqus by defining fire load, convection, and conduction parameters.

The fire load determined from the standard fire time-temperature curve is applied in the form of amplitude on the external boundary of the model. Convection is modelled through surface film condition interaction as heat flow from surrounding is through the model surface. Film coefficient is the same as defined above and is used along with sink temperature as 1 with sink amplitude same as fire load. Conduction between two surfaces in one element, from concrete to steel rebars of the beam passes through embedded constraint in Abaqus. This is achieved when the steel rebar is fully embedded in the host region concrete.

The model is divided into a number of finite elements. The mesh for both thermal and structural models should be the same to make them compatible. Mesh sizes 50mm, 25mm and 10mm are used to study the effect of mesh size on the convergence time and results. A mesh size of 25mm has been used in the current study, providing more accurate results in a reasonable time. The three-dimensional eight-node solid liner heat transfer element (DC3D8) with a temperature degree of freedom was used to model the concrete beams for thermal analysis. Similarly, a two-node heat transfer link element (DC1D2) with a temperature degree of freedom is used for reinforcing steel.

The input parameters required in heat transfer analysis include fire load and thermal material properties. Three different forms of fire load, including fire curve ISO-834 [8], ASTM E119 [9] and short design fire (data is chosen from a practical test performed by Kodur [6], are selected for the present study.

Thermal material properties like thermal conductivity, specific heat capacity, thermal expansion, density, and temperature-dependent elasticity modulus are required in heat transfer analysis. All this data is available in Eurocode 2004 Part 1-2 (EC 2) [10], except the thermal expansion coefficient which is taken from ASCE manual 78 [11] and expressed in equations below. In EC 2 [10] thermal elongation is given whereas input data required the thermal coefficient of material in Abaqus [4] therefore this value is taken from the ASCE [11] manual.

For siliceous and carbonate aggregate concrete

$$\alpha_c = (.008\theta + 12) 10^{-6} \text{ for } 20^\circ\text{C} \leq \theta \leq 800^\circ\text{C} \quad (1)$$

Similarly, for steel following expression can be used.

$$\alpha_s = (.004\theta + 12) 10^{-6} \text{ for } \theta < 1000^\circ\text{C} \quad (2)$$

$$\alpha_s = 16 \times 10^{-6} \text{ for } \theta \geq 1000^\circ\text{C} \quad (3)$$



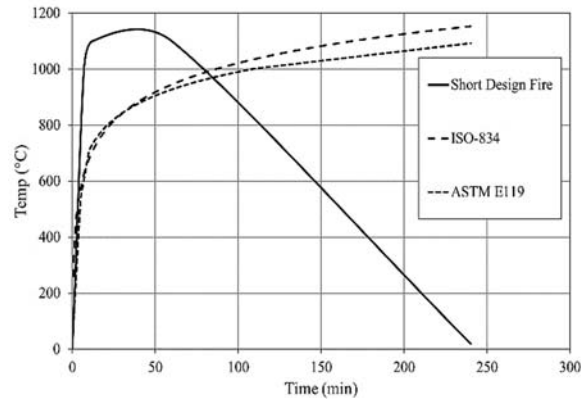


Figure 1. Time-dependent temperature curves. [6,8,9]

## 2.2. Thermal stress analysis

Structural analysis is performed in the second model using sequentially coupled thermal stress analysis. The second model uses the same heat transfer analysis model with further modification. In this model, concrete is discretized using eight-noded continuum elements (C3D8) with three degrees of freedom; namely three translations in x, y, and z directions, as they are capable of accounting for cracking of concrete in tension, crushing of concrete in compression, creep, and large strain [4]. Steel reinforcement is defined using two-noded link truss elements (T3D2). As it is assumed to be deformed by axial stretching only. They are pin jointed at their nodes [4].

Thermal structural stress analysis is performed in two steps. In the first step, the mechanical load is applied along with boundary conditions per the test specimen. In the second step, thermal load from heat transfer analysis is applied through predefined fields. The implicit solver available in Abaqus/Standard based on an iteration process to enforce equilibrium conditions is utilised for analysis. No bond slip is considered between concrete and steel, and temperature is considered uniform through the full length of the beam.

## 3. Material Modelling

Mechanical material properties like compressive and tensile strength of the material are required in stress analysis. Constitutive material models for steel and concrete are chosen from EC 2 [10], which implicitly include concrete transient strain. Also, only normal strength concrete is considered, so thermal spalling is negligible. The concrete material model is defined under the concrete damage plasticity material model (CDP) [4]. The input parameters for CDP models are shown in Table 1.

Table 1. CDP Model input parameters

Dilatation angle $\psi$	Eccentricity $\epsilon$	Fb0/fc0	K <sub>c</sub>	Viscosity parameter
35	.1	1.16	.666667	.0003

The problems related to achieving the convergence of the solution, caused by the non-linearity of the material model, were solved by viscosity stabilization  $\mu$  [12]. The selection of the viscosity parameter  $\mu$  was made iteratively after analyzing its impact on the convergence results. Finally, a value of 0.0003 was used, and the analysis shows that it completed the convergence in a reasonable time.

### 3.1. Concrete under compression

The concrete damage plasticity model is implemented with concrete compression hardening, concrete tension stiffening, and the concrete compression damage parameter. These parameters are modelled with the temperature



range. Concrete compression behaviour is defined through the stress-strain curve using a constitutive material model from EC2 [10]. Concrete strain is divided into two parts. So total strain  $\epsilon_t$  in the inelastic-cracking equals to cracking the strain  $\epsilon_{cr}$  and elastic strain  $\epsilon^{el}$  [4], it is explained in expression below.

$$\epsilon_{cr} = \epsilon_t - \epsilon^{el} \quad (4)$$

Similarly, damage parameter  $d_c$  is defined as the ratio of the cracking strain to the total strain. The value of  $d_c$  is valid only for descending branch of the stress-strain curve. The following expression [4] is used to calculate the damage parameter.

$$d_c = \frac{f_{cm} - \sigma_c}{f_{cm}} \quad (5)$$

### 3.2. Concrete under Tension

The tensile strength of the concrete reduces at high temperatures and is also calculated from EC 2 [10]. There is a software limitation to utilize concrete tension damage parameters along with temperature range. So, crack propagation in concrete under tension is modelled through fracture energy.

The fracture energy of concrete  $G_F$  [N/m], defined as the energy required to propagate a tensile crack of a unit area, should be determined by related tests. Without experimental data,  $G_F$  in [N/m] for ordinary, normal-weight concrete can be estimated from the following equation from fib Model 2010[13]. Fracture energy calculated through this expression has been used in the present study with reduced compressive strength at the high-temperature range.

$$G_F = 73. f_{cm}^{.18} \quad (6)$$

$f_{cm}$  is the mean compressive strength

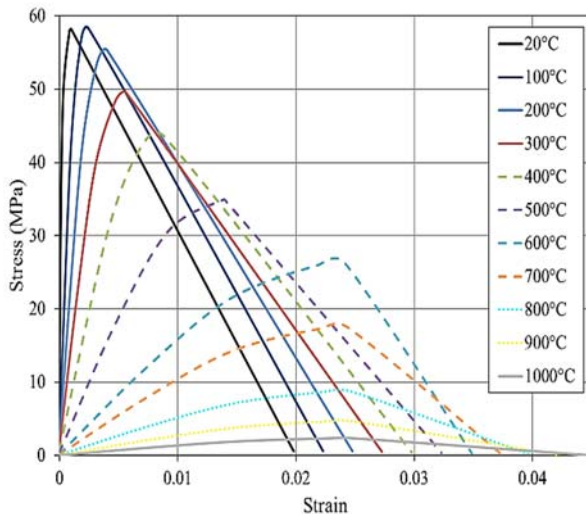


Figure 2. Stress-strain curves of concrete at elevated temperatures.

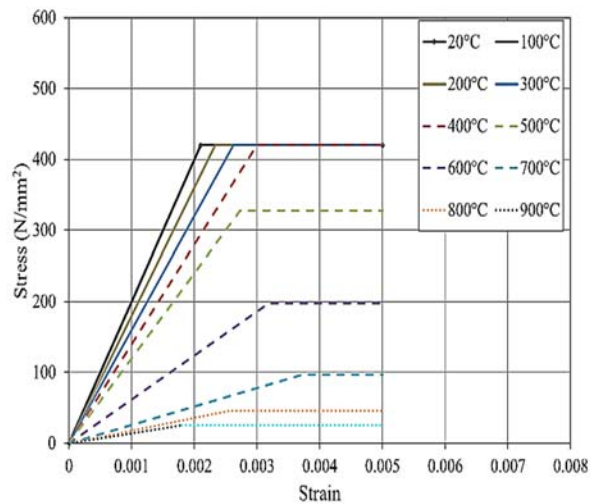


Figure 3. Perfect plastic material model for carbon steel at elevated temperatures.

### 3.3. Reinforcing Carbon Steel

Steel reinforcement can be modelled as perfectly plastic material with a single yield stress value per temperature [4]. In this material model, strain is increased elastically with increased stress, and once yield occurs, the material will deform plastically without increasing stress. Steel reinforcement is considered a perfectly plastic material and identical in tension and compression. The other option is miss yield surface to define isotropic yielding of steel reinforcement



and defined by uniaxial yield surface against uniaxial plastic strain along with the temperature. The plastic material data should be Cauchy stress and logarithmic strain. Following equations are used for converting simple nominal stress-strain to true stress, and logarithmic plastic strain is as follows [4]. Both models are utilized in this study.

$$\sigma_{true} = \sigma_{nom} = (1 + \epsilon_{nom}) \quad (7)$$

$$\epsilon_{ln}^{pl} = \ln(1 + \epsilon_{nom}) - \frac{\sigma_{true}}{E} \quad (8)$$

The constitutive material models of steel from EC 2 [11] are utilized to define isotropic steel yielding. The proportional limit is the end of an elastic region on the stress-strain curve. This is given as a ratio to yield strength in EC 2 [11], whereas, in the present study, it is taken as constant at 0.2% strain. The results produced from FEA using the new proposed proportional limits are in excellent agreement with the test results.

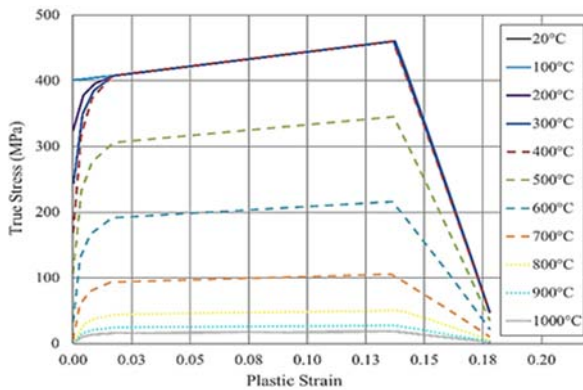


Figure 4. Stress-strain curve for carbon steel at elevated temperatures using EC 2 [10] material model.

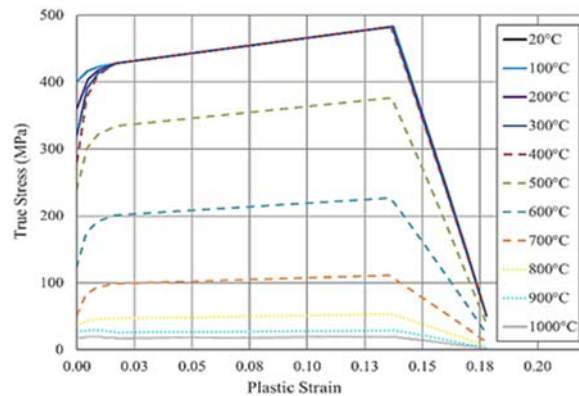


Figure 5. Stress-strain curve for carbon steel at elevated temperatures using EC 2 [10] material model considering 0.2% strain at the proportional limit

#### 4. Validation

RC beams tested under fire by Wu [14] and Dwaikat and Kodur [6], respectively, are chosen in the present study to validate the proposed FEA. The results show the capability and accuracy of the current FE model. These tests were selected because their results were thorough enough to allow for FE simulations and comparisons. The layout and arrangement of tested beams are given in subsequent sections. General properties are provided below.

Table 2. General properties of the tested beams.

Study	Beam designation	Fire exposure	Support condition	Concrete strength $f_c$ (MPa)	Aggregate type	Steel strength $f_y$ (MPa)	Applied Load (KN)
W. H. Wu	Beam slab 1	ISO 834	SS	21	Carbonate	240	Distributed load
Dwaikat and Kodur	B1	ASTM E119	SS	58.2	Siliceous	420	50
	B2	SF	AR	58.2	Siliceous	420	50



Three different types of beams are selected for the validation purpose to see the effect of different type of concrete strength, steel strength, fire exposure and support condition. The beam tested by Wu [14] was simply supported and exposed to ISO-834 [8] fire with low-strength concrete and carbonation aggregates. Whereas two different beams were tested by Kodur [6]. They have similar material properties as given in Table 2, but different fire exposure was applied. The beam exposed to the ASTM E119 [9] curve was simply supported, whereas the other beam was axially restrained (AR) and exposed to short fire (SF).

#### 4.1. Test by Wu et al.

The sample tested beam [14] was 5.1 m long in span, and 4.0 m of the internal span was exposed to fire, as shown in the figure below. An overlying slab of 80 mm thickness was placed on top of the beam during the fire test. An additional distributed load of 300 kg/m<sup>2</sup> was applied on the top of the overlying slab, so the total load acting on the beam was a combination of distributed load and overlying slab load.

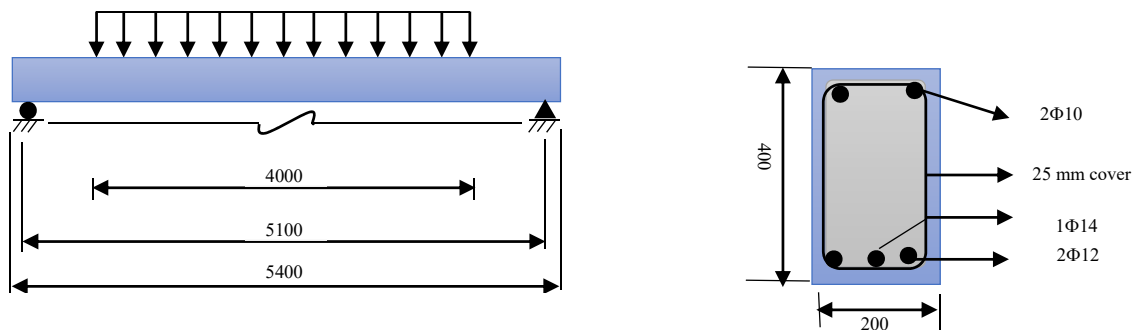


Figure 6 Test by Wu et al. [15]

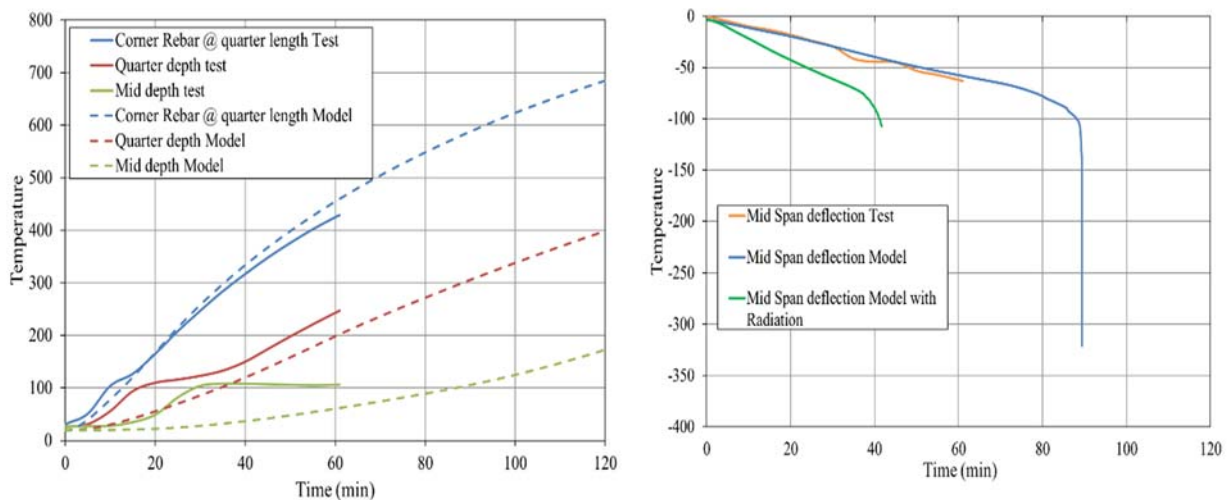


Figure 7. Comparison of predicted and measured rebar and concrete temperature and displacement.

Fire analysis of the sample beam was performed in Abaqus [4] using the abovementioned procedure. Heat transfer analysis was performed first considering radiation and then without it. Stress analysis results in figure (7) show that the FEA of the sample beam with radiation produced an early failure of the beam. In contrast, the model analyzed without radiation showed a closer deflection prediction with compression failure. The validity of the proposed methodology for heat transfer analysis is demonstrated by the close match between the FEA model and test outcomes.



#### 4.2. Test by Kodur et al.

Two concrete beams named B-1 & B2 were tested under different fire exposure by Dwaikat and Kodur [6]. They are analyzed by applying the above numerical procedure to validate the proposed approach of heat transfer analysis without radiation and the new proposed steel material model. The arrangement of the two beams is the same, except the fire load was different. The general layout is shown in figure 8.

The authors applied force 30 minutes before the start of the fire and sustained it until no more deformation could be recorded in the fire tests. This was chosen as the initial condition for the beam's deflection. After that, the load was kept constant for the duration of the fire exposure. B1 was exposed to ASTM E119 fire, and the short fire was applied to B2. Beam B1 failed to sustain load in fire after 180 mins. At the same time, B2 did not fail during fire exposure.

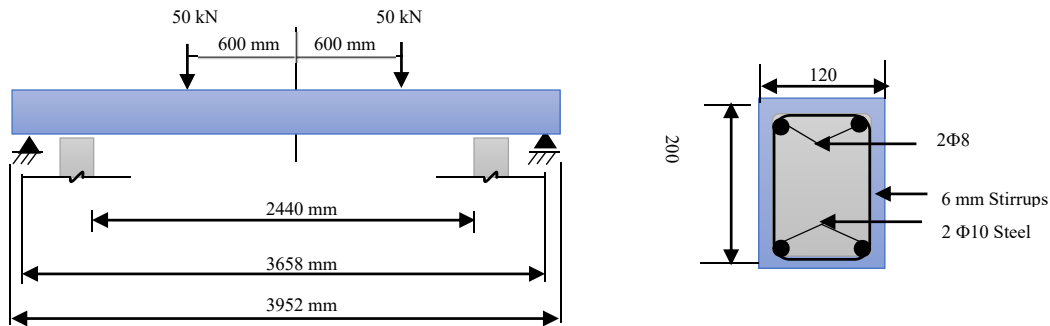


Figure 8. Test by Kodur et al. [6].

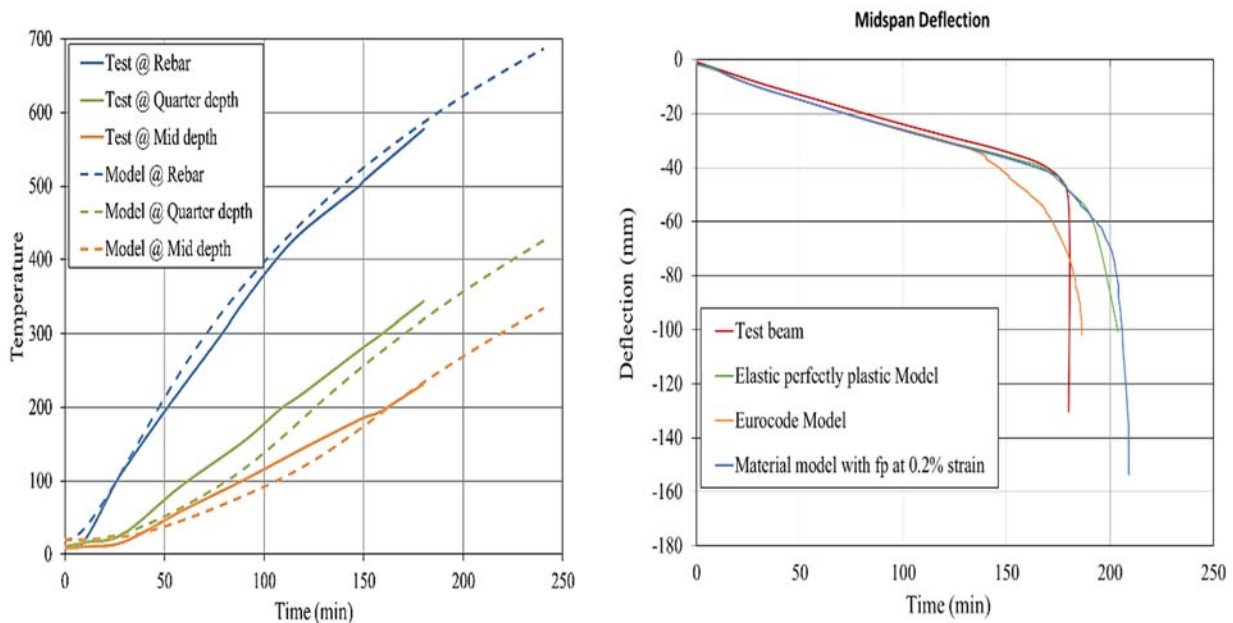


Figure 9: Comparison of predicted and measured rebar and concrete temperature and displacement for B-1.

Comparisons of results for the heat transfer model and structural analysis show that the two different assumptions made in this study, one for heat transfer analysis without radiation and the second for structural analysis with the



proposed steel material model, work well with the test results.

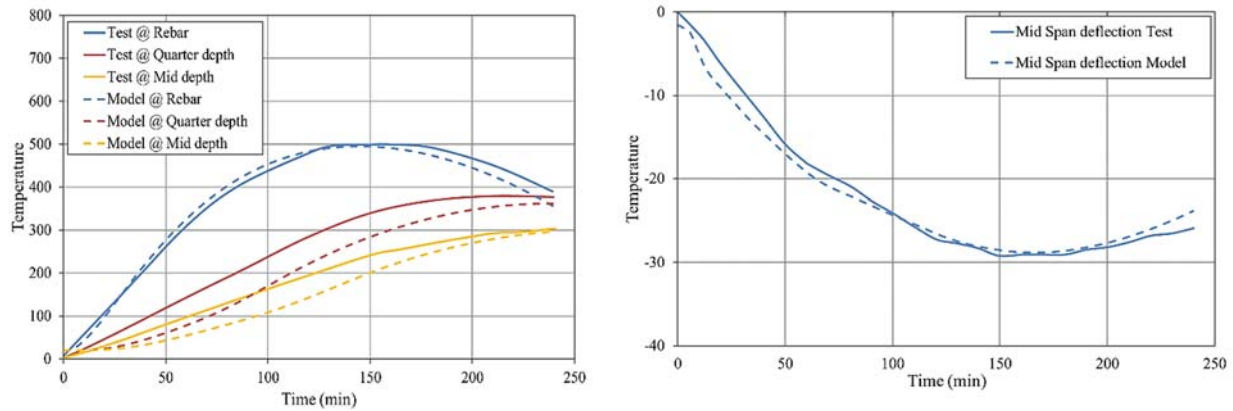


Figure 10. Comparison of predicted and measured rebar and concrete temperature and displacement for B-2.

The failure mode for B-1 is compression failure, whereas B-2 didn't fail due to short-term exposure to fire. The results are shown in figures (9) & (10) provide the comparison of the test beam and the numerical results.

## 5. Conclusion

A 3D FE model for predicting the behaviour of RC beams exposed to fire was discussed in this study. The heat transfer analysis without radiation and a new proportional limit for the steel material model is proposed in the current research, allowing for more accurate deflection predictions. The following conclusion can be drawn from this study.

- Heat transfer analysis in Abaqus [4] should be performed without taking the effect of radiation from surrounding fire unless a fire is modelled not in direct contact with RC beam.
- Elastic perfect plastic material model for steel rebar at elevated temperatures can be utilized in FEA. Strain hardening of steel at a given temperature can't be used due to the temperature rise during a fire.
- Plastic material model for steel rebar at elevated temperature can reduce the calculation time for the material model and a simulation time in Abaqus [4].
- New proposed proportional limit for steel rebar stress-strain curves at elevated temperature produces more accurate results.

## References

1. J. Beitel and N. Iwankiw, "Analysis of Needs and Existing Capabilities for Full Scale Fire Resistance Testing" NIST GCR 02-843, 2002.
2. L. Taerwe, "From Member Design to Global Structural Behaviour" International workshop, Fire Design of Concrete Structures-From Materials Modelling to Structural Performance, University of Coimbra Portugal, November 2007.
3. N.N. Brushlinsky, M. Ahrens, S.V. Sokolov, and P. Wagner, "World fire statistics", CTIF, International Association of Fire and Rescue Services, No. 23, 2018. Available at: [www.ctif.org/sites/default/files/ctif\\_report23\\_world\\_fire\\_statistics\\_2018\\_vs\\_2\\_0.pdf](http://www.ctif.org/sites/default/files/ctif_report23_world_fire_statistics_2018_vs_2_0.pdf)
4. 3DS/Simulia. ABAQUS/Standard: Abaqus Analysis User's Guide; 3DS/Dassault Systems, Providence, RI, USA, 2013.
5. W. Y. Gao, G. M. Chen, G. J. Teng, and J. G. Dai, "Finite element modelling of reinforced concrete beams exposed to fire" Elsevier Ltd, 52, pp. 488–501, 2013. doi: 10.1016/j.engstruct.2013.03.017.
6. M. B. Dwaikat and V. K. R. Kodur, "Response of restrained concrete beams under design fire exposure", Journal of Structural Engineering, vol. 135, no. 11, pp. 1408–1417, 2009.
7. J. H. Liao, Z. D. Lu, and L. Su, "Experimental and finite element analysis of shear strength of concrete beams subjected to elevated temperature" Journal of Tongji University (Nature Science), 41(6), 806–812, 2013.
8. ISO 834-1, "Fire Resistance Tests-Elements of Building Construction. Part 1: General Requirement, International Organization for Standardization", Geneva, Switzerland, 1999.
9. ASTM E119, "Standard methods of fire test of building construction and materials. American society of testing and materials", West Conshohocken, PA, 2008.



**4<sup>th</sup> Conference on Sustainability in Civil Engineering (CSCE'22)**  
Department of Civil Engineering  
Capital University of Science and Technology, Islamabad Pakistan



10. Eurocode 2," Design of concrete structures Part 1-2: General rules - Structural fire design Euro code", SS-EN-1992-1-1:2008, 3 July 2004.
11. T.T. Lie, "Structural Fire Protection" American Society of Civil Engineers (ASCE) Manual and Reports on Engineering Practice No. 78.
12. P. Kmiciek, M. Kamiński, "Archives Of Civil And Mechanical Engineering". XI (3), 623,2011. [http://dx.doi.org/10.1016/S1644-9665\(12\)60105-8](http://dx.doi.org/10.1016/S1644-9665(12)60105-8)
13. fib: Model Code for Concrete Structures 2010, Ernst and Son, 2013 (in press)
14. Wu, H. J.; Lie, T. T.; Hu, J. Y., "Fire Resistance of Beam-Slab Specimens: Experimental Studies" Internal Report (National Research Council of Canada. Institute for Research in Construction), no. IRC-IR-641, 1993-03.
15. Aliş, Betül, et al. "Investigation of Fire Effects on Reinforced Concrete Members via Finite Element Analysis." ACS Omega, vol. 7, no. 30, 2022, pp. 26881–26893., <https://doi.org/10.1021/acsomega.2c03414>.
16. Elshorbagy, Mohamed, and Mohamed Abdel-Mooty. "The Coupled Thermal-Structural Response of RC Beams during Fire Events Based on Nonlinear Numerical Simulation." Engineering Failure Analysis, vol. 109, 2020, p. 104297., <https://doi.org/10.1016/j.engfailanal.2019.104297>.



# REVIEW OF INFILL WALL MODELLING TECHNIQUES: MACRO AND MICRO MODELS

*<sup>a</sup> Fatima Khalid\*, <sup>b</sup> Samra Masood*

a: Department of Civil Engineering, NEDUET, Karachi [fatimak@neduet.edu.com](mailto:fatimak@neduet.edu.com)

b: Department of Civil Engineering, NEDUET, Karachi [samasood@neduet.edu.com](mailto:samasood@neduet.edu.com)

\* Corresponding author: Email ID: [fatimak@neduet.edu.com](mailto:fatimak@neduet.edu.com)

**Abstract-** Infilled masonry frames are integral part of reinforced concrete (RC) structures for almost 200 years. They are present in interior and exterior walls in both RC and Steel frames all around the world. The interaction of infills with the surrounding frames has a major influence on the structural response of the full composite structures. Their most influential property is that of a high initial stiffness and considerable strength. However, even today during the design process and during the assessment of the existing structures they are considered as non-structural members and their contribution in the structural response is overlooked. Numerous researchers have considered the influence of infills on the response of RC structures in the recent past and the need for inclusion of these members in the design and assessment of structures has been recognized. This study therefore aims to provide a thorough review of the work of several researchers to include the in-plane effect of infill panels in the behavior of RC frames.

**Keywords-** macro modelling, micro modelling, infill walls

## 1 Introduction

Buildings all over the world are usually designed without considering role of masonry wall enclosed within beam and columns known as infilled walls. With the advancement of research, it was found that infilled walls increase lateral strength and stiffness of the frame. However, if frames are not properly designed for aforementioned criteria, then it will eventually increase the risk of collapse. Despite of this, even today RC structures are designed without considering infill walls due to its complexity in modelling and giving the correct behavior. Therefore, still significant research considering the behavior and modelling of infill are in study [1], [2]. FEMA seismic assessment is usually carried out to see the behavior of building under earthquake loadings and considering all the aspects that are usually ignored in design.

In this study, a detailed review of existing techniques to model infill walls were conducted. Only in-plane behavior of infill walls for modelling was considered in this study. In Section 2 and 3, macro and micro models were discussed, respectively. Finally, conclusions were made in last section.

## 2 Macro Models

### 2.1 Equivalent Strut Model

Polyakov [3] has first replaced infill wall by an equivalent pin-jointed diagonal strut after conducting experiment on steel frames. The main properties required to model the diagonal strut is masonry material models in compression and the area of the strut. To find area of the strut different researchers has proposed the equivalent width of strut depending on infill aspect ratio and mode of failure of infill. The thickness for the strut is considered to be equal to the wall thickness.

Holmes [4] and Smith [5] proposed equivalent strut model with effective width of 33% of diagonal length of infill panel and different width for masonry panel ratio respectively. Smith [6] has proposed that effective width varies from 1/4<sup>th</sup> and





1/11<sup>th</sup> of diagonal length of infill panel for square and panels having aspect ratio of 5:1, respectively. Smith [6] further introduced stiffness parameter,  $\lambda_h$  which incorporate interaction between frame and infill in term of width as shown in (1) and (2), respectively.

$$\lambda_h = \sqrt[4]{\frac{E_m t \sin 2\theta}{4E_c I_c h_m}} \quad (1)$$

$$w = 0.58 \left(\frac{1}{H}\right)^{-0.445} (\lambda_h H')^{0.335} d_z \left(\frac{1}{H}\right)^{0.064} \quad (2)$$

Mainstone [7] proposed an empirical relation (3) based on  $\lambda_h$  which resulted in reduced value of effective width than proposed by [6]. Therefore it underestimated the lateral stiffness of the uncracked RC section as mentioned by Mehrabi [8].

$$w = 0.175 d_z (\lambda_h H')^{-0.4} \quad (3)$$

Kadir [9] has introduced new parameter  $\lambda_g$  (4) that needs to be incorporated while calculating width of strut.

$$\lambda_g = \sqrt[4]{\frac{E_m t \sin 2\theta}{4E_c I_g h_m}} \quad (4)$$

$$w = \frac{\pi}{2} \left( \frac{1}{4\lambda_h^2} + \frac{1}{4\lambda_g^2} \right) \quad (5)$$

Hendry (1990) presented that single strut width equals to half the width proposed by [6]. Paulay [10] concluded that wider strut width make structure stiffer resulting in higher seismic forces. Therefore, the proposed width was considered same as Holmes (1961) of diagonal strut

Liauw [11] studied that openings present in infill will affects the stiffness and strength of infills. Experimental and analytical study have been done to study the response of non-integral infilled frames incorporating material nonlinearities and proposed strut width as (6). FEMA has provision that infill wall with 25% opening do not need to be considered for equivalent compressive strut behavior.

$$w = \frac{0.95h \cos \theta}{\sqrt{\lambda_h H'}} \quad (6)$$

Decanini [12] provide several expressions for calculating effective strut width and concluded that with an increase in load, the strut width decreases significantly. Dawe [13] have proposed the formula based on Smith's and Kadir [9]  $\lambda_h$  and  $\lambda_g$  parameters. (7)

$$w = \frac{2\pi}{3} \left( \frac{\cos \theta}{\lambda_h} + \frac{\sin \theta}{\lambda_g} \right) \quad (7)$$

Durrani [14] provided an equivalent strut width semi-empirical formula (8) based on geometry of frame without considering relative stiffness parameter.

$$\frac{w}{d} = \gamma \sin 2\theta \quad (8)$$

$$\gamma = 0.32 \sqrt{\sin 2\theta} \left( (h^4 E_w t_w) / m E_c I_c h_w \right)^{-0.1} \quad (9)$$

Where

$$m = 6 \left( 1 + \frac{6E_b I_b h}{\pi E_c I_c L} \right) \quad (10)$$



$E$ ,  $I$  and  $h$  represents Elastic modulus, second moment of mass and height. The subscripts  $b$ ,  $c$  and  $w$  denote beam, column and wall, respectively.

Amato [15] proposed initially single concentric strut element that does not consider the local effects. Further, to incorporate local effects eccentric element was used. It also considers the influence of masonry dilation on the strut width. [16] has proposed the effective width formula as shown in (11)

$$w = 1.414 \frac{\pi}{2\lambda h} \quad (11)$$

Yekrangnia [17] proposed a single strut model to incorporate both local and global behavior of infill panels. Kumar [18] proposed single strut model for structures present in Pakistan with effective width equals 18% of diagonal length of infill wall.

## 2.2 Multiple Strut Model or Eccentric Model

Single strut model is not capable of producing the correct bending moment and shear force diagram. Increasing number of struts give better representation of internal forces as proved by Crisafulli et al. (2007). Zarnic [19] proposed an equivalent strut model based on their experimental results of 28 specimens of masonry infilled frames subjected to lateral cyclic loading. In this model, the diagonal strut is not connected to the beam-column joint to show the damage in the upper zone of masonry panel which behaved as a captive column i.e. more free to deform. Syrmakezis et al. [20] proposed multiple struts model and Schmidt (1989) proposed 2 struts which are not parallel to each other. Whereas Chrysostomou [21] proposed a 6 strut model, 3 parallel struts for compression and 3 parallel strut for tension as shown in Figure 1. The off diagonal struts are positioned by parameter  $\alpha$  that represents the fraction of the length or height of the panel. San Bartolomé [22] proposed 9-strut model for the infilled frame structure. El-Dakhakhni [23] proposed macro-model for concrete masonry infilled steel frames with 3 struts (one diagonal and two off-diagonal) for masonry panel as shown in Figure 2. The total area for the three struts is shown in (12).

$$A = \frac{(1-\alpha_c)\alpha_c h t}{\cos \theta} \quad (12)$$

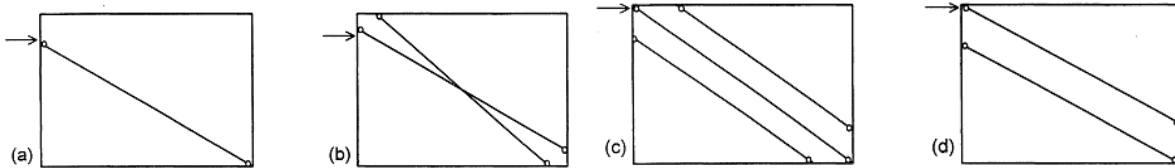


Figure 1 a) Zarnic et al. [19] b) Schmidt (1989) c) Chrysostomou [21] d) Syrmakezis et al. [20]

Thiruvengadam [24] proposed a complex model for dynamic analysis of infilled frame. In this model, infill was replaced by set of equivalent multiple struts which accounts for both frame-infill separation and infill openings. Fiorato [8] proposed “knee braced frame” to represent the masonry infilled behavior.

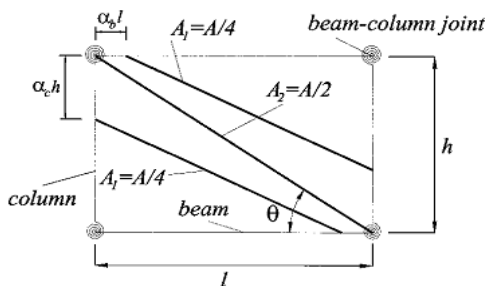


Figure 2 El-Dakhakhni [23] macro model

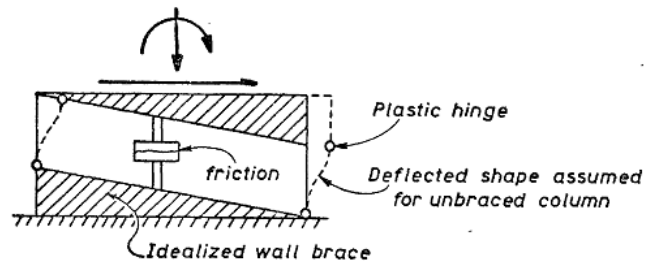


Figure 3 Leuchars et al. [8] model



### 2.3 Strut Model with Friction Element

Leuchars [8] proposed a double strut model with a friction element as shown in Figure 3. This model was portraying the internal forces including bending moment and shear in columns as well the friction mechanism along the cracks. This was just a hypothetical model that was never implemented.

Crisafulli [19] researched on three models as shown in Figure 4; single strut, double strut and three strut models. It was concluded that single strut model is not capable of capturing the local effects whereas multiple strut models can overcome this problem. Single strut model provides an adequate estimation of stiffness of the frame. But for refined analysis, multi strut models should be used without significant increase in the complexity.

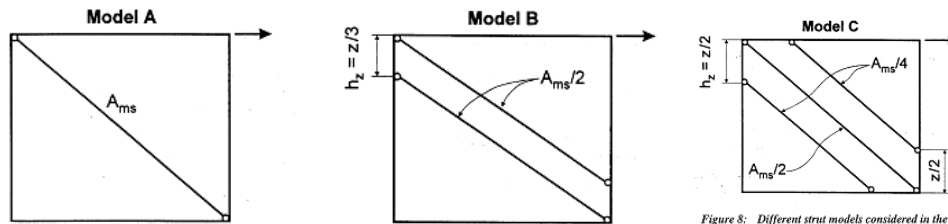


Figure 4 Proposed model for study by [19]

Further [19] proposed a new multi-strut model with shear spring as shown in Figure 5. This model accounts separately for compressive and shears behavior of masonry panel. This model depicts better the shear failure along mortar joints or diagonal tension failure when expected. The stiffness for whole masonry panel is divided into shear and axial compressive strut. This model is implemented in Ruaumoko (Carr, 2002) and SeismoStruct [25] software

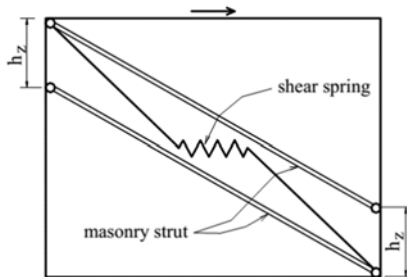


Figure 5 Crisafulli & Carr (2007) model

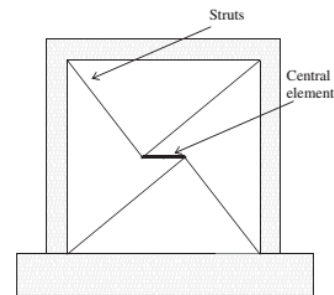


Figure 6 Rodrigues et al. (2010) model

Rodrigues [26] proposed an improved equivalent bi-diagonal compression strut model with a central strut element for representation of hysteretic behavior of masonry infill panels (Figure 6). Masonry panel is defined by 4-strut elements having rigid behavior and a central element where nonlinear hysteretic behavior is concentrated. This central element has purely compressive or tensile nature. The proposed model considers hysteretic behavior, strength and stiffness degradation, pinching, damage evolution and function of deformation demands, and implemented in Open Sees [27].

Samoilă [28] investigated several formulations for width of equivalent diagonal strut present in literature to find the best model. It has been concluded that the Paulay [10] formulation is the most appropriate choice, due to its consistency and simplicity.

Islam [29] used an open source computer program, STERA 3D to model infill frame with macro-element masonry (IFM2). They also discretized using a combination of nonlinear bending and shear springs together with axial and shear spring for frames and infills, respectively. A good match in the dataset was observed as the model was validated with existing literature.



Saneinejad and Hobbs [30] developed an inelastic analysis and design method using an equivalent diagonal strut for infill steel frames. Kakaletsis and Karayannis [31], also used equivalent strut model to assess the lateral resistance of masonry infilled RC frames with openings. Thiruvengadam [24] and Chrysostomou [32] introduced multiple struts to model infill walls and Klingner and Bertero [33] studied the behavior of RC block infilled reinforced concrete frames under cyclic loading. El-Dakhkhni [34] suggested the stiffness and the ultimate load capacity of concrete masonry infilled steel frames failed by corner crushing using an analytical approach. Mohyeddin [35] showed that even for same infill frames the strut properties can change for different values and location and number of struts can vary from infill to infill. Kareem and Panto [36] compared existing strut model and introduced 2D discrete macro model.

Srechai [37] developed a multistrut model based on experimental tests. Fiber-section truss elements are used for struts and equivalent stress-strain parameters were used to incorporate all potential failure modes. Empirical formulas were developed and calibrated based on experimental and statistical analysis. Their reliability was assessed through blind validation tests of empirical formulas and proposed model. Monotonic and cyclic load simulations of the infilled RC frames for single and multiple bays were conducted and compared with experimental results.

### 3 Micro Models

In micro-modeling, infill panels are modeled at different levels in detail using finite elements: mortar, bricks, and mortar/brick interface (Figure 7). It shows the behavior at local level so all possible modes of failure can be observed. It is the most accurate representation of infill panel behavior. But the computation time is high for large structures and numerous parameters need calibration.

Micro modeling can be further divided into three levels. The basic idea behind these levels is the variation in computational effort and accuracy [38].

1. Detailed Micro Modeling: In this approach, the continuum elements are used to model brick and mortar joints whereas interface between the brick and mortar is modelled by an interface discontinuous element.
2. Simplified Micro Modeling: In this approach, the continuum elements also known as expanded units are used to model bricks and joint and brick mortar interface is modeled using an interface element at mid thickness of mortar layer.
3. Homogenized Modeling: In this method, brick, mortar, and their interface is modeled as a homogenous continuum.

The level of micro modeling depends on level of refinement required in the research. The detailed micro-modeling approach is the most comprehensive approach in all modeling. It is precise for studying the local behavior of infill panels for both linear and non-linear behavior. But its modeling requires high level of knowledge of different parameters which require large number of tests. Apart from this, its computation time is highly consuming. On the other hand, the simplified micro-modeling or homogenized modeling is accurate for computing linear behavior of infills.

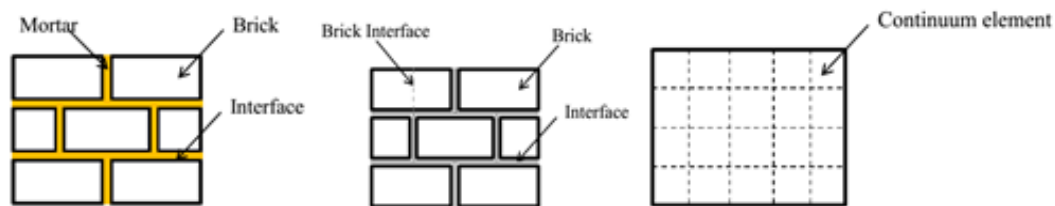


Figure 7 a) Detailed Micro Modeling b) Simplified Micro Modeling c) Homogenized Modeling

Several researchers worked on finite element modeling and presented different constitutive models to represent each unit of masonry wall. Firstly, Mallick [39] applied finite element approach as a micro modeling to address the issue of representing interface between frame and infill. It was modeled by contact elements but was not able to transfer tensile forces. Liauw [40] proposed a plastic approach in which three separate types of elements were used to study the behavior of infill frames. Three failure modes were identified which captures the corner crushing with failure in columns, beams and diagonal crushing of the infill.



A very close agreement has been observed between experimental and analytical results. Achyutha [41] investigated the elastic behavior of single storey infilled frame with opening. Slip, separation and contact conditions were modeled by single link elements at interface. The opening was also modeled by using very low value of thickness and modulus of elasticity of masonry. It was found that larger the opening, lesser will be the lateral stiffness of the structure. Dhanasekar [42] developed a model for brick masonry wall in which non-linear isotropic six-node elements were used for both the mortar and the bricks. The mortar joints are modeled as one-dimensional joint elements between infill and frame. Ali [43] proposed a finite element model similar to [42] having 4-node quadrilateral elements with a finer mesh near the loading point. This proposed model can be used for any brick mortar combination with any bond pattern. Mehrabi [8] proposed a complex constitutive model for modeling masonry joints interfaces. Compressive hardening behavior, the reversal of shear dilatancy, and the normal contraction of cementitious interfaces can be accounted in the proposed constitutive model. They used smeared cracked finite element model. It was concluded that the model can capture failure mechanisms and can approximate the lateral resistance of the frame. Syrmakizis [44] proposed a new finite element technique in which the frame-infill separation criterion is used to find the geometrical equilibrium condition. The basic difference of the analysis was that the contact lengths and stresses were estimated as an integral part of the solution. Stavridis presents a FEM scheme for assessing the nonlinear load-deformation behavior and failure mechanisms of masonry infilled RC frames through combination of the discrete and smeared-crack modeling approaches. Dorji [45] used gap element to model the interface between infill and frame. Mohyeddin [35] proposed a simplified micro-model where brick and mortar were modeled as a single smeared material and the mortar joints were modeled as zero-thickness interfaces or contact joints. Bhagyashri [46] studied two types of micro modelling techniques i.e. gap and link element method that were earlier proposed by Dorji [47] and Achutya [41]. It was concluded that both method give same results so they can be used in any FE software. Mohammad [42] proposed micro model parameters that were incorporated in ATENA software and were verified with existing results proposed by [6] for variant configuration of infill walls.

#### **4 Research Significance**

The significance of this work holds in the fact that although infills are not considered structural members they affect the structure's mass and lateral rigidities. Hence, to fully understand the behavior of the free vibration of the structure under seismic loads their contribution towards the behavior of frame shall not be neglected. Previously modeling infills and incorporating their contribution within the frame was a rather complex method. Studying the literature reveals that there are less complicated ways to include the effect of infills without compromising much on the overall behavior of the frames under dynamic loads. Thus, it is important to understand how these modeling methods are applied and which behavioral aspect of infilled frame can be covered by a certain technique. This research study gives an insight into all the modeling techniques which shall be included within the design in near future.

#### **5 Conclusion**

Extensive review of the existing studies that were proposed to model masonry infills to depict its behavior properly has brought following conclusions:

- Masonry infill significantly increase lateral strength and stiffness of the structures changing their time periods and mode shapes, consequently increasing the risk of collapse. Hence, they shall be incorporated in analysis to fully comprehend the behavior of masonry infilled RC frames;
- Despite of significant research, still infill walls are not considered while designing, though now researchers have started incorporating them into analysis. And it is revealed that incorporating them can be done at Macro, Micro or Meso levels, each having their own level of complexity;
- Macro modelling approach is easier and simpler as compared to micro modelling. However, it depicts only global behavior. Whereas, micro-modelling is time consuming and require large computations, but it captures failure modes and infill- frame interaction effects.

#### **Acknowledgment**

The authors would like to thank department of earthquake engineering who helped thorough out the research work. The careful review and constructive suggestions by the anonymous reviewers are gratefully acknowledged.



## References

- [1] S. Roosta and Y. Liu, "Development of a Macro-Model for concrete masonry infilled frames," *Eng. Struct.*, vol. 257, p. 114075, Apr. 2022, doi: 10.1016/J.ENGSTRUCT.2022.114075.
- [2] M. Donà, M. Minotto, N. Verlatto, and F. da Porto, "A new macro-model to analyse the combined in-plane/out-of-plane behaviour of unreinforced and strengthened infill walls," *Eng. Struct.*, vol. 250, p. 113487, Jan. 2022.
- [3] D. V MALLICK and R. T. SEVERN, "The Behaviour Of Infilled Frames Under Static Loading," *Proceedings of Institution of Civil Engineers*, vol. 38, no. 4, pp. 639–656, Jun. 2015.
- [4] M. HOLMES, "Steel Frames With Brickwork And Concrete Infilling.," vol. 19, no. 4, pp. 473–478, Jun. 2015,
- [5] B. S. Smith, "Lateral Stiffness of Infilled Frames," *J. Struct. Div.*, vol. 88, no. 6, pp. 183–199, Dec. 1962,
- [6] B. S. Smith, "Behavior of Square Infilled Frames," *J. Struct. Div.*, vol. 92, no. 1, pp. 381–404, Feb. 1966,
- [7] R. MAINSTONE, "Summary Of Paper 7360. On The Stiffness And Strengths Of Infilled Frames.," vol. 49, no. 2, p. 230, Jun. 2015,
- [8] A. B. Mehrabi, P. B. Shing, M. P. Schuller, and J. L. Noland, "Experimental Evaluation of Masonry-Infilled RC Frames," *J. Struct. Eng.*, vol. 122, no. 3, pp. 228–237, Mar. 1996, doi: 10.1061/(ASCE)0733-9445(1996)122:3(228).
- [9] MRA Kadir, "The structural behaviour of masonry infill panels in framed structures." PhD Thesis, University of Edinburgh, UK 1974
- [10] Paulay, T., & Priestley, M. J. N. "Seismic Design of Reinforced Concrete and Masonry Buildings." John Wiley & Sons, New York, 1997.
- [11] K. H. Kwan and T. C. Liauw, "Nonlinear analysis of integral infilled frames," *Eng. Struct.*, vol. 6, no. 3, pp. 223–231, Jul. 1984, doi: 10.1016/0141-0296(84)90049-X.
- [12] L. Decanini, F. Mollaioli, A. Mura, and R. Saragoni, "3 th World Conference on Earthquake Engineering Seismic Performance Of Masonry Infilled R/C Frames".
- [13] J. L. Dawe and C. K. Seah, "Analysis of concrete masonry infilled steel frames subjected to in-plane loads". In Proceeding of the 5th Canadian Masonry Symposium (pp. 329–40). Vancouver.
- [14] "Seismic retrofit of flat-slab buildings with masonry infills | In. Abrams, Daniel P., ed. Proceedings from the NCEER workshop on seismic response of masonry infills. Buffalo, N.Y, National Center for Earthquake Engineering Research, Mar. 1994. p.1-8, ilus, Tab. (Technical Report, NCEER 94-0004). | DESASTRES."
- [15] A. G. Amato, M. Fossetti, L. Cavaleri, and M. Papia, "An updated model of equivalent diagonal strut for infill panels," *Eurocode 8 Perspect. from Ital. Standpoint Work.*, no. January 2014, pp. 119–128, 2008.
- [16] A. Chethan, K and Babu, R Ramesh and Venkataramanna, Katta and Sharma, "Study on Dynamic Characteristics of 3D Reinforced Concrete Frame with Masonry Infill," *Power Res.*, vol. 5, pp. 11–18, 2009.
- [17] M. Yekrangnia and M. Mohammadi, "A new strut model for solid masonry infills in steel frames," *Eng. Struct.*, vol. 135, pp. 222–235, Mar. 2017, doi: 10.1016/J.ENGSTRUCT.2016.10.048.
- [18] M. Kumar, F. Khalid, and N. Ahmad, "Macro-modelling of reinforced concrete frame infilled with weak masonry for seismic action," *NED University J. Res.*, vol. 15, no. January, pp. 15–38, 2018.
- [19] F. J. Crisafulli and A. J. Carr, "Proposed macro-model for the analysis of infilled frame structures," *Bull. New Zeal. Soc. Earthq. Eng.*, vol. 40, no. 2, pp. 69–77, Jun. 2007, doi: 10.5459/bnzsee.40.2.69-77.
- [20] C. A. Syrmakzevis and V. Y. Vratsanou, "Influence of infill walls to RC frames response," in *8th European conference on earthquake engineering, Istanbul, Turkey*, 1986, pp. 47–53.
- [21] "Effects of degrading infill walls on the nonlinear seismic response of two-dimensional steel frames - ProQuest."
- [22] A. San Bartolomé, "Colección del Ingeniero Civil," *Libro*, no. 4, 1990.
- [23] W. W. El-Dakhkhni, M. Elgaaly, and A. A. Hamid, "Three-Strut Model for Concrete Masonry-Infilled Steel Frames," *J. Struct. Eng.*, vol. 129, no. 2, pp. 177–185, 2003, doi: 10.1061/(asce)0733-9445(2003)129:2(177).
- [24] V. Thiruvengadam, "On the natural frequencies of infilled frames," *Earthq. Eng. Struct. Dyn.*, vol. 13, no. 3, pp. 401–419, May 1985, doi: 10.1002/EQE.4290130310.
- [25] "Seismosoft Earthquake Engineering Software Solutions - Seismosoft." <https://seismosoft.com/> (accessed Jun. 30, 2022).
- [26] H. Rodrigues, H. Varum, and A. Costa, "Simplified Macro-Model for Infill Masonry Panels," vol. 14, no. 3, pp. 390–416, Mar. 2010,
- [27] "OpenSees | Pacific Earthquake Engineering Research Center." <https://peer.berkeley.edu/opensees> (accessed Jun. 30, 2022).
- [28] T. Kalman Šipoš and V. Sigmund, "Comparison of Non-Linear Masonry Infill Macro-Models," *Elektron. časopis građevinskog Fak. Osijek*, vol. 55, no. 2, pp. 44–55, 2014, doi: 10.13167/2014.8.6.
- [29] M. T. Islam, S. Noor-E-Khuda, and T. Saito, "A simple infill frame with macro element masonry model for the in-plane performance of infill walls," *Structures*, vol. 42, pp. 386–404, Aug. 2022, doi: 10.1016/J.ISTRUC.2022.06.014.
- [30] A. Saneinejad and B. Hobbs, "INELASTIC DESIGN OF INFILLED FRAMES".
- [31] D. J. Kakaletsis and C. G. Karayannis, "Influence of Masonry Strength and Openings on Infilled R/C Frames Under Cycling Loading," <http://dx.doi.org/10.1080/13632460701299138>, vol. 12, no. 2, pp. 197–221, Feb. 2008, doi: 10.1080/13632460701299138.
- [32] "Effects of degrading infill walls on the nonlinear seismic response of two-dimensional steel frames - ProQuest.>").
- [33] R. E. Klingner and V. V. Bertero, "Earthquake Resistance of Infilled Frames," *J. Struct. Div.*, vol. 104, no. 6, pp. 973–989, Jun. 1978,



- [34] W. El-Dakhkhni, W. W. El-Dakhkhni, M. Elgaaly, and A. A. Hamid, "Three-Strut Model for Concrete Masonry-Infilled Steel Frames Capacitance Sensor View project Drought Proneness Analysis of Southern Saskatchewan Province Using Markov Chain Model View project THREE STRUT MODEL FOR CONCRETE MASONRY-INFILLED STEEL FRAMES," 2003, doi: 10.1061/(ASCE)0733-9445(2003)129:2(177).
- [35] A. Mohyeddin, S. Dorji, E. F. Gad, and H. M. Goldsworthy, "Inherent limitations and alternative to conventional equivalent strut models for masonry infill-frames," *Eng. Struct.*, vol. 141, pp. 666–675, Jun. 2017
- [36] K. M. Kareem and B. Pantò, "Simplified macro-modelling strategies for the seismic assessment of non-ductile infilled frames: a critical appraisal," *J. Build. Eng.*, vol. 22, pp. 397–414, Mar. 2019
- [37] J. Srechai, S. Leelataviwat, W. Wararuksajja, and S. Limkatanyu, "Multi-strut and empirical formula-based macro modeling for masonry infilled RC frames," *Eng. Struct.*, vol. 266, p. 114559, Sep. 2022
- [38] F. Di Trapani, G. Macaluso, L. Cavaleri, and M. Papia, "Masonry infills and RC frames interaction: literature overview and state of the art of macromodeling approach," *Eur. J. Environ. Civ. Eng.*, vol. 19, no. 9, pp. 1059–1095, Oct. 2015
- [39] MALLICK DV and GARG RP, "effect of openings on the lateral stiffness of infilled frames," <https://doi.org/10.1680/iicep.1971.6263>, vol. 49, pp. 193–209, Jun. 2015, doi: 10.1680/IICEP.1971.6263.
- [40] L. Te-Chang and K. Kwok-Hung, "Nonlinear behaviour of non-integral infilled frames," *Comput. Struct.*, vol. 18, no. 3, pp. 551–560, Jan. 1984.
- [41] H. Achyutha, R. Jagadish, P. S. Rao, and S. S. Rahman, "Finite element simulation of the elastic behaviour of infilled frames with openings," *Comput. Struct.*, vol. 23, no. 5, pp. 685–696, Jan. 1986.
- [42] M. Dhanasekar and A. W. Page, "The influence of brick masonry infill properties on the behaviour of infilled frames.," <https://doi.org/10.1680/iicep.1986.463>, vol. 81, no. pt 2, pp. 593–605, Jun. 2015, doi: 10.1680/IICEP.1986.463.
- [43] S. S. Ali and A. W. Page, "Finite Element Model for Masonry Subjected to Concentrated Loads," *J. Struct. Eng.*, vol. 114, no. 8, pp. 1761–1784, Aug. 1988, doi: 10.1061/(ASCE)0733-9445(1988)114:8(1761).
- [44] C. A. Symakezis and P. G. Asteris, "Masonry Failure Criterion under Biaxial Stress State," *J. Mater. Civ. Eng.*, vol. 13, no. 1, pp. 58–64, 2001, doi: 10.1061/(asce)0899-1561(2001)13:1(58).
- [45] J. Dorji and D. P. Thambiratnam, "Modelling and Analysis of Infilled Frame Structures Under Seismic Loads," *Open Constr. Build. Technol. J.*, vol. 3, no. 2, pp. 119–126, Dec. 2009, doi: 10.2174/1874836800903020119.
- [46] P. Bhagyashri, N. Vinodh, K. Chethan, and B. P. Annapurna, "Micro Modelling of Masonry Infilled 3D RC Frames with Openings under Dynamic Loading," vol. 42, no. 3, pp. 1–16, 2022.
- [47] "Seismic performance of brick infilled RC frame structures in low and medium rise buildings in Bhutan | QUT ePrints." <https://eprints.qut.edu.au/29689/> (accessed Jun. 30, 2022).



# STRUCTURAL SYSTEMS IDENTIFICATION USING WEIGHTED TRANSMISSIBILITY OPERATOR UNDER FORCED VIBRATIONS

<sup>a</sup> *Shanza Arshad Khan\**, <sup>b</sup> *Faheem Butt*, <sup>c</sup> *Ahsan Ali*

a: Electrical Engineering Department, University of Engineering and Technology Taxila, shanza.arshad@students.uettaxila.edu.pk

b: Civil Engineering Department, University of Engineering and Technology Taxila, faheem.butt@uettaxila.edu.pk

c: Electrical Engineering Department, University of Engineering and Technology Taxila, ahsan.ali@uettaxila.edu.pk

**Abstract-** The structures are in a continuous state of deterioration due to aging, natural disasters, and other environmental agents, resulting in local or global damages after a specific time. The timely identification of such damages can prevent the huge loss of assets and it can provide an ample opportunity for repair and maintenance. Therefore the service lifespan of the structure can be enhanced by modeling the system and identifying its parameters. Operational modal analysis (OMA) is one of the efficient possible approaches for identifying an unknown, in operation structure and estimating its modal properties like mode shapes, natural frequencies, and damping ratios. Many system identification approaches are being investigated in the literature but most of them are based on time-domain system identification methods which have certain limitations. So there is a need to develop a frequency-based structural systems identification technique that provides clear modal peaks and is more efficient in suppressing fault peaks. In this work, Weighted transmissibility-based operational modal analysis (WTOMA) is applied to a three-floor structure excited by a randomly simulated earthquake. Three sensors are placed on three floors: one of them is attached to the ground floor to record the ground excitations and the remaining two are placed on two floors. The response of the structure in terms of acceleration -time is recorded. The proposed algorithm is then applied to the structural response to obtain its modal parameters.

**Keywords-** Singular values, Loading conditions, Weighted-transmissibility based OMA.

## 1 Introduction

The use of system identification(SI) methods in the civil engineering field has been increasing in recent years. The reason for this is the high success rate of the system identification methods in estimating the mathematical model. It allows civil engineers to make safer designs with the correct estimation of the mathematical model to ensure the integrity of structures. Because system identification plays a major role in reducing the gap between structural systems and their models, also it plays a major role in structural health monitoring(SHM) for damage identification. The system identification in the case of structural systems can be done in the form of obtaining structural response and identifying structural parameters. These parameters could be in the form of vibration signatures, stiffness, stress-strain energies, damping ratios, and mode shapes. In this paper SI will be used for dynamic systems, that is the structural systems that are subjected to dynamic loadings such as seismic, vehicular, wind, or impact loading. OMA is an output-only operational model analysis. It is a field of research that estimates and identifies model properties of operating structures based on output data.

This technique assumes that input to the system is white noise sequences which is the only drawback of the classical output-only techniques[1]. OMA techniques are categorized into three different classes; time domain, frequency domain, and time-frequency domain[2] [3] [4] [5]. Transmissibility is defined as a ratio of Fourier transformation of responses





located at different points in a system. [6]. Transmissibility-based OMA is an effective approach to identifying model parameters using the output data from ambient or forced vibrations. In the recent past, a new form of transmissibility that is based on power spectrum density transmissibility (PSDT) is introduced [7] to estimate modal parameters with single loading conditions. The fundamental approaches and applications of transmissibility-based system identification for structural health monitoring are discussed in [8]. A new OMA method based on combining PSDT under different load cases is proposed to enhance the robustness of current PSDT methods with non-white excitations[9].

An efficient approach based on a new concept, that is weighted transmissibility-based OMA (WTOMA) is utilized in this paper to find out and calculate the natural frequencies and mode shapes of a three-story building structure. SVD of the WTOMA matrix and calculation of averaged normalized weighted transmissibility (ANWT) functions are used to extract singular values, mode shapes, and natural frequencies of the system respectively. These functions depict clear modal peaks in the resulting spectra therefore WTOMA is an effective strategy to aid in peak picking [10]. Recently a new time-frequency domain method that combines weighted transmissibility and wavelet transform is proposed to properly identify modal properties of the numerical model under EI Centro earthquake excitation[11]. Another new approach based on deep learning enhanced image processing and PSDT is proposed to realize vibration measurements and identify natural frequencies from PSDT plots[12].

## 2 Research Methodology

### 2.1 Weighted Transmissibility Function

The Transmissibility function is obtained by taking the ratio of the Fourier transform of two output responses of a system at different locations[9].

$$T_{ij}(\omega) = \mathcal{F}\left(\frac{x_i}{x_j}\right) = \frac{X_i}{X_j} = \frac{H_{ik}(\omega)F_k(\omega)}{H_{jk}(\omega)F_k(\omega)} = \frac{H_{ik}(\omega)}{H_{jk}(\omega)} \quad (1)$$

In Weighted transmissibility, the transmissibility function gets divided by its absolute or mod value raised to some power gamma  $\gamma$ . Therefore the weighted transmissibility function is calculated as:

$$WT_{ij}(\omega) = \frac{T_{ij}(\omega)}{|T_{ij}(\omega)|^\gamma} \quad (2)$$

Whereas the weight function is given by:

$$W_{ij}(\omega) = \frac{1}{|T_{ij}(\omega)|^\gamma} \quad (3)$$

The parameter gamma “  $\gamma$  ” is chosen based on the required accuracy level. This parameter ‘ $\gamma$ ’ indicates the extent of difference that is allowed between the columns of the weighted transmissibility matrix. The weighted transmissibility matrix is given below:

$$WTM(\omega) = \begin{bmatrix} WT_{1j}^1(\omega) \cdots WT_{1j}^p(\omega) & WT_{1j}^{p+1}(\omega) \cdots WT_{1j}^N(\omega) \\ \vdots & \vdots \\ WT_{ij}^1(\omega) \cdots WT_{ij}^p(\omega) & WT_{ij}^{p+1}(\omega) \cdots WT_{ij}^N(\omega) \\ \vdots & \vdots \\ WT_{Nj}^1(\omega) \cdots WT_{Nj}^p(\omega) & WT_{Nj}^{p+1}(\omega) \cdots WT_{Nj}^N(\omega) \end{bmatrix} \quad (4)$$

here ‘j’ indicates a fixed reference DOF.

### 2.2 Weighted Transmissibility Based OMA

In this paper, a very efficient approach is investigated for the identification of the modal properties of any structure using the weighted transmissibility operator[9]. The decomposition of the weighted transmissibility matrix can be done using the SVD technique as follows[10].



$$[WTM(\omega)] = [U(\omega)][S(\omega)][V(\omega)]^H \quad (5)$$

The  $[V(\omega)]$  and  $[U(\omega)]$  are the right and left singular vectors of the transmissibility matrix. The matrix  $[S(\omega)]$  is a diagonal matrix consisting of the singular values with  $s_1(\omega) \geq s_2(\omega) \geq \dots \geq s_l(\omega)$  where “H” is representing the conjugate transpose.

By calculating the product of inverses of second singular values with different degrees of freedom obtained from  $WTM(\omega)$  can be used to calculate PIS ( $\omega$ ) function as follows:

$$PIS(\omega) = \prod_{j=1}^N \left( \frac{1}{S_2} \right)_j \quad (6)$$

Along with this, the mode shapes can also be derived by calculating the product between entities of left-most singular vectors  $[U_{1ij}(\omega)]$  and the function  $|T_{ij}(\omega)|^\gamma$  which is the inverse of the weight function  $W_{ij}(\omega)$  as follows:

$$\phi_{rij} = U_{1ij}(\omega) \frac{1}{N} \sum_{p=1}^N |T_{ij}(\omega)|^\gamma \quad (7)$$

### 3 Flowchart of the Algorithm:

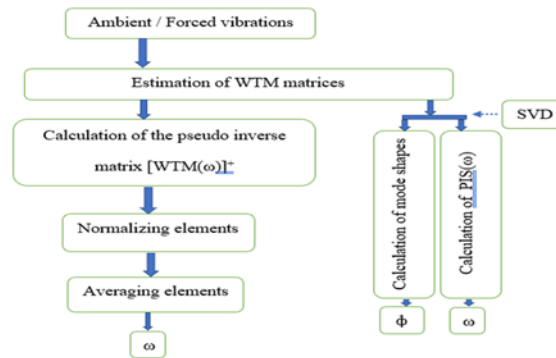


Figure 1: Flowchart of the WTOMA Algorithm

### 4 Experimental Procedures

The structure chosen for the current study is shown in Figure 2. The structure consists of three floors. The total length/width of the structure is 3600mm, the total height excluding footing is 7356mm, whereas each slab is 144 mm thick (Table 2). The total weight of the structure is 19.873 tons.

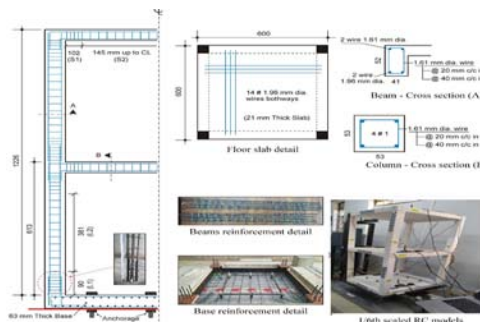


Figure 2: The prototype structure and its scaled model



Whereas the model used for analysis is obtained by scaling the structure and hence reduced model is obtained with a length/width of 600mm, a height of 1226mm, slab thickness of 23mm, and a total weight of 0.268tons. The structural scaling is performed by choosing a scale factor for each of the structure parameters and hence corresponding reduced model is shown in Table 1.

Table 1: Prototype Structural scaling details

Parameter	Scale Factor	Prototype Structure	Model (Provided)
Concrete	1	24 MPa	*Micro Concrete
Steel Reinforcement	1	Grade 60	*Grade 60
Column	Cross Section Area	36	900 cm <sup>2</sup>
	Rebar Diameter	6	19 mm
	Confinement Bar Diameter	6	10 mm
Beam 1 <sup>st</sup> Floor (B1)	Cross Section Area	36	690 cm <sup>2</sup>
	Bottom Rebar Diameter	6	19 mm
	Top Rebar Diameter	6	13 mm
	Confinement Bar Diameter	6	10 mm
Beam 2 <sup>nd</sup> Floor (B2)	Cross Section Area	36	690 cm <sup>2</sup>
	Bottom Rebar Diameter	6	13 mm
	Top Rebar Diameter	6	13 mm
	Confinement Bar Diameter	6	10 mm
Slab	6	10 mm	1.61 mm

. The dimensional details of both the prototype structure and its model are shown in Table 2.

Table 2: dimensional details of the prototype structure and its model

No.	Parameter	Prototype Structure	Model
1	Length/Width	3600 mm	600 mm
2	Height excluding footing	7356 mm	1226 mm
3	Column Size	300 mm × 300 mm	53 mm × 53 mm
4	Beam Size	230 mm × 300 mm	41 mm × 52 mm
5	Tie Beam	230 mm × 380 mm	63 mm thick footing pad
6	Slab Thickness	140 mm	23 mm
8	Weight	19.873 Tons	0.1239 Tons

## 5 Results

The results obtained through the investigated algorithm are shown below. The structure is excited by a randomly simulated earthquake. The response of the building structure i.e. acceleration – time history of the three sensors during the period of 100s is shown in Figure 3.

### 5.1 Use of Software

The software used for identifying and estimating the parameters of the structure is MATLAB.

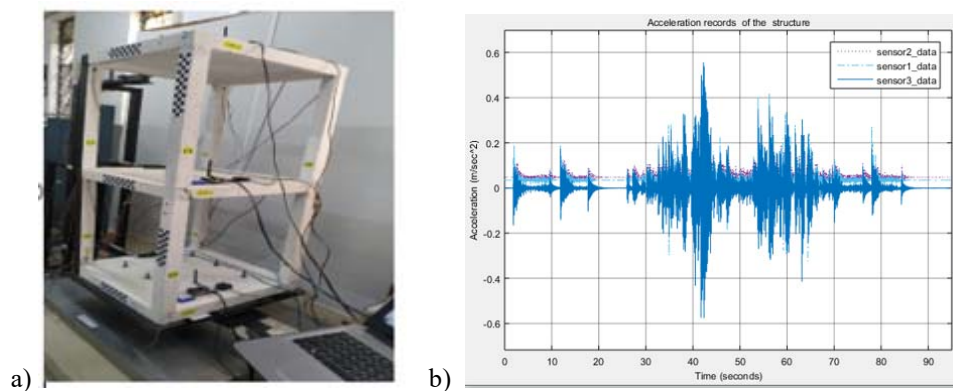


Figure 3: a. Building structure prototype with installed sensors b. sensors response time history

The first two natural frequencies obtained through the algorithm and the mode shapes corresponding to the two estimated natural frequencies are shown in Figure 4 and Figure 5.

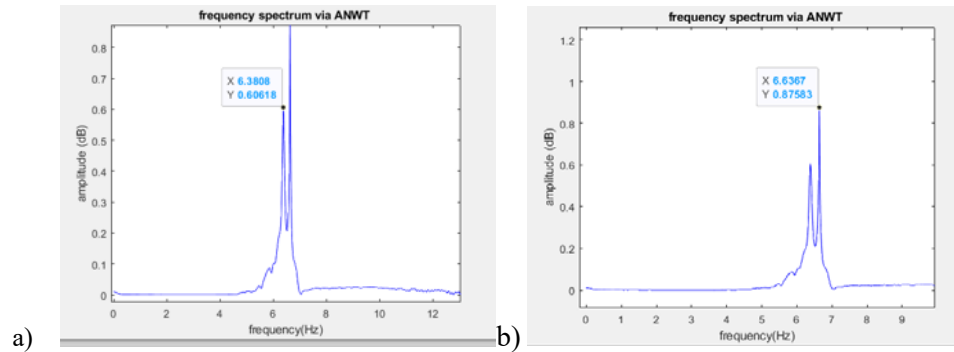


Figure 4: The natural frequencies obtained from WTOMA a. 1st natural frequency b. 2nd natural frequency

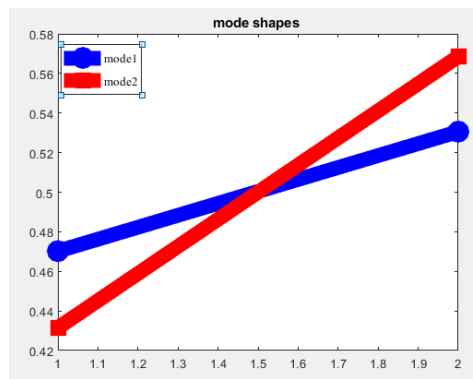


Figure 5: The mode shapes corresponding to the two frequencies

## 5.2 Comparison Of Results :

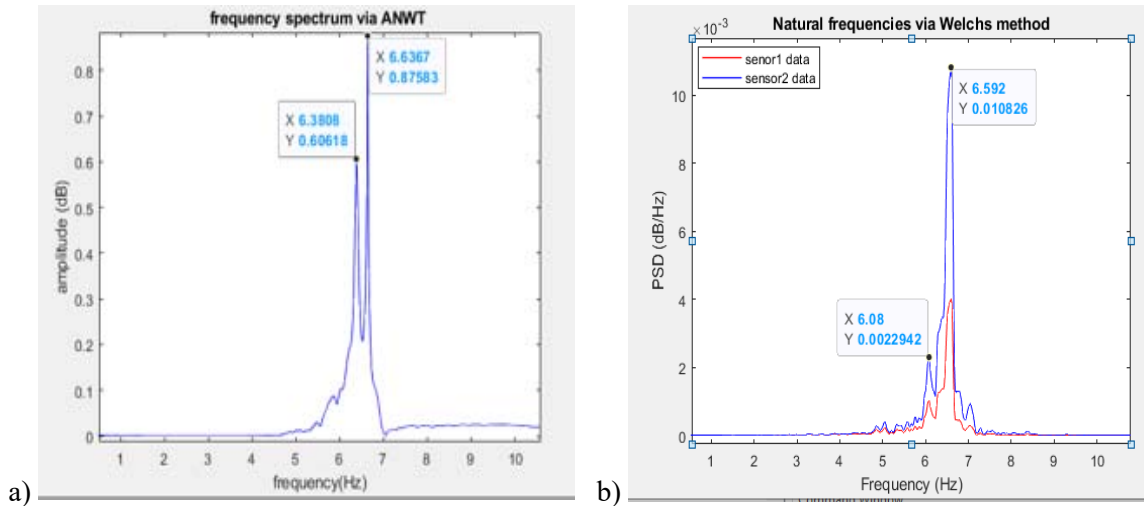


Figure 6: Comparison of a. WTOMA and b. Welch's averaged PSD

The results are compared with Welch's averaged PSD estimates, the frequencies obtained through the WTOMA algorithm are 6.38084Hz and 6.6367Hz respectively while the frequencies obtained from Welch's averaged are 6.08Hz and 6.592Hz respectively. As it can be seen that Welch's method suffers from noise sensitivity hence many false peaks are seen in the PSD plot. Whereas the WTOMA algorithm is more effective in displaying spectral peaks with strength and clarity. Along with this false peaks are minimized to a much extent and there is less spectral leakage as compared to Welch's averaged PSD.



## 6 Utilization Of Research Results:

The method can be used for identifying and estimating model parameters in real-time in operating systems such as bridges, buildings, and other engineering structures. The outcome of this research can be used for the prediction of structural failures and damage detection in the field of SHM.

## 7 Conclusion

The following conclusions can be drawn from the study conducted in this paper:

1. Spectral leakage is minimized hence strong and clear peaks occur in the resulting spectra.
2. Reduced noise sensitivity hence fewer false peaks.
3. Clearer mode shapes are obtained.

The results demonstrate that WTOMA is more effective in identifying modal parameters of a structure as it aids in the peak picking process hence strong spectral peaks occur in the resulting spectra. False peaks are minimized to a much extent and clearer mode shapes are obtained. Whereas Welch's method is more sensitive to noise and the concept of windowing function creates spectral leakages. Lower model order results in smoothing while higher order induces false peaks in Welch's method.

## Acknowledgment

The authors would like to thank Dr. Syed Saqib Mehboob from UET Taxila who provided the structural data to carry out this research. The careful review and constructive suggestions by the anonymous reviewers are gratefully acknowledged. The expertise has improved this study in many ways.

## References

- [1] C. Devriendt, G. De Sitter, S. Vanlanduit, P. J. M. s. Guillaume, and s. processing, "Operational modal analysis in the presence of harmonic excitations by the use of transmissibility measurements," vol. 23, no. 3, pp. 621-635, 2009.
- [2] B. Peeters and G. J. J. D. S. De Roeck, Meas., Control, "Stochastic system identification for operational modal analysis: a review," vol. 123, no. 4, pp. 659-667, 2001.
- [3] L. Zhang and R. Brincker, "An overview of operational modal analysis: major development and issues," in *Proceedings of the 1st International Operational Modal Analysis Conference, April 26-27, 2005, Copenhagen, Denmark, 2005*, pp. 179-190: Aalborg Universitet.
- [4] W. Weijtjens, J. Lataire, C. Devriendt, and P. Guillaume, *Transmissibility based OMA for time-varying loading conditions*. 2014.
- [5] R. Tarinejad, M. J. M. s. Damadipour, and s. processing, "Extended FDD-WT method based on correcting the errors due to non-synchronous sensing of sensors," vol. 72, pp. 547-566, 2016.
- [6] C. Devriendt and P. Guillaume, "Identification of Modal Parameters from Transmissibility Measurements," *Journal of Sound and Vibration*, vol. 314, pp. 343-356, 07/01 2008.
- [7] W. J. Yan, W. X. J. C. A. C. Ren, and I. Engineering, "Operational modal parameter identification from power spectrum density transmissibility," vol. 27, no. 3, pp. 202-217, 2012.
- [8] W.-J. Yan, M.-Y. Zhao, Q. Sun, and W.-X. Ren, "Transmissibility-based system identification for structural health Monitoring: Fundamentals, approaches, and applications," *Mechanical Systems and Signal Processing*, vol. 117, pp. 453-482, 2019/02/15/ 2019.
- [9] J. Kang, "Operational modal analysis method by combining power spectral density transmissibility functions under different load cases," *Mechanical Systems and Signal Processing*, vol. 180, p. 109433, 2022/11/15/ 2022.
- [10] M. Damadipour, R. Tarinejad, and M. H. Aminfar, "Weighted Transmissibility-Based Operational Modal Analysis for Identification of Structures Using Seismic Responses," *Iranian Journal of Science and Technology, Transactions of Civil Engineering*, vol. 45, no. 1, pp. 43-59, 2021/03/01 2021.
- [11] M. Damadipour and R. Tarinejad, "Structural system identification based on combining weighted transmissibility and wavelet transform," vol. 29, no. 2, p. e2868, 2022.
- [12] Z.-W. Chen, X.-Z. Ruan, K.-M. Liu, W.-J. Yan, J.-T. Liu, and D.-C. J. A. i. S. E. Ye, "Fully automated natural frequency identification based on deep-learning-enhanced computer vision and power spectral density transmissibility," p. 13694332221107572, 2022.



# STRENGTH PREDICTING OF FLY ASH-BASED CONCRETE VIA MACHINE LEARNING ALGORITHMS

*<sup>a, b</sup> Ayaz Ahmad \*, <sup>a, b</sup> Yadong Jiang, <sup>a, b</sup> William Finnegan*

a: Civil Engineering, School of Engineering, College of Science & Engineering, National University of Ireland, Galway, University Road, Galway, Ireland, [a.ahmad8@nuigalway.ie](mailto:a.ahmad8@nuigalway.ie); [yadong.jiang@nuigalway.ie](mailto:yadong.jiang@nuigalway.ie); [william.finnegan@nuigalway.ie](mailto:william.finnegan@nuigalway.ie);  
b: MaREI Centre, Ryan Institute, National University of Ireland, Galway, University Road, Galway, Ireland.

**Abstract-** The application of the support vector machine (SVM) and random forest (RF) algorithms to anticipate the compressive strength of fly ash-based concrete has been investigated in the study. A predictive performance comparison was performed for these two algorithms, where statistical metrics, such as coefficient of determination ( $R^2$ ), mean square error (MSE), root mean square error (RMSE), and mean absolute error (MAE), were used for the evaluation. The results reveal that the RF algorithm outperforms the support vector machine model in terms of predicting the compressive strength of concrete containing fly ash. The statistical checks and the investigation of k-fold cross validation also give confirmation of higher precision for the random forest model. The employed machine learning approaches successfully predicted the strength property of selected concrete and gives the indication that it can reduce the time, experimental efforts, and cost of the construction projects.

**Keywords-** concrete; fly ash; machine learning; modelling; validation.

## 1. Introduction

Portland cement is one of the most widely utilized ingredients in the concrete industry [1]. It is essential for developing the infrastructure required for social and economic growth but has a harmful influence on the environment [1, 2]. Cement manufacture results in substantial use of natural resources and substantial carbon dioxide ( $CO_2$ ) emissions [3, 4]. In addition, it is widely known that  $CO_2$  contributes to global warming. A few products or residues generated by various industrial sectors can react with calcium hydroxide to form calcium silicate hydrates similar to those formed during cement hydration [5-7]. These calcium silicate hydrates are referred to as pozzolans because they possess similar properties to Portland cement [8, 9]. The application of pozzolana in concrete can minimize the quantity of cement in it, which is one of the major causes of  $CO_2$  emission [10, 11]. Therefore, its use as a cement replacement appears to be a potential way to mitigate these issues [12]. The cement industry is responsible for around 8–10 percent of the world's anthropogenic  $CO_2$  emissions [13]. As the demand for construction materials in the developing world continues to rise, this level of output is becoming increasingly troublesome, and future developments are required for the construction sector to become ecologically sustainable [14, 15].

Fly ash (FA), a byproduct of burning coal, is now frequently used as a cement component in concrete, along with other pozzolans [16-18]. FA is also acknowledged as an environmentally benign substance because the use of this material helps to reduce the cement industry's overall carbon footprint [19]. Application of FA in concrete material as a partial replacement of binding material plays a positive role in reducing the emission of  $CO_2$  gasses [20, 21]. This approach not only helps to produce an environmentally friendly concrete but also fulfill the strength and durability requirements of the concrete [22].

Machine learning (ML) algorithms are widely using to forecast the strength properties of different types of concrete [23-25]. The connection of artificial intelligence with the field of engineering is of great interest for the researchers [26]. This approach not only reduces the effort of experiments but also minimizes the cost of the project [27]. A variety of ML



techniques such as bagging, decision tree, random forest (RF), multilayer perceptron, and gene expression programming are widely using for predicting the required outputs.

Investigating how well machine learning algorithms can predict outcomes is the purpose of this study. In order to forecast the compressive strength of selected concrete, both the support vector machine (SVM) and the RF approaches have been investigated. In order to validate the validity of the model, statistical checks and a method known as k-fold cross validation were incorporated. To estimate the compressive strength of fly ash-based concrete, this study makes use of two distinct kinds of algorithms—a single-label machine learning approach (SVM) and a multi-label machine learning ensemble technique (RF)—in order to break new ground. This approach is the primary innovation of the study. While individual techniques execute the model in the conventional fashion, an ensemble machine learning approach divides the actual models into a number of sub-models.

## 2. Materials and method

Python coding was introduced in the software for each employed ML technique to run the models. The data set used for the models was retrieved from the literature [24]. The comparison between the experimental result and the result obtained from the models was shown with the regression graphs, while the amount of difference between both the results was indicated with the error distribution graphs. The software automatically splits the data set into 80 percent for training the model and 20 percent for testing the model. However, k-fold cross validation approach was adopted for validation purpose. All the ingredients used to prepare the concrete materials were taken as the input parameters, and the result of the strength was taken as the output parameter. The descriptive statistics of the input parameters taken from the mentioned literature are listed in Table 1. However, the relative frequency distribution for the same parameters can be seen in Figure 1.

Table 1. Descriptive statistics of the variables

Parameters	Cement (kg/m <sup>3</sup> )	Fly ash (kg/m <sup>3</sup> )	Water (kg/m <sup>3</sup> )	SP (kg/m <sup>3</sup> )	CA (kg/m <sup>3</sup> )	FA (kg/m <sup>3</sup> )	Age (days)
Mean	282.13	77.29	180.95	5.45	1003.76	794.19	44.50
Standard Error	3.78	2.46	0.72	0.21	2.90	2.71	2.34
Median	252.00	100.40	185.70	5.70	1006.40	794.90	28.00
Mode	213.50	0.00	192.00	0.00	968.00	613.00	28.00
Standard Deviation	94.88	61.91	17.97	5.28	72.84	68.18	58.66
Sample Variance	9001.86	3832.72	322.86	27.89	5305.62	4648.69	3441.28
Range	405.30	200.10	88.00	28.20	324.00	351.00	364.00
Minimum	134.70	0.00	140.00	0.00	801.00	594.00	1.00
Maximum	540.00	200.10	228.00	28.20	1125.00	945.00	365.00
Sum	178026.90	48768.30	114176.60	3439.70	633370.90	501134.40	28082.00
Count	631.00	631.00	631.00	631.00	631.00	631.00	631.00

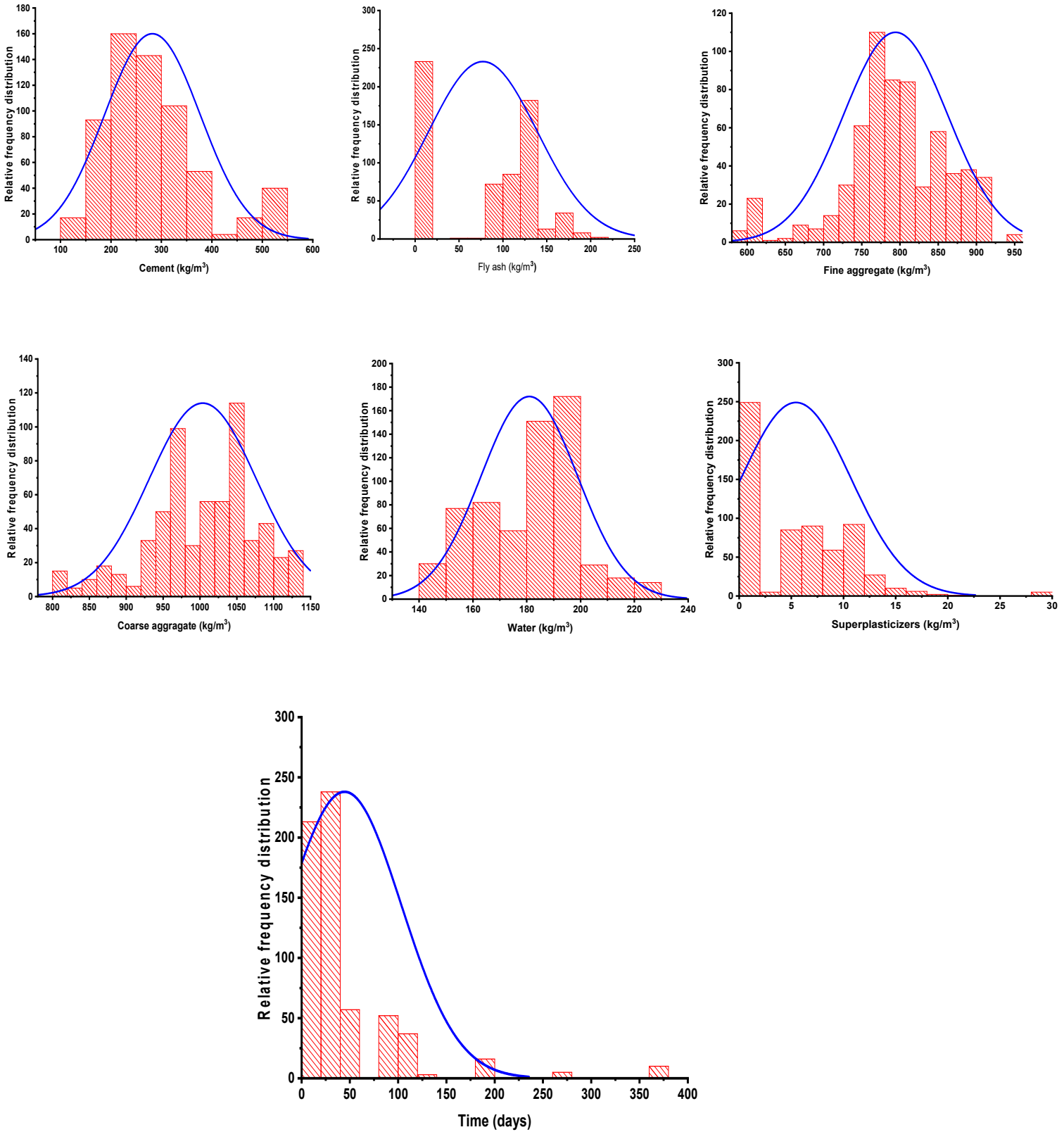


Figure 1. Relative frequency dispersal of the variables used for running the models





### 3. Employed Algorithms

A linear model that can be used for classification and regression issues is known as an SVM [28]. It is effective for a wide variety of real-world challenges and can solve both linear and non-linear issues. The basic notion of SVM is as follows: The algorithm draws a line or a hyperplane that divides the data into the appropriate categories. In recent years, one of the most effective machine learning approaches has been SVMs. SVMs have been successfully applied to numerous engineering related applications, including those of the petroleum and mining industries.

RF is a type of classification technique that is made up of several different decision trees [29]. When building each individual tree, it employs bagging and feature randomness to try to produce an uncorrelated forest of trees whose prediction by committee is more accurate than that of any individual tree. This forest of trees would then be used to make a prediction. This is among the most important aspects of the RF Algorithm, as it can handle a data set containing both continuous variables, which is used in the case of regression and categorical variables for classification. This capability is one of the most significant characteristics of the Random Forest Algorithm. The outcomes of categorization issues are improved, as a result of its use.

#### 3. 4. Result and discussion

##### 4.1. SVM algorithm's outcome.

The relationship between the experimental result for compressive strength (C-S) and the result obtained from the SVM model is depicted in the upper part of Figure 2 (a). The fact that the  $R^2$  value is equal to 0.95 demonstrates that the relationship is both reasonable and strong. Figure 2 (b), on the other hand, illustrates the disparity between the observed C-S data and the predicted data. The difference between these two values demonstrates that the highest value is equal to 9.16 MPa, while the lowest value that was reported was equal to 0 MPa.

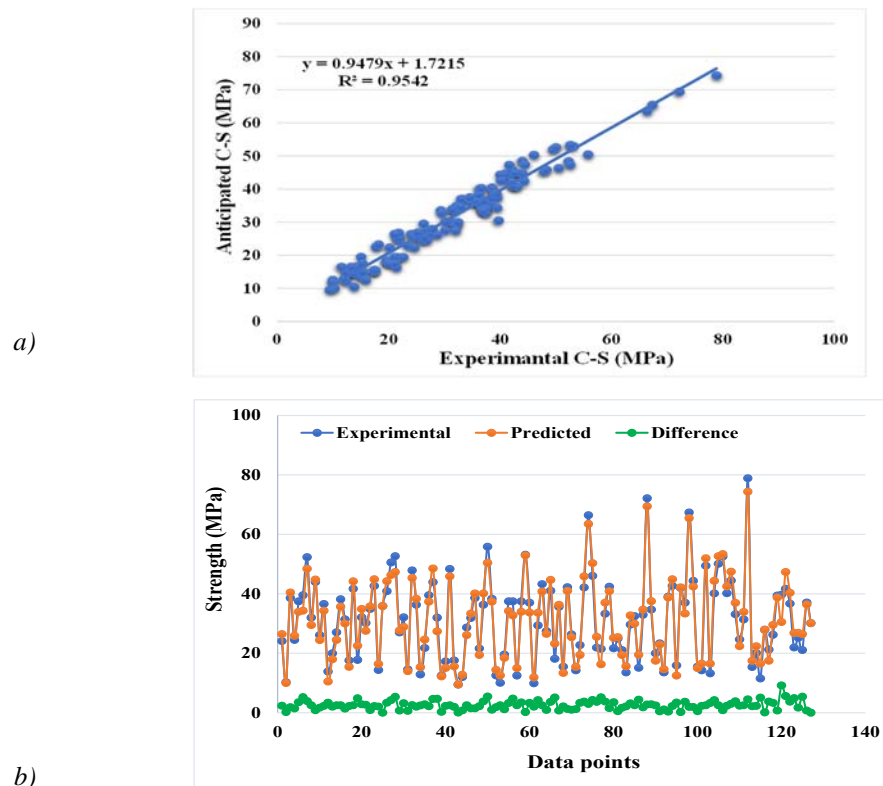


Figure 2. Regression and error's graphs: (2a) Experimental and predictive result's relationship of the C-S from SVM model; (2b) Difference of the predictive results and experimental C-S results from SVM model



#### 4.2. RF algorithm's outcome.

Figure 3 illustrates the relationship that exists between the actual C-S and the output that the model produces for the C-S. (a). When compared to the output of the SVM model, this relationship reveals a predictive result that is both more effective and accurate, as indicated by the R2 value, which is equal to 0.97. Figure b presents the error distribution that pertains to the RF model, which is another point of interest (b). This dispersal has a range of values, the lowest of which is 0.0092 MPa and the highest of which is 8.32 MPa.

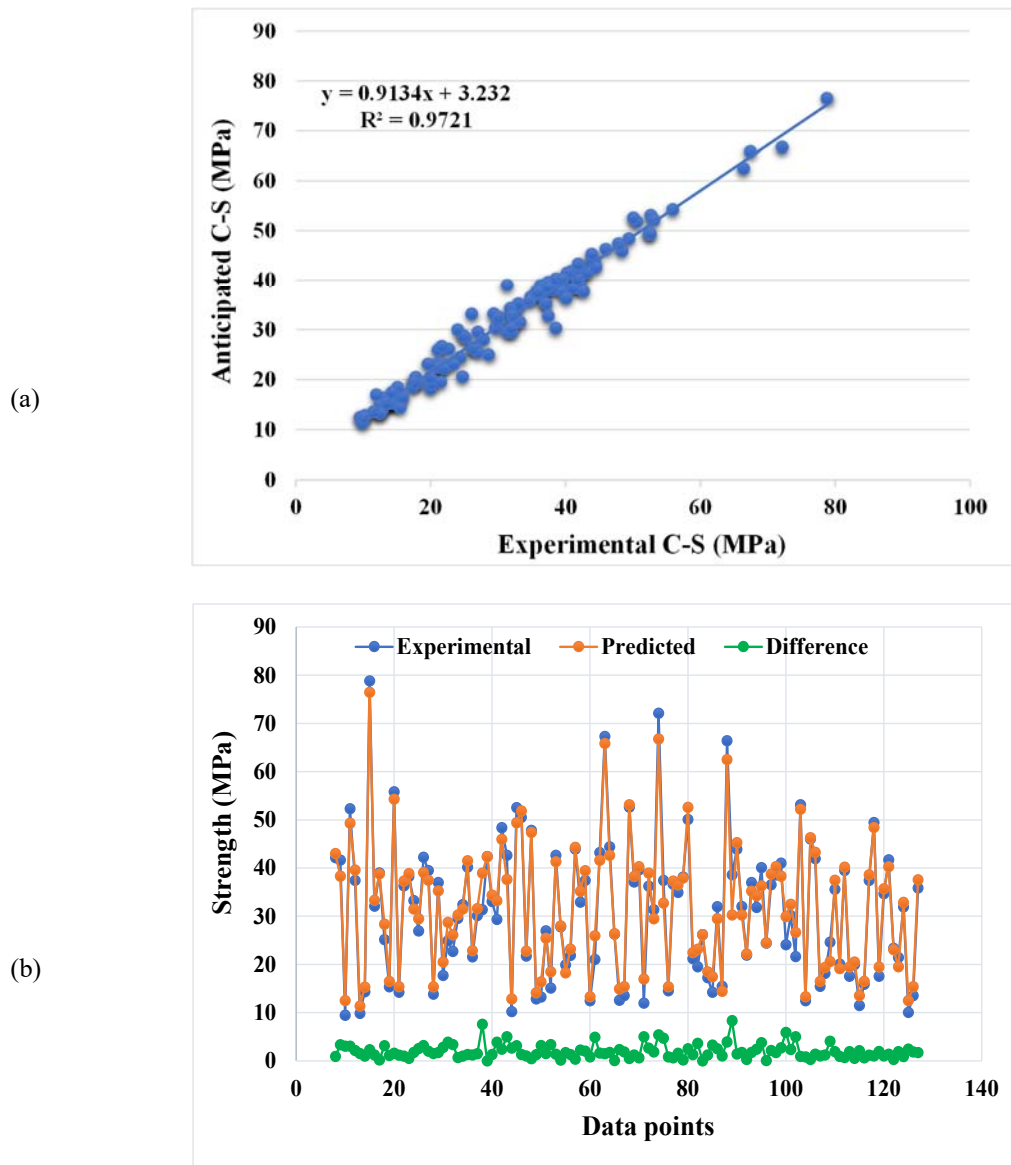


Figure 3. Regression and error's graphs: (3a) Experimental and predictive result's relationship of the C-S from RF model; (3b) Difference of the predictive results and experimental C-S results from RF model

## 5. K-fold cross validation (CV)

This method was used to validate the employed models. The legitimacy of the models was confirmed by the adoption of the CV approach. It uses nine out of ten subsets, with the exception of one subset that is utilized for the purpose of model



validation. The results of the C-V analysis are evaluated using the root mean square error (RMSE), the mean absolute error (MAE), the mean square error (MSE), and the correlation coefficient ( $R^2$ ). In comparison to the SVM model, the RF model demonstrates a significantly lower result of the specified errors and a significantly higher result of  $R^2$ . The average values of the MAE, MSE, RMSE, and  $R^2$  from the validation process for SVM models were 5.92 MPa, 8.14 MPa, 2.83 MPa, and 0.89, respectively, as shown in Figure 3 (a). Similarly, the average results for the same parameters from the RF model during the validation process were noted as 5.17 MPa, 6.24 MPa, 2.46 MPa, and 0.90, respectively, as depicted in Figure 3 (b).

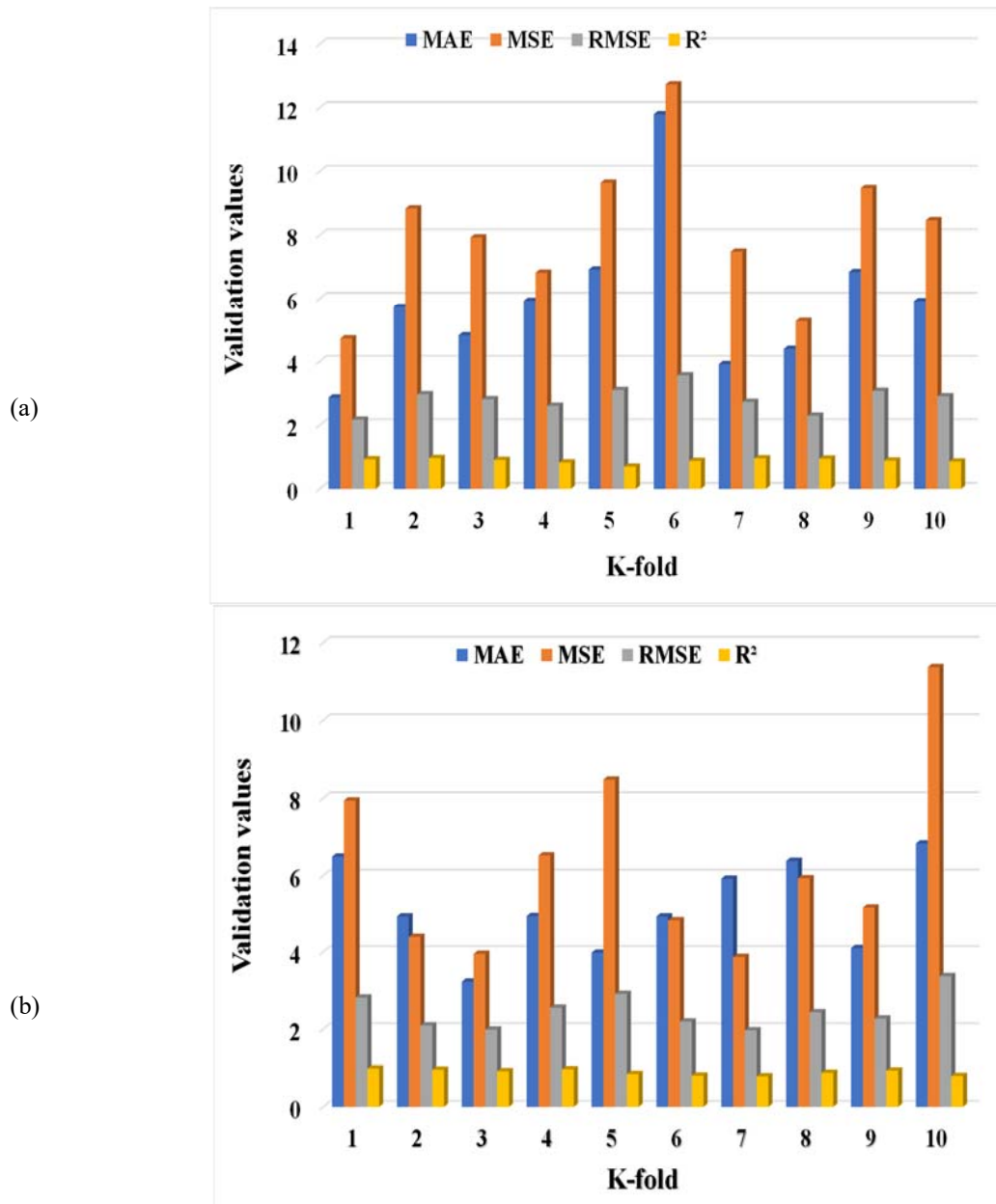


Figure 4. Validation results of the employed models (4a) K-fold CV for SVM algorithm; (4b) K-fold CV for SVM algorithm



Table 2. Statistical metrics for SVM and RF models

Algorithms	MAE (MPa)	MSE (MPa)	RMSE (MPa)
SVM	2.54	8.76	2.96
RF	1.97	6.25	2.50

## 6. Conclusions

This study describes the comparative study of two ML algorithms towards the prediction of C-S of concrete containing fly ash. The SVM and RF approaches have been introduced for the required outcome. However, the following conclusion can be drawn from the study.

- The RF model showed the affective predictive performance by giving an  $R^2$  value of 0.97 as compared to the SVM model's  $R^2$  value of 0.95.
- The lower values of the errors (MAE, MSE) also confirm the high accuracy of the RF model.
- The K-fold cross validation method was adopted to validate the employed models and confirm their legitimacy towards the predicted C-S of the concrete.
- The ML algorithms can be successfully applied to the selected data set to anticipate the required outcome.

This research has the potential to benefit the construction industries by reducing the overall cost of the projects that are being undertaken. The utilization of such techniques to predict the performance of composite materials in a limited time period is beneficial. This not only reduces the physical effort on the tests in the laboratory, but it also saves the valuable time of the project, which is a significant advantage.

## Acknowledgment

The authors would like to acknowledge the support of Science Foundation Ireland (SFI), through the MaREI Research Centre for Energy, Climate and Marine (Grant no. 12/RC/2302\_2).

## References

- [1] C. Meyer, "The greening of the concrete industry," *Cement and concrete composites*, vol. 31, no. 8, pp. 601-605, 2009.
- [2] A. Torres, L. Bartlett, and C. Pilgrim, "Effect of foundry waste on the mechanical properties of Portland Cement Concrete," *Construction and building materials*, vol. 135, pp. 674-681, 2017.
- [3] J. Hussain, A. Khan, and K. Zhou, "The impact of natural resource depletion on energy use and CO2 emission in Belt & Road Initiative countries: a cross-country analysis," *Energy*, vol. 199, p. 117409, 2020.
- [4] G. Habert *et al.*, "Environmental impacts and decarbonization strategies in the cement and concrete industries," *Nature Reviews Earth & Environment*, vol. 1, no. 11, pp. 559-573, 2020.
- [5] C. Hepburn *et al.*, "The technological and economic prospects for CO2 utilization and removal," *Nature*, vol. 575, no. 7781, pp. 87-97, 2019.
- [6] R. Heede, "Tracing anthropogenic carbon dioxide and methane emissions to fossil fuel and cement producers, 1854–2010," *Climatic change*, vol. 122, no. 1, pp. 229-241, 2014.
- [7] J. S. Gregg, R. J. Andres, and G. Marland, "China: Emissions pattern of the world leader in CO2 emissions from fossil fuel consumption and cement production," *Geophysical Research Letters*, vol. 35, no. 8, 2008.
- [8] A. H. Buchanan and B. G. Honey, "Energy and carbon dioxide implications of building construction," *Energy and Buildings*, vol. 20, no. 3, pp. 205-217, 1994.
- [9] S. D. Casler and A. Rose, "Carbon dioxide emissions in the US economy: a structural decomposition analysis," *Environmental and resource economics*, vol. 11, no. 3, pp. 349-363, 1998.
- [10] S. Ahmad, O. S. B. Al-Amoudi, S. M. S. Khan, and M. Maslehuddin, "Effect of silica fume inclusion on the strength, shrinkage and durability characteristics of natural pozzolan-based cement concrete," *Case Studies in Construction Materials*, vol. 17, p. e01255, 2022.
- [11] Y. Zhang, Y. Hua, and X. Zhu, "Investigation of the durability of eco-friendly concrete material incorporating artificial lightweight fine aggregate and pozzolanic minerals under dual sulfate attack," *Journal of Cleaner Production*, vol. 331, p. 130022, 2022.



- [12] A. A. Ramezaniapour, "Cement replacement materials," *Springer Geochemistry/Mineralogy, DOI*, vol. 10, pp. 978-3, 2014.
- [13] L. Barcelo, J. Kline, G. Walenta, and E. Gartner, "Cement and carbon emissions," *Materials and structures*, vol. 47, no. 6, pp. 1055-1065, 2014.
- [14] H. Jiang and C. Liu, "Forecasting construction demand: A vector error correction model with dummy variables," *Construction Management and Economics*, vol. 29, no. 9, pp. 969-979, 2011.
- [15] J. C. S. Tang, P. Karasudhi, and P. Tachopiyagoon, "Thai construction industry: demand and projection," *Construction Management and Economics*, vol. 8, no. 3, pp. 249-257, 1990.
- [16] M. D. A. Thomas, *Optimizing the use of fly ash in concrete*. Portland Cement Association Skokie, IL, USA, 2007.
- [17] K. Wesche, *Fly ash in concrete: properties and performance*. CRC Press, 1991.
- [18] R. C. Joshi and R. P. Lohita, *Fly ash in concrete: production, properties and uses*. CRC Press, 1997.
- [19] K. G. Babu and G. S. N. Rao, "Efficiency of fly ash in concrete with age," *Cement and concrete research*, vol. 26, no. 3, pp. 465-474, 1996.
- [20] U. N. Environment, K. L. Scrivener, V. M. John, and E. M. Gartner, "Eco-efficient cements: Potential economically viable solutions for a low-CO<sub>2</sub> cement-based materials industry," *Cement and Concrete Research*, vol. 114, pp. 2-26, 2018.
- [21] S. A. Miller, A. Horvath, P. J. M. Monteiro, and C. P. Ostertag, "Greenhouse gas emissions from concrete can be reduced by using mix proportions, geometric aspects, and age as design factors," *Environmental Research Letters*, vol. 10, no. 11, p. 114017, 2015.
- [22] A. I. Nicoara *et al.*, "End-of-life materials used as supplementary cementitious materials in the concrete industry," *Materials*, vol. 13, no. 8, p. 1954, 2020.
- [23] D.-C. Feng *et al.*, "Machine learning-based compressive strength prediction for concrete: An adaptive boosting approach," *Construction and Building Materials*, vol. 230, p. 117000, 2020.
- [24] K. Khan, A. Ahmad, M. N. Amin, W. Ahmad, S. Nazar, and A. M. Arab, "Comparative Study of Experimental and Modeling of Fly Ash-Based Concrete," *Materials*, vol. 15, no. 11, 2022.
- [25] A. Ahmad *et al.*, "Prediction of Geopolymer Concrete Compressive Strength Using Novel Machine Learning Algorithms," *Polymers*, vol. 13, no. 19, 2021.
- [26] W. Z. Taffese and E. Sistonen, "Machine learning for durability and service-life assessment of reinforced concrete structures: Recent advances and future directions," *Automation in Construction*, vol. 77, pp. 1-14, 2017.
- [27] M. Shang *et al.*, "Predicting the Mechanical Properties of RCA-Based Concrete Using Supervised Machine Learning Algorithms," *Materials*, vol. 15, no. 2, 2022.
- [28] S. Suthaharan, "Support vector machine," in *Machine learning models and algorithms for big data classification*: Springer, 2016, pp. 207-235.
- [29] G. Biau and E. Scornet, "A random forest guided tour," *Test*, vol. 25, no. 2, pp. 197-227, 2016.



# INVESTIGATION OF STRESSES IN A CONCRETE GRAVITY DAM UNDER COMBINED LOADINGS OF SEISMIC AND FLOOD WAVES

*<sup>a</sup> Muhammad Zeshan Khalil\*, <sup>b</sup> Naeem Ejaz, <sup>c</sup> Muhammad Waqas Malik, <sup>d</sup> Muhammad Shahrukh Pasha*

a: Department of Civil Engineering, University of Engineering & Technology Taxila, zeshankhalil18@gmail.com

b: Department of Civil Engineering, University of Engineering & Technology Taxila, naeem@uettaxila.edu.pk

c: Department of Civil Engineering, Capital University of Science and Technology-University-Islamabad, waqasmalikk@gmail.com

d: Department of Civil Engineering, Abasyn University-Islamabad Campus, pashahrukh@gmail.com

\*Corresponding author: Email ID: [zeshankhalil18@gmail.com](mailto:zeshankhalil18@gmail.com)

**Abstract-** This research is carried out to check the stability of a concrete gravity dam under the extreme loadings of combined seismic and flood waves. Concrete gravity dams are provided in highly seismic regions. These dams are not designed on experimental validation, but are simulated by finite element method on software. The environmental and other loadings and actions are then implemented on these simulated models and response of the system is checked. One drawback or ignorance of such system is, if a peak wave is generated and at the same time any seismic activity happens, then what will be the response of the dam, will it be stable in safe limit or not, will it survive combined loadings or not? That's why this study is based on such response prediction to evaluate the maximum stresses generated in the dam under such extreme loadings. In this study, a gravity dam is modelled on SAP2000 with finite element method. Blue Stone Dam from USA is selected and modelled on SAP2000. After that combined loadings i.e., seismic and flood wave are applied and response is predict of this simulation based model of the dam. After the successful run of the model, it is predicted that maximum stresses are generated on the top of the dam.

**Keywords-** Concrete gravity dam, Seismic loads, Flood wave loads, SAP2000, Finite element method

## 1 Introduction

Dams are obstacles that carry pounding of water or underground streams for different purposes such as power generation, storage of water, irrigation for agriculture, stabilization of flow, prevention of areas from floods, navigation, diversion of water channels and source of drinking water. The significance of these structures passes on the possibility of tragic disasters which can happen because of its failure, error in spillway design, piping through foundation, soil instability due to upstream fluctuation in water levels, poor maintenance, extreme precipitation events and flood waves, and seismic shocks and earthquakes [1]. The dynamic responses of concrete gravity dams due to earthquakes are affected by several factors. These factors include the dam's interaction with the water stored in the reservoir and foundation, sediments accumulation at reservoir's bed and non-linear behavior of dam's concrete. Recent studies indicated that the magnitude of the response of the concrete gravity dams is reduced generally due to the presence of sediments at the reservoir's bottom [2]. The concrete gravity dam's structures also face various flood wave loadings. These wave loadings occur in different scenarios including the wave loading relevant to the environmental data of the area is applied on the structural members together with gravity and buoyancy loads but without considering the wind loads (remote storm scenario) and the scenario where the load generated by extreme wave conditions, buoyancy and gravity loads are applied (extreme wave scenario) by neglecting wind load [3]. Different loadings are evaluated while design the concrete gravity dam. These loadings include earthquakes,



floods, sedimentation, ice and wind loads etc. In this study the combined effects of seismic and flood waves are investigated to predict the portion of the dam with maximum stresses. Designing earthquake-resistant dams and assessing the safety of existing dams both rely on a reliable analytical method that can identify the stresses and deformations brought on by an earthquake [4]. However, when taking into account the various definitions of a strong motion duration, it is still unknown how different durations may affect the seismic analysis of gravity dams. Furthermore, no definitive conclusion about the best option for the duration of a powerful ground motion has been reached. Due to its high accuracy and cheap computational effort for computing the dynamic reactions of structures, the endurance time analysis (ETA) approach, a high-efficiency seismic performance method, is frequently employed [5]. In this study, the stresses generated due to combined loading of earthquake and flood wave are evaluated. The response of the results shows that due to these combined loadings, damage in dam will be occurred at top portion of dam.

## 2 Research Methodology

### 2.1 Model Development.

Blue stone dam located in USA is selected to conduct this study [6]. The dam is modelled on SAP2000 software with Finite Element Method. Concrete is used as material and compressive strength of concrete is selected as 5000 psi. Solid body is selected to model it instead of members, due to the fact that dam is a solid body. The height of the dam is selected as 173 feet and length of the dam is selected as 600 feet. Six joints are provided in y-direction at interval of 100 feet for each and 4 joints are provided in z-direction at an interval of 34.7 feet each. To check the validation of model, the sum of masses in x-direction and y-direction for different modes of the model is computed more than 90% and the period is computed less than 8 seconds [7]. Hence the model developed for this study has shown validation. The model of the dam is shown the *Figure 1*.

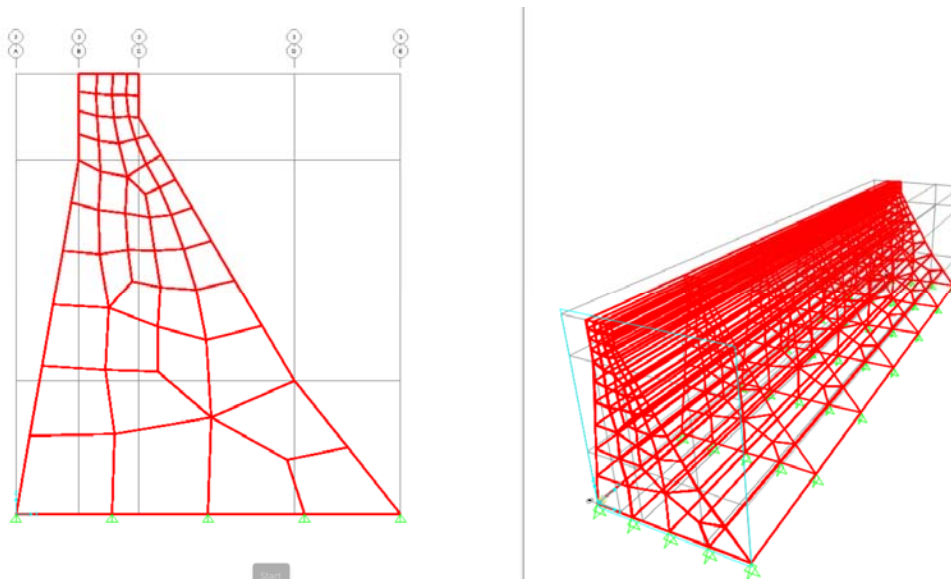


Figure 1: Model of dam developed on SAP2000

### 2.2 Load Definition.

For defining the load combination Time-History Analysis is used. Three earthquake loads are used and combined with peak flood wave of 6 feet height on the upstream side, in this study. Earthquake loads are downloaded from peer data base and imported in SAP2000 [6]. In this way 3 load combinations are created and model is run for these combinations. The earthquakes with magnitude greater than 6.5 are selected. The details of earthquakes used are available in *Table 1* and definition of flood wave is shown in *Figure 2*.



Table 1: Earthquakes used in this study.

Earthquake	Year	Magnitude	Epicentre Distance (KM)
Sitka Alaska	1972	6.68	34.61
El Centro	1940	6.95	6.09
Northridge	1994	6.61	7

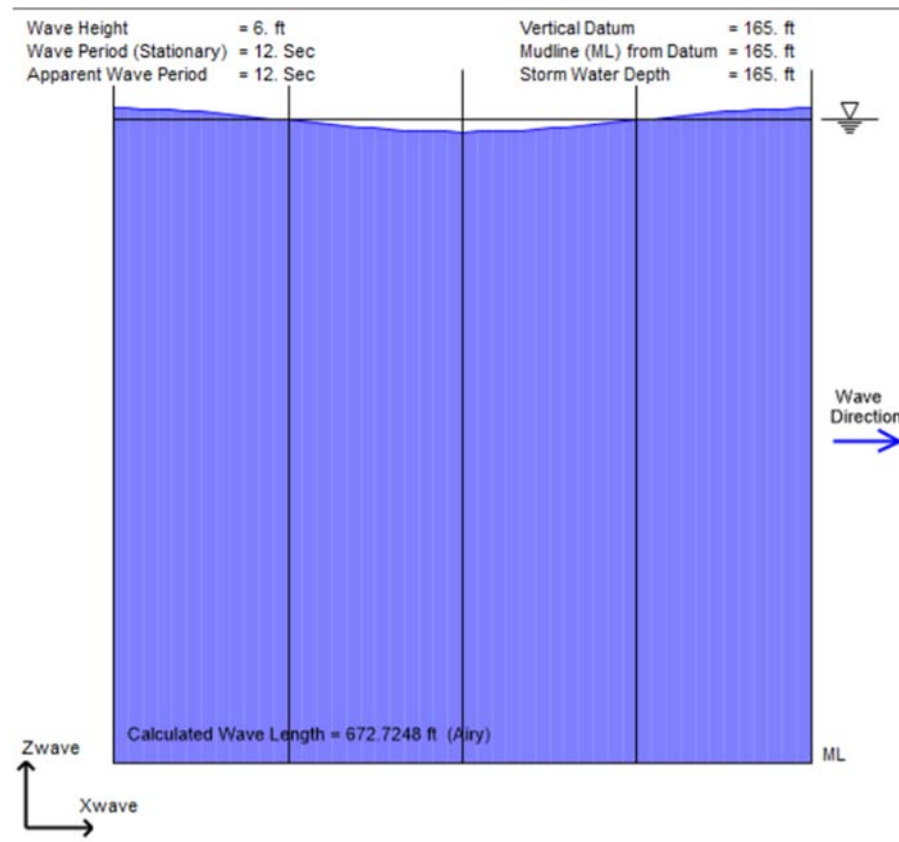


Figure 2: Definition of flood wave in SAP2000.

### 3 Results

The responses for the three earthquakes in combination with flood wave are represented below to check the stress contours for each case. The average of these three responses is taken to get the final results.

#### 3.1 Stress contours of Sitka Alaska Earthquake and Flood Wave

After running the model for load combination of Sitka Alaska earthquake and flood wave, the maximum stresses developed are found at top of the dam, equal to 8400 psi. The breach point of the concrete was selected as 5000 psi during modelling. So, it is predicted that as a response of aforementioned combination, the top of the dam will be damaged initially. The results of this combined loading have shown that there is 68% increase in the stresses at the top portion of the dam. The stress contours generated due to this type of combination in z-direction and y-direction are shown in Figure 3 a) and b) respectively. The stresses generated for a period of 4.35 seconds are presented in Table 2 and Graph 1.



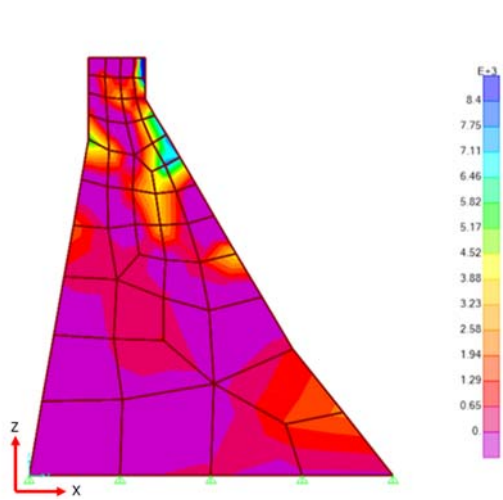


Figure 3 a): Stress contours in z-direction

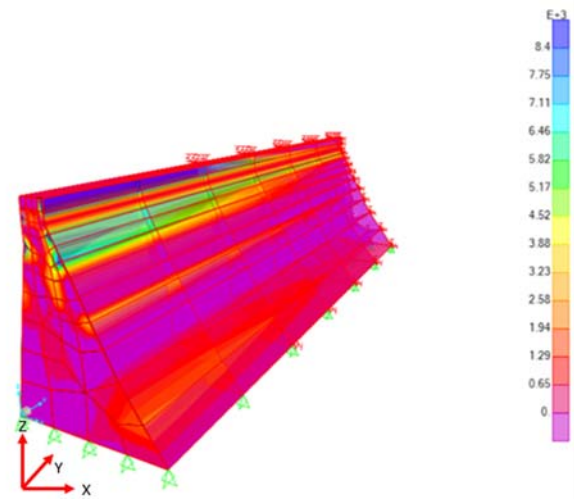
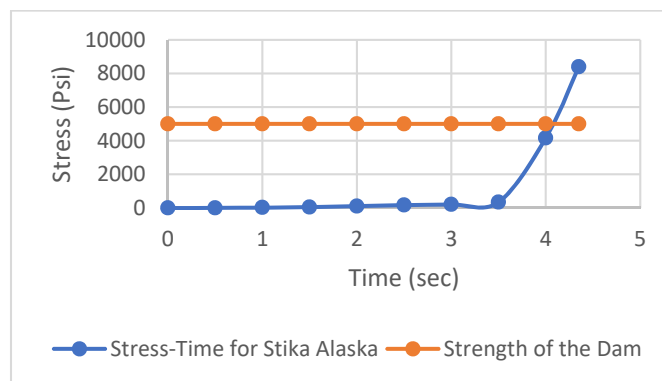


Figure 3 b): Stress contours in y-direction

Table 2: Stresses generated for a period of 4.35 seconds for Sitka Alaska Earthquake and Flood Wave

Sr. No.	Stresses (psi)	Time (Seconds)
1	0	0
2	4	0.5
3	28	1
4	52	1.5
5	104	2
6	175	2.5
7	208	3
8	347	3.5
9	4167	4
10	8400	4.35



Graph 1: Stresses generated for a period of 4.35 seconds for Sitka Alaska Earthquake and Flood Wave

### 3.2 Stress contours of El Centro Earthquake and Flood Wave

After running the model for load combination of El Centro earthquake and flood wave, the maximum stresses developed are found at top of the dam, equal to 7500 psi. The breach point of the concrete was selected as 5000 psi during modelling. So, it is predicted that as a response of aforementioned combination, the top of the dam will be damaged initially. The



results of this combined loading have shown that there is 50% increase in the stresses at the top of the dam. The stress contours generated due to this type of combination in z-direction and y-direction are shown in *Figure 4 a) and b)* respectively. The stresses generated for a period of 4.27 seconds are presented in *Table 3* and *Graph 2*.

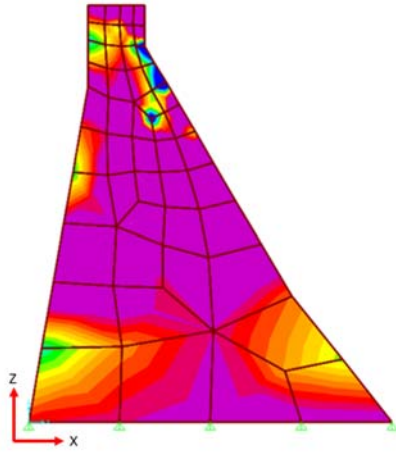


Figure 4 a): Stress contours in z-direction

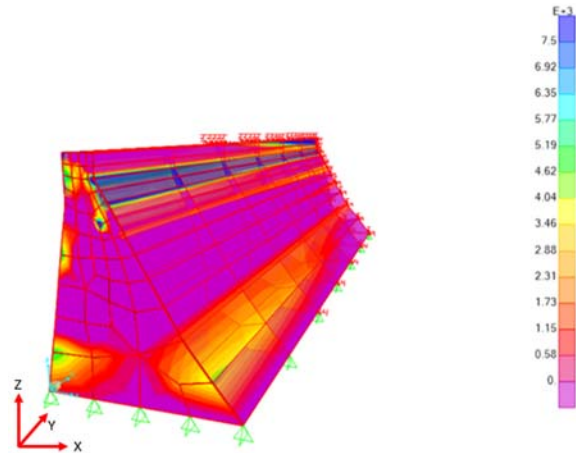
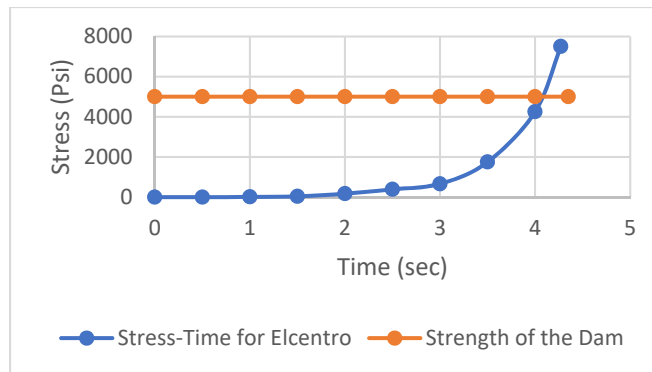


Figure 4 b): Stress contours in y-direction

Table 3: Stresses generated for a period of 4.27 seconds for El Centro Earthquake and Flood Wave

Sr. No.	Stresses (psi)	Time (Seconds)
1	0	0
2	0	0.5
3	14	1
4	39	1.5
5	175	2
6	393	2.5
7	664	3
8	1753	3.5
9	4254	4
10	7500	4.27



Graph 2: Stresses generated for a period of 4.27 seconds for El Centro Earthquake and Flood Wave

### 3.3 Stress contours of Northridge Earthquake and Flood Wave

After running the model for load combination of Northridge earthquake and flood wave, the maximum stresses developed are found at top of the dam, equal to 6200 psi.



The breach point of the concrete was selected as 5000 psi during modelling. So, it is predicted that as a response of aforementioned combination, the top of the dam will be damaged initially. The results of this combined loading have shown that there is 24% increase in the stresses at the top of the dam. The stress contours generated due to this type of combination in z-direction and y-direction are shown in *Figure 5 a) and b)* respectively. The stresses generated for a period of 4.12 seconds are presented in *Table 4* and *Graph 3*.

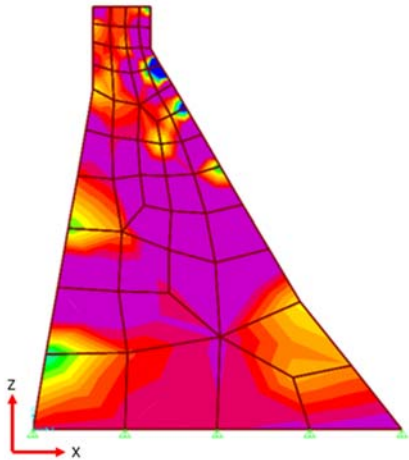


Figure 5 a): Stress contours in z-direction

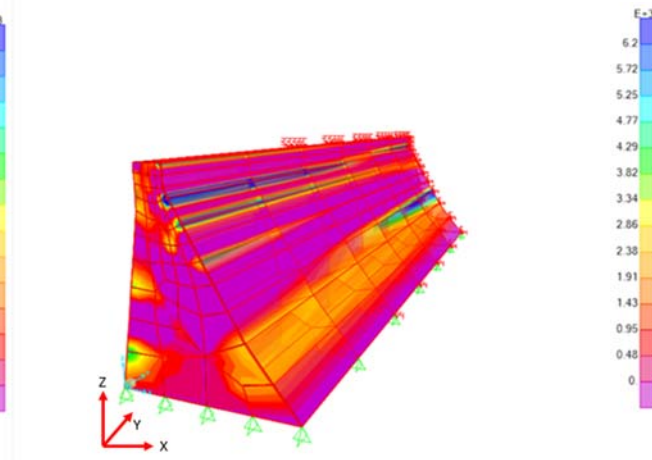
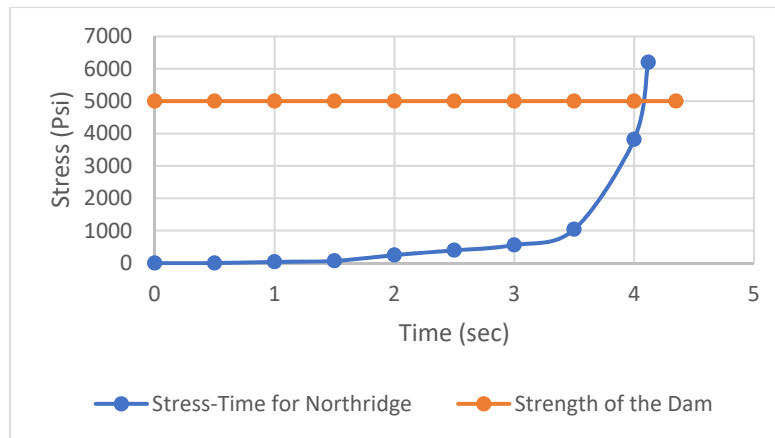


Figure 5 b): Stress contours in y-direction

Table 4: Stresses generated for a period of 4.12 seconds for Northridge Earthquake and Flood Wave

Sr. No.	Stresses (psi)	Time (Seconds)
1	0	0
2	1	0.5
3	36	1
4	66	1.5
5	248	2
6	393	2.5
7	556	3
8	1042	3.5
9	3819	4
10	6200	4.12



Graph 3: Stresses generated for a period of 4.12 seconds for Northridge Earthquake and Flood Wave



## 4 Practical Implementations

As this study is based on response prediction, the practical implementation of this research work can be verified by the future researchers by conducting experiments.

## 5 Conclusion

The results of this study have the following conclusions:

- 1 As an average response of three combinations, it is concluded that maximum stresses are produced at the top of the dam with strength greater than 5000 psi. Hence, the top portion of the dam will be damaged first under such type of extreme loadings.
- 2 Due to complex design of a concrete gravity dam, the combination of seismic and flood waves is ignored due to very less probability of such event to be occurred, but this study has shown some responses that have predicted that it should not be ignored.

The above study can also be carried out to predict the critical location of concrete gravity dams under such extreme loadings.

## Acknowledgment

The authors are very thankful to every person and department involved for helping throughout, especially Department of Civil Engineering-UET Taxila, Capital University of Science and Technology-Islamabad and Abasyn University-Islamabad Campus. Their efforts are gratefully acknowledged. The careful review and constructive suggestions by the anonymous reviewers are gratefully acknowledged.

## References

- [1] A. Dey<sup>1</sup> and M. Sawant, "Seismic response of a concrete gravity dam considering hydrodynamic effects."
- [2] M. N. El-Din and J. Kim, "Sensitivity analysis of pile-founded fixed steel jacket platforms subjected to seismic loads," *Ocean Engineering*, vol. 85, pp. 1-11, 2014.
- [3] K. Chatziioannou, V. Katsardi, A. Koukouselis, and E. Mistakidis, "The effect of nonlinear wave-structure and soil-structure interactions in the design of an offshore structure," *Marine Structures*, vol. 52, pp. 126-152, 2017.
- [4] S. Sarkhel, J. Padhi, and A. K. Dash, "Seismic analysis of a concrete gravity dam using ABAQUS," in *Recent Developments in Sustainable Infrastructure*: Springer, 2021, pp. 253-263.
- [5] Q. Xu, S. Xu, J. Chen, and J. Li, "A modified endurance time analysis algorithm to correct duration effects for a concrete gravity dam," *International Journal of Geomechanics*, vol. 22, no. 2, p. 04021285, 2022.
- [6] P. B. Tekie and B. R. Ellingwood, "Seismic fragility assessment of concrete gravity dams," *Earthquake engineering & structural dynamics*, vol. 32, no. 14, pp. 2221-2240, 2003.
- [7] K. Bandara and W. Dias, "Tsunami wave loading on buildings: a simplified approach," *Journal of the National Science Foundation of Sri Lanka*, vol. 40, no. 3, 2012.



# COST OVERRUNS AND DELAYS IN CONSTRUCTION: A STUDY ON CAUSES AND CONTROL MECHANISMS

*<sup>a</sup> Muhammad Usman Shahid\*, <sup>b</sup> Muhammad Adnan Sarwar, <sup>c</sup> Salman Ali Suhail*

a: Department of Civil Engineering, NFC- Institute of Engineering & Fertilizer Research, Faisalabad

b: The Architect, Karachi

c: Department of Civil Engineering, University of Lahore, Lahore.

\* Corresponding author: Email ID: [usman.shahid@iefr.edu.pk](mailto:usman.shahid@iefr.edu.pk)

**Abstract-** Triple constraints of a project i.e. cost, time and scope are considered as the key factors for defining the success of a project. At the same time, construction industry faced the challenges of time delays and cost overruns from the very beginning of its evolution till present. Multiple efforts are made by researchers in the past to identify the causes of such problems and proposed solution for them. This study focusses on the review of all the past studies conducted over the period of last decade. For this, number of relevant research papers are retrieved and filtered. After that frequency analysis was performed to find major factors throughout the world which significantly affect the project time and cost. Findings of this research show that lack of planning and design changes are the most important factors which affect the timely completion and total cost of a project. Further, emerging technologies like Building Information Modeling (BIM), Fuzzy techniques and Symbiotic Organism Search (SOS) can be used to control these problem in a project.

**Keywords-** cost overrun, fuzzy techniques, time and cost control, time delays

## 1 Introduction

Construction industry is considered as the main contributing factor to the development and economic growth of a country[1]. It accounts for approximately 10% of the global economy [2]. However, due to the uncertain and complex nature, it has been encountered by time delays and cost overruns over the years [3]. Researchers found that on average project time and cost changes 26% from its planned values [4, 5].

In order to reduce such kind of uncertainties from a project, critical factors need to be identified which directly or indirectly affect cost and duration of a project. Multiple studies have been conducted over the decades to determine these factors which are causing time delays and cost overrun [28-31]. This study will focus on reviewing these factors which appear in different past studies over the last one decade and synthesize the results. Further, this research will also provide insight about the methods for controlling time delays and cost overruns by using modern tools.

## 2 Causes of Time Delays:

Since the time delays do not only affect the timely completion of project but also it affects the project cost as well. Indirect cost which includes overheads, profits, and expenses etc. increases with the time. In Table 1, causes of time delays are reported in details from past studies conducted in different developed as well as developing countries. Most of the reported studies here are from one last decade.

## 3 Causes of Cost Overruns:

Similarly, causes of cost overruns in construction projects are also retrieved from one last decade studies which were conducted in developed as well as developing countries. Table 2 summarizes the results from 18 different research papers.



Table 1: Causes of Time Delays

<i>Reference</i>	<i>Country</i>	<i>Causes of Time Delay</i>
[6]	Oman	Site conditions, poor contract management, delayed payments, lack of skilled labor, late supply of materials, poor supervision, poor communication, change in drawings, change of policies, weather conditions, price escalation and inflation.
[7]	Indonesia	Delay in land acquisition, delay in approvals, site location, unions strikes, design changes, rework, performance of specialty contractors
[8]	Dubai, UAE	Changes in design, wrong estimation of project durations, delay in getting approvals from law agencies,, change of scope
[9]	Saudi Arabia	Modification of design and scope changes
[10]	Pakistan	Cultural Risks: Language barriers, Poor communication b/w parties. Financial Risks: Price escalation, inflation, budget overrun. Management Risks: Incompetency of project team, Improper planning of project, Poor relations with Governmental agencies, Inadequate organizational structure. Legal Risks: Lack of enforcement of legal laws. Political Risks: Change in policies, involvement of political partner in project, corruption
[11]	Malaysia	Poor weather conditions, poor construction material, poor estimation of productivity of equipment, unavailability of skilled labor, poor planning, and design changes.
[12]	Turkey	Security issues, high number of contracts to one contractor, poor labor productivity, design Change, poor supervision, poor construction material, change of drawings, poor planning
[13]	Australia, Malaysia and Ghana	Poor planning and scheduling, poor supervision, delayed payments, inexperienced contractor, complexity of project
[14]	Rwanda	Delay in payments, late material procurement, poor supervision
[5]	Denmark	Lack of project funding, delay in obtaining governmental approvals, lack of planning, lack of identification needs
[4]	Jordan	Site condition, weather condition, variation order, un-availability of trained labor, mistakes in design, Price escalation, inflation, payment delays, political influence, poor construction materials, poor planning
[15]	Malaysia	Cash flow problem and storage on site



Table 2: Causes of Cost Overruns

Reference	Country	Causes of Cost overruns
[16]	Vietnam	inflation, interest rate, costly equipment, incompetency of parties, poor communication
[6]	Oman	Change of scope, poor planning delay in payments, poor site conditions, inadequate trainings and experience, lack of skilled labor
[7]	Indonesia	Poor estimation of budget, price escalation, inflation, delays in payment, poor cash flow, weather conditions, rules and regulations
[8]	Dubai, UAE	Design changes, delays in approvals by client, wrong estimation of project costs, lack of capital availability of contractor, poor bidding method
[9]	Saudi Arabia	Poor cost and time estimation
[17]	India	Price escalation, inflation, poor bidding procedures, poor government policies, change of scope, wrong estimation of project cost,, change of design, weak cash
[18]	Pakistan	Payment delays, delays in approvals by client, poor contract management, poor financial health of contractor, lack of planning, change of scope
[10]	Pakistan	Violation of contract, contractual terms not clear, less availability of information, delays in payment
[19]	Qatar	Change of scope, poor planning and scheduling, lack of skilled labor, inflation, poor cot estimation, poor construction materials, poor estimation of project
[11]	Malaysia	Weather conditions, poor construction material, poor cost estimation, lack of cost planning, lack of understanding to local rules and regulations
[20]	Malaysia	Weather conditions, poor construction material, poor estimation of productivity of equipment, unavailability of skilled labor, poor planning, design changes, poor
[12]	Turkey	Lack of skilled labor, foreign contractor's dominance in industry, poor communication and cost control, scope changes, use of costly equipments,
[21]	Malaysia	Change of scope, poor communication among stakeholders, change in design, poor contract implementation, procurement problems, delay in payments, poor site
[14]	Rwanda	Design changes, lack of funds.
[5]	Denmark	Change of scope, design changes, inexperienced consultants, poor contract management
[4]	Jordan	Terrain condition, weather condition, variation order, un-availability of trained labor, mistakes in design, Price escalation, inflation, payment delays, political
[15]	Malaysia	Scope of work, tendering methods
[22]	Palestine	Political factor, escalation, unstable economy

So, it can be deduced from table 1 & 2 that these causes are related to each phase of project like planning, estimation, design, execution and supervision. Further, external factors such as political influence, change of policies, escalation and inflation also affect the projects in terms of time as well as cost. By controlling these factors, risks of time delays and cost overruns can be reduced.



#### 4 Research Method:

A comprehensive literature review was conducted by retrieving around fifty (50) papers from multiple journals such as “Alexandria Engineering Journal”, “International Journal of Engineering & Technology”, “International Journal of Project Management”, “Journal of management in engineering”, “International Advanced Researches and Engineering Journal”, “International Journal of Construction Management” and others. Then these papers were scrutinized and filtered depending upon its relevancy with the the research topic.

Initially, thirty four (34) factors, appearing in different journal and conference papers were identified which affect the project completion time. Considering the fact that factors appearing more frequently in different construction industries, will have significant effect on delays of project. So, these factors were shortlisted by using Equation-1, where frequency is considered the basic criteria for getting high score value. More the frequency of a factor means, more score value, more important that factor will be.

$$\text{Score} = \sum Fn/N \quad (\text{Equation-1})$$

Here:

**Fn**= Factor appearing in number of papers

**N**= Total number of papers

Similarly, twenty-nine (29) factors for cost overruns were identified and shortlisted in the same ways as explained earlier for time delays.

#### 5 Results and Discussion:

Based on the frequency analysis of past studies, it was synthesized that design changes and lack of planning are most influential factors that causes time delays as well as cost overruns as shown in Table 3. Similar results were also found in other studies that lack of planning and change of design are major factors of cost overrun and delay in time of a project [23-25]. The reason is that projects gets delayed in the absence of detailed planning, because there are no well-established baselines with which progress of project will be compared. In the absence of baseline schedule, it is very difficult to know either your project progress is up to the mark or not till date. Similarly, design changes ultimately cause the change of scope, where contractors have to perform rework sometimes, if that design change was suggested after construction of some elements. Therefore, this additional task demands extra time as well as extra money. So both of these factors discussed above significantly affect the time and cost of projects.

Further, lack of skilled labor and weather conditions are found as the other major causes of time delays and cost overruns. Since unskilled labor compromises the quality of work frequently and client rejects the work on the basis of poor quality. In that case, rework has to be performed. Further, weather conditions also affect the timely completion of project due to wastage of time in rainy season and then wait for site conditions to be dried. So time delays ultimately cause cost overrun as well because contractor has to bear project overheads (indirect cost). However, poor supervision, delayed payments, incompetent team and poor quality of materials are found as the influential factors only for time delays. On contrary, change of scope, inflation, poor estimation of cost and procurement issues such as awarding contract to lowest bidder are the factors which only affect the project cost significantly.

The major implication of this study is to provide the root causes of core issues of contraction industry since its inception i.e. time delays and cost overruns in the light of research conducted worldwide. The major issues found in this study are poor planning and design changes along with other factors as given in Table 3. So in order to overcome these issues detailed planning and right design should be ensured with help of BIM, Fuzzy techniques and SOS etc. at early stage of project life cycle.





Table 3: Ranking of most important factors affecting project time and cost

Ranking	Factors affecting Project Time	Score	Factors affecting Project Cost	Score
1	Design Changes	61.5%	Design Changes	44.4%
2	Lack of planning	46.2%	Lack of planning	44.4%
3	Poor supervision	38.5%	Change of Scope	38.9%
4	Delayed Payments	38.5%	Lack of Skilled Labor	33.3%
5	Incompetent Project Team	30.8%	Weather Conditions	27.8%
6	Weather Conditions	30.8%	Inflation	27.8%
7	Lack of Skilled Labor	30.8%	Poor estimation of schedule	27.8%
8	Poor Quality of Construction Material	30.8%	Procurement issues	27.8%

## 6 Conclusion and Recommendations:

It is concluded that design changes and lack of planning are the factors which significantly affect the performance of a project in terms of time and cost. Further, other factors such as lack of skilled labor and poor weather conditions also found as major causes of time delays and cost overruns. By controlling these factors through latest management tools, project performance in terms of time and cost can be improved.

It is recommended to overcome major causes such as lack of planning and design changes, change of scope, poor estimation and quality of construction materials, latest tools can be used. Amandin and Kule [14] studied that Gantt Bar Chart, Critical Path Networks/Method (CPM), Program Evaluation and Review Technique (PERT), Elemental Trend Analysis/Line of Balance (LOB), Precedence Network Diagram (PND), and Simulation are very much effective for controlling time delays and problem of poor planning. Further, design changes, scope changes, accurate estimation, clash detection and issues of quality control can be controlled through Building information modelling (BIM) [20]. Moreover, Fuzzy Analytical Network Processing, Fuzzy Artificial Neural Network, Fuzzy Monte-Carlo Simulation, and Fuzzy Bayesian Belief Network are used to understand the uncertainties in a project in terms of time delays and cost overruns [26]. After that Symbiotic Organism Search(SOS) algorithm can be used to find out multiple feasible solutions for project manager[27].Lastly, issues of procurement and lack of skilled labor can countered by adopting Quality Based Evaluation of firms and rigorous trainings of workers respectively.

## Acknowledgements

The careful review and constructive suggestions by the anonymous reviewers are gratefully acknowledged.

## References

- [1] A. Oke, D. Aghimien, C. Aigbavboa, and C. Musenga, "Drivers of sustainable construction practices in the Zambian construction industry," *Energy Procedia*, vol. 158, pp. 3246-3252, 2019.
- [2] S. Sharma and P. K. Goyal, "Cost overrun factors and project cost risk assessment in construction industry-a state of the art review," *International Journal of Civil Engineering (IJCE) Vol*, vol. 3, pp. 139-154, 2014.
- [3] S. Pehlivan and A. E. Öztemir, "Integrated risk of progress-based costs and schedule delays in construction projects," *Engineering Management Journal*, vol. 30, no. 2, pp. 108-116, 2018.



- [4] N. Al-Hazim and Z. A. Salem, "Delay and cost overrun in road construction projects in Jordan," *International Journal of Engineering & Technology*, vol. 4, no. 2, p. 288, 2015.
- [5] J. K. Larsen, G. Q. Shen, S. M. Lindhard, and T. D. Brunoe, "Factors affecting schedule delay, cost overrun, and quality level in public construction projects," *Journal of management in engineering*, vol. 32, no. 1, p. 04015032, 2016.
- [6] T. Amri and M. Marey-Pérez, "Towards a sustainable construction industry: Delays and cost overrun causes in construction projects of Oman," *Journal of Project Management*, vol. 5, no. 2, pp. 87-102, 2020.
- [7] R. Susanti, "Cost overrun and time delay of construction project in Indonesia," in *Journal of Physics: Conference Series*, 2020, vol. 1444, no. 1, p. 012050: IOP Publishing.
- [8] R. M. Johnson and R. I. I. Babu, "Time and cost overruns in the UAE construction industry: a critical analysis," *International Journal of Construction Management*, vol. 20, no. 5, pp. 402-411, 2020.
- [9] A. Bin Seddeeq, S. Assaf, A. Abdallah, and M. A. Hassanain, "Time and cost overrun in the Saudi Arabian oil and gas construction industry," *Buildings*, vol. 9, no. 2, p. 41, 2019.
- [10] M. A. Akhund, A. R. Khoso, A. A. Pathan, H. U. Imad, and F. Siddiqui, "Risk attributes, influencing the time and cost overrun in joint venture construction projects of Pakistan," *Engineering, Technology & Applied Science Research*, vol. 8, no. 4, pp. 3260-3264, 2018.
- [11] A. N. Haslinda, T. W. Xian, K. Norfarahayu, R. M. Hanafi, and H. M. Fikri, "Investigation on the factors influencing construction time and cost overrun for high-rise building projects in penang," in *Journal of Physics: Conference Series*, 2018, vol. 995, no. 1, p. 012043: IOP Publishing.
- [12] A. Rezaei and S. Jalal, "Investigating the causes of delay and cost-overrun in construction industry," *International Advanced Researches and Engineering Journal*, vol. 2, no. 2, pp. 75-79, 2018.
- [13] R. K. Shah, "An exploration of causes for delay and cost overrun in construction projects: A case study of Australia, Malaysia & Ghana," *Journal of Advanced College of Engineering and Management*, vol. 2, no. 1, pp. 41-55, 2016.
- [14] M. M. Amandin and J. W. Kule, "Project delays on cost overrun risks: A study of Gasabo district construction projects Kigali, Rwanda," *ABC Journal of Advanced Research*, vol. 5, no. 1, pp. 21-34, 2016.
- [15] Z. Shehu, I. R. Endut, A. Akintoye, and G. D. Holt, "Cost overrun in the Malaysian construction industry projects: A deeper insight," *International Journal of Project Management*, vol. 32, no. 8, pp. 1471-1480, 2014.
- [16] H. Pham, T.-V. Luu, S.-Y. Kim, and D.-T. Vien, "Assessing the Impact of Cost Overrun Causes in Transmission Lines Construction Projects," *KSCE Journal of Civil Engineering*, vol. 24, no. 4, pp. 1029-1036, 2020.
- [17] S. Sharma and P. K. Goyal, "Fuzzy assessment of the risk factors causing cost overrun in construction industry," *Evolutionary Intelligence*, pp. 1-13, 2019.
- [18] S. Sohu, A. H. Abdullah, S. Nagapan, A. A. Jhatial, K. Ullah, and I. A. Bhatti, "Significant mitigation measures for critical factors of cost overrun in highway projects of Pakistan," *Engineering, Technology & Applied Science Research*, vol. 8, no. 2, pp. 2770-2774, 2018.
- [19] M. Gunduz and O. L. Maki, "Assessing the risk perception of cost overrun through importance rating," *Technological and Economic Development of Economy*, vol. 24, no. 5, pp. 1829-1844, 2018.
- [20] T. Mohammed, N. Haron, A. Alias, I. B. Muhammad, and D. Baba, "Improving cost and time control in construction using building information model (BIM): A review," 2018.
- [21] P. Karunakaran, A. Abdullah, S. Nagapan, S. Sohu, and K. Kasvar, "Categorization of potential project cost overrun factors in construction industry," in *IOP Conference Series: Earth and Environmental Science*, 2018, vol. 140, no. 1, p. 012098: IOP Publishing.
- [22] I. Mahamid and N. Dmaidid, "Risks leading to cost overrun in building construction from consultants' perspective," *Organization, technology & management in construction: an international journal*, vol. 5, no. 2, pp. 860-873, 2013.
- [23] R. K. Muhammad, I. A. Rahman, and S. Nagapan, "Overrun Factors during the Construction Phase of Project," *International Journal of Sustainable Construction Engineering and Technology*, vol. 12, no. 3, pp. 96-102, 2021.
- [24] R. F. Herrera, O. Sánchez, K. Castañeda, and H. Porras, "Cost overrun causative factors in road infrastructure projects: A frequency and importance analysis," *Applied Sciences*, vol. 10, no. 16, p. 5506, 2020.
- [25] S. Sohu, A. Abdullah, S. Nagapan, T. Rind, and A. Jhatial, "Controlling measures for cost overrun causes in highway projects of Sindh province," *Engineering, Technology & Applied Science Research*, vol. 9, no. 3, pp. 4276-4280, 2019.
- [26] F. Afzal, S. Yunfei, M. Nazir, and S. M. Bhatti, "A review of artificial intelligence based risk assessment methods for capturing complexity-risk interdependencies: cost overrun in construction projects," *International Journal of Managing Projects in Business*, 2019.
- [27] D.-T. Nguyen, L. Le-Hoai, P. B. Tarigan, and D.-H. Tran, "Tradeoff time cost quality in repetitive construction project using fuzzy logic approach and symbiotic organism search algorithm," *Alexandria Engineering Journal*, vol. 61, no. 2, pp. 1499-1518, 2022.
- [28] Melaku Belay, S., Tilahun, S., Yehualaw, M., Matos, J., Sousa, H., & Workneh, E. T. (2021). Analysis of cost overrun and schedule delays of infrastructure projects in low income economies: case studies in Ethiopia. *Advances in Civil Engineering*, 2021.
- [29] Annamalaisami, C. D., & Kuppaswamy, A. (2021). Managing cost risks: Toward a taxonomy of cost overrun factors in building construction projects. *ASCE-ASME Journal of Risk and Uncertainty in Engineering Systems, Part A: Civil Engineering*, 7(2), 04021021.



**4<sup>th</sup> Conference on Sustainability in Civil Engineering (CSCE'22)**  
Department of Civil Engineering  
Capital University of Science and Technology, Islamabad Pakistan



- [30] Shoar, S., Yiu, T. W., Payan, S., & Parchamijalal, M. (2021). Modeling cost overrun in building construction projects using the interpretive structural modeling approach: a developing country perspective. *Engineering, Construction and Architectural Management*.
- [31] Enrica, M., Purba, H. H., & Purba, A. (2021). Risks leading to cost overrun in construction projects: a systematic literature review. *Advance Researches in Civil Engineering*, 3(1), 43-60.



# CONSTRUCTION COST ESTIMATION OPTIMIZATION USING BUILDING INFORMATION MODELLING (BIM)

<sup>a</sup> Muhammad Adeel\*, <sup>b</sup> Muhammad Asghar, <sup>c</sup> Junaid Asghar

a: Department of Civil Engineering, University of Engineering and Technology Taxila, [engradeel64@gmail.com](mailto:engradeel64@gmail.com)  
b: Department of Civil Engineering, University of Engineering and Technology Taxila, [asgharghani0078600@gmail.com](mailto:asgharghani0078600@gmail.com)  
c: Department of Civil Engineering, University of Engineering and Technology Taxila, [mjunaidasgharch@gmail.com](mailto:mjunaidasgharch@gmail.com)

\* Corresponding author: Email ID: [engradeel64@gmail.com](mailto:engradeel64@gmail.com)

**Abstract-** Compare commercially available BIM estimating tools, performance, and new construction workflows in a 5D BIM-based construction project. At this point in the design process, the cost of the project is usually approximated due to industry segmentation and the design line's segmentation. Very far along in the design process, which means it's too late to assist various stakeholders in making well-informed judgments. Perform In the design phase, value engineering and calculating early expenses have the ability to speed things up. High-quality, cost-effective buildings are the result of a more efficient project delivery procedure. There is a focus on changes in the workplace as part of the initiative. The Building Information Model (BIM) Estimation Process has been implemented in the construction project. Several BIM-based cost estimation software packages have been evaluated to support the various stages of design in this project. Examined the benefits and drawbacks of working with this software. The project's BIM-based estimation process was analyzed for its work practices and workflow [1]. Ultimately, we came up with a multi-stage technology adoption plan.

**Keywords-** BIM, Informed-decisions, multi-stage technology, Stakeholders, Workflows

## 1 Introduction

The cost of the design process is typically assessed over time due to the segmentation and percentage of the building industry. Because of this, it is a long way behind in terms of design. Assistance in decision-making for a wide range of stakeholders. Budget difficulties and the cost development process are typically highlighted in this Cost feedback [2]. The majority of construction engineering methods lower construction costs, performance, and quality of the build. There are numerous ways in which a company can speed up the process of producing high-quality, cost-effective projects, such as through value engineering. As long as BIM-based technologies have been available, expenses are based on just a few large ones. For construction companies, this functionality has been a boon.

CAD-based (Computer-Aided Design) documentation is being replaced with BIM-based (Building Information Modeling) documentation in today's business. One of the advantages of BIM over CAD drawings is that it has a huge amount of information that can be digitally extracted. Construction projects can benefit from the application of BIM-based cost estimating methods.

The primary goal of this project is to test and evaluate various workflows in BIM-based projects. As the first project to use BIM for cost estimating, this is an exciting step forward for the construction industry. Data and workflow modelling and comparison studies are the second building aspect. Lastly, to increase interest and awareness in implementing 5D BIM among key stakeholders of the Pakistan construction industry



## 2 Experimental Procedures

The modelling process begins with the selection of a representative design project. Building Information Modeling (BIM) will be used for the modelling process. Revit 2019 is the tool of choice for modelling applications. After the project has been modeled, cost information will be added to the building components. 5D BIM Cost Estimation will then be done using tools like Autodesk Navisworks Manage 2019 and Sigma Estimates. In order to complete this task, we must:

1. Several BIM-based cost estimating tools will be examined to assist different phases of design, including an assessment of current estimation methods and a comparison with BIM, suggested processes gathered from the literature (Eastman et al., 2011).
2. This software's advantages and drawbacks will be examined.
3. There will be a review of BIM-based estimating procedures and workflows.

### 2.1 Existing Estimation Processes and Workflows.

The estimating process in the classic design-build procurement paradigm is simple and easy. Paper-based and prescriptive bidding documents are still common. In order to establish a project budget for the purpose of validating sub-trades and supplier costs, documents are scanned for on-screen take-off and quantity data is entered into cost estimation software (MS Excel). There are many advantages to using integrated procurement modes, such as iterative cost and constructability validations or checks during the design phase (Figure 1).

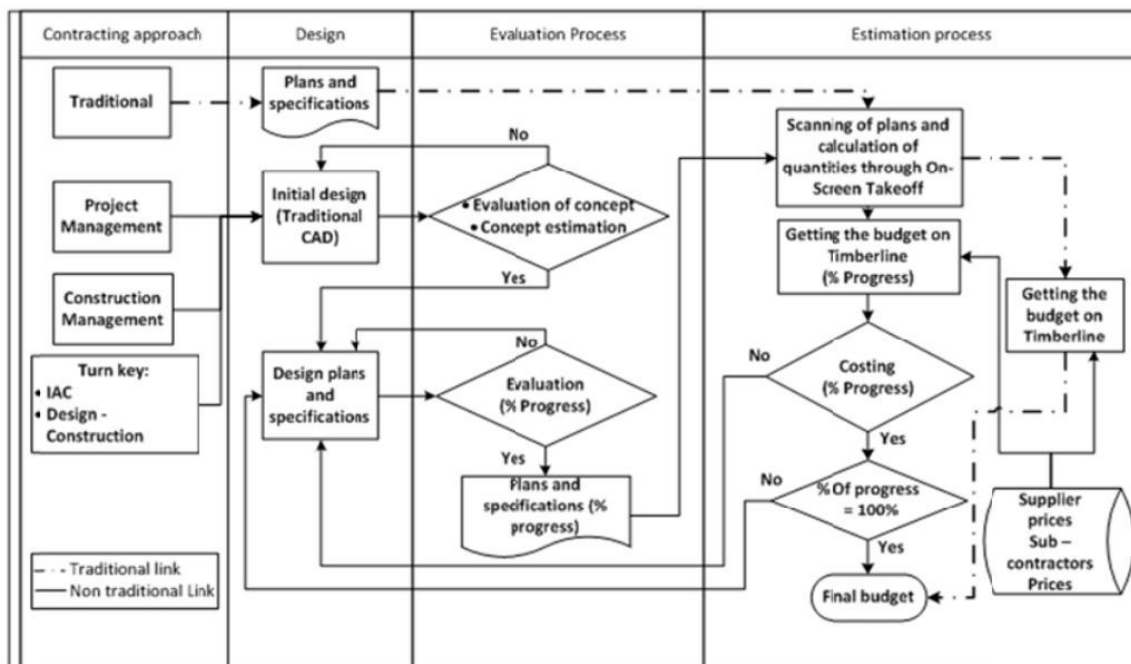


Figure 1: Existing Cost Estimation Workflows

## 3 Research Methodology

### 3.1 BIM-based Cost Estimation Using Autodesk Revit 2019

All views (with some exceptions) in Rivet are live demos of the model. This is done evenly to planning as well as Schedules. When it comes to Schedules, the model data appears in tabular form, but still offers a live view of the model. This means that there is no difference between the values shown in the schedule and the model and it also means that we can add and/or modify data in it (within logical limits) through the schedule itself.



### **3.2 BIM-based Cost Estimation Using Autodesk Navisworks Manage**

Navisworks® is a BIM (Building Information) project evaluation software that helps teams operate more efficiently together.

1. Streamline the design and construction process by integrating the two.
2. Before building begins, identify and resolve issues and countermeasures.
3. To better control the outcome, gather data from many deals.
4. Simulate model objects by animating and interfacing with them.
5. Sample projects can be used to generate schedules.
6. External project management programmes can be used to import schedules and costs.

Autodesk design applications like AutoCAD Architecture, AutoCAD Civil 3D, and Revit are common places to start a normal workflow. It is the job of an architect or engineer or other designers to determine what features (model, layouts, layers and features) to include in a design file before it is published. Once the content is selected, the drawing is published, and the file is sent to the Estimator. Designers may scan or save their work as an image file before sending it out for assessment. The process of rectifying the Quantification workflow begins after the files are received.

Open a design data source file in Navisworks. Open the Revit file by selecting Open and then browsing it.

1. Open the Workbook for Quantification
2. Create a project plan
3. Takeoff items can be created or selected.
4. Hide anything you don't want on display.
5. For objects that aren't listed in the catalogue, use measurement tools (for virtual takeoff).

Any time you wish to takeoff objects that aren't related to a model object or item, such as objects with geometry but no properties (or objects without geometry but no properties), you can use virtual takeoff. If you haven't saved the properties from the original design programme with your file, or if what you wish to remove doesn't exist in the model, this could be a problem. A viewpoint can be assigned to the virtual takeoff item in either case, making it easier to find it later on in the takeoff process. As soon as you remove the virtual object from the equation, you may begin to add characteristics to it.

### **3.3 BIM-based Cost Estimation Using Autodesk Revit and Sigma Estimates**

Software for estimating construction costs that is simple, quick, and accurate. The Live 5D Link between Revit and Sigma Estimate is the primary feature of this program.

Open the project and add the sigma estimate extension to it:

1. Select objects of the project and click on Element Properties as shown:
2. Link the objects with respective assemblies in Sigma. Make sure all objects have linked.
3. Click on Export to Sigma.
4. Select settings if required.
5. Open Sigma Estimate, see all the quantities extracted.



Go to Libraries and click update from library-it will connect the Revit model with sigma cost libraries. It will add prices to the activities. Check Resources Tab for all the resources required. Data can be exported to MS Project for scheduling and analysis.

## 4 Results

Based on our experience of these 5D BIM applications usage following are the results:

Table 1 Comparison of different software's for 5D Cost Estimation

Parameters	Autodesk Revit	Autodesk Navisworks	Sigma Estimates
Time Saving as compared to traditional methods	10 %	20 %	30 %
Accuracy of Cost Estimate	High	Medium	High
Difficulty Level of operating software	Low	High	Medium
Investment Cost for buying software	Low	Medium	High
Cost Analysis & Management	Low	Medium	High
Cost Databases	No	No	Yes
Suitable Stage for Estimation	Early Stage	After Final Design	All Stages
BOQ's	Short	Detailed	Highly Detailed

### 4.1 5D BIM Status in Pakistan

In spite of this, Pakistan has a long way to go in terms of infrastructure development due to shoddy construction methods in the industry (Maqsoom et al., 2013). It is clear that Pakistan's construction industry has a wide range of risks, including early failure and lack of facilities, planning and management changes in the scope of work/design, and corruption, complaints, and conflicts (Shabbar et al., 2017). Design errors and omissions, variations in drawing preparation and approval, deviations from drawings and specifications, unrealistic deadlines and cost estimates, improper planning, poor coordination among project stakeholders, and poor contract management have all been cited as the primary causes of the significant delay and increase in costs (Gardezi et al., 2014).

Contractors are expected to review construction drawings, specifications, and amendments as quickly as possible after they are presented to a contractor to begin building a facility and to notify any changes. In order to match CAD files and layout drawings, it requires time to analyze and compare the two. Inadequate vision, inaccuracies, and a lack of accurate information plague it (Fatima et al., 2015). As a result, the project manager will have to spend a lot of time and effort managing the site for valuable information (such as plans and specifications) and communicating with construction participants on the site and in the office (Park et al., 2016). Eventually, this results in conflict. Consequently, the Objectives of this project are on the line. A growing number of scholars in developing nations, such as Pakistan, have recognized the importance of BIM in today's building sector and have begun spreading the word about its advantages to all parties involved (Fatima et al., 2015).

In order to learn more about the current state of BIM models in Pakistan, we polled construction managers and project managers from organizations that are members of the Pakistan Engineering Council. BIM was found to be moderately well-known by 51% to 12% of respondents, while 8% were unaware of the advantages or uses of BIM. According to a survey conducted by (Maqsoom et al., 2014) [3], just 27 percent of AEC organizations in Pakistan employ BIM, while 73 percent of organizations are not involved in the BIM adoption process at all. According to these findings, Pakistan's construction industry is lagging behind in the adoption of BIM [4]. A few studies have examined Pakistani construction companies' reluctance to use BIM (Maqsoom et al., 2014). Problems that arose during the implementation of BIM were viewed as opportunities for awareness and instruction (Ismail et al., 2017 & Masood et al., 2014).



Drawings and construction data for an existing building should be redrafted using BIM concepts in order to illustrate the benefits of BIM to stakeholders in the construction sector in Pakistan. If you compare that to the typical way of doing things (Maqsoom et al., 2014) [5]. Our goal in creating this case study is to raise interest in and knowledge about the use of 5D BIM among Pakistan's construction industry's major stakeholders.

#### **4.2 Recommendations to implement 5D BIM in Pakistan**

1. BIM education should be made available in universities.
2. Complete courses of BIM should be introduced in degree programs in Architecture, Civil Engineering & Building Engineering.
3. Awareness of the benefits of 5D BIM should be given to engineers in practice by arranging seminars and workshops.
4. Private Cost database should be developed and should be available at a low price.

Technical experts of 5D BIM should be hired to get the maximum benefits of 5D.

## **5 Conclusion**

The construction sector is undergoing a paradigm shift as a result of the rise of BIM. Although it is possible to integrate more than five dimensions of information, the complexity of BIM implementation may increase significantly if more information is included. This initiative, therefore, aims to measure the next benchmark, 5D BIM, by conducting qualitative research. Observations clearly show that 5D BIM applications are practicable on a significant level. Decision-makers have been able to perform a sophisticated interpretation of information that is nearly impossible with the typical 2D CAD workflow because of information integration. A further finding implies that stakeholders who are unable to use BIM 5D may be unable to take full advantage of its features. Therefore, stakeholders who are unable to use BIM commit to building BIM capability benchmarking in the 5D BIM process. By virtualization of the 5D BIM, the project's clients will be able to participate in it with less of a learning curve. When the gap between expectations and results is filled, clients will be happier. Research on the development of best practices for 5D BIM is needed in general. Following extensive testing and evaluation, we can conclude that any of these tools can be used to create a more accurate, faster, and complete cost estimate, but it requires technical experience and expenditure.

## **Acknowledgment**

The authors would like to express their gratitude to everyone who contributed to the study, especially Engr. Muhammad Arshad Shahzad. The careful review and constructive suggestions by the anonymous reviewers are gratefully acknowledged.

## **References**

- [1] R. K. L. D. B. A. O. R. J. J. o. c. e. & m. Sacks, " Interaction of lean and building information modeling in construction.," pp. 968-980, (2010).
- [2] S. & K. A. Staub-French, "3D and 4D modeling for design and construction coordination: issues and lessons learned," Journal of information technology in construction (ITcon), vol. 12, no. 26, pp. 381-407, 2007.
- [3] A. C. C. & A. M. Maqsoom, " Internationalization process of Pakistani contractors: (pp).," An exploratory study. In ICCREM 2013: Construction and Operation in the Context of Sustainability, pp. 59-72, 2013.
- [4] B. Z. H. M. K. M. & M. A. Ali, " BIM implementation in public sector of Pakistan construction industry," American Society of Civil Engineers Reston, VA, pp. 42-51, 2018.
- [5] M. K. J. M. T. J. A. E. & M. D. Rekola, "Towards integrated design and delivery solutions: pinpointed challenges of process change," vol. 6, no. 4, pp. 264-278, (2010).





# BARRIERS TO IMPLEMENT BIM IN PAKISTAN

<sup>a</sup> Muhammad Usama\*, <sup>b</sup> Muhammad Saad Khan, <sup>c</sup> Hafiz Aiman Jamshaid

a: Department of Civil Engineering, University of Central Punjab, [muhammadusama104@outlook.com](mailto:muhammadusama104@outlook.com)

b: Department of Civil Engineering, University of Central Punjab, [saadkhan45a@gmail.com](mailto:saadkhan45a@gmail.com)

c: Department of Civil Engineering, University of Central Punjab, [aiman.jamshaid@ucp.edu.pk](mailto:aiman.jamshaid@ucp.edu.pk)

Corresponding Author Email ID: [muhammadusama104@outlook.com](mailto:muhammadusama104@outlook.com)

**Abstract-** Building Information Modeling (BIM) is a 3-D Model-Based process of creating and managing data, which assists designers, contractors and engineers. Moreover, contemporary technologies are assisting engineers to fulfill the expectations of customers in an effective way, as the demands of designs are getting complicated with every passing day. As a result, by utilizing the theory of BIM, engineers can build, design and handle infrastructures and buildings in a facile way. The implementation of BIM in Pakistan is very low as compared to the gulf and other developed countries. In Pakistan, the ratio of BIM is only 11% [1] because of using traditional methods, which can easily be handled with the help of BIM. BIM is more economical than using traditional methods of construction in terms of cost and time. The implementation of BIM in Pakistan faces many barriers, for instance, awareness issues, shortage of BIM professionals, problems of investment in new technologies, etc. This paper aims to identify the problems that hinder the acquisition of Building Information Modelling (BIM) in Pakistan. Also, we highlight the solutions to implement Building Information Modelling (BIM) in Pakistan. Furthermore, we have suggested a roadmap to improve the implementation of BIM in Pakistan.

**Keywords-** Building Information Modelling (BIM), Barriers in BIM implementation, Solutions, Road map.

## 1 Introduction

Building Information Modeling (BIM) is a 3-D Model-Based process of creating and managing data, which assists designers, contractors and engineers. Moreover, contemporary technologies are assisting engineers to fulfill the expectations of customers in an effective way, as the demands of designs are getting complicated with every passing day. As a result, by utilizing the theory of BIM, engineers can build, design and handle infrastructures and buildings in a smooth way, as it assists professionals having better collaboration by yielding vital insights of the under considered project. BIM is not only a 2D or 3D modeling process of visualization, but it is more about providing details and information about how buildings will function effectively. The model components are correlated, and design parameters are defined with the help of the data in the model. By varying the parameters of the model, whole window gets updated with respect to the variations in terms of elevation, sheet views and section. The management of building design and project data in digital form across the course of a building's life cycle is now possible thanks to the new approach known as BIM, which also allows for information sharing and interoperability among stakeholders. Construction industry players have adopted it and are increasingly implementing it in a variety of fields due to its potent benefits for reducing costs and time while enhancing production and efficiency [2].

BIM is very popular in the world because, in BIM based software's like Revit, we can collaborate with Structural, MEP (Mechanical, Electrical, and Plumbing), and Architectural. When we open a file in Revit, then Structural, Architect, and MEP can access the file and start their working. Since its release in 1997, Revit has been revolutionizing the field of architecture and construction. Contrary to other software's that are dependent upon one thing, in Revit, we can perform



Structural, MEP, and Cost Scheduling work simultaneously, and in fact, Interior, Exterior, and landscape views are also visualized in Revit through BIM. In BIM software's, we can quickly generate a design during the planning by automatically generating the view in 3-D on an alternate window. The main and the most important feature of BIM is collaboration and communication, so that builders and architects can do their work on the same project without any disturbance. Also, the model gets updated when one work is done, while others who are associated with the project can access it. BIM is significantly vital in terms of improving efficiency, particularly during the time intervals of construction and designing, as it assists in decreasing the required time without compromising on cost and efficiency. Furthermore, better clearness can be achieved, if we opt for BIM from starting to the completion of a construction project. It enables important stakeholders to view digestible, day-to-day pictures of development on the construction site, in addition to the benefits provided for subcontractors.

These real-time summaries aid communication and reduce the amount of rework that a project requires overtime. Because all subcontractors on the project have access to the same centralized BIM designs, they can communicate with one another and share critical information. If someone is making a change in the project, then everyone who is associated with the project can see it. By using old methods of construction, there are lots of chances in terms of materials wastage like cement, sand, bricks. A BIM based 3-D model can also assist in reducing the quantity of the required materials. With the help of BIM, we can know the material quantity by cost scheduling during the pre-construction. For example, if we want to construct a wall of building, then we will already have the estimations such as how much bricks and mortar are required to construct the wall, as we already have visualized the wall in 3-D. Actually, BIM can be applied in variety of disciplines in terms of construction life cycle, from conception to implementation of the finished structure. Kreider & Messner used BIM 25 times during the project, from start to finish. Because of many factors such as cost, time, and resources, the specific usage is dependent on the project's goal [3].

In the planning phase, we create the 3-D of the project and then we move to the existing condition modelling in which we create the 3-D model of the present situation of the site along with the available facilities on the site. This model can be created in many ways like by conducting surveys depending on which method is suitable for the present condition. We can make cost estimation more accurately and in a detailed way using BIM. It has ability to attach information about materials and their cost, and we can make changing for the future. We then move to the phase planning stage in which we make the scheduling (4D) that tell us the start and the finish time for our project. The site analysis for that BIM/GIS tool is then utilized to compute the parameters in the desired region to compute the most favourable site region for the upcoming experiments. The design phase involves scheduling and estimation (4D&5D). The scheduling ensures the building will be ready within the time and the estimation gives the idea about the cost of the materials. We then analyse our structures to establish the distribution of internal forces, moments, stresses, and displacement on the building to investigate the stability of the structure. Energy analysis can also be done to calculate the building energy performance. After completing the design process, the next step is to start the construction. As we have already computed the estimated cost and scheduling, we will have the idea, such as which and how much required amount of materials are needed to be purchased from the market. BIM assists to manage price and schedules, improving accuracy, efficiency and quality during the construction. In terms of operation, it involves the building maintenance scheduling, which proves to be quite beneficial in maintaining buildings along with their working functionally. The building system analysis then assesses how well a structure performs in comparison to its design. This entails how a building's mechanical system works along with the power consumptions. We then come to the asset management and disaster planning of the building [4]. The purpose of this paper is to identify the barriers that Pakistan is facing in way for the implementation of BIM, its solutions. At last provided a road map to implement BIM in Pakistan.

## **2 Literature Review**

Building information modelling (BIM) is a procedure that turns the building industry's fragmented, antiquated methods into a seamless, modern one. To collect, generate, analyze, and manage the digital representation of the produced project model, many tools, technologies, and contracts are used. Scheduling, costing, and facilities management are just a few of the applications of BIM, a well-known n-D modelling platform for effective communication and cooperation. The construction sector benefited greatly from the deployment of BIM across the project life cycle [5]. BIM has demonstrated its ability to increase productivity and efficiency during the design phase. BIM can combine automatic scheduling and cost analysis during the construction stage, allowing for improved project delivery coordination and quality [5]. BIM's origins



may be traced back to the 1950s, when computer-aided design, or CAD, was first used. During 1960s, Hanratty created the first commercial Computer-Aided Machining (CAM) in 1957. In 1963, Ivan Sutherland created CAD software by developing a Sketchpad, which is a graphical user interface. Actually, Sketchpad was an application that allowed the user to create drawings. Interface with the application graphically using a display, a light pen for drafting, and a pair of tabs on which the designer could input settings and limitations. In 1970s, during the transition from two-dimensional (2D) to three-dimensional (3D), CATIA was created by the French Aerospace Company. CATIA is a well-known software program. Actually, the creation of BIM takes us to the era of 1970s, when AIA journal published a paper, written by Charles M. Eastman, related to the prototype functioning which debated on the vital parameters that collect information from facades, maps, sections, and viewpoints. Moreover, instead of entering changes many times, all the relevant drawings get updated with merely a single change, which helps in the computation of cost with the aim of having the desired supplies and tools being accessible rapidly [6].

### **2.1 Barriers in BIM Implementation**

Most people in our country do not know about BIM because there is a lack of awareness. They complete their projects without using BIM. The ratio of BIM used to complete projects in Pakistan is quite low due to using old methods of construction which enhance both cost and time. Also, the initial investment cost of BIM software and Hardware is quite high, as the training is also expensive and there are not enough resources available to install BIM in system hardware. It is expected that BIM will yield crucial advantages to industries (AEC), but its adoption and execution demands price as with contemporary devices. The implementation of BIM technology requires a lot of financial resources in terms of training, education, administrative and initial investments, and costs during the transitional period. Due to the requirements of high financial resources, mostly large industries opt for BIM. Also, we require high storages devices and certain software's for the execution of BIM, which further enhances the required amount. These high-cost issues enhance the distance between professionals and BIM in terms of its adoption [7&8]. There are less experts in Pakistan who can implement BIM in the construction sector because of the BIM software issues in terms of learning and complexity among the engineers, and they prefer the old method to complete the project. The construction firms of our country are also not affiliated with BIM, and they complete their construction projects without using it. In fact, clients also don't know about BIM; therefore, they do not demand to complete their projects by using BIM [9]. The lack of skilled or well-trained BIM professionals is one of the main obstacles in terms of adopting BIM in the development section, since productivity of BIM is completely dependent on the qualification of the person using the BIM tool. For the successful implementation of BIM, the project team members must be skilled in their respective specific field regarding BIM. Implementation of BIM has the barrier of several legal aspects. One of the most important aspects is related to the ownership of data. There is always a conflict of interest among the owner and developer, but sometimes the claims are also made by architects and designers. There is no universal solution to this problem, but can be managed by case to case and project to project depending upon the circumstances of each project. Another important problem in this field is related to the rights of accessing and controlling the data, as every partner claim to possess access and rights to keep, modify and control the data. In case of multiple accesses, the issue of inconsistency, inaccuracy, and irregularity of data may happen, and no one will be ready to take responsibility of that issue [10].

### **2.2 Solutions**

The top three strategies for increasing the adoption of BIM in Pakistan are Workshops, Lectures, and Conference Events [11]. To familiarize people with BIM, it is required to conduct workshops, arranging seminars, and group discussions to spread awareness of BIM among people. The advantages of BIM should be emphasized to the organization's decision-makers, so that they support and set up seminars, conferences, and workshops on BIM for their staff. By providing incentives and compensation, businesses should keep their skilled and knowledgeable workforce. The next step is to open coaching centers to teach about BIM with no or minimum amount of fees. Top management should train workers on contemporary advancements in the field to overcome conventional ways of thinking.

By overcoming the reluctance to co-operate with other BIM professionals [12], clients should be informed about the benefits of BIM technology so they can better understand its uses. A standardized approach should be taken by the government when deploying new technologies. Consistent policy should be followed and legal difficulties should be



resolved [13]. It is essential to equip students with the theory of BIM in educational institutes with the aim of improving the skills of upcoming young generation. Conference events should be organized to enhance public awareness.

### 2.3 BIM in Pakistan

Undoubtedly, the development sector is considered as the backbone of Pakistan's economy. It is one of the most employment-producing sectors in Pakistan. From 2016 to 2017, Pakistan has witnessed a growth of approximately 9.05 % in the development sector [14]. Unfortunately, the percentage of using BIM in Pakistan is only 11% [1]. This is because we are still using traditional methods of construction which enhance the cost and time. Also, the development sector of Pakistan is experiencing serious issues due to inadequate organizing, misconduct problems, alternations in the design and scope, and quality problems [15]. Moreover, in addition to the above discussed issues, other issues, such as improper designs, time problems, delays in terms of accepting projects, disputed between the organizing staff members, insufficient actions, and the communications issues between the required organizations [16].

Meanwhile, BIM is utilized in many developed nations, such as in Germany, it is 90%, in the U.S.A, it is 79%, in Canada, it is 78%, in the U.K, it is 74%, in China, it is 67%, in Europe, it is 42%, in the Middle East, it is 25%, in India, it is 22%, and in Pakistan, it is only 11% [1]. We can see the difference in terms of implementing BIM in developed countries and other developing countries like Pakistan. It is pivotal to resolve the issues of development sector by introducing national policies at the government level. It is essential to make action plans at the national level along with taking all the required steps in terms of resolving the issues of the construction industry [17].

## 3 Future Frame Work

The Higher Education Commission (HEC) may start BIM as an academic course in colleges and universities to aware people about BIM. In Pakistan, most of the clients do not want to create their house or building in a 3D model because they do not want to spend money creating 3D models, as they are unaware about the benefits of BIM. Therefore, the benefits are required to be discussed with customers with the aim of raising awareness related to BIM applications.



Figure 1: Proposed plan to improve the implementation BIM in Pakistan

The Implementation of BIM in Pakistan is only 11% [1], which is extremely less by comparing it with other developed nations. To increase the implementation of BIM, we will have to initiate some important steps ourselves by creating a BIM society and engage with people which are interested in BIM like architects and engineers working in different firms of Pakistan. After creating the society of BIM, we can possibility expand it towards different major cities across Pakistan where the construction ratio is high like Islamabad, Karachi, Lahore, Peshawar, and Quetta, and also advertise it on social media platforms as possible. People in developing countries like Pakistan do not know BIM. They complete their construction project without BIM because the implementation of BIM is quite low. Furthermore, the people of the society like architects, and engineers working in different firms should share the advantages of BIM with their clients, so that the



maximum number of people get interested to complete their construction project by using BIM. In addition, the BIM society should collaborate with the government and raise our concerns about the implementation of BIM. For its implementation, we should open coaching centers to teach about BIM. BIM society which is working across Pakistan should conduct more workshops, and conference events on a domestic level and also some lectures in the universities, so that people have better information about BIM. Conducting workshops, and conference events will help to deliver our message to more people, allowing more interest of people in this field along with helping to create more BIM professionals. As the number of BIM professionals increases, there will be more chances of increasing the implementation of BIM in Pakistan.

#### **4 Relevance of Research**

The purpose of this paper is to implement BIM practically in those regions where the ratio of BIM is very low. So, the results of this paper will prove useful for them to implement BIM practically in their field.

#### **5 Conclusions**

The following conclusions can be drawn from the conducted study:

1. BIM is a suitable platform for the AEC professionals because it helps to eradicate communication gap among various stakeholder's communication, collaboration, and reduce fragmentation. As a result, understanding the concept of BIM is required to assist stakeholders in the AEC industry in adopting and implementing BIM.
2. There will be less wastage of time and materials in construction, as BIM aids in finding the exact material quantity, cost estimation and scheduling during the pre-construction phase. BIM is helpful in detecting the clashes amongst various models of any construction project prior to the real execution. Thus, it reduces the design and execution complexities.

#### **6 Recommendations**

Following recommendations can be drawn from the conducted study:

- 1 Workshops, seminars, lectures, and conferences on BIM can help spreading awareness about the benefits of BIM. They will also help in bringing the professionals at different levels in contact with each other.
- 2 A dedicated society of BIM can play a vital role in the implementation of BIM at gross levels even in developing countries.
- 3 Collaboration with BIM professionals at national and international levels can help in capacity building of developing countries.

#### **Acknowledgment**

We would like to thank our parents, respected teachers who helped thorough out the research work, especially Civil Engineering department. The careful review and constructive suggestions by the anonymous reviewers are gratefully acknowledged.

#### **References**

- [1] Imtiaz Ali Bhatti, Abd Halid Abdullah, Sasitharan Nagapan, Nbi Bux Bhatti, Samiullah Sohu and Ashfaque Ahmed Jhatial, "Implementation of Building Modelling(BIM) in Pakistan Construction Industry," Engineering, Technology and Applied Science Research, vol. 8, No. 4, 2018, 3199-3202.
- [2] Ilhan B, Yaman H. Meta-Analysis of Building Information Modeling Literature in Construction. Int. J. Eng. Innov. Technol. 2013;3(4):373-9.
- [3] Wan Nur Syazwani Bt Wan Mohammad, Mohd Rofdzi Bin Abdullah and Sallehan Ismail, " Understanding the Concept of Building Information Modeling: A Literature Review," Vol. 8 , No.1, January 2018, , E-ISSN: 2222-6990.
- [4] <https://www.letsbuild.com/blog/a-history-of-bim>
- [5] C. Eastman, P. Teicholz, R. Sacks, and K. Liston, A Guide to Building Information Modeling for Owners, Managers, Designers, Engineers, and Contractors
- [6] Branz, "Productivity Benefits of BIM



**4<sup>th</sup> Conference on Sustainability in Civil Engineering (CSCE'22)**  
Department of Civil Engineering  
Capital University of Science and Technology, Islamabad Pakistan



- [7] Bilal Manzoor, Idris Othman, Syed Shujaa Safdar Gardezi and Ehsan Harirchian, "Strategies for Adopting Building Information Modeling (BIM) in Sustainable Building Projects: A Malaysian case study, *Buildings* 2021, 11, 249.
- [8] Olawumi TO, Chan DW, Wong JK, Chan AP, "Barriers to the integration of BIM and sustainability practices in construction projects, " A Delphi survey of international experts,*Journal of Building Engineering*. 2018; 20:60–71.
- [9] Umar farooq, Dr. Kashif ur rehman, Rafaqat sohaib, Nasir khan and Adnan haider, "Adoption and Awareness of Building Information Modelling (BIM) in Pakistan," 1<sup>st</sup> Conference on Sustainability in Civil Engineering, August 01, 2019, Capital University of Science and Technology, Islamabad, Pakistan, Paper ID:308.
- [10] Liu S, Xie B, Tivendal L, Liu C, "Critical barriers to BIM implementation in the AEC industry, " *International Journal of Marketing Studies*. 2015, 7(6), pp. 162.
- [11] Memon AH, Rahman IA, Memon I, Azman NIA, "BIM in Malaysian construction industry: status, advantages, barriers and strategies to enhance the implementation level, " *Research Journal of Applied Sciences, Engineering and Technology*. 2014; 8(5):606–14.
- [12] Fida Siddiqui, Muhammad Akram Akhund, Tauha Hussain Ali , Shabeer Hussain Khahro, Ali Raza Khoso and Hafiz Usama Imad Vol 12(25), DOI: 10.17485/ijst/2019/v12i25/142325, July 2019
- [13] Sardar Kashif ur Rehman, Arbab Faisal, Mohammed Jameel, Fahid Aslam *Appl. Sci.* 2020, 10, 7250; doi:10.3390/app10207250
- [14] Pakistan economic survey August 2018
- [15] Shabbar, H.; Ullah, F.; Ayub, B.; Thaheem, M.; Jamaluddin; Gabriel, HF, "Empirical evidence of extension of time in construction projects, "*J. Leg. Aff. Disput. Resolut. Eng. Constr.* 2017, 9, 04517008.
- [16] BIM Process through A360 Cloud. Available online: <https://bimandbeam.typepad.com/.a/6a00d83453439169e201b7c73706ed970b-pi> (accessed on 14 August 2020)
- [17] Haron, A.T.; Marshall-Ponting, A.J.; Aouad, G, "Building information modelling in integrated practice,". In *Proceedings of the 2nd Construction Industry Research Achievement International Conference (CIRIAC 2009)*, Kuala Lumpur, Malaysia, 3–5 November 2009.



# FIBERGLASS AS AN INSULATION LAYER IN ROOF GARDENING

<sup>a</sup> Hoorab Shoaib\*, <sup>b</sup> Hafiz Aiman Jamshaid, <sup>c</sup> Hassan Sardar Cheema, <sup>d</sup> Umar Waqas

a.: Department of Civil Engineering, University of Central Punjab, [hoorabshoaib6@gmail.com](mailto:hoorabshoaib6@gmail.com)  
b: Department of Civil Engineering, University of Central Punjab, [aiman.jamshaid@ucp.edu.pk](mailto:aiman.jamshaid@ucp.edu.pk)  
c: Department of Civil Engineering, University of Central Punjab [umarwaqas1998@gmail.com](mailto:umarwaqas1998@gmail.com)  
d: Department of Civil Engineering, University of Central Punjab,  
Corresponding Author Email ID: [hoorabshoaib6@gmail.com](mailto:hoorabshoaib6@gmail.com)

**Abstract** - The purpose of this case study, document review is to create awareness among people about the benefits of fiberglass insulation and to recommend its use to reduce heat loss in summer as well as prevent heat loss in winter. A low-cost option is based on the use of a fiberglass insulation layer to ensure light barriers and insulation with reflective elements. Anyone can use it and install it on the roof of their house. The insulation layer is one of the essential layers of roof gardening. After providing insulation material to the roof building use less energy for heating and cooling. Just like in summer it prevents the building from overheating and in winter it prevents the building from getting too cold. So fiberglass insulation is the best way to protect the building from overheating. Fiberglass insulation makes building more energy-efficient. There is a lot of pollution in Pakistan cities like noise pollution, water pollution, and air pollution. Fiberglass keeps noise out of our homes. The major purpose of writing this paper is to make fiberglass more efficient and economic so that people can easily use it as insulation material in buildings to prevent heat and cold.

**Keywords** – Insulation layer, roof gardening, advantages of roof gardening, cost estimation.

## 1 INTRODUCTION

Roof gardening is simply defined as a garden on the roof of our houses. Roof gardens provide a lot of benefits. These include increment in oxygen, reducing pollution, cleaning the environment, reducing the heat of building, reducing the energy cost, and protecting our roof from moisture in the rainy season. With the increment in population, pollution is also increasing over time. People use different vehicles that produce harmful gases and these gases affect human health. Air pollution is a major problem today because it causes dangerous diseases in humans. So rooftop gardening is a great way to keep the air clean and free of hazardous gases. This study emphasizes knowledge based on journals, Various reports from research organizations, the Internet, and a visit to an Urban Landscape Architectural firm called eGarden.

The visit to eGarden was essential to understand the benefits, components, materials, and alternatives (depending on the condition of a roof), and their cost. Roof gardening consists of some key components. The components include the following layers : Waterproofing, Protection layer, Lightweight fills and thermally insulating layers, Drainage, Filter layer, The soil layer, Vegetation, Irrigation, and Maintenance considerations. Roof gardening also provides fresh food, fruit, and vegetables.

Pakistan is one of the main victims of climate change. In Pakistan, the rapid population growth, and poor urban planning have resulted in an unhealthy and fragile environment in the major cities like Karachi and Lahore. Still, the Government of Pakistan does not have any specific policy provision or legislation that promotes urban agriculture or rooftop garden in particular. So roof gardening is the cheapest way to enhance gardening, reduce pollution and make the environment healthy.

Roof gardening consists of different layers that protect our roof from damage. These layers involve the waterproofing layer, protection layer, insulation layer, drainage layer, and vegetation layer. Every layer has its purpose. These layers protect our roof in different ways. My aim is to discuss the insulation layer, its types, and



its advantages. Insulation material is used to control the entrance of heat, cold, and noise from entering the building. Now a day's people have a lot of options to use insulation material but the best insulation material is fiberglass.

Fiberglass is the best insulation material. It is made of special fine glass fibers. It has high tensile strength. It is used in different types of insulation materials like batts, rolls, and loose fills. It is also used in the form of rigid boards. Fiberglass can get molded into different difficult shapes. Just like we can use fiberglass in boats, roofing, and aircraft as well. We have a variety of materials that provide insulation to our home by creating small spaces, where air pockets can control the flow of heat.

Fiberglass insulation does the same job. Fiberglass is made up of small, thin glass fiber that forms several air pockets that help control the flow of heat and cold [2]. So the main purpose of writing this paper is to inform people about the major benefits of fiberglass insulation which are saving of money and sound control. Installing fiberglass insulation helps you maximize your home's energy efficiency and saves your money each year by reducing your heating and cooling costs.

## **2 LITERATURE REVIEW**

Below are the common types of insulation material,

### **2.1 Cellulose insulation**

It is the oldest form of insulation that people can use in their houses. It is in form of loose-fill or blow-in insulation. Both these forms can be used in both old and new houses. Cellulose is fiber insulation. It is used in enclosed existing walls and unfinished floors. Now a day's mostly companies make cellulose insulation. It is primarily made from recycled newsprint. Mostly 75-85% of cellulose insulation is made by recycling paper [3].

### **2.2 Polyurethane foam**

Polyurethane foam insulation is a new and effective method of insulation for buildings. Labour applies it by spraying, in this way it reaches the smallest of gaps. Its perfect installation is an important step. It provides the damage-resistant insulation of a house. It also improves living comfort and reduces bills.

### **2.3 Mineral wool**

Mineral wool is also known as mineral fiber and mineral cotton. It is made of fibrous material which is formed by spinning molten mineral or rock material like slag and ceramics. It is used for soundproofing. Most people avoid it because it is an expensive type of Insulation. The high cost of mineral wool is its major drawback

### **2.4 Fiberglass**

Fiberglass is the best insulation material. It is made of special fine glass fibers. It is used in different types of insulation materials like batts, rolls, and loose fills. It is also used in the form of rigid boards. Now a day's mostly manufacturers made medium and high-density fiberglass batt insulation because these have a higher R-Value than simple and low-density fiberglass batts, according to the U.S Department of Energy [2]. Most people use batt because it is a common type of batt.

- Less in weight
- High strength
- Less brittle

These batts are available in different thicknesses mostly in the range of 3 to 6 inches. Fiberglass is primarily used in all types of buildings to prevent or slow down the transfer of heat in summer and cold in winter. Fiberglass is a great option for homeowners who want to save money cheaply. The properties of fiberglass are as follows,



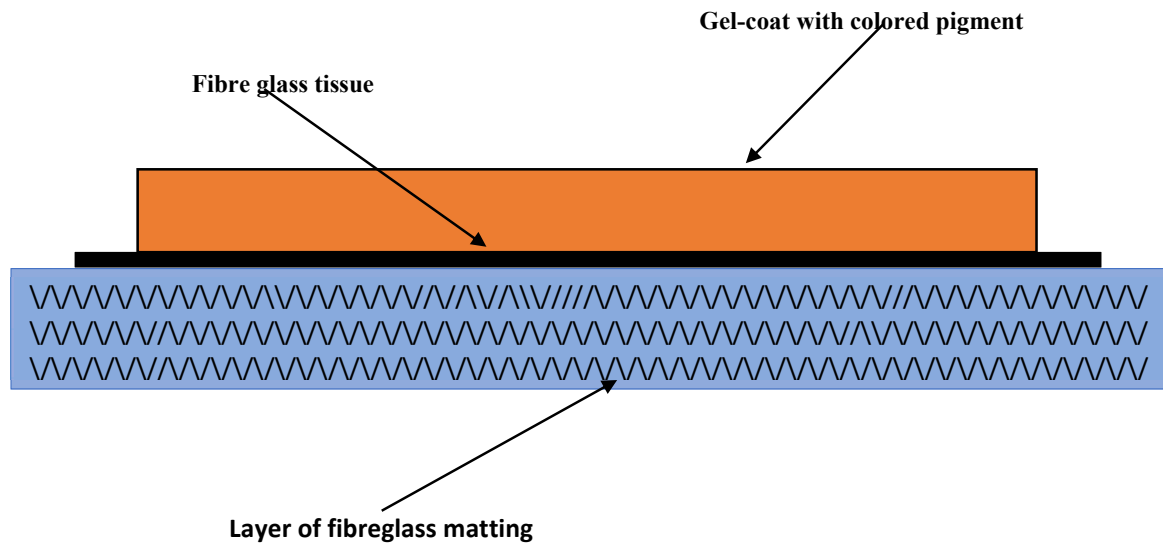


Figure 1 : Fibreglass insulation diagram

#### 2.4.1 Types of fiber insulations

Nowadays manufacturers are making several different types of Fibreglass insulation. We've to carefully choose it according to our house area like if we're only looking to install insulation in the roof so it is different from wall insulation. There are three main types of Fibreglass insulation which are as follows:

#### 2.4.2 Batt insulation

This is the most common insulation type used to insulate walls and ceilings. The insulation batts are long having circular shapes like rolls. These batts are made of a very fine layer of fine glass stands. It is a very thick blanket. Batt insulation can also be made from cotton or stone wool.

The hugest advantage of batt insulation is its lowest price. It is the least expensive way that we can use for our home insulation. So most people have to prefer this insulation for their houses. People can save their electricity bills most cheaply. Secondly, it is so easy to install. We can also install it in our houses by ourselves and in this way, we can reduce labor costs as well.

#### 2.4.3 Loose-fill insulation

Loose fill is made of cellulose, fiberglass, and mineral wool. All these materials are produced by recycling the waste materials. It consists of small particles of fiber and foam. So we can easily conform them to any place in our house.

It gives us the following advantages

1. We can install it in any roof shape
2. It can provide better insulation by up to 22% [2]
3. We can achieve a higher R-value starting with a loose fill
4. Not too much expensive/cheap
5. Only 2 persons can install it easily

#### 2.4.4 Rigid fiberboard insulation

It is mainly made of fiberglass or mineral wool material. It is mostly used for insulating air ducts in homes. It is also used in places where the temperature is high. Its range is 1 – 2.5 inches. It gives us the following advantages:



1. High R-value
2. It can control moisture
3. We can use it on both sides of the wall or ceiling
4. It prevents air leakage

### 3 METHODOLOGY

This study emphasizes knowledge based on journals, Various reports from research organizations, the Internet, and a visit to an Urban Landscape Architectural firm called eGarden. The visit to eGarden was essential to understand the benefits, components, materials, and alternatives (depending on the condition of a roof), and their cost. The thickness of the glass wool insulation has a great influence on the audile and thermal insulation value. The thickness of fiberglass insulation starts at 60 mm and increases to 20 mm (80, 120, 140, 160, 180,...)[6]. A minimum thickness of 160 mm is recommended to insulate a pitched roof. You can also work with two alternating layers to make sure there are no seams[6]. Insulation values and properties of blankets and fiberglass batts are;

1. High storage capacity : 800 J/kgK
2. Lamda value : 0.032 to 0.040 W/mL-K
3. Density : 25kg/m<sup>3</sup>
4. Diffusion resistance : 1

The important point about fiberglass insulation is its R-value and its thickness. The R-value tells us about the efficiency of insulation material. The greater the R-value shows the more efficiency of insulation material. Simply the R-value tells us about the resistance of heat transfer through the 2D barrier. These barriers can be a layer of insulation, a window, or a complete wall or ceiling. If you want to know about the perfect type of fiberglass insulation so it depends on the thickness of the batt. According to the US Department of Energy reports that if you want to use 3.5-inch thick fiberglass batt so it will offer an R-value of R-15 at (68 -80 Rupee)[1]. If you want to use 8-inch thick batt so it'll offer an R-value of R- 25 at (74 -90 Rupee) per square foot [1].

TYPES OF INSULATION	R-VALUE
BATTS	3.1 – 3.4 per inch of thickness
LOOSE FILL (WALL)	3.7 - 4.3 per inch of thickness
RIGID FIBROUS	4 – 5 per inch of thickness

Now if we talk about the synthesis of fiberglass, it is made of limestone, soda ash, feldspar, nepheline syenite, and silica sand. Silica sand is commonly used as a precursor to glass in fiberglass. The limestone and soda ash are used to help reduce melting temperatures. We need to carefully add all the ingredients to make the perfect quantity and quality of fiberglass. During the formation of Fibreglass insulation, all the materials are sampled at various steps in the process of formation just to maintain the quality.

One of these steps is the batch of raw materials is fed into the melter then the glass fiber leaves the machine and last, the final cured fiberglass insulation product appears from the end of the production line. Most manufacturers of fiberglass insulation follow different ASTM testing procedures to adjust, measure and optimize the product's sound barrier performance and noise absorption. Manufacturers efficiently control their physical properties by adjusting the manufacturing variables like binder content, bulk density, fiber diameter, and the thickness of fiberglass insulation.

### 3 COST ESTIMATION

However, fiberglass insulation is not too much expensive. Most house owners can easily install this in their houses. The average cost to install fiberglass insulation starts at (175 – 320 Rupees) per square foot [5]. Installing fiberglass insulation in our houses reduces our electricity bills and saves our money. Its cost also depends on its installation method.



## 5 RESULT

Make rooftop gardening a trend in Pakistan as its every layer offers many benefits. In this paper I have only explained the insulation layer and its benefits. If we talk about other layers then each layer is providing individual benefits. The biggest advantage of these layers is that you can use them individually on the roof of your homes. Now if you talk about insulation layer then following are the results that people will get after installing it.

### 5.1 *Energy Efficient and saves the bills*

Normally fiberglass insulation can reduce our electricity bills by up to 40-50%. It can also reduce noise pollution. Fiberglass insulation reduces heat in the summer and cools your roof.

### 5.2 *Environment friendly and flexible*

30 % Fiberglass is made from recycling waste material. This factor makes it environment-friendly. People can easily install it on their roofs because it is flexible. Its flexible nature reduces its cost.



Figure 2 : Installation of fibreglass insulation in the walls and ceilings [9]

### 5.3 *Easily available and less expensive*

Fiberglass insulation is easily available in the market. Manufacturers mostly made batts and these are available at low prices in the market. The low cost of fiberglass insulation makes it the most useable insulation material.

### 5.4 *Incombustibility*

Fiberglass is a mineral material, it is incombustible in nature. It does not support a flame. It does not emit smoke or toxic products when exposed to heat.

### 5.4 *Practical implementation*

In this paragraph I've briefly explain the practical implementations of fibreglass as an insulation material. The best thermal barrier for industrial gaskets is a high temperature insulating material. Because fiberglass is enduring,



safe and offers superior insulation, fiberglass is one of the widely preferred materials in industrial gaskets. It also provides safety of machinery and professional manpower. Its biggest practical use is to wrap pipes and tanks because it can protect cold and hot surfaces from -60°F to 650°F. Fiberglass grating is used in bottling lines and wineries. Due to the salt water of the sea, the docks rust and fiberglass is used to protect it[8].

## **6 CONCLUSION**

Fiberglass insulation is one of the cheapest types of insulation. Now the weather is very hot in summer and very cold in winter. People use air conditioners to reduce the heat from their homes in summer and this increases their electricity bills. So the best solution to this problem is to install fiberglass insulation in homes. It resists heat waves in summer and keeps our homes cool. It also reduces electricity bills by up to 50%. Plus, it's easy to install and less expensive. Nowadays, with the increase in population, noise pollution is increasing day by day. The atmosphere is getting hot and humid. Therefore, the installation of fiberglass insulation in your home also reduces noise pollution.

## **ACKNOWLEDGEMENT**

The authors would like to thank every person/department who helped thorough the research work, particularly the CE department. The careful review and constructive suggestions by the anonymous reviewers are gratefully acknowledged.

## **REFERENCES**

- [1] <https://www.attainablehome.com/the-r-value-of-fiberglass->
- [2] <https://www.forbes.com/advisor/home-improvement/what-is-fiberglass-insulation/>
- [3] [https://en.wikipedia.org/wiki/Cellulose\\_insulation](https://en.wikipedia.org/wiki/Cellulose_insulation)
- [4] <https://www.buildwithrise.com/stories/fiberglass-insulation>
- [5] <https://www.homeadvisor.com/cost/insulation/>
- [6] <https://www.insulation-info.co.uk/insulation-material/fibreglass-insulation>
- [7] <https://blog.gltproducts.com/blog/the-value-of-mineral-wool-in-fabricated-pipe-insulation-0-0-0-0>
- [8] <https://phelpsgaskets.com/blog/fiberglass--types-properties-and-applications-across-industries>
- [9] <https://blog.certainteed.com/2021/09/benefits-of-fiberglass-insulation/>



# AN OVERVIEW ON THE 3D PRINTING TECHNOLOGY IN CONSTRUCTION INDUSTRY

<sup>a</sup> *Muhammad Abrar*

a: Department of Civil Engineering, University of South Asia Lahore, [enr.m.abrar@outlook.com](mailto:enr.m.abrar@outlook.com)

**Abstract-** Innovations have started to emerge in the construction sector with the developing technology. One of these innovations is the utilization of 3-dimensional printing technology. Civil engineers build structures using materials and techniques available in the times. 3D printing technology attracts attention since it is faster than traditional construction, less costly, less labor and less error margin in today. It is possible to produce structures with complex designs and small scaled various products, under favor of this technology. First of all, 3D model design is needed in order to produce structures with 3D printing printers. Optimized cement-based mortar material is used in 3D printing printers. In order to be able to build layers on top of each other without collapse, and to perform 3D printing without shrinkage cracks, a building material recipe should be prepared by obtaining appropriate mixing ratios. While placing the building material, layered production is made without using a mold, and the width and thickness of the printing layer is constantly controlled during placement. Attention is paid to the use of sustainable building materials in buildings built using this technology. In addition, studies are carried out for zero waste in the use of materials. In this study, it is aimed to briefly introduce this new generation method along with its benefits, shortcoming and possible use as future of construction industry after eliminating these shortcomings.

**Keywords-** 3D printing, Cementitious material, Construction automation, Digital construction, Sustainability.

## 1 Introduction

Industries have begun to re-establish their production systems with the developing technology. 3D printing technology has also been improving of late years, along with additive manufacturing. 3D printing technologies enable design optimization and have advantages over traditional manufacturing methods. It is necessary to keep up with the new age in order to survive in the variable sector with the increase in the competitive environment. The construction industry is also under the pressure of change due to technological developments. Therefore, it is attracting great attention in the construction industry as a new strategic challenge [1]. The application of 3D printers has taken its place in the field of engineering, especially in the field of medicine and automotive. There have been developments in additive production technology in layers with cement and various materials. This technology has emerged as a joint product of materials science, robotic coding and architectural design studies, using the advantages of shotcrete and self-compacting concrete. In this type of printing, the ability to pump, workability and construct of fresh concrete and the strength of hardened concrete are of great importance [2][3]. Rheological properties such as viscosity and yield stress are also considered critical properties to control the printable property of printer concrete.

The lack of a certain standard in the mixture design and the insufficient number of studies affect these properties negatively [4]. Ultra-high strength concrete was also developed by [5] and it was revealed that the concrete samples printed by 3D printing technology provided high toughness than conventional method. A few researchers have also developed ways to print foam concrete by the 3D printing technology for various civil engineering applications. The type of concrete was found as sustainable and lightweight. This foam concrete developed by those researchers is applicable where the weight of structure matters [6]. The main purpose of this paper is to briefly review 3D printing technology and its applications in



the construction industry. The studies discuss the future of 3D printing technology in the field of construction and suggestions are made for possible uses in the construction industry.

## 2 3D Printing Technology

Traditional manufacturing methods are based on the principle of subtracting material from the raw material during the manufacture of parts. In additive manufacturing, which is one of the new production techniques that has become widespread today, unlike traditional manufacturing methods based on material reduction techniques from the part, the part is produced directly from the material. The device used in manufacturing manufactures the part layer by layer by following a tool path derived from the geometry of the part to be produced. It is possible to produce parts with complex geometries and the loss of material during manufacturing is at a minimum level due to this unique feature of additive manufacturing [7]. The foundations of the additive manufacturing method date back to the 1980s. It is known that the SLA-1 device produced by the 3D System company is the first 3D printer system [8]. Additive manufacturing is one of the modern manufacturing methods that has gained importance in recent years. It is a form of manufacturing in which the 3D model is obtained by adding layer by layer the powders to be built using geometric data. With additive manufacturing methods, parts with complex geometry can be obtained quickly [9]. The 3D manufacturing process is divided into subclasses such as SLA (Stereolithography), SLS (Selective Laser Sintering), FDM (Fused Deposition Modelling), DLP (Digital Light Processing), EBM (Electron Beam Melting) and LOM (Laminated Object Manufacturing) according to the materials used and the principle of combining materials. Table 1 shows a comparison of some additive manufacturing methods [10].

Table 1 Comparison of additive manufacturing methods [11]

Method	FDM	SLA	SLS	EBM	LOM
Working principle	Extrusion Stacking Technique	Solidification of photopolymer material with UV light	Sintering of powder with CO2 laser	Electron Beam Melting	Laser Cutting and Gluing of Sheets
Material used	ABS, polyamide, polycarbonate, polyethylene, polypropylene and investment casting wax.	Resin-based materials, acrylic epoxy, polypropylene.	Polyamide, polystyrene, carbon fiber and Aluminum added polyamide, polycarbonate, stainless steel, cobalt chrome, nickel chrome, titanium, ceramic.	Cobalt chrome and titanium alloys, ceramics.	Paper, plastic foam, metal and ceramic powder impregnated materials.
Resolution	Medium	Good	Weak	Weak	Medium
Strength	Good	Medium	Good	Good	Medium
Roughness	Medium	Good	Weak	Good	Medium

3D printing technology, which has caused changes by breaking new ground in diverse sectors, has moreover affected the construction sector. Building production in construction contains of significant stages like design, projecting and implementation. With the improvement of innovation, digital manufacturing has been used for a long time in the design and projecting phase of buildings. The design and projection of the building is supported two-dimensional (2D) drawings and scale models. Today, 2D drawings and prototypes are replaced by three-dimensional (3D) modelling techniques. Designers, architects and engineers have had the advantage of making the necessary changes in their projects easily, seeing the problems that may arise before the implementation and making the changes that occur in unforeseen situations during the implementation phase with digital modelling methods. The implementation phase of building production, on the other hand, did not change as fast as the design process and remained dependent on the traditional method of building production.



In the last years, the interest in 3D printing technology has increased because of the fact that it provides design freedom, less error margin, less material wastage, less waste material, and reduced cost compared to the traditional method in the

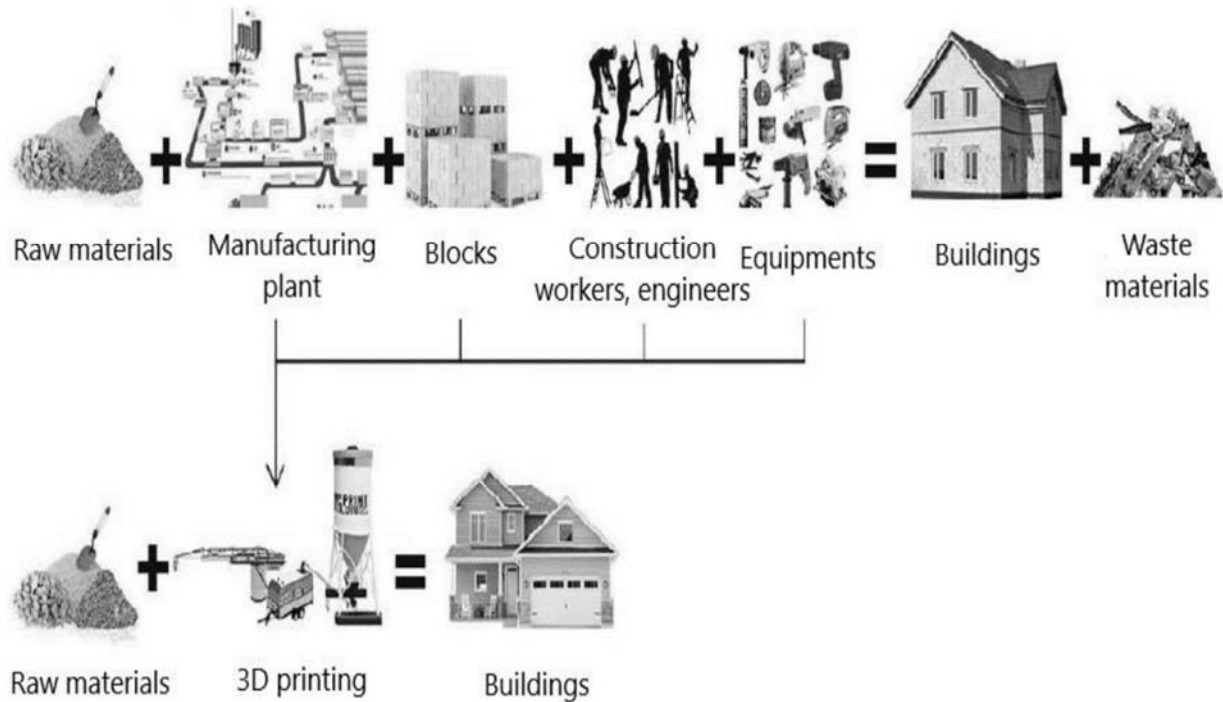


Figure 1: Comparison diagram of 3D printing automated building production with the traditional method [11]

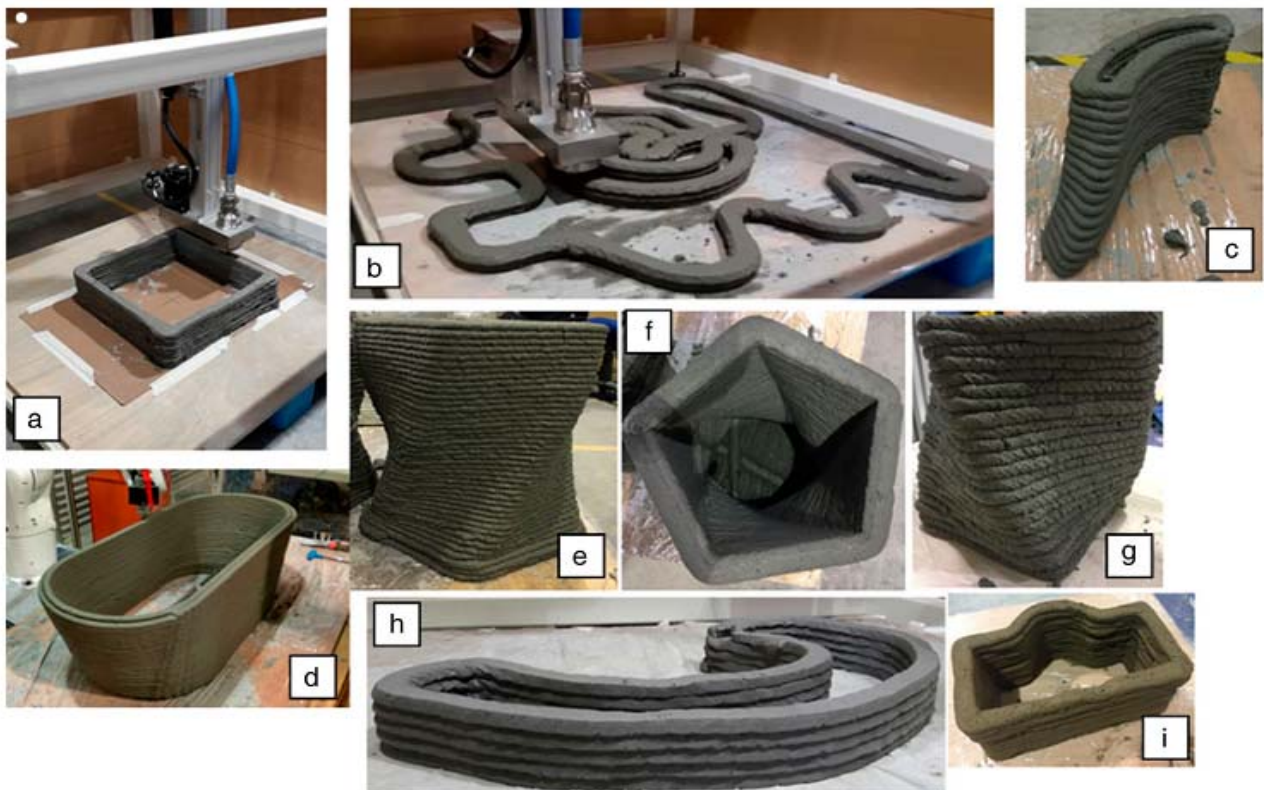


Figure 2: 3D concrete printed objects at SC3DP (prototype) [12]



construction industry [11]. Figure 1 shows the comparison of 3D printing and conventional methods whereas figure 2 shows the 3D concrete printed objects. A Chinese construction company produced 2 buildings with 3D Printer. Recycled concrete was used to produce the structures with a 3D Printer. After the 1100 m<sup>2</sup> building was produced in the factory, it was moved to the place where the building will be installed to be combined. A 3D Printer cement-like material is used to produce parts with a length of 32 m, a width of 10 m and a height of 6 m. This proprietary material includes fiberglass, concrete powder, sand and hardening material. It is also stated that it is a very earthquake proof material [13]. This 3D printed building is shown in figure 3. There are many restrictions which are imposed by material processing constraints but on the other hand progress of 3D printing study is quite rapid. Due to this phenomenon the additive manufacturing technology's potential can be fully utilized [14]. Biomimicry and bio-inspiration provides the background for the making new structures and low consumption of materials at same time so, this idea is critical. However, these techniques provide high sustainability and better mechanical qualities [15]. The primary importance is the evaluation of printing techniques and about thirty 3DCP initiatives has been taken around the globe. In 3DCP, by the use of material stacking deposition, target components are formed. The precision of extrusion control is a major concern during extrusion quality control [16]. In this regard, the use of real-time feedback control is a workable option. Real-time control systems have been developed by the researchers that not only controls the motions of robot arm use in 3D printing but also monitors the extrusion parameters. Conventional building techniques cause high accidents and rates of injuries are also countless while traditional techniques of building are connected with higher prices, lower efficiency and labor resilience [17].



(a) Connection details of the 3-D printed villa



(b) The concrete mould printed

Figure 3 (a & b): 3D printing production by WinSun [18]

### 3 Usability of 3D Printing Technology

Kazemian et al. (2017) carried out several experiments on the workability, printing accuracy and durability, and ease of printing of cementitious printing mixtures. In the experimental results, it was observed that the use of silica fume and Nano-clay for four types of mixtures increased the stability of the printing mixtures considerably [19]. Hojati et al. (2018) investigated the physical and mechanical properties of 3D printer concrete. The rheological properties of the mixture were considered in the design of the appropriate printhead. In addition, the length of the fiber to be included in the mixture in accordance with the diameter of the print head was investigated in the relationship between the interlayer bonding. The 3D printer machine consists of a fixed pump with a 15 mm diameter printer head and a 6-axis robotic arm that can provide various movements in different axes so that the material can be extruded properly. Consequently, it was defined that the hardening speed of the material should be adjusted well for printing and the width of the 3D printer head should be compatible with the fiber to be used, otherwise it is possible to clog the pump during the extruding process. In addition, it was concluded that attention should be paid to the ability of the material to carry the layer that will come on top of the layers [20]. Xia et al. (2019) developed geopolymers binder materials using only slag mixtures for use in powder-based 3D printers. With the research, geopolymer materials that can be used in powder-based 3D printers have been expanded with





mixtures of fly ash and slag. The effect of the amount of fly ash on the 3D printability properties of the geopolymer mixture and its compressive strength were investigated. As a result of the research, it was observed that the increase in the amount of fly ash did not affect the mixture settleability, but negatively affected the wettability and compressive strength of the mixture. It was determined that the best mixture was the samples containing 50% slag and 50% fly ash [21].

Arunothayan et al. (2020) have conducted research to produce ultra-high-performance fiber reinforced concrete with a 3D printer. Fiber less and 2% fiber reinforced UYPFRB was fabricated by 3D printer and compared with standard manufactured UYPFRB. As a result of the experimental study, the printability and shape stability of the UHPFRC were adequately provided. However, the compressive strength of the one poured into the normal mold was higher [22]. Marchment and Sanjayan (2020) discussed the problems affecting interlayer adherence, which has become one of the disadvantages of 3D printer concrete. They stated that the printing material should be fluid for the pumping process, but the mixture recipe created should not decrease the strength while affecting the consistency [23]. Ma et al. (2020) investigated the inadequacy of compatibility between adhering layers, which is one of the biggest problems of 3D printer concrete in the construction industry. A new cement mortar with additives was developed and cellulose fiber was used. When the mixture used is pumped, the amount of moisture on the surface of the printed layers is at the maximum level. Cellulose fiber retained excess water on the surface and contributed as an internal curing agent. Small amounts of clay and superplasticizer additives are used to optimize the rheological properties. Silica fume was used to improve water retention, silica powder was used to increase material density and fill micropores. According to the SEM results, the compatibility between the layers was significantly improved [24].

#### 4 Comparison of Benefits and Shortcomings for Use of 3D Printing

About 8% of the world anthropogenic CO<sub>2</sub> is produced by cement industry. The 3DCP places the concrete in a precise manner so the consumption of material is reduced by 3DCP [25]. 3DCP has also many positive characteristics like sustainable building materials can be used, save money time and energy. It also lowers the pollution caused by construction without compromising in mechanical properties of concrete. Also, majority of 3DCP is extrusion-based [26]. On the other hand, the idea of digital concrete is quite wide and surrounds the different types of methods which have potential to create bio-based structures. 3D printing formwork was investigated in both in-situ and prefabricated by [27]. 3DP concrete reinforcement building formworks are well defined as compared to the reinforcement construction of 3DPC on-site and its components. The transportation and preparation of concrete, casting of concrete, formwork's printing in factory, transportation of elements and assembly with its use as in-situ assembly are all components of prefabricated 3D printing formwork [28]. The workability of concrete plays a vital role in fresh and hardened properties of concrete [29], [30]. A good workable mix is desired for 3D printing so that desired mechanical properties may achieve. There is need of time research out 3DCP technologies so that it may transfer from laboratory testing phase to real life. No doubt, sand is a natural resource but with the passage of time is becoming limited in many areas; a number of nations are running out of this for utilization in civil engineering applications. By 3D printing recycled aggregates can be used a sustainable construction material. The preparation of mix for 3D printing requires special admixtures for maintaining workability so it takes extra economy. There is need to mitigate these shortcomings to use 3D printing in civil engineering construction industry.

#### 5 Conclusion

In this paper 3D printing technology and usability of 3D printing are described by the state-of-the-art review. The comparison of its shortcoming and benefits along with its possible use in future is briefly discussed. Based upon this study following conclusions have been made:

1. 3D printing is a technique that can be predicted to be used in the construction industry and can provide economic and environmental advantages. The use of this technique depends on the accuracy of printing, printing material, cost and time.
2. The use of 3D printing is dependent on conditions such as usability in large construction, development of building information modelling, production diversity and life cycle cost.
3. This technique will be used at the highest level once these conditions have been successfully overcome. Powder bed fusion (PBF) and directed energy deposition (DED) methods are the most suitable 3D printing techniques to



be used in the construction industry. These methods allow proper fabrication of the structure, but are constrained by cost, time, and maximum element size.

4. The transportation of robot arm, repairing, specific usage of admixtures makes it costly process so it increased the overall cost of the project.
5. Due to higher cost of operation and mixing of materials, it is not recommended on large scale use.

It is suggested to find new ways to make 3D printing economical process as sustainable construction can be performed by 3D printing as it requires less man power and provides greater efficiency.

## Acknowledgment

The author would like to thank every person who have helped in this research. The careful review and constructive suggestions by the anonymous reviewers are gratefully acknowledged.

## References

- [1] İ. E. Öztürk and G. B. Öztürk, "The Future of 3D Printing Technology in the Construction Industry: a Systematic Literature Review," *Eurasian J. Civ. Eng. Archit.*, vol. 2, no. 2, pp. 10–24, 2018, Accessed: Jun. 24, 2022. [Online]. Available: <https://dergipark.org.tr/en/pub/ejcar/issue/39134/434066>
- [2] Z. Wu, A. M. Memari, and J. P. Duarte, "State of the Art Review of Reinforcement Strategies and Technologies for 3D Printing of Concrete," *Energies*, vol. 15, no. 1. 2022. doi: 10.3390/en15010360.
- [3] C. Liu *et al.*, "Effect of sulphoaluminate cement on fresh and hardened properties of 3D printing foamed concrete," *Compos. Part B Eng.*, vol. 232, 2022, doi: 10.1016/j.compositesb.2022.109619.
- [4] H. G. Şahin and A. Mardani-Aghabaglou, "Assessment of materials, design parameters and some properties of 3D printing concrete mixtures; a state-of-the-art review," *Construction and Building Materials*, vol. 316. 2022. doi: 10.1016/j.conbuildmat.2021.125865.
- [5] Y. Yang, C. Wu, Z. Liu, H. Wang, and Q. Ren, "Mechanical anisotropy of ultra-high performance fibre-reinforced concrete for 3D printing," *Cem. Concr. Compos.*, vol. 125, 2022, doi: 10.1016/j.cemconcomp.2021.104310.
- [6] C. Liu *et al.*, "Influence of HPMC and SF on buildability of 3D printing foam concrete: From water state and flocculation point of view," *Compos. Part B Eng.*, 2022, Accessed: Jun. 27, 2022. [Online]. Available: <https://www.sciencedirect.com/science/article/pii/S1359836822004516>
- [7] A. Lou and C. Grosvenor, "Selective laser sintering, birth of an industry," *Dep. Mech. Eng. Univ. Texas, Austin, TX*, vol. 8, 2012.
- [8] D. Bourell *et al.*, "Materials for additive manufacturing," *CIRP Ann. - Manuf. Technol.*, vol. 66, no. 2, pp. 659–681, 2017, doi: 10.1016/j.cirp.2017.05.009.
- [9] K. Özsoy and B. Duman, "Eklemeli İmalat (3 Boyutlu Baskı) Teknolojilerinin Eğitimde Kullanılabilirliği," *Int. J. 3D Print. Technol. Digit. Ind.*, vol. 1, no. 1, pp. 36–48, 2017, Accessed: Jun. 24, 2022. [Online]. Available: <https://dergipark.org.tr/en/pub/ij3dptdi/issue/33982/376178>
- [10] I. Celik, F. Karakoc, M. C. Cakir, and A. Duysak, "Rapid Prototyping Technologies and Application Areas," *J. Sci. Technol. Dumlupinar Univ.*, vol. 31, no. 8, pp. 53–70, 2013, Accessed: Jun. 24, 2022. [Online]. Available: <https://dergipark.org.tr/en/pub/dpufbed/issue/35926/404617>
- [11] T. Uygunoğlu *et al.*, "3D TEKNOLOJİSİ İLE YAPI MALZEMESİ ÜRETİMİNDEKİ GELİŞMELER," *Int. J. 3D Print. Technol. Digit. Ind.*, vol. 03, pp. 279–288, 2019, Accessed: Jun. 24, 2022. [Online]. Available: <https://dergipark.org.tr/en/pub/ij3dptdi/issue/51591/559782>
- [12] Y. Wei Daniel Tay, B. Panda, S. Chandra Paul, N. Ahamed Noor Mohamed, M. Jen Tan, and K. Fai Leong, "3D printing trends in building and construction industry: a review," *Taylor Fr.*, vol. 12, no. 3, pp. 261–276, Jul. 2017, doi: 10.1080/17452759.2017.1326724.
- [13] "No Title," 2015. <http://priyoid.com> (accessed Jun. 24, 2022).
- [14] C. R. Rollakanti and C. V. S. R. Prasad, "Applications, performance, challenges and current progress of 3D concrete printing technologies as the future of sustainable construction - A state of the art review," *Mater. Today Proc.*, Apr. 2022, doi: 10.1016/j.matpr.2022.03.619.
- [15] G. H. Andrew Ting, T. K. Noel Quah, J. H. Lim, Y. W. Daniel Tay, and M. J. Tan, "Extrudable region parametrical study of 3D printable concrete using recycled glass concrete," *J. Build. Eng.*, vol. 50, 2022, doi: 10.1016/j.jobbe.2022.104091.
- [16] G. S. Lakshmi Devi and P. Srinivasa Rao, "Flexural Behavior of Quaternary Blended Fiber Reinforced Self Compacting Concrete Slabs Using Mineral Admixtures," in *IOP Conference Series: Materials Science and Engineering*, 2020, vol. 1006, no. 1. doi: 10.1088/1757-899X/1006/1/012020.



- [17] G. S. L. Devi, C. V. S. R. Prasad, and P. S. Rao, "Influence of mineral admixtures on structural behaviour of Quaternary Blended Self Compacting Concrete reinforced beams with addition of crimped steel fibers," *Mater. Today Proc.*, vol. 57, pp. 2325–2329, 2022, doi: 10.1016/j.matpr.2022.01.125.
- [18] P. Wu, J. Wang, and X. Wang, "A critical review of the use of 3-D printing in the construction industry," *Automation in Construction*, vol. 68, pp. 21–31, 2016. doi: 10.1016/j.autcon.2016.04.005.
- [19] A. Kazemian, X. Yuan, E. Cochran, and B. Khoshnevis, "Cementitious materials for construction-scale 3D printing: Laboratory testing of fresh printing mixture," *Constr. Build. Mater.*, vol. 145, pp. 639–647, 2017, doi: 10.1016/j.conbuildmat.2017.04.015.
- [20] H. Maryam *et al.*, "3D Printing of Concrete: a Continuous Exploration of Mix Design and Printing Process," *42nd IAHS WORLD Congr. Hous. Dign. Mank.*, no. May, pp. 1–14, 2018, Accessed: Jun. 24, 2022. [Online]. Available: [https://www.researchgate.net/profile/Maryam-Hojati/publication/325076823\\_3D\\_Printing\\_of\\_Concrete\\_a\\_Continuous\\_Exploration\\_of\\_Mix\\_Design\\_and\\_Printing\\_Process/links/5af5384c4585157136ca447a/3D-Printing-of-Concrete-a-Continuous-Exploration-of-Mix-Design-and-](https://www.researchgate.net/profile/Maryam-Hojati/publication/325076823_3D_Printing_of_Concrete_a_Continuous_Exploration_of_Mix_Design_and_Printing_Process/links/5af5384c4585157136ca447a/3D-Printing-of-Concrete-a-Continuous-Exploration-of-Mix-Design-and-)
- [21] M. Xia, B. Nematollahi, and J. Sanjayan, "Printability, accuracy and strength of geopolymer made using powder-based 3D printing for construction applications," *Autom. Constr.*, vol. 101, pp. 179–189, 2019, doi: 10.1016/j.autcon.2019.01.013.
- [22] A. R. Arunothayan, B. Nematollahi, R. Ranade, S. H. Bong, and J. Sanjayan, "Development of 3D-printable ultra-high performance fiber-reinforced concrete for digital construction," *Constr. Build. Mater.*, vol. 257, 2020, doi: 10.1016/j.conbuildmat.2020.119546.
- [23] T. Marchment and J. Sanjayan, "Penetration Reinforcing Method for 3D Concrete Printing," in *RILEM Bookseries*, vol. 28, 2020, pp. 680–690. doi: 10.1007/978-3-030-49916-7\_68.
- [24] G. Ma, N. M. Salman, L. Wang, and F. Wang, "A novel additive mortar leveraging internal curing for enhancing interlayer bonding of cementitious composite for 3D printing," *Constr. Build. Mater.*, vol. 244, 2020, doi: 10.1016/j.conbuildmat.2020.118305.
- [25] Y. Chen *et al.*, "Mechanical anisotropy evolution of 3D-printed alkali-activated materials with different GGBFS/FA combinations," *J. Build. Eng.*, vol. 50, 2022, doi: 10.1016/j.jobe.2022.104126.
- [26] S. Nazar, J. Yang, B. S. Thomas, I. Azim, and S. K. Ur Rehman, "Rheological properties of cementitious composites with and without nano-materials: A comprehensive review," *Journal of Cleaner Production*, vol. 272, 2020. doi: 10.1016/j.jclepro.2020.122701.
- [27] G. Cesaretti, E. Dini, X. De Kestelier, V. Colla, and L. Pambaguian, "Building components for an outpost on the Lunar soil by means of a novel 3D printing technology," *Acta Astronaut.*, vol. 93, pp. 430–450, 2014, doi: 10.1016/j.actaastro.2013.07.034.
- [28] C. Gosselin, R. Duballet, P. Roux, N. Gaudillière, J. Dirrenberger, and P. Morel, "Large-scale 3D printing of ultra-high performance concrete - a new processing route for architects and builders," *Mater. Des.*, vol. 100, pp. 102–109, 2016, doi: 10.1016/j.matdes.2016.03.097.
- [29] M. Abrar, "WORKABILITY OF BANANA FIBERS REINFORCED CONCRETE FOR EASY POURING," *3rd Conf. Sustain. Civ. Eng.*, no. 21, pp. 5–9, 2021.
- [30] M. Abrar and M. Ali, "Workability of Concrete Having Hybrid Natural Fibers of Different Lengths for Easy Pouring," pp. 1–6, 2021.



# APPRAISAL OF DESERT SAND AS A SOURCE OF SUSTAINABLE DEVELOPMENT

<sup>a</sup> Muhammad Arif, <sup>b</sup> Muhammad Usman Arshid\*, <sup>c</sup> Abdul Waheed

a: Department of Civil Engineering, University of Engineering and Technology Taxila, [marifkhattak99@gmail.com](mailto:marifkhattak99@gmail.com)  
b: Department of Civil Engineering, University of Engineering and Technology Taxila, [usman.arshid@uettaxila.edu.pk](mailto:usman.arshid@uettaxila.edu.pk)  
c: Department of Civil Engineering, Military College of Engineering Risalpur, [waheed\\_mce@yahoo.com](mailto:waheed_mce@yahoo.com)  
\* Corresponding author: [usman.arshid@uettaxila.edu.pk](mailto:usman.arshid@uettaxila.edu.pk)

**Abstract-** Sustainable development demands exploring innovative construction materials and waste recycling techniques. However, the desert sand present in huge volumes remains unexplored for its suitability as construction material for decades. The stone processing industry produces large volumes of marble dust (WMD) waste, and its uncontrolled disposal poses a serious environmental hazard. The current study aimed to evaluate the physical and engineering properties of dune sand collected from Thal, a famous desert in Pakistan. After the initial exploration, the research work further evaluated the effectiveness of WMD as an additive for improving this sand. WMD was mixed with sand in proportions varying from 5-30 %. The experiments yielded promising improvements in dry density and unconfined compressive strength (UCS). Fifteen Percent (15%) by volume was identified as the optimum dosage of the WMD. The research work paves the path for utilizing desert sand in civil engineering projects and proposes fruitful recycling of WMD, reducing environmental pollution. Further studies are recommended to expand the scope of the investigation to evaluate its suitability as a mortar for masonry works and a potential concrete ingredient.

**Keywords-** Desert, WMD, Soil Improvement, Pollution, Dune sand.

## 1 Introduction

The Thal desert is situated in the southwestern part of the Punjab province in Pakistan. The geographic coordinates taken at the sample collection points are 31° 10' N and 71° 30' E. It has an approximate length of 190 miles (306 km) with a maximum breadth of 70 miles (113 km). The total area of the Thal desert is about 10,000 km<sup>2</sup> (3,900 sq mi). The Thal desert soil is alluvial with sandy textured dunes covering 50 to 60 per cent of the area. The maximum and minimum temperatures of the Thal desert are recorded at about 44 °C and less than 0 °C, respectively. The average annual precipitation varies from 385 mm in the north-east to 170 mm in the south. Approximately three-fourths of annual rainfall is received during monsoon. [Source: Thal Development Authority]

A large quantity of waste marble dust is produced while cutting and processing different stones. Almost twenty-five (25%) of the raw marble stone is lost in the form of dust. During the fiscal year 2016-2017, 4.9 million tons of wastage were generated in Pakistan. More than 2.15 million tons were generated in Khyber Pakhtunkhwa province (KPK), 1.92 million tons in Baluchistan, and 0.82 million tons in the previous FATA region. [1] Waste marble dust is hazardous if it is not controlled or recycled. If mixed with soil in some proportions, the results may favour geotechnical properties and effective waste management. [2]. Various industries regularly produce ceramic and marble waste everywhere in Algeria and worldwide. It is a big problem for the waste management authorities of every country. This type of waste poses serious health hazards and environmental pollution. We can recycle these types of waste to improve different soil types and waste management policies [3]. Huge volumes of waste marble dust, especially colloid, deteriorate the air quality index. It is the utmost requirement of the time to reduce the production of WMD by introducing modern processing and recycling techniques. Sustainable development requires the utilization of waste materials in the construction industry. The utilization of WMD as a slurry has been evaluated and reported to produce encouraging results [4]. Sand dunes have very low



resilience; if disturbed, it becomes very difficult to stabilize again to their original position. [5]. The waste marble dust was mixed with desert sand in Oman in different proportions. Its effect on the physical properties of soil was studied and reported to produce considerable improvement in the studied properties [6]. The utilization of WMD as a fine aggregate has also been studied, and a mixture of sand and WMD in 80:20 proportion was found to produce better consistency and flexure strength [7]. Waste marble dust is not only mixed with sand, but it can also be used in black cotton soil, and it gave good results in the index properties of black cotton soil. [8]. The effectiveness of recycled waste marble dust as a grout for in situ soil improvement and deep mixing has been evaluated and reported to improve considerably. Its utilization as grouting material can be environment-friendly recycling of the WMD [9]. In geotechnical engineering, the practice of improving the strength of loose soil with waste marble materials has been increasing [10]. Expansive soil requires treatment to provide a stable foundation for roads and buildings. The studies concluded that the waste marble dust and plastic strips increase unconfined compressive strength and decrease the free swell of soil.[11, 12].

It is evident from the presented literature that researchers have been trying and testing the effectiveness of WMD for various purposes in civil engineering applications. The current study aimed to explore locally produced waste marble dust and desert sand and evaluate their raw physical and mechanical properties. Further to initial exploration, this research also evaluates WMD's potential for improving the target geotechnical properties. The purpose of this research is the maiden appraisal of geotechnical properties of dune sand of Thal desert in Pakistan.

## 2 Experimental Procedures

The desk study and literature review exercise was followed by a reconnaissance survey of the sample collection site, i.e. Thal desert of Pakistan (Noor Pur Thal). Visual Inspection of the soil characteristics and acquisition of geographic coordinates, followed by collecting samples for the detailed investigation in a laboratory. All the tests enlisted in Table 1 were performed according to the relevant ASTM standards. The standards and procedures followed for each test were carried out on natural and modified soil. Table 2 presents the proportion of sand: WMD and their assigned matrix IDs. The tests enlisted in Table 1 were repeated on all the mixes presented in Table 2.

Table 1 Test Description and Standard Reference

Test	Specification
Atterberg limits	ASTM D4318
Specific gravity	ASTM D854
Compaction Test (OMC and MDD)	ASTM D1577
USC-Unconfined compressive strength	ASTM D2166

Table 2 Mix Proportions and Matrix IDs

S.no	Soil (%)	WMD (%)	Notation
1	100	0	NAT
2	95	5	WMD 1
3	90	10	WMD 2
4	85	15	WMD 3
5	80	20	WMD 4
6	75	25	WMD 5
7	70	30	WMD 6

## 3 Research Methodology

A comprehensive work plan was devised to streamline the research execution, which is presented below. The Desk study included exploration of the existing data related to the study area, dune sand and the potential additive to improve the studied properties of the geomaterials. The flow chart is shown in figure 1.

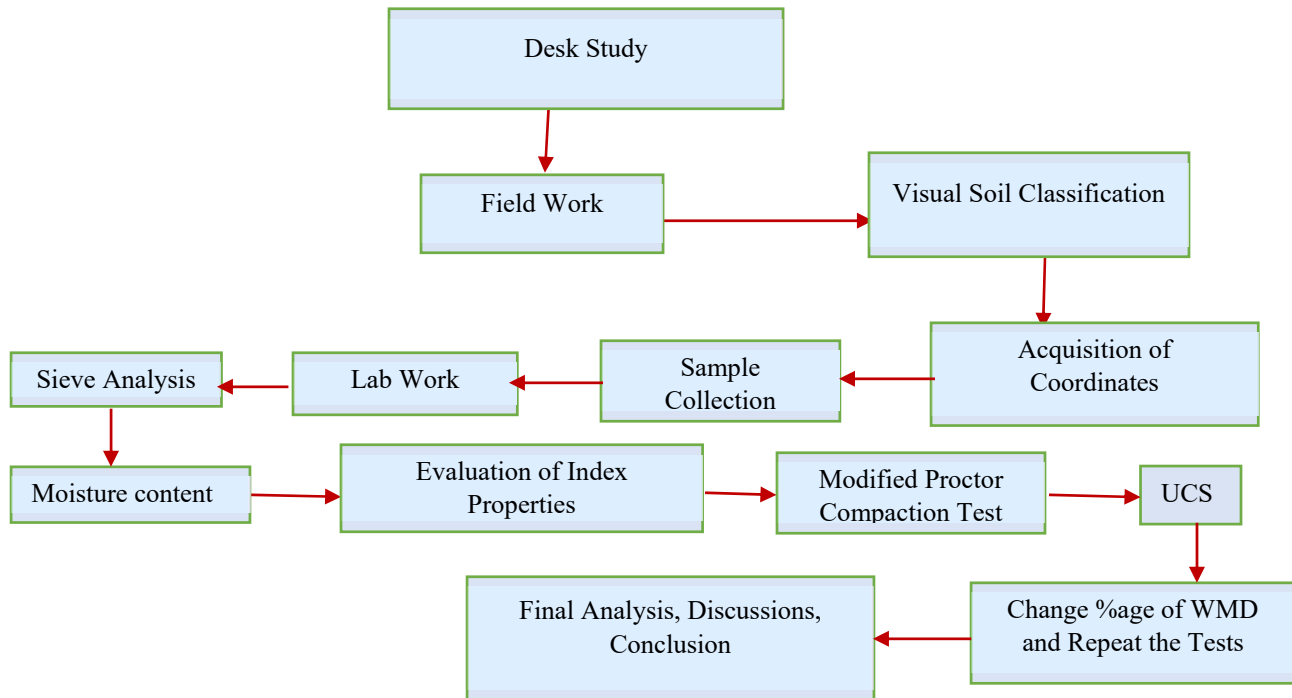


Figure 1: Flowchart

### 3.1 Material

The dune sand collection point is located near Noor Pur Thal of district Khushab Punjab. The geographic coordinates taken at the site are 31<sup>o</sup> 10' N and 71<sup>o</sup> 30'. The basic tests were performed to evaluate the physical and chemical properties of sand and are presented in Table 3 below

Table 3. Physical and chemical composition of soil

Test Description	Property Determined	Unit	Value
AASHTO Classification			A-2-4
Physical properties	Natural Moisture content	%	9.3
	Specific gravity		2.71
Atterberg limits	Liquid limit	%	NP
	Plastic limit	%	NP
	Plasticity index	%	N.P
Modified proctor Test	OMC	%	9.3
	MDD	lb/cft	109.
Strength test	UCS	kg/cm <sup>2</sup>	0

### 3.2 Additives

The additive used for this research is Waste Marble Dust (WMD), collected from the marble industry located near Taxila, Pakistan. Waste marble dust is high in calcium oxide content which is cementing property, but it produces many environmental hazards. That's why we select WMD as an additive for desert sand. The Chemical composition of Waste marble dust is shown in Table 4.



Table 4 Chemical composition of WMD.

Oxide Concentrations %	CaO	Al <sub>2</sub> O <sub>3</sub>	SiO <sub>2</sub>	Fe <sub>2</sub> O <sub>3</sub>	MgO
WMD	42.45	0.52	26.35	9.40	1.52

## 4 Results

### 4.1 Index properties

Basic index properties (LL, PL & PI) and gradation were determined to classify further collected soil samples. The Atterberg's limits tests were attempted on all the mixes, but all the mixes remain non-plastic even at the maximum dosage of WMD, i.e. 30 %. The gradation presented in figure 2 led to the classification of raw soil as A-2-4. It means our soil is silty or clayey gravel sand. The gradation curve of WMD is shown in figure 3.

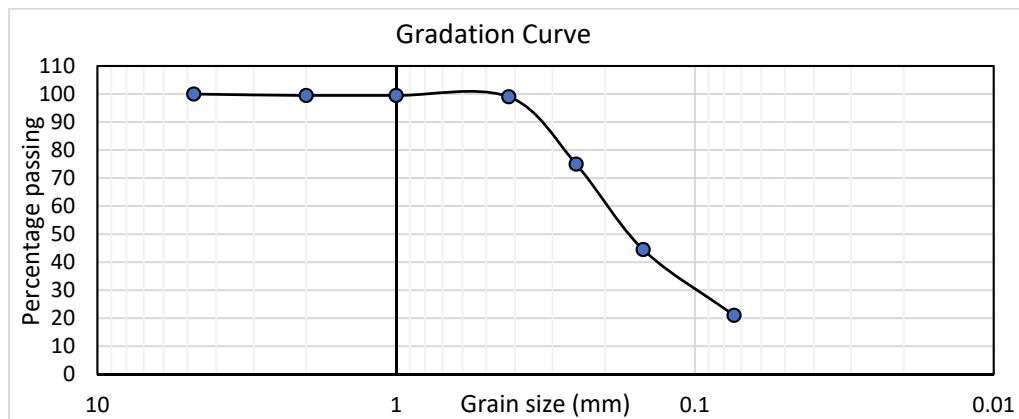


Figure 2: Gradation Curve of Dune Sand

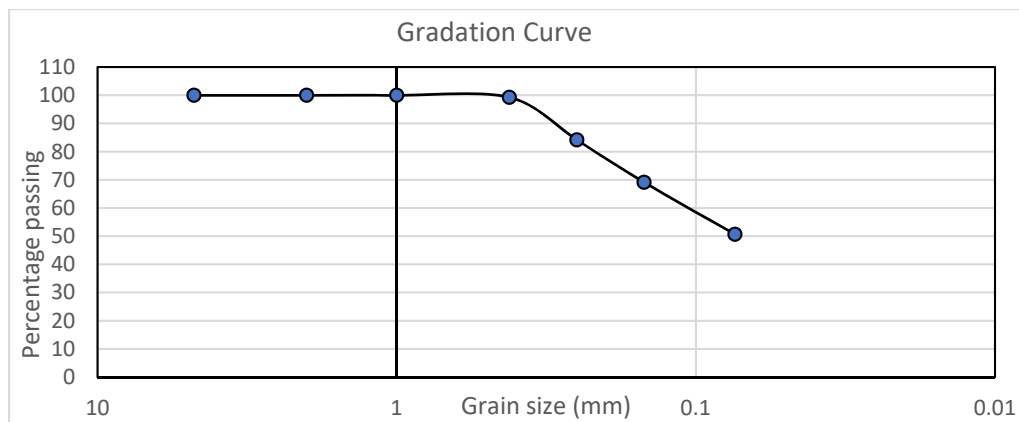


Figure 3: Gradation Curve of WMD

### 4.2 MDD

We performed a modified proctor compaction test according to ASTM D1557. Each test was performed twice to determine the effect of waste marble dust on MDD and OMC of soil. The results show that the waste marble dust increases the MDD of the soil, as shown in figure 4. The MDD of raw sand (pure sand without additive) was 109.3 lb/ft<sup>3</sup>. The MDD increased to 115.9 lb/ft<sup>3</sup> with the addition of WMD, showing a 6 % increase with 30% WMD. The MDD increased due to the cementitious effect of CaO present in waste marble dust and the replacement of waste marble dust particles having a high specific gravity of mixes.

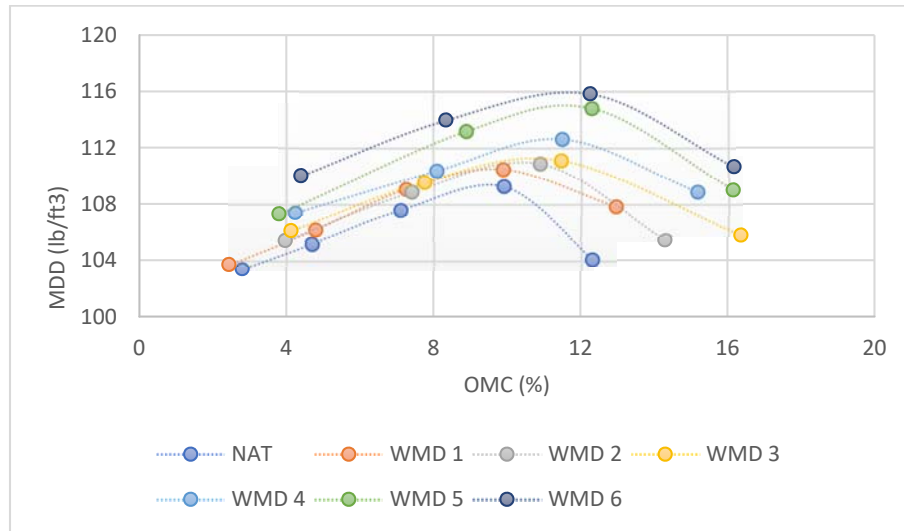


Figure 4: Effect of WMD on compaction tests

### 4.3 OMC

An increase in OMC was observed with the addition of waste marble dust. The OMC increased from 9.3% to 11.8% by adding 30% WMD, as shown in figure 4. OMC increase shows that an increase in a dry unit weight of soil sample improves the soil properties and reduces the permeability in soil. Hence, mixing waste marble dust in desert sand improves the geotechnical behaviour of that sand.

### 4.4 Unconfined Compressive Strength Test

Unconfined compressive strength test was performed on raw soil and soil: WMD mixes twice on all the mixes. The pure sand's unconfined compressive strength was zero while increasing to 0.15 (kg/cm<sup>2</sup>). The improvement in UCS for all the mixes is shown in figure 5. Adding waste marble dust to soil produces a cohesive effect in the soil and achieved 0.15(kg/cm<sup>2</sup>) unconfined compressive strength by adding 30% of waste marble dust. Hence, by adding waste marble dust to desert sand, the compressive strength of that sand increased.

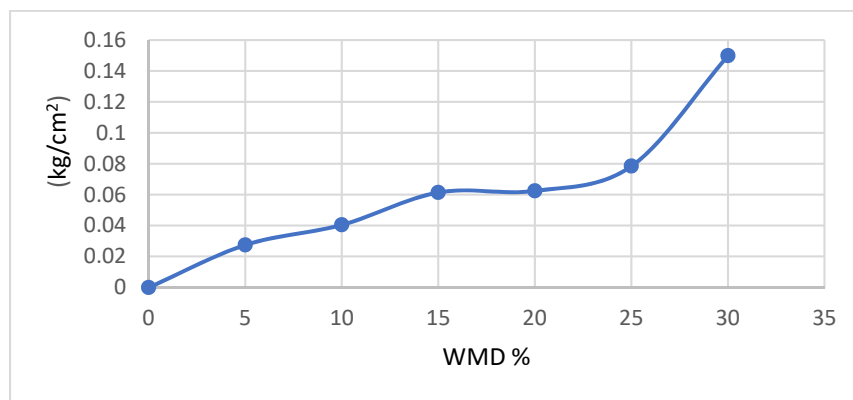


Figure 5: Combine result of UCS with varying percentages of WMD

## 5 Conclusion

This paper presented a maiden appraisal of the geotechnical characteristics of dune sand in the Thal desert. The initial appraisal also includes an evaluation of WMD as an additive for the dune sand. The experimental study proves WMD's effectiveness for stabilizing dune sand. The following conclusions have been drawn from this study:





1. The current study evaluated the physical and engineering properties of dune sand collected from Thal, a famous dessert in Pakistan, and waste marble dust's effectiveness in improving dune sand's physical and mechanical properties.
2. The Desert/dune sand is an abundant material, and the current study paves the way for its effective utilization in the construction industry.
3. The physical and engineering properties of desert sand can be improved by adding waste marble dust; hence WMD has been identified as an effective additive soil improvement.
4. Using waste marble dust as an additive can reduce environmental hazards posed by its uncontrolled disposal.

This research recommends expanding the investigation's scope to evaluate its suitability as a mortar for masonry works and a potential concrete ingredient.

## References

- [1] A. Ghani, Z. Ali, F. A. Khan, S. R. Shah, S. W. Khan, and M. Rashid, "Experimental study on the behavior of waste marble powder as partial replacement of sand in concrete," *SN Applied Sciences*, vol. 2, no. 9, pp. 1-13, 2020.
- [2] A. Waheed, M. U. Arshid, R. A. Khalid, and S. S. S. Gardezi, "Soil Improvement Using Waste Marble Dust for Sustainable Development," *Civil Engineering Journal*, vol. 7, no. 9, pp. 1594-1607, 2021.
- [3] S. Deboucha, Y. Sail, and H. Ziani, "Effects of ceramic waste, marble dust, and cement in pavement sub-base layer," *Geotechnical and Geological Engineering*, vol. 38, no. 3, pp. 3331-3340, 2020.
- [4] S. S. Kushwah and S. Gupta, "EFFECT OF MARBLE SLURRY DUST AND LIME STABILIZATION ON GEOTECHNICAL PROPERTIES OF FINE SAND," *International Journal of research in Engineering and Technology (2011)*, pp. 62-72, 2017.
- [5] R. A. Khan, "Creating forests resources in Thal desert for combating land degradation," *World Environment Day 16th June-2011*. [http://pecongress.org.pk/images/upload/books/\(8\)%20Creating%20Forests%20Resources](http://pecongress.org.pk/images/upload/books/(8)%20Creating%20Forests%20Resources), vol. 20, 2011.
- [6] M. U. Qureshi, B. Al-Sawafi, M. Al-Washahi, M. Al-Saidi, and S. Al-Badi, "The Sustainable Use of Fine Marble Waste Powder for the Stabilization of Desert Sand in Oman," in *International Congress and Exhibition "Sustainable Civil Infrastructures: Innovative Infrastructure Geotechnology"*, 2017, pp. 303-313: Springer.
- [7] L. Kherraf, H. Hebhouh, A. Abdelouahed, and W. Boughamssa, "Comparative study on the performance of sand-based mortars from marble, floor tile and cinder block waste," *Journal of Building Engineering*, p. 103433, 2021.
- [8] P. S. Singh and R. Yadav, "Effect of marble dust on index properties of black cotton soil," *Int J Engg Res Sci Tech*, vol. 3, pp. 158-63, 2014.
- [9] M. Z. Alnunu and Z. Nalbantoglu, "Performance of Using Waste Marble Dust for the Improvement of Loose Sand in Deep Soil Mixing," *Arabian Journal for Science and Engineering*, pp. 1-14, 2021.
- [10] N. W. Jassim, H. A. Hassan, H. A. Mohammed, and M. Y. Fattah, "Utilization of waste marble powder as sustainable stabilization materials for subgrade layer," *Results in Engineering*, p. 100436, 2022.
- [11] S. Amena and W. F. Kabeta, "Mechanical Behavior of Plastic Strips-Reinforced Expansive Soils Stabilized with Waste Marble Dust," *Advances in Civil Engineering*, vol. 2022, 2022.
- [12] A. Waheed, M. U. Arshid, R. A. Khalid, and S. S. S. J. C. E. J. Gardezi, "Soil improvement using waste marble dust for sustainable development," vol. 7, no. 9, pp. 1594-1607, 2021.



# CONCEPTUAL DESIGN OF RESIDENTIAL BUILDINGS FOR DAYLIGHT EMPLOYING CONTEMPORARY BEST PRACTICES

*<sup>a</sup> Nida Azhar, <sup>b</sup> Faiza Saeed, <sup>c</sup> Farrukh Arif\**

a: Department of Urban & Infrastructure Engineering, NEDUET, [nazhar@cloud.neduet.edu.pk](mailto:nazhar@cloud.neduet.edu.pk)

b: Department of Civil Engineering, NEDUET, [faizasaeed@cloud.neduet.edu.pk](mailto:faizasaeed@cloud.neduet.edu.pk)

c: Department of Civil Engineering, NEDUET, [farrukh@cloud.neduet.edu.pk](mailto:farrukh@cloud.neduet.edu.pk)

\* Corresponding author: Email ID: [farrukh@cloud.neduet.edu.pk](mailto:farrukh@cloud.neduet.edu.pk)

**Abstract-** With the increasing energy demands and greenhouse gas emissions, daylight has been considered one of the crucial aspects of passive design strategies to be incorporated in buildings. The literature review indicated a lack of studies to guide the utilization and suitability of such daylight systems for buildings. This article studies contemporary passive daylight incorporating strategies that can be adopted in buildings considering the local context's thermal and visual comfort and privacy. After a thorough review, this study recommends having WWR near 50% for the sun-facing walls with a light shelf and solitude to be part of the conceptual design.

**Keywords-** Energy Efficiency, Daylight, Building envelope, Residential units.

## 1 Introduction

Building energy consumption accounts for almost 40% of the world's energy consumption [1]. Current energy production is mainly based on fossil fuels, and its demand is increasing daily across the globe. In Pakistan, an increase in the urban population in recent decades has led to rising energy demand and, consequently, increased carbon dioxide (CO<sub>2</sub>) emissions [2]. Several countries across the globe are striving to shift their electricity generation to renewable resources. Still, the downside of this shift is energy from such resources is often inconsistent and intermittent [1].

There can be two aspects to resolving the energy problem: reducing energy consumption and improving the energy efficiency in buildings. While focusing on making buildings energy efficient, passive design strategies can be incorporated to reduce the energy demand of residential buildings. The passive design includes orientation of the main façades and windows, wall thickness, thermal insulation, window details, sunroom for passive solar heating, shading devices, etc. [3]. Passive buildings require less energy as they strike a balance between the heat losses and the heat gains concerning the particular climatic condition of the building's location.

Natural light is vital in improving buildings' environmental quality and energy efficiency [4]. This study is focused on the utilization of daylighting to reduce the consumption of energy during the daytime using relevant passive design strategies. In a residential building, daylight can penetrate through windows, window glasses, or other openings. This study discusses several contemporary practices, which are discussed in detail, can better utilize daylight and reduce energy demand.

Designers need to understand the importance of not only the utilization of daylight but its impact on visual and thermal comfort. A study focused on suitable daylight intensity for local residential units reports that the daylight factor is higher than what is recommended by the Chartered Institute of Building Service Engineers (CIBSE) [5]. Incorporating thermal comfort in design is challenging due to the unavailability of commonly accepted standards. Moreover, no globally agreed glare metric for visual comfort can be applied to various conditions [6]. Therefore, this study provides a conceptual design



strategy through a review of contemporary practices. Hence, daylight can be utilized more efficiently in residential designs considering thermal and visual comfort at the same time.

## **2 Scope**

The scope of this study is to study design alterations in building envelopes focused on daylight optimization for residential units keeping in mind the thermal and visual comfort aspects of daylight.

## **3 Objective**

The objective of this study is to propose a conceptual design of a residential unit based on contemporary best practices incorporating thermal and visual comfort and privacy as per social norms.

## **4 Methodology Design**

The review has been conducted from codes, reputed journal publications, and conference proceedings from 2017-2022. The review methodology is focused on a few design alterations such as Window Wall Ratio (WWR), Atrium Solatube, Light Shelf, and Kinetic Shading System.

## **5 Review of Contemporary Passive Design Strategies for Daylight Utilization**

Before discussing the strategies, it is essential to understand how to measure daylight in buildings. The following discussion offers the various methods used for the measurement of daylight. A lux meter can measure the luminance level in a room. Daylight factor (DF) is a daylight availability metric that expresses as a percentage the amount of daylight available inside a room (on a work plane) compared to the amount of unobstructed daylight available outside under overcast sky conditions [7]. Useful daylight illuminance (UDI) is a daylight availability metric that corresponds to the percentage of the occupied time when a target range of illuminances at a point in space is met by daylight [8]. It can be calculated with simulations. Multiple simulation engines are available for daylight analysis; one study used Integrated Environmental Solution-Virtual Environment (IES-VE) for daylight analysis [9]. Notably, desirable illuminance thresholds for residential buildings are still argued. BREEAM and LEED take 300 lux as the benchmark for general visual tasks, and 3000 lux is a typical upper threshold for the overlit issue [10].

Pakistan, a country with many sunny days, can considerably use this resource of natural daylight for its energy demands. Over the years, many passive design strategies have been incorporated to use daylight in residential units efficiently. This study discusses the building envelope aspect of energy efficiency. Since building envelope has been proven essential for decreasing energy consumption and providing thermal comfort and healthy internal spaces [11].

Within the building envelope, the Window to wall ratio (WWR) also needs to be considered in the passive design for better illuminance and proper distribution of daylight. A study of the apartment building in Kathmandu valley recommends that the Window to wall ratio be 24% [12]. ASHRAE 90.1-2010 suggests WWR capped at 40%. WWR for local conditions is suggested to increase from 26% to 50% [13]. As far as thermal comfort is concerned, the increased window size will cause an increase in heat gain because the thermal resistance of the window glass is lower than wall thermal resistance [14]. This issue can be resolved by employing another passive technique and increasing WWR to ensure thermal comfort. For visual comfort, a study found that having less than 50% WWR cause unacceptable visual comfort and illuminance performance. Hence, the recommended WWR ratio will provide visual comfort [15].

Atriums have been proven to increase daylight for many years. It is equally effective today to reduce buildings' energy usage in cold and warm climates by supplying daylight and natural ventilation to interiors if appropriately designed. Atriums, if not, adequately designed atriums can increase energy consumption or cause visual and thermal discomfort [9]. Atrium can have different sizes and geometry. It must be carefully considered because the physical characteristics of the atrium, along with roof configuration, enclosing surfaces, and adjacent spaces, influence the amount of daylight reaching the interior spaces [9]. Due to the complexity of the atrium design, suitable design needs to be explored carefully for the local context before implementation. Therefore, achieving a suitable design of the atrium will lead to a cost-efficient way of making the building energy efficient. Figure 1 illustrates different forms of the atrium.

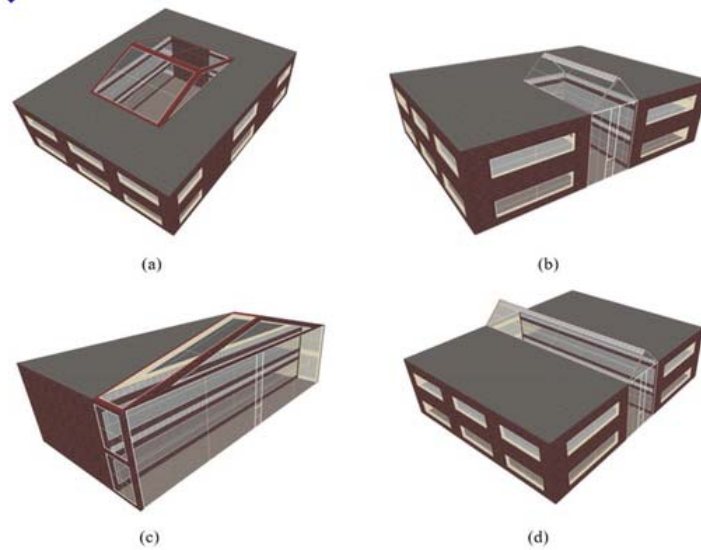


Figure 1: Four forms of atriums [9]

To capture daylight in a building, solatube technology has gained tremendous popularity due to its positive environmental impact and the resulting internal health conditions. The significant advantage of solatube is that it transfers daylight efficiently while blocking excessive heat and providing visual comfort [16]. The basic principle behind the solatube is multi reflections on the highly reflective internal surfaces of the tube. It has three zones, the capture zone, which is the receiving part of the light; the transfer zone, which is the reflecting tube; and the delivery zone, which emits light.

The initial cost of this system is high, and energy savings, in the long run, are not merely enough to make people convinced to use it. Nevertheless, the other benefits solatube offers, such as visual comfort, environment pollution, healthy conditions, indoor environmental quality, and productivity improvements, can make customers inclined towards it [16]. Figure 2 shows the working of a Solatube.

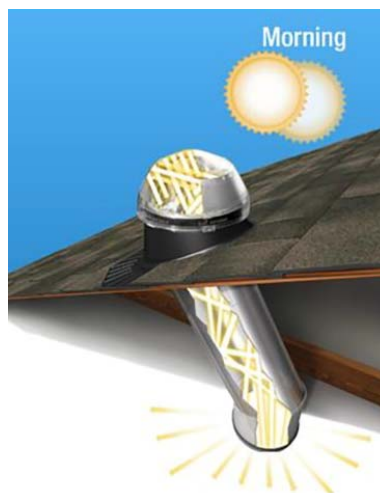


Figure 2 Solatube [16]

A light shelf is one of the light-guiding system (LGS) technology. LGS is easy to install compared to conventional sun shading devices such as solar screens and roller blinds, which block natural light penetration, thus reducing natural light distribution in buildings. LGS reflects, refracts, or deflects sunbeams from facades [17]. Contrary to conventional techniques, they improve light distribution in the room and reduce glare and overheating. If an optimal light shelf is used, thermal comfort can improve up to 81% [18]. Light shelves are also an efficient tool for optimizing and controlling indoor



daylight delivery, thus increasing visual comfort [19]. One of the reasons light shelves are gaining popularity in exploration and research during recent years is because light shelves are very cost-efficient solutions to utilize daylight [20]. Figure 3 shows a Daylight reflector.

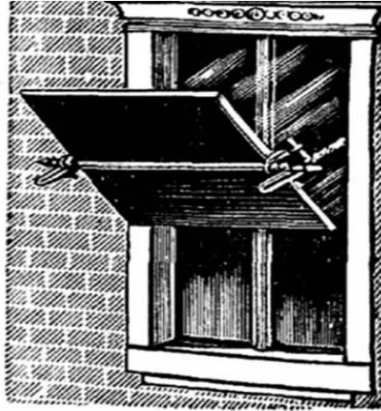


Figure 3: Daylight reflector by W. Hanifch and Co. [20]

A kinetic shading system is another mechanism that works independently and maximizes daylight while preventing direct daylight. A kinetic shading system can decrease the indoor temperature by 2-3 degrees, thus ensuring thermal comfort [21]. This system also diffuses daylight equally, reducing low glare and over-illumination [22], providing visual comfort. Construction cost is the major drawback of kinetic shading systems; otherwise, optimal design for movement and rotation of shader has been achieved [23]. Figure 4 shows an Exterior view of kinetic shading



Figure 4: Exterior view of kinetic shading [22]

## 6 Discussion and Conceptual Design

Passive design strategies are very effective, and this area has been explored for many years. However, lack of awareness and perception of the high cost hinders it from becoming part of regular residential building design in different world areas [24]. Passive design strategies are climate-sensitive. With the prevailing extreme climate changes, it is challenging to implement strategies evaluated a long time ago. Therefore, relying on contemporary studies is recommended [25].

For hot climates, it is essential to consider daylight variables before simulating design strategies for results, including external shading system, WWR, and type of glazing [26].

According to the design alterations described earlier in this study, different strategies can be compiled in the following Table 1.



Table 1: Comparison of Alternate Passive Design Strategies

Category	Passive Design Element	Initial Cost	Thermal Comfort	Visual Comfort
Light capturing devices	Window to Wall Ratio (WWR)	✓	×	✓
	Atrium	✓	✓	✓
	Solatube	×	✓	✓
Shading devices	Light Shelf	✓	✓	✓
	Kinetic Shading System	×	✓	✓

Since WWR is one of the daylight design variables, studies for local scenarios suggest that recommended size would make better use of daylight. Therefore, it should be part of our residential unit design. It does not have any extra cost of construction, and if coupled with a light shelf, it can counteract the drawback of thermal discomfort due to large windows and reduce glazing. Since windows are already part of an existing design, having windows with light shelves will not cause hindrance from the client for implementation.

Atriums, along with light shelf, is the one that provides thermal comfort and visual comfort at the same time while employing daylight at a lower cost. Consequently, atriums need to be included in our conceptual design.

Solatube is a relatively new design aspect, but its cost is comparatively lower due to less technological intervention. In addition, the solatube also preserves privacy and offers daylight without transmitting heat along with visual comfort.

## 7 Study Significance

Although much work has been done for daylight utilization, it is not part of our typical designs compared to its full potential. This study gives a brief on five strategies considering daylight significant variables to increase their use in residential designs practically.

## 8 Conclusions & Recommendations for Future Research

The following conclusions can be drawn from the review:

Considering the local context, complexity, and economy of design alterations, the window wall ratio (WWR) is recommended to be 50% along with a light shelf.

The atrium, an ancient way of daylight utilization, is found to provide thermal and visual at low cost, making it highly suitable to be incorporated in energy-efficient residential design.

Solatube (also called light pipes) can be included in the design to make residential units energy efficient. Despite being costly, they offer many other benefits that surpass the initial cost concern since each penny is worth it.

Kinetic shading systems are equally efficient in daylight utilization. Kinetic shading systems can be explored further for cheaper technological advancement to reduce cost and make it economical to be a part of the design in Pakistan.

This study was limited to a few passive design strategies; this area can be explored further for different strategies available since Pakistan has excellent potential to consume daylight.

## Acknowledgment

The study presented in the paper is part of research project NRPU-9626 funded by the Higher Education Commission of Pakistan under its National Research Program for Universities. The corresponding author is PI of the project.



## Reference

- [1] Nadeem, Ahmad, and Arshad. "PRECON: Pakistan residential electricity consumption dataset." In Proceedings of the *tenth ACM international conference on future energy systems*, pp. 52-57, 2019.
- [2] Ghafoor, Zareen, Sharif, U. Khan, Hayyat, Farhan, and Shahzad. "Energy consumption and carbon dioxide emissions of residential buildings in Lahore, Pakistan." *Polish Journal of Environmental Studies* 29, no. 2 pp 1613-1623, 2020.
- [3] Omrany, Hossein, and Marsono. "Optimization of building energy performance through passive design strategies." *British Journal of Applied Science & Technology* 13, no. 6, pp 1-16, 2016.
- [4] Fadle, M., Abu, M., Lukman, N. I. K., Ibrahim, N. I. K. & Sopian, K. "The Performance of External Shading Devices and Daylighting Rule of Thumb for a Tropical Climate of Thumb". *Latest Trends in Renewable Energy and Environmental Informatics*, 130–134, 2013.
- [5] Yousuf, Sumra, Alamgir, Afzal, Maqsood, and Arif. "Evaluation of daylight intensity for sustainability in residential buildings in cantonment cottages Multan." *Mehran University Research Journal of Engineering and Technology* 36, no. 3 597-608, 2017.
- [6] Shafavi, Seyed, Zomorodian, Tahsildoost, and Javadi. "Occupants visual comfort assessments: A review of field studies and lab experiments." *Solar energy* 208, 249-274, 2020.
- [7] Hopkinson, Galbraith. "Architectural Physics: Lighting." 1963.
- [8] Samadi, Sahba, Noorzai, Beltrán, and Abbasi. "A computational approach for achieving optimum daylight inside buildings through automated kinetic shading systems." *Frontiers of Architectural Research* 9, no. 2, 335-349, 2020.
- [9] Omrany, Hossein, Ghaffarianhoseini, Berardi, Ghaffarianhoseini, and HW Li. "Is atrium an ideal form for daylight in buildings?" *Architectural Science Review* 63, no. 1, 47-62, 2020.
- [10] Ji, Guanzhou. "Daylight Availability And Occupant Visual Comfort In Seattle Multi-Family Housing." *ASHRAE Topical Conference Proceedings*, pp. 93-102, 2020.
- [11] Al-Qahtani, Elgizawi, "Building envelope and energy saving case study: a residential building in Al-Riyadh, Saudi Arabia", *International Journal of Low-Carbon Technologies*, 15, 04, pp 555–564, 2020.
- [12] Sangraula, Birat, and Uprety. "Window to wall ratio for daylighting in context of apartment building in Kathmandu valley." *Journal of Building and Environmental Engineering*, 08-14, 2020.
- [13] Arif, Khalid, and Azhar. "Identification of Energy Efficiency Improvement Measures of an Existing Residential Building Using Audit-Assisted Energy Simulation and Analysis." *Engineering Proceedings* 12, no. 1, 18, 2021.
- [14] Elghamry, Rania, and Hamdy Hassan. "Impact of window parameters on the building envelope on the thermal comfort, energy consumption and cost and environment." *International Journal of Ventilation* 19, no. 4, pp 233-259, 2020.
- [15] Ochoa, Carlos, Aries, Loenen, and Hensen. "Considerations on design optimization criteria for windows providing low energy consumption and high visual comfort." *Applied energy* vol 95, 238-245, 2012.
- [16] Balabel, A., M. Alwetaishi, A. Abdelhafiz, U. Issa, I. A. Sharaky, A. K. Shamseldin, M. Al-Surf, and M. Al-Harthi. "Potential of Solatube technology as passive daylight systems for sustainable buildings in Saudi Arabia." *Alexandria Engineering Journal* 61, no. 1, 339-353, 2022.
- [17] Wong, Liang. "A review of daylighting design and implementation in buildings." *Renewable and Sustainable Energy Reviews* 74, 959-968, 2017.
- [18] Ebrahimi-Moghadam, Amir, Ildarabadi, Aliakbari, and Fadaee. "Sensitivity analysis and multi-objective optimization of energy consumption and thermal comfort by using interior light shelves in residential buildings." *Renewable Energy* 159, pp 736-755, 2020.
- [19] Bahdad, Salem, Fadzil, Onubi, BenLasod. "Sensitivity analysis linked to multi-objective optimization for adjustments of light-shelves design parameters in response to visual comfort and thermal energy performance." *Journal of Building Engineering*, 44, pp 102996, 2021.
- [20] Kontadakis, Antonis, Tsangrassoulis, Doulos, and Zerefos. "A review of light shelf designs for daylit environments." *Sustainability*, 10, no. 1, pp 71, 2017.
- [21] Ahmed, Mostafa MS, Ali K. Abdel-Rahman, Bady, and Mahrous. "The thermal performance of residential building integrated with adaptive kinetic shading system." *International Energy Journal*, 16, pp. 3, 2016.
- [22] Ahmed, M., Rahman, Bady, E. Mahrous, and M. Suzuki. "Optimum energy consumption by using kinetic shading system for residential buildings in hot arid areas." *International Journal of Smart Grid and Clean Energy*, 5, no. 2, 2, 2016.
- [23] Samadi, Sahba, Noorzai, Beltrán, and Abbasi. "A computational approach for achieving optimum daylight inside buildings through automated kinetic shading systems." *Frontiers of Architectural Research*, 9, no. 2 pp 335-349, 2020.
- [24] Alkali, M. A., Jie, Dalibi, and Danja. "Hindrances to the Utilization of Climate Responsive Architecture Principles for Residential Design in Northeast Nigeria." *environment*, 9, pp 10, 2020.
- [25] Wang, Shangyu, Liu, Cao, Li, Yu, and Yang. "Applicability of passive design strategies in China promoted under global warming in past half century." *Building and Environment*, 195, 2021.
- [26] Al-Dossary, Mohammed, and Kim. "A study of design variables in daylight and energy performance in residential buildings under hot climates." *Energies*, 13, no. 21, 5836, 2020.



# OPERATIONAL ENERGY LIFE CYCLE ASSESSMENT OF RESIDENTIAL HOUSES – ANALYTICAL STUDY OF AN URBAN DISTRICT OF PAKISTAN

<sup>a</sup> Farrukh Arif\*, <sup>b</sup> Muhammad Taha Jawed, <sup>c</sup> Waleed Ahmed Khan

a: Department of Civil Engineering, NED University of Engineering & Technology, [farrukh@cloud.neduet.edu.pk](mailto:farrukh@cloud.neduet.edu.pk)  
b: Department of Civil Engineering, NED University of Engineering & Technology, [jawed.pg13806@cloud.neduet.edu.pk](mailto:jawed.pg13806@cloud.neduet.edu.pk)  
c: Department of Civil Engineering, NED University of Engineering & Technology, [waleedahmedkhan@neduet.edu.pk](mailto:waleedahmedkhan@neduet.edu.pk)

\* Corresponding author: Email ID: [farrukh@cloud.neduet.edu.pk](mailto:farrukh@cloud.neduet.edu.pk)

**Abstract-** Energy consumed by the buildings at their operational stage is considered one of the main factors burdening the environment. This consumed energy releases greenhouse gases (GHG) emissions due to the rising energy demands from cities' domestic and residential sectors. The domestic sector of Pakistan consumes 45.9 % of its annual energy. Heating, ventilation, air conditioning (HVAC), and lighting appliances consume about half of the total building energy. There is a rising need for more innovative and sustainable approaches to buildings operations to cope with this global issue. To fill this gap in sustainable construction and operations of residential buildings efficiently, this research was conducted based on Energy Life Cycle Assessment (ELCA) methodology for the residential houses. Researchers collected data from 13 houses in district Central of Karachi. It included information related to building envelope and operational energy details. The life cycle assessment framework was applied over the collected inventory data, and life cycle inventory analysis was performed, leading to the integration of the Life Cycle Impact assessment. The results evaluated that studied houses produce 48120 Tons of carbon footprint throughout the life cycle stages of the buildings for a reference study period of 60 years. Global warming potential was found to be the highest, followed by acidification and eutrophication potential.

**Keywords-** Life cycle assessment, energy efficiency, Energy, Carbon footprint

## 1 Introduction

The domestic sector of Pakistan consumes 45.9 % of its annual energy. About half of the total energy is consumed by buildings and/or heating, ventilation, air conditioning (HVAC), and lighting appliances [1]. With rising population demands, there is a noticeable need for energy-efficient buildings to reduce environmental impacts, such as; global warming, acidification, ozone depletion, etc. Statistics and research from the last decade reveal that the climate is changing globally [2] and will continue to do so. Overall, environmental burden of buildings can be reduced by using LCA as an instrument, which provides trade-offs associated with pressures, health and wellbeing and the consumption of natural resources [3]. Buildings play a significant role in the consumption of energy throughout the world, and the pattern of rising energy demands from this sector questions the urgency of mitigating environmental impacts caused by these buildings. This paper presents implementing an operational energy life cycle assessment framework in the district Central of Karachi in which data from 13 houses were collected and analyzed. The research was carried out by creating energy models for existing houses, and after energy auditing; results were compared with the simulation results extracted from BEM (Building Energy Model) and ELCA (Energy Life Cycle Assessment). The study will result in quantification of total carbon footprint for reference period of sixty years and the factors, which contribute towards these carbon footprints, will be analyzed.





## 2 Literature Review

### 2.1 Life Cycle Assessment

LCA is a process that quantifies and assesses the flow of energy and material within a system. Steps that include upstream (material extraction, manufacture, transport, and assembling), usage, and downstream (demolishing and disposal) of goods, products, or services network are usually inventoried first. Life cycle assessment is constantly evolving; it has been carefully constructed over the years to help manage and develop different working standards. One such development done on a global scale on quality standards is the international standard organizations (ISO) standards; 14,000 and above, with ISO 14,040 series establishing a focus on the LCA approach [4]. In the LCA approach, the information is processed through four main stages [5]: (1) Life cycle assessment (2) Life Cycle Inventory Analysis (3) Life Cycle Impact Assessment (4) Impact Categories. The impact categories, which have been observed and confirmed from various standards, handbooks, and reading materials [6], [7], [8] include; Global Warming, Climate Change, Land use, Water use, Acidification, Eutrophication, Stratospheric ozone layer depletion, Abiotic Resource Depletion Potential, Abiotic Resource Depletion potential of fossil fuels, Human Toxicity and Eco Toxicity.

### 2.2 Energy Life Cycle Assessment (ELCA)

The ELCA process of a building or product comprises two levels [5]. The method caters to all of a building's energy inputs throughout its life cycle. This analysis includes the energy utilization of the following phases: the manufacture, usage, destruction, and finally, disposal [6]. Usage includes all operations that the building uses throughout its life span. Manufacturing usually involves the production and transfer of building materials and engineering equipment used to install and reconstruct structures. The different types of tools and inventories available for level 1 and level 2 analysis are provided in the following sub-sections.

#### 2.2.1 Level-1

Product comparison tools include; Building for Environmental and Economic Sustainability (BEES), National Renewable Energy Laboratory's (NREL), U.S. Life-Cycle Inventory (LCI) Database, SimaPro, Integrated Assessment, and Life Cycle Explorer.

#### 2.2.2 Level-2

These software tools improve the decision-making process by providing a detailed project analysis. Some of these support tools are Envest 2, Eco Calculator, and Athena. These are the tools specialized in LCA and Sustainable Architecture.

## 3 Research Methodology

A literature review was the first step of the methodology. It was necessary to benchmark ELCA concepts, elicit secondary, data and development of ELCA framework for houses in alignment with international standards. Following the literature review was the step of energy life cycle assessment which included; gathering inventory data, calculation of annual utility consumption, identification of emission factors, identification of LCA tool, calculation of impact categories, and finally calculation of overall carbon footprint of the studied houses. The inventory data was collected for the 13 houses located in district central. The inventory data collected included; architectural plans, 12 months' utility bills (electricity, natural gas, and water), number of occupants, and covered area of the building which were used in the life cycle assessment. This data was utilized to calculate the LCA of the houses during their operational phase. Since the water, consumption data was unavailable for most of the houses, it was calculated based on water demand estimation for the district central in Karachi. As per Karachi Water and Sewage Board (KWSB), the per capita water demand is 54 gallons or 246 liters per day. The said values were used to estimate the total annual water consumption of the household based on the number of occupants in that particular house. Emission factors were taken from LCA inventory data provided in the One-Click LCA inventory (online LCA tool) which are provided in Table 1. An emissions factor is a representative value that attempts to relate the quantity of a pollutant released to the atmosphere with an activity associated with releasing that pollutant. These factors are usually expressed as the weight of the pollutant divided by a unit weight, volume, distance, or duration of the activity emitting the pollutant (e.g., kilograms of particulate emitted per mega gram of coal burned). Such factors facilitate the estimation of emissions from various sources of air pollution. In most cases, these factors are averages of all available data of acceptable quality. They are generally assumed to be representative of long-term averages for all facilities in the source



category (*the United States Environmental Protection Agency, n.d.*). District central of Karachi was considered as case study area for performing the analysis with the view of implicating the findings generally in other urban areas of Pakistan.

*Table 1 Emission factors for Pakistan. (Values taken from One Click LCA, Bionova Ltd)*

Consumption Category	Profile	Global Warming Kg CO <sub>2</sub>	Acidification Kg SO <sub>2</sub>	Eutrophication on Kg PO <sub>2</sub>	Ozone depletion potential Kg CFC11	Formation of ozone of lower atmosphere Kg Ethene
Electricity/ KWh/Year	Electricity (World Data)	0.741675281	0.005276896	0.001199800	0.000000035742	0.000182250
Natural Gas/ Cft/Year	Natural gas	0.064132221	0.000189243	0.000012695	0.000000005045	0.000012853
Water/ Cft/ Year	Tap water, clean	0.008495054	0.000046002	0.000023274	0.000000000000	0.000002071

Special care was taken to adapt the values from the website for profiles from Pakistan. For electricity consumption, production emission factors for thermal power generation were taken from world profile. This was based on literature review findings and assumption that thermal power generation will result in similar emissions for Pakistan as well due to similarity in generation plants' technology.

#### 4 Life Cycle Assessment Calculation

The equation that derives the LCA calculation is simple and is given below:

$$EEI = OEC \times EF \text{ ----- (1)}$$

Where;

*EEI = Estimated Environmental Impact annually*

*OEC = Operational Energy Consumption*

*EF = Category Emission factor*

The above equation gives the annual carbon emission values for the calculated household. To calculate its LCA over its operational life cycle, another variable is required i.e., the reference study period/ calculation period for LCA study. This period usually ranges between 0 to 80 years for a household, mainly depending on design life. The reference study period has been assumed 60 years for this research. For the calculations performed in studied houses, Life cycle impact values were calculated using equation (2).

$$LCI = EEI \times n \text{ ----- (2)}$$

Where;

*EEI = Estimated Environmental Impact annually*

*n = study period/reference period for LCA*

Table 2 shows the emissions for houses of district Central based on their Electricity consumption.



Table 2 Annual Emission Calculations for Electricity for District Central

House Code	Plot Size in yards	GWP Kg CO <sub>2</sub>	AP Kg SO <sub>2</sub>	EP Kg PO <sub>2</sub>	ODP Kg CFC11	POCP Kg Ethene
H1	200	1981.76	14.10	3.21	0.000096	0.49
H2	120	2985.98	21.24	4.83	0.000144	0.73
H3	120	2750.87	19.57	4.45	0.000133	0.68
H4	100	3533.34	25.14	5.72	0.000170	0.87
H5	400	4916.57	34.98	7.95	0.000237	1.21
H6	120	2024.77	14.41	3.28	0.000098	0.50
H7	100	1288.29	9.17	2.08	0.000062	0.32
H8	80	2516.65	17.91	4.07	0.000121	0.62
H9	120	2516.65	17.91	4.07	0.000121	0.62
H10	120	2516.65	17.91	4.07	0.000121	0.62
H11	240	1948.38	13.86	3.15	0.000094	0.48
H12	240	1948.38	13.86	3.15	0.000094	0.48
H13	240	1948.38	13.86	3.15	0.000094	0.48
H14	260	1948.38	13.86	3.15	0.000094	0.48
H15	505.66	4916.57	34.98	7.95	0.000237	1.21

Table 3 shows the emissions for houses of district Central based on their Natural Gas consumption.

Table 3 Annual Emission Calculations for Natural Gas for District Central

House Code	Plot Size in yards	GWP Kg CO <sub>2</sub>	AP Kg SO <sub>2</sub>	EP Kg PO <sub>2</sub>	ODP Kg CFC11	POCP Kg Ethene
H1	200	48291.56	142.50	9.56	0.003799	9.68
H2	120	75868.42	223.87	15.02	0.005968	15.20
H3	120	55730.90	164.45	11.03	0.004384	11.17
H4	100	24049.58	70.97	4.76	0.001892	4.82
H5	400	67210.57	198.33	13.30	0.005287	13.47
H6	120	56692.88	167.29	11.22	0.004460	11.36
H7	100	34246.61	101.06	6.78	0.002694	6.86
H8	80	55910.47	164.98	11.07	0.004398	11.21
H9	120	55910.47	164.98	11.07	0.004398	11.21
H10	120	55910.47	164.98	11.07	0.004398	11.21
H11	240	48291.56	142.50	9.56	0.003799	9.68
H12	240	48291.56	142.50	9.56	0.003799	9.68
H13	240	48291.56	142.50	9.56	0.003799	9.68
H14	260	48291.56	142.50	9.56	0.003799	9.68
H15	505.66	34246.61	101.06	6.78	0.002694	6.86

Table 4 shows the emissions for houses of district Central based on their Water consumption.

Table 4 Annual Emission Calculations for Water for District Central

House Code	Plot Size in yards	GWP Kg CO <sub>2</sub>	AP Kg SO <sub>2</sub>	EP Kg PO <sub>2</sub>	ODP Kg CFC11	POCP Kg Ethene
H1	200	80.81	0.44	0.22	0	0.02
H2	120	53.87	0.29	0.15	0	0.01
H3	120	80.81	0.44	0.22	0	0.02
H4	100	161.62	0.88	0.44	0	0.04
H5	400	188.56	1.02	0.52	0	0.05
H6	120	161.62	0.88	0.44	0	0.04
H7	100	161.62	0.88	0.44	0	0.04
H8	80	53.87	0.29	0.15	0	0.01



House Code	Plot Size in yards	GWP Kg CO <sub>2</sub>	AP Kg SO <sub>2</sub>	EP Kg PO <sub>2</sub>	ODP Kg CFC11	POCP Kg Ethene
H9	120	80.81	0.44	0.22	0	0.02
H10	120	80.81	0.44	0.22	0	0.02
H11	240	161.62	0.88	0.44	0	0.04
H12	240	161.62	0.88	0.44	0	0.04
H13	240	161.62	0.88	0.44	0	0.04
H14	260	175.09	0.95	0.48	0	0.04
H15	505.66	340.52	1.84	0.93	0	0.08

## 5 Results of Energy Life Cycle Assessment

Table 5 summarizes the overall carbon footprint generated by the studied houses of district Central that generate emissions of 48120 Tons. The Overall footprint is represented in the equivalent of CO<sub>2</sub>. The reference study period for this study is 60 years, and the generated results are stated.

Table 5 Summary of Carbon Emission of district central

Carbon Metric	Central
No. of Houses	13
Global Warming CO <sub>2</sub> (Kg)	799081.31
Acidification SO <sub>2</sub> (Kg)	2528.62
Eutrophication PO <sub>2</sub> (Kg)	219.95
Ozone depletion CFC11 (Kgs)	0.06
Ethene (POCP) (Kgs)	162.04
Carbon Footprint/Year (Kgs of CO <sub>2</sub> )	801991.98
Reference Study Period (Years)	60
Carbon Footprint for Life Cycle (60 Years)	48119519 Kgs
Total (In Tons)	48120

The annual overall emission results for studied houses of the district Central are graphically illustrated in Figure 1. It provides the emission results and carbon footprints per year are found to be highest while the most negligible value is of ozone depletion CFC11. CO<sub>2</sub> is the leading cause of Global warming that is why it is high in magnitude, which is followed by acidification and eutrophication due to sulphurdioxide-ammonia reaction and deposition to the changes in the chemical composition of the soil and surface water.

## 6 Practical Implementation of the study

Using similar approach as presented in the study, more localities with high carbon footprints can be identified. This can help to identify energy efficiency improvement measures that can reduce carbon footprints. The authors have worked on the same idea in an extended study under same project.

## 7 Conclusions

After analyzing 13 houses located in the district central of Karachi 48120 tons carbon footprint was found for the reference period of 60 years. Among different parameters, which contribute in the calculation of carbon footprint, carbon dioxide (CO<sub>2</sub>) emissions that is global warming potential ranks first, acidification (SO<sub>2</sub>) ranks second and Eutrophication (PO<sub>4</sub>) ranks third.

## 8 Recommendations

The findings of this assessment along-with similar assessment of houses studied in other districts were combined to perform building energy efficiency assessment using building information modeling, and energy analysis to propose energy efficiency improvement measures. The potential measures can reduce energy use intensity (EUI) and hence, life cycle impact of operational energy use. These measures included; using R-38 Roof Insulation, R- 2 CMU Wall for the



construction, Double Glazed Window Glass, window shades of at least 1/6<sup>th</sup> of the Window height, Providing Daylight & Occupancy controls, reducing Plug Load Efficiency to 6.46 watts/m<sup>2</sup> or less, reducing Lighting Efficiency to 3.23 watts/m<sup>2</sup>. It was estimated that an integrated application of improvement measures can help reduce carbon footprint of one of the houses (i.e., H12) by approx. 62%. The results obtained from this study can be used to predict the parameters for other parts of Pakistan as well by considering them as benchmark.

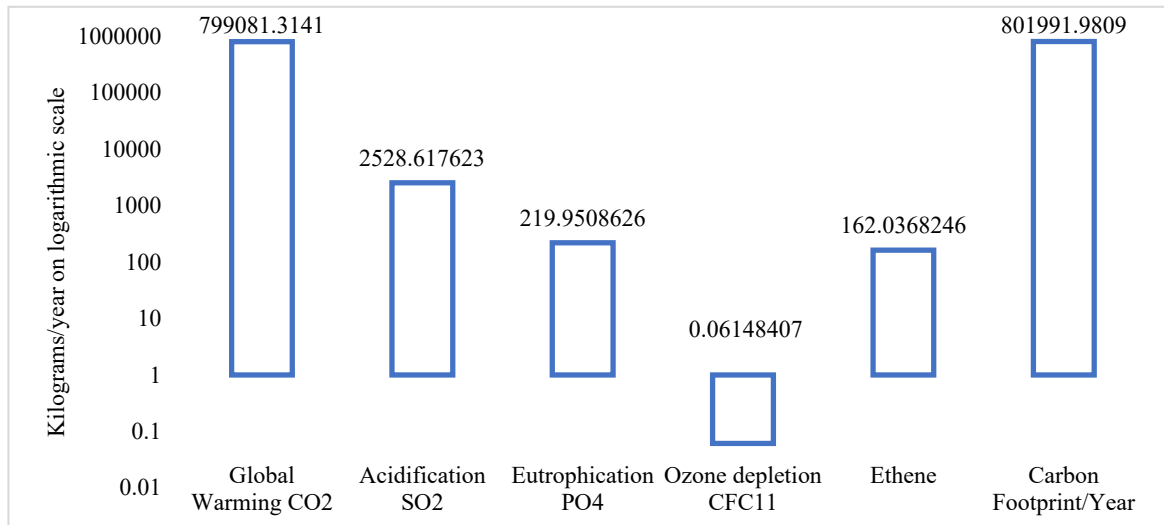


Figure 1 Emission results for houses studied in District central

## Acknowledgment

The study presented in the paper is part of research project NRP-9626 funded by the Higher Education Commission of Pakistan under its National Research Program for Universities. The corresponding author is PI of the project.

## Reference

- [1] Sohail, M., & Qureshi, M. U. D. (2011). Energy-efficient buildings in Pakistan. *Science Vision*, 27–38. [http://inis.iaea.org/search/search.aspx?orig\\_q=RN:46043546](http://inis.iaea.org/search/search.aspx?orig_q=RN:46043546)
- [2] Stocker, T. F., Clarke, G. K. C., Le Treut, H., Lindzen, R. S., Meleshko, V. P., Mugara, R. K., Palmer, T. N., Pierrehumbert, R. T., Sellers, P. J., Trenberth, K. E., & Willebrand, J. (2001). Physical Climate Processes and Feedbacks. *Climate Change 2001: The Scientific Bases. Contribution of Working Group I to the Third Assessment Report of the Intergovernmental Panel on Climate Change*, 881.
- [3] Abdulrahman et.al (2022), “The application of life cycle assessment in buildings: challenges and directions for future research”. *The International Journal of Life Cycle Assessment* (2022) 27:627–654
- [4] Pré Consultants. (2006). *ISO 14040*. <https://www.iso.org/standard/37456.html>; 2020 [accessed 12 December 2020]. *Lci*, 1–6.
- [5] Cabeza, L. F., Rincón, L., Vilariño, V., Pérez, G., & Castell, A. (2014). Life cycle assessment (LCA) and life cycle energy analysis (LCEA) of buildings and the building sector: A review. *Renewable and Sustainable Energy Reviews*, 29, 394–416. <https://doi.org/10.1016/j.rser.2013.08.037>
- [6] Birgisdóttir, H., & Rasmussen, F. N. (2016). Introduction to LCA of Buildings. Danish Transport and Construction Agency, 1–18. [https://www.trafikstyrelsen.dk/~media/Dokumenter/09\\_Byggeri/Baredygtigt\\_byggeri/TBST-2016-02-Introduction\\_LCA\\_english.pdf](https://www.trafikstyrelsen.dk/~media/Dokumenter/09_Byggeri/Baredygtigt_byggeri/TBST-2016-02-Introduction_LCA_english.pdf)
- [7] Carbon Leadership Forum. 343(2019). *Life Cycle Assessment of Buildings: A Practice Guide*. 33. <http://carbonleadershipforum.org/projects/lca-practice-guide/>
- [8] European Committee for Standardization. (2011). *UNE-EN 15978:2011 Sustainability of construction works - Assessment of environmental performance of buildings - Calculation method*. International Standard, November.



# APPLICATION OF CONSTRUCTION AND DEMOLITION WASTE FOR SUSTAINABLE PAVEMENT CONSTRUCTION- A REVIEW

*Adeem Waqar Hashmi*

National Engineering Services Pakistan (NESPAK), [www.nespak.com.pk](http://www.nespak.com.pk)  
Email ID: [adeemwaqarhashmi@gmail.com](mailto:adeemwaqarhashmi@gmail.com)

**Abstract-** Over the past few decades, there has been a sharp rise in the production of construction and demolition waste (CDW) on a global scale, which has led to environmental issues as a result of its unregulated disposal. The use of recycled materials has increased within the same time period, mostly for sustainable development and environmental protection. In lieu of inefficient disposal and management of this type of trash, the objective of this research is to examine the HMA production for pavement construction utilizing recycled construction and demolition waste aggregates. These materials can be utilized to construct unbound layer like base, sub-base, and subgrade of pavement. For the preservation of natural resources, sustainable pavements composed of recyclable materials have recently become essential. In place of natural aggregates like broken rocks, CDW has been considered as a recycling material, potentially lowering environmental effects and boosting the economic potential of recycling. It has been demonstrated that doing so reduces the carbon footprint of the construction industry, conserves natural resources, reduces hazardous emissions, and lowers total costs for paving construction and maintenance. This paper examines the investigations that have been conducted on the usage of aggregates made from building and demolition waste in asphalt and unbound pavement layers. Therefore, the primary goal of this paper has been to conduct a literature review that would identify alternate strategies to use CDW in pavement projects. In order to encourage highway administrations to create new technical criteria and recommendations on CDW recycling, this paper aims to propose techniques that will do just that. This study seeks to announce the beginning of a new age of economic innovation in pavement engineering.

**Keywords-** Construction, Demolition, Pavement, Sustainability.

## 1 Introduction

Construction and demolition waste (CDW) production has grown remarkably as a result of the expansion of the construction industry. This has exacerbated issues brought on by ineffective administrative practices, like the uncontrolled and disorganized disposal of CDW, specifically in huge cities. Urban building is an ideal section for promoting the responsible use of waste materials and industrial by-products. As buildings, roads, walkways, bridges, and other structures are constructed and demolished, this business uses a lot of raw materials and produces a lot of garbage. Wood, plaster, concrete blocks, ceramics, mortar, asphalt concrete mills, bricks, simple and reinforced concrete make up the majority of this waste [1].

Maintaining natural resources now requires sustainable pavements made of recycled materials. In order to reduce possible environmental effects and increase the possible economic worth of recycling, CDW has been investigated as a material for recycling in place of natural aggregates like crushed rocks. Explicitly in structural layers like pavement sub base and base, recycled construction and demolition waste (RCDW) aggregate has been strongly employed as a granular material. RCDW



aggregate's makeup can vary greatly based on the elements that make up its components (e.g., mortar, cement concrete, crushed stones, and ceramic) [2, 3].

The introduction of enormous volumes of these materials into the highway industry still stands as one of the most practical strategies. Despite the fact that there have been a variety of attempts to reduce accumulated CDW stockpiles. This is because large-scale asphalt projects are required. Which depend on enormous amounts of paving materials. Roadways continue to be the most accessible and pervasive form of transportation in the globe when compared to other transport forms (railway, airway, maritime, and multimodal). Any nation would have to make a significant financial expenditure to build long-lasting roadways made up of pavement layers placed at top of a compacted subgrade. The majority of total waste content (65–70%) is made up of concrete since reinforced concrete structures account for a significant share of common CDW globally. However, the use of any reclaimable/recyclable/reusable aggregates as a substitute material is anticipated to be more cost-effective, sustainable, environmentally safe, and satisfactorily consistent with the needed criteria as compared to natural substances. [4].

Huge quantities of CDW are typically disposed of at landfills, thus reduces the land's capacity and degrades the environment. In order to increase sustainability, recycled CDW has been used in subgrade construction, which not only reduces the need for building materials but also lessens the environmental harm that CDW causes to the environment. As an outcome, CDW recycling and utilization are essential for the growth of the sustainable construction industry [5].

Improved knowledge of CDW production and management, along with the environmental effects resulting from its management, is necessary to execute sustainable recycling initiatives. According to reports, recycled aggregates are environmentally sustainable in regions where virgin materials must be transported over great distances or where natural resources are extremely rare. In order to create sustainable CDW management systems, environmental and management challenges should be properly assessed. [6].

In figure 1. A generalized classification scheme for CDW depending upon its origin of resources is shown. It is generally recognized that depending on the regions in which they are produced, the amount and makeup of any residue, and in particular, CDW, can vary greatly. These influences include population development, topography, regional planning, soil characteristics legislation, building materials, and technologies. [7, 8].

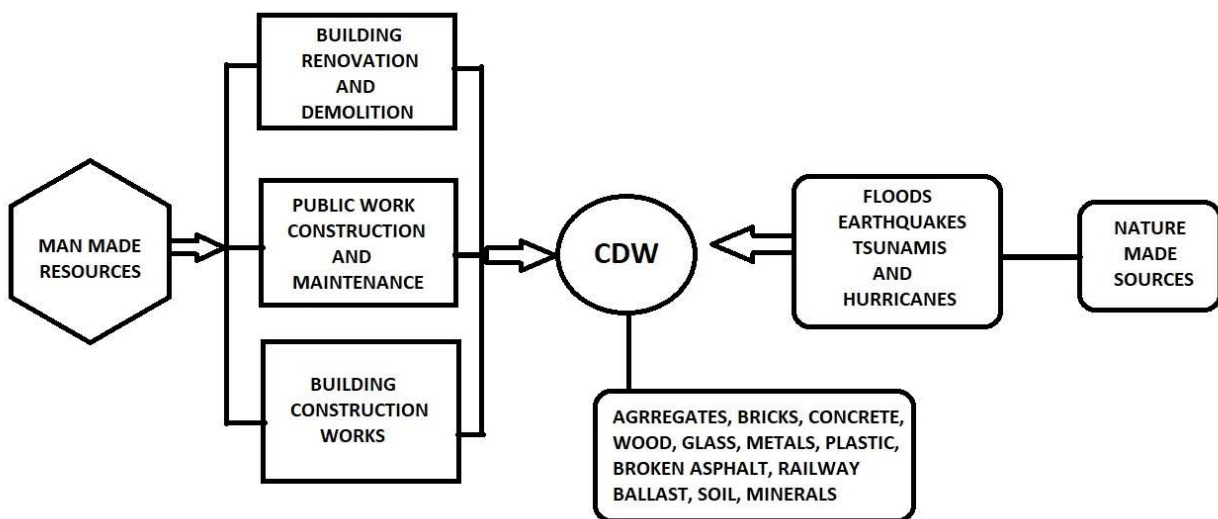


Figure 1: CDW classification based on source of origin

In light of this, the purpose of this study is to first outline numerous advantages of CDW recycling before attempting to increase current understanding of potential CDW incorporation into paving materials. This review study aims to inspire future ground-breaking research that will remove current barriers to the widespread use of CDW in flexible pavements



in underdeveloped nations by providing background information. Future research in this area should also look into ways to modify asphalt plants of the present and the future generations in order to encourage states, municipalities, and contractors to work together even more closely on CDW recycling projects.

## **2 Issues Related to Construction and Demolition Waste (CDW)**

Solid wastes are typically used to describe the construction and demolition (C&D) materials produced by some construction and demolition activities. Solid wastes generated during the building, remodelling, and repair of individual homes, businesses, and other civil related projects are referred to as construction waste. Generally speaking, demolition trash are the leftovers from razed buildings and roadways. The environment is under a great deal of pressure due to the recent development of massive amounts of solid waste created throughout the world, with the construction and demolition industries producing the majority of these wastes.

In 2014, construction and demolition (CD) operations produced about 0.530 billion tonnes in the United States and 1130 million tonnes in China. Comparatively speaking, the construction industry in Europe generates 35% of the overall amount of garbage, which is double and quadruple times greater than total amount of home waste produced in the United States and Europe, accordingly. The European Union as a whole has accomplished the 2020 recovery horizon, including backfilling. Out of the 19 member nations, 11 still need to strengthen their recovery capacities in order to meet the EU goal. More over 0.368 billion tonnes of demolition and construction garbage were produced in the 28 EU members plus the United Kingdom in 2018 [9, 10].

Untreated C&D waste has been accumulated in landfills and rural regions, posing a serious hazard to the environment and public health. The C&D garbage landfill uses up valuable land and raises issues with water contamination, soil deterioration, and global warming. Investigating inefficient and sustainable development models is essential to recycle C&D waste. Construction and demolition waste (CDW) from initiatives like building new superstructures and infrastructures, as well as from rehabilitation and repair work on existing structures, is currently overflowing global landfills. The techniques used to get rid of this trash is a serious issue as well. The dumping of these substances, which is typically haphazard, has a serious pessimistic impression on the surroundings, contaminating the air, water, and soil. As well as exhausting places that might otherwise be livable [11].

Trash produced during the building, maintenance, restoration, and destruction of bridges, roads, building, and other infrastructure is referred to as construction and demolition (C&D) waste. It has certain negative environmental effects that include consuming valuable land space, depleting landfills, using energy and non-energy resources, depleting resources, and polluting the environment [12].

## **3 Use of CDW for sustainable pavement construction**

The majority of total waste content (65–70%) is made up of concrete since reinforced concrete structures account for a significant share of common CDW globally. In comparatively low level applications, like the road building industry, it is being proposed that the concrete obtained from regular CDW can be crushed and then utilized to replace all or at least a portion of freshly quarried (primary) aggregates.

However, in recent years, interest in the Super paver design that is based on the volumetric characteristics of HMA has grown. These basic volumetric characteristics of asphaltic mixtures include air voids, voids filled with bitumen, dry bulk density, and voids in mineral aggregate. Asphaltic pavement's in-situ performance is directly influenced by the design's dependability, the quality of the materials used, the construction methods used, the amount of traffic, the environment, and the pavement's functional and structural resistance to deterioration. The volumetric and mechanical characteristics of HMA by CDW have been described in a wide variety of research up to this point.

The use of coarser RCA (Recycled Concrete Aggregate) enhanced efficiency in the form of stiffness and stability, according to the results of earlier experiments. This noticeable improvement is related to the transformation of RCA particles into surfaces that are severely crushed and have sharp edges, which immediately increases friction force in the HMA matrix. [13]- [16].





In instance, structural layers such as pavement base sand sub bases have effectively utilized recycled construction and demolition waste (RCDW) as a granular pavement material. However, the applications of scrap tyres in civil engineering projects are widely known. These applications include reuse for generating plastic and rubber goods, producing feedstock of carbon black, burning for the creation of steam, and building cement as a fuel for the kiln. Crumb rubber (R) is used in applications in civil engineering because it offers great soundproofing, good acid resistance, strong water resistance, absorbs plastic energy, and has a significant impact resistance. The porosity, strength, and deformability of the C&D aggregates including rubber were affected by the effects of high temperature, and it was determined that adding rubber to the aggregates would improve their response to significant temperature exposure in terms of deformability and strength. [17, 18].

Over the past few decades, production of construction and demolition (C&D) materials, such as recovered concrete aggregate (RCA) and dragging asphalt fragments (DAP), has significantly increased. Demolition of concrete structures yields the RCA, whereas demolition of asphalt pavements yields the DAP. In recent years, these materials have been extensively used in modern road constructions, particularly in the subgrade layer, thereby lowering their potential environmental impact and achieving sustainability on a global scale. The issues of inelastic response to high dynamics loads were solved by increasing energy absorption by introducing clay towards the RCA and DAP materials. As the moisture content being used compaction rose, the swelling percentages observed with the CBR tests dropped. This implies that in order to lessen the economic and environmental problems throughout the world, the C&D materials in the manner used here may be blended with clay at relevant content for subgrade of road pavement [19]- [21].

Some of the innumerable advantages of potential CDW recycling include conserving the planet's limited natural resources, reducing manufacturing dependence on raw materials, saving the money, getting rid of waste stockpiles, lowering main disposal costs, and - unquestionably - making the world's environment cleaner and more sustainable. [22].

#### 4 CDW Recycling Advantages and Consequences

Table 1. Also exemplifies some of the countless advantages of CDW recycling, some of which include conserving the planet's limited natural resources, reducing manufacturing dependence on raw materials, saving money, getting rid of waste stockpiles, lowering main disposal costs, and - without a doubt - making the world's environment cleaner and more sustainable [23]-[25].

Table 1 CDW Recycling advantages and consequences

Advantages	Consequences
Financial Resource Savings	Energy decrease for virgin materials process, refining, extracting and transportation
Decrease in Raw material dependency	High industrial material use and low use of earth resources
Natural resource preservation	Future protection of natural habitats
Environment protection	Prevention of change in climate
Waste stock elimination	Decrease in water and air pollution and greenhouse gas emission
Decrease in expenses related to disposal	Landfilling and haulage cost decrease

There is a lot of possibility for CDW to be recycled and used again. Aggregates made from CDW are highly sought-after on the market for usage in construction materials and projects. Numerous studies have been conducted in recent years to determine whether it is feasible to use CDW in projects including ceramic materials, mortar, and concrete, a landfill cover layer, asphalt, and roadways [26]- [28].



## 5 Conclusion

The viability of employing CDW as paving materials for new construction was assessed in this study. This review paper's major finding can be summed up as follows:

1. This study explores the practicality of using recycled construction and demolition waste aggregates to manufacture hot asphalt mixtures for roadways in order to decrease the environmental effect caused by incorrect management and disposal of building and demolition waste.
2. Due to its exceptional strength and bearing capacity, using CDW-derived materials in the construction of roadway bases and sub bases is another advantageous option.
3. Before being used in subgrades, the primary CDW are complex mixtures that require careful manufacturing processes to be completed, and before pavement is constructed, the water content and maximum particle sizes of the preparatory CDW materials must comply with criteria.
4. Given that their acceptance can be gauged based on their real laboratory and field determined properties, in pavements the use of CDWs is probably one of their greatest applications. Their constituents are typically natural aggregates, which is typically advantageous for their application as unbound layers.
5. Using CDWs in pavement construction has shown to be a practical way to take advantage of their remaining good characteristics. The quality of the finished product is greatly influenced by the recycling procedures and the proper selection and classification of the raw waste materials.

In order to mitigate the environmental issues caused by the improper management and waste disposal. This study explores the practicality of using recycled construction and demolition waste aggregates to manufacture hot asphalt mixtures for paving urban roadways in order to decrease the environmental effect caused by incorrect management and disposal of building and demolition waste. Numerous habitats and species, and also climate change and air pollution are negatively impacted by poor waste management.

## Acknowledgment

The author would like to thank every person/department who helped thorough out this review. The constructive suggestions by my colleagues and the careful review and constructive suggestions by the anonymous reviewers are gratefully acknowledged.

## References

- 1: A. Ossa, J. García, L., & E. Botero, "Use of recycled construction and demolition waste (CDW) aggregates: A sustainable alternative for the pavement construction industry," *Journal of Cleaner Production*, vol.135, PP. 379-386, 2016.
- 2: I. Beja, A., R. Motta, & L. Bernucci, B, "Application of recycled aggregates from construction and demolition waste with Portland cement and hydrated lime as pavement subbase in Brazil," *Construction and Building Materials*, vol.258, PP.119520, 2020.
- 3: H. Baghban, A. Arulrajah, G. Narsilio, A., & S. Horpibulsuk, " Assessing the performance of geothermal pavement constructed using demolition wastes by experimental and CFD simulation techniques," *Geomechanics for Energy and the Environment*, vol.29, PP.100271, 2022.
- 4: A. Gedik, "A review on the evaluation of the potential utilization of construction and demolition waste in hot mix asphalt pavements. *Resources, Conservation and Recycling*, vol.161, PP.104956, 2020.
- 5: L. Liu, Z. Li, G. Cai, J. Zhang, & B. Dai, "Long-term performance of temperature and humidity in the road embankment constructed with recycled construction and demolition wastes," *Journal of Cleaner Production*, vol.356, PP.131851,2022.
- 6: N. Ferronato, G.E Guisbert Lizarazu, M.A Gorritty Portillo, L. Moresco, F. Conti, & V. Torretta, "Environmental assessment of construction and demolition waste recycling in Bolivia: Focus on transportation distances and selective collection rates," *Waste Management & Research*, vol.40(6), PP.793-805,2022.
- 7: G.Reis, S, D, M. Quattrone, W. Ambrós, M., B. Grigore Cazacliu, & C. Hoffmann Sampaio, "Current applications of recycled aggregates from construction and demolition: A review," *Materials*, vol.14 (7), PP. 1700, 2021.
- 8: M.Contreras-Llanes, M. Romero, M. Gázquez, J, & J.Bolívar, P, "Recycled Aggregates from Construction and Demolition Waste in the Manufacture of Urban Pavements," *Materials*, vol 14(21), PP.6605, 2021.
- 9: S. Pourkhorshidi, C. Sangiorgi, D. Torreggiani, & P. Tassinari, "Using recycled aggregates from construction and demolition waste in unbound layers of pavements," *Sustainability*, vol.12 (22), PP.9386, 2020.
- 10: X.Zhao, R.Webber, P.Kalutara, W.Browne, & Pienaar, J, "Construction and demolition waste management in Australia: A mini-review," *Waste Management & Research*, vol.40 (1), PP.34-46, 2021.



- 11: J. Zhang, A.Zhang, C.Huang, Yu, H, & C.Zhou, "Characterising the resilient behaviour of pavement subgrade with construction and demolition waste under Freeze–Thaw cycles," *Journal of Cleaner Production*, vol. 300, PP.126702, 2021.
- 12: M. Mohanty, S.Mohapatra, S, & S.Nayak, "Efficacy of C&D waste in base/subbase layers of pavement–current trends and future perspectives: A systematic review," *Construction and Building Materials*, vol. 340, PP.127726, 2022.
- 13: D. Vega A, L, J. Santos, & G. Martinez-Arguelles, "Life cycle assessment of hot mix asphalt with recycled concrete aggregates for road pavements construction," *International journal of pavement engineering*, vol. 23(4), PP.923-936, 2022.
- 14: G.Zou, J.Zhang, X.Liu, Y.Lin, & H.Yu, "Design and performance of emulsified asphalt mixtures containing construction and demolition waste," *Construction and Building Materials*, vol. 239, PP.117846, 2020.
- 15: C. Lu, J. Chen, C.Gu, J. Wang, Y. Cai, & T.Zhang, "Resilient and permanent deformation behaviors of construction and demolition wastes in unbound pavement base and subbase applications," *Transportation Geotechnics*, vol. 28, PP.100541, 2021.
- 16: M. Arab, G, M.Alzara, W.Zeiada, M.Omar, & A. Azam, "Combined effect of compaction level and matric suction conditions on flexible pavement performance using construction and demolition waste," *Construction and Building Materials*, vol. 261, PP.119792, 2020.
- 17: F. Maghool, A.Arulrajah, B.Ghorbani, & S.Horpibulsuk, "Strength and permanent deformation properties of demolition wastes, glass, and plastics stabilized with foamed bitumen for pavement bases," *Construction and Building Materials*, vol. 320, PP.126108, 2022.
- 18: M.Saberian, J.Li, M.Boroujeni, D.Law, & C.Li, Q, "Application of demolition wastes mixed with crushed glass and crumb rubber in pavement base/subbase. *Resources*," *Conservation and Recycling*, vol. 156, pp.104722, 2020.
- 19: A.Cabalar, F, O.Zardikawi, A, & M. Abdulnafaa, D, "Utilisation of construction and demolition materials with clay for road pavement subgrade," *Road Materials and Pavement Design*, vol. 20(3), PP. 702-714, 2019.
- 20: J.Zhang, L.Ding, F.Li, & J.Peng, "Recycled aggregates from construction and demolition wastes as alternative filling materials for highway subgrades in China," *Journal of Cleaner Production*, vol.255, PP. 120223, 2020.
- 21: F.Maghool, M.Senanayake, A.Arulrajah, & S.Horpibulsuk, "Permanent deformation and rutting resistance of demolition waste triple blends in unbound pavement applications," *Materials*, vol. 14(4), PP.798, 2021.
- 22: S.Salehi, M.Arashpour, J.Kodikara, & R.Guppy, "Sustainable pavement construction: A systematic literature review of environmental and economic analysis of recycled materials," *Journal of Cleaner Production*, vol. 313, PP. 127936, 2021.
- 23: H.Strieder, L, V.Dutra, F, P, A.Graeff, G, W.Núñez, P, & F.R.M Merten, "Performance evaluation of pervious concrete pavements with recycled concrete aggregate," *Construction and Building Materials*, vol. 315, PP. 125384, 2022.
- 24: M.Contreras Llanes, M.Romero Pérez, M.J.Gázquez González, & J.P. Bolívar Raya, "Construction and demolition waste as recycled aggregate for environmentally friendly concrete paving," *Environmental Science and Pollution Research*, vol. 29(7), PP.9826-9840, 2022.
- 25: Y.Tang, J. Xiao, Q. Liu, B. Xia, A. Singh, Z. Lv, & W. Song, "Natural gravel-recycled aggregate concrete applied in rural highway pavement: Material properties and life cycle assessment," *Journal of Cleaner Production*, vol. 334, PP. 130219, 2022.
- 26: P.R.L Lima, M.B. Leite, & E.Q.R Santiago, "Recycled lightweight concrete made from footwear industry waste and CDW," *Waste management*, vol.30(6), PP.1107-1113,2010.
- 27: X.Pan, Q. Xie, & Y. Feng, "Designing recycling networks for construction and demolition waste based on reserve logistics research field," *Journal of Cleaner Production*, vol.260, PP.120841,2020.
- 28: T.K.L. Nguyen, H.H. Ngo, W. Guo, T.L.H. Nguyen, S.W. Chang, D.D. Nguyen, & L. Deng, "Environmental impacts and greenhouse gas emissions assessment for energy recovery and material recycle of the wastewater treatment plant," *Science of The Total Environment*, vol.784, PP.147135,2021.



# CHALLENGES FOR INCORPORATING BIM BASED LCA IN A NEW COMMERCIAL BUILDING PROJECT & CONSTRUCTION FIRM IN PAKISTAN: A REVIEW

<sup>a</sup> Ali Junaid\*, <sup>b</sup> Umair Ahmed

a: Gren Construction (SMC-Pvt) Ltd, Islamabad, [ali.grencon@gmail.com](mailto:ali.grencon@gmail.com)

b: Gren Construction (SMC-Pvt) Ltd, Islamabad, [umair.grencon@gmail.com](mailto:umair.grencon@gmail.com)

\* Ali Junaid: Email ID: [ali.grencon@gmail.com](mailto:ali.grencon@gmail.com)

**Abstract-** This paper presents the gap in current infrastructure development method in Pakistan's construction industry and other. Construction Industry consumes the natural raw material to turn it into usable construction product which release embodied carbon dioxide in environment which has highest percentage in Green House Gases (GHGs), which trap heat in atmosphere. Gradual annual temperature increases per year due to global warming caused by the conventional practice by both developed and developing nations construction industry has sparked an outrage in common people. Hence, environment friendly construction techniques were developed. Building Information Modelling (BIM)-based Life Cycle Assessment Technique (LCA) is critically reviewed for its usage in a developing country. By utilizing BIM based LCA, the environmental load can be reduced, however, lack of resources and data is the biggest hurdle for unlocking its true potential.

**Keywords-** Building Information Modeling, Commercial Building, Construction Industry, Life Cycle Assessment.

## 1 Introduction

A Commercial building in real estate sector is defined as income generating property either in form of capital gains or rental income. A Commercial building is ultimately considered economy activity generator of the locality which dictates and forms the living standard of the nearby society. A commercial building can be utilised to present a number of small scale business in the area. The building can be utilised by hospitality management segment, retail outlets, private Small and Medium Enterprise (SMEs) offices, healthcare, multifamily apartments, educational institutes, and large scale industry offices. A Commercial building usually operates on the timely in-flow and out-flow of the payments under certain condition, resulting in wealth rotation in lower and upper segments of the society. In-flow of the cash means to attain rent, operating expense recovery, fees in term of utility provision (security, water supply, electricity), proceeds of any sale made in any portion of building, tax collection and dispensation, tax crediting. Whereas, Out-flow entails initial building construction cost, all operating costs, government taxes on income, costs upon sale and maintenance expenditure. Pakistan is a developing nation in which construction industry and real estate sector plays a major role in its contribution towards Gross Domestic Product (GDP).

The business of new building construction in developing countries is flourishing because of its key role in providing work status to the local community, whereas, it also creates more opportunities for exchanging culture and resources [1]. The design of GDP per capita and the commitment of construction industry in the all-out GDP of the nation is generally agreed upon principle, importance in the developing phase of the economy, The GDP increments at a quicker rate, then, at that point, levels off lastly go down at more elevated levels of monetary turn of events. This implies, that it extraordinarily impacts the economy of a nation; while it additionally adds to-wards its current circumstances. The working of other industries is directly influenced by the efficiency and progress of construction development along with its industry. Retarded functioning of this industry can effectively contribute to creating impediments in the growth of the personal lives of a nation.



Building Construction Industry plays a twofold role in providing both food and shelter [2]. For a developing country, the economy is directly related to the construction industry. This relation has been studied by many authors. Similarly, building along with its pre-requisite infrastructure development by the construction industry is linked with the usage of energy by direct or indirect means [3]. In the present day, the ramification of conventional construction industry performance pattern has brought attention from every walk of life because of harm done to the environment and ecosystem. According to IPCC 2018 report, the increase of 1.5° centigrade per year on average presents a stark image of the drastic changes that occur in environment due to current practices [4]. If, the current practices are adopted as same an increase of 2° centigrade on average per year will resultantly wipe the entire eco-system [5]. Gases that trap heat and radiations in Earth's atmosphere are referred to as Green House Gases (GHGs), furthermore, they are a major cause of temperature increment. The construction industry which comprises roads, roads materials, bridges, buildings, building materials, and components are responsible for 40% of Carbon Dioxide (CO<sub>2</sub>) emission in the world which is the major constituent of Green House Gases (GHGs) [6].

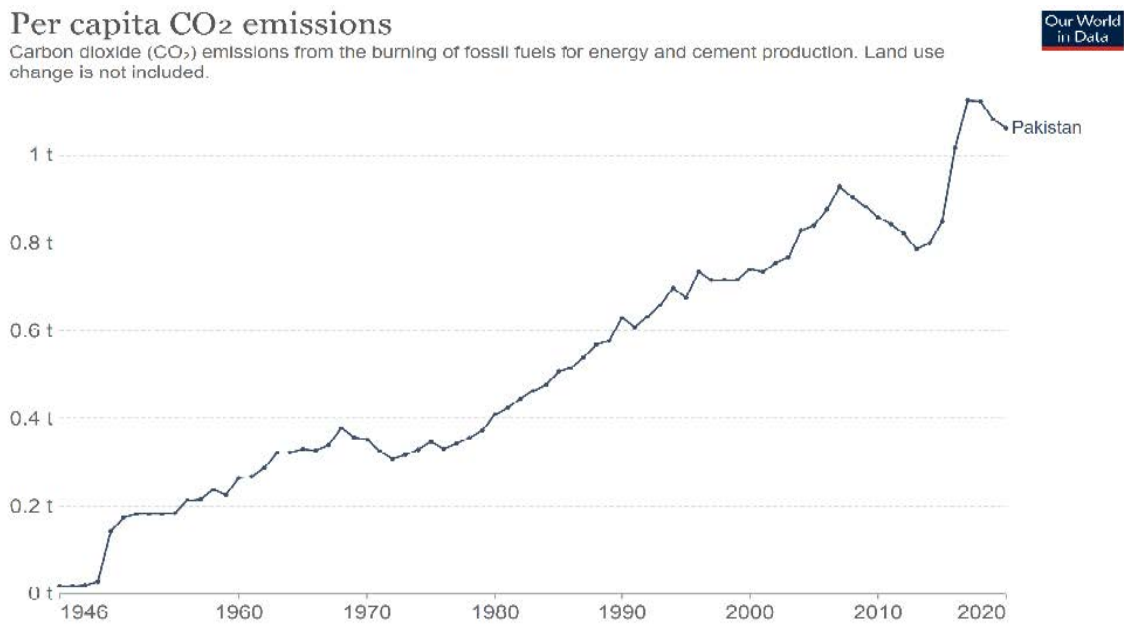


Figure 1: Emissions of Carbon Dioxide (CO<sub>2</sub>) per capita by Pakistan over the years [7].

Figure 1 aforementioned shows the upward increment in CO<sub>2</sub> emission per capita over the years by Pakistan. Natural resources of the world are depleting as the population and demand grow. Harm to the natural environment continues to occur with the emission of Green House Gases (GHGs) caused as a result of using natural resources. 65% of Green House Gases (GHGs) consist of Carbon Dioxide (CO<sub>2</sub>) which in turn are globally produced due to current construction industry practices [8]. This has resultantly put pressure to find sustainable and environmentally friendly methods to curb carbon emissions. Currently, after effects of climate change are being faced by the people all over world. Every year millions of people relocate in essence to find better opportunities but detrimental effect of climate change is also key element in order to vindicate their relocation [9]. Global warming induce melting of glaciers which rise the sea level, rapid urbanization has put cities on exaggerated path towards unliveable temperatures [10]. Water shortage or water scarcity is also a major challenge for country like Pakistan [11]. Therefore, an existential threat persists on mankind by degradation and current annual temperature rise demographs because of current human practices, which makes it all the more substantial for developing countries like Pakistan to adopt environmentally viable construction techniques. This paper focuses on the applicability of BIM based LCA for countries like Pakistan in order to develop sustain construction practices, techniques and tools based on local resources using modern tools available in market, learn how developed countries have utilized the modern tools and techniques to found environment friendly construction methodologies.

## 2 Building Construction

Food and shelter are the basic requirement for humans to survive. Literal mean of construction is that it is the science and art of putting objects together in systematic organization. Building construction usually means making and erection of



structures used for provision of shelter. It involves phases from initial gathering of financing, planning, design and continues till the time a structure is built and ready to use. Construction also makes up process of repair and maintenance, improve, extend and expand the building from original shape. It concludes at the demolition, decommissioning or dismantling. The idea of having shelter against the harsh weather and animal species developed in Neolithic times or stone age. First huts and shelters were built from simple tools or by hands [12]. As the time advanced many technological advancements were made in the field of building construction.

In order to find livelihood, people started working in set of teams of to provide shelter to other peoples. Initially, people were dominated by force and only slaves were used to build shelters. As time went on people gained mastery to provide certain skill set in shelter construction therefore, demanding something in return. The prevailing concept of barter system was used to trade shelter for something in return. The idea for building shelters for commercial activity developed in 2000 BCE [12]. In modern times, the concept of commercial building can be predated to 1800s where buildings were used to in order to gain income from them [13].



Figure 2: Conventional method of commercial building construction in Pakistan.

Figure 2 depicted supra shows the conventional method of building construction in Pakistan. Whereas, new techniques are available in the market which would allow for sustainable development to take place. The construction industry pays a lot of Gross Domestic Product in Pakistan so the idea of sustainable construction practices will be instrumental in decreasing the carbon emission as a whole and will allow new market trends based on the positive impact on health, to grow.

### 3 Incorporation of BIM based LCA to reduce embodied carbon footprint emissions

Embodied Carbon emissions are referred as those carbon emissions which take place in materials and construction processes throughout the whole lifecycle of the infrastructure. Therefore, it includes the material extraction, transportation to manufacturer or production plant, during manufacturing or production, transportation to site for use, while application in construction phase, transportation to end of life facilities and beyond the life cycle of the product [5]. Transportation infrastructure helps in mass mobility of people and goods from one place to another. The continuous construction of infrastructure cause large sum of material extraction, production, and utilization, therefore, releasing a huge sum of Green House Gases (GHGs) [14]. Building infrastructure is essential for human development which in turn arises sustainability challenge to cater for. Overall, the construction sector and carbon emission are directly proportional to each other [3]. To achieve sustainable environmental infrastructure without causing any further environmental degradation is an arduous task for policy makers.



In addition, demand-driven innovation policies coupled with booming GDP growth in developing countries have improved energy efficiency. Macro-level economic policy serves as a productive primary tool for managing the structure of market demand and supply. In the current situation, manufacturers are benefiting from meeting potential demand by launching new and improved products as barriers to entry for new companies have been removed. , has supported a high-price strategy to stimulate innovation activity for demand-driven policy innovation. Many developing and emerging economies are striving to implement demand-side innovation policies in consumer policy, government procurement, and key market reforms to highlight social needs and market failures. Developed for function and energy saving. Building on existing theory and research, many empirical articles examine the dynamic links between innovation and environment in different economies and regions., [15].

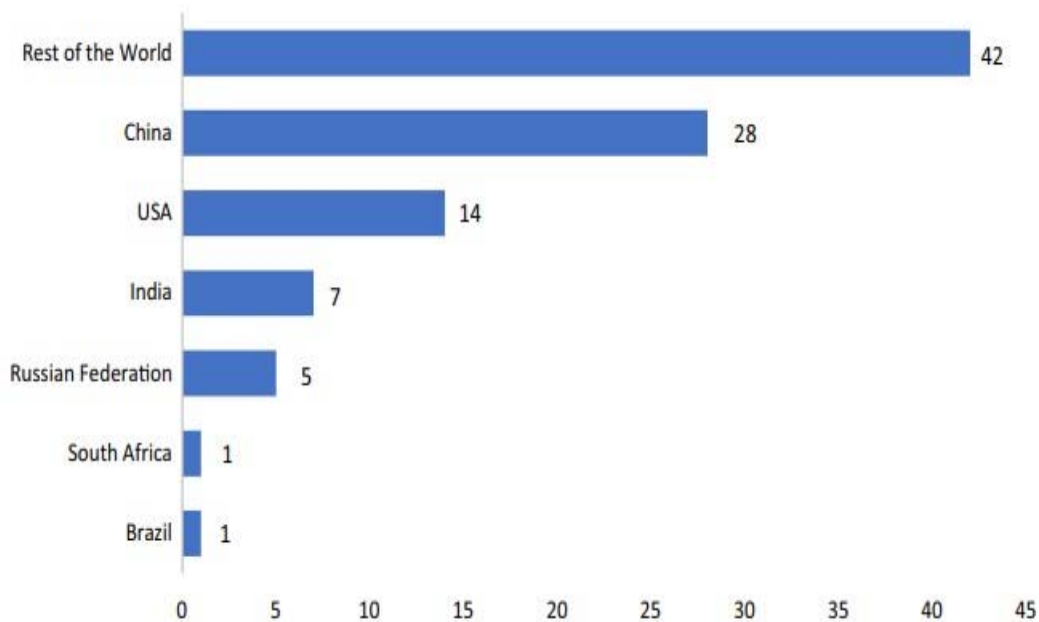


Figure 3: Global CO<sub>2</sub>E Emitting Economies in year 2020 [15]

Figure 3 illustrated above shows that the of conventional practices of carbon intensive industries is still a problem even in developed countries. Whereas, Fundamental initiatives are being undertaken worldwide by scholars to find alternative, cost efficient, and environment friendly practices needed today to maintain the overall functionality of the building facility.

Literature suggest that there are many techniques utilized now a days to hamper the on-going environmental degradtaion. Building Information Modeling is a new technology which help policy makers in applying environmentally viable, socially acceptable and economically feasible materials or practices from the line design stage to completion including maintenance and operational phase of the infrastructure which also includes immediate service restoration in case of break down. [16]. It is a new roboust method to calculate environmental load of buildings which are either constructed or in construction phase. It is desirable to use the BIM tool in early stage of construction however, due to lack of information, resource and data available the usage of BIM is restricted and limited. A bidirectional path is required to transfer information in order to successfully execute Life Cycle Assessment for the project under consideration. This tool allows one to practically integrate building-related environmental sustainability requirements into BIM projects and carry out desired changes to reduce its environmental impact.

#### 4 Literature Review

Various scholars have researched on making building construction environmentally viable and make future living condition better for all humanity. A summary of their working is explained in table 1.



Table 1 Literature Review for Limiting Embodied Carbon Footprint by BIM Based LCA

Authors	Study Area	Year	Summary of Using BIM based LCA for Limiting Embodied Carbon Emission.
Dauletbek and Zhou [17]	China	2022	It was concluded that BIM-based life cycle assessment is a powerful tool for assessing homes in operation and maintenance phase as it comprehensively evaluates the environment, energy efficiency and economics.
LLatas, et al. [18]	Spain	2022	A data driven BIM based LCA was proposed for the locality, which indicated most CO <sub>2E</sub> emitting materials for which alternatives can be worked out.
Cheng, et al. [19]	China	2022	It was concluded that steel, timber and bricks were the top most contributing factors, whereas, interior alternatives and carbon sinks can be worked out to balance the negative output.
Maierhofer, et al. [20]	Austria	2022	It was found out that 68% of the building GHGs release to the environment was related operational integration system and BIM based LCA can hamper down the negative impact if applied in design phase. This is now a regulation under the European Union standard building procedure.
Ansah, et al. [21]	China	2021	Under consideration study proved that the BIM based LCA provides a systematic and detailed assessment of the building project and by adopting real local data driven BIM based LCA, we can improve the design robustness and performance of building environmentally.





Decision-makers on the national level should set out a solid policy for setting targets for carbon dioxide emission reduction. National-level policy devised keeping in mind the sustainable development is based upon three main challenges, in essence, interpretation of the development work keeping in mind the future use, information structuring to maintain a defined level of service while catering influencing need. As Pakistan is developing, sustainability-oriented strategies must involve all environmental, social, and economic parameters so that due input is taken from stakeholders. Developing a national-level strategy would mainly depend upon the contribution from the private sector. For that purpose, the policymakers, should initially roll out plans for helping the local sector to couple up to the advanced stage, then only, discourage the conventional practices. Afterward, the system of incentives and restrictions should be imposed to ascertain and enforce the policy in true letter and spirit.

Unavailability of data and lack of reliable data results in over designing of structure to ensure the smooth operation of the public or private facility. Efficiency and reliability in testing results should ensure the proper designing of public infrastructure. This would result in the reduction of material wastage inherently reducing the embodied carbon emission. Alternative materials should be incorporated resulting in better environmental performance as compared to simple design. Building Information Modeling also helps a great deal in this regard to keep track of the development work completed. This will not only help inefficient operation but significantly reduce the wastage of resources in repair and maintenance. The exact quantities can be calculated and end of life recycling or refurbishment can be planned

## **5 Discussion**

The growing human need for infrastructure provision is a massive challenge while keeping in mind the prospects of that human livelihood and standard of living. The construction industry provides the infrastructure for daily activity by mankind in the movement of goods and people, however, conventional methods of construction are causing a detrimental effect on the environment [22]. The rapid increase of population results in massive building infrastructure needs for survival therefore, the development of building projects is occurring on a massive scale. Natural fossil fuels are the key elements of the construction industry whereas, blatant use of these resources results in Carbon Dioxide (CO<sub>2</sub>) emissions both directly and indirectly [23]. Pakistan is currently amongst the countries with the lowest carbon emissions rating, however, developing countries will suffer the most from climate change [24]. Therefore, it is imperative for developing countries like Pakistan to develop policy frameworks, adopt sustainable practices, adopt material alternatives, improve processes and develop national strategies from now so that corrective actions taken beforehand will resultantly allow new markets and trends to flourish which will be sustainable in the long run and provide better living condition to future generations. Adopting BIM based LCA will be a step in right direction in order to provide the desired level of service to the client whereas, promoting sustainability criteria for future construction in the locality. This opens up new market trend to flourish, which initially increases the boost of construction sector in country's GDP, Furthermore, allowing more environment friendly construction to take place.

## **6 Conclusions & Recommendations**

Following conclusions can be drawn based on literature review: -

1. Developing Countries like Pakistan emit the least amount of embodied carbon footprint in environment, whereas, will be bearing the major consequences.
2. Building Information Modelling (BIM) is a new tool that has been introduced by Autodesk in Architecture, Engineering and Construction domain. Though, there is a resource deficiency for expertise in this new software tool, there has been a lot of effort to gain maximum utility of this software; Which has proven it to be worthy.
3. BIM based Life Cycle Assessment is a new technique that is being adopted by developed countries and that has performed in excellent manner in order to reduce the embodied carbon emission of the new infrastructure construction.
4. The versatility of technique can be enhanced much further by utilizing local area based carbon emission factors data and by utilizing the technique from initial design phase till completion.
5. Locally available environment friendly material alternatives should be accessed and factored in so that building performance can be judged as a whole.



Following are the recommendations that should be adopted to counter the effect of carbonised environment :-

1. National Coordinated effort to develop a policy framework and road map to modern tool usage solutions.
2. Roadmap to convert existing infrastructure towards environment friendly alternatives. Government policy to strictly achieve zero carbon emission in new building projects.
3. All developers to committ to relevant industry roadmap and require disclose of supply chain data.
4. All manufactures to comply and committ to road map developed to achieve environment friendly materials.
5. Future curriculum must include the harmful impact of unregulated construction practices.
6. Upcoming research should be focused on improving energy efficiency of existing infrastructures, private buildings, public buildings and new construction of any facility using BIM based LCA in operational and maintenance phase as well.

## Acknowledgment

The author would like to thank Allah Almighty for his divine blessing particular thanks to Brig. Engr. Muhammad Ayub (Retd), teachers, and colleagues who have helped throughout this research work. The careful review and constructive suggestions by the anonymous reviewers are gratefully acknowledged.

## References

- [1] O. S. Neffati *et al.*, "Migrating from traditional grid to smart grid in smart cities promoted in developing country," vol. 45, p. 101125, 2021.
- [2] P. Manu, A.-M. Mahamadu, T. T. Nguyen, C. Ath, A. Y. T. Heng, and S. C. J. S. s. Kit, "Health and safety management practices of contractors in South East Asia: A multi country study of Cambodia, Vietnam, and Malaysia," vol. 107, pp. 188-201, 2018.
- [3] Y. Su, Z. Zou, X. Ma, and J. Ji, "Understanding the relationships between the development of the construction sector, carbon emissions, and economic growth in China: Supply-chain level analysis based on the structural production layer difference approach," *Sustainable Production and Consumption*, vol. 29, pp. 730-743, 2022.
- [4] U. Nations, "Intergovernmental Panel on Climate Change Special Report," vol. Special Edition, 2018.
- [5] W. G. B. Council, "Bringing Embodied Carbon Upfront," 2019.
- [6] M. Ö. A. Akan, D. G. Dhavale, and J. J. J. o. C. P. Sarkis, "Greenhouse gas emissions in the construction industry: An analysis and evaluation of a concrete supply chain," vol. 167, pp. 1195-1207, 2017.
- [7] M. R. a. P. R. Hannah Ritchie, "'CO<sub>2</sub> and Greenhouse Gas Emissions Pakistan'," 2020.
- [8] M. Asif, T. Muneer, R. J. B. Kelley, and environment, "Life cycle assessment: A case study of a dwelling home in Scotland," vol. 42, no. 3, pp. 1391-1394, 2007.
- [9] B. Halder, A. M. S. Ameen, J. Bandyopadhyay, K. M. Khedher, and Z. M. Yaseen, "The impact of climate change on land degradation along with shoreline migration in Ghoramara Island, India," *Physics and Chemistry of the Earth, Parts A/B/C*, p. 103135, 2022.
- [10] P. Han, Z. Tong, Y. Sun, and X. Chen, "Impact of Climate Change Beliefs on Youths' Engagement in Energy-Conservation Behavior: The Mediating Mechanism of Environmental Concerns," *International Journal of Environmental Research and Public Health*, vol. 19, no. 12, p. 7222, 2022. [Online]. Available: <https://www.mdpi.com/1660-4601/19/12/7222>.
- [11] B. Chen, J. Cui, X. Man, W. Dong, C. Yan, and X. Mei, "The climate cost of saving water by different plastic mulching patterns," *Journal of Cleaner Production*, vol. 359, p. 132011, 2022/07/20/ 2022, doi: <https://doi.org/10.1016/j.jclepro.2022.132011>.
- [12] C. J. A. j. o. A. Runnels, "Review of Aegean prehistory IV: the Stone Age of Greece from the Palaeolithic to the advent of the Neolithic," vol. 99, no. 4, pp. 699-728, 1995.
- [13] T. H. Witkowski, "The Commercial Building as a Promotional Tool in American Marketing History, 1800-1940," in *Proceedings of the Conference on Historical Analysis and Research in Marketing*, 2001, vol. 10, pp. 199-210.
- [14] S. M. H. Shah, A. Junaid, R. H. Khan, and S. S. S. Gardezi, "Assessment of Embodied Carbon Footprint of an Educational Building in Pakistan Using Building Information Modeling (BIM)," in *Collaboration and Integration in Construction, Engineering, Management and Technology*: Springer, 2021, pp. 235-239.
- [15] Z. Weimin, M. Z. Chishti, A. Rehman, M. J. E. Ahmad, Development, and Sustainability, "A pathway toward future sustainability: assessing the influence of innovation shocks on CO<sub>2</sub> emissions in developing economies," vol. 24, no. 4, pp. 4786-4809, 2022.



**4<sup>th</sup> Conference on Sustainability in Civil Engineering (CSCE'22)**  
Department of Civil Engineering  
Capital University of Science and Technology, Islamabad Pakistan



- [16] A. Alasskar and P. Jagannathan, "BIM in Construction and Maintenance of Infrastructure Projects," Singapore, 2022: Springer Singapore, in *Advances in Construction Management*, pp. 481-499.
- [17] A. Dauletbek and P. Zhou, "BIM-based LCA as a comprehensive method for the refurbishment of existing dwellings considering environmental compatibility, energy efficiency, and profitability: A case study in China," *Journal of Building Engineering*, vol. 46, p. 103852, 2022.
- [18] C. LLatas, B. Soust-Verdaguer, A. Hollberg, E. Palumbo, and R. J. A. i. C. Quiñones, "BIM-based LCSA application in early design stages using IFC," vol. 138, p. 104259, 2022.
- [19] B. Cheng, K. Lu, J. Li, H. Chen, X. Luo, and M. J. J. o. C. P. Shafique, "Comprehensive assessment of embodied environmental impacts of buildings using normalized environmental impact factors," vol. 334, p. 130083, 2022.
- [20] D. Maierhofer, M. Röck, M. R. M. Saade, E. Hoxha, A. J. B. Passer, and Environment, "Critical life cycle assessment of the innovative passive nZEB building concept 'be 2226' in view of net-zero carbon targets," p. 109476, 2022.
- [21] M. K. Ansah, X. Chen, H. Yang, L. Lu, and P. T. J. E. I. A. R. Lam, "Developing an automated BIM-based life cycle assessment approach for modularly designed high-rise buildings," vol. 90, p. 106618, 2021.
- [22] R. Spence and H. J. H. i. Mulligan, "Sustainable development and the construction industry," vol. 19, no. 3, pp. 279-292, 1995.
- [23] L. Huang, G. Krigsvoll, F. Johansen, Y. Liu, X. J. R. Zhang, and S. E. Reviews, "Carbon emission of global construction sector," vol. 81, pp. 1906-1916, 2018.
- [24] U. Nations, "Intergovernmental Panel on Climate Change Special Report," vol. Special Edition, 2014.



# EXPERIMENTAL STUDY OF SCOURING AROUND ELLIPTICAL PILE-CAP BY USING THE SUBMERGED BROAD CRESTED TRAPEZOIDAL WEIR AT DOWNSTREAM

*<sup>a</sup> Muhammad Ashgar\*, <sup>b</sup> Naeem Ejaz, <sup>c</sup> Muhammad Aleem, <sup>c</sup> Hafiz Ubaid Ur Rehman*

a: Department of Civil Engineering, University of Engineering and Technology Taxila asgharghani0078600@gmail.com

b: Department of Civil Engineering, University of Engineering and Technology Taxila naeem@uettaxila.edu.pk

c: Department of Civil Engineering, University of Engineering and Technology Taxila, engrm.aleem@gmail.com

c: Department of Civil Engineering, University of Engineering and Technology Taxila, ubaidsiddiqui1964@gmail.com

\* Corresponding author: Email ID: asgharghani0078600@gmail.com

**Abstract-** Bridge piers fail for a variety of reasons but scouring around the pier is the most common. It is during the scouring procedure that the piers are decontaminated. As a result, the foundation of the bridge is exposed, which ultimately results in its collapse. The scouring effect around bridge piers was reduced by employing a different method. An Elliptical Pile-Cap of dimension (D) six centimeters by six centimeters was installed at the upstream side of a submerged trapezoidal broad crested weir (TBCW), and the height of the weir (Z) was five centimeters without piers and with weirs at various separation distances (S), two-dimensionally (S), and four-dimensionally (S). The experiment was conducted in a channel at the Hydraulics Engineering Laboratory, University of Engineering and Technology Taxila, utilizing a uniform bed material, flow depth-flowing under clear water conditions. The upstream face of the pier had its scouring depth compared to the local scouring in both the presence and absence of TBCW. Experiment results demonstrate that by using the submerged TBCW- at downstream  $S = 2D$ ,  $S = 4D$ , as opposed to without it, the scour depth at Elliptical Pile-Cap may be reduced by 48%.

**Keywords-** Elliptical Pile, Trapezoidal Broad Crested Weir, Reduction, scouring

## 1 Introduction

Local scour holes around bridge piers are almost inevitable in alluvial channel beds subjected to the erosive force of oncoming river flows. Building bridges that span alluvial channels demands expertise or at least the ability to design and construct them [1]. This estimate is as close to being precise as feasible in order to predict the maximum scour depth that may occur near the piers over the course of the bridge's expected lifespan. Scour depth estimation is in its infancy because of the complexity of scour problems, which necessitates the development of a unifying theory. This type of scouring is most common during floods, which have unstable flows and may even change direction (Wardhana et al. 2022) [2]. Scrubbing occurs when three-dimensional boundary-layer separation occurs at the dock, resulting in bed material being eroded by high-turbulence and vorticity local flow structures. The examination of scour at bridge piers has been ongoing for several decades. For a variety of approach flows, sediment sizes and grades, pier types and sizes, and other variables, researchers have studied local pier scour extensively in alluvial channels and produced several prediction models to determine the maximum scour depth at bridge pilings [3]. For the hydrodynamic forces in the scour hole to stop removing particles, the local scour persists for an adequate amount of time at the bridge pier's piers. Equilibrium is reached at this point in the scour hole and the scour depth does not change much unless flow conditions or bed material changes (Mohammad Vaghefi et. al 2022) [4].

## 2 Experimental Procedures

All the experiment was performed in the Water resources & Hydraulics Engineering Laboratory of Department of Civil Engineering, University of Engineering and Technology, Taxila. The channel had specifications of 20 m length, 1 m wide and 0.75 m deep glass-sided flume with an adjustable tailgate at the channel-end to regulate the flow depth used for the experimental depth. Through the centrifugal pump, discharge was supplied to the tank then inter to the main channel by aligned honeycomb diffuser in the direction of flow for smooth and uniformly distribution of flow cross-wise. At the tail of channel water enter in the sediment tank after filling and trapping the flowed sediments, the flow discharges in the main channel. Plan view of the Laboratory channel and experimental setup shown in Figure 1. Also, pictorial representation of experimental setup shown in Fig 2

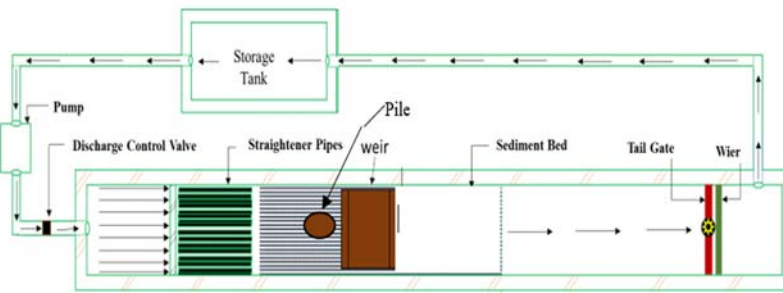


Figure 1: Plan View of Channel

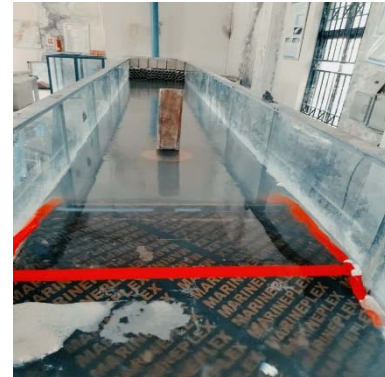


Figure 2: Pictorial View of Experimental Setup

Fig 1: Plan View of Channel A 9m long, 0.20m deep and .96m wide false bottom of uniform, medium size ( $d_{50}=.51\text{mm}$ ) bed material and pier base was introduce, sand size considered in this study stood in compliance to the condition of  $D/d_{50} > 50$  in order to dominate the sediment size effect on the scour evolution process guaranteeing non ripple-forming sand (Raudkivi & Ettema, 1983) ( Ettema, Melville, & Barkdoll, 1998). The diameter of the pile was not more than 10% of the channel width to prevent the effect of walls on scouring (Chiew and Melville, 1987) [5], therefore double square pile modelled by 0.06m dimension of wood material. The trapezoidal broad crested weir (TBCW) modelled by wood material, weir width equal to the full width of channel, crest length was 50cm, the weir was 5cm above the flat bed, the sides slopes of the TBCW was 1V:2H, which is more stable and seepage control. (Fritzi & Hager, 1998). The dimension of TBCW was within the limits (Sturm, 2001) (Henderson 1966) (Chanson, 2004) [6].

Elliptical Pile was placed at the equal distance the from edges of the flume, at the upstream of the TBCW. In start the elliptical pile was placed near the upstream of the weir, separation distance from the TBCW was 0D, then increase the separation distance (S) with respect to the diameter of pier as 2D and 4D. The sand bed was carefully levelled to flat bed with upstream and downstream flume bed, before performing every experiment. The discharge was then allowed to enter flume gradually and attained the flow depth and velocity became low with the help of tailgate channel. The discharge was set and flow depth was regulated manually to maintain constant and then stabilized flume slowly. After the completion of drainage, point gauge was used to measure the scouring around the pier having an accuracy of  $\pm 0.5$  mm. The experimental minimum time, allowed to run was 3 hours for each experiment. The suitable equilibrium time is 3 hours for the experiment (Karimi et al., 2017). Therefore, average time taken for each experiment was 3 hours. After completion of the above procedure, measured the geometrical dimensions of the scoured hole.

## 3 Research Methodology

There were three distinct discharges tested, with Froude numbers ranging from 0.189 to 0.26, to see if scouring around an elliptical pile cap was possible. Two studies were conducted using a Broad crested trapezoidal weir at the downstream end of each discharge. The third set of trials used a Broad crested trapezoidal weir at downstream and an elliptical pile cap at three different discharge distances (0D, 2 D and 4 D), all of which were done simultaneously. All the tests were completed in crystal-clear water with a constant depth of flow and three distinct discharges.



## 4 Results

Table 1: Experimental Condition and Result

Case	S (m)	Q (m <sup>3</sup> /s)	T (hr)	h (m)	ys_f (cm)	ys_f/D
1	Without weir	0.023	3	0.15	5.3	1.03
2		0.027	3	0.15	5.8	1.08
3		0.032	3	0.15	6.4	1.15
4	2D	0.023	3	0.15	3.3	0.65
5		0.027	3	0.15	4.0	0.73
6		0.032	3	0.15	4.7	0.84
7	4D	0.023	3	0.15	5.1	0.88
8		0.027	3	0.15	5.6	0.95
9		0.032	3	0.15	5.2	1.04

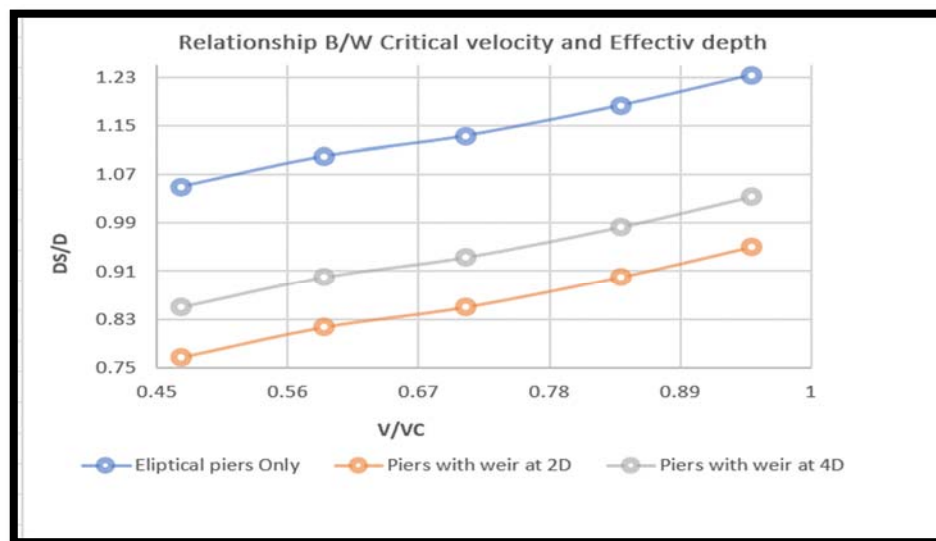


Figure 3: Scour Depth verses flow intensities

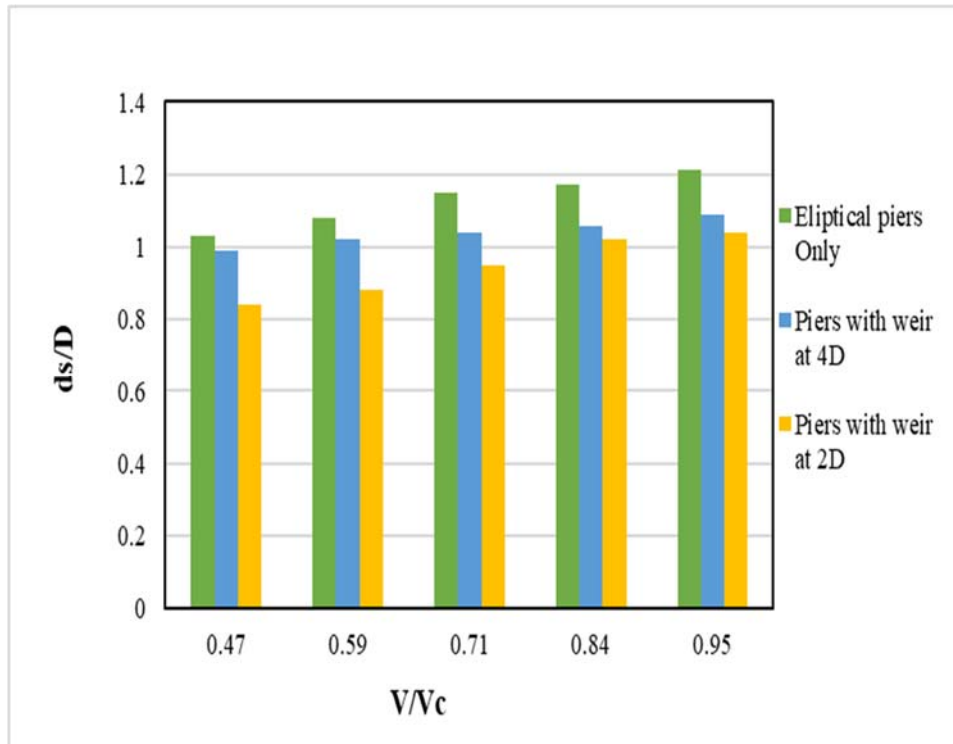


Figure 4: Comparison of elliptical piers only, TBCW at 2D, and 4D

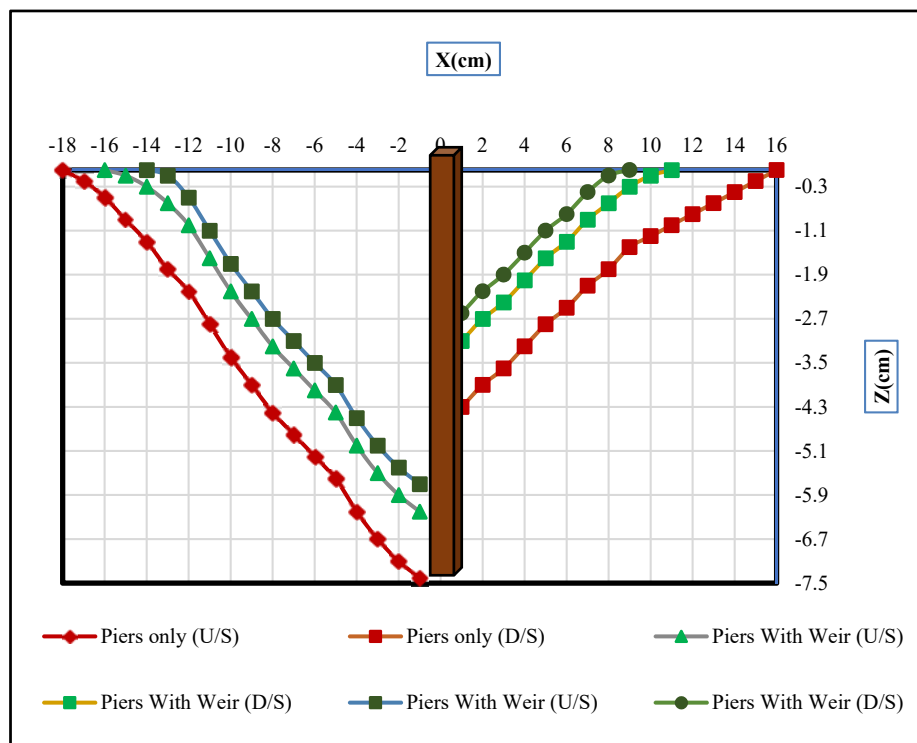


Figure 5a: Longitudinal Scour Profile

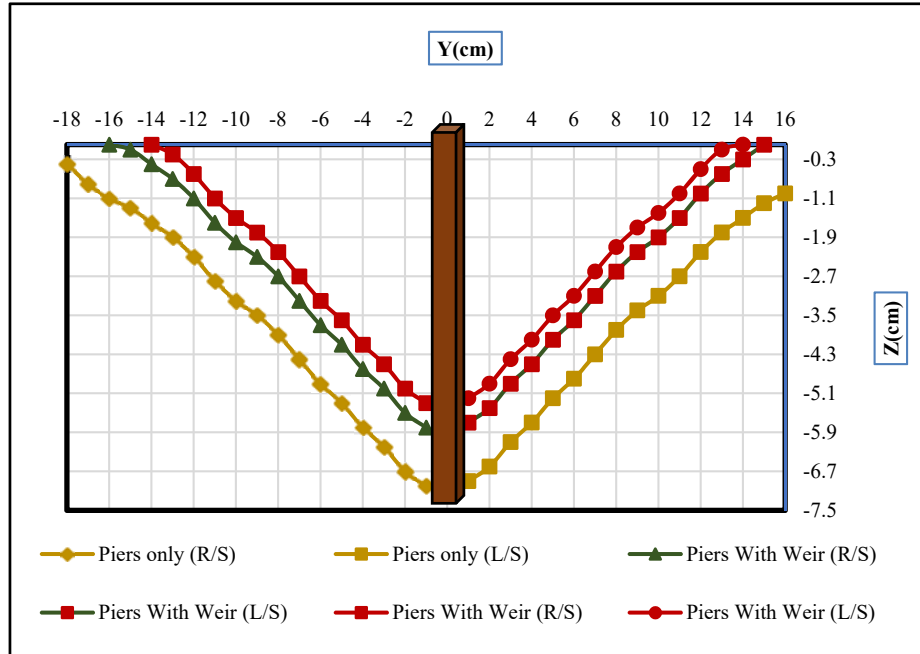


Figure 5b: Lateral Scour Profile

In first case scouring around Elliptical pile-cap was measured without presence of TBCW, then installed the Elliptical pile-cap at the upstream of submerged TBCW and varies the separation distance ( $S$ ) between TBCW with respect to pier dimension of pier as  $2D$ , and  $4D$  measure the scouring around the pier and compare the result of elliptical pier scouring with or without presence of submerged TBCW. During experiment it was observed that scouring was minimum when the piers was installed at distance of  $2D$  from the upstream sides of weir and it will increase as we move from the upstream of weir at  $2D$  and  $4D$ .

Fig. 3 represents the plot of pier scour depth versus various flow intensity shows that the pier scour depth increases with the increase in flow intensity and vice versa. It is since due to the increase in intensity that both the flow depth and velocity increases, which in turn cause an increase pier scour depth. This trend is shown in Fig1 for elliptical piers only, piers with *TBCW* at  $2D$ , and  $4D$  separation distance ( $S$ ) for time interval of  $3h$ , respectively. Fig. 4 shows the comparison between pier installed without *TBCW* and piers installed with weir separation distance between the pier and weir.

Fig 5 (a and b) shows the scour the longitudinal and lateral profiles of scour holes which shows that the scour hole was increased due to increasing the flow intensity. Fig. 5a shows that the scour depth on upstream side of the pier was approximate same as the scour depth of the lateral profiles of the piers due to swirling effect generated along the sides of the pier as shown in Fig. 5b

## 5 Conclusion

This study concluded that:

- The Scouring depth around the pile increases by increasing Froude Number in clear water condition.
- The depth of scour hole increases with the increase of distance from the weir.
- By the increase of separation distance from  $2D$  to  $4D$  between elliptical pile and weir, scouring reduction is reduced; 42% reduction in scouring at  $2D$  and 33% reduction in scouring at  $4D$ .
- Reduction in scouring was 27% around elliptical pile-cap without presence of TBCW; 6% greater reduction than previous study with only Elliptical pile.





## Acknowledgment

The authors would like to express their gratitude to everyone who contributed to the research, especially the Civil Engineering department, Prof Dr Naeem Ejaz. The anonymous reviewers' diligent review and constructive comments are greatly appreciated.

## Reference

- [1] M. & B. Ettema, Scale effect in pier-scour experiments., Vols. Vol. 124, No.6., Journal of Hydraulic Engineering, (1998).
- [2] C. G. R. C. F. & C. A. H. Grimaldi, "Countermeasures against local scouring at bridge piers: Slot and combined system of slot and bed sill," *Journal of Hydraulic Engineering*, vol. 135, no. 5, pp. 425-431, (2009b).
- [3] R. T. A. & C. F. Gaudio, "Gaudio, R., Tafarojnoruz, A., & Calomino, F. (2012). Combined flow-altering countermeasures against bridge pier scour. Journal of Hydraulic Research, (1), 35 43," *Journal of Hydraulic Research*, vol. 50, no. 1, pp. 35-43, (2012).
- [4] L. M. B. W. G. D. & W. C. N. Wang, "Wang, L., Melville, B. W., Guan, D., & Whittaker, C. N. (2018). Local scour at downstream sloped submerged weirs, (8)," *Journal of Hydraulic Engineering*, vol. 144, no. 8, p. 18, 2018.
- [5] P. a. E. T. a. B. M. Gautam, " Experimental study of Scour around a complex pier with elliptical pile-cap," in *ICSE 2016 (8th International Conference on Scour and Erosion*, Oxford,UK, 2016.
- [6] A. L. M. A. & C. Marion, "Marion, Effect of sill spacing and sediment size grading on scouring at grade-control structures," *Earth Surface Processes and Landforms*, vol. 29, no. 8, pp. 983-993, 2004.



# Experimental Analysis of Scouring Around the Round Nose Bridge Pier Using Different Bed Material Conditions

<sup>a</sup> Hafiz Ubaid Ur Rehman\*, <sup>b</sup> Naeem Ejaz, <sup>c</sup> Muhammad Aleem, <sup>d</sup> Muhammad Asghar

a: Department of Civil Engineering, University of Engineering and Technology Taxila, [ubaisiddiqui1964@gmail.com](mailto:ubaisiddiqui1964@gmail.com)

b: Department of Civil Engineering, University of Engineering and Technology Taxila, [naeem@uettaxila.edu.pk](mailto:naeem@uettaxila.edu.pk)

c: Department of Civil Engineering, University of Engineering and Technology Taxila, [engrm.aleem@gmail.com](mailto:engrm.aleem@gmail.com)

d: Department of Civil Engineering, University of Engineering and Technology Taxila, [asgharghani0078600@gmail.com](mailto:asgharghani0078600@gmail.com)

\* Corresponding author: Email ID: [ubaisiddiqui1964@gmail.com](mailto:ubaisiddiqui1964@gmail.com)

**Abstract**-Unexpected weather events, manufacturing defects, shoddy workmanship and poor building maintenance are all common causes of bridge collapse. However, scour damage to bridge pilings is far and away the most common cause of serious damage. Sediment is removed from bridge piers by running water's hydraulic force, a process called scouring. Scour around the piers of a bridge must be taken into account when determining its safety. It's been studied in a number of different ways. Through the use of three different discharge rates (0.32-0.37-0.032m<sup>3</sup>/s), the round nose bridge was successfully integrated into the sandbed, which was measured at 0.57mm in diameter by this research team's team of engineers and engineers. A uniform distribution of particles in the bed resulted in a geometric standard deviation (g) of grain sizes between 1.22 and 1.30. sg of gravel particle size distribution is less than 1.4, and the round nose bridge pier was incorporated into a gravel bed with gravel sizes from 4.1 mm to 14.25 mm Flexible vegetation should be used at distances of 0, 4, and 6 D from the round Nose Bridge Pier, where D is the diameter of the round nose of the Pier. Vegetation upstream served as a water filter. Each test required three hours to complete. At each of the diagonals (upstream, downstream, left, right, and upstream and downstream) a point gauge was lowered into the water to measure the depth of local scour. In an experiment, scouring around the round nose bridges pier employing flexible vegetation was reduced by up to 50% at 0D, 38.11 percent at 4D, and 30.15 percent at 6D distances. Stubborn vegetation reduces scouring by 33.44 percent, 30.92 percent, and 27.38 percent at zero, four and six dimensional distances. A lower scouring rate was observed for flexible vegetation than for rigid vegetation in the vicinity of round nose bridge pilings. A distance between the pier and the vegetation was increased in order to reduce scouring caused by flexible and rigid vegetation.

**Keywords**- Wide Crested Trapezoidal Weir, Scour Depth; Flexible Vegetation; Rigid Vegetation

## 1 Introduction

Scouring is the process by which the hydraulic force of flowing water removes sediment from bridge piers and abutments. Horseshoe vortices are formed around bridge supports and piers due to redirected water flows. Cleaning can be accomplished in three ways: by local scouring, contraction scouring, or by aggravations or degrading substances. Scouring around obstructions in a stream is called "local scouring" in this context. When a bridge collapses due to local scour, the most common cause is a collapsed foundation. Horse shows have vortex systems, for example, which are secondary flows [1]. Local scouring relies heavily on three vortex systems: the one in the wake, the one in the trailing wake, and the one in the bow wave. The bed material rises to the floor in a wake vortex system. The pier's shape and water depth influence the system's strength. When the piers are submerged, the trailing vortex system does not exist in practise. The fragmentation of the piers' upstream flow creates a horseshoe vortex system. Because of the horseshoe vortex, the upstream side of the bridge pier is particularly vulnerable to bed scouring. Different types of waves, such as horseshoe vortex and bow wave, appear on the water's surface [2].



Octagonal, square, circular and oval pilings were all used to estimate the scour depth around the pilings in order to determine the scour depth. Compared to the square piling, the scour depth of the piling was found to be between 10% and 20% greater. If something were to happen, the circular and oval faces of the piling would be in the path of most traffic as compared to the square piling (Ghani & Mohammadpour, 2016) [3].

## 2 Experimental Procedures

"It was done one sand and gravel at a time to fill in the main channel. Testing was carried out on a sand or gravel bed 8 metres by 15 centimetres deep and the same length. This component is used to carry out all scour studies. With regard to the flume's centerline and at a distance of 4 metres from the sand bed, a bridge pier was constructed in the test section. Three discharge rates (0.023 m<sup>3</sup>/sec, 0.027 m<sup>3</sup>/sec, and 0.032) were used in each experiment to measure Froude Numbers [4]. Measurement of flow discharge after the tailgate was accomplished by placing a trapezoidal weir at the channel's end (Reca et al. 2006). The flow depth,  $h$ , is maintained at 15 cm for each set of trials.

### 2.1 Laboratory Channel.

The Hydraulic Laboratory, Civil Engineering Department, University of Engineering & Technology Taxila, and the Pakistani Institute of Science and Technology conducted all of the trials in the laboratory channel. The following are the main components of the laboratory flume.

1. Pipe leading to the inlet 2. The primary means of communication. 3. Setting basin as a foundation 4. Excessive waste Pipe Weir's number five



Figure 1: Laboratory Channel

### 2.2 Material.

The channel's middle was marked with a 6-cm-diameter round nose bridge pier for testing purposes. For the tested pier sizes,  $B/D$  ratios greater than 10 are required for the flume width and pier nose diameter (i.e.  $D=6\text{cm}$ ). As an alternative to real plants, the flexible model array was constructed from conventional broom heads and was used to study hard-vegetated channels. For the flexible vegetation, stacked broom heads with a diameter of 0.04 mm each were used and were inserted into the sand bed with Hole sizes of 3 millimetres are perforated evenly across the surface [5].

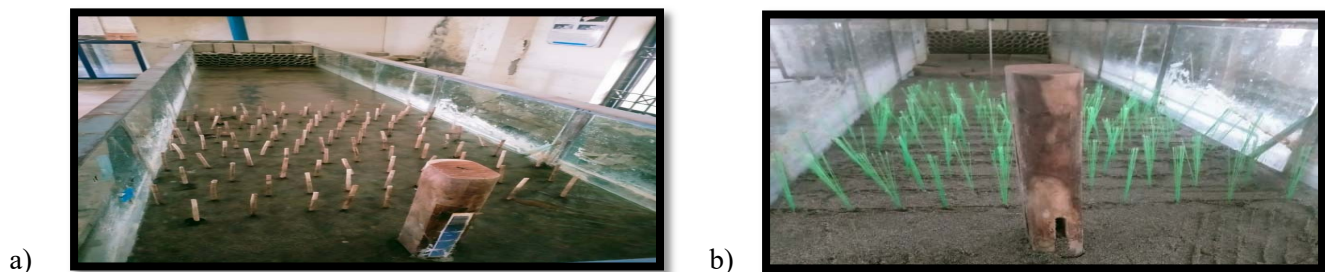


Figure 2 : Round Nose Bridge Pier a) With rigid Vegetation b) With Flexible Vegetation



### 3 Research Methodology

The experiment was conducted on a sediment bed of 10 metres long. With this final one-third of sediment bed zone covered, we were confident that all velocity profiles had been established (Vaghefi, Akbari, & Fiouz, 2016). Perpendicular to the centerline, the pier was set up and ranged accordingly. When it came to B and D, there was a 16:1 ratio. According to Ballio, Teruzzi, and Radice, the contraction effects on scour depth are present at W/D 3. (2009). B/D 5 was found to have a reduced contraction effect by Lança, Fael, Maia, Pêgo, and Cardoso (2013). As a result, the contraction effect had no impact on the findings of this study.

Experiments were conducted on a round nose bridge pier with three different flow discharges, i.e., 22,27,32 l/s.. Weirs at the end of the canal after the tailgate were used to measure discharge flow rates (Reca et al. 2006). For each set of trials, the flow depth, h, is maintained at 15 cm. It was determined that  $B/h > 5$ ,  $D/h > 0.7$  was met in order to reduce the impact of water depth and eliminate secondary flows (Melville and Hadfield 1999). All experiments were carried out at Froude Numbers 0.189, 0.22, and 0.26 at 0.023m<sup>3</sup>/s, 0.027m<sup>3</sup>/s, and 0.032m<sup>3</sup>/s. The flow discharge was measured by a trapezoidal weir at the end of the canal after the tailgate (Reca et al. 2006). 42 experiments in the laboratory channel used sand and gravel as the bed material. Tests were conducted on the round nose bridge pier with and without various types of artificial vegetation (Artificial Flexible and Rigid). a three-hour equilibria was maintained in all experiments (Karimi et al. 2017). Melville and Chiew (1999) defined the equilibrium period for scour depth as the time during which the scour depth does not fluctuate by more than 5% of the pier diameter at any given point in time. At the end of each test, the flume was gently drained, and the depth of the scour hole was recorded.

### 4 Results

A pier's scour depth is directly related to its flow velocity. It is also true that an increase in flow velocity increases the scour depth due of its erosive activity, until it hits the critical velocity, which causes a drop in the pier scour depth. As vegetation is erected and distances between pier and vegetation diminish, the maximum scour depth ( $d_s/D$ ) falls, indicating that round-nose piers with sand beds are most susceptible to scour

#### 4.1 Graphs

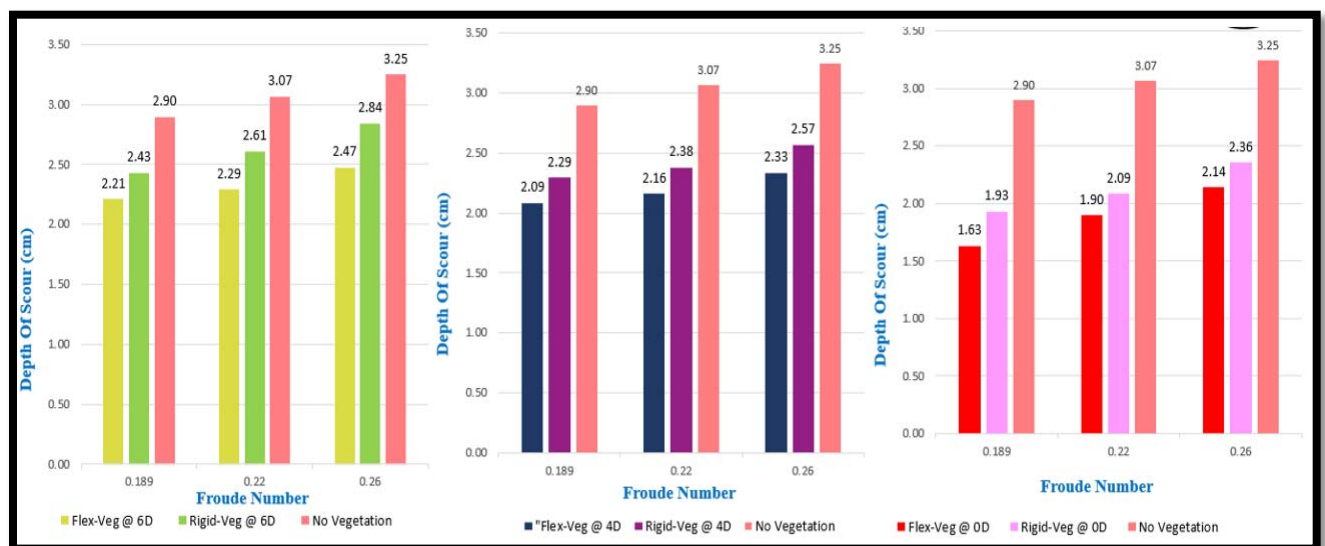


Figure 3: Relationship between scour depth ( $d_s$ ) and Froude Number for sand bed material.

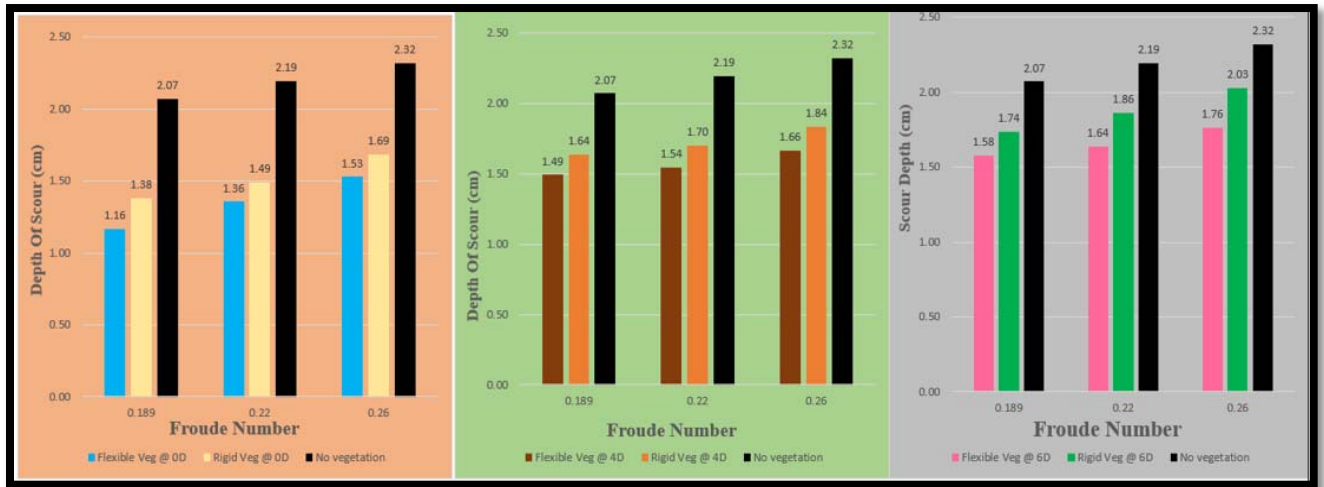


Figure 4: Relationship between scour depth ( $d_s$ ) and Froude Number for gravel bed material.

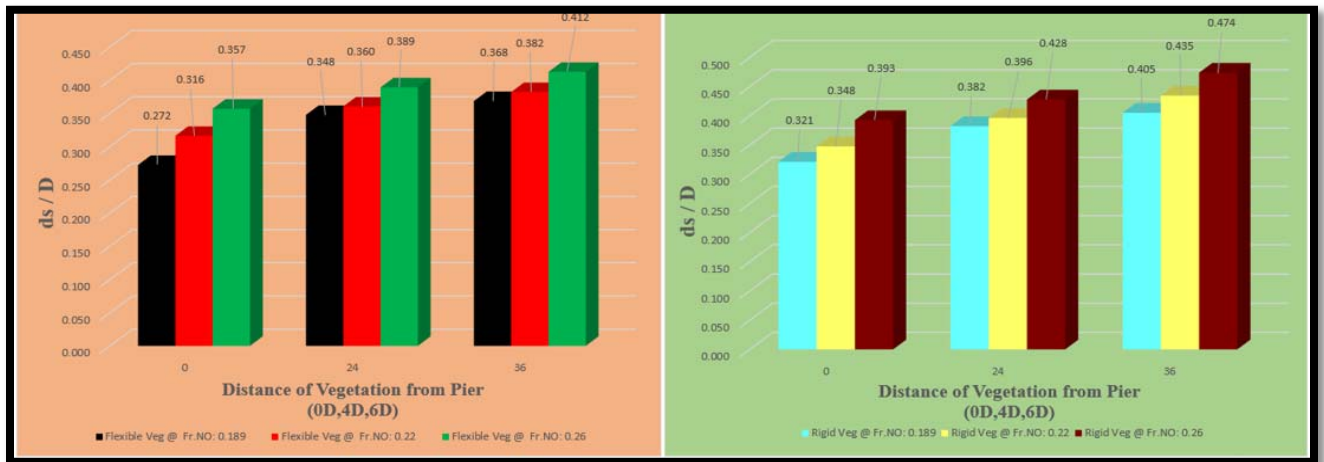


Figure 5: The  $d_s/D$  versus Distance b/w vegetation and the pier having sand bed installed at upstream side.

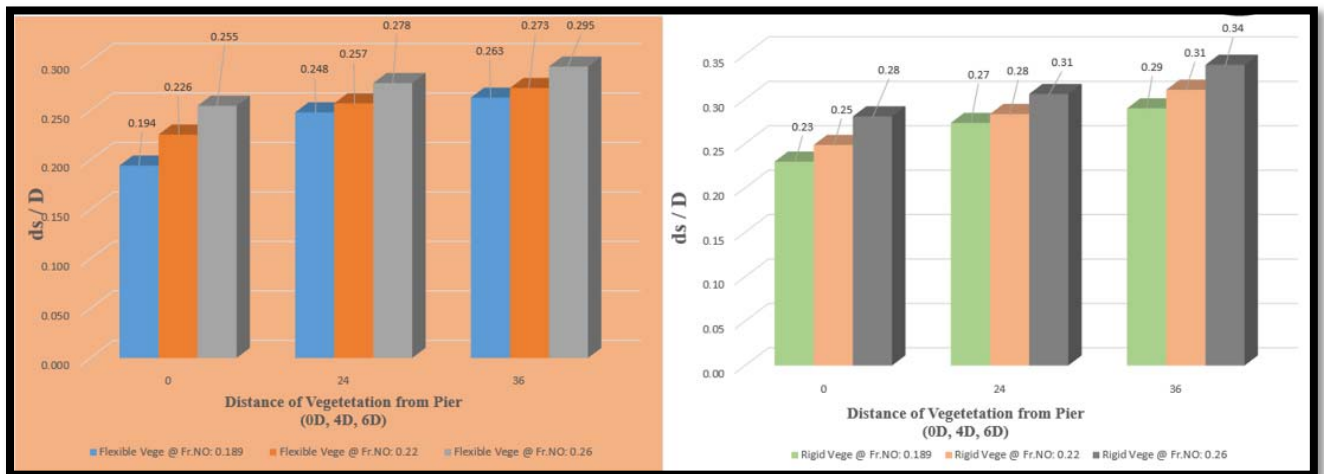


Figure 6: The  $d_s/D$  versus Distance b/w vegetation and the pier having gravel bed installed at upstream side.

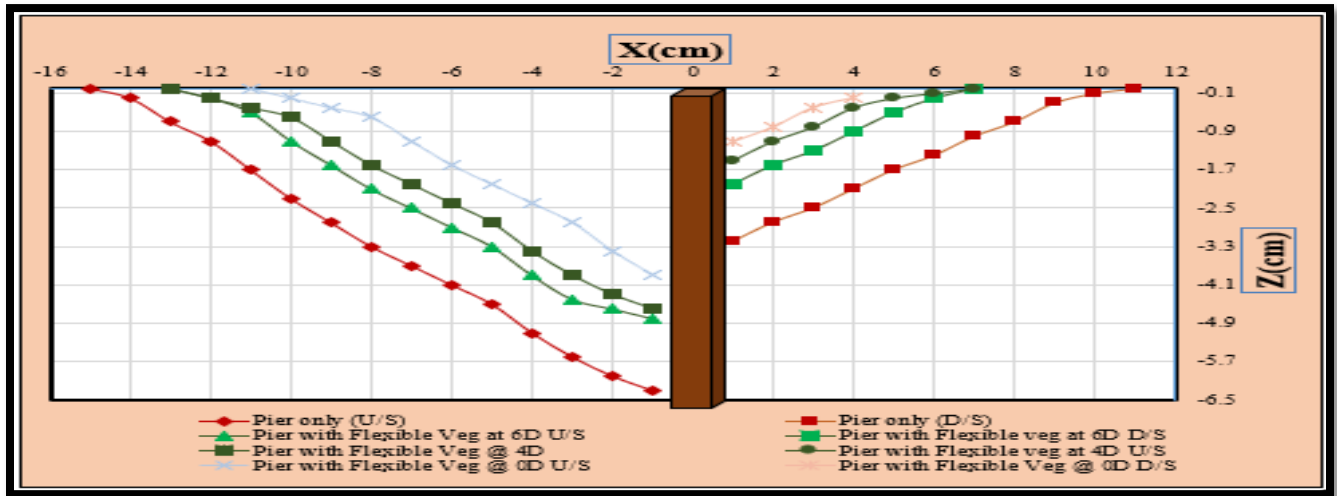


Figure 7: With and Without Flexible Vegetation, the lateral scouring profile of the Round Nose Bridge Pier.

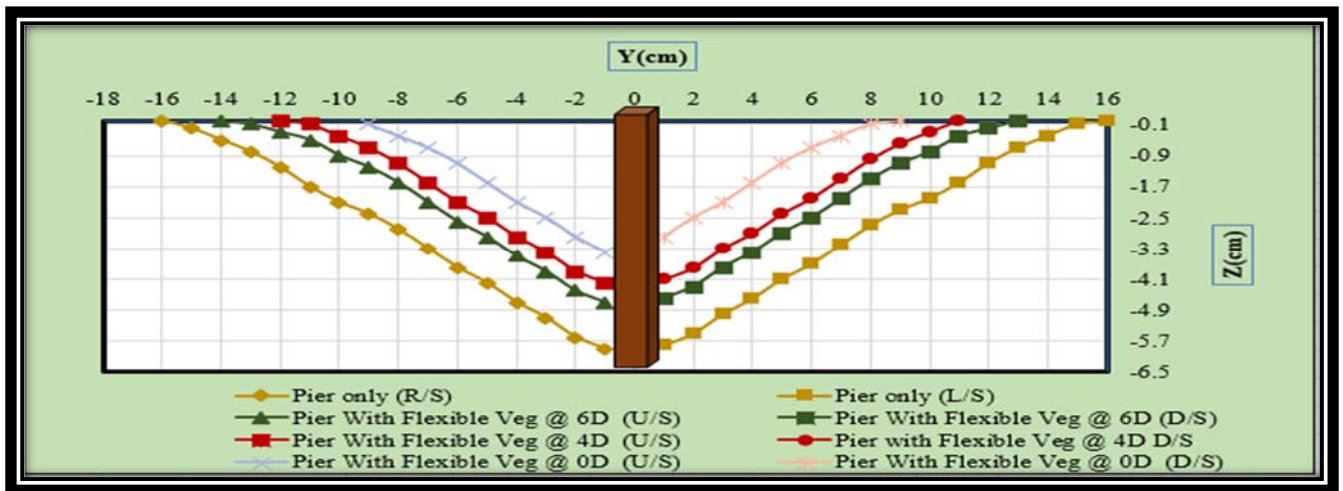
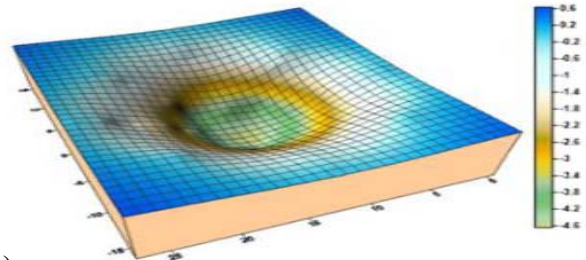
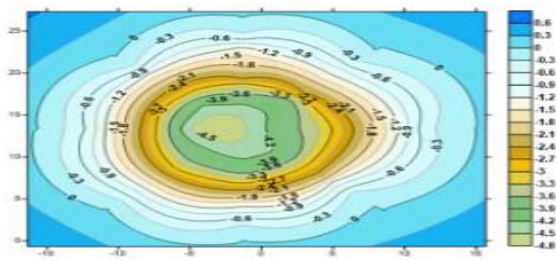


Figure 8: With and without Rigid vegetation, the longitudinal scouring profile of a round-nose bridge pier.

## 4.2 Use of Software

To produce a contour map and 3D geometry for all tests, Golden SURFER Software surveyed the bed topography around the pier. Not only do scour depth contour maps reveal information about the scour process, its dimensions, and its topography, but they can also be used to devise countermeasures for scouring protection under various flow circumstances.



a)

Figure 9: Scour Hole around Pier without ve;

b)

n a) Contour map & b) 3D Geometry.

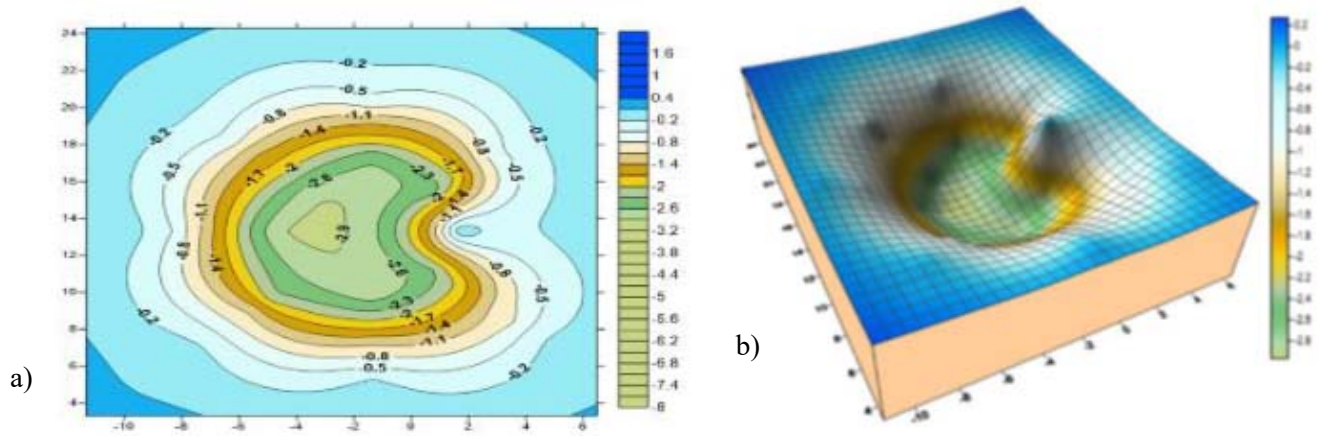


Figure 10: Scour Hole around Pier with flexible vegetation at 0D a) contour map and b) 3D geometry.

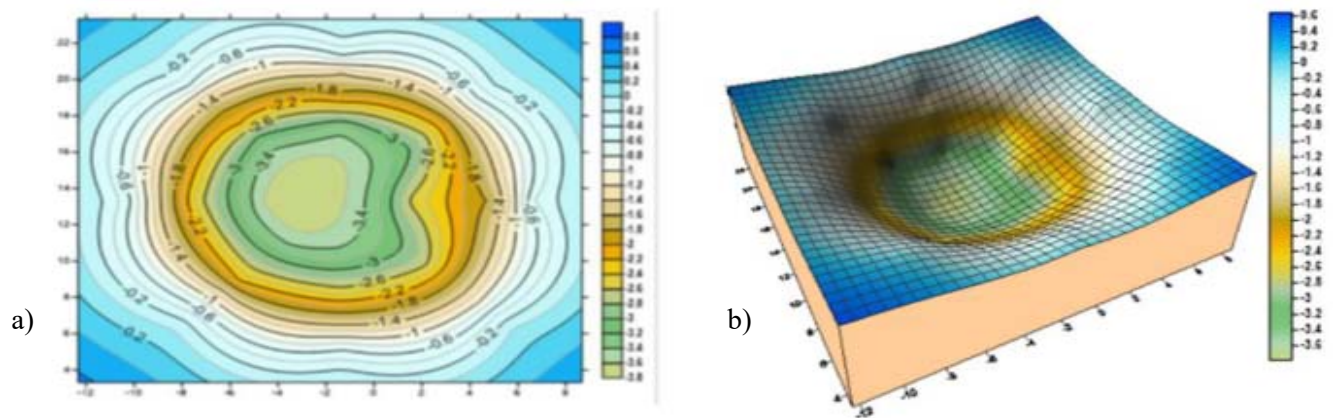


Figure 11: Scour Hole around Pier with flexible vegetation at 4D a) contour map and b) 3D geometry.

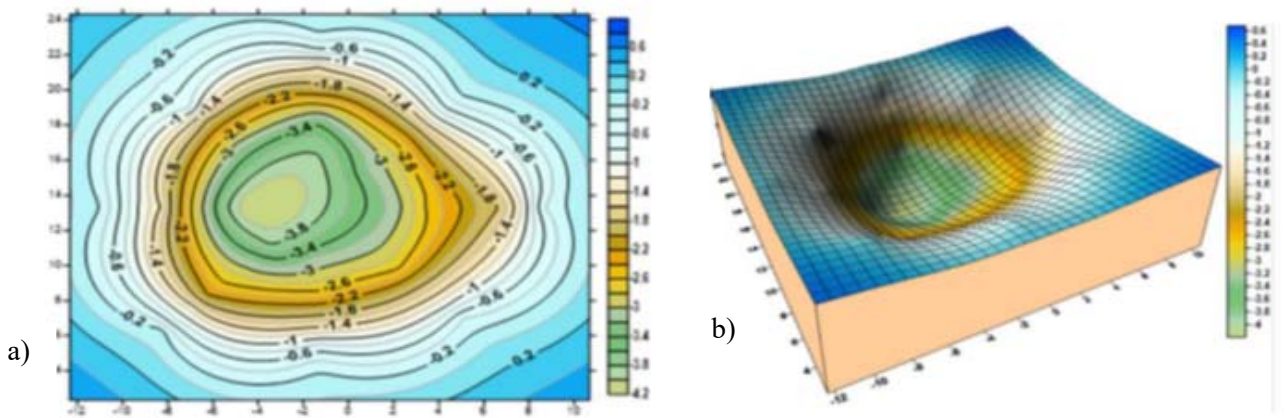


Figure 12: Scour Hole around Pier with flexible vegetation at 6D a) contour map and b) 3D geometry.



## 5 Conclusion

According to this study, the following findings can be drawn:

1. The scouring depth increases with increasing Froude Number in clear water.
2. When the distance between the pier and vegetation was as close as possible, the scouring around the pier decreased the most.
3. When there is a minimum distance between a floating pier and flexible vegetation, scouring around the pier is reduced by 43.79.0 percent. Vegetation that is more adaptable at distances of four and six dimensions reduces scouring by 38.11% and 34.15%, respectively. Scouring is reduced by 33.44%, 31.92%, and 27.38% at 0, 4, and 6 degrees.
4. When the distance between the pier and the flexible vegetation is at its smallest or 0D, scouring around the pier decreases by up to 52%. Flexible vegetation also reduces scouring by 44.21 percent and 38.35 percent when used at 4D and 6D distances. When scouring is compared to rigidity in vegetation, flexibility in vegetation reduces it by the most, by 37.44%, 34.92%, and 32.38% for various ds/D ratios (0D, 4D, and 6D).
5. Scours and corrective measures are clearly depicted in maps generated under a variety of flow, sediment, and vegetation conditions.

## Acknowledgment

It is with sincere appreciation that we thank Prof. Dr. Naeem Ejaz and the Civil Department at UET TAXILA for all of their assistance with this study. We are grateful to the anonymous reviewers for their thorough work and thoughtful suggestions.

## References

- [1] A. L. M. A. & C. Marion, "Effect of sill spacing and sediment size grading on scouring at grade-control structures.," *Earth Surface Processes and Landforms*, vol. 983 993, p. 29(8), F. (2004)..
- [2] ". R. T. A. & C. R. T. A. & C. F. Gaudio, "Combined flow-altering countermeasures against bridge pier scour.," *Journal of Hydraulic Research*, (1), 35 43," *Journal of Hydraulic Research*, vol. 50, no. 1, pp. 35-43, (2012)., Vols. vol. 50, no. 1., pp. pp. 35-43, (2012)..
- [3] H. M. O. a. M. N. Hamidifar, "Reduction of scour using a combination of riprap and bed sill," in *Institution of Civil Engineers-Water Management*. , Thomas Telford Ltd, 2018.
- [4] ". A. L. M. A. & C. Marion, "Effect of sill spacing and sediment size grading on scouring at grade-control structures," *Earth Surface Processes and Landforms*, Vols. vol. 29, no. 8., pp. pp. 983-993, 2004..
- [5] M. & B. Ettema, "Scale effect in pier-scour experiments.,," *Journal of Hydraulic Engineering*, , Vols. Vol. 124, No.6, (1998).
- [6] ". R. T. A. & C. R. T. A. & C. F. Gaudio, "Combined flow-altering countermeasures against bridge pier scour.," " *Journal of Hydraulic Research*, (1), 35 43., Vols. vol. 50, no. 1., pp. pp. 35-43., F. (2012). .





# DESIGN OF CIVIL COMPONENTS OF MICRO HYDRO POWER PLANT: A CASE STUDY

*<sup>a</sup> Majid Khan\*, <sup>b</sup> Adil Khan, <sup>c</sup> Muhammad Shakeel, <sup>d</sup> Asad Ullah Khan*

a: Department of Civil Engineering, University of Engineering and Technology Peshawar, majidayubbi@gmail.com

b: Department of Civil Engineering, University of Engineering and Technology Peshawar, 18pwciv5027@uetpeshawar.edu.pk

c: Department of Civil Engineering, University of Engineering and Technology Peshawar, 18pwciv5186@uetpeshawar.edu.pk

d: Department of Civil Engineering, University of Engineering and Technology Peshawar, asadullahk636@gmail.com

\* Corresponding author: Email ID: majidayubbi@gmail.com

**Abstract-** Northern areas of Pakistan are endowed with vast hydropower generation potential. Many micro-hydropower plants (MHPP) working in private and public sectors are without proper engineering design. The proposed project has been designed on a stream in the peochar valley, Swat, Pakistan. The stream is having enough discharge and most importantly adequate head that can be easily available to generate electricity. The flow data of the stream was collected from SRSP's office. For suitable positioning of civil components of the hydropower plant, a survey has been made to mark proper points. Such point was marked which had a large head because greater the head, the more is the capacity of the plant. A favorable point on the stream was selected where diversion works were designed to divert a part of water from stream to a canal. Canal conveys water to the settling basin and forebay. Through the penstock, water strikes the blade of turbine and generate electricity. The net head obtained at the site is 76ft. The designed discharge was determined to be 10 cusec. After determining these parameters, the design of civil components was undertaken. The approach channel dimensions were designed to be 2.5 ft × 2.24 ft. Settling basin forebay were designed according to the design discharge. This plant was designed to have a power generation capacity up to 40 kW.

**Keywords-** Micro-hydro power plant, Hydropower generation, Stream water flow, Green Energy

## 1 Introduction

There is a very rapid depletion of non-renewable resources for generating electricity and the electricity demand is increasing due to the growing population and the desire for standard living. According to an estimation, presently more than 1.5 billion people are deprived of access to electricity throughout the world [1]. Pakistan is also facing multifaceted challenges in the power sector and almost 50 million people are having no access to the electric grid [2]. Alternatively, harnessing water, tidal and solar energy can overcome the power shortages and to meet the electricity. Subsequently, MHPP is considered one of the desirable sources for power generation because of its environment-friendly nature and extensive potential available throughout the world [3]

The energy of the moving water is used for the generation of hydropower. The energy production from moving water dates back to ancient Greek times. Ancient Greek used to grind wheat into flour by rotating wheels through moving water. The water wheel is placed in a stream that picks up the moving water in buckets. The kinetic energy of the flowing water turns the wheel and is converted into mechanical energy that grinds the wheat into flour. In the late 19<sup>th</sup> century, a tremendous development had been made to generate electricity from hydropower. Many MHPP working in private and public sectors are without proper engineering design. In the present study, the work has been carried out to propose and design MHPP on a stream in the peochar valley, Swat, Pakistan. The stream is having enough discharge and most importantly, sufficient



head that can be easily used to generate electricity for the local people. The flow data of the stream was collected from SRSP's office.

## 2 Design Methodology

Design methodology deals with the numerical background related to design of the micro hydro power plant. It involves the identification of some basic equations and relation to be used for the project. In the present work, two types of design methodology are involved: 1) Hydraulic design and 2) structure design.

### 2.1 Hydraulic design of civil components of MHPP

#### 2.1.1 Weir and intake structure

A side intake is normally located at the bank of diversion works and consists of an opening called orifice through which water is entered and drawn to the downstream approach channel. The majority of small hydropower schemes are of the run-of-river kind, where water used for the power generation is brought back to the river at tail-race (downstream). Also, in run-of-river hydropower project electricity is generated from discharges larger than the minimum required to operate the turbine.

##### 2.1.1.1 Design of orifice for side intake

The typical section through weir and section through submerged orifice is illustrated in Figure 1. The discharge through orifice of an intake when in submerged condition can be calculated as;

$$Q=A \times V=A \times C \sqrt{2g(H_r-H_h)} \quad (1)$$

Where; Q= discharge (m<sup>3</sup>/sec), V= velocity (m/sec), C= coefficient of discharge of the orifice

$H_r - H_h$ =Difference between the river and the headrace canal water level

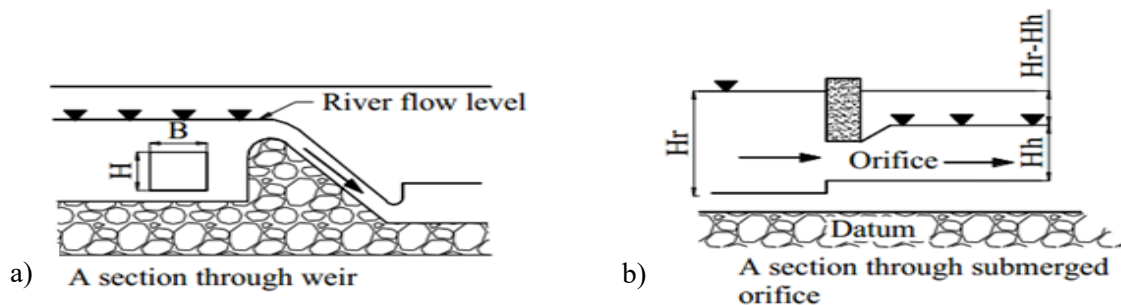


Figure 1: a. A section through weir, b. A section through submerged orifice

The size of slope and cross-section of an approach channel should be designed in such a way that the required turbine discharge (design discharge) can be economically traveled to the head tank (fore-bay). Generally, the size of cross-section and slope are interrelated. During the designing of a channel, the slope should be not higher to prevent more head loss. This gentler slope will produce low velocity and ultimately result in greater cross-section. On contrary, when the slope is steep, the velocity will be higher and resulting in smaller cross-section but the head loss, in this case, will be more. The cross-sectional shape of canal is decided according to the site conditions and stability. It may be rectangular, trapezoidal or some other possible shape. By using Manning's equation find the depth and width of the channel.

$$Q = \frac{1.49 \times A \times R^{2/3}}{n} \quad (2)$$



Here, the channel is rectangular, so:

$$\frac{Q \times n}{1.49 \times \sqrt{S}} = \frac{A^{5/3}}{49.49} = 1.26 H^{8/3} \quad (3)$$

The equation (3) provided the height of approach channel. Provided with height, calculating the width and Cross-sectional area of the channel by  $W = 2H$  and  $A = W \times H$  respectively.

When the flow is diverted from stream or river, there are some suspended particles. The settling basin is used to settle down these suspended particles. Settling basin has two portions: the first portion is called sand trap which settles down smaller size particles and the second portion is called gravel trap which settles down larger particles. There are different components of settling basin like, inlet zone, settling zone and outlet zone as shown in Figure 2.

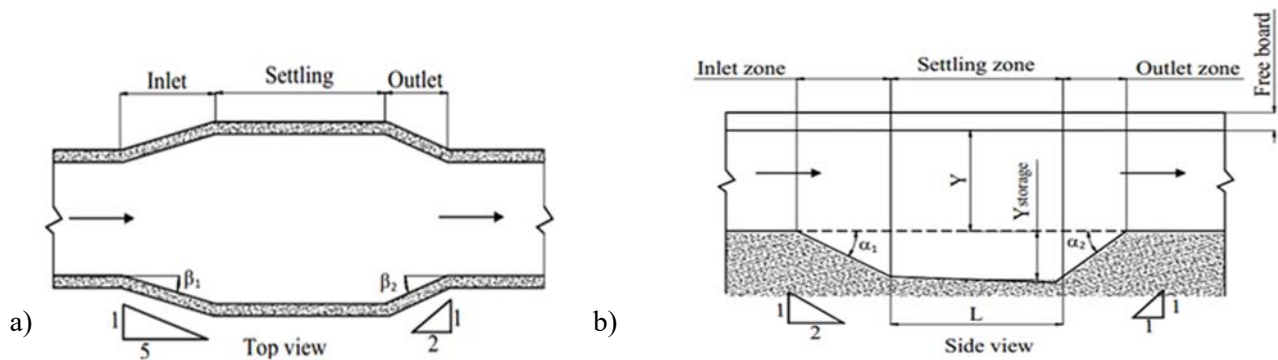


Figure 2: a. Top view of settling basin, b. Side view of settling basin

$$L_s = \frac{2 \times Q}{(W_s \times V_v)} \quad (4)$$

Where,  $Q$  = design flow in  $m^3/s$ ,  $W_s$  = Basin width

$V_v$  = fall velocity, taken as 0.03m/s for the value for 0.3mm particles.

$$D_c = \frac{V O_s}{(L_s \times W_s)} \quad (5)$$

Where,  $D_c$  = average collection depth,  $V O_s$  = volume of silt stored in the basin in  $m^3$  and  $L_s$  = Basin length

#### 2.1.4 Design of fore-bay

Structurally, the fore bay and settling basin are same but in forebay, outlet transition is replaced with a trash rack. The typical fore bay for MHPP is shown Figure 3. The recommended size for forebay should be such that a person can go inside for cleaning and at least once a year to repair.

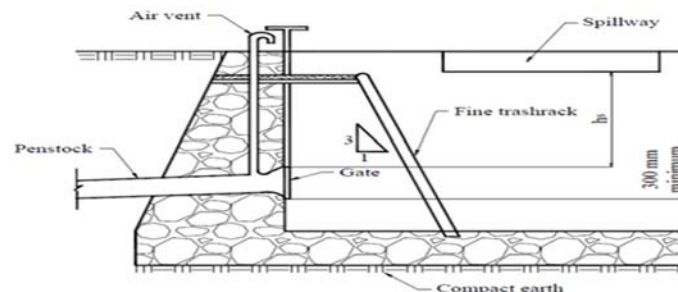


Figure 03: Typical Fore bay in MHPP



It has been recommended that the minimum submergence head for a penstock should be calculated as below:

$$h_s \geq \frac{v^2}{2g} \quad (6)$$

For the design of the weir and approach channel, different moments are calculated and sliding and overturning stability checks are applied to check the stability. For the structural design of the settling basin, determine the dimension (length, width and height) of the tank from hydraulic design. The tank should be designed according to the situation (whether the length to width ratio is more or less than 2), so in this case it is more than 2. Thus, assuming the long wall is a cantilever and the short wall to act like a beam with both ends fixed. In the present study the shape of the tank is rectangular. The tank that is resting on ground the slab, the slab should be designed in such a way that it can safely transfer water weight and the structure self-weight to the ground. Normally, the floor slab thickness ranges from 150 mm to 250 mm with a minimum of 3% reinforcement.

### 3 Results and discussion

#### 3.1 Hydraulic Design

##### 3.1.1 Intake structure

The intake structure dimensions and flow characteristics are determined and summarized in Table 1.

Table 1: Intake structure Hydraulic Design

Intake structure					
Discharge (Q)	Velocity of Water Through Orifice (V)	Area of Orifice (Q/V)	Height of Orifice (H)	Width of Orifice (W)	Depth of Weir (D)
10 cusecs	4.815 ft/sec	2.068 ft <sup>2</sup>	0.75 ft	2.77 ft	2.75 ft

##### 3.1.2 Approach channel

In the present study, the channel is a rectangular channel and the slope is found out from the site topography. Approach channel design values have been summarized in Table 02.

Table 2: Approach channel Hydraulic design

Approach Channel							
Discharge (Q)	Slope (S)	Max Velocity (V <sub>max</sub> )	Height (H)	Width (W)	Area (A)	Actual Velocity (V)	Depth of Approach Channel
10 cusecs	1/500	4.92 ft/sec	1.24 ft	2.48 ft	3.09 ft <sup>2</sup>	3.23 ft/sec	2.24 ft



### 3.1.3 Design of settling Basin

According to [4] the thumb rule for the width of the settling basin is 2 to 5 times the width of the approach channel. Assume the width of the settling basin will be two times the width of the channel. All others dimensions of settling basin have been calculated and summarized in Table 03.

Table 3: Hydraulic Design of settling Basin

Design of settling basin							
Discharge (Q)	Width of Settling Basin (Ws)	Settling Velocity of Particles (Vv)	Settling Basin Length (Ls)	Silt Load (S <sub>l</sub> )	Silt Density (S <sub>d</sub> )	Volume of Silt (V <sub>O<sub>s</sub></sub> )	Collection Depth required for settling basin (D <sub>c</sub> )
10 cusecs	4.94 ft	0.197 ft/s	16.2 ft	12096 kg	73.68 kg/ft <sup>3</sup>	328.34 ft <sup>3</sup>	4.1 ft

### 3.1.4 Design of Forebay

The hydraulic analysis provided the dimensions for the forebay which is shown in Table 04. The minimum submergence head required for the penstock is done in accordance with the standard [5].

Table 4: Hydraulic Design of forebay

Design of forebay									
Discharge (Q)	Storage Capacity of Fore-bay	Volume (V)	Length (L)	Width (W)	Actual Depth	Velocity in Penstock	Min head in Fore-bay Req above crown (h <sub>s</sub> )	Storage Depth (d <sub>b</sub> )	Min Depth (h <sub>s</sub> + d <sub>b</sub> )
10 cusec	60 sec	600 ft <sup>3</sup>	16.1ft	4.94 ft	7.5 ft	9.8 ft/sec	2.25 ft	1 ft	3.25 ft

## 3.2 Structure Design

All the structural components of MHPP have been designed in accordance with the standard.

### 3.2.1 Structure design of Approach channel

Multiple checks and standards applied to the check the stability of retaining the wall, designed for approaching the channel and the designed values are provided in Table 05. The retaining wall's structure dimension has been provided in Table 06.



Table 5: Approach channel structure design

Approach Channel							
Discharge (Q)	Slope (S)	Max Velocity (V <sub>max</sub> )	Height (H)	Width (W)	Area (A)	Actual Velocity (V)	Depth of Approach Channel
10 cusec	1/500	4.92 ft/sec	1.24 ft	2.48 ft	3.09 ft <sup>2</sup>	3.23 ft/sec	2.24 ft

Table 6: Retaining wall of approach channel

Structure Design Walls of approach channel				
Top Width of Retaining Wall	Bottom Width of Retaining Wall	Height of Retaining Wall	Unit Weight of PCC ( $\gamma_c$ )	Unit of Water ( $\gamma_w$ )
0.75 ft	1.5 ft.	2.24 ft.	150 lb/ft <sup>3</sup>	62.4 lb/ft <sup>3</sup>

### 3.2.2 Structure design of forebay and settling basin

The reinforcement details for the design of settling basin and forebay is mentioned in Table 07.

Table 7: Structure design of settling basin and forebay

Structure design of settling basin and forebay				
Design of long wall		Design of short wall	Design of base slab for settling basin and forebay	
Thickness of the Wall (d)	Vertical & Horizontal Reinforcement	Vertical & Horizontal Reinforcement	Thickness of the Slab	Reinforcement in Both Directions (Mesh)
12 inches	#4 bar @ 9in c/c	#4 bar @ 9in c/c	6 inches	#4 bar @ 9in c/c

## 4 Conclusion

In this study, the design of different components of Peochar MHPP is done by using standard rule and procedure. The different components include; the intake structure, approach channel, settling basin and forebay are designed. From the



hydraulic design the sizes of these components are determined. The results obtained from the redesign are more economical as compared to the existing MHPP at the site. MHPP will tremendously improve the socio-economic life in northern regions of Pakistan. This will ultimately reduce the wood cutting issue which northern people are using for energy consumption, particularly in the winter season. This will result in discouraging deforestation and ultimately preserve the ecosystem.

## 5 Recommendations

The following recommendations have been suggested in these studies:

- The proposed project in the present studies, is economically viable and it can be attractive for private investors. Therefore, the government of KPK should invite and encourage the private sector to take up this project for implementation.
- A single turbine unit has been proposed. In future, a design scheme having two smaller turbine units equivalent in capacity to a single unit could be worked out. This would be beneficial in a way that during lower flows a single turbine unit would be operational while during full design flow both the units will be working.
- In the proposed scheme, economic analysis is done by doing an economic comparison between the proposed MHPP and an equivalent capacity thermal power plant. Another way of doing this economic analysis is through Long Run Marginal Cost Method (LRMC). An economic study based on LRMC could be done in the future.

## References

- [1] K. Sørnes, "Small-scale Water Current Turbines for River Application," p. 24, 2010.
- [2] F. Z. Hussain Samad, "Electrification and Household Welfare evidence from Pakistan," *South Asia Region Office of chief economist*, 2018.
- [3] A. Wube, "Design and Analysis of Small Hydro Power for Rural Electrification," vol. 16, no. 6, 2016.
- [4] BINOD PANDEY 2011, "design of micro hydro power plant"
- [5] Anil Kunwar, 2012, Bachelor degree Thesis on "Technical Specifications of Micro Hydropower System Design".



# ANALYZING THE LAND-USE IMPACT ON FLOOD REGIME IN SOAN BASIN

<sup>a</sup> Usama Nazar\*, <sup>b</sup> Muhammad Shahid, <sup>c</sup> Hamza F Gabriel

a: SCHOOL OF CIVIL AND ENVIRONMENTAL ENGINEERING, NICE, NUST H-12 Campus, usama.mcs21@gmail.com

b: SCHOOL OF CIVIL AND ENVIRONMENTAL ENGINEERING, NICE, NUST H-12 Campus, m.shahid@nice.nust.edu.pk

c: SCHOOL OF CIVIL AND ENVIRONMENTAL ENGINEERING, NICE, NUST H-12 Campus, hamza.gabriel@nice.nust.edu.pk

**Abstract-** Increase in population results in rapid urbanization. As a result, imperviousness increases, infiltration decreases, runoff discharge, and flood peak rise. Different patterns of urbanization and understanding its impact on flood responses are getting the attention of researchers. This study focuses on the changing urbanization impact on the flood peak of the Soan basin (SRB) using HEC-HMS v. 4.9 (Hydrologic Engineering Center - Hydrologic Modeling System). The input variables for the HEC HMS model were estimated using the Digital elevation model, Land use/ Land cover maps, and Soil and rainfall data. The urbanization trend has been increasing in the 20<sup>th</sup> century and the Soan river basin (SRB) has been experiencing an expansion from 3% to 17% from 1997 to 2020. The response to land use land cover (LULC) change on the calibrated event of 1997, simulated peak discharge for 1997 land use land cover (LULC) was 2383 m<sup>3</sup>/sec, for 2010 land use land cover (LULC) it was 2442 m<sup>3</sup>/sec and for 2020 land use land cover (LULC) LC it was 2462 m<sup>3</sup>/sec. HEC- HMS modeling shows an elevated increase in simulated peak discharges (flood flow) and runoff volume as shown in (Table 1) due to an increase in a built-up area in (SRB) between 1997 and 2020. The study showed that urbanization has a larger impact on flood peaks rather than flood volume.

**Keywords** Flood intensity, Flooding, HEC-HMS, HEC Geo-HMS

## 1. INTRODUCTION:

Due to the rise in imperviousness, sudden changes in land use in emerging economies and an increase in extreme rainfall events may be significantly raising the danger of flooding, especially in metropolitan areas [1]. Extreme storm occurrences that cause urban floods are of great interest to several scholars worldwide. The likelihood of severe rainfall occurrences rises as the world's temperature rises. The changing patterns of rainfall events demonstrate the need for flood modeling. Changes in land use land cover (LULC) have a significant effect on the watershed ecosystem, economic activity, and hydrological processes. In addition to environmental vulnerabilities, land use land cover (LULC) shifts are important drivers of environmental change on a global scale, with potential negative effects on human well-being and way of life [2]. Land-use changes within a basin have a wide range of temporal and spatial effects on hydrological processes. It may have an effect on hydrological processes including interception, infiltration, evaporation, and an increase in runoff.

The rapid increase in the built-up area has adverse effects on the hydrological, it increases perviousness as a result increases surface runoff, and decreases groundwater flow, and lag time. The changes in land use with climate change have negative impacts not just on environments but on urban infrastructure in South Asia's tropical region [1]. On -average, metropolitan basins lose 90% of their storm precipitation to surface flow, while nonurban, wooded basins retain 25% of their rainwater. It is well known that increased impervious surface areas contribute to the effects of urbanization on hydrological processes [3].

The identification of appropriate techniques to analyze the influence of land-use change on storm runoff generation remains a critical issue. In various case studies, land-use patterns and rainfall events were inputs to an event-based hydrological model to evaluate the basin's hydrological responses to actual or expected precipitation events. These strategies have





provided a warning of the likelihood or severity of future hydrologic reactions. Few methodologies exist for estimating peak discharges from projected land use patterns [4].

HEC-HMS describes the spatial patterns of a basin using a basin model by dividing a basin into relatively homogeneous sub-basins. The HEC-HMS system of hydrological modeling techniques aims at identifying sub-basin peak discharge hydrographs and directing flows through channels to the study outlet. In this study, the Curve Number (CN) was employed to find surface flow and peak discharges as land use distribution at the regional scale, and the curve number (CN) could be created and hydrologically validated. Similarly, Du et al., 2019 [3] in the Xiang River Basin, China, employed SCS CN to anticipate the effects of LULC change on flooding behavior caused by shifting urban patterns.

Kumar et al. 2022 [5] carried out a study on the combined effect of hydrological variations and Land use land cover change in the USRI watershed, India, and found out that due to increasing urbanization and reduction in water bodies and green cover there has been an increase in streamflow. Umukiza et al. 2021 [2] employed an event-based method to explore the effects of fast LULC change on peak discharge and flow volume and observed that peak flow/ discharge depends on the curve number (CN), which relies on the LULC scenario. If growth in built-up areas is pursued, strategic countermeasures that do not enhance the area's susceptibility must be implemented. Younis et al. 2018 used a lumped model and event-based model (HEC-HMS) and LANDSAT data to study the evaluate the impacts of LULC changes on hydrology in the upper Indus basin, including forest area, bare land, and impervious increases. The LULC change research was conducted on a small scale in the Mansehra metropolitan district (16 km<sup>2</sup>). Soil and built-up area rose from 69 percent and 8.2 percent in 2000 to 78 percent and 13.76 percent in 2010, respectively, while river flow increased by 33.61 percent from 2000 to 2010, suggesting a significant positive relationship between LULC and river discharge on a regional scale [6]. The flood response to the built-up area by utilizing the HEC HMS model was done by Emam. et. al 2016 [1]. The peak discharge based on precipitation to a 50-year return period in 2030 increased by 130%, due to land use cover and change. The aims of this research are to (1) analyze the flooding process and identify the significant land-use changes and their spatial distribution from 1980-to 2020; (2) investigate the land-use pattern changes effects on the flood regime of the Soan basin.

## 2. DATA AND METHODOLOGY:

### 2.1 Study region:

The Soan River is a significant tributary of the Indus River and a key hydrological unit of Pakistan's Potohar plateau, with its source in the Murree Mountains. The Soan River passes via the Chirah and Dhoke Pathan hydrological gauging stations before flowing into the Indus River. Both the Chirah sub-basin and the Dhoke Pathan sub-basin are located above the hydrological gauging stations at Chirah and Dhoke Pathan, respectively. The Soan basin as shown in (Figure 1) is 6842 km<sup>2</sup> in size and has an elevation range of 262 to 2264 m. The basin's slope ranges from mild to severe, and monsoon-fed streams account for virtually all of the basin's flow. Simly dam being the primary drinking water supply for Islamabad, the capital of Pakistan, receives water from the Soan River. It also serves as the Potohar plateau's primary irrigation water supply [7].

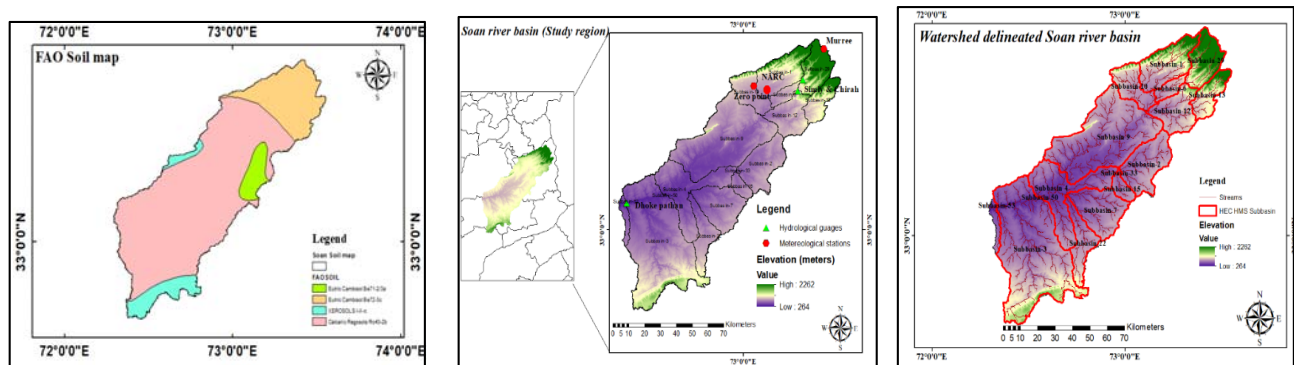


Figure 1 a) FAO soil map of study area. b) Study area map of SRB (Soan river basin) c) Delineated Soan basin



## 2.2 Data sets:

The daily precipitation data is provided by PMD (Pakistan meteorological department), WAPDA, and NARC of three gauging stations, and stream flow data at two gauging stations (Chirah and Dhoke Pathan) from 1960 to 2013 were collected. The two flood events were identified in July-1997, and July 2010, and the precipitation data and flow data have been used.

The soil types as shown in (Figure 1) were extracted from the data-sharing site of the Food and Agriculture Organization soil map. The HSG (hydrologic soil group) A, B, C, and D classifications, are used to represent high to low permeability rates when the soils are fully saturated and not have vegetation cover, and experiencing a high-intensity rainstorm

The Land Use and Land Cover data for 1997 and 2010 were extracted from a data-sharing site of glovis.org and re-classified into a water body, bare land, Vegetation land, forest, and Built-up area. The hydrologic soil group “D” covers most of the area of the Soan basin, followed by the group “C” [3].

## 2.3 Hydrological engineering center- hydrologic modeling system rainfall-runoff simulation procedure:

In contrast to fully-distributed hydrological models, HEC-HMS separates an entire basin model into homogenous sub-basins basis on the area threshold established in the model. It takes various sub-basins changing surface conditions into account. Evapotranspiration and snowmelt have not been considered in the HEC-HMS model since short-term flood events are depicted as being driven by high-intensity rainfall. To estimate the hydrological impact of LULC modifications solely, LULC maps are employed in conjunction with the precipitation data [8]. As a result, the semi-distributed model is preferable for simulating flood occurrences at a broad basin size. HEC HMS v4.9 was used in this work to predict surface runoff using different LULC maps.

HEC-HMS uses the following steps to run the simulation:

1. Basin model shows the physical characteristics of the study area.
2. Meteorological model takes rainfall data as input associated with each sub-basin.
3. Control specifications show the start and end and a time step of the simulation.
4. Time series data manager has observed discharge data and rainfall gauge data.

All of the above-mentioned models are combined to simulate by defining the following parameters:

1. *SCS-curve number- excess precipitation or runoff*: The SCS-CN (Soil Conservation Service Curve Number) is a function of total rainfall, land cover, soil characteristics, and moisture. CN value ranges from 30 for permeable soil to 100 for water bodies, being the most important parameter CN value is used to represent the urbanization level. CN (Curve number) grid was created to extract individual curve numbers for each sub-basin, using the LULC maps and FAO soil maps in conjunction with the HEC-Geo HMS extension of Arc Map and using the CN lookup table, provided by the SCS report [9] and Juan Du. et.al 2019 [3] in Xiang River Basin, China.
2. *SCS-UH (Soil Conservation Service Unit Hydrograph)*: SCS unit hydrograph was used to calculate the direct runoff, the average UH resulting from runoff, and rainfall at gauges in agriculture basins.
3. *Baseflow method*: The Recession Model is used as a tool to explain the drainage processes from natural retention in basins. The river depth where additional runoff accumulates is defined by the baseflow parameter in flood studies.

## Results:

### 3.1 Land-use land-cover change analysis:

Supervised classification of LANDSAT images of 1997, and 2010 (Figure 2) and applied algorithm of maximum likelihood. The images were classified into; Waterbody, Bare-land, Forest, Vegetation, and Settlements. LULC analysis was carried out by estimating the areas of LULC in 1997, and comparing them to the areas of land cover in 2010 and 2020 as shown in (Figure 3). As of 1997 the bare land covered most of the Soan river basin, forest, and vegetative land covered



25%, Built-up area covered 3% and water body covered approx. 1% of the total Soan basin. In the year 2010, vegetative and bare land covered most of the area by 39%, and 38% respectively, with 13% of the area as forest and built-up area covered 9% and water bodies covered approx. 1% of the total Soan basin. In 2020, 55% of vegetative land covered most of the area of the Soan Basin, the built-up area has slightly increased to 17% of the total area, and forest and bare land covered 14% and 13% of the total Soan river basin area.

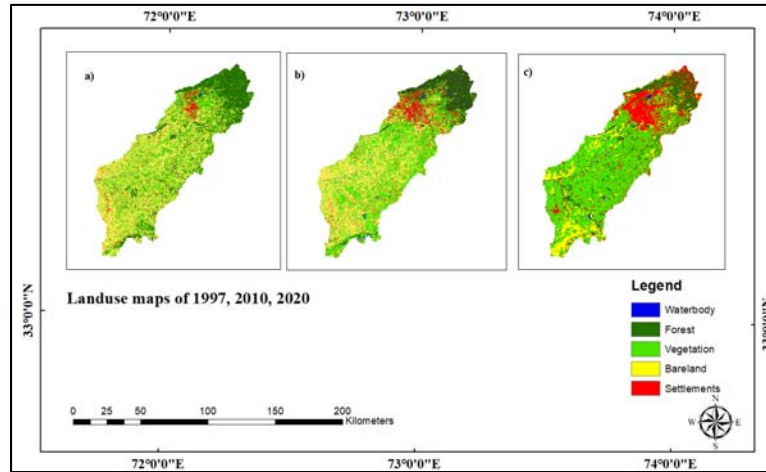


Figure 2 Land use maps a) 1997 b) 2010 c) 2020

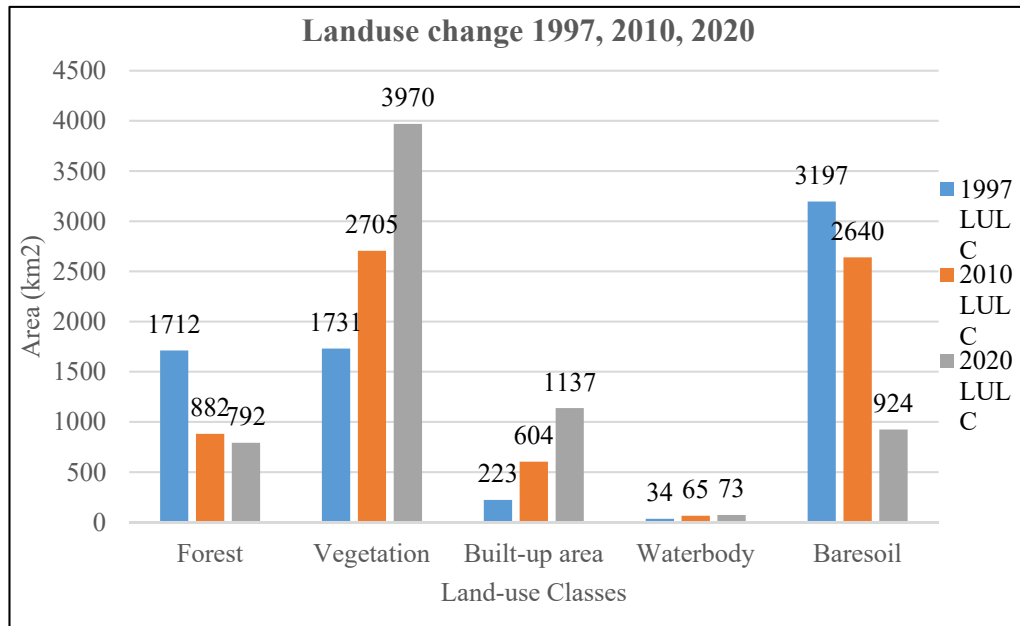


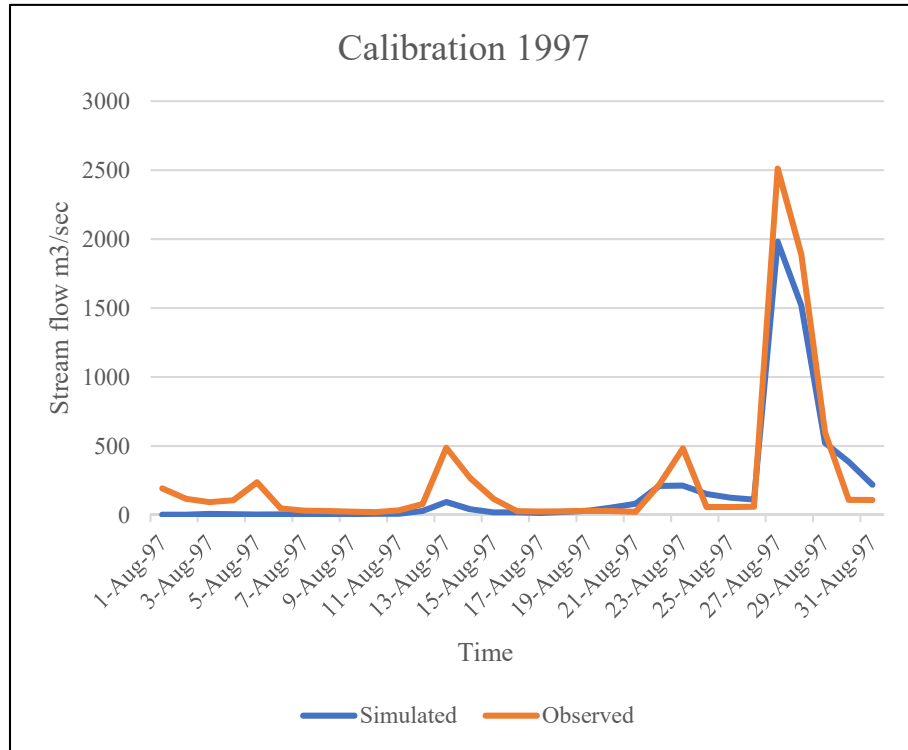
Figure 3 LULC comparisons (1997, 2010, 2020)

### 3.2 Impact of land use/land cover change on peak flood flows:

The rainfall-runoff is the result of a combination of climatic and topographical conditions. The HEC HMS model was calibrated for the event of July 1997 (Figure 4) and validated for the event of 2010 as shown in (Figure 5). The calibrated HEC HMS model for the 1997 event is used to simulate the flood responses to different LULC conditions (Curve number and impervious percent) of 1997, 2010, and 2020 as shown in (Figure 6).



Split sample methodology and streamflow observation data gathered at the watershed's outlet were used in the calibration and validation of the HEC-HMS model.



NSE: 0.886  
R<sup>2</sup>: 0.94  
RMSE: 0.3

NSE: 0.790  
R<sup>2</sup>: 0.86  
RMSE: 0.5

Figure 4 Calibration

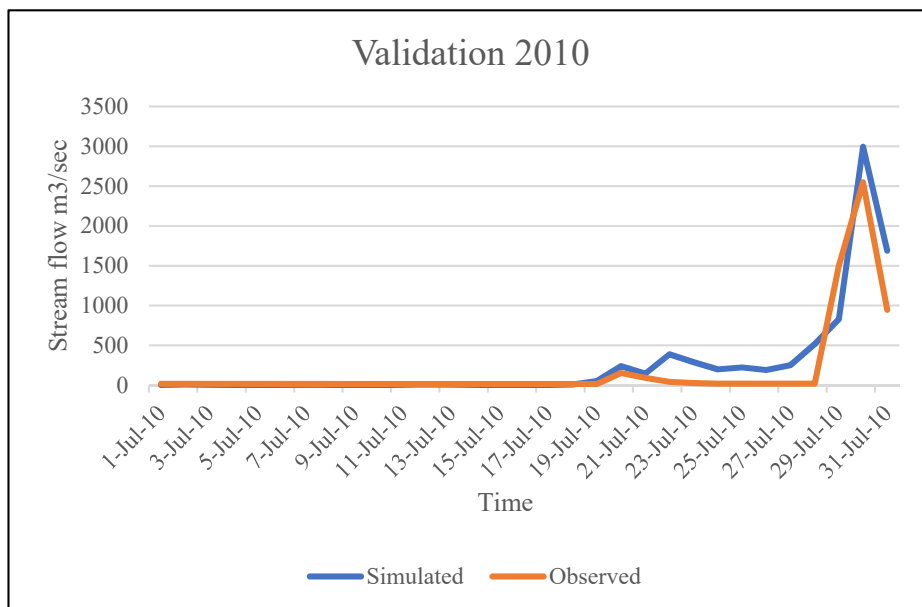


Figure 5 Validation of 2010

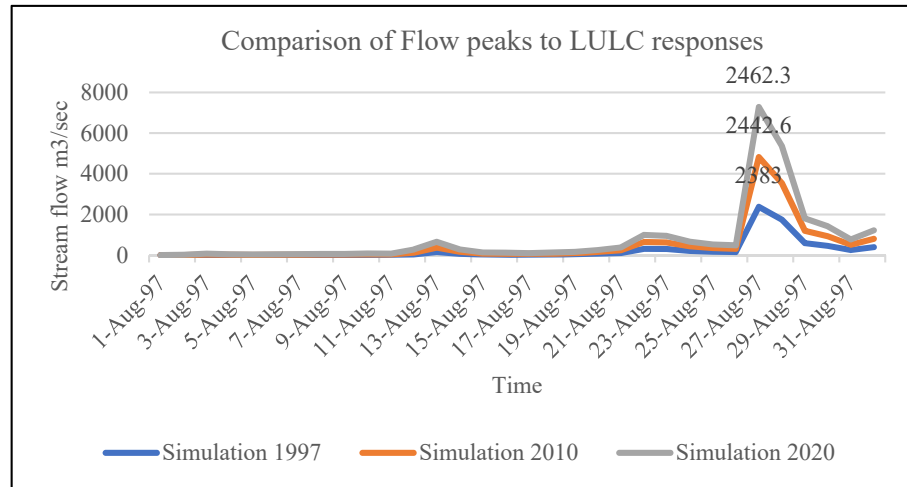


Figure 6 LULC change impact on flow peak

Table 1 Responses of the peak flood flow to the land use changes of 1997, 2010, 2020

Catchment	LULC conditions	Impervious percent	Simulated peak flow m³/sec	Increase m³/sec	Flow volume (mm)
Soan River basin	1997	3	2383	0	95.5
Soan River basin	2010	9	2442	59	102.68
Soan River basin	2020	17	2462	79	108.77

## Conclusions

The following conclusion has been drawn from this study:

1. The Land-use land cover change varied spatially such as the artificial surfaces increased from 1997 to 2020 i.e., from 3% to 17%. The significant land-use change in SRB was vegetative cover (Agriculture, grass, etc) increased from 25% in 1997 to 55% in 2020. The major urbanization or urban area expansion rate occurred at Rawalpindi and Islamabad of approximately 500 km<sup>2</sup> in 2020.
2. The peak flood flow and flood volume increased from 1997 to 2020 by 79 m<sup>3</sup>/sec and 13 mm with increasing urbanization and the flows were observed at the outlet. Soan river basin has most of the area covered by an arable or vegetative cover which is why it had little effect on the elevated peak. Acknowledgments:

## ACKNOWLEDGEMENTS:

This acknowledgment will hardly justify my sense of profound veneration for my research supervisor Dr. Muhammad Shahid, and the Head of the Department Dr. Hamza Farooq Gabriel for their indelible help, unprecedented enthusiasm, constructive criticism, and perceptive encouragement. The careful review and constructive suggestions by the anonymous reviewers are gratefully acknowledged.

## References:

- [1] A. R. Emam, B. K. Mishra, P. Kumar, Y. Masago, and K. Fukushi, "Impact assessment of climate and land-use changes on flooding behavior in the upper ciliwung river, jakarta, Indonesia," *Water (Switzerland)*, vol. 8, no. 12, 2016, doi: 10.3390/w8120559.



**4<sup>th</sup> Conference on Sustainability in Civil Engineering (CSCE'22)**  
Department of Civil Engineering  
Capital University of Science and Technology, Islamabad Pakistan



- [2] E. Umukiza, J. M. Raude, S. M. Wandera, A. Petroselli, and J. M. Gathenya, "Impacts of land use and land cover changes on peak discharge and flow volume in kakia and esambumbur sub-catchments of narok town, kenya," *Hydrology*, vol. 8, no. 2, Jun. 2021, doi: 10.3390/hydrology8020082.
- [3] J. Du, L. Cheng, Q. Zhang, Y. Yang, and W. Xu, "Different Flooding Behaviors Due to Varied Urbanization Levels within River Basin: A Case Study from the Xiang River Basin, China," *International Journal of Disaster Risk Science*, vol. 10, no. 1, pp. 89–102, Mar. 2019, doi: 10.1007/s13753-018-0195-4.
- [4] M. Ali, S. J. Khan, I. Aslam, and Z. Khan, "Simulation of the impacts of land-use change on surface runoff of Lai Nullah Basin in Islamabad, Pakistan," *Landscape and Urban Planning*, vol. 102, no. 4, pp. 271–279, Sep. 2011, doi: 10.1016/j.landurbplan.2011.05.006.
- [5] M. Kumar, D. M. Denis, A. Kundu, N. Joshi, and S. Suryavanshi, "Understanding land use/land cover and climate change impacts on hydrological components of Usri watershed, India," *Applied Water Science*, vol. 12, no. 3, Mar. 2022, doi: 10.1007/s13201-021-01547-6.
- [6] S. M. Z. Younis and A. Ammar, "Quantification of impact of changes in land use-land cover on hydrology in the upper Indus Basin, Pakistan," *Egyptian Journal of Remote Sensing and Space Science*, vol. 21, no. 3, pp. 255–263, Dec. 2018, doi: 10.1016/j.ejrs.2017.11.001.
- [7] M. Shahid, Z. Cong, and D. Zhang, "Understanding the impacts of climate change and human activities on streamflow: a case study of the Soan River basin, Pakistan," *Theoretical and Applied Climatology*, vol. 134, no. 1–2, pp. 205–219, Oct. 2018, doi: 10.1007/s00704-017-2269-4.
- [8] J. de Niel, A. Vermeir, Q. Q. Tran, S. Moustakas, and P. Willems, "Efficient approach for impact analysis of land cover changes on hydrological extremes by means of a lumped conceptual model," *Journal of Hydrology: Regional Studies*, vol. 28, Apr. 2020, doi: 10.1016/j.ejrh.2020.100666.
- [9] "SCS2000".



# EXPERIMENTAL STUDY OF BRIDGE PIERS OF DIFFERENT SHAPE SURROUNDED BY MESH WIRE TO MINIMIZE THE LOCAL SCOUR

*<sup>a</sup> Muhammad Anees\*, <sup>b</sup> Naeem Ejaz, <sup>c</sup> Muhammad Aleem, <sup>c</sup> Ghulam Abbas*

a: Department of Civil Engineering University of Engineering and Technology Taxila, [anees\\_soomro89@yahoo.com](mailto:anees_soomro89@yahoo.com)

b: Department of Civil Engineering University of Engineering and Technology Taxila, [naeem@uettaxila.edu.pk](mailto:naeem@uettaxila.edu.pk)

c: Department of Civil Engineering University of Engineering and Technology Taxila, [engr.aleem@gmail.com](mailto:engr.aleem@gmail.com)

Corresponding author: Email ID: [anees\\_soomro89@yahoo.com](mailto:anees_soomro89@yahoo.com)

**Abstract** -It is the local scour that is causing the most serious damage to the bridge. One of the most important considerations in pier design is how to minimize scouring. The experimental decrease of scouring around various kinds of bridge piers using mesh wire is investigated in this paper. There are many kinds of mesh wires that are put above the streambed level around the piers of bridges to decrease scouring. Using mesh wire to around the circular pier gave us the finest results. Compared to conventional bridge piers, scouring on the circular pier with mesh wire was reduced by up to 52% after 48 hours of testing. In comparison to square and rectangular bridge piers with mesh wire, the scouring on circular and square bridge piers was reduced by 52% each. This means that the most effective mesh wire bridge pier is a circular bridge pier.

**Keywords:** Scouring; mesh wire; Rectangular Bridge Pier; Scour Reduction, Piers

## Introduction

Small scour holes around bridge piers are inevitable in alluvial channel beds exposed to the erosive action of approaching river flows. Bridges that span alluvial channels need to be designed and built with a knowledge of the maximum scour depth that may occur near the piers over the expected lifetime of the bridge [1]. Scour depth at piers is still in its infancy because of the intricacy of the scour challenges. Floods, with their unpredictable and even counter-flowing flows, are ideal conditions for major scouring. The local flow structure, which has a high degree of volatility and vorticity, causes bed material erosion, resulting in scour, which is caused by a three-dimensional boundary-layer separation at the pier. Researchers have been studying scouring at bridge piers for some years now. Alluvial channel scour has been studied extensively, and researchers have developed a set of prediction equations to estimate the maximum scour depth at bridge piers under diverse approach flow, sediment size and gradation, and pier type and size situations. [2]. It takes time for the hydrodynamic forces in the scour hole to no longer remove particles from the pier scour hole, which is why it persists for a long period. When the scour hole achieves this equilibrium, the scour depth does not fluctuate much until the flow conditions or bed material changes. The purpose of this paper to minimize the scouring around the different shapes of bridge piers by placing the mesh wire at the bottom of piers on the bed of the ground [3]. however, the aim of this research is to investigate the scouring around the different shapes of piers using the mesh wire and compare their results in reduction of the scouring.

## Experimental Procedures

All the experiment was performed in the Water resources & Hydraulics Engineering Laboratory of Department of Civil Engineering, University of Engineering and Technology, Taxila. The channel had specifications of 20 m length, 1 m wide and 0.75 m deep glass-sided flume with an adjustable tailgate at the channel-end to regulate the flow depth used for the experimental depth. Through the centrifugal pump, discharge was supplied to the tank then inter to the main channel by



aligned honeycomb diffuser in the direction of flow for smooth and uniformly distribution of flow crosswise. At the tail of channel water enter in the sediment tank after filling and trapping the flowed sediments, the flow discharges in the main channel. Plan view of the Laboratory channel and experimental setup shown in Figure 1: Plan View of Channel A 9m long, 0.20m deep and .96m wide false bottom of uniform, medium size ( $d_{50}=0.51\text{mm}$ ) bed material and pier base was introduced, sand size considered in this study stood in compliance to the condition of  $D/d_{50} > 50$  in order to dominate the sediment size effect on the scour evolution process guaranteeing non ripple-forming sand [4]. The diameter of the pier was not more than 10% of the channel width to prevent the effect of walls on scouring [5]. therefore double square pier modelled by 0.06m dimension of wood material. The trapezoidal broad crested weir (TBCW) modelled by wood material, weir width equal to the full width of channel, crest length was 50cm, the weir was 5cm above the flat bed, the sides slopes of the TBCW was 1V:2H, which is more stable and seepage control [6] The dimension of TBCW was within the limits [7]. The mesh wire of size 0.5" X 0.5" is used in addition to the foundation which is placed at ground level of the bed to encounter the scouring.

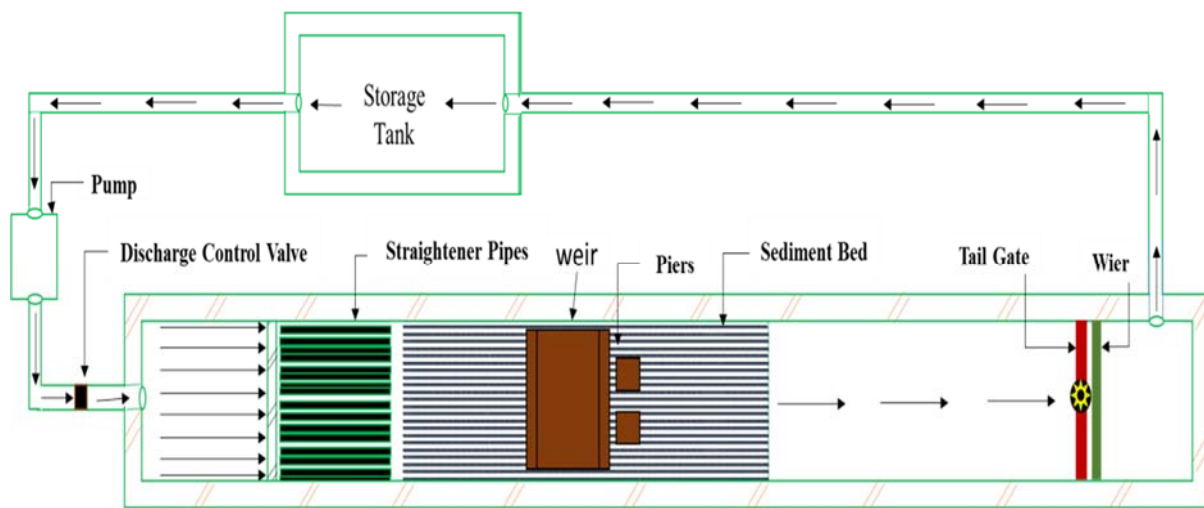


Figure 1: Plan View of Channel

## Research Methodology

- The experimental setup took place in the hydraulic lab's open channel.
- Wooden bridge piers of all shapes and sizes are used.
- Square mild steel wire mesh of size: 0.5" X 0.5" & Diameter 1.2mm is used at the bottom of bed of different shapes of bridge piers of size 6"x6" after scaling down.
- A flume is used to test the effectiveness of scouring on various pier configurations.
- Each inclined bridge pier's scour depth is recorded.
- used to determine distance and/or surface roughness

### 1.1 Equation

Clear water conditions were used for all the trials. The following equation should be used to calculate the discharge value.

$$Q = \frac{2}{3} C_{rd2} \sqrt{2g} b_2 h_2^{3/2} + \frac{2}{3} C_{rd1} \sqrt{2g} (2b_1) h_1^{3/2} + \frac{8}{15} C_{td} \sqrt{2g} \tan(\theta/2) h_{1e}^{5/2}$$

Alternately, we may say that  $b$  is the width of the weir and the angle of the notch. Discharge coefficient for rectangular sharp-crested weirs and triangular sharp-crested weirs, respectively. Weir crest water head ( $h$ ), effective head ( $h_e$ ), and gravitational acceleration ( $g$ ) are all measured in feet.





## Results

Table 1: Experimental Condition and Result

Case	Pier Shape	Q (m <sup>3</sup> /s)	T (hr)	h (m)	ys_f (cm)	ys_f/D
1	Circular Pier with mesh wire	0.020	2	0.15	6.3	0.75
2		0.029	2	0.15	6.8	0.78
3		0.038	2	0.15	7.4	0.81
4	Square Piers with mesh wire	0.020	2	0.15	4.3	0.88
5		0.029	2	0.15	5.0	0.9
6		0.038	2	0.15	5.7	0.933333
7	Rectangular piers with mesh wire	0.020	2	0.15	5.1	1.03
8		0.029	2	0.15	5.6	1.09
9		0.038	2	0.15	6.2	1.12

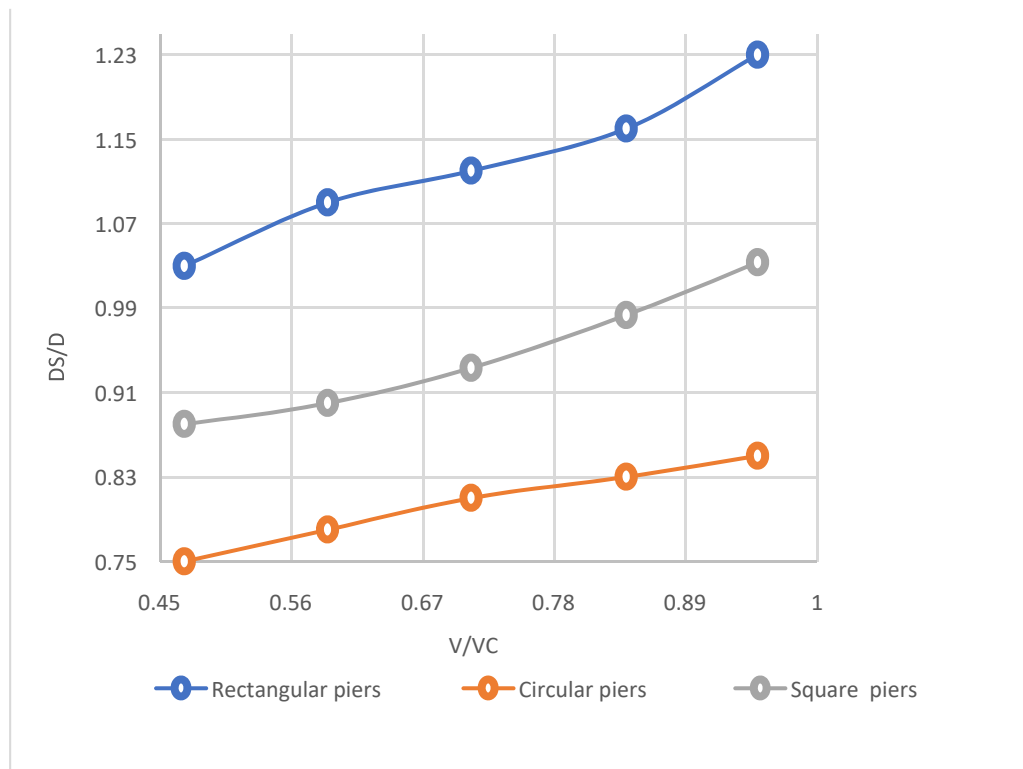


Figure 2: Relationship b/w Effective depth and effective velocity of different piers with mesh wire

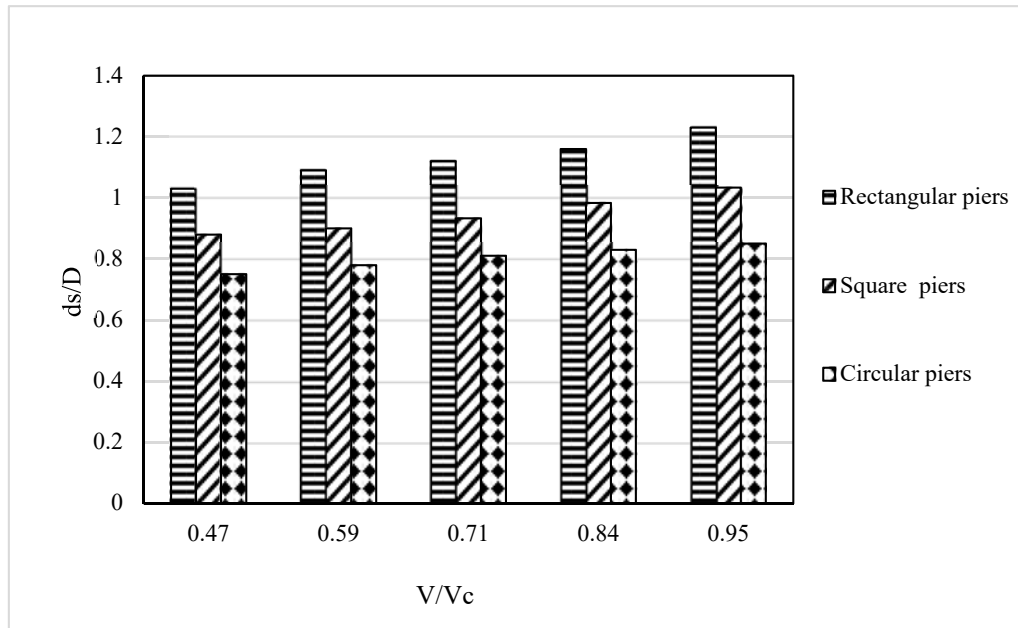


Fig 3: Scouring depth near the different shapes of Piers with mesh wire

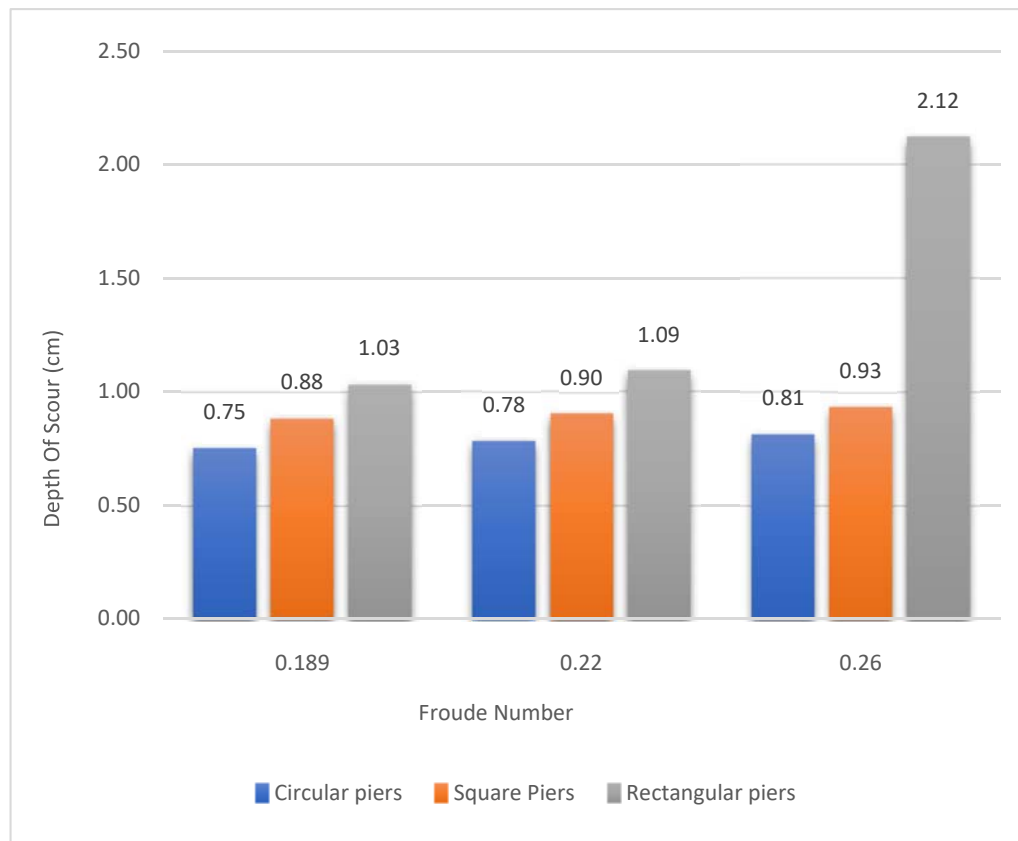


Fig 4: Relationship B/W scouring depth with Froude number using different shapes of bridge piers with mesh wire

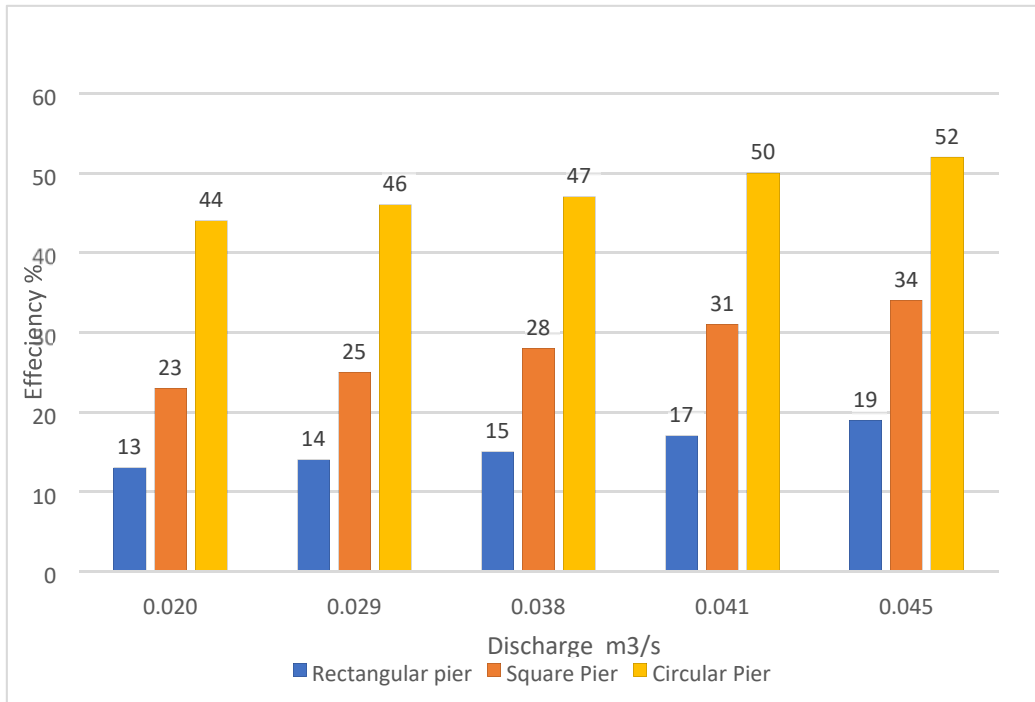


Fig5: Relation b/w efficiency % and Discharge with mesh wire

Table 1: shows the Experimental Condition and carried out in lab with different shapes of piers (Rectangular, Square, Circular) with mesh wire at the three different discharges Fig 1 and Fig 2 shows the scouring around the different shapes of piers it shows that the effective velocity increases the scouring depth around the piers increased. The scouring depth is maximum for the rectangular shapes bridge piers i.e., 1.12 and minimum for the circular shapes piers i.e., 0.75

Fig 3 Shows the relationship between the Froud number and depth of scouring of different shapes of bridge piers with mesh wire shows that as the Froud number increased the scouring depth around the bridge piers increased mean Froud number has the directly relation with Scouring depth. From this Fig 3 we noted that the Scouring depth is minimum i.e., 0.81 for circular shape pier for each Froud number and Scouring depth is maximum i.e., 2.12 for rectangular shaped pier for each Froud number. Fig 4 Shows that the percentage reduction in scouring is maximum for the circular pier with mesh wire i.e., 52% and for the square pier with mesh wire is 34% and for the rectangular pier with mesh wire is 25%. Hence the most efficient pier with mesh wire is circular pier. Scouring can be minimized by using mesh wire for circular pier.

It's far expected that the research carried out in this research will contribute to the development of opportunity substances in successfully reducing bridge pier scour. There's big ability for this subject matter to end up value effective and sustainable even as also being completely operational. It's far predicted that the varying parameters used inside the checking out will immediately make contributions to the reduction or enhancement of a scour hollow across the bridge pier. Wire mesh technique can be employed in bridge piers like the gabion wall used for protection.

## Conclusion

An open channel experiment was used to test the effectiveness of various bridge pier forms utilizing mesh wires in this study.

1. Based on the results of this experiment, the following conclusions were drawn:
2. A reduction in the scouring depth is achieved by using mesh wire around the different shaped piers.
3. Increasing the channel discharge minimized scouring using mesh wire around different-shaped bridge piers.
4. Rectangular Bridge pier with mesh wire at the bed level outperformed all other types of bridge piers, with a 52 percent efficiency rating. With the round bridge pier, the scouring is decreased by up to 52% compared to the traditional bridge-piers.



## Acknowledgment

It is with gratitude that the authors express their gratitude to all those who contributed to the study, in particular Professor Dr. Naeem Ejaz of the Civil department and Engineer Muhammad Aleem. We appreciate the anonymous reviewers' thoroughness and thoughtfulness in providing their insights.

## References

- [1] M. Ali, "Role of post-tensioned coconut-fiber ropes in mortar-free interlocking concrete construction during seismic loadings," *KSCE Journal of Civil Engineering*, vol. 22, pp. 1336-1343, 2018.
- [2] Lenzi, M. A., Marion, A., & Comiti, F. (2003). Local scouring at grade-control structures in alluvial mountain rivers. *Water Resources Research*, 39(7). <https://doi.org/10.1029/2002WR001815>
- [3] Ningombam Bishwajit Singh, Thiyam Tamphasana Devi & Bimlesh Kumar (2022) The local scour around bridge piers—a review of remedial techniques, *ISH Journal of Hydraulic Engineering*, 28:sup1, 527-540, DOI: 10.1080/09715010.2020.1752830
- [4] Marion, A., Lenzi, M. A., & Comiti, F. (2004). Effect of sill spacing and sediment size grading on scouring at grade-control structures. *Earth Surface Processes and Landforms*, 29(8), 983-993. <https://doi.org/10.1002/esp.1081>
- [5] Hamidifar, H., M.H. Omid, and M. Nasrabadi. Reduction of scour using a combination of riprap and bed sill. in *Proceedings of the Institution of Civil Engineers-Water Management*. 2018. Thomas Telford Ltd.
- [6] Abdel-Aal, G., Y. Mohamed, and E.-D.J.C.E. Waheed, O. and El-folly, M.,(2008), Local scour mitigation around bridge piles using protective plate (collar), *Scientific bulletin. Faculty of engineering. Ain Shames University. Faculty of engineering*
- [7] Zarrati, A.R., et al., Scour countermeasures for cylindrical piers using riprap and combination of collar and riprap. 2010. 25(3):p. 313-322.



# TO STUDY THE IMPACT OF FLOATING DEBRIS ON BRIDGE PIER

<sup>a</sup> Muhammad Umar Hayyat Jam\*, <sup>b</sup> Usman Ali Naeem, <sup>c</sup> Faheem Butt

a: Civil Engineering Department, University of Engineering & Technology, Taxila, [umerjam36@gmail.com](mailto:umerjam36@gmail.com)

b: Civil Engineering Department, University of Engineering & Technology, Taxila, [usman.naeem@uettaxila.edu.pk](mailto:usman.naeem@uettaxila.edu.pk)

c: Civil Engineering Department, University of Engineering & Technology, Taxila, [faheem.butt@uettaxila.edu.pk](mailto:faheem.butt@uettaxila.edu.pk)

\* Corresponding author: Email ID: [umerjam36@gmail.com](mailto:umerjam36@gmail.com)

**Abstract-** Storms and flooding caused significant damage to buildings and bridges. The waterborne debris created during such natural disasters will cause significant damage to many structures unless they were designed for these loads. Flood field survey findings suggested large objects such as wooden logs, cars, vessels, storage barrels, and other containers intensify the damage. For this cause, a driftwood approach was established to test tree washout, floating trees movement, and collisions with the pier. This paper addressed the findings of experimental analysis on the frameworks to measure the debris impact force and dynamic properties on pier. It also analyzed the formulas, which were defined with the experiment results in the recently released design guidelines (FEMA P-646, 2012). This resulted in impact force on bridge pier (different shapes of pier) with different debris mass and also vibrational characteristics (dynamic properties) of pier by using sensors. Moreover, different hydraulic jumps were observed while observing water surfaces in different situations.

**Keywords-** Experimental modeling, Flood born debris, Floods, Flow channel.

## 1 Introduction

Flooding is typically defined as a large volume of water overflowing outside of its normal parameters. Floods can cause extensive damage to structures, bridges, properties, and human life. Flooding is the accumulation of a large volume of fluid (typically water) from a nearby body of water that saturates the ground, which is normally dry all year. The most common causes of inland flooding are intense rains over a watershed, either a reservoir or a levee breach, or snow covers in northern areas rapidly melting [1, 2]. Understanding flood loads will thus contribute to the design and installation of flood-resistant buildings. The current construction and building guidelines pursued by [3] recommend specific methods for characterizing the debris effect load, but these are not well developed.

Flood waters in urban rivers caused by bridge obstructions by various floating debris can cause significant damage to local property, infrastructure, and members of the public, and such blockages have become more common in recent years [4-7]. These debris can include various types of vegetation, such as wooden logs, shrubs and trees, as well as urban material, including shopping trolleys, swept vehicles, and floating containers [4].

Bridge structural susceptibility in flood flows is commonly modelled. It is determined by the water depth and flow rate combined. Although the Guidelines are derived from historical flood data, their empirical investigation is extremely limited. The need to resolve the considerable number of major problems associated with such processes encourages the recent shift toward more established and simple deterministic risk assessment methodologies. Post-disaster findings have confirmed that vegetation helps to mitigate the negative consequences of natural disasters. A few notable ones from around the world are discussed briefly here. The density and thickness of the vegetation on the upstream side both contribute to the increase in backwater. A forest, depending on its configuration and thickness, can provide adequate resistance to a



flood force. Experimental and numerical studies of the influences of vegetation density disclosed that increasing the aspect ratio of the vegetation limits both the water level and velocity behind the vegetation. [8]. The floating debris carried by a flood can collide with buildings and bridges, causing additional damage. Not only is vegetation important, but several factors contribute to catastrophic variations in floods. The experimental findings show that, even in sparse conditions, two rows of vegetation generated more driftwood than a single row of vegetation. More driftwood develops as the aspect ratio continues to improve. Inland forest trees can resist the stress of floating debris as well as trapped debris depending on flow velocity and Froude number [9]. Tanaka and Ogino [10] thoroughly investigated the Impulse force on locally constructed bridge pier caused by the collision of water-borne floating debris. The impact of waterborne debris on bridge piers in the presence and absence of vegetation on structural buildings is investigated in this paper.

During flood events, debris makes contact with bridge piers in the flood water's path, causing an impact, hydrostatic and hydrodynamic loading on bridge pier. Floodwater debris strikes residential or other structures in the floodplain. The above implications slow down the debris and apply force to the bridge pier. The intensity of the force can indeed be large enough to cause significant, if not disastrous, structural damage. The aim of this study is to evaluate impact forces on bridge pier due to floating debris depending on mass and velocity of prototype floating woody debris by experimental procedure as well as numerical analysis.

## 2 Experimental Procedures

### 2.1 Forces On Bridge Pier Due To Flood Born Debris.

The structural fragility of bridge pier is determined by both demand (loading) and structural sustainability (capability). This study focuses on the structural loading caused by the flood. During catastrophic disasters, the advancement of floodplains in high-risk areas can be subject to a variety of forces, including impact forces.

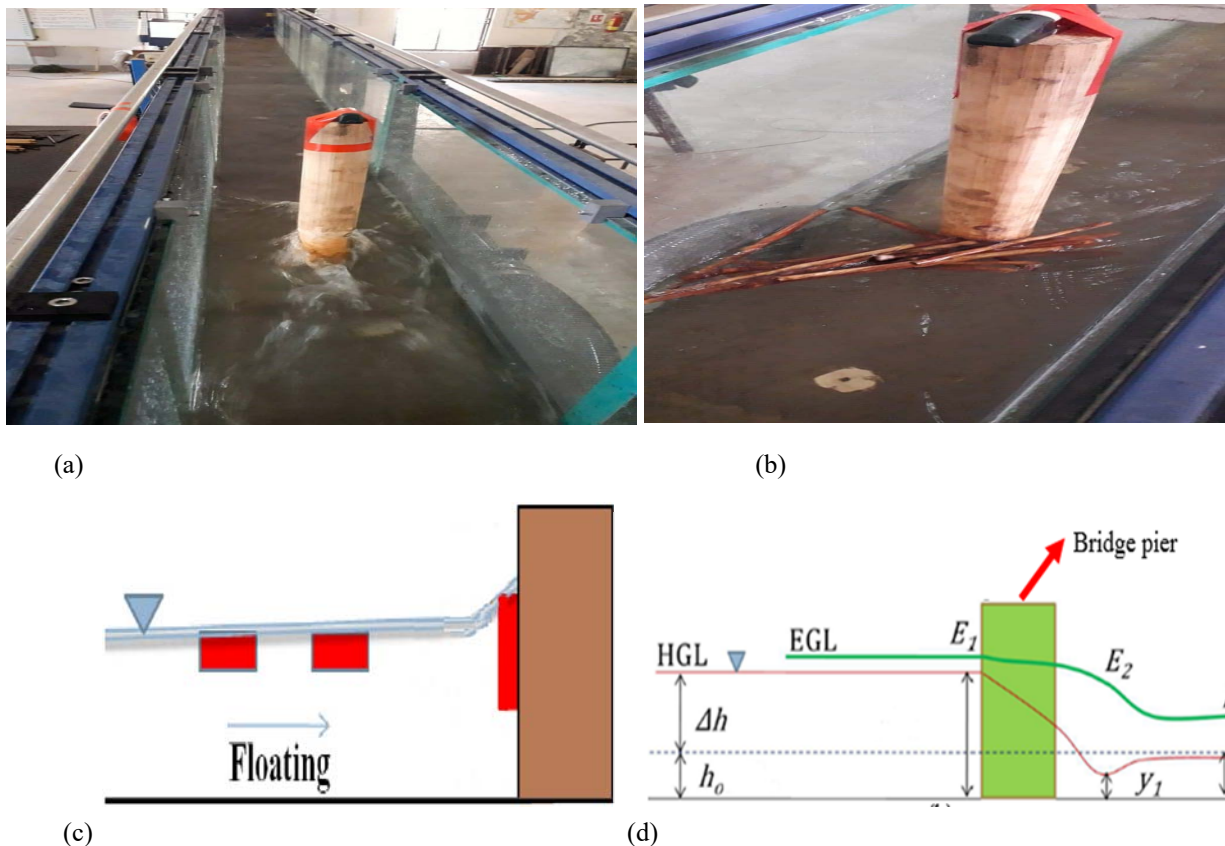


Figure 1: Schematic view of (a) flow channel with pier (b) Debris impact with pier (c-d) Flow behavior and difference of different parameters in the presence of floating debris with bridge pier



## 2.2 Impact force

FEMA P-55(2011) suggested an equation to determine impact force which is

$$F_i = WVC_D C_{str} C_B \quad (1)$$

Wherein  $F_i$  is the impact force,  $W$  is the debris weight,  $V$  is the debris velocity,  $C_D$ ,  $C_{str}$  and  $C_B$  are the depth, building structure, and blockage coefficients, respectively. Based on the flow depth the depth and blocking coefficients range from 0-1. Meanwhile,  $C_{str}$  is based on the form of structure, the direction, the natural phase, and the period of the impact. The coefficients in Eq.1 are obtained from laboratory results as well as engineering conclusions.

The FEMA P-646 (2012) [7] introduced the formula to determine debris impact forces that differed from the previous version, and the following is:

$$F_i = 1.3 u_{max} \sqrt{km_d(1+c)} \quad (2)$$

For which,  $u_{max}$  refers to the maximum velocity of flow close to the structure. The velocity of the moving debris is believed to be equal to the velocity of flowing water.  $k$ ,  $m_d$ ,  $c$  refers to the combined rigidity of the impacted structures, the mass of the debris, and the hydrodynamic mass coefficient respectively. As per FEMA P-646 [11] for wooden debris, for debris that flows parallel to the flow direction,  $c = 0$ , for debris with a transverse orientation towards flow direction  $c = 1$ , Whereas for debris such as 20-ft and 40-ft cargo ships,  $c = 3$  and  $c = 2$  respectively.

## 2.3 Hydrostatic force.

The horizontal hydrostatic force is extracted from the change in water level on wall upstream and downstream sides. It is given per unit length by:

Where  $\rho$  and  $g$  are the density of water and the gravitational acceleration respectively while as  $h_{us}$  and  $h_{ds}$  are referred to as depth of water upstream and downstream of the wall.

## 2.4 Hydrodynamic Force.

Hydrodynamic force is resulted from a composite of inertia and drag, while as it depends on both kinematics and dynamics of the flow and characteristics of structure respectively. The following concise expression is, in general, followed for the Hydrodynamic force per unit length is.

$$F = C_d \cdot \rho \cdot g \cdot h \cdot u^2 \quad (3)$$

Where  $C_d$  is the drag coefficient,  $h$  and  $u$  are the depth of water near wall and velocity component orthogonal to the object respectively.

## 3 Research Methodology

In a glass-sided water flume (constant bed slope 1/500) that is 10 m long, 0.30 m wide, and 0.34 m high at the University of Engineering and Technology Taxila, laboratory tests were performed under various conditions. The schematic figure of the water channel is shown in Fig.1 (c-d). A small scale (1/45) of a bridge pier was designed to test the relationship of the bore structure and the effect of debris on the structure. This bridge pier has a height of 0.55 m, a width of 0.03 m, and a length of 0.10 m and provided an equal building height of 675 cm, a length of 457 cm, and a real building width of 457 cm. As per the horizontal impact of debris, Eq.2 was used to measure the impact forces on the bridge pier. A high-speed digital camera was used to monitor the behavior of the structure model and the velocity, direction, and effect of debris flow with the bridge pier. To study the change of vibrational characteristics (dynamic properties) of bridge pier by using sensors.

Different pieces of wooden planks collide in the staggered arrangement shown in Fig. 1(b) each with various sizes, diameter, and weights, was used to measure the effect caused by the wood debris. Moreover, the wooden pier model in the open channel is shown in Fig.1 (a). The debris weight was then selected to fit target weights of 0.42 g, 0.43 g, 0.48 g, and 0.49 g to reflect the debris scale of 1/45. The complete detail of debris used in the present experimental work is given in shown in Fig.1 (d) and table 2.



Table 2: Debris used in the present work are;

Debris Type	Length (mm)	Diameter (mm)	Weight (gm)
D1	97	12.65	14.3
D2	153	18.2	17.6
D3	266	19.34	18.24
D4	255	18.7	29.55

## 4 Results

### 4.1 Debris Impact Forces.

Fig. 2 represents the experimentally derived values on the composition of the debris. They were determined using the formulas given in the design guidelines. FEMA P-646 (Eq. 2) is to investigate the impact force (Fig.2) of all debris given in table 2. The Forces displayed in Fig. 2 are based on the velocity of the debris that is measured experimentally. For wooden log debris, FEMA P-646 [11] suggested  $C=1$  and  $k=2.4 \times 10^6$ .

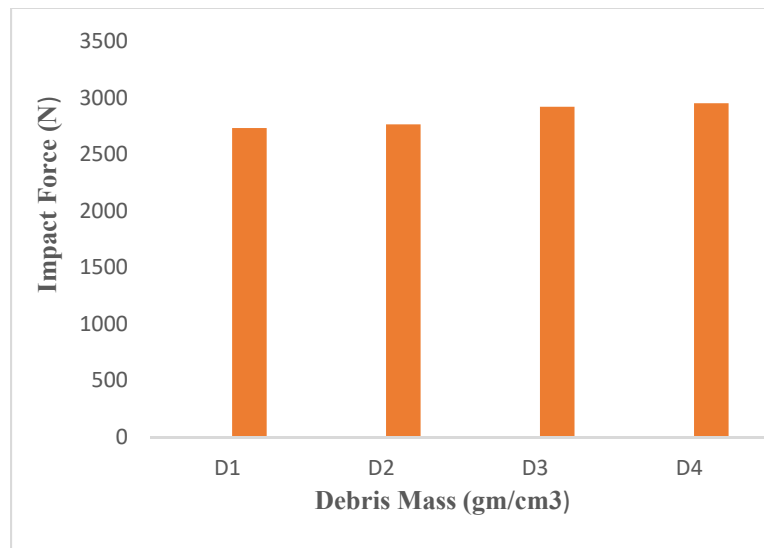


Figure 2: Impact force of different debris mass on bridge pier

The impact force was related directly to the mass of debris, as shown in Fig. 2. The highest value of impact force was noticed for D4, while the lowest value was noted for D1. Similarly, in terms of impact force, which is dependent on  $u/s$  and  $d/s$  water head, D3 had the highest value due to its longer length (26.6 cm) when compared to other debris (D1, D2, and D4). D2 debris had a lower value due to its shorter length (9.7 cm) and lower diameter value (1 cm). The lower hydrodynamic magnitude reflected the lower values of water accumulation upstream of the pier. Because the dynamic force was affected by flow velocity, the D2 type of debris had the highest value in comparison to the D3 type of debris, which had the lowest value. Because the flow velocity and debris velocity were the same, the experiment confirmed that higher flow depth due to longer length reflected the lower velocity shown in Fig. 2.





## 4.2 Use of Software.

There are number of softwares available which can mimic the process involved in research work and can produce the possible results. One of such type of software is MATLAB. The data of vibrations of piers was collected by using sensor, when debris of different masses collided with piers of different shapes. The vibrational characteristics (dynamic properties) of bridge pier was obtained by using MATLAB software and it eased the process of paper writing.

As by adopting the above practices all dynamic properties of bridge pier of a research paper can be written and together compiled to form complete research ready for Peer review.

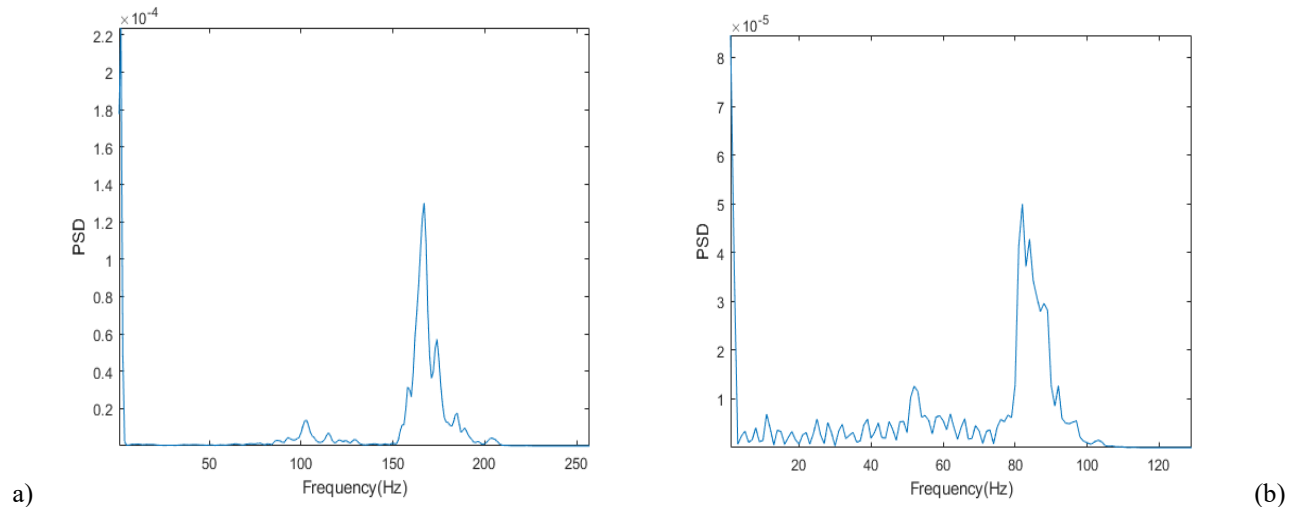


Figure 3: (a) Vibrational characteristics of original pier (b) Vibrational characteristics of scrapped pier

## 5 Conclusion

Following conclusions can be withdrawn from the conducted study:

- 1 The analysis of stability of structures in flood-prone areas is a key problem in assessing flood-induced risks, particularly given the high correlation of life loss throughout these tragic events.
- 2 The highest value of impact force was observed for D4 (2950.6 N) while the minimum value for the debris D1 (2731.6 N).
- 3 During the analysis, it was found that the FEMA P-646 equation provided a better and more accurate calculation of the impact forces.
- 4 It was observed that dynamic properties of pier has more stiffness at dominant frequency (170Hz) when pier in original shape and less stiffness at frequency (85Hz) when pier is scrapped.

## Acknowledgment

The authors would like to express their gratitude to the University of Engineering and Technology, Taxila, for offering the Hydraulics Lab. The anonymous recommendations are gratefully acknowledged for their thorough examination and positive comments.

## References

- [1] D. Palermo, I. Nistor, T. Al-Faesly, and A. Cornett, "Impact of tsunami forces on structures: The University of Ottawa experience," in *Proceedings of the fifth international tsunami symposium, Ispra, Italy*, 2012, pp. 3-5.
- [2] M. Saatcioglu, A. Ghobarah, and I. Nistor, "Performance of structures in Indonesia during the December 2004 great Sumatra earthquake and Indian Ocean tsunami," *Earthquake Spectra*, vol. 22, no. 3\_suppl, pp. 295-319, 2006.



**4<sup>th</sup> Conference on Sustainability in Civil Engineering (CSCE'22)**  
Department of Civil Engineering  
Capital University of Science and Technology, Islamabad Pakistan



- [3] B. Ellingwood, *Development of a probability based load criterion for American National Standard A58: Building code requirements for minimum design loads in buildings and other structures*. Department of Commerce, National Bureau of Standards, 1980.
- [4] E. Rigby, M. Boyd, S. Roso, P. Silveri, and A. Davis, "Causes and effects of culvert blockage during large storms," in *9th International Conference on Urban Drainage*, Eric W. Strecker, Wayne C. Huber, Editors Portland, Oregon, USA, 2002: Citeseer.
- [5] K. T. Lee, Y.-H. Ho, and Y.-J. Chyan, "Bridge blockage and overbank flow simulations using HEC-RAS in the Keelung River during the 2001 Nari typhoon," *Journal of Hydraulic Engineering*, vol. 132, no. 3, pp. 319-323, 2006.
- [6] J. Xia, F. Y. Teo, B. Lin, and R. A. Falconer, "Formula of incipient velocity for flooded vehicles," *Natural Hazards*, vol. 58, no. 1, pp. 1-14, 2011.
- [7] N. P. Wallerstein and S. Arthur, "A new method for estimating trash screen blockage extent," in *Proceedings of the Institution of Civil Engineers-Water Management*, 2013, vol. 166, no. 3: Thomas Telford Ltd, pp. 132-143.
- [8] G. A. Pasha and N. Tanaka, "Undular hydraulic jump formation and energy loss in a flow through emergent vegetation of varying thickness and density," *Ocean Engineering*, vol. 141, pp. 308-325, 2017.
- [9] G. A. Pasha and N. Tanaka, "Effectiveness of finite length inland forest in trapping tsunami-borne wood debris," *Journal of Earthquake and Tsunami*, vol. 10, no. 04, p. 1650008, 2016.
- [10] N. Tanaka and K. Ogino, "Comparison of reduction of tsunami fluid force and additional force due to impact and accumulation after collision of tsunami-produced driftwood from a coastal forest with houses during the Great East Japan tsunami," *Landscape and Ecological Engineering*, vol. 13, no. 2, pp. 287-304, 2017.
- [11] D. Bass and V. Koumoudis, "FEMA's Coastal Construction Manual Update—Flood-Resistant Design," in *Advances in Hurricane Engineering: Learning from Our Past*, 2013, pp. 128-135.



# FEM-BASED APPROACH TO STUDY THE IMPACT OF DRAINAGE ON HYDRAULIC BEHAVIOUR OF EARTH DAMS

*<sup>a</sup>Qazi Umar Farooq\*, <sup>a</sup>Muhammad Tayyab Naqash,*

a: Department of Civil Engineering, Islamic University of Madinah, Saudi Arabia [umar@iu.edu.sa](mailto:umar@iu.edu.sa); [tayyab@iu.edu.sa](mailto:tayyab@iu.edu.sa);

\* Corresponding author: Email ID: [umar@iu.edu.sa](mailto:umar@iu.edu.sa)

**Abstract-** Small homogenous dams are an integral part of the water resource management system yet their failures are common and result in massive life and economic losses. Piping, uplift, and porewater pressure buildup, are the primary reasons behind the hydraulic failure of the dams. The dam drainage system is of great importance in the hydraulic stability of the retaining structure. In this paper, FEM-based analysis has been done to examine the effect of drainage material's geotechnical properties on the hydraulic behavior of homogenous small-scale earthen dams. The study results reflect the extent of variation in, pore water pressure, flow net patterns, and overall seepage velocity with changes in the toe drainage characteristics. With the selection of appropriate drainage material, more than 10-m of head loss has been reported at downstream. The results can be applied for the upgrading of hydraulic and geotechnical considerations for the design of homogenous dams.

**Keywords-** Toe Filter, Porewater Pressure, Flow Nets, Hydraulic Conductivity

## 1 Introduction

This paper presents a part of ongoing research on small-scale dams at the Islamic University of Madinah. Water resource conservation and development are key global issues under changing climatic conditions. Water resource management has been targeted by various international, regional, and national future visions such as the kingdom of Saudi Arabia vision 2030, the middle east green initiative[1], and the national water vision of Pakistan. With an estimated population of 227 million by 2025, Pakistan's current water availability of less than 1100 cubic meters per person, down from 5000 cubic meters in 1951, classifies it as a "water-stressed" country that is headed towards becoming a "water-scarce" country if action is not taken urgently [2]. According to the records of the International Commission on Large Dams, there are approximately 150 dams in Pakistan. The majority of them are located in Punjab and Khyber Pakhtunkhwa (KPK), where the River Indus and its tributaries flow from the northern hilly areas to the southern regions of Sindh and fall into the Arabian Sea [3]. Most of these dams are homogeneous and are constructed from the middle of the 1960s to 1975. Earthen or concrete dams of reasonable height are common hydraulic structures built to impound water [4]. Since large dams require huge capital, special geological and geographic conditions, and environmental consequences[5] small scale dams will be the easiest solution for Pakistan's water problems.

Small dams still withstand a reasonable quantity of water; therefore, proper investigations of dams are required to prevent downstream devastation due to any failure. These failures can range from minor to catastrophic, impairing human life and property damage [6]. Piping failures in dams are pretty common; the mechanism of "piping associated with heaving" was introduced by Terzaghi [7]. Piping failures are attributed to the uncontrolled seepage or unsuitable zonation of materials and filters in earthen dams. Other causes of piping that lead to the failures in earth dams can be Hydraulic, Seepage, and Structural failures [8]. The unfamous 1976 incident of Teton dam failure in Idaho, USA was primarily due to the piping[9]. Another issue with the failure of dams is the dry-wet cycle which can cause cracks in the soil structure and destabilize the dam [10]. The piping and undesirable seepage can be effectively controlled by placing an appropriate dam drainage system. Various studies have been found in the literature on the design and implementation of dam drainage systems [11][12]. The



FEM analysis has also been extensively used for the structural and dynamic stability of the embankments[13]. This study particularly focuses on the hydraulic behavior of the earthen dams while considering the material characteristics of the toe drainage system. The objective of this research is to highlight the effectiveness of different economically viable geomaterials in the toe drainage system.

## 2 Materials and Method

The hydraulic behavior of the dam system has been demonstrated by three different material components. The homogenous embankment, the dam foundation, and the targeted drainage systems. The dam drainage system's main component i.e., the toe filter has been modeled by using three different geomaterials. The geotechnical property of the filter varies in terms of porosity and permeability. The details of the material properties for all the dam components and the three tested filters are tabulated in Table 1.

Table 1: Material properties of various dam components

Dam Component	Geotechnical Properties			
	Dry Unit weight ( $\gamma_d$ ) kN/m <sup>3</sup>	Porosity ( $n$ ) %	Hydraulic Conductivity ( $k$ ) m/s	
Embankment	18	40	$1 \times 10^{-9}$	
Foundation	17.5	42	$3 \times 10^{-8}$	
Toe Filter	TF-1	16	36	$3 \times 10^{-7}$
	TF-2	15	37	$5 \times 10^{-6}$
	TF-3	14	38	$1 \times 10^{-6}$

The FEM analysis for the dam model has been performed by a 2-D dam system. The geomechanics module of the COMSOL Multiphysics program has been used for the analysis. The model geometry with distinguished features is shown in Figure 1.

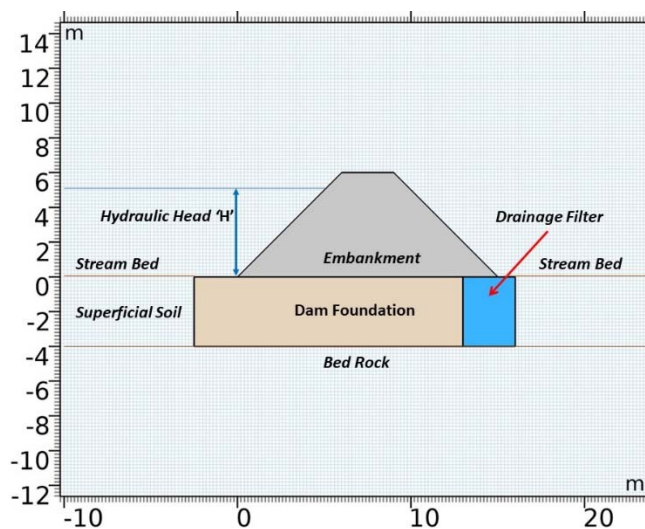


Figure 1: Cross-section of the dam and boundary conditions



The small-scale earth dam system comprises a homogeneous trapezoidal embankment. The main dam embankment has a 6-m long base with a 2-m wide crown, while the dam height is assumed as 6-m. Considering a 1-m freeboard the maximum hydraulic head that can be applied to the dam is 5-m. The dam system is overlaying on the bedrock with very low permeability. The foundation is 4-m deep and comprises the same soil as that of the main embankment, however, it is more porous than the embankment. The more porous foundation creates a longer seepage path and avoids the concentration of flow nets in the main dam body. The study cases are differentiated by the material properties of the toe drainage filter. Three drainage filters namely TF-1, TF-2, and TF-3 were considered in this analysis, where 'TF-1' was the least permeable filter. The density, porosity, and hydraulic conductivity of the filters can be controlled by field compaction. In this study, the porosity of filters varies from 36 to 38 %, while the coefficient of permeability of the least permeable filter is three times less than the maximum one.

### 3 Results and Discussions

The FEM analysis presented in this section is based on Richard's equation for flow through porous media under partially saturated conditions. The flow nets for the dam system under the hydraulic head of 5-m at equilibrium with TF-1 and TF-2 filters are respectively shown in Figure 2a, and Figure 2b. The flow net pattern for both cases is quite similar with flow lines concentrated in a more permeable foundation and relatively high permeable drainage filter. Nevertheless, the hydraulic head at different dam sections is diverse in the two figures and more porous filter TF-2 has better head loss at downstream.

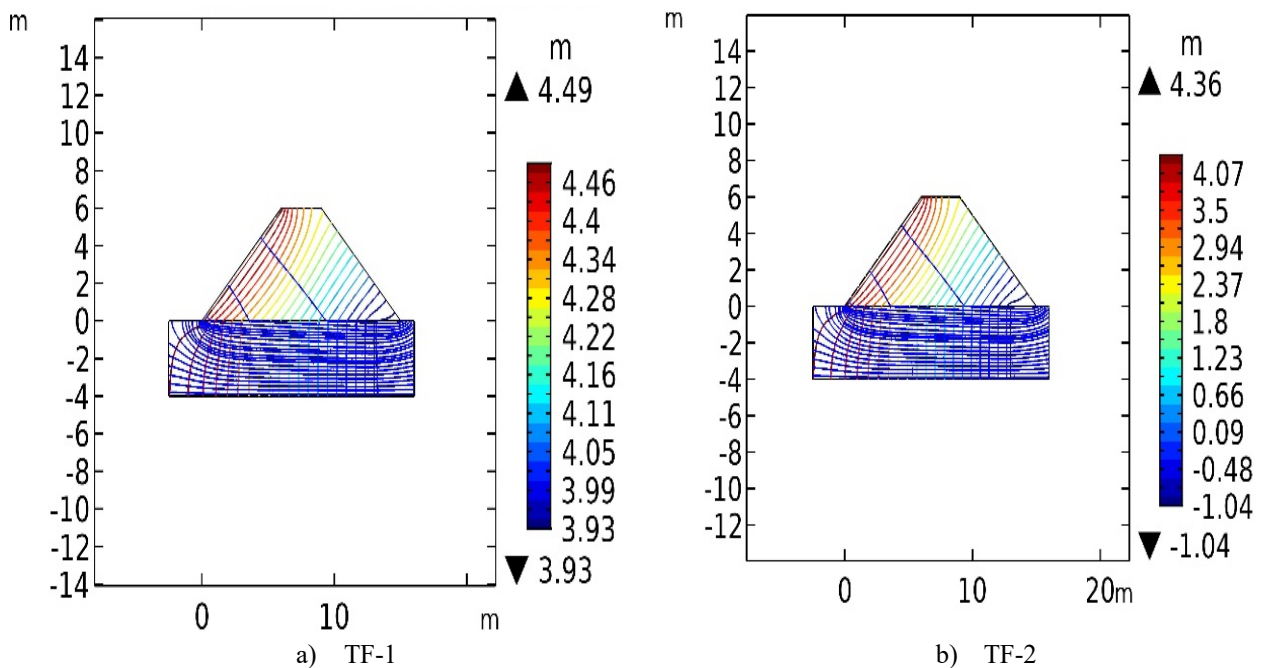


Figure 2: Flow net patterns with different filters, the legend shows the hydraulic head.

The effectiveness of the filter can be better reflected by comparing the water pressure diagram. The porewater pressure situation at equilibrium under the 5-m hydraulic head for the three filters is shown in Figure 3. The dam system with the least permeable TF-1 filter has a very limited partially saturated zone, near the dam crown, (Figure 3a). With an increase in drainage the partly saturated zone increases this can be seen in Figures 3a to 3c.

The improved drainage also increases the seepage velocity across the dam sections which is not an encouraging indication. The seepage velocities for the three considered cases are compared in Figure 4. With drainage improvement the minimum and the maximum seepage velocities in the system increase.

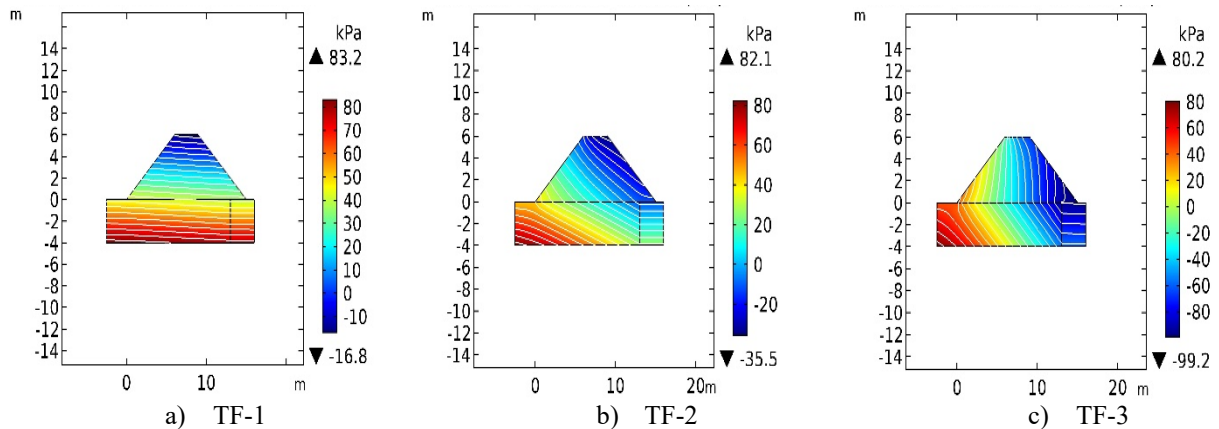


Figure 3 Pressure Distribution concerning Filter Properties

The widespread velocity lines with an increase in higher velocity red zone at the embankment foundation junction on the upstream side can be seen in the figure. The seepage velocities at some locations can reach the critical value and cause scoring which can lead to piping.

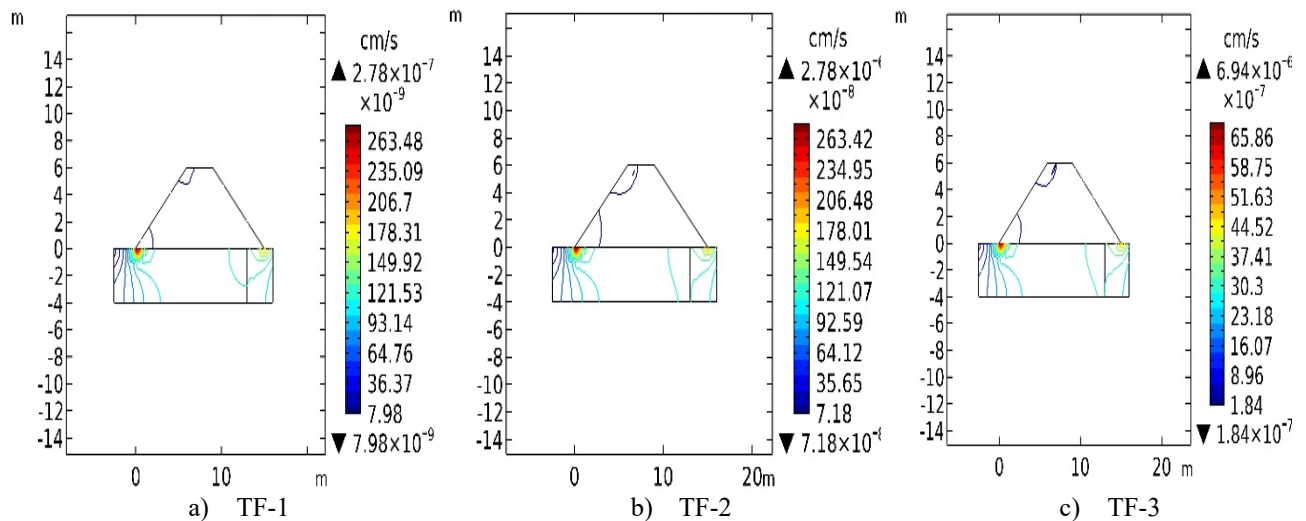


Figure 4: Net Seepage velocity (cm/s) Patterns

The summary of the FEM analysis is presented in Figure 5. With the increase in outflow seepage velocity, the overall system head loss ( $h_l$ ) enhances almost exponentially, however, more data sets are required to establish an allowable range and an appropriate mathematical relation.

The head loss reflects the pore pressure drop at various dam sections and hence an increase in hydraulic stability. However, the higher seepage velocities can lead to internal erosion and effects long-term stability therefore, a reasonable maximum allowable seepage velocity is required to be determined for each dam element. The maximum allowable seepage velocity through a porous media mostly depends on the critical hydraulic gradient, material porosity, and soil gradation.

The study results show that the drainage filter characteristics greatly affect the hydraulic stability of an embankment dam. The filter placement shall be strictly monitored during the construction. In situ compaction and permeability tests must be done at greater frequency and any misalignment with the filter design shall be referred to the geotechnical engineer.

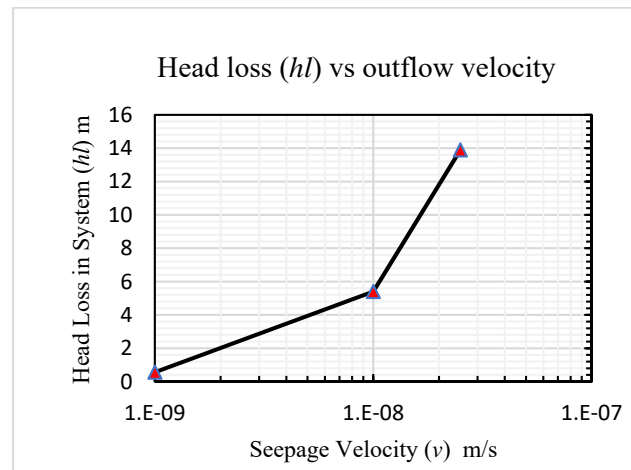


Figure 5: Filter Drainage and Dam performance

## 4 Conclusion

Richards's approach for partially saturated flow in soils can be utilized in FEM-based models to economically study the hydraulic behavior of small-scale homogeneous embankment dams. The study results can be concluded as follows:

1. The efficacy of the toe drainage is critical in terms of dam stability and can alter the pore water pressure distribution, and seepage velocity patterns in the dam system.
2. The increase in system outflow velocity remarkably decreases the water pressure at various dam sections however, it also results in higher seepage velocities which may lead to scoring. Therefore, an optimal solution is required for the specific site conditions and available materials.
3. The dam design engineers are encouraged to utilize FEM-based tools through industry-academia linkage for the optimal selection of design parameters and geomaterials.

## Acknowledgment

The authors would like to acknowledge the technical support and other facilities provided by the department of civil engineering, Islamic University of Madinah.

## References

- [1] Q. U. Farooq, M. T. Naqash, and A. T. Ahmed, "Numerical Evaluation of Embedded Smart Irrigation System for Deep-Rooted Desert Trees," *Civil Engineering and Architecture*, vol. 10, no. 2, pp. 470–476, Mar. 2022, doi: 10.13189/cea.2022.100207.
- [2] Planning Commission, "Pakistan Vision 2025," *Government of Pakistan*, 2014. .
- [3] T. Hussain, A. Basit, and M. N. Javed, "Climate Change Effects on Water Resources and Need of Dams in Pakistan," *Global Mass Communication Review*, 2021, doi: 10.31703/gmcr.2021(vi-i).24.
- [4] Y. Li, A. Chen, L. Wen, P. Bu, and K. Li, "Numerical simulation of non-cohesive homogeneous dam breaching due to overtopping considering the seepage effect," *European Journal of Environmental and Civil Engineering*, 2022, doi: 10.1080/19648189.2020.1744481.
- [5] S.-Y. Han, S.-J. Kwak, and S.-H. Yoo, "Valuing environmental impacts of large dam construction in Korea: An application of choice experiments," *Environmental Impact Assessment Review*, vol. 28, no. 4–5, pp. 256–266, May 2008, doi: 10.1016/j.eiar.2007.07.001.
- [6] J. D. Pisaniello, T. T. Dam, and J. L. Tingey-Holyoak, "International small dam safety assurance policy benchmarks to avoid dam failure flood disasters in developing countries," *Journal of Hydrology*, vol. 531, pp. 1141–1153, Dec. 2015, doi: 10.1016/j.jhydrol.2015.09.077.



- [7] K. Terzaghi, *Theoretical Soil Mechanics*. 1943.
- [8] I. Singh Saluja ZHCET, A. Mohammad Athar ZHCET, and A. A. Sarfaraz Ansari ZHCET, “Causes of Failure of Earthen Dams and Suggested Remedial Measures,” *Prof. Sarfaraz A. Ansari International Journal of Computer & Mathematical Sciences IJCMS*, 2018.
- [9] “Teton Dam failure - at last the complete story.,” *CONSTR. NEWS*, no. 5501, Mar. 10, 1977. 1977.
- [10] W. Ye and F. H. Ma, “Study on the effect of dry-wet cycle on the dam slope stability,” *MATEC Web of Conferences*, 2019, doi: 10.1051/mateconf/201927201050.
- [11] M. M. Aboelela, “Control of Seepage through Earth Dams Based on Pervious Foundation Using Toe Drainage Systems,” *Journal of Water Resource and Protection*, vol. 08, no. 12, pp. 1158–1174, 2016, doi: 10.4236/jwarp.2016.812090.
- [12] A. Pak and M. Nabipour, “Numerical Study of the Effects of Drainage Systems on Saturated/Unsaturated Seepage and Stability of Tailings Dams,” *Mine Water and the Environment*, vol. 36, no. 3, 2017, doi: 10.1007/s10230-017-0468-y.
- [13] K. Fuławka, A. Kwietniak, V. Lay, and I. Jaśkiewicz-Proć, “Importance of seismic wave frequency in FEM-based dynamic stress and displacement calculations of the earth slope,” *Studia Geotechnica et Mechanica*, vol. 44, no. 1, 2022, doi: 10.2478/sgem-2022-0002.





# TO CALCULATE THE DISCHARGE COEFFICIENT FOR A BROAD CRESTED WEIR WITH NON-SUBMERGED FLEXIBLE VEGETATION

<sup>a</sup> Nauman Khan\*, <sup>b</sup> Usman Ghani, <sup>c</sup> Zakir Ullah

a: Department Of Civil Engineering, University of Engineering and Technology Taxila, Pakistan, [enr.naumankhan800@gmail.com](mailto:enr.naumankhan800@gmail.com)

b: Department Of Civil Engineering, University of Engineering and Technology Taxila, Pakistan, [usman.ghani@uettaxila.edu.pk](mailto:usman.ghani@uettaxila.edu.pk)

c: Department Of Civil Engineering, University of Engineering and Technology Taxila, Pakistan, [zakir6897@gmail.com](mailto:zakir6897@gmail.com)

\* Corresponding author: Email ID: [enr.naumankhan800@gmail.com](mailto:enr.naumankhan800@gmail.com)

**Abstract-** Broad crested weirs are generally used as an embankment weir in flood plains for discharge measurement. Due to erosion these weirs are susceptible to failure. To avoid failure of these structures the energy of flowing water must be dissipated. In this research work, flexible vegetation with varying density were used to investigate their effect on the discharge coefficient and energy dissipation of broad crested weir (BCW). For this an experimental study was performed in the hydraulic laboratory of Civil Engineering Department UET Taxila. Flexible vegetation cover was installed over the crest of BCW, and three different densities of vegetation were used. Coefficient of discharge ( $C_d$ ) and energy dissipation ( $\Delta E$ ) were calculated for non-submerged condition of the vegetation. From experimental work it was observed that, as the density of vegetation was changed from dense to sparse, the value of  $C_d$  increases. Lowest value of  $C_d$  was observed for 2cm c/c spacing (maximum density) and highest value of  $C_d$  was observed for 6cm c/c spacing (minimum density). It was also observed that for non-submerged condition of weir, overflow head ( $H$ ) increases with increasing discharge values. As far as the energy dissipation is concerned, the  $\Delta E$  decreases as the vegetation density is reduced from denser to sparse vegetation cases. Highest value of  $\Delta E$  was observed in case of 2 cm c/c spacing, and lowest value of  $\Delta E$  was observed in case of 6 cm c/c spacing.

**Keywords-** Broad crested weir, Discharge, Coefficient of Discharge, Energy dissipation.

## 1 Introduction

Weir is a hydraulic structure constructed across the river to raise the water level and divert a portion of the river flow for irrigation, power generation, water supply schemes and measure discharge [1]. These are normally overflow structures build as a rigid wall of concrete, brick masonry, stone masonry and compacted earth. Sometimes weirs are provided with gates. The gates regulate only a small portion of water. The major portion of water is regulated through crest. Normally weir is provided at right angle to the axis of the river, but oblique weir may also be provided. There are broad crested earthen weirs, with sloping ramps on upstream as well as on downstream sides. Such a weir is also used in flood plains to measure discharge. Broad crested embankment weir has higher discharge capacity as compare to broad crested weir with vertical faces. Embankment weir has a normal slope of 1V: 2H to provide proper stability of slope and control the seepage through embankment weir [2]. The increase in the upstream slope of weir also increases the head loss through the weir and vice-versa. Also it has been concluded that head loss decreases as the downstream water depth increase [3]

Broad crested embankments weirs are overflow hydraulic structures. Due to overflow condition these are more susceptible to failure due to continuous erosion of the crest. Now a day's environmental friendly materials (such as rip-rap, stone



pitching and gabions) are used to increase the surface roughness and provide maximum resistance to the flow. In embankment weir discharge is reduced by increasing the roughness of surface. The roughness of the crest had its effects on velocity distributions and shear stress [4]. The effect of weir height is directly proportional to discharge coefficient, while the effect of surface roughness is inversely proportional to discharge coefficient [5].

Plants and vegetation also play a vital role in reducing the effect of high velocity of the flow. Plants are provided in flood plains to minimize the effects of flood and reduce transport of sediments. To design safe embankments, the vegetated weirs play an important role in raising the flood water level. It has also been investigated that vegetation cover over the crest of embankment causes much loss in the head of flood water [6]. Vegetation occurs naturally on embankment and creates maximum turbulent behavior for the flow. Due to turbulence behavior in the zone of vegetation, energy is dissipated. As compare to smooth embankment weirs, vegetative embankment weirs offers greater turbulence and resistance to flowing water. It is also investigated that upstream water head is directly proportional to the roughness of the embankment weir, because of the availability of vegetation over it [7]. The flow resistance varies with stem diameter, vegetation density and elastic properties of vegetation [8]. Hydraulic performance of semi circular increases by 45% with the increase of particle size of roughness material [9]. As compare to other slopes, slope of 1:3 for downstream ramp was most appropriate for discharge coefficient [10].

In the present research, the impact of flexible vegetation cover with varying density on the discharge coefficient of a broad crested weir has been investigated. The energy loss has also been investigated. The results have been shown in the graphs.

## 2 Experimental Procedure

All the experimental work was executed in the hydraulic laboratory of civil engineering department, University of Engineering and Technology Taxila. A glass walled open channel with rectangular x-section was used for all the experiments (Fig. 2.1a). The channel is fitted with six tanks below it which supply water to the channel through a pump. These tanks were filled manually using a water pipe.

A model of BCW was prepared using plywood and it was installed in the channel (Fig. 2.1b). The weir model was trapezoidal in shape. Model had an upstream ramp, a crest and a downstream ramp. A slope of 1V: 2H was provided both for upstream & downstream ramps. The crest of the weir was 25cm in length, whereas the crest height & width were 11cm and 31cm respectively. Circular holes of diameter 0.9cm were drilled at a distance of 2cm center to center over the crest of the weir in a square pattern

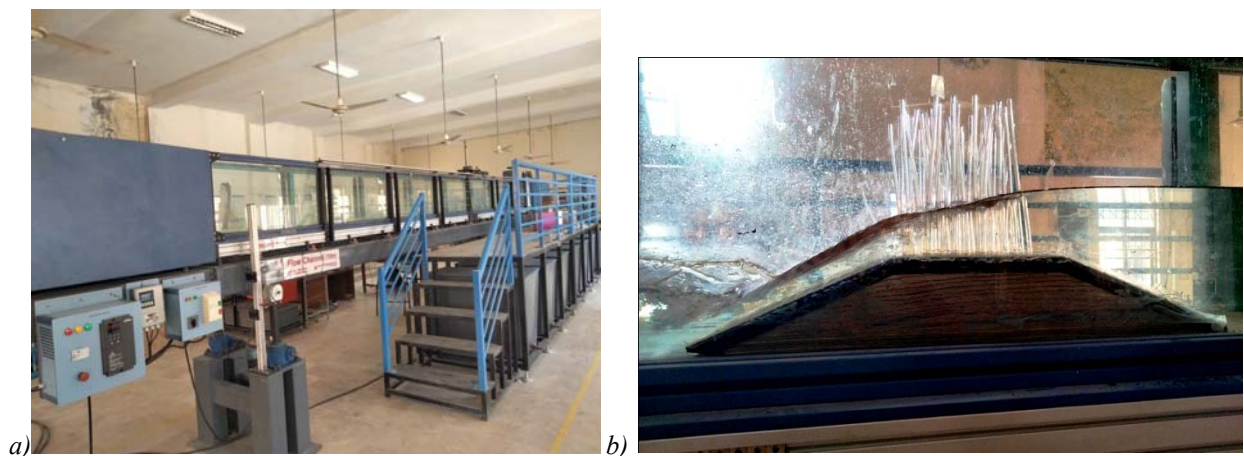


Figure 2.1: a. Rectangular glass channel, and b. Weir model inside the channel

Weir model were installed 4m downstream from the inlet of the open channel. Different pattern of flexible vegetation were fixed at the crest of weir model with varying density. A movable scale was fixed over the channel, which was used to measure the depth of water at two measuring stations.



Vegetation used over the crest of the weir was flexible. Flexible sticks made of silicon were used as flexible vegetation over the crest of the weir. The flexible sticks were 22.5cm long and had a diameter of 0.8cm. These sticks were transparent and could bend with the flow of water.

### 3 Research Methodology

Three cases of flexible vegetation cover over the crest of the weir were studied in this research work. This has been shown in Fig. 3.1.

- Case-1: Flexible vegetation with 2cm c/c spacing (max. density)
- Case-2: Flexible vegetation with 4cm c/c spacing (intermediate density)
- Case-3: Flexible vegetation with 6cm c/c spacing (min. density)

For each case of vegetation cover, four different flow rates (Q) were used. These flow rates were 0.21ft<sup>3</sup>/s, 0.36 ft<sup>3</sup>/s, 0.51 ft<sup>3</sup>/s and 0.59 ft<sup>3</sup>/s..

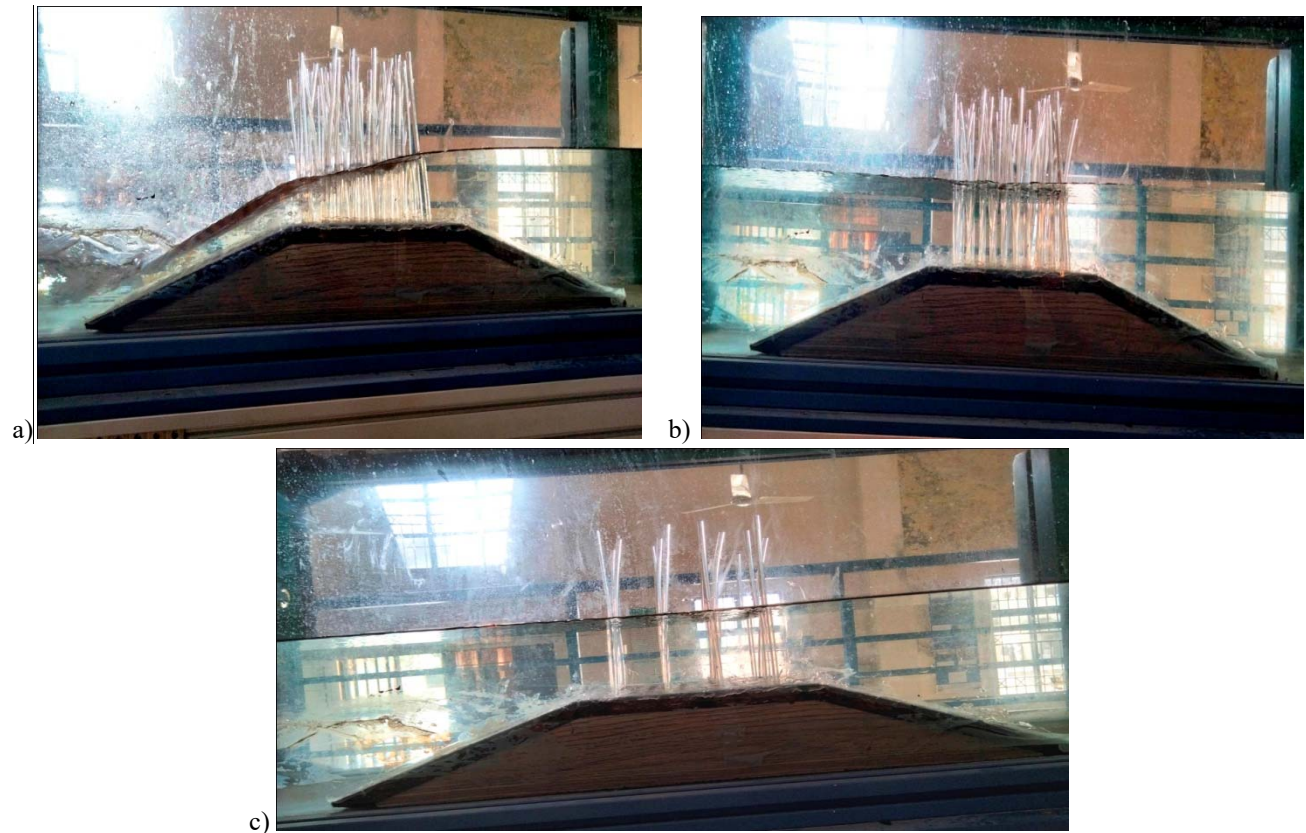


Figure 3.1: Flexible vegetation with a. 2cm c/c spacing, b. 4cm c/c spacing, c. 6cm c/c spacing

#### 3.1 Calculation for $C_d$ and $\Delta E$

Discharge passing through broad crested trapezoidal weir was calculated using Eq.1 [11]

$$Q = C_d * B * \sqrt{g \left( \frac{2}{3} * H \right)^3} \quad (1)$$

Where;

Q = Discharge (ft<sup>3</sup>/s)

B = width of weir (ft)

H = Overflow head over the crest of the weir (ft)

$C_d$  = Co-efficient of Discharge



Coefficient of discharge can be found using Eq.2

$$C_d = \frac{Q_{act}}{Q_{theo}} \quad (2)$$

Energy dissipation ( $\Delta E$ ) through the weir was calculated using following general equation

$$\Delta E(\%) = \frac{E_1 - E_2}{E_1} * 100 \quad (3)$$

$$E_1 = Y_1 + \frac{V_1^2}{2g} \quad (4)$$

$$E_2 = Y_2 + \frac{V_2^2}{2g} \quad (5)$$

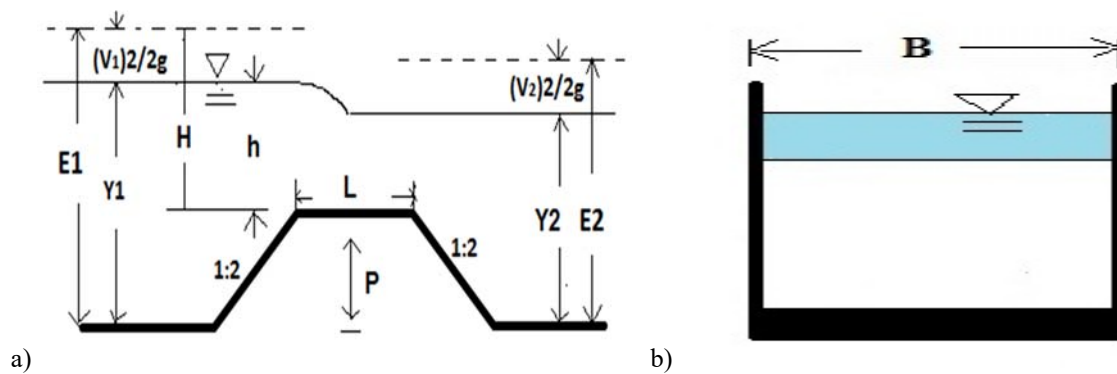


Figure 3.2: a. Profile of weir, and b. suppressed rectangular sharp crested weir

### 3.2 Calculation of actual discharge in channel

The actual discharge ( $Q_{act}$ ) in the channel was calculated using sharp crested rectangular suppressed weir (Fig.3.2b). It was installed at a distance of 4m d/s of the inlet. Discharge was calculated using the following equation for suppressed rectangular sharp crested weir [12].

$$Q = 3.33 * B * H^{3/2} \quad (6)$$

Where;

B = width of weir (ft) (here B=3.10 ft)

H = depth of water over the crest (ft)

Q = discharge (ft<sup>3</sup>/s)

## 4 Results & discussions

By measuring the flow depths at u/s and d/s of the broad crested weir, the coefficient of discharge ( $C_d$ ) and energy dissipation ( $\Delta E$  %) were calculated for all the three vegetation cases against various discharge values. Results of all the three densities were compared and following graphs were plotted.

Figure 4.1(a) shows the variation of  $C_d$  values for different densities of vegetation. As the density of vegetation change from max. to min., the values of  $C_d$  increases. Hence it is concluded that  $C_d$  is inversely proportional to the density of vegetation cover. Vegetation provides resistance to the flow by increasing Head over the crest. So discharge is reduced.  $C_d$  has lowest values for 2cm spacing (max. density) of vegetation at the corresponding depths, and highest values for 6cm spacing (min. density).

Figure 4.1(b) shows that for non-submerged condition of weir, overflow head (H) increases with increasing discharge (Q) values. From Equation of flow it is obvious that Flow (Q) is directly proportional to Head (H), so the results are justified.

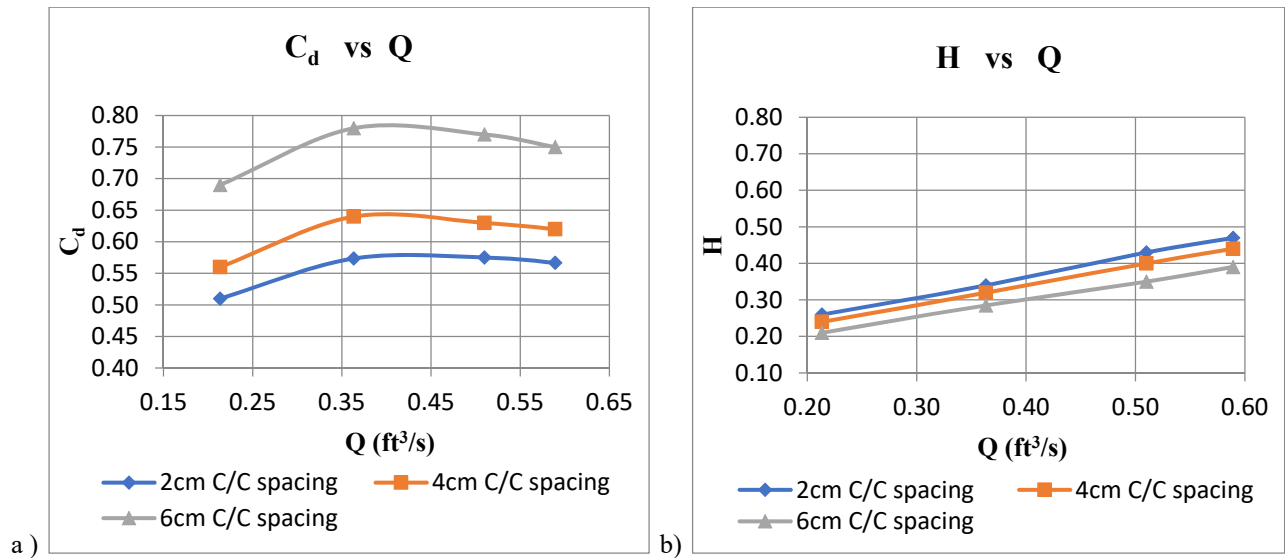


Figure 4.1: a.  $C_d$  vs.  $Q$  results for flexible vegetation with different densities, b. Over flow head ( $H$ ) vs.  $Q$  results for different densities of flexible vegetation.

Following graph show the relationship between energy dissipation and downstream water depth ( $Y_2$ ). Figure 4.2 shows the values of  $\Delta E$  for different densities of vegetation. As the density of vegetation change from dense to sparse, the values of  $\Delta E$  decrease. Due to Vegetation U/s head is increases and the velocity of the flow decreases. Thus creating a deep pool of water for maximum energy dissipation. Energy dissipation is highest for 2cm c/c spacing (max. density) and lowest for 6cm c/c spacing (min. density).

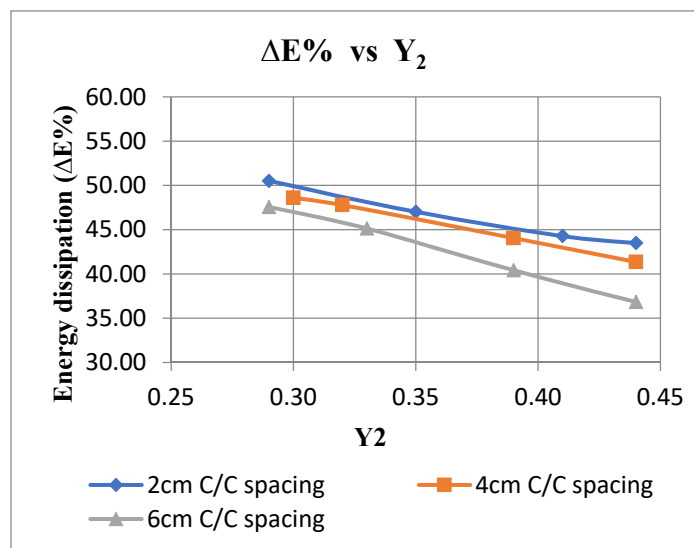


Figure 4.2: Effect of density variation on  $\Delta E$  for flexible vegetation

This research may be applied practically in flood plain for the safety of Embankment weirs against failure. Flexible vegetation over the crest of weir structure increases surface roughness and energy dissipation. So the risk of Crest Erosion is minimised. Apart from vegetation we may also use gabions, stone-pitching and rip-rap over crest to increase surface roughness.



## 5 Conclusion

Following conclusions could be drawn from this research work:

- 1  $C_d$  values were maximum for 6cm c/c spacing (min. density) and was minimum for 2cm c/c spacing (max. density).
- 2 It was also observed that for non-submerged flow condition, the overflow head (H) increases with increasing discharge.
- 3 Maximum value of energy dissipation was observed for 2cm c/c spacing (max. density) and was minimum for 6cm c/c spacing (min. density).

## Acknowledgment

The authors would like to thank every person who helped throughout the research work. The careful review and constructive suggestions by the anonymous reviewers are gratefully acknowledged.

## References

- [1] Experimental Study of Flow Characteristics Over Single Step Broad Crested Weir. Bashir Tanimu, Aliyu Bamaiyi Usman, Al-Amin Danladi Bello, Surajo Abubakar Wada, Khalid Sulaiman. 2021, JOURNAL OF SCIENCE TECHNOLOGY AND EDUCATION 9 (2), JUNE, 2021, p. 246.
- [2] HYDRAULICS OF EMBANKMENT WEIRS. Hermann M. Fritzi, Willi H. Hager, Fellow, ASCE. 1998, JOURNAL OF HYDRAULIC ENGINEERING, p. 1.
- [3] Laboratory study of head loss for trapezoidal weirs with vegetation elements. M.A Siddique, U.ghani,A.Latif,S.Ali,T.sultan,M.U Rashid. Taxila pakistan : s.n., 2016, Technical journal,University of Engineering and Technology (UET) Taxila,Pakistan, Vol. 21, p. 3.
- [4] Hydraulic Performance of an Embankment Weir with Rough Crest. Stefan Felder, Nushan Islam. 2016, Journal of Hydraulic Engineering, p. 1. ISSN 0733-9429.
- [5] Effect of Height and Surface Roughness of a Broad Crested Weir on the Discharge Coefficient: Experimental Study. Rafid Alboresha, Uday Hatem. s.l. : IOP Publishing, 2021. IOP Conf. Series: Materials Science and Engineering. p. 2. doi:10.1088/1757-899X/1090/1/012087.
- [6] Flow resistance of vegetated oblique weir-like obstacles during high water stages. S. Ali, W. S. J. Uijtewaal. 2013, Hydrology and Earth System sciences, p. 5513.
- [7] Experimental Investigation for Discharge Coefficient of an Embankment Weir Using Smooth and Vegetated Embankments. Hafiz Muhammad Aamir, Usman Ghani, Muhammad Kaleem Ullah, Ghufraan Ahmed Pasha. Lahore : MUET, Pakistan, 2019. 2nd International Conference on Sustainable Development in Civil Engineering. p. 724 & 728.
- [8] Performance of flexible emergent vegetation in staggered configuration as a mitigation measure for extreme coastal disasters. L. Noarayanan, K. Murali, V. Sundar. s.l. : Nat Hazards, 2012. p. 1. DOI 10.1007/s11069-012-0089-5.
- [9] PERFORMANCE COMPARISON OF SEMICIRCULAR WEIRS WITH VARYING CREST ROUGHNESS. Mujahid Muhammad Muhammad, Terhile Thaddeus Jen, Abubakar Ismail, Aliyu Dandajeh Adamu, Basiru Abdulsalam. 2022, Vol. 8, p. 1. <https://doi.org/10.48422/IMIST.PRSM/ajees-v8i1.31473>.
- [10] Flow through a sluice gate over a broad crested weir under free- and submerged-flow conditions. Amin Seyedzadeha, Mehdi yasi,javad farhoudi,Andreas Malcherek. 2022, ISH Journal of Hydraulic Engineering . <https://doi.org/10.1080/09715010.2022.2094733>.
- [11] Bélanger, J.B. (1841). Notes sur l'Hydraulique. ('Notes on Hydraulic Engineering.') Ecole Royale des Ponts et Chaussées, Paris, France, session 1841-1842, 223 pages (in French)
- [12] USDA. part 650 National engineering Handbook. [book auth.] United states department of Agriculture (USDA). *National Engineering Handbook*. United states : USDA, feb 2022, p. 57



# EXPERIMENTAL STUDY OF T-SHAPED SPUR DIKE WITH DIFFERENT INCLINATION TO MINIMIZE THE LOCAL SCOUR

<sup>a</sup> Nayab Tariq, <sup>b</sup> Naeem Ejaz, <sup>c</sup> Ghulam Abbas, <sup>d</sup> Muhammad Asghar

a: Department of Civil Engineering, University of Engineering and Technology Taxila, [Nayabtariq23@gmail.com](mailto:Nayabtariq23@gmail.com)

b: Department of Civil Engineering, University of Engineering and Technology Taxila, [naeem@uettaxila.edu.pk](mailto:naeem@uettaxila.edu.pk)

c: Department of Civil Engineering, University of Engineering and Technology Taxila, [ghulamabbas696@yahoo.com](mailto:ghulamabbas696@yahoo.com)

d: Department of Civil Engineering, University of Engineering and Technology Taxila, [asgharghani0078600@gmail.com](mailto:asgharghani0078600@gmail.com)

\* Corresponding author: Email ID: [Nayabtariq23@gmail.com](mailto:Nayabtariq23@gmail.com)

**Abstract-** River bank erosion is controlled through spur dikes. The River banks scouring around spur dikes is complex, especially when they are engaged in the straight position. This is due to the interaction of the spur dike's flow pattern with the vortex helical currents. Experiment findings are presented in this research that flow around a T-shaped spur dike minimize through inclination. The impact of the inclination of the spur dike with unique geometry. Experiments are carried out in a rectangular channel with a recirculating flow. The findings indicate that the minimum scour depth, as well as the volume and dimensions of the scour hole, decreases as the inclination of the T-shaped spur dike rises. The height of the ridge downstream of the spur dike grows as the length of the spur dike is increased. The highest scour depths are found at a 0<sup>0</sup> inclination of T-Shaped dyke. After 36 hours of experiment, showing a maximum of 58% reduction in scouring for 15<sup>0</sup> inclination compared spur dyke without inclination. So, the more efficient T-shaped spur dyke with inclination.

**Keywords:** Scouring, Inclination, Spur dykes, Depth, Flume, T- shape

## 1 Introduction

A spur dike is a river training construction that extends away out from bank into to the channel. It diverts the flow stream away from the bank, protecting the bank against erosion. Another side after construction of spur dike velocity of flow become maximum around spur dike due to this channel bed scouring occurs. The main channel's depth is increased due to the flow limitation produced by the spur dike[1]. Over the years, this purpose of spur dikes, that can provide greater defense against bed scouring, has been chosen as the primary aim of spur dike development[2]. Spur dikes are constructed at an angle to the main flow. Depends upon construction material spur dikes are made of stone, gravel, rock, earth, concrete and wood[3]. Spur dikes are constructed to maintain a bottomless, straight channel for improved navigation, and they are also helpful in preventing ice jamming. Spur dikes are of various types that can be distinguished according to their appearance, construction and action on stream flow. Depends upon design, geometry of spur dikes the most important consideration[4]. A unified theory for determining scour depth at spurs dike is still very much in early stages due to the intricacy of the scour challenges. Major scouring occurs often during floods, which feature unstable flows and, in certain cases, flow directions that are opposite to those of typical flows. Scour is caused by three-dimensional boundary-layer separation near the dyke's end, which causes bed material erosion due to the high volatility and vorticity of the local flow structure[5]. Numerous experimental studies of local dike's shear failure in alluvial streams were conducted, and researchers developed a series of prediction methods to estimate the scour depth at various spur dikes to inclination under various flow dynamics, sediment size and differentiation. Experiments were carried out to study the scouring arrangement from around spur dike at various angles relative to the flow axis. The bed failure caused by aggressiveness of flow due to which it is always have a difficult and dangerous problem for hydraulic engineers. It has been known from the previous research that the scouring has a



considerable effect by the shape and inclination of spurs and the location of maximum scour depth is highly dependent on the spur dike inclination angle.

## 2 Experimental Procedures.

All the experiment is performed in the Water resources & Hydraulics Engineering Laboratory of Department of Civil Engineering, University of Engineering and Technology, Taxila. The channel had specifications of 20 m length, 1 m wide and 0.75 m deep glass-sided flume with an adjustable tailgate at the channel-end to regulate the flow depth used for the experimental depth. Through the centrifugal pump, discharge is supplying to the tank then inter to the main channel by aligned honeycomb diffuser in the direction of flow for smooth and uniformly distribution of flow crosswise. At the tail of channel water enter in the sediment tank after filling and trapping the flowed sediments, the flow discharges in the main channel. Plan view of the Laboratory channel and experimental setup shown in (Figure 1): Plan View of Channel A 9m long, 0.20m deep and .96m wide false bottom of uniform, medium size ( $d_{50}=0.60\text{mm}$ ) bed material and T-shaped spurs dyke is introduce, sand size considered in this study stood in compliance to the condition of  $D/d_{50} > 50$  in order to dominate the sediment size effect on the scour evolution process guaranteeing non ripple-forming sand (Raudkivi & Ettema, 1983) ( Ettema, Melville, & Barkdoll, 1998). The thickness of the spur dykes was 10 mm which is not more than 10% of the channel width to prevent the effect of walls on scouring (Chiew and Melville, 1987). The trapezoidal broad crested weir (TBCW) modelled by wood material, weir width equal to the full width of channel, crest length was 50cm, the weir was 5cm above the flat bed, the sides slope of the TBCW was 1V:2H, which is more stable and seepage control. (Fritzi & Hager, 1998). The dimension of TBCW was within the limits (Sturm, 2001) (Henderson 1966) (Chanson, 2004).

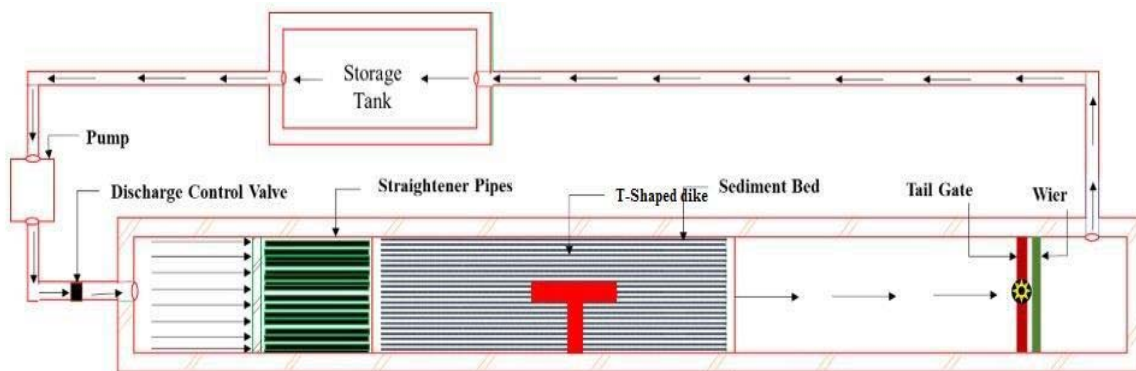


Figure 1: Plan View of Channel

## 3 Research Methodology

- Open channel in hydraulic lab will be used for experimental setup.
- The shape of spur dikes made of wooden will be used.
- To the evaluation of scouring around the different inclination of 0, 9, 15, spur dike will be placed in flume.
- The slope of the channel bed will be uniform and having sediments of the average diameter 0.71mm
- Scour depth will be measured around T-shaped spur dike with scour gauge or laser distance meter.

### Equation:

Experimental work all were carried out in Hydraulics lab of civil engineering department, theoretical discharge equation used for measuring Discharge value.

$$Q_t = 2/3 C_{rd} \sqrt{2g} (b_2 h_2^{3/2}) + 2/3 C_{rd} \sqrt{2g} (2b_1) h_1^{3/2} + 8/15 C_{td} \sqrt{2g} (\tan(\theta/2)) h_1 e^{5/2}$$





Where;

$\theta$  = Notch angle,  $b$  = Width of weir,  $C_{rd}$  = Coefficient of discharge of the rectangular sharp-crested weir,  $C_{td}$  = Coefficient of discharge for triangular sharp-crested weir,  $g$  = gravitational acceleration,  $h$  = Water head on the weir crest,  $h_e$  = Effective head

## 4 Results:

Table 1: Experimental Condition and Result

Dyke inclination	Q (m <sup>3</sup> /s)	T (hr)	h (m)	ys_f (cm)	ys_f/D
0°	0.023	3	0.20	6.3	0.81
	0.031	3	0.20	6.8	0.83
	0.042	3	0.20	7.4	0.81
9°	0.023	3	0.20	4.3	0.89
	0.031	3	0.20	5.0	0.95
	0.042	3	0.20	5.7	0.90
15°	0.023	3	0.20	5.1	0.76
	0.031	3	0.20	5.6	0.75
	0.041	3	0.20	6.2	0.65

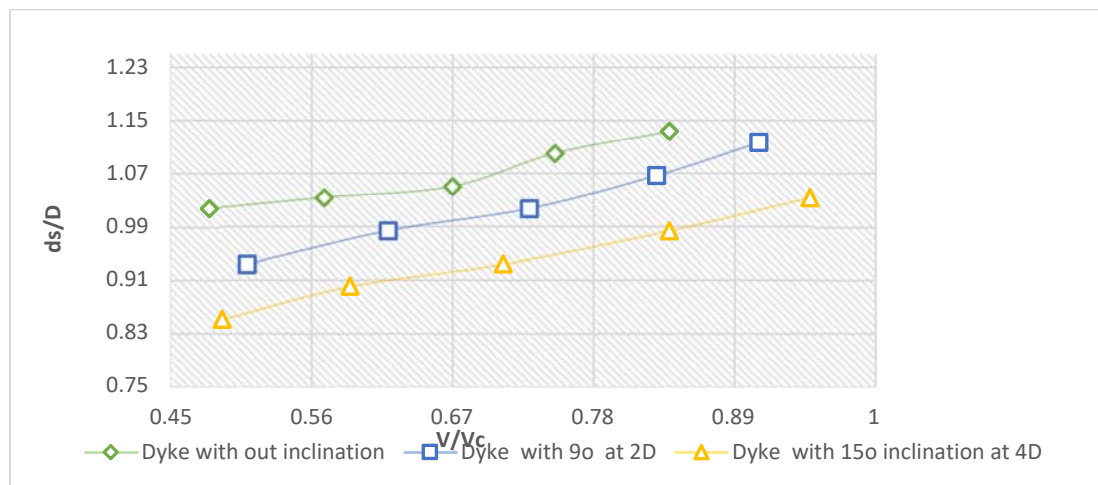


Figure 2: Relationship b/w Effective depth and effective velocity of different dyke inclination

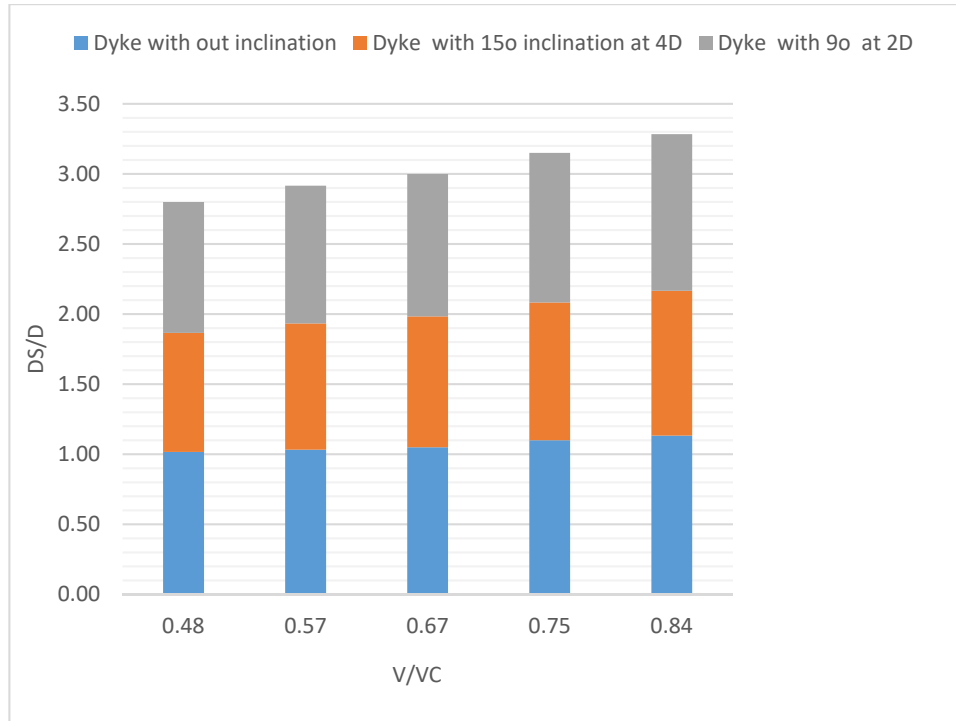


Figure 3: Scouring depth at different inclination



Figure 4: Relationship B/W scouring depth with Froude number

Geometry and inclination of spur dike effects the local scouring of bed channel. Like (Figure 2) explain that scouring depth is maximum where spur dikes are without inclination and values of local scouring depth is minimum due to different spur dike inclination. Similarly, in (Figure 3) the relationship between the Froude number and depth of scouring with different inclination of spur dikes. Experimental work shows that spur dike local scouring is inverse relation with flow condition.



The Scouring depth is minimum for spur dikes with maximum inclination for each Froude number and similarly Scouring depth is maximum for spur dikes without inclination as shown in (Figure 4). The purpose of this research is to control the channel bed scouring after construction of T-shaped spur dike with different inclination.

## 5 Conclusion

In this work, the efficiency of T-shaped spur dykes studied with different inclination by experimentally dykes placed in an open channel.

The following conclusions were drawn from this experimental work

1. Scouring depth decreases with the use of T-shaped spur dykes with inclination
2. The scouring around the T-shaped spur dykes with inclination decreased with increasing the discharge in channel.
3. The T-shaped spur dykes with 15<sup>o</sup> inclinations is most efficient that's reduced scouring up to 58% as compared to without inclination spur dyke.

## Acknowledgment

The authors would like to thank every person/department who helped thorough out the research work, particularly Prof Dr Naeem Ejaz and Engr Ghulam Abbas. The careful review and constructive suggestions by the anonymous reviewers are gratefully acknowledged.

## References

- [1] C. Özyaman, C. Yerdelen, E. Eris, and R. Daneshfaraz, "Experimental investigation of scouring around a single spur under clear water conditions," *Water Supply*, vol. 22, no. 3, pp. 3484–3497, Mar. 2022, doi: 10.2166/WS.2021.389.
- [2] P. Esmaeli, S. Boudaghpour, M. Rostami, and M. Mirzaee, "Experimental investigation of permeability and length of a series of spur dikes effects on the control of bank erosion in the meandering channel," *Ain Shams Engineering Journal*, vol. 13, no. 4, Jun. 2022, doi: 10.1016/j.asej.2022.101701.
- [3] Y. Moussa and M. Atta, "Simulation of scour at bridge supports," *Gradjevinar*, vol. 72, no. 9, pp. 793–801, 2020, doi: 10.14256/JCE.2506.2018.
- [4] R. P. Tripathi and K. K. Pandey, "Experimental study of local scour around T-shaped spur dike in a meandering channel," *Water Science and Technology: Water Supply*, vol. 21, no. 2, pp. 542–552, Mar. 2021, doi: 10.2166/ws.2020.331.
- [5] M. A. Lenzi, A. Marion, and F. Comiti, "Local scouring at grade-control structures in alluvial mountain rivers," *Water Resources Research*, vol. 39, no. 7, 2003, doi: 10.1029/2002WR001815.



# AN OVERVIEW OF SUSTAINABLE REPAIR STRATEGIES FOR POTHoles IN FLEXIBLE PAVEMENTS DURING REHABILITATION PHASE

<sup>a</sup> Haider Abrar, <sup>b</sup> Minhas Shah\*

a: Riphah School of Leadership, Riphah International University, [a.haider@live.com](mailto:a.haider@live.com)

b: Department of Civil Engineering, Capital University of Science and Technology, Islamabad, [shahminhas96@yahoo.com](mailto:shahminhas96@yahoo.com)

\* Corresponding author: Email ID: [shahminhas96@yahoo.com](mailto:shahminhas96@yahoo.com)

**Abstract-** The formation of distresses on pavement causes the Pavement Management System to provide an activity of rehabilitation which not only costs money but also has environmental impacts. A pothole is the most occurring flexible pavement distress that not only causes comfort issues but also leads to the degradation of the remaining pavement. It is very significant to address this problem in a sustainable way that would decrease the effect on the environment. This paper aims to study different researches on pothole formation and its repair strategy that would not only increase the capability of the pavement but also be a sustainable solution. A number of research has been done on potholes to find feasible and sustainable solutions. An extensive literature review has been carried out in this paper regarding different materials that are helpful in minimizing the moisture susceptibility of flexible pavement distresses mainly potholes. The analysis indicates that pothole formation is dependent upon many factors including the type of aggregate, binder type, and external factors like moisture infiltration. Moreover, the binder type is a significant factor. The combination of non-woven fabric and ultra-thin asphalt overlay is very susceptible to reducing pothole formation which is also considered to be more environmentally friendly as compared to other strategies like rubber-modified asphalt and hence can be called a sustainable solution.

**Keywords-** Potholes, Sustainable pavement solution, Pothole repair

## 1 Introduction

Road network is considered the backbone of any economy and hence road projects are included in major national projects. Road projects have a major impact during the construction and also during the maintenance phase of the project at the same time the appearance of distresses is also a major liability to the project that not only affects the user comfort but also has a very deep impact is the prospect of sustainability. Out of these distresses Potholes is major occurring distress. Hence it is very significant to discuss this distress in view of the maintenance phase of a road project. The composition of the flexible pavement consists of aggregates and bitumen. The structure is provided by the aggregates which provide the skid resistance and resist the load of the vehicles, whereas the bitumen acts as a binder in this mixture. With the advent of time the deterioration process of the pavement takes place this happens mainly due to the bitumen degradation leading to bitumen brittleness, and environmental exposition. Moreover, there are very bright chances of infiltration of moisture into the pavement that later, due to the phenomenon of freeze and thaw causes the initiation of cracks. These cracks can initiate at the bottom or from the top. The continuous loading on the pavement for long periods also causes distress to appear on the surface if rehabilitation and maintenance are not done at specified intervals, these cracks propagate until they form a bowl shape and this bowl-shaped distress is called a pothole. Potholes cause a reduction in the service level of the pavement and it is considered the most infuriating distress in pavements [1]. The properties of the materials that can help in avoiding potholes require being durable to the environment, cohesion and good workability, rutting potential, durability to traffic loading, and free-thaw potential [2]. To repair a pothole there is a variety of methods and materials that have been



previously studied. These repair materials contain (i) Cold Mix Asphalt (ii) Hot-mix Asphalt (iii) other additives and polymeric resins and materials. Generally, it is accepted that the hot mix asphalt which is actually the combination of Bitumen and fine and coarse aggregates is the best possible conventional repair methodology, yet its applicability is limited due to the fact that there are constraints of laying temperature and batch requirement. Contrarily, a low-quality repair is achieved by the Cold mix asphalt which is the combination of the bitumen emulsion and cementitious material and aggregates but higher flexibility of the application exists, for instance, individual potholes can be repaired using a small amount of packages disregard of the weather conditions. Furthermore, modern research has helped in the use of polymeric materials in the pavements as admixtures. These polymeric materials and resins have the potential to repair the potholes with higher efficiency. Polymeric materials like rapid setting urethane resins and DCPD i.e. dicyclopentadiene are good examples. These materials are no doubt expensive and their common use is not possible but with the advancement of technology further materials can be discovered that are sustainable in all three aspects. Shrivastava et al [19] developed a new technique for the identification of potholes using modern machine learning technology. This method would help identify potholes at a very early age hence giving enough time to apply repair strategies. Zhang et al. [20] performed an experimental study in which they used waterborne polyester concrete for cold patching of the potholes. The usage of this modified concrete proved to be very time-saving as the patched surface could be opened for traffic after just 2 hours.

Typically, the selection of the material for the repair of potholes is dependent on the resources available, distress level, and administrative and political conditions. In this article, to assess the significance of a pothole repair during the maintenance and rehabilitation phase, pothole distress along with the characteristics of flexible pavement and the selection of sustainable remedy has been reviewed based on the available literature. Different researches on pothole formation and its repair strategy in the last few years have been studied to find techniques that would not only increase the capability of the pavement but also be a sustainable solution. A number of research has been done on potholes to find feasible and sustainable solutions. An extensive literature review has been carried out in this paper regarding different materials that are helpful in minimizing the moisture susceptibility of flexible pavement distresses mainly potholes.

## **2 Flexible pavement characteristics and Pothole formation**

The structure of a flexible pavement consists of a subgrade, which is actually the foundation layer, upon this layer, there is a sub-base composed of granular material, on top of the sub-base, a base course is laid which is a combination of fine and coarse aggregate and on top of this layer is the asphaltic wearing course. Using the linearized theory of elasticity, the stresses and the strains on the pavements are evaluated. During the design phase of the flexible pavements, the thickness of the layers is considered based upon allowable values of the stresses and the strains in the flexible pavement. The characteristics of the surface of the pavement include frictional resistance, ride quality, the potential for hydroplaning, sound absorption properties, texture, and wholesome performance of the pavement. The focus on pavement research is due to the growing interest in pavement surface concerns and characteristics about performance, traffic noise, and safety. Flexible pavements are considered different in terms of behavior under loading along with the aging process of the roads. Further research into this topic of flexible pavement can lead to the knowledge of the changes and overall effect on the pavements which can help in optimizing the design and hence come forward as a sustainable solution to different flexible pavement-related problems.

A bowl-shaped depression on the surface of the flexible pavement is called a pothole. The size of the pothole ranges from six inches to almost three feet. During the service period of a road, it is subjected to heavy traffic loads along with environmental conditions. These moving loads displace the small fragments of the surface which deteriorate further and cause different distresses like crocodile cracking which advances to become potholes [14]. These potholes first appear only on the uppermost layer of the structure but with time water pounds and infiltrate the bottom layers, inducing stress, and hence this pothole spreads, depth-wise, further and the stability of the areas decreases further [3]. Potholes are the distresses that are localized and are interrupted in the pavement surface and on that region of the pavement the part of the pavement has split away, causing a depression of shallow depth [4]. Potholes can be categorized as distress that is a depression on the surface of the road in an irregular fashion and the main reason for the formation of this distress is the logging water on the roads [5].

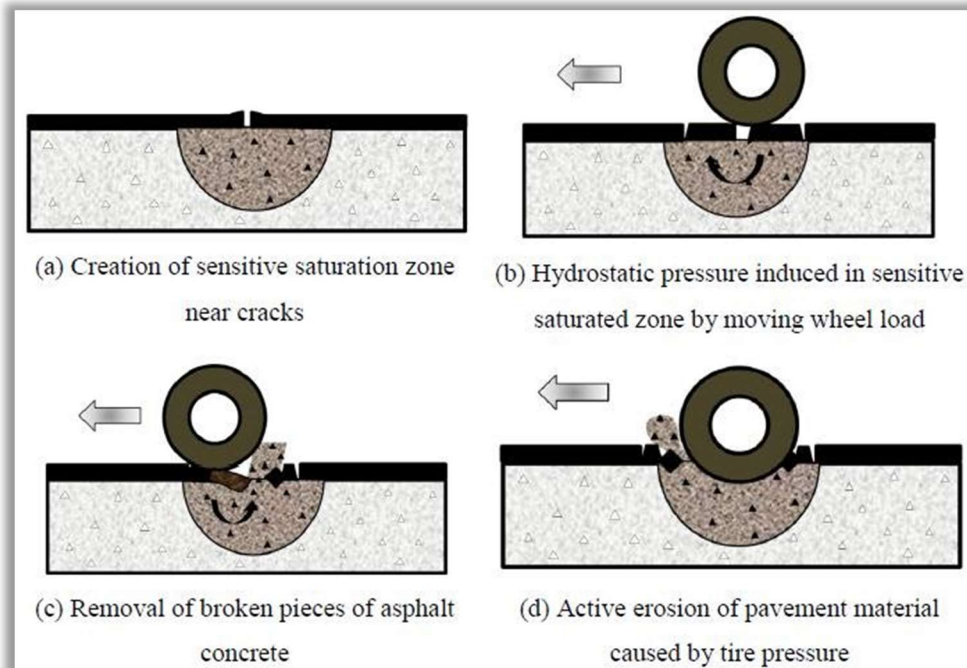


Figure 1: Pothole formation sketch [14].

### 3 Different Repair Methods

Due to the need to be constructed from time to time the maintenance and repairing of potholes remains to be a severe problem. In suburban and rural areas, pothole maintenance is very rarely done because of the availability and cost of the maintenance. With the intense growth in the construction industry along with the population, the management of waste material has become a major problem for most of the world where a large amount of plastic waste is generated and disposed of in the environment due to the non-degradation property of plastic it would remain as a part of the environment forever causing pollution. Therefore, it is the current need of the country to utilize the waste plastic in road projects. At the same time, the upgradation of roads that takes place due to the spreading of the road network causes the insufficiency of the original materials, simultaneously the waste produced from the demolition of the old structure is also disposed of in the countryside contributes to the increment of land pollution along with traffic congestion. On the bright side, this waste can be used in pavements as the replacement of fillers and aggregates with better performance.

The addition of recycled mixture in bitumen for the maintenance activities like repair of potholes reveals a greater efficiency in Improving the mixtures and saving cost. It was established after the study of the recycled materials that the recycled asphalt mixtures are preferable due to their reasonable performance and affordability as compared to the mixtures that are composed of conventional asphalt [6]. Commonly, the use of recycled materials in Hot Mix Asphalt is preferred due to the benefits in regard to environmental sustainability. In alternative to the in aggregate, pavements, made of recycled aggregate, is also cost-effective [7]. In the SBDP pothole interface, the use of ultra-thin asphalt overlay UTAO along with NWF, that is the non-woven fabric, can help in the mitigation of the stresses that are in a horizontal state [8]. In a research study done on the poly ethylene plastics that were used as 10%, 8%, 6% and 4% admixtures in bitumen, and it was found out that the optimum results were achieved at 8% for mix. Similarly, the demolished waste was used in replacement for the original aggregate. During the aggregate tests it was found that the demolished aggregate has the capacity to be used in the village roads and district roads [9]. In another study that was performed to compare the properties of cold mix asphalt with a mixture of waterborne epoxy and Styrene-Butadiene rubber asphalt, it was found that the later gave bright results in terms of forming strength, excellent in initial strength, low temperature construction workability, high temperature stability, low temperature crack resistance, and water stability [10].

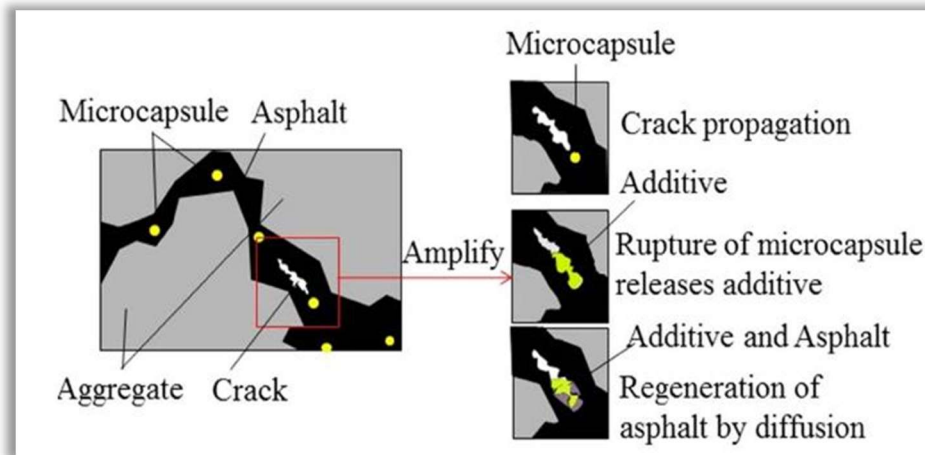


Figure 2: Microcapsule-based self-healing technique [11].

An advanced technique for the prevention of crack propagation that leads to the formation of potholes is the use of microcapsules as shown in figure 1. The healing capsule moves under siphoning action towards the micro-cracks then the catalyst in the asphalt mixture polymerizes this capsule hence filling the crack and making a micro crack bond [11]. When the cracks propagate, they initiate the ignition of microcapsule by rupturing it hence releasing the additive which diffuses with the concrete to seal the crack. When used from 0-0.9% by weight of bitumen at different ratios of air voids it showed good results by decreasing the moisture susceptibility and enhancing the properties of bitumen of asphalt mixtures. Using the Nano silica at every content of air void improved the resistance to moisture [12]. Nanocomposite along with granite and limestone aggregates to test its resistance to stripping. It was seen that the resistance to pothole formation was greatly improved along with the increase of resistance of hot mix asphalt using these admixtures combined [13].

#### 4 Selection of sustainable method

The pavement system uses a substantial amount of resources, which results in the degradation of the environment. To reduce the consumption of pavement construction materials it is very significant to understand the environmental impacts, for proper and effective decision making and for designing sustainable pavements. Hence it is very important to select materials that are environmentally friendly and have better durability and reliability as compared to conventional materials [15]. An overview of the different pothole materials has been provided in table 1 which shows that synthetic binder has more functionality towards damage as compared to conventional repair methods. In this table each type of applied binder has been divided on the basis of application and composition i.e. hot applied, cold applied, and synthetic binder. These binders have been further divided on the basis of durability, equipment used for laying, the limitation for application, environment required for application, their possibility of recycling, and distress type that is mostly experienced in that type of binder.

Table 1 Pot hole repair materials overview on material type basis [15]

	Hot applied asphalt	Cold applied asphalt	Cement	Synthetic binder
Est. durability	Cat I, Cat II, Cat III	Cat I, Cat II	Cat I, Cat II	Cat I, Cat II, Cat III
Equipment	Comprehensive	Limited	Limited	Limited
Application limitation	None	None	Pothole<1/2m dia	Temp >10 deg celsius
Working environment	Special education	None	None	Special education
Possibility of recycling	Yes	Yes	No	No
Type of distresses	Adhesion failure cracks in repair, immersed chipping	Fretting, Loss of material	Adhesion failure, Cracks in repair	Loss of material, loss of chippings, pavement cracks, Cracks in repair



The selection of most sustainable option and the best available option is required for the maximum welfare. Using the state of the art techniques for sustainability the service life of the flexible pavements can be extended using maintenance strategies [16]. If the maintenance budget is increased 2% to account for sustainable maintenance decisions like full-depth repair, cold in-situ recycling, whose emission of greenhouse gasses is lower than other options. It has also been observed that micro surfacing and functional asphalt overlay are more feasible options when there are low financial restrictions [17]. Flexible pavements require periodic maintenance ultimately causing the cost of life cycle to increase [18]. Hence, considering all these aspects three materials can be short listed, the use of waterborne epoxy would be a suitable selection in this case as it gives very fine results in terms of performance but due to its excess cost this admixture cannot be recommended, using synthetic binders have also better results and comparatively are low cost. The use of ultra-thin asphalt overlay UTAO along with NWF, that is the non-woven fabric, can be considered the best option for pothole repair.

## 5 Practical Implementation

With the increasing rates of materials and the maintenance cost it is the need of the hour to identify techniques that can result in more durable pavements requiring low maintenance. The national highway authorities need to be educated in this regard. Moreover, the wastage of material is of great concern that needs to be looked into. With this study being done the modern methods and materials that have been discussed in this article can be implemented practically. To ensure efficient performance, guidelines provided by the authors should be taken into consideration by the development authority and the techniques should be first applied to small sections of roads and continuous monitoring of that section will be required to confirm the real time performance of the applied technique. Moreover, developing societies should use these modern methods for local streets mainly as the traffic load on these streets is not much. As already mentioned that the cost of the waterborne epoxy is more and it is not economically viable solution for pothole, as compared to this technique the use of UTAO used with non-woven fabric is a sustainable method for repairing potholes. The thin overlay reduces the cost, and also helps sealing cracks that have very minimum width hence stopping cracks to propagate any further. Due to their property of penetration, higher softening point, good ductility this material can be considered fit for pothole repair.

## 6 Conclusion

The environmental sustainability of the pavement systems can be enhanced by the use of environmentally friendly and recycled materials. The findings of this review article provide valuable information that can be helpful in the selection as well as the design of pavement structures that are sustainable, mainly in regions which are highly urbanized and has scarce resources. Following are the conclusions drawn from the literature study.

1. Pavement deterioration and other pavement distresses are mainly the cause of potholes.
2. Pothole is affected by many factors this includes aggregate type, mix design, asphalt binder type, variation in temperature, method of construction, traffic loads, sensitive saturation zone, and accumulation of water.
3. The cheapest and most sustainable type of repair solution is the use of hot mix asphalt with the addition of waste material.
4. The current trend regarding Pothole formation is bent towards sustainability and specifically, the use of waste materials as additives.
5. The film thickness of the asphalt binder is one of the significant factors that affects the resistance to crack formation. Hence, increasing the film thickness of asphalt around the aggregate surface along with some filler material can enhance the life of pavements.
6. Use of microcapsule self-healing technology is also an effective way of avoiding pothole formation.

On the basis of the conclusion drawn from the literature, it can be said that the main cause of pothole formation is actually other distresses that include alligator cracking, raveling, longitudinal and transverse cracking and, mainly water infiltration that expands and contracts with the variation of temperature. Once a particle from the surface is displaced all other particles in the vicinity become vulnerable hence leading to pothole formation. Hence using strategies that reduce the chances of





crack formation will actually reduce the probability of pothole formation.

## Acknowledgment

The authors would like to acknowledge the help received from teachers, especially Dr. Majid Ali. The help received from our parents is also greatly acknowledged. The careful review and constructive suggestions by the anonymous reviewers are gratefully acknowledged.

## References

- [1] Y. Yang, Z. Qian, X. Song, A pothole patching material for epoxy asphalt pavement on steel bridges: fatigue test and numerical analysis, *Constr. Build. Mater.* 94 (2015) 299–305.
- [2] Q. Dong, B.S. Huang, S. Zhao, Field and laboratory evaluation of winter season pavement pothole patching materials, *Int. J. Pavement Eng.* 15 (4) (2014) 279–289.
- [3] Oshone, M., Dave, E. v., & Sias, J. E., Asphalt mix fractures energy-based reflective cracking performance criteria for overlay mix selection and design for pavements in cold climates. *Construction and Building Materials*, 211 (2019) 1025–1033.
- [4] Kanoungo, A., Sharma, U., Goyal, A., Kanoungo, S., & Singh, S. (2021). Assessment of Causes of Pothole Development on Chandigarh Roads. *Journal of The Institution of Engineers (India): Series A*, 102(2), 411-419.
- [5] Rahiman V, A. (2021). Pothole Detection and Volume Estimation Based on Disparity Transformation with Histogram Thresholding.
- [6] AlKheder, S. (2022). Environment-friendly recycled asphalt pavement design for road maintenance applications. *Environment, Development and Sustainability*, 1-25.
- [7] Durrani, A. (2021). nalysis of Reclaimed Asphalt Pavement (RAP) Proposed for Use as Aggregate in Microsurfacing and Chip Seal Mixes for Local Roadways Applications in Ohio.
- [8] Chen, L., Liu, G., Zhang, X., & Pan, G. (2021). An innovative interface reinforcement method for steel bridge deck pavement pothole repair. *Construction and Building Materials*, 298, 123838.
- [9] Singh, J. (2021, November). Durability of potholes filled with waste materials. In *IOP Conference Series: Earth and Environmental Science* (Vol. 889, No. 1, p. 012056). IOP Publishing.
- [10] Zhang, W., Zhang, Z., & Zhao, Q. (2022). Laboratory Performance Evaluation of a Waterborne Epoxy-Modified Asphalt Mixture with Styrene-Butadiene Rubber for Cold Patching Applications. *Journal of Materials in Civil Engineering*, 34(6), 04022111.
- [11] Mirabdolazimi, S. M., Kargari, A. H., & Pakenari, M. M.. New achievement in moisture sensitivity of Nano-silica modified asphalt mixture with a combined effect of bitumen type and traffic condition. *International Journal of Pavement Research and Technology*. 2020, 14, 105–115.
- [12] Yan, C., Huang, W., Zheng, M., Zhang, Y., & Lin, P.. Influence of ageing on high content polymer modified asphalt mixture stripping, cracking and rutting performances. *Road Materials and Pavement Design*. 2021, 22(8), 1824-1841.
- [13] Golestani, B., Moghadas, F., Saeed, S., & Galooyak, S.. Performance evaluation of linear and nonlinear Nano-composite modified asphalts. *Construction and Building Materials*. 2012. 35, 197–203
- [14] Dhali, M. K., & Biswas, M. (2019). MCA on mechanism of river bed potholes growth: a study of middle Subarnarekha River basin, South East Asia. *Environment, Development and Sustainability*, 21(2), 935-959.
- [15] Hajj, R., & Lu, Y. (2021). *Current and Future Best Practices for Pothole Repair in Illinois*. Illinois Center for Transportation/Illinois Department of Transportation.
- [16] Scope, C., Vogel, M., & Guenther, E. (2021). Greener, cheaper, or more sustainable: Reviewing sustainability assessments of maintenance strategies of concrete structures. *Sustainable Production and Consumption*, 26, 838-858.
- [17] Torres-Machi, C., Osorio-Lird, A., Chamorro, A., Videla, C., Tighe, S. L., & Mourgues, C. (2018). Impact of environmental assessment and budgetary restrictions in pavement maintenance decisions: Application to an urban network. *Transportation Research Part D: Transport and Environment*, 59, 192-204.
- [18] Hamim, O. F., Aninda, S. S., Hoque, M., & Hadiuzzaman, M. (2021). Suitability of pavement type for developing countries from an economic perspective using life cycle cost analysis. *International Journal of Pavement Research and Technology*, 14(3), 259-266.
- [19] Shrivastava, A., Srivastava, D. K., & Shukla, A. (2023). Review of Road Pothole Detection Using Machine Learning Techniques. In *Information and Communication Technology for Competitive Strategies (ICTCS 2021)* (pp. 95-104). Springer, Singapore.
- [20] Zhang, Z., Zhang, H., Lv, W., & Yang, Y. (2022). Road performance of waterborne unsaturated polyester concrete cold patching materials for potholes in bituminous pavement. *Construction and Building Materials*, 348, 128689.



# RUTTING-DENSIFICATION MITIGATION MEASURES FOR PAVEMENTS OF PAKISTAN-SUSTAINABLE WAY FORWARD

<sup>a</sup> *Ammad Hassan Khan\**, <sup>b</sup> *Zia ur Rahman*, <sup>c</sup> *Saeed Ahmad*

a: Department of Transportation Engineering, University of Engineering & Technology Lahore, chair-tem@uet.edu.pk

b: Department of Transportation Engineering, University of Engineering & Technology Lahore, gzia718@uet.edu.pk

c: Department of Transportation Engineering, University of Engineering & Technology Lahore, 2016te28@student.uet.edu.pk

\* Corresponding author: Email ID: [chair-tem@uet.edu.pk](mailto:chair-tem@uet.edu.pk)

**Abstract-** The concept of having layers in flexible pavement is to sustain and distribute the heavy traffic load of the vehicles to the subsequent layers. Due to insufficient compaction of the asphalt concrete, the surface layers (wearing and base) continue to densify under loads resulting in the rutting densification. Rutting in the pavement considerably reduces the service life. For this purpose, different factors resulted into insufficient compaction of pavements in Pakistan need to be identified. Mitigation measures for rutting densification are required to be proposed for improvement of pavement life-cycle. Roads exhibiting rutting-densification were identified. Core samples of asphalt concrete surface layers (wearing and base) were collected from the roads. Density of these core samples were determined and compared with volumetric of mix design adopted during construction. The laboratory samples were prepared in accordance with volumetric of the extracted road core samples. These samples were tested in wheel tracking machine for determination of the rut-depth. Rutting depth determined in laboratory is compared with actual field data of rutting. Results indicate that NHA class B is 43% more susceptible to rutting than NHA class A. Effects of different factors like mix volumetric, aggregates shape, and asphalt content etc. on laboratory and field rutting were evaluated. Necessary mitigation measures to control rutting densification phenomenon for future sustainable pavements in Pakistan are also proposed.

**Keywords-** mitigation, pavements, rutting densification, sustainable

## 1 Introduction

The design of pavements should be such that it must withstand the stresses against axle loads, moisture change and environmental temperatures. The design of pavements should also meet the major distresses like rutting, fatigue, cracking etc. acceptance criteria. Pavements should have sufficient skid resistance for the smooth movement of the vehicles. The elastic modulus is the parameter which reflects the densification of asphalt mix. Densification of asphalt mix is a function of aggregates, asphalt mixing methodology, asphalt mix volumetric, field preparation and compaction, temperature and moisture damage etc. inappropriate/insufficient densification of asphalt mixes lead towards rutting in surface course as shown in Figure 1. Rutting is the most important type of distress occurred during the life cycle of the pavement. Therefore, it is desirable to minimize the rutting. Rutting normally occurs in three types as shown in Figure 1. Rutting densification majorly observed in the top of Asphalt concrete pavements. Asphalt concrete pavements have shown variations in the performance so there is a need to correlate the asphalt concrete properties to the pavement performance. (Rizvi, Khan et al. 2021).

Rutting is the load related distress. Although all the pavement layers (base, subbase, subgrade) contribute to rutting but the contribution of asphalt concrete layer towards rutting is very significant. The pavement network in Pakistan experiencing premature rutting in asphalt concrete layer. The structural design of pavements is based primarily of the



empirical relationships developed through research and field experience. Today the design methodologies for the flexible pavement falls in two categories, empirical and mechanistic-empirical. Main aim of both these design considerations is to limit the horizontal tensile strain at the bottom of asphalt layer to limit fatigue cracking and to limit the vertical compressive strain at the top of subgrade to prevent rutting. Extensive rutting lead towards structural failure of pavement and cause serious issues like hydroplaning. Rutting in the asphalt concrete layer is generally due to the lateral distortion and shear deformation.

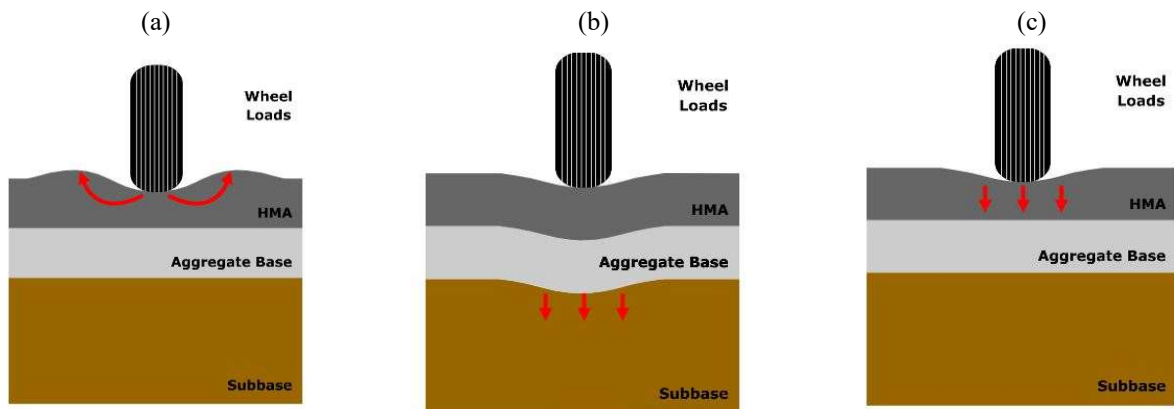


Fig 1: Rutting types a) mix rutting b) subgrade rutting c) densification Source: <https://pavementinteractive.org/>

Asphalt rutting is the permanent deformation in the wheel path in the longitudinal direction on the surface of the pavement due to repeated application of heavy vehicles. The main causes of asphalt rutting is plastic deformations due to the exposure of moisture in the mix design, traffic consolidation and stripping of asphalt. Asphalt rutting negatively effects the life cycle of pavement. The main reason of asphalt rutting is change in temperature of environment, stiffness of mix design and increase in traffic loads. Rutting mostly occurs at high temperature and low frequency loading. Rut depth and width is also affected by thickness of HMA layer, material quantity, traffic loads and environmental condition. There are three stages for the development of rut in the asphalt layer. Initial, intermediate, and final stages according to load repetitions. In the initial stage, the densification occurs at a very fast rate primarily due to consolidation (volume change). In the intermediate stage, the constant rutting occurs throughout the life of the pavement. In the final stage, accelerated rutting occurs primarily due to shear deformation (plastic flow).

When densification occurs in HMA layer the aggregate rearrange themselves result in the decrease in air void content when densification increases with time and traffic the stability of the mix increased due to which the rate of rutting decreased. This is called strain hardening. Generally, the void content in newly constructed HMA pavement is 7% which reduces considerably (3-5%) in a period of two years. At that point the density of the mix is called ultimate density (at which the shear deformation is usually optimized for meeting the demands of traffic). The factor affecting the ultimate density are degree of initial compaction, material Properties, mix design, weather conditions, traffic, HMA thickness[16]

Pavement sustainability is defined as pavement having longer life, good reliability, minimum acceptable life cycle cost and environmental impacts. The failure of pavement earlier than design life is common problem. We lack in best practices and lesson learnt from the design and construction of the pavement. The current design methodologies of designing flexible pavement are not sufficient to explain sustainability in pavement construction. Sustainable policies are needed for evaluating the pavement in terms of environmental, performance, economic and optimized solution from given alternatives for design and construction. Using local available construction material, recycled use of aggregates and using green technology can contribute to sustainable pavements. The criteria of sustainable pavements are optimizing the use of natural resources, reduce the GHG emissions, reduce air, water and noise pollution and improving health, safety and comfort. Sustainability must be incorporated in every activity from the initial planning to the final phase of the construction. To



prevent rutting the proper mix design methods, workmanship during construction, proper material specifications, proper compaction at the site are necessary.[18]

The most advance technique to reduce rutting is the use of geo-synthetic reinforcement and minimizing the exposure of moisture in the mixture during the construction quality control. The use of open graded, dense graded and stone filled aggregates in the mixture also reduce the rutting considerably [15]. Following are the objectives of the study

- To identify the roads in and around Lahore that exhibit rutting densification
- To evaluate the characteristics of identified roads materials
- To determine rutting of identified road mixes in field and laboratory
- To compare field and laboratory rutting
- To propose suitable measures to reduce rutting densification

## 2 Experimental Procedures

Table 1 presents the summary of tests carried out under the experimental programme.

*Table 1 shows the experimental procedures employed for carrying out this study.*

Sr. No	Test Name	ASTM Designation
1	Sieve Analysis of aggregates	ASTM D6913
2	Loss of abrasion, wear (%)	ASTM C131
3	Plasticity index value	ASTM D4318
4	Softening point	ASTM D36
5	Penetration at 25°C,100 g,5 sec	ASTM D5
6	Penetration of residue % of original	ASTM D5
7	Ductility at 25°C,5cm/min	ASTM D113
8	Ductility of residue at 25°C, 5cm/min	ASTM D113
9	Loss on heating, 163°C, 5 hours (%)	ASTM D6
10	Solubility (%)	ASTM D4
11	Specific Gravity at 25°C	ASTM D792
12	Stability(kg)	ASTM D6927
13	Flow-0.25(mm)	ASTM D6927
14	Voids in mineral aggregates (VMA %)	ASTM D6995
15	Voids in filled with asphalt (VFA %)	ASTM D6995
16	Unit weight (PCF)	ASTM D2726
17	Loss in stability (%)	ASTM D6927
18	Resilient Modulus	ASTM D7369

## 3 Research Methodology

Following methodology was adopted to achieve the objective of study

### *Extensive review of possible reasons of rutting densification across the globe*

Various national and international conference proceedings, journals, books etc. were consulted related to review of literature and existing practices in control of rutting and its necessary remedies. The review of literature reveals that mix design and mix laying are two crucial factors in rutting densification [1-7]. Few noticeable works include [17] indicates that rutting can occur due to softening of base, sub-base and roadbed material. The major reason is the moisture infiltration. Rutting can be countered due to softening of binder at elevated temperatures as well as insufficient construction practices [18]. Rutting can also be encountered due to overloading of vehicles. Due to inadequate structural design of thickness the probability of rutting increases. Rutting generates in asphalt layers due to three mechanisms: loss of materials, densification and lateral plastic flow (or shear-related deformation), of which the shear-related deformation constitutes the majority of current studies associated with rutting.



### ***Selection of pavement conditioning survey criteria for evaluation of rutting densification***

Highway distress identification manual for the long term pavement performance programme criteria was used to describe the rutting. The method described in Figure 2 was used for the determination of the rutting. Straight-edge of 1.2m is placed transversely over the portion of the road where rutting was occurred. The maximum vertical distance from the bottom of the straight edge to the top surface of the pavement is measured with a gauge and is reported nearest millimetre as the rut depth. [19]

Rutting (Overall Condition) (Asphaltic Concrete Pavement)

Slight: Rutting 6.35mm to less than 12.7mm deep.

Moderate: Rutting 12.7mm to less than 25.4mm deep.

Severe: · Rutting 25mm deep or greater

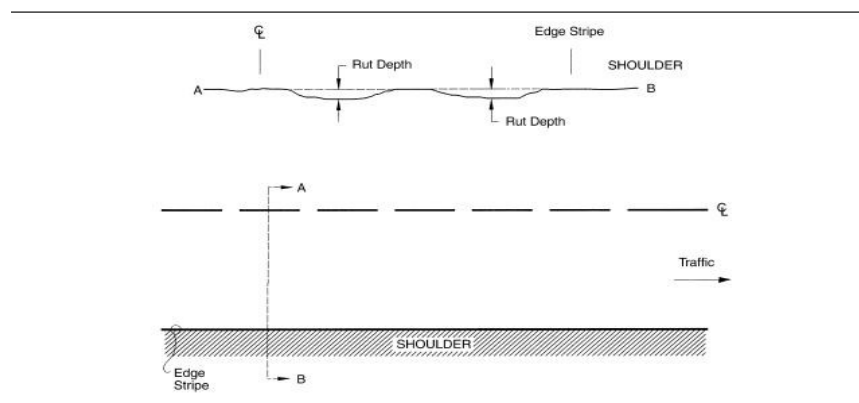


Figure 2: Pavement conditioning survey criteria

### ***Identification of roads prone to rutting densification***

The pavement section selection was accomplished by surveying the routes physically. The main criterion used in this selection is that the selected sections should represent the spectrum of pavement cross section, paving materials and traffic volume. Rut depth of these roads were measured. Inspect, measure and record the extent and severity of rutting. Roads exhibiting rutting were identified and labelled as test site in a survey and described in figure 3.



Figure 3: Identification of roads



### ***Collection of core samples & test pits samples of surface course from rut prone roads***

Core samples of two roads having NHA A class and NHA B class exhibiting rutting were collected and described in figure 4. Cores were obtained by using a power auger equipped with 6/4-inch coring bit. For thin AC layers 6 inch diameter coring bit was used and for thicker layer 4 inch coring bit was used. These produced enough material for testing according to ASTM. Most of the cores obtained from wheel paths were utilized for measurement of bulk specific gravity, layer thickness and extraction testing to determine material properties.



Figure 4: Collection of core samples of rut prone roads

### ***Preparation of laboratory mix samples as per gradations found at roads for wheel tracker tests***

Various laboratory tests were conducted to assess the physical and engineering properties of core materials obtained from the test site. The cores sample size 150mm diameter and 75 mm height may be obtained by compacting to a target height or by sawing one face (which will, subsequently, be the “bottom” face of the test specimen) to desired height. It is not permitted to saw both faces of the specimen to obtain the required specimen height for laboratory evaluation of two sample of NHA class A and NHA class B, samples are prepared in field and described in figure 5.





Figure 5: Preparation of laboratory mix sample

#### ***Performance of wheel tracker test for determination of laboratory rutting of the mixes observed at road***

Laboratory evaluation for the rutting performance is done by performing the wheel tracking test (WTT). Different types of devices were developed to carry out this test under the principle of measuring the permanent deformations that occur in the mixture when it is subjected to a loaded wheel. The rut depth was measured on the sample at 1 min intervals with a linear variable differential transformer (LVDT) as shown in figure 6.



Figure 6: Wheel Tracker Test

#### ***Wheel tracker test:***

The wheel tracking test (WTT) has been widely used as a standard laboratory test to evaluate the rutting resistance of asphalt mixtures. One sample of each NHA class A and NHA class B are prepared. Specimen diameter is 150mm and height is 62mm. Test samples can be in the form of beams or cylinders. Beams are typically compacted with the asphalt vibratory compactor while cylinder samples are typically compacted with the Super pave Gyratory Compactor (SGC). Cylindrical samples compacted to 4-percent air voids and beam samples compacted to 5-percent air voids resulted in wheel tracker laboratory test results that were more closely related to field rutting performance than did cylindrical and beam samples compacted to 7-percent air voids. The system must take rut depth measurements at least every 100 passes of the wheel. Test temperature significantly affects measured rut depths. As test temperature increases, APA rut depths



increase. Samples tested at a test temperature corresponding to the high temperature PG specification better predicted field rutting performance than did samples tested at 6°C higher. Rut depth at every 5000, 10,000, 15,000, 20,000 passes and at the failure of sample is recorded.

#### ***Assessment of possible reasons causing the rutting densification on the roads by comparing the pavement design criteria with actual post construction parameters***

- 1- Traffic consolidation
- 2- Stripping of asphalt
- 3- Improper compaction at site
- 4- Stiffness of mix design
- 5- High temperature

The performance criterion for total permanent deformation is defined in terms of maximum rut depth in the wheel path. Typical maximum rut depth for total permanent deformation are on the order of 7 to 12mm. Design should not exceed HMA rutting level of 10mm within design period.

## **4 Results**

### ***Results of extensive review of possible reasons of rutting densification across the globe***

Rutting is one of the most common distress observed in asphalt mixes. Various factors can contribute towards the propagation of rutting in asphalt mixes. Various agencies described their own criteria's for the identification and evaluation of rutting in asphalt mixes. Asphalt mix inappropriate design and its inappropriate laying in the field using desired resources are the key components that result into rutting-densification of asphalt mixes.

### ***Results of selection of pavement conditioning survey criteria for declaration of rutting densification***

For declaration of rutting densification the procedure described in highway distress identification manual was used as shown in figure 7. Straight-edge of 1.2m is placed transversely over the portion of the road where rutting was occurred. The maximum vertical distance from the bottom of the straight edge to the top surface of the pavement is measured with a gauge and is reported nearest millimetre as the rut depth.

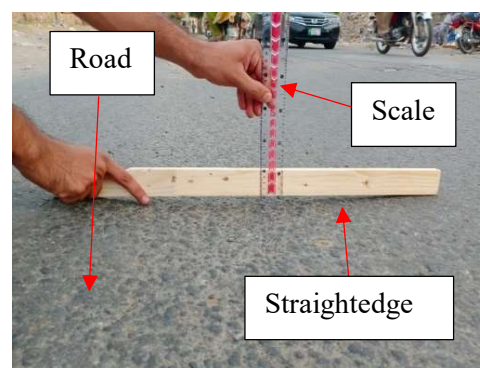


Figure 7: Rutting measurement in accordance with the distress identification manual

### ***Results of identification of roads prone to rutting densification***

Rutting in asphalt layer is caused by combination of volume change and shear deformation due to the application of traffic load. It has been observed that shear portion is more significant than the volumetric one. The major portion of the rutting occurs during initial loading. Using the above described procedure and the material parameters in Tables, the rutting was measured 3mm as measured with 1.2m straightedge as shown in figure 8.



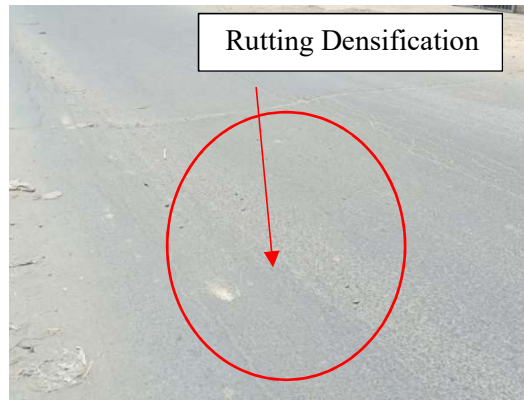


Figure 8: Rutting identification in the field

**Results of collection of core & test pits samples of surface course from rut prone roads**

From NHA class A and B roads cores are collected and tests are conducted on it at binder, aggregate and mix level and results are shown in table 2, 3, 4 and 5.

Table 2: Asphalt test of sample NHA class A & B

Test Parameter	Temperature	Units	Results (NHA Class A)	Results (NHA Class B)	Method
Penetration		-----	63	66	ASTM D5
Penetration of Residue% of original	25°C	%	78	74	ASTM D5,D6
Ductility			Above 100	Above 100	ASTM D113
Ductility of residue	25°C	cm	Above 100	Above 100	ASTM D113,D6
Loss on heating	163°C	%	0.06	0.07	ASTM D6
Solubility	-----	%	99.8	99.70	ASTM D2042
Flash Point	-----	°C	305	298	ASTM D92
Softening Point	-----	°C	46.5	47	ASTM D36

Table 3: Optimum bitumen content of NHA class A & B

Mix Type	Asphalt Wearing Course
Proposed optimum A.C % by Weight of mix (Class A)	4.25 $\pm$ 0.3%
Proposed optimum A.C % by Weight of mix (Class B)	4.0 $\pm$ 0.3%

Table 4: Aggregate gradation of NHA class A & B

Sieve Size	% Passing (NHA Class A)		% Passing (NHA Class B)	
	Obtained	Required Limits (Class-A)	Obtained	Required Limits (Class-B)
1"	100	100	----	----



3/4"	95	95-100	100	100
1/2"	---	---	82	75-90
3/8"	42.50	56-70	70	60-80
No.4	29	35-50	50	40-60
No.8	8.50	23-35	30	20-40
No.16	10	5-12	10	---
No.50	---	---	---	5-15
No.200	5	2-8	5	3-6

Table 5: Asphalt mix properties of sample NHA Class A & B

Test Property	NHA Class A	NHA Class B	Required
	Obtained	Obtained	
Stability(kg)	1106	1063	1000 min
Flow-0.25(mm)	13	12.5	8-14
Voids in mineral aggregates (VMA %)	15.5	15.25	12-20%
Voids in filled with asphalt (VFA %)	73.25	72.5	65-75
Unit weight(PCF)	144.41	148.9	Not specified
Loss in stability (%)	13	15	20 max
Resilient Modulus (0.1 sec)	8000 MPa	7000 MPa	5000+
Resilient Modulus (0.3 sec)	6000 MPa	6400 MPa	5000+

#### Comparison of rut depth of NHA class A & B:

Field data of rutting of two roads having NHA class A and B is compared and results are shown in figure 9.

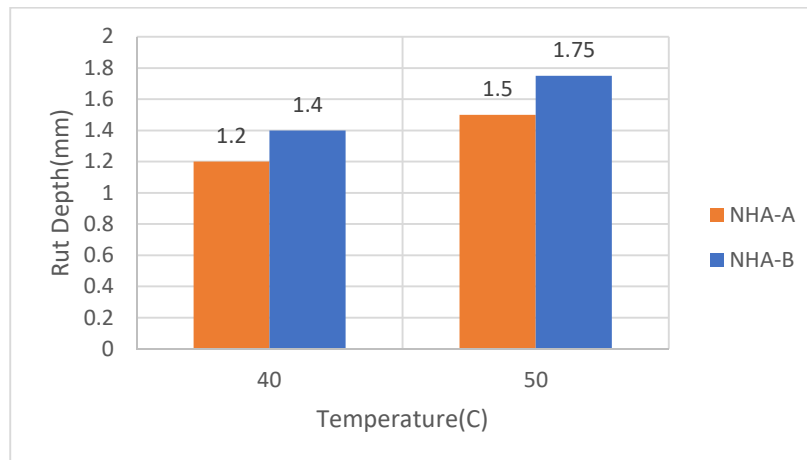


Figure 9: Rut Depth vs. NHA class A and B



## 5 Practical Implementation:

Every year both provincial and federal governments of Pakistan allocate having budgets for rehabilitation overlaying and improvement of roads. This research helps to provide guidelines and database for stockholders engaged in road maintenance and design for optimization of cost and performance.

## 6 Conclusions

Following conclusions may be drawn from the finding of this research.

- It was observed during survey that rutting densification was mostly occurred under the wheel path of vehicles. Rutting was observed more pronounced at a distance of 1m from centerline and edge on both sides of 6m wide under study city roads. The roads where asphalt wearing course was laid with asphalt mix designation NHA B exhibited 43% more rutting than roads laid with NHA A mixes under almost comparable traffic loading.
- Resilient modulus is the most important characteristics of asphalt mix material to control the rutting densification. NHA class A having resilient modulus 8000MPa at 0.1 sec is greater than the resilient modulus value of NHA class B having value 6000 MPa at 0.1 sec (25%greater). NHA class A having resilient modulus 7000MPa at 0.3 sec is greater than the resilient modulus value of NHA class B having value 6400 MPa at 0.3 sec (9%greater).
- The major reasons contributing towards rutting densification can be ranked as below
  - Overloading of vehicles
  - Maintenance issues
  - Non-adoption of performance mixes
  - Lateral movement of material
  - Softening of base, sub-base due to moisture infiltration

To prevent rutting the proper mix design methods, workmanship during construction, proper material specifications, proper compaction at the site are necessary. The most advance technique to reduce rutting is the use of geo-synthetic reinforcement and minimizing the exposure of moisture in the mixture during the construction quality control. The use of open graded, dense graded and stone filled aggregates in the mixture also reduce the rutting considerably.

## References

- [1] Aman, M. Y., Alnadish, A. M., Rohani, M. M., Danial, D. B., & Tahir, M. M. (2020, May). Effect of the Densification of the Reinforced Asphalt Mixtures on the Permanent Deformation. In *IOP Conference Series: Earth and Environmental Science* (Vol. 498, No. 1, p. 012027). IOP Publishing.
- [2] Archilla, A. R., & Madanat, S. (2000). Development of a pavement rutting model from experimental data. *Journal of transportation engineering*, 126(4), 291-299.
- [3] Allen, D. L., & Deen, R. C. (1980). Rutting Models for Asphaltic Concrete and Dense-Graded Aggregate from Repeated-Load Tests.
- [4] Barroso, L. X., de Rezende, L. R., & de Farias, M. M. (2019, March). Study of the relationship between the aggregates gradation, binder properties and densification indexes for an asphalt concrete rutting resistance. In *5th International Conference on Road and Rail Infrastructure*.
- [5] Behiry, A. E. A. E. M. (2012). Fatigue and rutting lives in flexible pavement. *Ain Shams Engineering Journal*, 3(4), 367-374.
- [6] Button, J. W., Perdomo, D., & Lytton, R. L. (1990). Influence of aggregate on rutting in asphalt concrete pavements. *Transportation Research Record*, (1259).
- [7] Coleri, E., Harvey, J. T., Yang, K., & Boone, J. M. (2012). A micromechanical approach to investigate asphalt concrete rutting mechanisms. *Construction and Building Materials*, 30, 36-49.
- [8] Emmanuel, O. E., & Dennis, B. E. (2009). Fatigue and rutting strain analysis of flexible pavements designed using CBR methods. *African Journal of Environmental Science and Technology*, 3(12), 412-421.
- [9] Ford Jr, M. C., & Ford Jr, M. C. (1988). *Pavement densification related to asphalt mix characteristics* (No. 1178).
- [10] Huang, J., & Sun, Y. (2020). Effect of modifiers on the rutting, moisture-induced damage, and workability properties of hot mix asphalt mixtures. *Applied Sciences*, 10(20), 7145.
- [11] Hu, S., Zhou, F., & Scullion, T. (2011). Development, calibration, and validation of a new ME rutting model for HMA overlay design and analysis. *Journal of Materials in Civil Engineering*, 23(2), 89-99.



**4<sup>th</sup> Conference on Sustainability in Civil Engineering (CSCE'22)**  
Department of Civil Engineering  
Capital University of Science and Technology, Islamabad Pakistan



- [12] Javilla, B., Fang, H., Mo, L., Shu, B., & Wu, S. (2017). Test evaluation of rutting performance indicators of asphalt mixtures. *Construction and Building Materials*, 155, 1215-1223.
- [13] Kandhal PS, Mallick RB. Effect of Mix Gradation on Rutting Potential of Dense-Graded Asphalt Mixtures. *Transportation Research Record*. 2001;1767(1):146-151. doi:10.3141/1767-18
- [14] Stroup-Gardiner, M., Newcomb, D. E., Olson, R., & Teig, J. (1997). Traffic densification of asphalt concrete pavements. *Transportation research record*, 1575(1), 1-9.
- [15] Tarefder, R. A., Zaman, M., & Hobson, K. (2003). A laboratory and statistical evaluation of factors affecting rutting. *International Journal of Pavement Engineering*, 4(1), 59-68.
- [16] Zhang, Y., Ling, M., Kaseer, F., Arambula, E., Lytton, R. L., & Martin, A. E. (2022). Prediction and evaluation of rutting and moisture susceptibility in rejuvenated asphalt mixtures. *Journal of Cleaner Production*, 333, 129980.
- [17] Roy-Chowdhury, A. B., Saleh, M. F., & Moyers-Gonzalez, M. (2022). Finite element modelling of permanent deformation of hot mix asphalt tested in the Modified Wheel Tracker (MWT). In *Eleventh International Conference on the Bearing Capacity of Roads, Railways and Airfields, Volume 2* (pp. 497-507). CRC Press.
- [18] Rizvi, M. A., et al. (2021). "Evaluation of Linear Deformation and Unloading Stiffness Characteristics of Asphalt Mixtures Incorporating Various Aggregate Gradations." *Sustainability* **13**(16): 8865.
- [19] Perera, R. W., Kohn, S. D., & Rada, G. R. (2008). *LTPP manual for profile measurements and processing* (No. FHWA-HRT-08-056).



# SMART AND SUSTAINABLE BRIDGE ABUTMENTS - A CASE STUDY

<sup>a</sup> Gaia Corelli, <sup>b</sup> Paula Hidalgo Manrique, <sup>c</sup> Furqan Qamar\*

a: WSP UK,

b: WSP UK

c: WSP UK

\* Corresponding author: Email ID: [furqan.qamar@wsp.com](mailto:furqan.qamar@wsp.com)

**Abstract-** The use of off-site manufactured (OSM) elements is increasing in the Construction industry due to its benefits in terms of cost, site labour and speed of construction. It is commonly acknowledged that off-site production also offers other advantages, that are less evident, but still bring significant improvements on both Health & Safety and Sustainability if compared to more traditional in-situ construction methods. The aim of this paper is to explain how the design and use of OSM reinforced concrete abutment panels contributed to a smarter delivery of the A34 new Overbridge in Perry Barr, Birmingham, UK. After describing the site and project specific constraints, the paper shows the options considered for the new bridge abutments in the early design stages and the factors that contributed to the final choice. Details of the definitive solution are then illustrated with a focus on Health & Safety and Sustainability improvements. The paper then highlights a few key aspects that were considered in the design to ensure accurate production in the factory and efficient assembly on site for the abutment panels. The conclusion then summarises the direct and indirect savings and benefits that the use of OSM abutment panels brought to the project.

**Keywords-** off-site manufactured (OSM), bridge abutments, embodied carbon, sustainability.

## 1 Introduction

Modern methods of construction describe different techniques of industry which differ significantly from traditional construction approaches [1,2]. These new techniques include various concepts like novel construction, off-site manufacturing, and pre-fabrication [3]. All these techniques provide opportunities of continuous improvement in the processes of construction industry. This results in reduction of waste and offers improvement in sustainability indicators. Offsite manufacturing includes manufacture and preassembly of elements before execution on a site and is considered as one of the techniques of modern methods of construction [5]. In the study by Davies, 2013[4], it was described how the lack of repetition of end products in the construction industry as compared to other sectors makes off site manufacturing more challenging. There are many benefits of OSM technique which include better quality of product, lower costs, faster construction and reduced labour reworks on site [1]. In addition, OSM technique with reduced site activities also helps to overcome restrictions associated with difficult sites and reduces wastes up to about 90% [6,7,8].

In this paper a case study is considered to explain the benefits of use of OSM abutment units. The case study is based on design and construction of a new overbridge in Perry Barr, Birmingham, UK. Perry Barr is located approximately 4 miles north of Birmingham city centre. The area covered by this scheme is located along the A34, which is part of Birmingham's Strategic Highway Network and provides a key arterial route from the M6 motorway and Walsall into central Birmingham. The aspiration of Birmingham City Council (BCC) was to deliver a programme of infrastructure improvements at Perry Barr to support regeneration of the area.



In section 2 of this paper, it is explained which methodology was used to decide the geometry of OSM abutment units at design stage. Then in the following section, the outcome of final geometry for OSM abutment units is discussed. In the last section, benefits of use of novel OSM abutment units are concluded.

## 2 Challenges

Implementation of OSM techniques as compared to conventional form of construction poses many challenges. In this case study for a new overbridge in Perry Barr, there were a number of constraints. These included construction of bridge foundations in close proximity to existing structures, strict traffic management restrictions and a tight construction programme. The new bridge had to be designed and subsequently constructed within the limited area enclosed by two existing overbridges and retaining structures. Most of the construction works also had to be undertaken while the junction was operating as per BCC requirements and only occasional lane closures were allowed. Figure 1 below shows a photograph that was taken during the OSM abutment units installation.

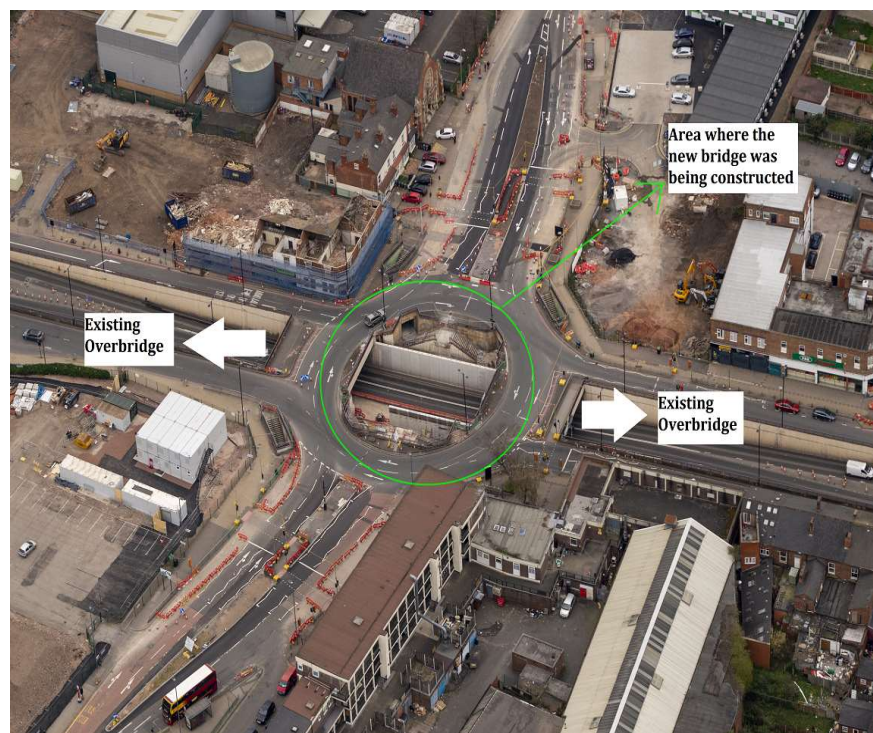


Figure 1 – Construction site for the new overbridge.

During the Design & Build tender process, in-situ reinforced concrete (RC) abutments on piled foundations had been considered because of the limited information available. During detailed design, on availability of more information, options for OSM abutment units were explored. The key driver for this was the need for ease and speed of construction on one side, and the will to provide a sustainable and innovative solution. The final proposal for the new bridge abutments consisted of OSM RC leaf abutment panels. The original abutments were 1.20m thick and required a series of in-situ concrete pours, while the panels were slimmer and totally precast, which was an added value as they could save time and eliminate risks associated with fixing rebar and concrete casting. As the abutment stiffness is key in the load distribution of integral bridges, a reduced 0.50m thickness was investigated by implementing a preliminary 2D frame model. The subsequent ideas of backfilling the substructures with no-fines concrete and using a void former at the back of the abutments to create a gap also helped reduce the horizontal pressure in favour of a 0.50m thickness.

To finalise the geometry of the OSM abutment units and to decide their width, two main aspects were considered. These included limiting the self-weight of any element to 23 tonnes, due to site lifting constraints, and the type of superstructure, which consisted of 25no. MY5 prestressed beams with 150 mm solid deck cover slab. Figure 2 shows the geometry of a standard unit of pre-cast abutment.

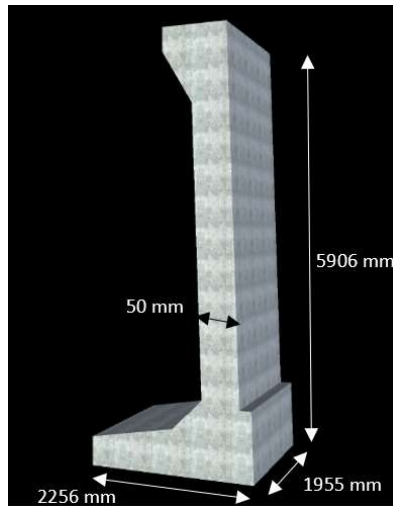


Figure 2 – Pre-cast abutment, standard unit.

As expected, the revised abutments type reduced the amount of moment being transferred to the foundations because a lower stiffness attracts less moment. At that point it was decided to evaluate spread foundations as opposed to piled foundations, since the existing bridges, adjacent to the new structure, sit on spread foundations, suggesting good ground conditions. It was also found that contemporary photos, originating from construction in 1961, show rock cuts in the existing ground and confirming suitability. Spread foundations would be cheaper, quicker to build and less disruptive, hence more sustainable. In Table 1 and accompanying Figure 3, key challenges encountered in the selection of OSM abutment units' spread foundation and resolutions are listed. Figure 4 shows a 3D view of the new bridge.

Table 1 – Challenges and resolutions to enable use of spread foundations.

Challenge	Our resolution
Keeping the total vertical action acting on the foundation within its middle-third.	<ul style="list-style-type: none"> <li>- It was ensured that bending moment being transferred to the foundations was determined appropriately. By applying a full rotational restraint at the base of 2D frame, the bending moment value was overestimated.</li> <li>- Methods for factoring soil stiffness into Finite Elements (FE) bridge models were found. The method proposed by E.C. Hambly in 'Bridge Deck Behaviour' considered to be suitable and considered.</li> <li>- A sensitivity analysis was carried out by using half and twice the provided Young Modulus.</li> <li>- Values of moment and axial force were used that maximised the eccentricity.</li> </ul>
Bridging over the existing 1830mm sewer pipe with spread foundations.	<ul style="list-style-type: none"> <li>- To ensure spread footings could bridge over the existing 1830mm pipe, an in-situ continuity slab at the back of some precast units over the pipe was considered.</li> <li>- Checks were carried out to assess how many units were required to be stiffened, based on a 2D analysis, to help spreading the load from the superstructure onto the areas either side of the pipe.</li> </ul>

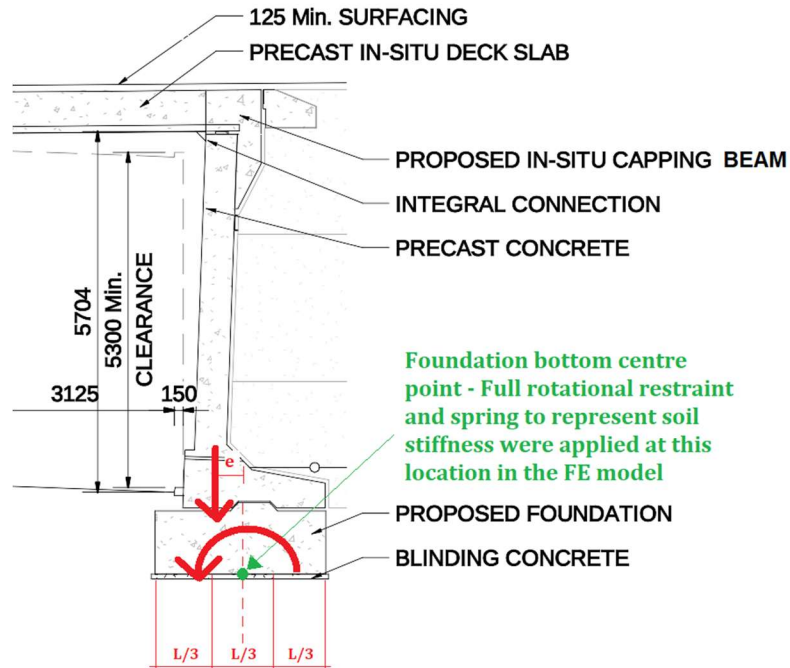


Figure 3 – Main actions being transferred to the foundations.

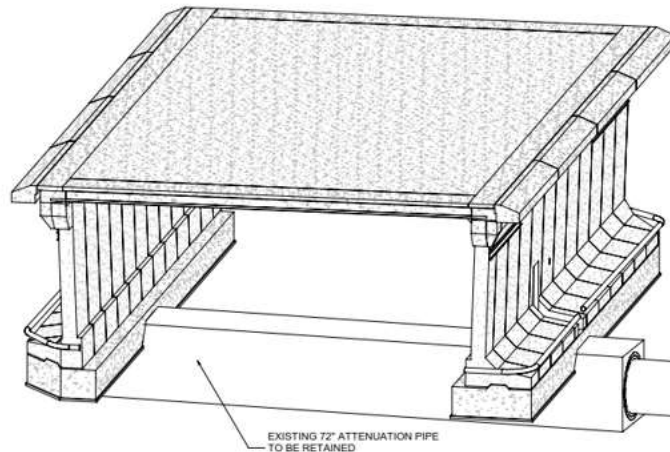


Figure 4 – Bridge Revit model

### 3 Results and implementation

Following continuous engagement with the contractor, understanding of the site constraints and completion of feasibility checks, the geometry of the OSM abutment units was finalised. The width of standard units was 1955mm and the height of all the units was 5906mm.

Considering the constraints within the site area, 4 different types of OSM abutment units were developed:

1. 19no. Type 1 standard units.
2. 1no. Type 2 unit with an opening to retain access to an existing pump room.
3. 2no. Type 3 units with a corbel on the side to fit the width of the bridge deck required.
4. 2no. Type 4 units with a corbel on the side and a tapered base to fit within existing structures.



Figure 5 below shows the position of the different types of OSM abutment units within the new bridge, while Figure 6 summarises the main construction stages for the new bridge.

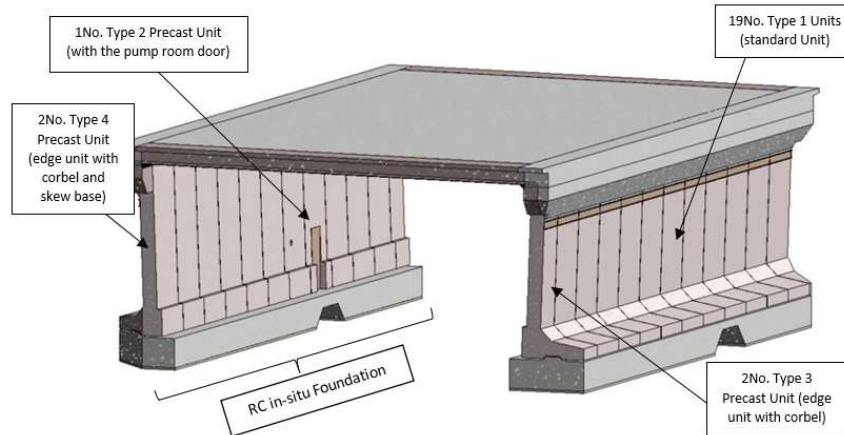


Figure 5 – New bridge, OSM abutment units.

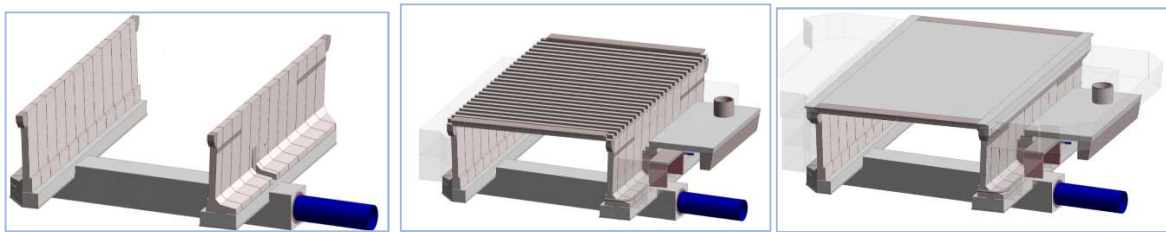


Figure 6 – New bridge, construction stages summary.

The comparison between in-situ concrete abutments and the OSM abutment units was carried out and it was found that the OSM option is a more sustainable solution. They are an environmentally friendly solution, with minimal waste during manufacture and reduced carbon emissions compared to in-situ concrete. Figure 7 shows the comparison between the embodied carbon emissions for traditional in-situ abutments and OSM abutments for the specific case of the new bridge in Perry Barr. In order to determine the carbon footprint for the two solutions, the impact of site machinery, transport to site and labour was considered. Carbon emissions for these three aspects were calculated based on fuel consumption by considering specific mileage for transport and labour and time usage of site machinery.

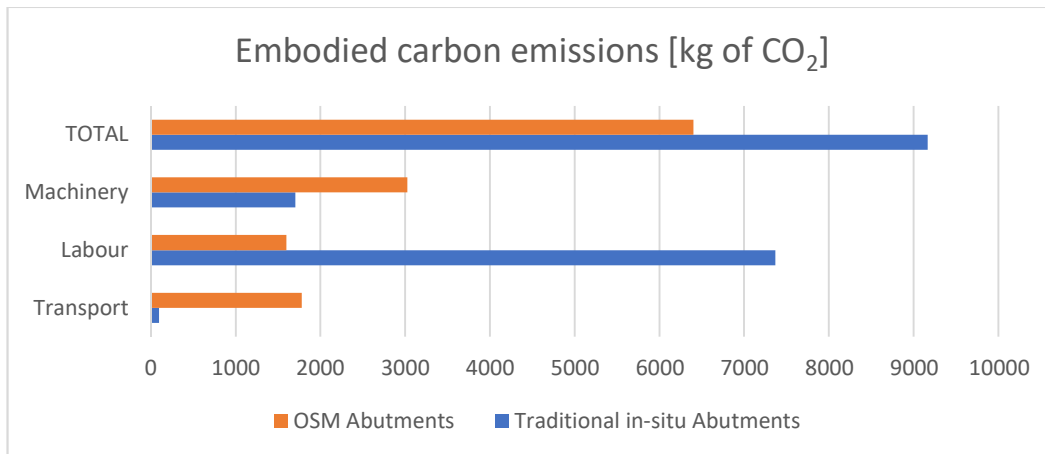


Figure 7 – New bridge abutments, embodied carbon emissions in-situ vs. OSM [Data courtesy of Tarmac]



From a social impact point of view, the time spent in placing these units and disruption to local traffic were considerably less than the ones necessary to cast in-situ concrete abutments. The Contractor had an overall time saving of 2 weeks by using the proposed OSM abutment panels. In addition, the OSM panels were installed within 8 night-time road closures as opposed to the 20-night shifts that would have been necessary for in-situ abutments.

The Health and Safety benefits are also worth mentioning. No site operatives were required to climb down into the layby area to fix rebar cages and work next to live traffic. Risks associated with traffic management were significantly reduced and minimised. On the other hand, the use of OSM abutment units added risks associated to the transport of heavy and large elements. These are however smaller in comparison with the ones that have been eliminated and reduced. In addition, they could be safely managed by competent precast concrete manufacturer and contractor. While OSM elements are generally more expensive to manufacture than equivalent in-situ elements, in this case their use saved significant time. This resulted in labour and traffic management cost savings, which outbalanced the increased manufacturing cost and led to an overall reduced construction cost.

When dealing with OSM elements, the design needs to also focus on production in the factory and installation on site, which are both complex stages for the overall construction process. Supporting the production of high quality OSM elements since design stage is key to minimise waste of resources, optimise timescales, achieve higher quality standards and have a reduced embodied carbon for the asset. In this sense, design approach consisted of:

- Getting early precast manufacturer involvement at preliminary design stage to discuss the construction process and ensure all the parties involved understood the construction sequence.
- Making sure the interface between different structural elements, both precast and in-situ, was clearly and correctly reflected in the new bridge drawing set.
- Ensuring concrete outlines and reinforcement drawings for the precast abutment panels were thoroughly checked by different design engineers and issued to the manufacturer as early as possible.
- Checking the fabrication drawings by the manufacturer and clarifying any doubt on reinforcement detailing before production began.

The described approach enabled the manufacturer to better plan the production of the OSM abutment units and, reduced the chances of having delays to the construction programme. As it is generally acknowledged, precast concrete elements achieve higher quality standards than their in-situ equivalents. This is beneficial for the asset future maintenance, that will likely be reduced for precast elements if compared to in-situ, resulting in an operational carbon reduction. The case study discussed in this paper shows as a collaborative approach between the different parts involved in a scheme can maximise the benefits of using OSM elements.

When it comes to installation of OSM elements on site, generally there are significant benefits in terms of Health & Safety, which have been previously described in this paper. Many common risks related to in-situ reinforced concrete can be eliminated by using OSM elements, on the other hand there are risks which cannot be eliminated and need to be carefully managed. In the case of the new bridge in Perry Barr and the OSM abutment panels, these residual risks were essentially related to the potential instability of the panels during installation and construction. The following measures were adopted to proactively address this hazard and minimise the risk of instability:

- The shape of the panels was designed to be stable on their own during construction.
- Holding down bolts were provided as a further safety measure, in case anything accidentally hit one of the panels during the works.
- A shear key between in-situ foundations and OSM units was provided as a precaution against accidental sliding actions during construction.
- A temporary steel tie at the back of the 3 end units was provided to secure Type 4 units, whose tapered bases would make the 2no. end units unstable if left to stand independently.

Figures 8 to 10 show some key stages of the installation of the OSM abutment panels.



Figure 8 – Installation of OSM abutment panels, preparation [Photo courtesy of Tarmac]

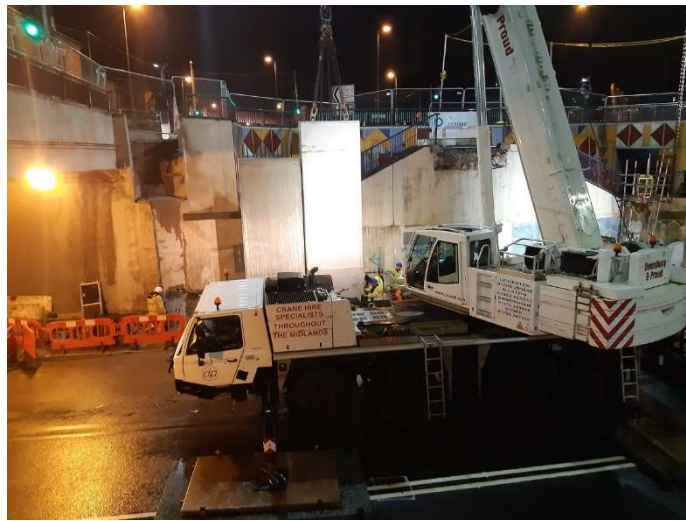


Figure 9 – Installation of OSM abutment panels, panel positioning [Photo courtesy of Tarmac]



Figure 10 – Installation of OSM abutment panels, back view of the panels [Photo courtesy of Tarmac]



## 4 Conclusion

The case study discussed in this paper for use of OSM abutment units presented several challenges at design and construction stages. The application of strong engineering principles together with great construction capabilities ensured the successful delivery of the new bridge in Perry Barr with an innovative type of OSM abutments. The OSM abutment units represent a solution that, compared with traditional in-situ substructures, is safer and more sustainable due to:

1. OSM abutment units having 34% lower embodied carbon footprint for the new bridge as compared to traditional in-situ construction.
2. The Contractor being able to reduce construction time by approx. 2 weeks by using OSM abutment units.
3. Installation of OSM abutment units being carried out in 8 nights as compared to 20-night shifts for traditional in-situ construction, reducing disruption to local communities.
4. The above reduction leading to reduced construction cost.
5. OSM abutment units carrying a reduced number of risks to Health & Safety associated to production and installation.

The results from this case study showed that the use of OSM abutment units offered great benefit as compared to conventional in-situ construction. This technique needs to be considered and developed for other structural elements in the future.

## Acknowledgment

The authors would like to thank WSP UK Ltd (Designer) and Tarmac (Contractor) as Organisations who have given the opportunity to carry out this study. The careful review and constructive suggestions by Jonathon Dickson are gratefully acknowledged.

The careful review and constructive suggestions by the anonymous reviewers are also gratefully acknowledged.

## References

- [1] Goulding, J.S., Arif, M., Pour-Rahimian, F. and Sharp, M.D, "Offsite construction: sustainable innovation futures using SMART approaches proceedings of the CIB world building congress", *Construction and Society Conference*, 2013.
- [2] Goulding, J., Rahimian, F.P., Arif, M. and Sharp, M, "Offsite construction: strategic priorities for shaping the future research agenda", *Architectonica*, Vol. 1 No. 1, pp. 62-73 2012.
- [3] Farmer, M. "Modernise or Die: Time to Decide the Industry's future-The Farmer Review of UK Construction Labour", Construction Leadership Council, 2016.
- [4] Davies, G, "Designing for manufacture and assembly eng". Excellence journal laing o'Rourke, 2013.
- [5] Sean, R.S., Wood, J.B. and Hairstans, R. "Increasing need for offsite construction and manufactured infrastructure in the UK economy", Proceedings of CIAT Symposium, 2015.
- [6] Pinsent Masons (2017), Modular Construction in UK Housing, Pinsent Masons, 2017.
- [7] Jaillon, L. and Poon, C.S, "Design issues of using pre-fabrication in Hong Kong", *Construction Management and Economics*, Vol. 28 No. 10, pp. 1025-1042, 2010.
- [8] Niu, Y., Lu, W., Chen, K., Huang, G.G. and Anumba, C, "Smart construction objects", *Journal of Computing in Civil Engineering*, 2015.



# USE OF MARBLE DUST AS A FILLER MATERIAL IN FLEXIBLE PAVEMENTS

<sup>a</sup> Adil Khan\*, <sup>b</sup> Majid Khan, <sup>c</sup> Shahid Ali, <sup>d</sup> Mubashir Khattak

a: Department of Civil Engineering, University of Engineering and Technology Peshawar, [18pwciv5027@uetpeshawar.edu.pk](mailto:18pwciv5027@uetpeshawar.edu.pk)

b: Department of Civil Engineering, University of Engineering and Technology Peshawar, [majidayubbi@gmail.com](mailto:majidayubbi@gmail.com)

c: Department of Civil Engineering, COMSATS University Islamabad-Abbottabad Campus, [shahid.ali0627@gmail.com](mailto:shahid.ali0627@gmail.com)

d: Department of Civil Engineering, COMSATS University Islamabad-Abbottabad Campus, [mubashir.khattak.52@gmail.com](mailto:mubashir.khattak.52@gmail.com)

\* Corresponding author: Email ID: [18pwciv5027@uetpeshawar.edu.pk](mailto:18pwciv5027@uetpeshawar.edu.pk)

**Abstract-** Pakistan is leading towards a major motorway system. Infrastructure growth especially highways and most of the roads are flexible pavements which have higher susceptibility to Rutting. To overcome this issue we have to find ways to solve these problems. Keeping in view the current economic conditions, one must find material which is cost effective and locally available. One such material is the use of Marble Dust with the replacement of filler material in Flexible Pavements. Therefore different tests were conducted to investigate the effect of Marble Dust, on various Mechanical Properties such as Marshall Stability, Dynamic Stability and Rutting resistance. Marble Dust is cheap and locally available material. The modified asphalt mix were prepared by wet process which involves direct mixing of bitumen (60/70 penetration grade) and Marble dust at a high temperature (160-165°C) followed by aggregates during mixing process. The modified asphalt concrete specimens were prepared with the Marble dust percentages of (1%, 2%, 3%, and 4%). Both modified and un-modified Samples were prepared by Marshall Mix design (ASTM D6926), using NHA Class A gradation. Prior to sample preparation, the bitumen (60/70 penetration grade) and aggregates (Margalla aggregate) were tested to check their compatibility according to the standards of NHA. The optimum binder content (OBC) 4.4% was found using Marshall Mix design (ASTM D6926), which was then used in the preparation of both conventional and modified samples. Performance tests including Marshall Stability, flow, Rutting resistance and Dynamic stability were performed to check performance of modified mixes. The tests results revealed that modified mix containing 50% replacement of filler material with marble dust of the total replacement percentage provides best resistance against rutting and enhances dynamic stability of flexible pavement than the other modified percentages. The whole analysis concluded that replacement of filler material with marble dust gives better results regarding pavement performance.

**Keywords-** National highway authority, optimum binder content, hot mix asphalt, specific gravity

## 1 Introduction

Marble dust production contributes significantly to environmental problems [1]. Normally 25% of marble dust is produced by cutting marble blocks. In the world in many countries, marble dust is settled down by the sedimentation process which is then left in situ and causes the appearance of the environment ugly. It also produces dust which jeopardizes both agriculture and health [2]. The original reason for using marble dust is economy, sustainability, and the advantages offered in terms of the durability of optimum binder content [3]. The marble generation amount is considerable which is in the range 5-6 million tons [4].

Since ancient times, marble has been used as a construction material. As a result, marble waste being a by-product is a very important material that requires appropriate environmental disposal attempts. Marble dust, which is a solid waste material produced mostly from the actions on marble can be used as a filler material in road pavements in the preparation of bituminous concrete [5]. The production of economic and more long-lasting bituminous concrete using marble waste can help the civil engineer profession to ensure the economy in the construction project and rectify the environmental problems. This study aims to evaluate the effect of marble dust as filler material on the strength and stiffness-related



properties of bituminous mixes. Marble dust is the residue that is collected from cutting marble blocks into smaller pieces to achieve the required smooth and aesthetic shape. The waste utilization will not only be economical but may also help in creating a sustainable and pollution-free environment. Leaving the marble dust in an open environment will cause environmental problems. In this study, the rutting resistance of Marble dust modified hot mixed asphalt will be evaluated. The effect of different percentages of Marble dust on the performance of HMA mixtures will also be evaluated and the possibility of using Marble dust as a filler material will also be assessed. The main focus of this study is to find that optimum percentage of marble dust as a filler replacement in HMA with having low rutting and high dynamic stability.

## 2 Research Methodology

### 2.1 Phases of Research

**2.1.1 Phase-1** In this phase of the research, the required material (aggregate and bitumen) was collected from the respective sources.

**2.1.2 Phase-2** Both aggregate and bitumen were then tested to check their quality as per NHA specifications in this phase of the project. All tests were performed in accordance with their respective ASTM/ AASHTO/ BS standards as shown in table 1 and table 2.

**2.1.3 Phase-3** This phase consists of the preparation of Marshall Mix Design. The blending of different sizes (coarse & fine) of aggregate was done to achieve the gradation according to NHA specifications. The bitumen was added to different percentages of 3.5%, 4%, 4.5%, and 5%. For each blend Gmb, Gmm, Marshall Stability, flow, and volumetric properties were determined. The results were then plotted and optimum bitumen content was determined to be used in the design.

**2.1.4 Phase-4** In this phase, the filler material was replaced by marble dust in varying percentages in the asphalt mix, and checked its Gmb, Gmm, stability, flow, and volumetric properties.

**2.1.5 Phase-5** In the last phase of this research project, the performance of HMA was checked for Rutting and Dynamic Stability of the modified and control mixes.

Table 1: Aggregate tests

S.No	Test Name	Standard	Objective
1	Sieve Analysis	ASTM C-136	Helps in obtaining the proportion of different aggregate sizes to be used in Marshall Mix samples.
2	Aggregate Impact Value Test	ASTM D5874-02	This test aims to determine the toughness of aggregates.
3	Los Angeles Abrasion Test	ASTM C 535	This test aims to determine the hardness of aggregates.
4	Aggregate Crushing Value Test	BS: 812	This test aims to determine the crushing value of aggregate.
5	Specific Gravity of Coarse Aggregates	ASTM C127-12	This test is performed to find out the specific gravity by density bottle method.
6	Flakiness & Elongation Test	ASTM D 4791-99	It is performed to determine the percentages of flaky and elongated particles.
7	Liquid & Plastic Limit Test	ASTM D4318 – 17	This test is performed to find out the liquid limit, plastic limit, and the plasticity index of soils.



Table 2: Bitumen and other tests

S.No	Test Name	Standard	Objective
1	Penetration Test	ASTM D5-95	It is used to find the hardness or consistency of bitumen which helps in evaluating the grade of bitumen.
2	Flow & Stability Test	ASTM D6927-06	It is conducted to measure the maximum load experienced by the bituminous material at a loading rate of 50.8 mm/minute.
3	Rutting Resistance	ASTM D2974	A Rutting resistance test is performed to evaluate the deformation that occurs due to heavy traffic with the wheel of vehicles.

### 3 Results and Discussion

Different tests were performed to evaluate the rutting resistance of HMA samples. Results of the tests are given below in table 3.

Table 3: Results of the tests

S.No	Test Name	Result	S.No	Test Name	Result		
1	Sieve Analysis	The final approved JMF is shown in table 4 and it's graph in figure 1	5	Specific Gravity of Coarse Aggregates	Aggregate Size	Specific Gravity	
					3/4 inch	2.66	
					1/2 inch	2.51	
2	Aggregate Impact Value Test	19.52 % (Excellent)	6	Specific Gravity of fine Aggregates	Aggregate Size	Specific Gravity	
					Crushed Sand	2.57	
					Filler	2.40	
3	Los Angeles Abrasion Test	29.06 %	7	Flakiness & Elongation Test	Aggregate Size	Flakiness	Elongation
					3/4 inch	12.44%	7.03%
					1/2 inch	10.31%	8.92%
					3/8 inch	11.67%	10.82%
4	Aggregate Crushing Value Test	19.28%	8	Liquid Limit of filler material & Plastic Limit Test of filler material	Moisture Content	No. of blows	
					35 %	16	
					31%	21	
					24.5%	34	
					5.43%		



Table 4 shows the Job mix formula which determines the contribution of each size of aggregate in the preparation of HMA samples. The upper and lower limit indicates the NHA Class A specifications. HMA samples were prepared according to these specifications and the results are shown in tabular form below.

Table 4: Final approved JMF

Project: Use of Marble dust as a Filler Material in Flexible Pavements															
FINAL APPROVED JMF															
Nominal Maximum Size		19.0 mm										Approved Design Gradation *		NHA Specification Limits Part - 2 - Table 1 b	
stock piles		3/4"		1/2"		3/8"		Crushed Sand		Filler					
Combination Percentages		27.00%		0.00%		27.00%		42.00%		4.00%					
Sieve No.	Sieve Size	Individual stockpile	Percentage	Individual stockpile	Percentage	Individual stockpile	Percentage	Individual stockpile	Percentage	Individual stockpile	Percentage				
inch	mm		27.00 %		0.00%		27.00 %		42.00 %		4.00%		Lower	Upper	
1	25	4.26	100.0%	27.0%	100.0%	0.0%	100.0%	27.0%	100.0%	42.0%	100.0%	4.0%	100.0%	100%	100%
3/4	19	3.76	72.6%	19.6%	100.0%	0.0%	100.0%	27.0%	100.0%	42.0%	100.0%	4.0%	92.6%	90%	100%
1/2	12.5	3.12	5.3%	1.4%	95.0%	0.0%	100.0%	27.0%	100.0%	42.0%	100.0%	4.0%	74.4%		
3/8	9.5	2.75	2.5%	0.7%	74.0%	0.0%	76.4%	20.6%	100.0%	42.0%	100.0%	4.0%	67.3%	56%	70%
No 4	4.75	2.02	0.0%	0.0%	3.1%	0.0%	1.0%	0.3%	100.0%	42.0%	100.0%	4.0%	46.3%	35%	50%
No 8	2.36	1.47	0.0%	0.0%	0.0%	0.0%	0.0%	0.0%	55.0%	23.1%	100.0%	4.0%	27.1%	23%	35%
No 16	1.18	1.08	0.0%	0.0%	0.0%	0.0%	0.0%	0.0%	12.3%	5.2%	100.0%	4.0%	9.2%	5%	12%
No 80	0.18	0.46	0.0%	0.0%	0.0%	0.0%	0.0%	0.0%	7.1%	3.0%	100.0%	4.0%	7.0%		
No 200	0.075	0.31	0.0%	0.0%	0.0%	0.0%	0.0%	0.0%	6.0%	2.5%	43.0%	1.7%	4.2%	2%	8%
Pan	0	0	0.0%	0.0%	0.0%	0.0%	0.0%	0.0%	0.0%	0.0%	0.0%	0.0%			

Following is the graphical representation of JMF as shown in figure 1. The blue line shows upper limits, the orange line shows lower limits of NHA specifications and the yellow line shows the design gradation of HMA samples.

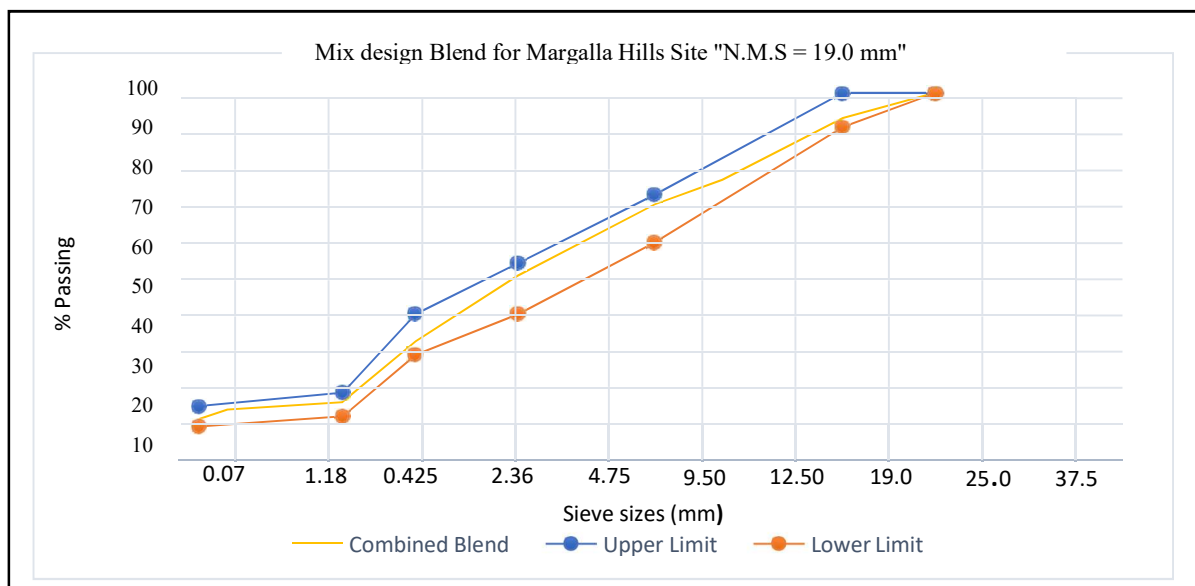


Figure 1 Graphical Representation of Final Approved JMF





### 3.1 Marshall Mix Design

The purpose of the Marshall mix design is to select the asphalt binder content that satisfies the minimum stability and range of flow values at the desired density.

#### 3.1.1 Flow and Stability Tests

Flow & stability tests were performed with increments of 0.5% of binding material used in HMA samples. These tests were carried out to find out the optimum binder content (OBC) used in HMA samples. The results produced are given below in table 5.

Table 5: Determination of OBC

% Bitumen Content by Mass of Aggregate	3.50	4.00	4.50	5.00
Unit weight ( $G_{mb}$ )	2.336	2.339	2.356	2.352
Maximum theoretical specific gravity ( $G_{mm}$ )	2.493	2.462	2.465	2.426
Stability (kN)	9.14	9.91	10.48	10.89
Air voids (% $V_a$ )	6.29	5.01	4.46	3.04
VMA %	14.05	14.39	14.24	14.82
VFA %	55.27	65.22	68.70	79.48
Flow (mm)	1.97	2.30	2.67	2.90

The results of HMA standard samples prepared at OBC were compared with specifications, which showed that the samples comply with NHA specifications.

#### 3.1.2 Flow & Stability Results of Modified Samples

The modified samples are prepared at OBC with the replacement of marble dust with the filler at different percentages from (25-100) %.

Following are the results of unit weight ( $G_{mb}$ ), Flow & Stability, % Air voids, % Air voids in mineral aggregates (VMA), and % Air voids filled with the bitumen (VFA) of Marshall Mix samples prepared at OBC as shown in table 6.

Table 6: Results of modified HMA sample

Percent replacement of filler with marbledust	0%	25%	50%	75%	100%
Unit weight ( $G_{mb}$ )	2.338	2.505	2.523	2.536	2.469
Max theoretical specific gravity ( $G_{mm}$ )	2.348	2.509	2.528	2.545	2.476
Stability (kN)	11.05	12.27	12.70	14.67	12.35
Air voids (% $V_a$ )	4.4	4.40	3.71	3.19	5.78
VMA %	14.8	15.64	14.58	13.67	16.86
VFA %	70	71.85	74.55	76.63	65.71
Flow (mm)	0.91	3.41	3.54	4.16	3.94



### 3.1.3 Results of Rutting Test and dynamic stability of Standard & Modified HMA Samples

The following table 7 shows the results of the rutting test performed on standard and modified samples of HMA. Table 8 shows the results of the dynamic stability of standard and modified HMA samples.

Table 7: Rutting Test Results

Percentage of Filler Replacement	Average Rutting Values (mm)
0	4.407
50	3.95
100	4.29

Table 8: Dynamic Stability Test Results

Percentage of Filler Replacement	Average Dynamic Stability Values (kN/ m <sup>2</sup> )
0	1513
50	2163
100	1623

The results of rutting of standard and modified HMA samples prepared with 50% and 100% replacement of filler material with marble dust. The value of rutting is minimum at 50% replacement of filler material as shown in figure 2. Also, the value of dynamic stability is maximum at 50% filler replacement with marble dust. If we increase the filler replacement above 50%, the value of dynamic stability (DS) decreases as shown in figure 3.

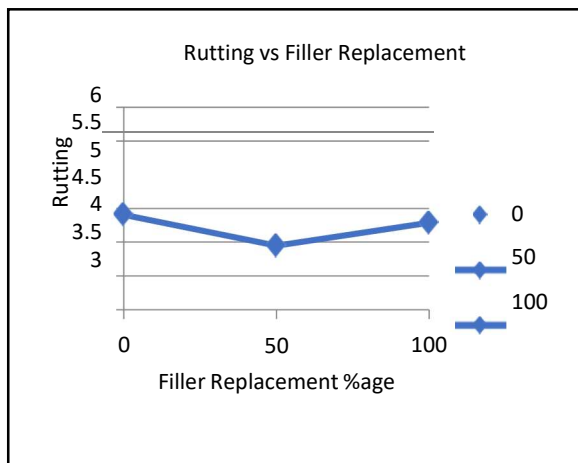


Figure 2: Graph of Rutting vs Filler Replacement %

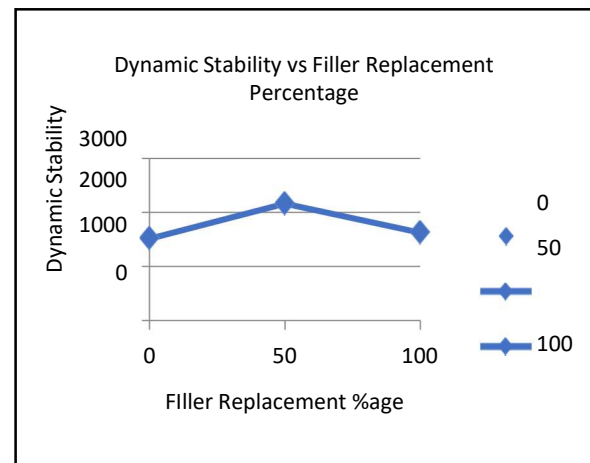


Figure 3: Graph of DS vs Filler Replacement %

## 4 Conclusion

Following are the conclusions from the conducted study:

- 1 When 50% filler is replaced with marble dust, the stability and flow of the hot mix asphalt have improved that is 2163 KN/m<sup>2</sup>, at 0% of marble as a filler replacement the dynamic stability of HMA is 1513 KN/m<sup>2</sup>, and at 100% of filler replacement the dynamic stability is 1623 KN/m<sup>2</sup>. Adding the filler improves the Dynamic Stability and Rutting Resistance of the HMA.
- 2 50% replacement gives a maximum improvement in resisting the Rutting and Dynamic Stability of the HMA that is 3.95mm, at 0% of marble as a filler replacement the rutting of HMA is 4.407mm, and at 100% of filler replacement the rutting of HMA is 4.29mm.



## References

- [1] Ahmed S. Eltwati, & Fares Saleh. (2020). Improvement of Subgrade Soils by Using Marble Dust-(Libya, Case Study). *THE INTERNATIONAL JOURNAL OF ENGINEERING AND INFORMATION TECHNOLOGY (IJEIT)*, 06.
- [2] Deepti Mehta, & Saurabh Tege. (2020, July 07). STUDY OF MARBLE WASTE AND ITS UTILIZATION. *International Research Journal of Engineering and Technology (IRJET)*, 07, 5.
- [3] Jayvant Choudhary, Brind Kumarb, & Ankit Gupta. (2019). Performance evaluation of asphalt concrete mixes having copper. *World Conference on Transport Research – WCTR 2019*, (p. 12).
- [4] Mr. Ranjan Kumar, & Shyam Kishor Kumar\*. (2015, August). Partial Replacement of Cement with Marble Dust Powder. *Mr. Ranjan Kumar Int. Journal of Engineering Research and Applications*, 05(8), 10.
- [5] Virendra Singh Shekhawat, Dr. Bharat Nagar, & Parvez Choudhary. (2017, October). USE OF MARBLE DUST AS FILLERS IN ASPHALT PAVEMENT. *International Journal of Modern Trends in Engineering and Research (IJMTER)*, 04(10), 9.



# TO EVALUATE THE SELF-HEALING OF ASPHALT MATERIALS AT DIFFERENT TEMPERATURES

<sup>a</sup> Moazam Sattar\*, <sup>b</sup> Muhammad Tariq, <sup>c</sup> Muhammad Aleem

a: Civil Engineering Department, University of Engineering and Technology Taxila, moazam.malik59@gmail.com

b: Civil Engineering Department, University of Engineering and Technology Taxila, tariqdaud2@gmail.com

c: Civil Engineering Department, University of Engineering and Technology Taxila, engrm.aleem@gmail.com

\* Corresponding author: Email ID: [moazam.malik59@gmail.com](mailto:moazam.malik59@gmail.com)

**Abstract-** It is common for asphalt pavement to develop micro cracks over time, largely owing to weather and traffic conditions. Pavement fatigue life is shortened as a result of these fissures. When the temperature of an asphalt mixture rises, cracks that previously appeared begin to close. The purpose of this study is to use microwave induction to determine the effect of temperature on the self-healing ability of asphalt pavement material. Asphalt's fatigue resistance was measured using a four-point beam fatigue apparatus. This experiment required a certain amount of condition time and temperature. Before and after conditioning, the specimens were tested. The first recovery cycle results in a significant loss of fatigue resistance, however the loss of fatigue resistance from the second healing cycle to the third healing cycle was minimal. Asphalt's self-healing properties improved with temperature, too. Temperature was shown to be the most important determinant in asphalt's ability to self-heal. Temperatures ranging from 37 to 40 degrees Celsius had the highest healing index.

**Keywords-** Four-point beam test, Microwave oven heating, Self-Healing,

## 1 Introduction

The pleasant operating experience and low cost of asphalt pavement make it an attractive option for highway construction. However, degradation occurs quickly once the road is put into service because to traffic volumes, bitumen ageing, and environmental factors such as moisture damage, temperature influence, and UV radiation. Meanwhile, minor cracks emerge in the asphalt pavement, which gradually deepen and produce more major problems including travel, potholes, and fracturing [1]. Road safety is jeopardised by these deteriorations, which also necessitate costly maintenance. Fractures in asphalt mixtures start out as micrometer-sized cracks, but they can quickly grow due to traffic and environmental factors. As a result, preventive maintenance programme measures must always be used to extend the life of asphalt pavements. Additionally, asphalt mixtures can self-heal without the need for human intervention. Blacktop can also self-heal if they are not subjected to traffic forces that can worsen fractures. As a result, complete healing could lay hold of a handful of months, which is impossible to achieve in practice due to the constant drift of Lorries. Asphalt is a stuff that can mend itself. According to Bazin and Saunier [2], and the role of temperature in self-healing is critical. Although bitumen's viscosity is proportional to temperature, at a certain temperature threshold (i.e., 30–70 °C), it tends to flow into cracks by capillary and gravity and seal the fissure [3]. During the summer, cracks in asphalt pavement that are evident in the winter will disappear, but it is necessary to heat asphalt concrete so that it will heal faster due to temperature. [4]. the high temperature created by microwave heating is very difficult to control; it can exceed asphalt's flash temperature limit, damaging its chemical structure. Consequently, the time spent in the heating process should be closely survived [5].

Out of three types of metallic waste examined by Bowen et al., (HBSS) had the best microwave absorption performance [6]. It is common practice to employ lubricating and extender oils rich in maltene components (also known as



"rejuvenators") in pavement repair since these oils may be used to reconstitute the asphalt binder's chemical makeup in order to utilize rejuvenators in asphalt pavements, they must fulfil the following five requirements. Bitumen compatibility, high temperature stability, capacity to endure mixing and construction circumstances, healing temperatures between 30 and 40 degrees Celsius, and the ability to heal continuously or several times are all important considerations [7]. Asphalt concrete's thermal capacity and solar radiation would have no extra thermal impact. A decrease in composite viscosity and an increase in rutting resistance were both achieved by using microwave-preprocessed ground tire rubber, as shown by Xu et al. Gallego et al. looked at the efficiency of a new thermo mechanical treatment for enhancing the healing capacity of hot asphalt mixes. A self-healing asphalt mixture including waste metals was studied by Yalcin using induction warming and microwave heating [8]. The aim of this paper is to evaluate and compare the self-healing properties of asphalt material by using Microwave induction Method.

## 2 Experimental Procedures

Asphaltic pavement materials may be tested for stiffness modulus and fatigue resistance using bending tests. In CEN, AASHTO, and Chinese test requirements, four-point bending tests are included. Controlled strain or regulated stress techniques of loading are possible for the prismatic beam specimen. Servo pneumatics, an increased digital data collection and control system, and user-friendly software make up the CRT-SA4PT-BB Standing Alone Four Point Bend Beam Machine. Microsoft Excel™-compatible format test data is saved to the disc during testing, which includes both graphs and tables. Beam height and breadth may be adjusted to meet AASHTO specifications despite the fact that the clamps are spaced at 118.5mm centers (the distance between outer ends is 335.6mm (fourteen inches)). Mixing aggregates and bitumen, we created asphalt material slabs before dividing them into 4 beams of asphalt mixture. Beam measured 12 inches in length, 2 inches in breadth, and 2 inches in depth when estimated over its whole surface area. There were a total of twenty asphalt material beams constructed. Asphalt beams were subjected to a Fatigue test using a four-point Beam test device. The device's frequency ranged from 0.1 to 30 Hz. Temperatures and frequencies were varied throughout the testing process to see what effects were seen. The initial fatigue cycle is the number of times before fractures appear.

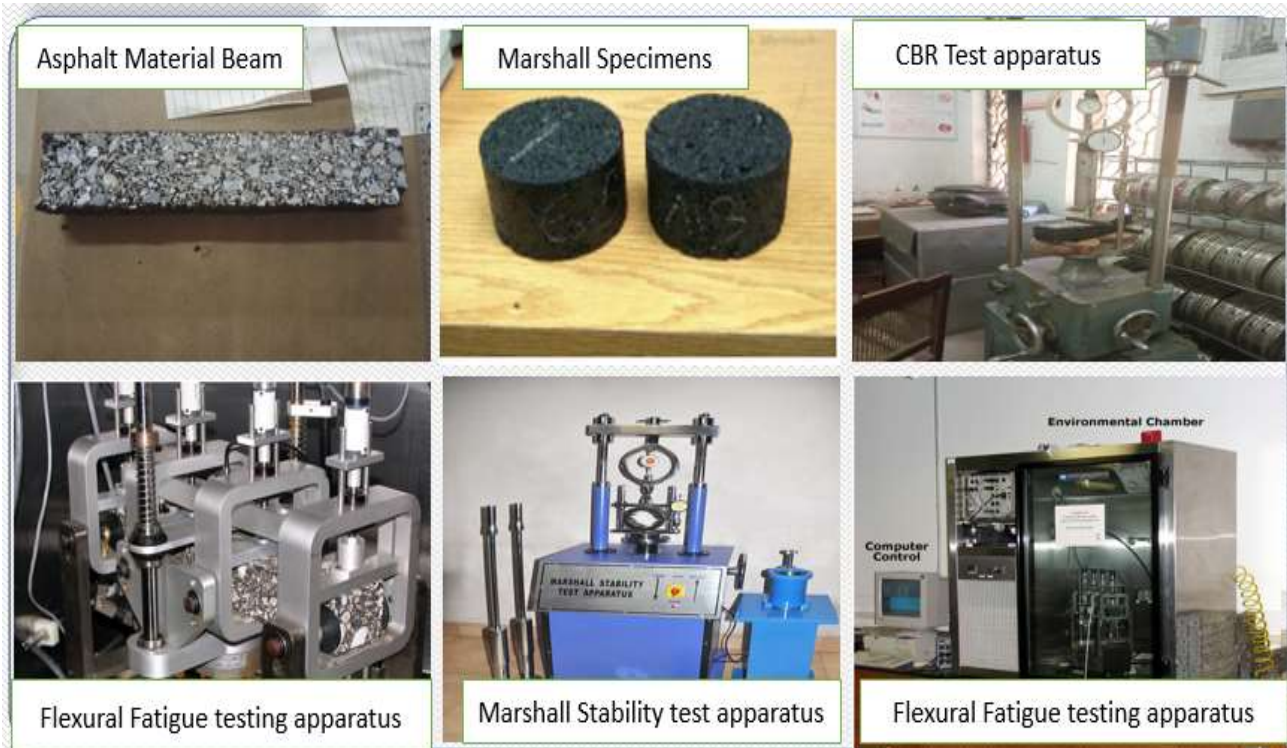


Figure 1: Experimental Setup



### 3 Research Methodology

To meet the goals of the research, a three-phase procedure was devised. The initial step was to narrow down the options for raw materials. A single aggregate supply and three local asphalt binder were chosen. Bitumen from the Attock Oil refinery's 80/100 penetration grade and 60/70 penetration aggregates were utilized. Second, several binder tests on asphalt binder were done in order to discover binder requirements. Phase 2. It was tested for penetration, ductility, viscosity and softening point. Third, the self-healing of asphalt mix was performed utilizing microwave induction. i.e. asphalt mixture design specimens were made. This phase's primary test was a four-point beam fatigue test. Tests were performed during self-healing to compare the asphalt material beam's fatigue resistance. This was the era in which the Healing Index was discovered. Analyzing the data was the last step in the study technique. Asphalt 60/70 and 80/100 mixture healing indices were studied. In first phase two different local asphalt binders and Margalla aggregates were chosen to make preparation of the asphalt mixture. In Second phase specimens were made ready for both qualitative as well as quantitative tests. To check the qualities of the chosen asphalt, both conventional and rheological experiments were carried out. In the third phase of research methodology, Self-Healing of asphalt mixture was accomplished by using Microwave oven. The flowchart of research Methodology is given below in Figure 2.

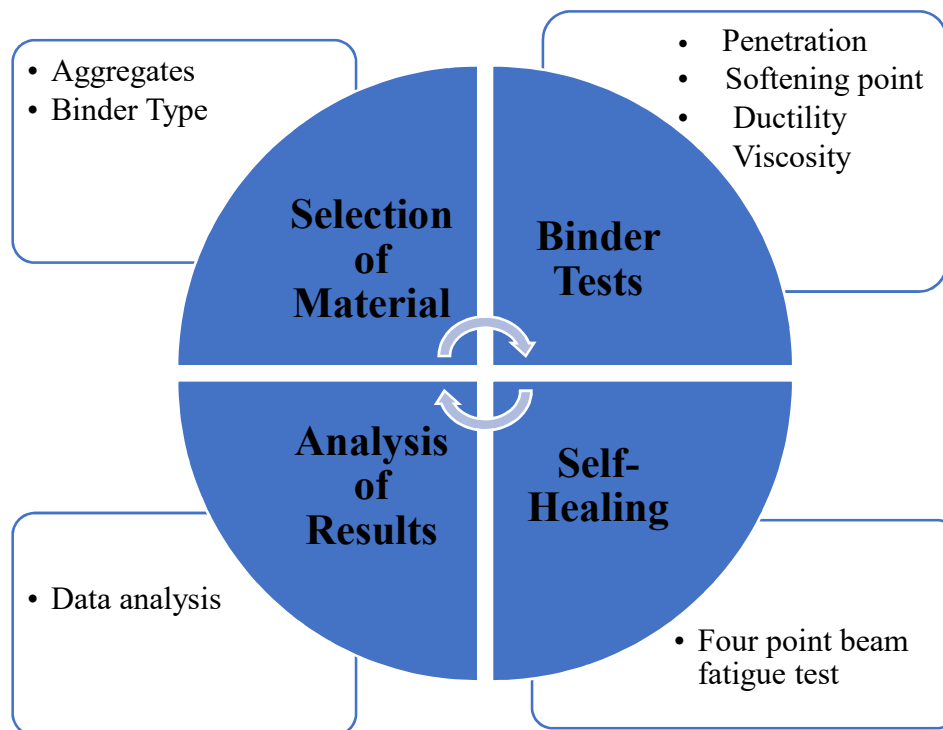


Figure 2; Flowchart of Research Methodology

## 4 Results

### 4.1 Fatigue resistance of healed specimen

A considerable decrease in fatigue resistance was seen after the first healing cycle, however there was no such decrease between the second and third healing cycles, as shown by the results of cyclic loading. Because certain aggregate grains were shattered during the initial 4 PB test, they were unable to completely restore their strength when microwave treatment was applied. When it came to the third and final measure of fatigue resistance, however, the two were almost tied. Broken aggregates, in other words, impede healing to a certain extent. Figure 2 shows the results of cyclic loading when 60/70 grade bitumen was used. Figure 4 shows that 1st fatigue resistance of asphalt material 80/100 was less than that of 60/70.



Healing performance of 80/100 asphalt mixture was greater than that of 60/70. Results of cyclic loading for both grades of bitumen are shown in Figure 3 and Figure 4. Because 80/100 grade binder is softer than 60/70, so healing performance of 80/100 is greater than that of 60/70. Different vehicles load apply, remove and reapply on road which is an example of cyclic loading. Self-healing of asphalt mixture occurs in periods without traffic and under high temperatures, starting between 30oC and 70oC depending on the type of bitumen used. The main healing mechanism of asphalt mixture is the capillary flow of the bitumen through the cracks at high temperatures. This is a very slow process and cracks may need many days to fully self-heal. By increasing temperature, Healing capability can be increased as shown in fig.

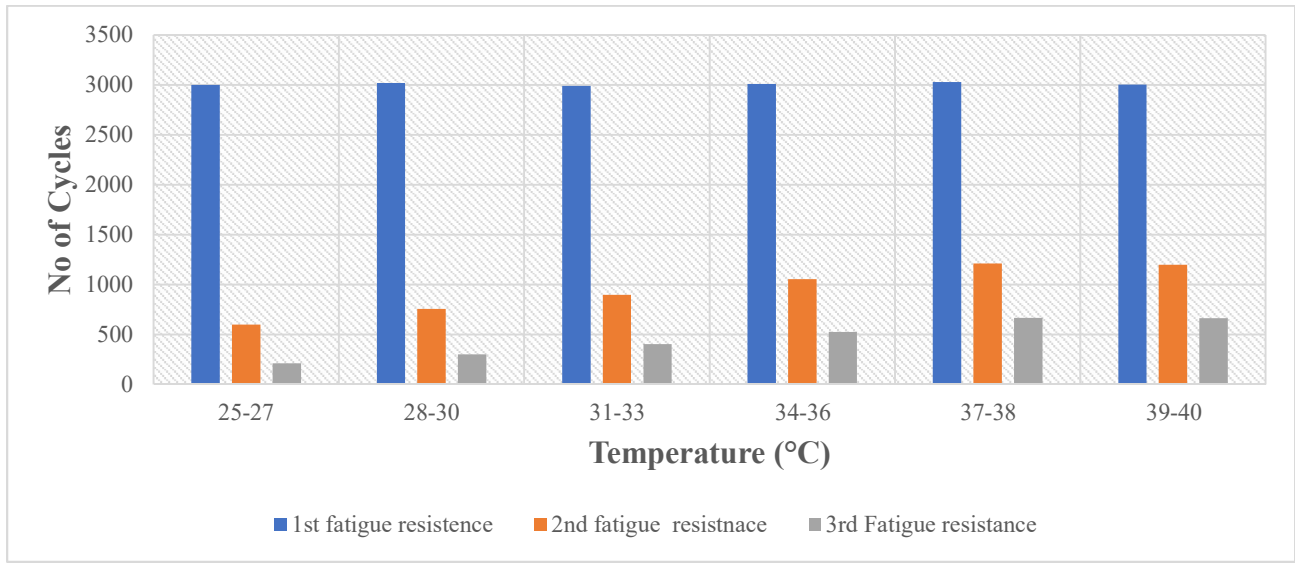


Figure 3: Effect of temperature on fatigue resistance (60/70)

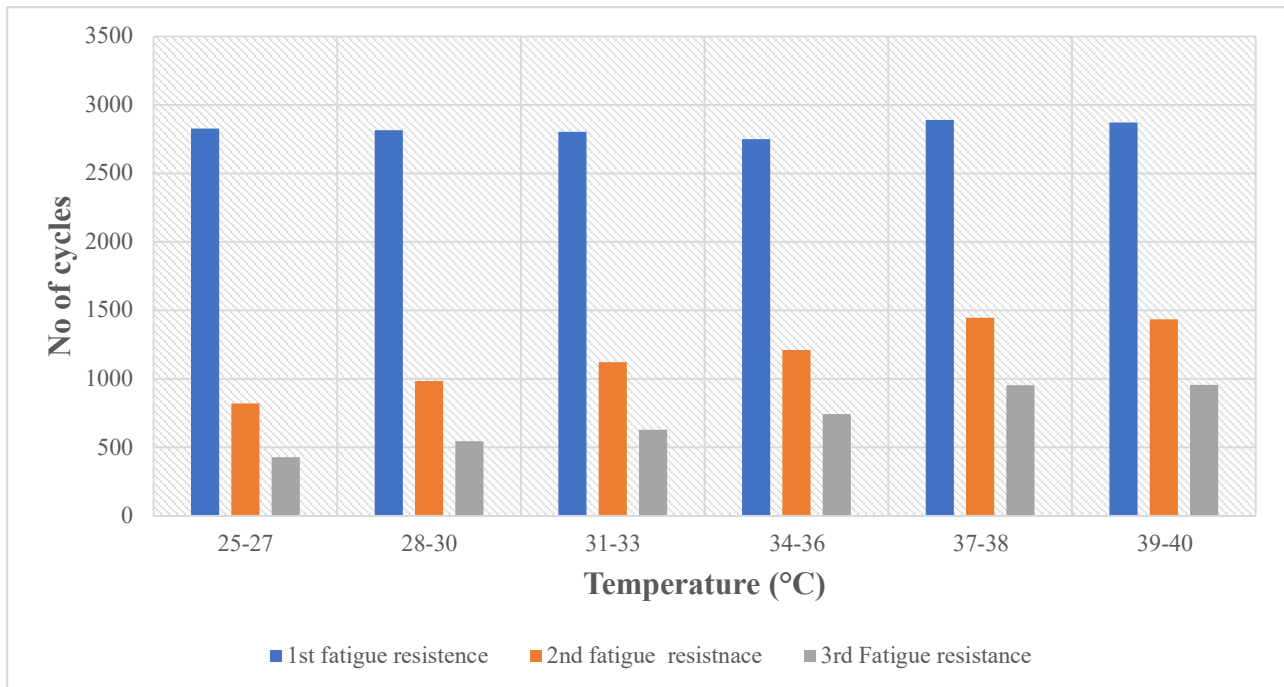


Figure 4: Effect of temperature on fatigue resistance (80/100)



## 5 Practical Implementation

Fig 5 shows the working mechanism of the microwave heating vehicle. While moving, the automobile heats the pavement via the microwave unit. Additional equipment, because the crusher and the shovel, are set up for mincing the ice layer and pushing the ice to the road side. The authors 'purpose turned into the deicing of the pavement, however plainly comparable systems may be used for different heating pavement applications.

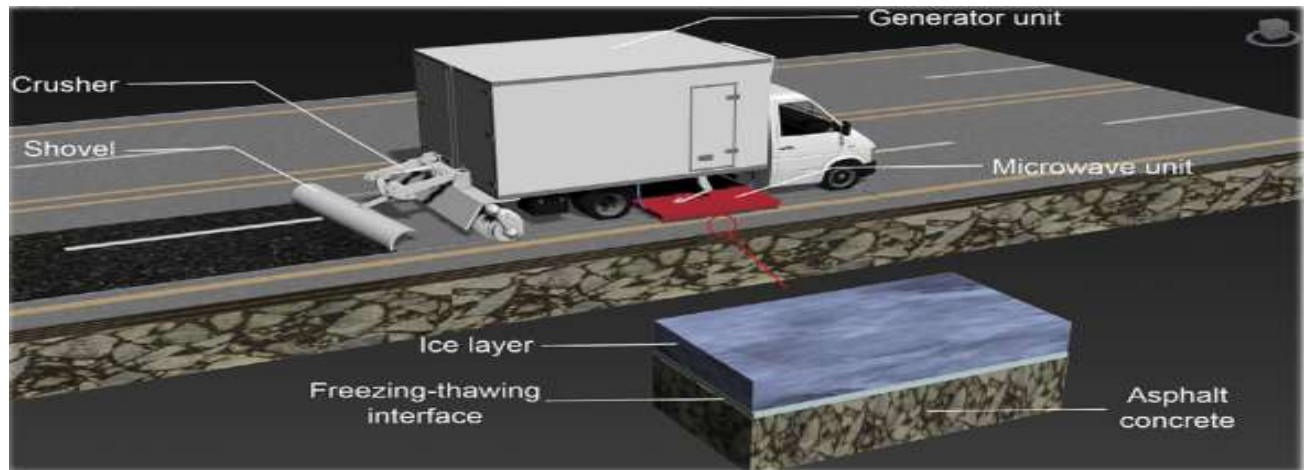


Figure 5: Working mechanism of the microwave heating vehicle

## 6 Conclusion

In the light of results attained, conclusions are summarized as:

- 1 High temperatures improve pavement fatigue life because asphalt material fractures mend faster at high temperatures. It is reported that cracks seen within the asphalt pavement in winter disappear in summer, however to enhance temperature related healing performance, it's necessary to heat asphalt concrete artificially. Self-healing of asphalt material also enhanced with increasing time up to some extent and then decreases.
- 2 Based on experimental data, healing performance of 80/100 grade bitumen was higher than that of 60/70 grade bitumen.

## References

- [1] S. Xu, A. García, J. Su, Q. Liu, A. Tabakovic', E. Schlangen, Self-Healing Asphalt Review: From Idea to Practice, *Adv. Mater. Interfaces*, 2022. 1–21 p. ISBN 10-1002-201800536.
- [2] P. Bazin, J. Saunier, Deformability, Fatigue and Healing Properties of Asphalt Mixes, in: *International Conference on The Structural Design of Asphalt Pavements*, Ann Arbor, Michigan, 1967. 553–569 p. ISBN 100855.
- [3] A. Menozzi, A. Garcia, M.N. Partl, G. Tebaldi, P. Schuetz, Induction healing of fatigue damage in asphalt test samples, *Constr. Build. Mater.*, 2015. 162–168 p. ISBN 10.1016-10-034.
- [4] Q. Liu, S. Wu, E. Schlangen, Induction heating of mastic asphalt for crack control, *Constr. Build. Mater.*, 2013. 345–351 p, ISBN 10-1016-2012-11-075.
- [5] E. Lizasoain-Arteaga, I. Indacochea-Vega, P. Pascual-Muñoz, D. Castro-Fresno, Environmental impact assessment of induction-healed asphalt mixtures, *J. Cleaner Prod.*, 2018.1546–1556 p. ISBN 10-1016-2018-10-223.
- [6] L. Baowen, S. Aimin, L. Yupeng, W. Wentong, L. Zhuangzhuang, J. Wei, C. Xin, Effect of metallic-waste aggregates on microwave self-healing performances of asphalt mixtures, *Constr. Build. Mater.*, 2022. 246 p. ISBN 118510.
- [7] X. Liu, Y. Zhao, Z. Wei, D. Zhang, Microwave absorption enhancement of asphalt concrete with SiC-Fe<sub>3</sub>O<sub>4</sub> mixtures modifier, *Constr. Build. Mater.*, 2022. 254 p. ISBN 119209.
- [8] O. Xu, M. Li, D. Hou, Y. Tian, Z. Wang, X. Wang, Engineering and rheological properties of asphalt binders modified with microwave preprocessed GTR, *Constr. Build. Mater.*, 2022. 256 p. ISBN 119440.





# EFFECT OF RAINFALL INTENSITY AND DURATION ON STABILITY OF NATURAL SLOPES OF UNSATURATED FINE SOILS

*"Sohaib Naseer\* & "Robert Evans*

a: Department of Civil Engineering, School of Architecture, Design and Build  
Environment Nottingham Trent University, United Kingdom  
\*Corresponding author: sohaib.naseer2019@my.ntu.ac.uk

**Abstract** - Rainfall infiltration is a major cause of slope failures in soft and cohesive soils. The water infiltration increases the pore water pressures, ground water level and decreases the matric suction of unsaturated soils, which has been proved as a critical factor for stability of slopes. As a result of increased pore water pressure and decrease in matric suction, the shear strength of the soil decreases which increases the likelihood of the failure of slope. This paper investigates the failure mechanism of natural slopes subjected to high and low intense rainfall with various duration of rainfall events. Finite element analysis was carried out using commercially available PLAXIS 2D software, which is considered to be a comprehensive tool for geotechnical modelling. It was observed that in addition to slope geometry, soil physical characteristics and hydraulic properties, rainfall intensity and duration also play a key role in stability of unsaturated soil slopes.

**Keywords**- unsaturated slopes, matric suction, pore pressure, slope stability.

## 1 Introduction

Rainfall-triggered slope failures are widespread geological disasters in many parts of the world, especially in the high tropical areas, which are extensively covered with residual soils. [1]; [2]; [3]. These slope failures are normally shallow with usual depth of slip surface of 1 to 3 m oriented parallel alongside the slope surface [4]; [5]; [6]. During the rainfall events, the water infiltrates into the soil which causes reduction in matric suction, which causes a significant reduction in shear strength of soil and hence failure occurs. [7]; [8]; [9][10][11]. Numerous researchers have conducted numerical studies as well as laboratory experimentations to get detailed understanding of failure mechanisms of slope failures due to rainfall infiltration. (i.e. [12]; [13];[14]). Merat et al. ([15]) conducted a study on 84 landslide events occurs in the Tizi-Ouzou region of North of Algeria, and reported that more than 65% of landslides occur because of climate change including rainfall and snow. The study showed a great relationship between landslides and climate conditions. Stability controlling parameters of slopes, which have been studied by different researchers [16], [15]; [18], include the permeabilities of soils, saturation degree, slope geometry, existence of ground water table, duration and intensity of rainfall event. Various computational programs can be used to simulate the rainfall events for stability analysis including PLAXIS, Geo-Studio, ABAQUS, etc. Usually, limit equilibrium methods are adopted by researchers due to their simplicity, but they have limitations. With advancements in numerical methods, couple flow-deformation analysis options have been included in different tools. It allows researchers to simulate the flow analysis and stability analysis at same time.

A parametric study [15] conducted with different stability controlling factors including the rainfall intensity and duration, degree of saturation, and hydraulic properties of soils concluded that these parameters play an important role in stability of slopes. The pore water pressure varies with variation of these parameters and hence factor of safety varies. [19]



conducted finite element modelling for stability analysis of unsaturated soil slopes and reported that rainfall infiltration causes a reduction in matric suction and increase in moisture content, which increase pore water pressure and thus results in reduction of safety factor for slope.

Rainfall events are thought to play a key role in rainfall-induced slope failure due to their intensity, length, antecedent condition, resolution, and pattern. [8], [20], [21]; [22]. Intense rainfall has been identified as a triggering factor for many slope failures worldwide, and it is widely accepted that many slope failures have occurred during prolonged rainfall. [23]. It is well understood that antecedent rainfall significantly contributes to rainfall-induced failures of low-hydraulic conductivity slopes, but probably contributes less significantly to those of high conductivity slopes. [24]. Rainfall resolution is often critical in determining the amount of precipitation infiltration that might contribute to slope failures since rainfall intensity varies. Thus, in the investigation of rainfall-induced slope collapse, using high-resolution rainfall data (hourly rather than daily rainfall data) may yield more accurate results, as suggested by [20]. Furthermore, a specific rainfall pattern caused the least stable slopes, the lowest minimum factor of safety, and the shortest time to reach the minimal factor of safety (high intensities in the beginning, followed by a constant decline towards the end of the rainfall)[21]. The relationship between rainfall events and soil hydraulic characteristics influences the quantity of rainwater penetration required to decrease surficial soil suction, which can cause a slope failure. When the rainfall intensity is almost equivalent to the soil hydraulic conductivity, the incident rainfall can theoretically be completely absorbed into the soils. Rainwater infiltration in this situation is most capable of decreasing surficial soil suction to a critical level. Rainfall of modest intensity will penetrate completely into the surficial soil, but it may not be enough to decrease the soil's suction. When rainfall is especially intense, however, rainwater will move to runoff in part. Because strong rainfall is usually of shorter duration, precipitation penetration may be insufficient to lessen soil suction. Matric suction is a crucial factor in shallow slope failures, according to several studies [12], [25] [26], [8]. When precipitation infiltrates the slope surface, matrix suction decreases and the wetting front slides down until it reaches a depth where the slope's shear strength can no longer sustain slope stability. This type of failure occurs more frequently on slopes with low hydraulic conductivity than on slopes with high hydraulic conductivity, such as clean sand. [12]. Infiltration can only attenuate suction of the surficial soils to shallow depths in the first example, resulting in a shallow slope collapse mechanism. Given the fact that rainfall and soil parameters are the determining factors, coupled investigations of seepage and slope stability are now routinely used to assess rainfall-induced slope instability. In both seepage and slope stability analyses, the deterministic approach is widely used. This paper investigates the failure mechanism of slope subjected to low and high intense rainfall of short and long duration. A uniform soil slope with same shear strength is analyzed using finite element methods. The results of finite element analysis is presented in following sections.

## 2 Slope geometry and material properties

Commercially available finite element tool PLAXIS 2D was used for this study which is a persuasive program which can help users in characterizing geotechnical problems in a realistic manner. This study investigates the impact of low and high intense rainfall with short and long duration on factor of safety and total displacements. For this purpose, a series of finite element analyses were done. The two-dimensional finite element method was used with 15-node plane strain model using the PLAXIS 2D computer program. The studied parameters include the rainfall intensity (mm/hr), and durations of the rainfall (hours). Figure 1 shows the typical geometry of the slope used in the numerical analysis. Two sets of rainfall events were considered, high-intensity rainfall (60mm/hr, 90mm/hr and 120mm/hr) and low-intensity rainfall (5mm/hr, 10mm/hr and 20mm/hr) with different durations (01hr, 03hrs, 06hrs, 12hrs, 24hrs, 48hrs and 96hrs). The hardening soil model was used to model the nonlinear behavior of the soil. This constitutive model is an advanced soil models and can be used to simulate various types of soil. Published literature provided the material parameters of the soil employed in this investigation. The soil index and shear strength properties are summarized in Table 1 and Table 2, respectively. The Van Genuchten model was used to simulate the soil-water characteristic curve which is a significant parameter in terms of unsaturated slope stability. Figure 1 displays the typical generated mesh for full-scale slope geometry and boundary conditions. The vertical boundaries of the model were supposed to be deformable vertically and fixed laterally, whereas the bottom boundary was assumed to be fully fixed. For the flow water boundary conditions, the vertical boundary conditions were assumed to be permeable and the bottom boundary was assumed to be impermeable. It is assumed that the water table is located 20 m below the ground surface.

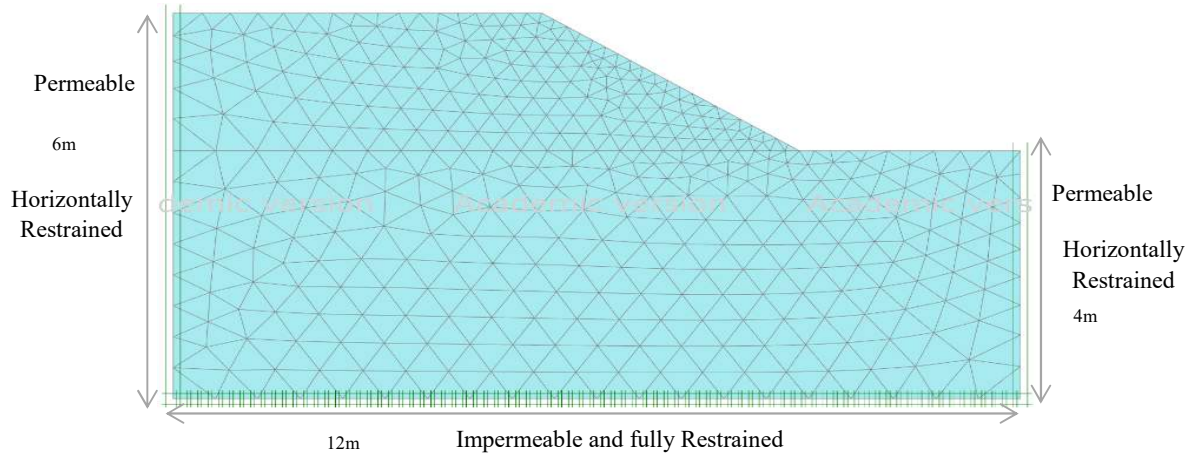


Figure 1: Slope Geometry and typical mesh

Table 1: Index Properties of Soil used for this study [27]

Properties	Moisture Content (%)	Liquid Limit (%)	Plastic Limit (%)	Soil Classification	Specific Gravity	Unsaturated unit weight (kN/m <sup>3</sup> )	Saturated unit weight (kN/m <sup>3</sup> )
Values	32	76	42	High Plastic silt (MH)	2.64	13.2	17.00

Table 2: Shear Strength and unsaturated parameters of Soil used in this study [27]

Parameters	Young's Modulus (kN/m <sup>2</sup> )	Effective Cohesion (kN/m <sup>2</sup> )	Effective friction angle (°)	Hydraulic conductivity (m/s)	Poisson's ratio	$g_a$	$g_n$	$g_t$
Values	10000	8.0	32.0	$2.32E^{-7}$	0.33	0.7	1.8	0.5

### 3 Results and discussions

Rainfall intensity and duration are the key influencing factors for rainfall induced slope failures. An idealized homogenous slope with gradient of 1V:1.5H was analyzed under different rainfall intensities and duration. The figure 2 shows the rainfall intensity, rainfall durations applied on slope and variations in factor of safety. Rainfall intensity of 5mm/hr, 10mm/hr and 20mm/hr are classified as low intense whereas, 60mm/hr, 90mm/hr and 120mm/hr are classifies as high intense. Rainfall with high intensity and short duration does not have a significant effect, whilst rainfall with low intensity and long duration reduces the factor of safety up to the critical condition. This is due to the permeability of soils which allows rainfall water to infiltrate into the slope. For 1 hour duration, the safety factor does not change significantly, as a result of the hydraulic properties of the soil. For rainfall intensity of 5mm/hr, the factor of safety doesn't change significantly because the infiltration of water was not enough to increase pore water pressure up to critical conditions, and hence the slope remains stable with a high safety factor. However, 20mm/hr rainfall intensity was found to be most crucial



for slope stability as the safety factor reduced to 1.062 (i.e. on the verge of failure). Rainfall infiltration into the soil body decreases the factor of safety due to the reduction in matric suction and increase in pore water pressure.

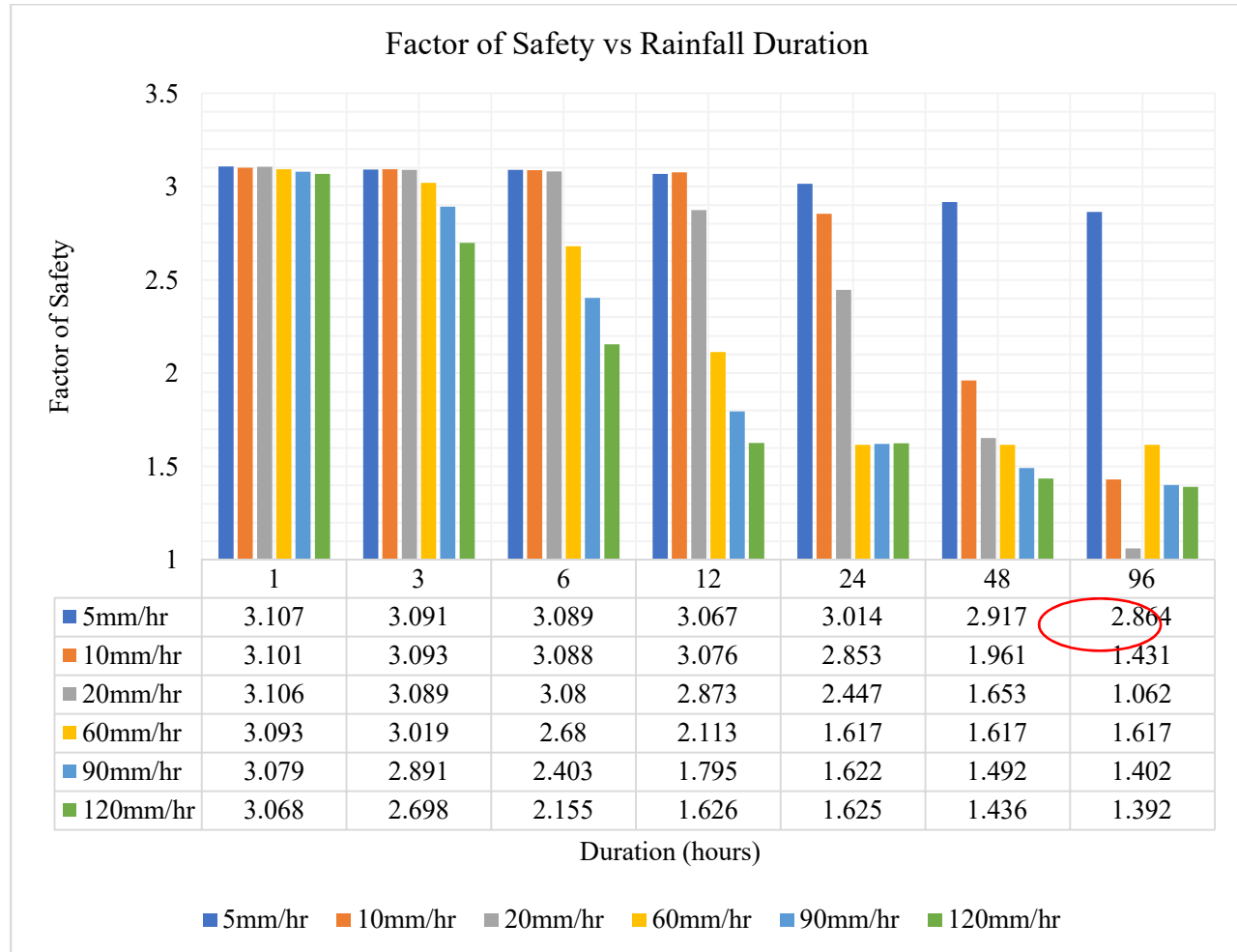


Figure 2: Variation in safety factor with different rainfall intensity and duration

### 3.1 Safety Factors of slope subjected to low and high intense rainfall

To investigate slope instability and the failure zone subjected to rainfall infiltration, the critical slip surfaces were assessed. Figure 3 shows the critical slip surfaces for modelled slope under different rainfall duration (01 hr & 24 hrs) and with higher intensity (120mm/hr) and low intensity (5mm/hr). A shallow slip surface can be seen against short duration while a deep failure surface was observed for prolonged rainfall events. Due to the hydraulic properties of fine soils, the rainfall water takes more time to infiltrate into the slope and hence delayed the failure. The slope remains stable during the rainfall events and fails after some time, depending upon the soil permeability and amount of water infiltrated into the slope. Researchers (Mahmood et al. 2011, Tsaparas et al. 2002) have proved that if the ratio of rainfall and saturated permeability ( $q/k_{sat}$ ) is higher, less water will infiltrate into the ground and more water will disappear as runoff water and hence slope remain stable. Further, if the ratio is low then more water will infiltrate into the ground, resulting in an increase in pore water pressure which leads to the failure of slope. If the ratio is very low, in case of rainfall with 5mm/hr intensity, then pore water pressure would not be affected.

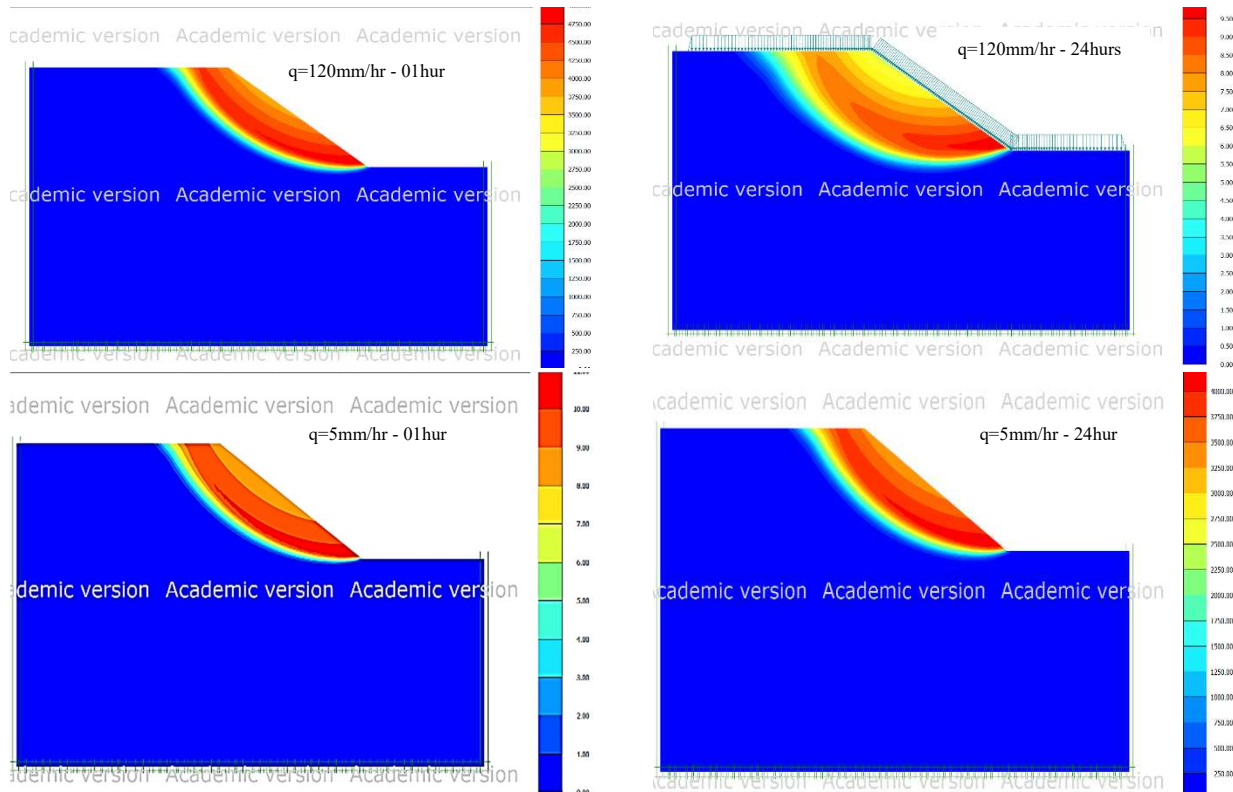
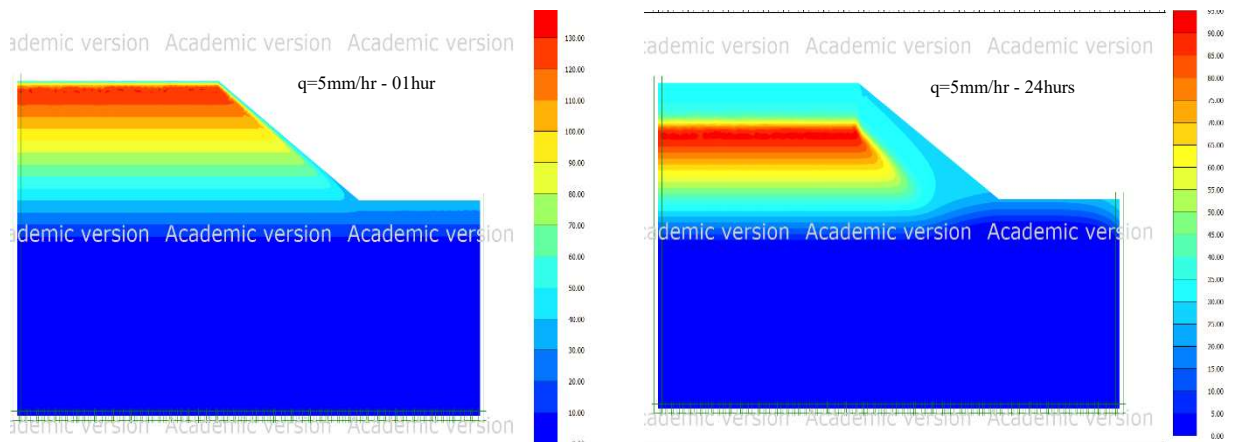


Figure 3: variation in slip surface with rainfall of different duration and different intensities

### 3.2 Variation in pore water pressure and matric suction

It has been proved that slope failure occurs due to the reduction in matric suction and a resulting increase in pore water pressure. Matric suction is the foremost variable for susceptibility analysis of rainfall induced slope failures. Slope failure is mainly dependent on the initial matric suction conditions of soils at surface and subsurface. Figure 4 shows the fluctuations in matric suction due to the rainfall infiltration. It can be observed that rainfall with short duration does not reduce matric suction significantly, whilst rainfall with longer duration does. Also, it can be seen that matric suction reduction decreased with the slope depth. Maximum suction was observed near the face of the slope whereas, with higher depth, its decreased. This is because of the presence of ground water table at higher depths.



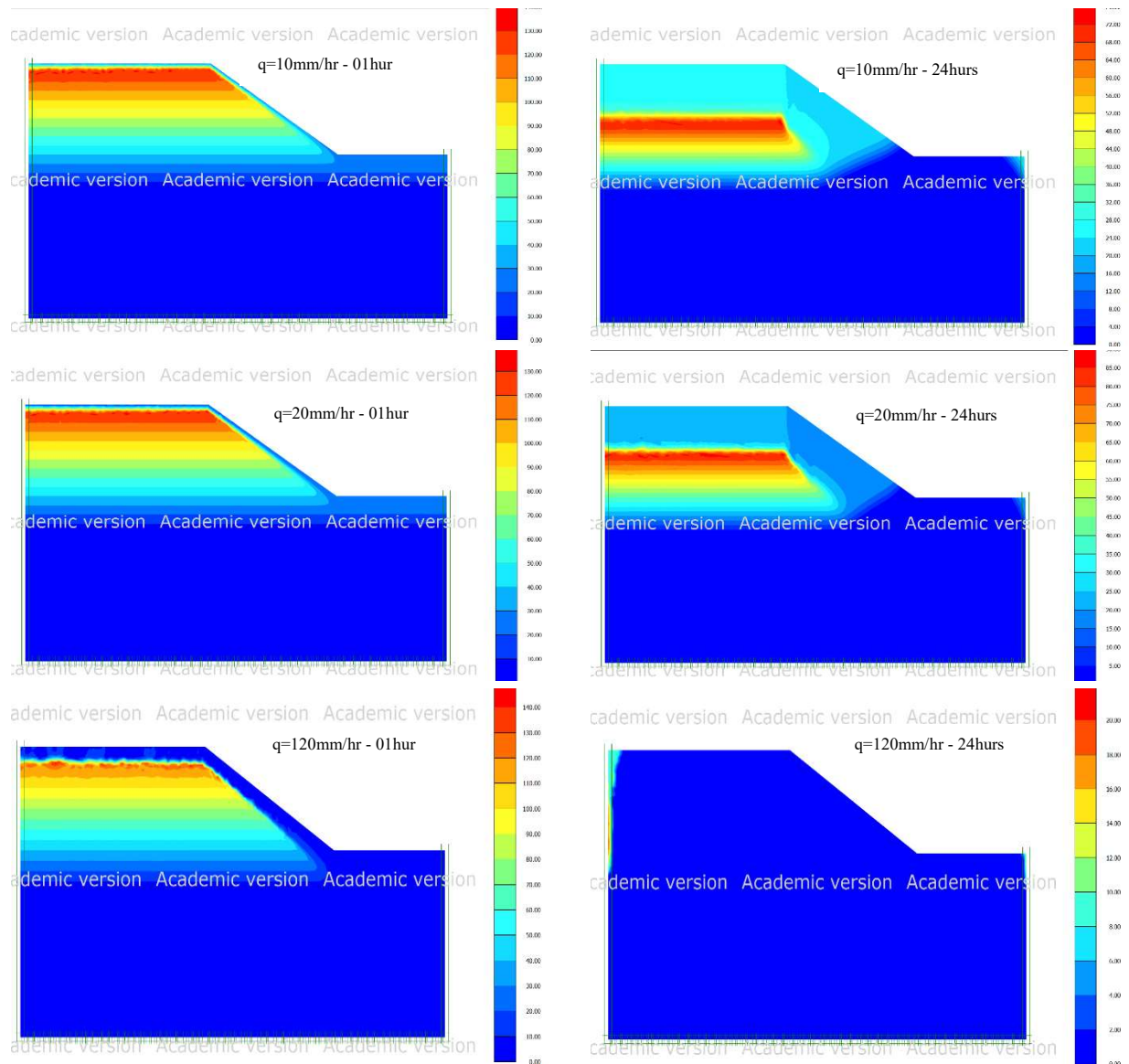


Figure 4: Variation of matric suction with different rainfall intensities and duration

## 4 Conclusions

The purpose of the current study was to investigate the impact of rainfall duration and intensity on slopes with low hydraulic characteristics. Finite element based numerical analysis was carried out on an idealized slope with 1V:1.5H gradient. Coupled flow-deformation analysis was carried out which allows seepage and deformation analysis at the same time. Based on this study, the following conclusions can be derived:

- In addition to the soil strength characteristics, and slope geometry, rainfall duration and intensity plays an important role in stability of slopes. The amount of infiltration depends on the hydraulic properties of soil.
- The variation in climate changes resulted in variation of matric suction profile with different time durations. There is an optimum value among low rainfall intensities at which the factor of safety is critical. 20mm/hr intensity resulted the minimum factor of safety



- The rainfall with low intensity and prolonged duration are more critical as compared to the high intensity and short duration.

## Acknowledgment

This study was conducted in Nottingham Trent University and is part of a PhD research project. The authors highly appreciated the support and guidance provided by the University and all technical staff. Moreover, the careful review and constructive suggestions by the anonymous reviewers are gratefully acknowledged.

## References

- [1] E. W. Brand, "Landslides in Southeast Asia, A state-of-the art report," 1984.
- [2] L. Shaw-Shong, "Slope failures in tropical residual soil," *Trop. Residual Soil Eng.*, pp. 71–102, 2004.
- [3] B. B. K. Huat, F. H. Ali, and S. Mariappan, "Effect of surface cover on water infiltration rate and stability of cut slope in residual soils," *Electron. J Geotech Eng*, vol. 10, 2005.
- [4] J. R. Muller and S. J. Martel, "Numerical models of translational landslide rupture surface growth," *Pure Appl. Geophys.*, vol. 157, no. 6, pp. 1009–1038, 2000.
- [5] J. Kim, S. Jeong, S. Park, and J. Sharma, "Influence of rainfall-induced wetting on the stability of slopes in weathered soils," *Eng. Geol.*, vol. 75, no. 3–4, pp. 251–262, 2004.
- [6] Y. Matsushi, T. Hattanji, and Y. Matsukura, "Mechanisms of shallow landslides on soil-mantled hillslopes with permeable and impermeable bedrocks in the Boso Peninsula, Japan," *Geomorphology*, vol. 76, no. 1–2, pp. 92–108, 2006.
- [7] D. G. Fredlund and H. Rahardjo, *Soil mechanics for unsaturated soils*. John Wiley & Sons, 1993.
- [8] A. B. Fourie, D. Rowe, and G. E. Blight, "The effect of infiltration on the stability of the slopes of a dry ash dump," *Geotechnique*, vol. 49, no. 1, pp. 1–13, 1999.
- [9] Q. B. Travis, S. L. Houston, F. A. M. Marinho, and M. Schmeeckle, "Unsaturated infinite slope stability considering surface flux conditions," *J. Geotech. geoenvironmental Eng.*, vol. 136, no. 7, pp. 963–974, 2010.
- [10] M. F. Ayazi and A. Tangri, "Stabilization of soil nailed slope by flexible materials," *Mater. Today Proc.*, vol. 49, pp. 1950–1955, 2022, doi: 10.1016/j.matpr.2021.08.134.
- [11] M. Nasiri and M. Hajiazizi, "An experimental and numerical investigation of reinforced slope using geotextile encased stone column," *Int. J. Geotech. Eng.*, vol. 15, no. 5, pp. 543–552, 2021, doi: 10.1080/19386362.2019.1651029.
- [12] D. Pradel and G. Raad, "Effect of permeability on surficial stability of homogeneous slopes," *J. Geotech. Eng.*, vol. 119, no. 2, pp. 315–332, 1993.
- [13] H. Rahardjo, X. W. Li, D. G. Toll, and E. C. Leong, "The effect of antecedent rainfall on slope stability," in *Unsaturated soil concepts and their application in geotechnical practice*, Springer, 2001, pp. 371–399.
- [14] J. Zhou, H. Li, Y. Zhou, J. Zhang, and G. Fan, "Initiation mechanism and quantitative mass movement analysis of the 2019 Shuicheng catastrophic landslide," *Q. J. Eng. Geol. Hydrogeol.*, vol. 54, no. 2, 2021.
- [15] S. Merat, L. Djerbal, and R. Bahar, "Numerical analysis of climate effect on slope stability," in *PanAm Unsaturated Soils 2017*, 2017, pp. 308–318.
- [16] J. M. Gasmo, H. Rahardjo, and E. C. Leong, "Infiltration effects on stability of a residual soil slope," *Comput. Geotech.*, vol. 26, no. 2, pp. 145–165, 2000.
- [17] H. Rahardjo, T. T. Lee, E. C. Leong, and R. B. Rezaur, "Response of a residual soil slope to rainfall," *Can. Geotech. J.*, vol. 42, no. 2, pp. 340–351, 2005.
- [18] S. Pradhan, D. J. Toll, N. J. Rosser, and M. J. Brain, "Field monitoring of soil-moisture to understand the hydrological response of a road-cut slope.," EDP Sciences, 2020.
- [19] C. W. W. Ng and Q. Shi, "A numerical investigation of the stability of unsaturated soil slopes subjected to transient seepage," *Comput. Geotech.*, vol. 22, no. 1, pp. 1–28, 1998.
- [20] A. J. Hearman and C. Hinz, "Sensitivity of point scale surface runoff predictions to rainfall resolution," *Hydrol. Earth Syst. Sci.*, vol. 11, no. 2, pp. 965–982, 2007.
- [21] A. Rahimi, H. Rahardjo, and E.-C. Leong, "Effect of antecedent rainfall patterns on rainfall-induced slope failure," *J. Geotech. Geoenvironmental Eng.*, vol. 137, no. 5, pp. 483–491, 2011.
- [22] S. Pradhan, D. G. Toll, N. Rosser, and M. J. Brain, "An investigation of the combined effect of rainfall and road cut on landsliding," *Eng. Geol.*, p. 106787, 2022.
- [23] C. I. Massey, D. N. Petley, and M. J. McSaveney, "Patterns of movement in reactivated landslides," *Eng. Geol.*, vol. 159, pp. 1–19, 2013.
- [24] I. Tsaparas, H. Rahardjo, D. G. Toll, and E.-C. Leong, "Infiltration characteristics of two instrumented residual soil slopes," *Can. Geotech. J.*, vol. 40, no. 5, pp. 1012–1032, 2003.
- [25] H. Rahardjo and D. G. Fredlund, *Soil Mechanics for Unsaturated Soils*. New York; Toronto: Wiley, 1993.
- [26] S. W. C. Au, "Rain-induced slope instability in Hong Kong," *Eng. Geol.*, vol. 51, no. 1, pp. 1–36, 1998.
- [27] R. Ullah, R. Abdullah, A. Kassim, N. Z. M. Yunus, and H. Sendo, "ASSESSMENT OF RESIDUAL SOIL PROPERTIES FOR SLOPE STABILITY ANALYSIS," *GEOMATE J.*, vol. 21, no. 86, pp. 72–80, 2021.



# HELICAL PILE: AN INNOVATIVE AND SUSTAINABLE FOUNDATION TECHNIQUE

<sup>a</sup> Hamza Ahmad Qureshi \*, <sup>a</sup> Muhammad Safdar, <sup>b</sup> Muhammad Haseeb Khan, <sup>c</sup> Hazarat Bilal

a: Earthquake Engineering Center, Department of Civil Engineering, University of Engineering and Technology, Peshawar, Pakistan.

b: Department of Civil Engineering, University of Engineering and Technology, Peshawar, Pakistan.

c: Department of Civil Engineering, Abasyn University Peshawar, Pakistan.

\* Corresponding author: Email ID: [18pwciv4995@uetpeshawar.edu.pk](mailto:18pwciv4995@uetpeshawar.edu.pk)

**Abstract-** Helical pile is an advanced sustainable deep foundation technique. Its importance in the construction sector is growing very hastily. However, being an advanced foundation technique, there is still an ambiguity about its usage, that whether to use helical piles or conventional piles in a construction project. The main objective of this paper is to compare helical piles with the conventional piles (i.e., Driven piles and Cast-in-situ piles) on the basis of different factors and draw conclusion between them. These factors include axial capacity, lateral capacity, method of installation, soil condition, cost, impact on environment and construction time. After extensive literature review the authors of the paper came to a conclusion that helical piles in many aspects are far better than conventional piles. Moreover, they cover several aspects of green construction like, less cost, fast construction, less carbon emission, low environmental impact, reusability etc.

**Keywords-** Cast in Situ Piles, Driven Piles, Helical Piles, Sustainable Foundation Technique

## 1 Introduction

This state-of-the-art literature review effectively shows the differences between helical piles (see Figure 1) and conventional piles in terms of several fundamentals. Helical piles, which were originally designed to support lighthouses and moorings, but they are now used to support the foundations of both old and new buildings because of their drastic improvement in term of efficiency and practicality. When soil becomes soft or oversaturated, it settles and compacts over time. This can cause the entire structure to shift out of alignment, which is dangerous. Helical piles, due to their high bounce resistance, are an excellent foundation choice for structures subject to frost heave or expansive soils [1]. Besides their advantages, the use of helical screw piles is limited by certain flaws like disturbance of the soil during installation within the pile helices' affected zone, the high displacement required to fully mobilize the bearing component of their bearing plates, and the low buckling resistance of their slender shaft under compression loading [2]. In recent years, the field of pile foundations has experienced a sharp increase in the use of helical piles [3]. Because of their high bearing capacity, fast installation and better recovery, they are now used in the foundation of offshore wind turbines [4]. The Christchurch earthquake caused only minor damage to a number of helical pile-supported structures in New Zealand, proving the viability of helical piles as a foundation material in seismically active regions [5].



Figure 1: Helical Pile [6].





The factors which were used to draw comparison between conventional and helical piles, and which make helical piles an innovative and sustainable foundation technique, includes axial capacity, lateral capacity, method of installation, soil condition, cost, impact on environment and construction time. Each one of them is discussed briefly as under;

## **2 Axial Capacity**

According to Elkasabgy [7], when site subsurface conditions were taken into account, the ultimate capacity of a single-helical pile was approximately 18% greater than that of a conventional pile, while the ultimate capacities of double-helical piles were almost 45 to 85 % greater than that of a conventional pile. This extra increase in the capacity of the helical pile was due to the presence of double helixes. Similarly, Sakr [8] also conducted out full-scale tests in Alberta, Canada. He discovered that helical piles with same embedment depths provide approximately 230% to 290% larger capacities in cohesive soil than driven piles. Hence, he concluded that helical piles have higher capacities due to the use of single or multiple helices with diameters greater than the shaft diameter. Sakr [9] further conducted field test on high-capacity helical piles, using 5% failure criterion, he computed that the axial compressive capacities of helical piles ranged from 1500 to 2500 kN, while their uplift capability range from 1500 to 2000 kN. Hence, we can say that helical piles typically have axial uplift capacities of 60% to 70% of their axial compressive capacities. Similarly, another researcher Malik [10] analyses the axial capacities of helical and conventional piles in the same ground and soil conditions, taking into account the effect of increased overburden pressure. He uses dry Toyoura sand that has been compacted to 70%, 80%, and 92% relative density in his test. He found that around settlement equals 10% of pile tip diameter, the load settlement curve for conventional piles plunges downward without increasing load, but around settlement equals 15% of pile tip diameter, the load settlement curve for helical piles plunges. Helical piles with helix-to-shaft diameter ratios of 2–4.1 demonstrated 2–12 times greater end bearing capacity than conventional piles with comparable pile shaft diameter. Another researcher Ali [11] concluded from his experimental work that Screw piles (helical pile) have a high tensile and compressive strength (up to three times that of a conventional pile) and can be utilized in a range of soil strata above and below water.

## **3 Lateral Capacity**

Wind loads, earthquakes, imbalanced ground pressures, snow loads, axial force on pipes, and load eccentricity are all elements that affect lateral loads and moments on piles. As a result, deep foundations are often constructed to resist such loads, and thus helical piles are also used to counteract horizontal forces. Sakr [12] conducted field test on high-capacity helical piles installed in dense to exceptionally dense clayey soil, he computed that helical piles can withstand high lateral load resistance as compared to conventional piles. He also investigated that shaft length was nearly involve in controlling the lateral load behaviour. Bien [13] conducted experimental study on helical and conventional piles with the same shaft diameter and wall thickness. According to his results, helical and driven piles show identical long-term lateral behaviour. His research discovered that the lateral resistance of both helical and driven piles is predominantly controlled by shaft diameter and embedment depth. However, when he inspected the piles after four years of their installation, he found that the helical piles' long-term lateral resistance increased by an average of 10% to 20%, outperforming the driven piles. The lack of total stiffness of the coupling joints along the pile shaft can impact pile performance under lateral loads [14]. Therefore, grouting technology was used to overcome the limits of helical screw piles, resulting in "Grouted Helical Pile." The concept of a grouted helical pile can be characterised as placing a cylindrical grout column around the helical pile's thin shaft to strengthen its buckling resistance, stiffen the coupling joints, and boost pile capacity by increasing the pile shaft resistance contribution to overall pile capacity [15].

## **4 Method of Installation**

The method of installation of conventional piles and helical piles is brilliantly explained in this paper, which will essentially be an effective comparison analysis. The purpose of this comparison is to show how their installation methods affect the environment and the long-term sustainability of civil engineering works. In order to install conventional piles, A standard pile is made up of a cylindrical steel shaft with an open or closed end and the installation characteristics of open-ended and closed-ended piles are different. Because there is less driving resistance, installing an open-ended pile is significantly easier



[10]. To install conventional piles, we have two basics techniques;

#### **4.1 Displacement Piling Installation**

The method of installing piles into the ground without removing any soil or other material is known as displacement piling installation method (i.e., Dropping weight, Vibration, Jetting).

##### **4.1.1 Dropping Weight**

A hammer about the weight of the pile is raised to recommended height and then released to strike the pile head, which is a simple dropping hammer technique.

##### **4.1.2 Vibration**

Vibratory hammers are composed of helical contra-rotating unusual pieces within a covering affixed to the pile's head and are either electrically or hydraulically propelled.

##### **4.1.3 Jetting**

Water jetting can help piles penetrate sediment or gravel-filled soil. This method, on the other hand, has had little impact on stiff clays or terrain with a lot of coarse gravel, cobbles, or pebbles.

#### **4.2 Non-Displacement Piling Installation**

Similarly, by removing any soil or other material is known as non-displacement piling installation method (i.e., The Continuous Flight Auger and Underreaming method)

##### **4.2.1 Continuous Flight Auger (CFA)**

The Continuous Flight Auger (CFA) is a mobile foundation carrier with a porous flight drill that is dragged in the soil to the required piling depth. As the pile is being lifted from the ground, concrete is poured via the flight auger to create it.

##### **4.2.2 Underreaming**

An underream is created by inserting an underreaming tool into the straight part of a pile shaft and then enlarging it at the pile's bottom. After installation and before concrete is put, a man carrying cage is normally dropped and the pile's shaft and underream are inspected.

#### **4.3 Drilling of Pile (Helical Pile Installation)**

For installation of Helical piles, Helical piles are driven in the earth in the same way that a screw is implanted into wood, but on a much greater scale. They are screwed into the ground using machine-mounted hydraulic or electrically powered drilling tools as shown in Figure 2. The benefit of helical piles is that the torque demonstrated during installation can be linked to axial capacity [10]. The torque-to-capacity ratio is monitored in real time during installation, therefore helical piles have built-in quality control. Another feature that sets helical piles apart from ordinary piles for bridge applications is the speed with which they can be installed while producing the least amount of noise and vibration [9]. Due to their ease of installation, rapid use, and other advantages over conventional pile systems, helical piles have become more popular as a deep foundation for a range of structures [11].

## **5 Soil Condition**

Except for expansive soil, conventional piles may be installed in any type of soil. However, helical piles are best suited for expansive soils of any kind of soils. But there are still some conditions (e.g., hard strata and granular soils) in which conventional piles are preferred. Borehole data and professional experience can be used to assess the likelihood of discovering hard or soft soil layers that require advanced methods and equipment. The degree of soil consistency, whether



cohesive or non-cohesive, is strongly connected to the difficulties of installing helical piles in the ground.



Figure 2: Drilling of Helical Pile [16].

The three soil types (dense to very dense sand, hard till, and hard clay) plus "gravel/cobble" are considered relatively difficult for helical pile placement [17]. Khazaei [18] stated that helix plates might break during installation process, as a result, helical pile technology is not suitable for foundations in gravelly or stiff soil. Similarly, Safdar [19] also stated that helical piles can't be used in very hard, thick, or gravelly soils because the helical plate will get damaged or the helical pile's direction might change when it comes into contact with the hard stratum. Helical piles have a high tensile and compressive strength (2 to 3 times that of a conventional pile) and can be employed in a variety of applications for a variety of soil strata both above and below the surface of the water [20].

## 6 Cost of Construction

The process of constructing a concrete foundation is not only time-consuming, but also costly. A third-party company digging the hole, constructing (and dismantling) the shuttering/forming, pouring the concrete, and removing any residual soil can cost a significant amount of money as well as construction time. A helical pile system, on the other hand, should be less expensive because we only require a helical pile and a hydraulic machine [21]. Helical piles are thought to be more cost-effective because they require less people, don't require expensive equipment when used onshore, and can be recycled [22]. A report published by Almita Piling Inc. in 2015 stated clearly that helical pile is cost effective than driven piles and cast in situ piles as shown in table 1. For example, a cost comparison is made between helical pies system and conventional pile systems in the following categories: Material cost, Shipping cost, Labour cost, Equipment cost, Other Direct cost, and Total cost, of power substation project near High River City, Calgary, Canada.

Table 1: Cost Comparison of the Three Pile Systems

Pile Type	Material Cost (\$)	Shipping Cost (\$)	Labor Cost (\$)	Equipment Cost (\$)	Other Overhead Cost (\$)	Project Duration (day)	Total Cost (\$)
Helical Pile	468,084	18,450	236,912	128,240	41,282	29	892,968
Driven Pile	459,552	97,580	270,570	207,785	64,698	32	1,089,585
CIP Pile	242,346	4,100	508,300	464,278	54,098	53	1,305,974



According to Almita Piling Inc., among the pile systems designed and installed for the defined project (power substation project near High River City, Calgary, Canada), the helical pile has the lowest installation cost, being the cheapest from conventional pile as they have the highest installation cost [23].

## 6 Installation Time

The installation of helical pile is much faster and easier than that of conventional pile. Rapid installation, immediate loading, relatively accurate capacity verification, and installation in all-weather conditions, are all advantages of helical pile construction [24]. With the help of two crew members, 10 m of helical pile may be installed in just 30 minutes [25]. The helical piles are drilled directly into the ground by machine-mounted hydraulic or electrically driven drilling equipment and can be joined in groups with a steel load transfer grillage. The relationship between (1) torque, (2) installation time, (3) soil layer, and (4) depth may exist in particular patterns in helical and conventional piles which affect the construction time rates. The construction time of helical piles is substantially faster than that of conventional heaps, since conventional piles must be hammered into the earth, which takes longer than helical piles. Helical piles can also be loaded right after installation and installed without casings through groundwater [26]. The U.S. Army Corps of Engineers in New York turned the Stony Brook University campus into a temporary field hospital, converting 255,676 square feet of space to provide care for up to 1,028 non-coronavirus patients and low acuity coronavirus patients. Helical piles, as compared to ordinary piles, were the best foundation solution since they can be swiftly installed and removed when the hospitals are no longer required [27].

## 7 Impact on Environment

Conventional piles generate noise and vibration during the process of installation. With more stringent environmental restrictions, it is becoming increasingly vital to determine if the foundation should be able to completely removed or not, during demolition of the building. To get higher bearing capacity, drilled shafts or conventional piles are installed in deeper depths and in stronger areas, then they are difficult to remove entirely during plant deconstruction. Helical foundations provide outstanding building performance and are simple to install even in difficult-to-reach situations. Furthermore, helical piles offer the environmental benefit of being easy to take out, as well as the economic benefit of being recyclable as compared to conventional pile [28]. All across the world, cementitious materials are widely used in construction. However, the cement business has a significant impact on the environment due to Carbon dioxide emission and the use of natural resources for manufacturing energy. As a result, lowering cement use is critical for achieving long-term green construction practises. Helical piles are utilised, because they are composed of steel rather than cement, to achieve long-term green construction standards. Conventional piles are pure cementitious works, which have a major impact on the environment owing to carbon dioxide emissions [15]. In New Forest England, according to Chestnut Farm Mobile Dwelling project, several houses needed to be constructed, so due to low impact on environment and aesthetic view, helical piles were used in these prefabricated mobile homes (as shown in Figure 3) [29].



*Figure 3: Chestnut Farm Mobile Dwelling project [29].*



## Conclusion

The authors of this research study came up to a conclusion that helical piles are considerably superior to conventional piles in many ways after conducting a thorough literature review. Some of the outcomes are given as under;

1. The ultimate capacities of single-helical piles were roughly 18% greater than those of conventional piles, while those of double-helical piles ranged from nearly 45 to 85 percent higher. Another researcher stated that the end bearing capacity of helical piles with helix-to-shaft diameter ratios of 2-4.1 was 2–12 times larger than that of conventional piles with similar pile shaft diameters. This extra increase in the capacity of the helical pile was due to the presence of helixes.
2. The helical piles' long-term lateral resistance increased by an average of 10% to 20%, outperforming the driven piles. To increase their lateral resistance further, grouting technique will be used.
3. They can be easily installed with the help of hydraulic machine, without making any noise and vibration thus making it environmentally friendly and green construction technique.
4. Helical piles are best suited for expansive soils or any kind of soil, however they can't be used in very hard, thick, or gravelly soils because the helical plate will get damaged or the helical pile's direction might change when it comes into contact with the hard stratum.
5. Helical piles require less people, does not require expensive equipment when used onshore, higher capacity (thus less number of piles will be required) and can be recycled, making it cost effective construction material.
6. With the help of two crew members, 10 m of helical pile may be installed in just 30 minutes, thus fast installation technique.

## Acknowledgment

The authors of the paper would like to thank their final year project supervisor **Dr Muhammad Safdar**, for his continuous guidance, proper supervision, valuable suggestion, encouragement and full co-operation in the course of the project. We are also very thankful to **Engr. Akib Ahmed** research assistance, for his immense guidance and help during the long and tiring experimental work. We are also grateful to the staff of **soil mechanics lab, concrete lab** and **material testing lab** of **Uet Peshawar** for their technical support during experimental test in laboratory. Also, the careful review and constructive suggestions by the anonymous reviewers are gratefully acknowledged.

## Reference

- [1] H. A. Qureshi, N. Ahmad and M. Safdar, "Parametric Study for Lateral Capacity of Helical Piles: A State-of-the-Art Literature Review," *Journal of Applied and Emerging Sciences*, vol. 11, no. 2, 2021.
- [2] F. Bagheri and M. H. El Naggar, "Effects of the Installation Disturbance on the Behavior of the Multi-Helix", Montreal City, Quebec, Canada: . 66th Canadian Geotechnical Conference, 2013.
- [3] K. Shao, Q. Su, J. Liu, K. Liu, "Optimization of inter-helix spacing for helical piles in sand", *Journal of Rock Mechanics and Geotechnical Engineering*, Volume 14, Issue 3, June 2022.
- [4] Y. Lin *et al.*, "Bearing Characteristics of Helical Pile Foundations for Offshore Wind Turbines in Sandy Soil", *Journal of Marine Science and Engineering*, volume 10, 2022.
- [5] M. K. Elsaywy, M. H. El Naggar *et al.*, "Seismic performance of helical piles in dry sand from large-scale shaking table tests", *Geotechnique*, Volume 69 Issue 12, 2019.
- [6] "Helical Pile, John Lawrie Tubulars LTD," 2022. [Online]. Available: <https://www.johnlawrietubulars.com/products/helical-piles>.
- [7] M. Elkasabgy and M. H. El Naggar, Axial compressive response of large-capacity helical and driven, University of Western Ontario canada: *Can. Geotech. J.*, 2014.
- [8] M. Sakr, Comparison between high strain dynamic and static load tests, Sherwood Park, Alb., Canada T8H 0G2: *Geotechnical Engineering*, Elsevier, 2013.



**4<sup>th</sup> Conference on Sustainability in Civil Engineering (CSCE'22)**  
Department of Civil Engineering  
Capital University of Science and Technology, Islamabad Pakistan



- [9] M. Sakr, "High Capacity Helical Piles- A New Dimensions for Bridge," in *8th International Conference on Short and Medium Span Bridges*, Niagara Falls, Canada, 2010.
- [10] A. A. Malik, J. Kuwano, S. Tachibana and T. Maejima, "End bearing capacity comparison of screw pile with straight pipe," *Acta Geotechnica*, 2016.
- [11] O. K. Ali and H. O. Abbas, "Performance Assessment of Screw Piles Embedded in Soft Clay," *Civil Engineering Journal*, vol. 5, no. 8, 2019.
- [12] M. Sakr, "Performance of laterally loaded helical piles in clayey soils established from field experience," *The Journal of the Deep Foundations Institute*, 2018.
- [13] B. Dinh, J. Liu, J. Dunn, J. Zhang, P. Huang, "Long-term Lateral Resistance of Helical Piles in Cohesive Soils," *Almita Piling Inc., Ponoka, Alberta, Canada, Geo Regina*, 2014.
- [14] R. A. Vickars and S. P. Clemence, "Performance of Helical Piles with Grouted Shafts. In New Technological," in *In New Technological and Design Developments in Deep Foundations GeoDenver*, Reston, Virginia, USA, 2000.
- [15] M. Mansour, M. Aboutabikh, A. M. Soliman and M. H. E. Naggar, "Sustainable Grouted Helical Piles: Materials and Performance," in *Conference: CSCE 2016 Annual General Conference*, London, Ontario, Canada, 2016.
- [16] A. J. Lutenecker, "Foundation Alternatives for Ground Mount Solar Panel Installations," *Geotechnical and Structural Engineering Congress*, 2016.
- [17] Yi, Chaojue, Li, Baocheng, Zheng, Chaoyu and Lu, Ming, "Simulation Based Contingency Estimating for Helical Pile Installation," *Leadership in Sustainable Infrastructure*, 2017.
- [18] Khazaei, Javad, and A. Eslam, "Geotechnical Behavior of Helical Piles via Physical Modeling by Frustum Confining Vessel (FCV)," *International Journal of Geography and Geology*, Vols. 5, no. 9, 2016.
- [19] M. Safdar and H. A. Qureshi, "Practical Applications of Helical Piles: A State-of-the-Art Literature Review," *Technical Journal*, vol. 26, no. 4, 2021.
- [20] Al-Baghdadi, M. J. Brown, J. A. Knappett and A. H. Al-Dafae, "Effects of Vertical Loading on Lateral Screw Pile Performance," in *Institution of Civil Engine, Geotechnical Engineering 170*, 2017.
- [21] W. C., "Super Tiny Houses," 2021. [Online]. Available: <https://www.supertinyhomes.com/screw-pile-foundations-for-tiny-houses-and-backyard-offices/>.
- [22] P. P. Kumar, Patar and Haldar, "A Critical Review on Design Aspects of Screw Piles for Renewable Energy Devices," in *1st International Screw Pile Symposium on Screw Piles for Energy Applications*, Scotland, 2019.
- [23] C. Yi and M. Lu, Foundation Construction Cost Comparison: Helical Pile, Driven Pile, and CIP Pile, University of Alberta, 2015.
- [24] H. A. Perko, Helical Piles: A Practical Guide to Design and Installation, Wiley, 2009.
- [25] M. Safdar, H. A. Qureshi, F. Shah and N. Ahmad, "Parametric Study and Design Method for Axial Capacity of Helical piles: A Literature Review," *Journal of Applied and Emerging Sciences*, vol. 11, no. 2, 2021.
- [26] D. E. Bobbitt and S. P. Clemence " Helical Anchors: Application and Design Criteria," in *9th Southeast Asian Geotechnical Conference*, Bangkok, Thailand: 6-105 to 6-120., 1987.
- [27] "IDEAL", Helical Pile Foundations for Covid-19 Field Hospitals in New York, 2020. [online]. Available: <https://www.idealfoundationsystems.com/helical-pile-foundations-for-covid-19-field-hospitals-in-new-york/>
- [28] J. Bak, B.-h. Choi, J. Lee, J. Bae, K. Lee and D. Kim, "Behaviour of Single and Group Helical Piles in Sands from Model Experiments," in *2nd International Conference on Building Materials and Materials Engineering (ICBMM)*, Republic of Korea, 2018.
- [29] "Screw Fast Foundation", Chestnut Farm Mobile Dwelling, 2022. [online]. Available: <https://www.screwfast.com/case-study/chestnut-farm-mobile-dwelling/>.



# EXPERIMENTAL STUDY ON LOAD CARRYING CAPACITY OF INDIVIDUAL PILES IN A PILED RAFT FOUNDATION SYSTEM

<sup>a</sup> Muhammad Zubair\*, <sup>b</sup> Naveed Ahmad, <sup>c</sup> Irfan Jamil, <sup>d</sup> Abrar Ullah

a: Civil Engineering, University of engineering and technology Taxila, [xubikhan.edu@gmail.com](mailto:xubikhan.edu@gmail.com)

b: Civil Engineering, University of engineering and technology Taxila, [naveed.ahmad@uettaxila.edu.pk](mailto:naveed.ahmad@uettaxila.edu.pk)

c: Civil Engineering t, University of engineering and technology Peshawar, [irfanuop@hotmail.com](mailto:irfanuop@hotmail.com)

\* Muhammad Zubair : Email ID: [xubikhan.edu@gmail.com](mailto:xubikhan.edu@gmail.com)

**Abstract-** Raft foundations are provided, in case isolated footing fills more than 70 % area of building under a superstructure. The term "piled raft foundation" refers to a foundation that incorporates the usage of piles and rafts. When high-rise buildings are constructed on soil of low bearing capacity or on fill material, piled raft foundation system have proven to be cost-effective without compromising serviceability and bearing capacity requirements. The use of tactically positioned piles beneath a raft can increase the raft's load bearing capacity and decrease differential settlements. Current study is focused on evaluation of individual piles' load carrying capacity in a piled raft foundation system embedded in poorly graded sand with relative density of 35 %. A small-scaled model was prepared in the laboratory containing galvanized iron piles and aluminum raft. The piles were instrumented through strain gauges in order to measure the load resisted by each pile. The piled raft model was placed in the center of sand container and subjected to vertical load. It was found that the load bearing capacity of piled raft is much greater as compared isolated pile and raft only.

**Keywords-** Piles, Raft, Piled raft foundation system, Load sharing capacity, small scaled model

## 1 Introduction

Foundations are the most significant and important part of civil engineering structures. The main function of foundation is, to take load from superstructure and transfer it into underlying soil to ensure structure stability and serviceability requirements. As foundation is one of the most important and critical part of any civil engineering structure so it should be designed very carefully because foundation failure will lead to failure of whole structure. The three main types of foundations for high rise buildings are, raft foundation, pile foundation and piled raft foundation. When the subsoil is having good bearing capacity like gravel and dense sand, raft foundation system is most economic option for high-rise buildings. Example are Trianon tower, Trianon tower is about 190 m high, and Main Plaza tower which is about 90 m high, both are good examples, in Frankfurt in which settlements are less than 100 mm and tilting less than 1:800 [1]. When upper soil layer is weak, having low bearing capacity and unable to support load from superstructure, piles foundations are provided to transfer the load to hard strata. The load from superstructure is transferred to soil via skin friction or end bearing or by the combination of end bearing as well as skin friction. Piled raft foundation is an amalgamation of raft which is called shallow foundation, and piles (deep foundation) in which load is shared between raft and piles to enhance load carrying capacity of soil and reduce structural settlements. Arrangement of piles can be adjusted to reduce differential settlement of foundation system and improve load bearing capacity of raft. In traditional design philosophy of piled raft foundation, it was assumed that the total load from superstructure is resisted by piles while ignoring the contribution of raft [2]. As raft is directly get in touch with soil, so it bears a considerable portion of load from superstructure, making the traditional method of design of piled raft too conservative. If contribution of raft is ignored, the number and length of piles



will be increased, making the design uneconomical. The design philosophy for piled raft foundation system is now changing, acknowledging the contribution of raft in a piled raft foundation system. Piles are not only designed to take load from superstructure but also work as to reduce settlements [3]. A piled raft foundation has composite soil structure interaction. Care be required to be taken in the analysis of pile soil interaction, raft soil interaction, pile, pile interaction and pile raft interaction [4]. For high rise buildings, the majority of piled raft foundations were constructed on Frankfurt clay using settlement-reducing piles[5]. The tactically positioning of piles can improve the raft's load bearing capacity and tend to decrease differential, settlements [6]. Davids conducted experimental study and showed that the load from superstructures is shared between raft as well as piles, in which piles resist about 50 to 80 % of the total applied load while the remaining load was beard by raft [7]. The part of vertical loading from the super structure is transferred to the underneath soil via raft contact pressure, which varies from 30 to 60 % of the total vertical applied load; depending on the condition of soil under raft. The above percentage is not constant, as the pile length decreases, the load carried by raft increases. Also, load carrying capacity of raft increases while increasing spacing between piles. They also demonstrated that, in the case of weak soil or soft clay, the piled raft system is suitable for high-rise buildings in terms of bearing capacity and serviceability requirements [8]. Hemsley predicted that, the contribution of raft is about 50 % of the total load from superstructure[9]. When designing a piled raft system, it was revealed that the raft resisted load in a piled raft foundation system ranged from 25 to 51 % of the total applied load applied, with an average assessment of 36 %. The load from superstructure is divided among raft and piles, while the piles system usually resisting about 50 to 80 % of the total applied load and transferring such load in deeper strata [10]. From previous few decades, high rise buildings especially in Gulf area has been constructed, on piled raft foundation system. Few of them include as Burj Khalifa in Dubai and QIPCO tower in Doha[11]. According to available research study, most of researcher worked on combined load bearing capacity of piles in a piled raft foundation system. The main purpose of this study is to explore the individual piles load sharing capacity in piled raft foundation system.

## 2 Experimental Study

### 2.1 Scope

The core purpose of this study is to evaluate the load sharing capacity of individual piles in a piled raft foundation system under vertical load. For this purpose, a small scale model was prepared in the laboratory and subjected to vertical loading to predict individual piles load sharing capacity, as inadequate research has been carried out on individual behavior of piles under vertical loading. So the modern age demand to conduct experimental study using small scale model to predict individual piles load carrying capacity. This study also aims for the estimation of piled raft settlement against applied vertical load.

### 2.2 Test Equipment

To study the individual piles' load sharing capacity in a piled raft foundation system, a small scale piled raft model was prepared in the laboratory and filled with loose sand. The raft was modeled square with dimension of 30 x 30 cm and 2.54 cm thickness. The raft was made of aluminum with modulus of elasticity 69 GPa. Holes were provided within raft surface for installation of piles in different configurations. In total 25 holes with 1.3 cm diameter and 6.35 cm center-to-center spacing were drilled into raft surface. The piles were made of Galvanized iron having modulus of elasticity of 200 GPa. The piles were made circular and hollow from inner side. Diameter of the piles was 1.905 cm and they were attached with raft using nut bolts assembly. Nine (09) piles were manufactured in the laboratory having length of 45 cm. Calibrated strain gauges were installed on each pile to predict the load taken by individual piles. A calibrated vertical load cell with maximum capacity of 08 ton was also installed to verify the load taken by piles as observed by strain gauges. LVDTs (Liner Variable Displacement Transducer) with their tips placing vertically on raft were installed on each side of raft. The accuracy of LVDTs was 0.01 mm and their purpose was to measure vertical displacements (Settlements) and rotation of piled raft in case of differential settlement. The general view of the load test equipment and description of each part is shown in figure.1





Figure 1: General view of vertical loading test arrangements

- |                               |                                   |          |
|-------------------------------|-----------------------------------|----------|
| 1. Vertical load arrangements | 4. Sand container                 | 7. LVDTs |
| 2. Vertical load cell         | 5. Frame supporting for pluviator |          |
| 3. Raft                       | 6. Data logger                    |          |

Load was applied concentrically and vertically on the piled raft model and vertical displacement (settlements) were recorded with the help of LVDTs as installed at raft surface via data logger. The soil container was rectangular with dimensions of 1.50 m height, 1.20m length, and 0.90m width and was made of steel. The dimension of sand container is large enough to satisfy boundary condition. The sand container was made large enough in order to satisfy boundary conditions. The soil container was strengthened by providing supports to the side walls of container. The purpose of providing extra supports was to prevent the container from bulging while applying load on pile raft model. The piled raft model was placed accurately in the center of sand container. To ensure the horizontal and vertical leveling of test model, spirit level was used.

### 3 Experimental Procedures

The soil used for this study was poorly graded sand. Grain size distribution analysis was carried out using a set of sieves as per ASTM D-422. The grain size distribution curve has been plotted and presented in figure 2. Coefficient of curvature ( $C_c$ ) and uniformity coefficient ( $C_u$ ) calculated were 0.72 and 3.12, respectively. The sand has been classified as poorly graded. The properties of sand have been listed in table 1. As per ASTM D-4254 and D-4253, the minimum and maximum unit weights were 106 pcf and 92 pcf, respectively. Testing was carried out at relative density of 35%. This density was obtained through mobile pluviator. The mobile pluviator was calibrated by falling sand from sand cone through different heights. The desired density was obtained by falling sand from height of 9.5 inch. In order to maintain uniformity of sample a shutter with 13mm holes is attached at the bottom of sand cone. As the height of sand container is 1.50 m so it was filled in 10 layers while each layer of sand is 15 cm.

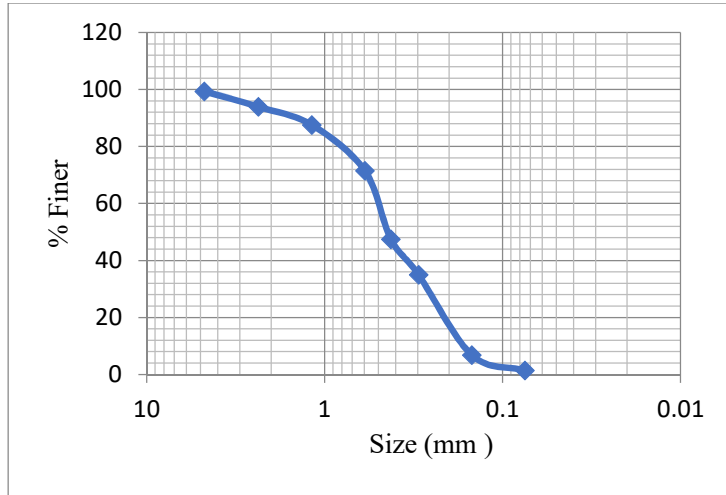


Figure 2: Sieve Analysis

Parameter	Value	Remarks
D60	0.5	
D50	0.46	
D30	0.24	
D10	0.16	
Coefficient of Uniformity (CU)	3.12	SP because $C_u < 6$ and $C_c < 1$
Coefficient of curvature (CC)	0.72	
Maximum unit weight	106 PCF	
Minimum unit weight	92 PCF	

Table 1: Properties of sand

## 4 Results and Discussion

Following different configurations were made and will be discussed in subsequent sections.

- Single pile only
- Raft only
- 04 piled raft

### 4.1 Single pile

Load bearing capacity of single pile was determined by subjecting pile to vertical load. The pile was installed at the centre of sand container and LVDTs were installed to measure settlement. At a load of 272 N, a very high settlement value of 6.8mm was measured, that is about 36% of pile diameter. Load settlement curve for tested pile has been shown in figure 3. A linear relationship was observed.

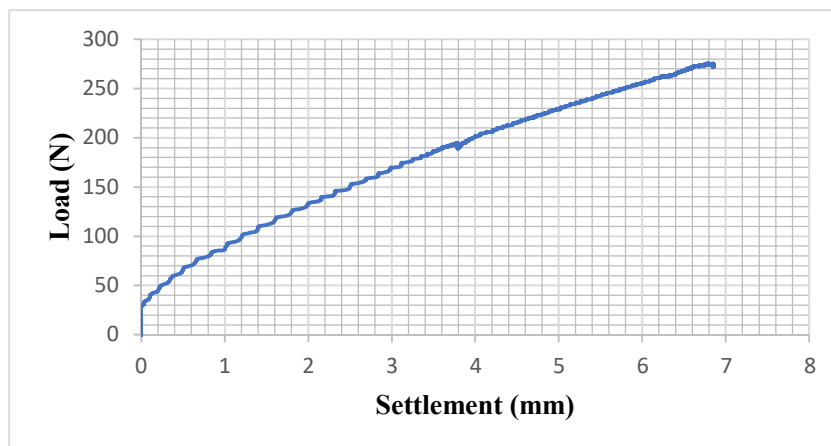


Figure 03: Load versus Settlement curve of single pile



#### 4.2 Raft only

The behaviour of raft to vertical loading was observed by placing raft in the centre of sand container after sand pluviation. 5000 N vertical load was applied and load versus settlement curve was plotted as illustrated in figure 4. From figure, it is clear that the raft settles 7.6 mm at 5000 N load. Although, settlement to load ratio for raft is less than that of single pile but still it is too high to be not allowed for practical situations.

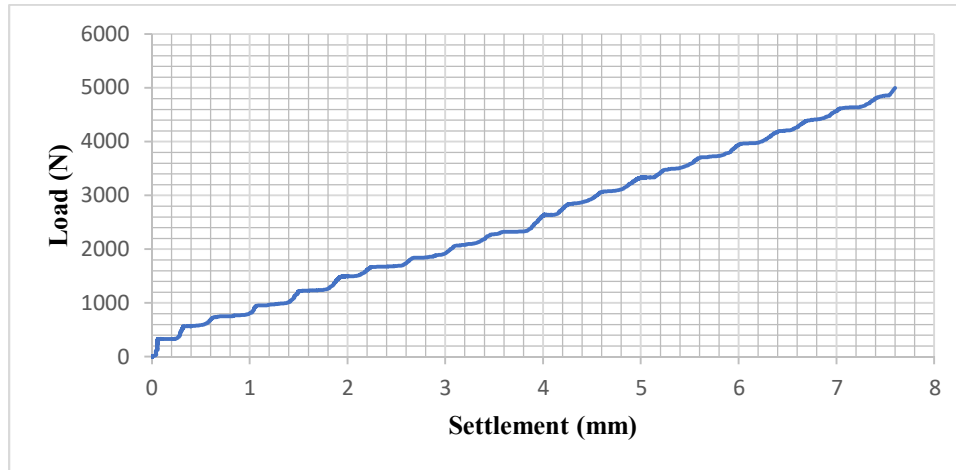


Figure 4: Load versus settlement curve of raft

#### 4.3 Piled Raft

Four piles were attached rigidly with the help of nut and bolt to raft with centre to centre distance of 25 cm and subjected to vertical loading up to 5000 N. The contributions of piles to vertical loading are presented in figure 5. As it is clear from graph that a total of 5000 N vertical load was applied to piled raft. The load taken by piles in this case was 57.7% and load beard by raft was 42.3% at settlement of about 3.6 mm. Initially the contribution of raft is less but as vertical load increases, the soil beneath the raft gets compacted and stiffness of soil increases causing an increase in its load sharing. It is clear from figure that with further increase in load, the contribution of raft increases, at some point beyond 4.1mm the raft contribution to load reaches to 50 %. So, it is clear that for a piled raft foundation system constructed on loose sand, initially load sharing of raft is less but with increase in load, the soil gets compacted and raft contribution tend to increase.

Load shared by individual piles in a piled raft foundation system is presented in figure 6. From figure, it is clear that all the piles carry almost same amount of load. So, we can say that some portion of load was beard by raft and remaining load was uniformly shared with piles. Figure 7 summarized the above discussion by presenting the percentage load carried by raft, piles and individual piles.

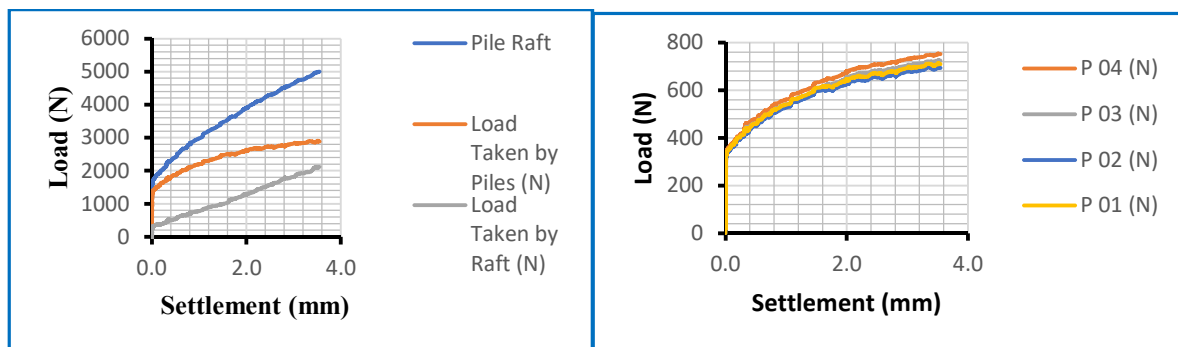


Figure 5: Load versus settlement curve of 04 piled raft

Figure 6: Load versus settlement curve of individual piles piledraft

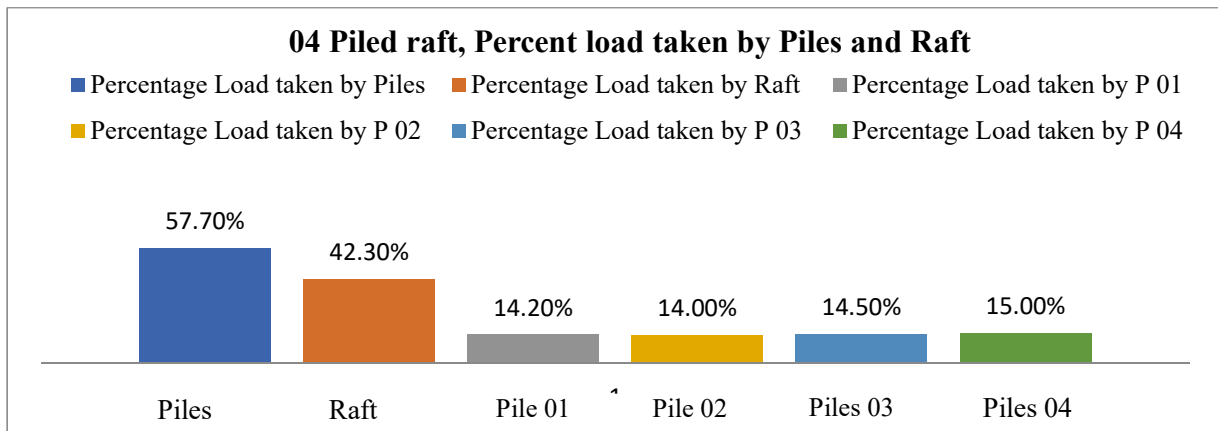


Figure 7: Percentage load taken by piles and raft

## 5 Conclusions

Based on current experimental study, the following conclusions can be made:

1. Single pile is not efficient to take vertical loads and settles down significantly under nominal load. By providing raft, settlement will be reduced.
2. In piled raft foundation, the piles not only take load as transferred via raft but also act settlement reducer.
3. Raft with no pile bears load of 5000 N at a settlement of 7.6 mm but with the addition of 4 piles with the same raft and same loading conditions, the settlement was reduced to 3.6mm. With the addition of 4 piles the settlement was reduced about 50%.
4. In a piled raft foundation system with four piles, applied vertical load is uniformly distributed among all the piles.

## References

- [1] Phung Duc Long. "Piled raft - A new foundation design philosophy for high rises" Geotechnics for Sustainable Development-Geotec Hanoi 2011, Phung .Construction Publishing House ISBN 978-604-82-000-8.
- [2] J.B. Burland, B.B. Broms, V. Demello, "Behavior of Foundation and Structures" in: Proc. 9th. ICSMFE, Tokyo, 1977, pp. 495-546
- [3] Burland, J.B, Broms, B.B, De Mello, V.F.B. (1977). Behavior of foundations and structures. Proc. 9th ICSMFE, Tokyo, Vol. 2, 495-546
- [4] Yilmaz, B., (2010), "An Analytical and Experimental Study on Piled Raft Foundations", MSc. Thesis, Middle East Technical University, Ankara.
- [5] Katzenbach, R., Schmitt, A., Turek, J.(2003).Reducing the costs for deep foundations of high-rise buildings by advanced numerical modeling. ARI The Bulletin of the Istanbul Technical University, Vol. 53, No.2.
- [6] A.Z. Elwakil, W.R. Azzam 2015. Experimental and numerical study of piled raft system. Alexandria Engineering Journal (2016) 55, 547-560.
- [7] A. Davids, A postcard from Dubai design and construction of some of the tallest buildings in the world, in: Proc. of the CTBUH 8 the World Congress, 3-5 March, Dubai, 2008.
- [8] Leung et al, Role of linear elasticity in pile group analysis and load test interpretation, J. Geotech. Geo-environ. Eng. ASCE 136 (12) (2010) 686-694
- [9] H.G. Poulos, The Piled Raft Foundation for the Burj Dubai Design and Performance: A presentaco Programa pos Graducaoem Geotencia-Brasilia-DF, 2010.



# AN EXPERIMENTAL STUDY ON LATERAL CONTRIBUTION OF RAFT AND PILE IN A PILED RAFT FOUNDATION SYSTEM

*<sup>a</sup>Abrar Ullah\*, <sup>b</sup>Naveed Ahmad, <sup>c</sup>Kiramatali*

a: Civil Engineering, University of Engineering and Technology Taxila, [enr.abrarullah@gmail.com](mailto:enr.abrarullah@gmail.com)

b: Civil Engineering, University of Engineering and Technology Taxila, [Naveed.ahmad@uettaxila.edu.pk](mailto:Naveed.ahmad@uettaxila.edu.pk)

c: Civil Engineering, University of engineering and Technology Peshawar, [kiramatali30@gmail.com](mailto:kiramatali30@gmail.com)

\* Corresponding author: Email ID: [enr.abrarullah@gmail.com](mailto:enr.abrarullah@gmail.com)

**Abstract-** In the recent past, with increasing height of the buildings, the pile raft foundation is becoming an efficient choice to transmit the load safely to the ground. The high rise buildings and communication towers are exposed to vertical loads from superstructure and lateral loads from earthquake, wave action and wind etc. In such situation, to increase the load carrying capacity of the foundation and to decrease lateral and vertical displacement, piles are provided under the raft. This type of foundation system is call piled raft foundation system. In pile raft foundation system, the load is distributed between the piles and the raft, making the system economical as compared to old traditional methods in which the piles were taking all the loads. A lot of research work has been carried out on vertical contribution of raft in the pile raft foundation system. There is very limited literature available on contribution of raft to resist lateral loads. If raft contribution to resist lateral loads is considered, foundation design could be made more economical. In this research work, a small-scale model pile raft foundation model was used for experimentation. It was observed that a considerable amount of lateral load was resisted by the raft component. From the test results it came to know that with increasing the number of piles, the load carrying capacity/ contribution of raft decreases. It was also observed that rear piles resist more lateral load compared to the front piles in a pile group.

**Keywords-** Pile raft foundation system, Deep foundation, High rise structure, Lateral load contribution

## 1 Introduction

For many years, pile foundations have been used as load bearing and transferring systems. During the early days of civilization, the load bearing capacity of the ground was improved by driving timber piles into the ground by hand or digging holes and filling them with sand and stones. In 1740, after the invention of pile driving equipment by Christoffoer Polhem, the use of pile foundation gained more popularity. During the designing of Tower Latinoamericana, Mexico in 1956, Dr. Leonardo Zeevaert introduced the concept of combined piled raft system to enhance the loading carrying capacity of underneath weak compressible soil. This was the first high rise building in which combined pile raft foundation was used; otherwise, the pile foundation was the only option for tall buildings before this concept. The tower gained attention of geotechnical society when it withstood at 7.9 magnitude earthquake in 1957. Now-a-days, if bearing capacity of soil is sufficient, raft foundation is provided under tall buildings to transfer the load to underneath soil safely, otherwise piles are provided in combination of raft to transfer the imposed loads to underlying soil strata [1]. In [2], the optimization of pile location in piled raft foundation and its effect on the reduction of differential settlement are studied.

In [3], the piled raft foundation which was designed for Messeturm tower in Frankfurt is studied, with more piles organized near the corners. It was determined from this practical case that the reduction of total and differential settlement is dependent on pile configuration and comparative stiffness of raft-soil system.

In [4], small scale piled raft model in the centrifuge test were studied with different pile configuration. The experimental study concluded that centralizing piles surrounding point load (i.e., where columns are located) reduces total as well as differential settlements, improving design cost-effective but also efficient. According to [5], load resisting of pile's varies with their position in a group, and ultimate lateral resistance within pile group is reduced due to stress zone overlapping in the surrounding soil. They also came to the conclusion that the lateral resistance of a pile group is function of row position within a group. Results in [6] demonstrated that, for a given displacement, piles in leading row sustained more load than



piles in tailing row, and that, due to group effect; all piles in the group take less load than a single pile. It was discovered in [7, 8] that pile spacing is directly related to average lateral resistance and group interaction has a considerable impact on lowering pile lateral resistance. Several experiments are also conducted to investigate pile behavior under various load combinations. The influence of lateral load and bending moment on load carrying capacity of a single pile and a pile group was calculated, and presence of lateral loads or bending moment resulted in significant decrease in vertical load carrying capacity [9]. According to [10, 11], the lateral displacement of piled raft foundation increases under combined loads. According to the available literature, most researchers have done work on lateral response, but they only calculated lateral deflection with the conclusion that the raft contributes to lateral load resistance. The purpose of this research is to determine the potential of raft and piles in resisting lateral load in a combined piled raft foundation System using experiments on instrumented small scale models.

## 2 Experimental Study

### 2.1. Scope

The main purpose of this research is to study the lateral load contribution of piles and raft in a combined piled raft foundation system under a constant vertical load. For this purpose, a small-scale model was prepared in the laboratory and subjected to uniformly increasing lateral loading in the presence of constant vertical loading. The contribution of piles and raft is determined against every lateral loading.

### 2.2. Experimental Setup and Equipment

To study the lateral load contribution in a combined piled raft foundation system, a small scale instrumented piled raft model was prepared in the laboratory. The container was filled with loose sand having relative density of 35%. The modeled raft was square in shape and made of aluminum with dimension of 30 x 30 cm and 2.54cm thickness. Total 25 holes with 1.3 cm diameter and 6.35cm center-to-center spacing were drilled into raft surface for installation of 1.905cm diameter galvanized iron piles in different configurations. The piles were made circular and hollow from inner side having length of 45cm. They were attached with raft using nut and bolts assembly. Calibrated strain gauges were installed on each pile to measure the lateral load contribution of each pile connected in combined piled raft model. A calibrated vertical load cell with maximum capacity of 08 ton was also installed to measure the applied vertical loads. Linear Variable Displacement Transducers (LVDTs) with their tips resting laterally on raft were installed on each side of raft. The accuracy of LVDTs was 0.01 mm and their purpose was to measure lateral displacements. The Schematic and pictorial view of the experimental setup and its parts are shown in Figure1 and Figure 2, respectively.

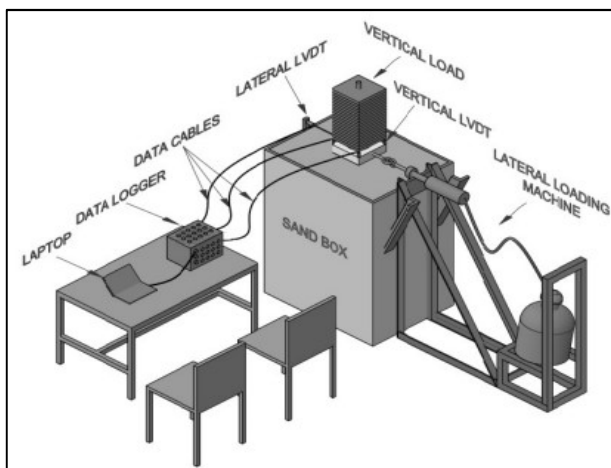


Figure 1: Schematic view of experimental setup



Figure 2: Pictorial view of experimental setup

The piled raft model was placed accurately in the center of rectangular soil container with dimensions of 1.5m height, 1.2m length and 0.9m width as shown in Figure 3. The soil container was filled with sand of required relative density of 35%



using mobile pluviator as shown in Figure 4. Two pile configurations were used during current study. Four piles with center to center spacing of 254mm and 5 piles with same layout but having an extra pile in the middle of the 4 piles setup were used for testing purposes. The lateral load was applied perpendicular and concentrically to the raft under constant vertical load of 5000N. The lateral displacement was noted with the help of LVDTs via data logger.

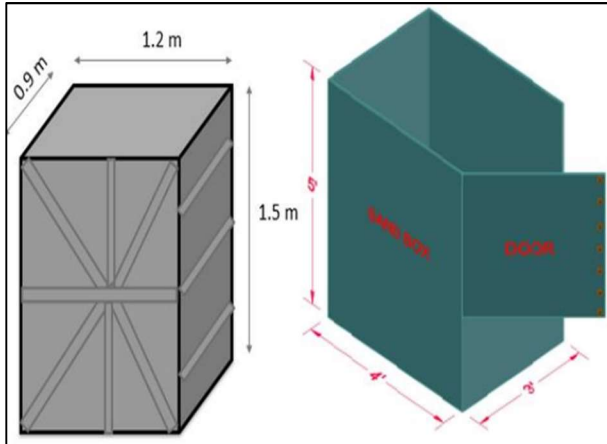


Figure 3: Model sand container

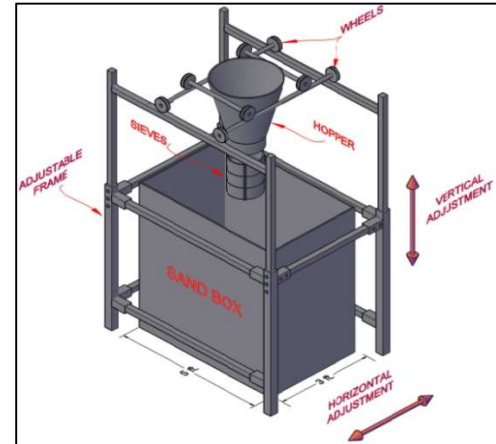


Figure 4: Mobile pluviator

### 2.3. Experimental Procedures

The grain size distribution curve was plotted after carrying out of sieve analysis on the testing soil according to ASTM D-422 as shown in Figure 5. The uniformity coefficient ( $C_u$ ) was 3.12 and the coefficient of curvature ( $C_c$ ) was 0.72 as per the plotted grain size distribution curve. The testing soil was classified as poorly graded sand. The maximum and minimum unit weight of the testing soil found 106pcf and 92pcf respectively as per ASTM D-4253 and D-4254.

The piled raft modes testing were conducted in testing soil having relative density of 35%. The targeted relative density of testing soil was achieved through sand raining technique using mobile pluviator. Several trials were carried out to find the exact height of fall to achieve 35% required relative density. The required relative density was achieved by falling sand from a height of 9.5 inches. In order to maintain uniformity of sample, a shutter with 13mm holes was attached at the bottom of sand cone and the 1.5m high sand container was filled in 10 layers with each layer of 15cm thickness.

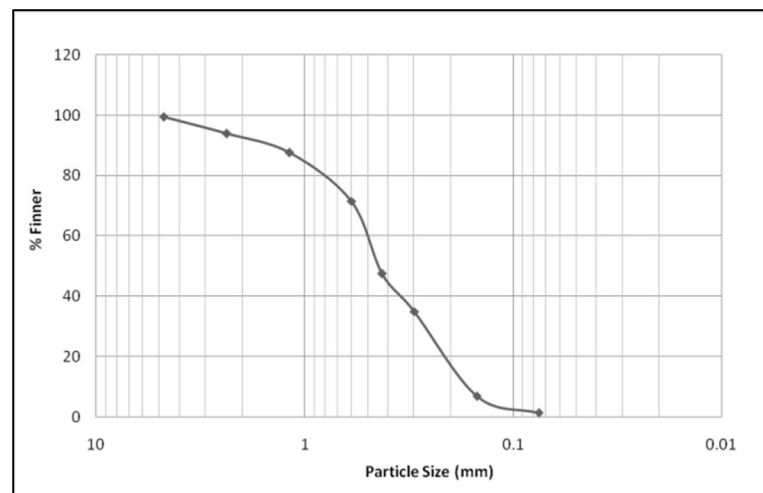


Figure 5: Grain size distribution curve



The piles were placed at their respective location when the container was filled up to 1.2m height. After placing the piles, the sand raining again started till the container filled completely. The raft was then fixed by a nut and bolt system with the already placed piles, and a little downward pressure was applied on the raft to make full contact of the raft with the soil. The schematic and pictorial representations of the detailed experimental study are shown in Figure 1 and 2. The installed load cells, strain gauges and LVDTs were connected with data logger to record the required data. Lateral load was applied after application of a constant vertical load of 5000N and data was recorded.

### 3 Results and Discussion

Two cases with following pile and raft configuration were used for this study:

- Four piles attached with raft as shown in Figure 6 and 8.
- Five piles attached as shown in Figure 7 and 9.

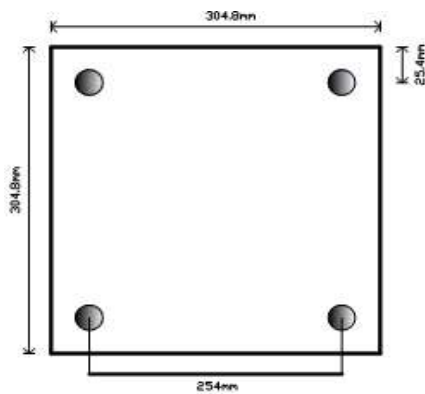


Figure 6: Plan view of 4-Piled Raft Model

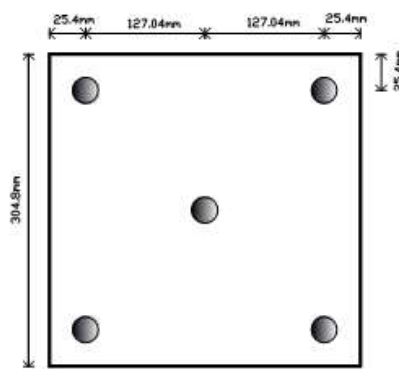


Figure 7: Plan view of 5-Piled Raft Model

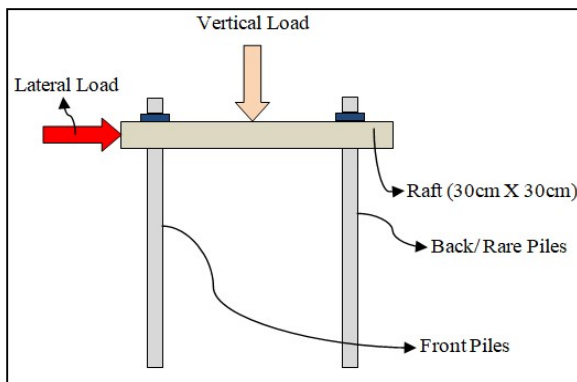


Figure 8: Sectional view of 4-Piled Raft Model

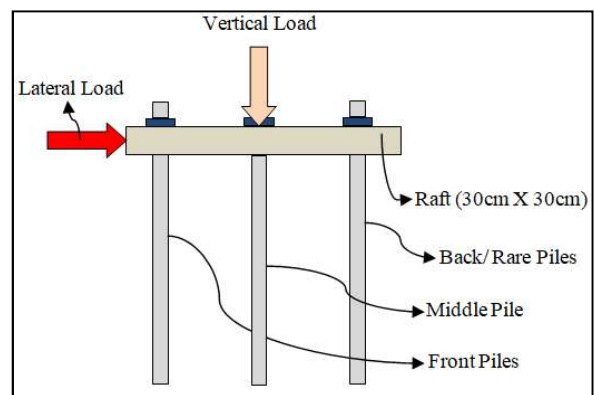


Figure 9: Sectional view of 5-Piled Raft Model

#### 3.1 4-Piled Raft Model

Four piles with center-to-center distance of 254mm were rigidly connected to the raft by nut bolt system as shown in Figure 9. Initially, the system was subjected to constant vertical load of 5000N followed by lateral loading through hydraulic jack. Figure 10 shows that initially all the load is taken by raft due to high stiffness and it mobilizes at very small strain. Raft contribution to resist lateral load is also dependent on the lateral displacement because at large displacement the contact between the soil and the raft may vanish. At approximately 2 mm lateral displacement, the pile contribution exceeds the raft contribution as the soil in front of the piles gets compacted and hence results in an increase in soil stiffness.





Figure 11 shows that back piles take more load throughout the lateral displacement, compared to front piles. This is because the soil available in front of the back piles has high stiffness due to confinement. This behavior is against the pile group where front piles take more load because the front pile leaves free space behind and due to this free space, the soil stiffness decreases in front of the back piles.

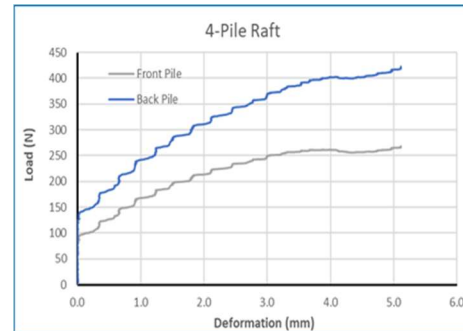
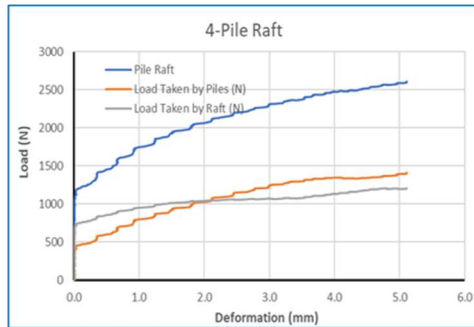


Figure 10: Load distribution b/w piles, raft and piled raft model    Figure 11: Load distribution b/w front pile and back pile

### 3.2. 5-Piled Raft Model

The same layout was maintained as in pile raft with 4 piles with an additional pile installed at the center of raft. Before application of lateral load, a constant vertical load of 5000N was applied. Figure 12 shows that initially total load is resisted by raft. After raft mobilization, the piles started resisting lateral load. Initially, the raft showed very high stiffness, followed by sudden degradation of stiffness. This is because the raft resists lateral load only by skin friction between raft and the underlying soil. In contrast to the 4-Pile raft, where the pile contribution exceeded the raft contribution at 2 mm, in this case the raft and pile contribution continued and never cross each other. This is because the center pile provides resistance to avoid overturning/tilting of the system. As piles number increased from 4 to 5, the raft load reduced from 750 N to 200 N at 1mm displacement. From Figure 13, it is clear that again back piles take more load, but up-to 1 mm displacement the difference between the loads taken by piles is very small. After 1 mm lateral displacement, the difference gets predominant. The middle pile and back pile take same load upto 1.5 mm displacement after that the stiffness of middle pile decreased, reaching a constant stiffness at very high displacement.

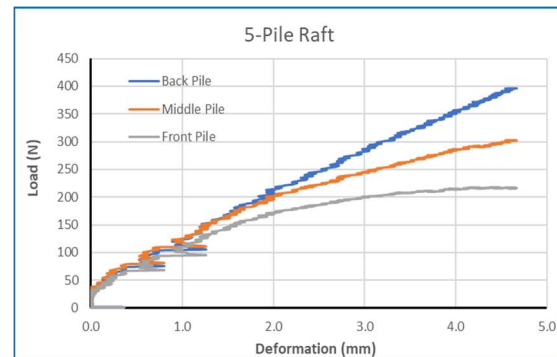
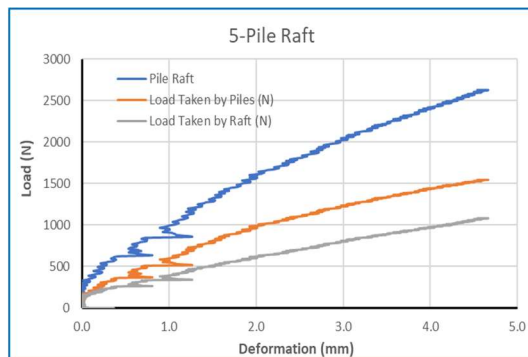


Figure 12: Load distribution b/w piles, raft and piled raft    Figure 13: Load distribution b/w front piles, middle and back piles.

## 4 Conclusions

- 1) At small or no lateral strain, more lateral load is taken by the raft compared to piles. After 2mm displacement, the soil in front of the piles gets compacted increasing stiffness of the piles and so their contribution in lateral load sharing.
- 2) Contrary to group piles behavior, back piles take more load compared to front piles in case of pile raft foundation system.



- 3) With increase in number of piles, the load sharing by raft decreases and that of piles increases at a given lateral displacement value.

## Acknowledgment

I am thankful to Civil Engineering Department, University of Peshawar for allowing me to use their experimental setup for this research work. This research work would be impossible without their support.

## References

- [1] Poulos H. G., "Piled raft foundations: design and applications", *Geotechnique* 51.2 (2001) 95-113.
- [2] Kim K. N., Lee S. H., Kim K. S., Chung C. K., Kim M. M., Lee H. S., "Optimal pile arrangement for minimizing differential settlements in piled raft foundations", *Computers and Geotechnics* 28, no. 4 (2001) 235- 253.
- [3] Katzenbach R., Bachmann G., Boled-Mekasha G., Ramm H., "Combined pile raft foundations (CPRF): An appropriate solution for the foundations of high-rise buildings", *Slovak Journal of Civil Engineering (SJCE)* (2005) 19-29.
- [4] Nguyen D. D., Kim D. S., Jo S. B., "Settlement of piled rafts with different pile arrangement schemes via centrifuge tests", *Journal of Geotechnical and Geoenvironmental Engineering* 139.10 (2013) 1690-1698.
- [5] Brown D. A., Morrison C., Reese L. C., "Lateral load behavior of pile group in sand", *Journal of Geotechnical Engineering* 114.11 (1988) 1261- 1276.
- [6] Rollins K. M., Peterson K. T., Weaver T. J., "Lateral load behavior of fullscale pile group in clay", *Journal of geotechnical and geoenvironmental engineering* 124.6 (1998) 468-478.
- [7] Comodromos E. M., Ptilakis K. D., "Response evaluation for horizontally loaded fixedhead pile groups using 3D non-linear analysis", *International Journal for Numerical and Analytical Methods in Geomechanics* 29.6 (2005) 597-625.
- [8] Kim B. T., Yoon G. L., "Laboratory modeling of laterally loaded pile groups in sand", *KSCE Journal of Civil Engineering* 15.1 (2011) 65-75.
- [9] Meyerhof G. G., Yalcin A. S., "Pile capacity for eccentric inclined load in clay", *Canadian Geotechnical Journal* 21.3 (1984) 389-396.
- [10] Davisson M. T., Robinson K. E., "Bending and buckling of partially embedded piles", *Proceeding of the 6th International Conference on Soil Mechanics and Foundation Engineering*. Montreal; (1965) 243-246.
- [11] Stacul, Stefano and Nunziante Squeglia. "Analysis of Laterally Loaded Piled Raft Foundation." *Proceedings of the 4th World Congress on Civil, Structural, and Environmental Engineering* (2019)
- [12] Jamil, I., & Ahmad, I. (2019) "Bending moments in raft of a piled raft system using Winkler analysis". *Geomechanics and Engineering*, 18(1), 41-48. (2019).



# EXPERIMENTAL STUDY OF INFLUENCE THE BEARING CAPACITY OF SANDY SOIL BY USING CEMENT GROUTING

<sup>a</sup> Muhammad Adil Nawaz\*, <sup>b</sup> Muhammad Ashgar, <sup>c</sup> Muhammad Aleem, <sup>d</sup> Hammad Raza

a: Department of Civil Engineering, University of Engineering and Technology Taxila, [adilqaisrani786@gmail.com](mailto:adilqaisrani786@gmail.com)  
b: Department of Civil Engineering, University of Engineering and Technology Taxila, [asgharghani0078600@gmail.com](mailto:asgharghani0078600@gmail.com)  
c: Department of Civil Engineering, University of Engineering and Technology Taxila, [engrm.alcem@gmail.com](mailto:engrm.alcem@gmail.com)  
d: Department of Civil Engineering, University of Engineering and Technology Taxila, [hammad.raza@uettaxila.edu.pk](mailto:hammad.raza@uettaxila.edu.pk)  
\* Corresponding author: Email ID: [adilqaisrani786@gmail.com](mailto:adilqaisrani786@gmail.com)

**Abstract-** Due to the presence of weak soil with poor engineering features, such as structures built in the coastal zone require deep foundations. In these places, the soil profile is primarily loose sand, which is subsequently underlain by clayey soil at a depth of 3 to 4 meters. The constructions that have been built here have seen a lot of settlement. To improve this type of sand grouting is used to increase the bearing capacity of soil to decrease settlement in this study. The shear strength of the grouted sand improves as the cement quantity increases, effects of cement grouting sand shear strength and bearing capacity of the soil improves to experimental findings show that 4% cement grout is more effective than 2% and 6% cement grout. The findings of numerous studies indisputably show that grouting may be utilized to greatly improve the strength properties and reduce the permeability of sandy soils.

**Keywords-** Cement Grouting, Sand replacement, Permeation

## 1 Introduction

Grouting is a ground improvement technique that involves injecting a fluid-like substance capable of producing a gel and adhering soil particles. Permeation grouting, compaction grouting, and hydraulic fracturing are all options for grouting. The unrestricted flow of grouting into the soil cavities with minimum influence is referred to as permeation grouting. Solution grouts and suspension grouts are two types of grout. The method of permeation grouting is commonly employed to lower ground permeability and regulate the ground flow of water, but it may also be used to reinforce and stiffen the ground. [1, 2]. The soil sample in coastal areas is frequently made up of relatively loose sandy soils that extend 3 to 4 meters below ground level and are loamy by clayey soils of medium stiffness. Excessive settlements may occur in buildings erected on such soils, resulting in punched shear collapse. Grouting is an effective technique for repairing poor soil. [3]. In 1958, post-grouting innovation was first used on the pile foundation design of the Maracaibo bridge, in which the load-carrying capacity of the footings was increased by grouting prefabricated piles, and a study on the development of a low-cost shake table was conducted (Zhou, Xu et al. 2021). This technique is applied to various engineering infrastructure projects and has offered substantial social and economic benefits due to its simplicity, speed, and low cost [4]. Because of its ability to tackle several common foundation problems, such as the development of low- to intermediate constructions over soft to extremely soft clayey soil of vast depth, larger capacity micro piles are in high demand today. For this sort of soil, the standard approach of constructing large cast-in-situ masonry piles is both costly and time-consuming. The group behavior of cast-in-situ filled with concrete micro piles in densely packed clayey soil is explored in this research. The experimental data on the behavior of micro piled rafts under static axial horizontal compressive force are discussed in this work [5]. The influence of sand particle size distribution on cement mortar flow behavior and bonding strength was investigated. The coarse sand filler used 25–30% less water than the fine sand filler in the cement-based mortar [6].



Compaction grouting might be an efficient way to prevent vulnerable soils from liquefying. Grouting resulted in the biggest improvement in the sand. Although the silts were improved, the grouting was less successful[7].

## 2. Experimental Procedures

### 2.1 Material

The kind of granular media and the aim of grouting influence the choice of grouting materials. Grouting materials often used for granular media grouting include cement, bentonite, clay, and lime. The sand was employed as the grouting media and cement will be used as the filling material in this investigation. For the production of cement grouts, grade Portland Cement (OPC) that conforms to PS 232-2008 will be utilized that properties of cement shown in Table 1,2. The cement sacks are stored in airtight containers to prevent any changes in their qualities over time.

Table 1: The properties of the cement utilized

Trial No.	Weight of Cement (gm)	Water (cc)	Water(%)	Needle Penetration (mm)
01	400	100	25	15
02	400	110	27.5	27
03	400	112	28	34

Standard consistency = 28%

Table 2: Cement properties

<b>Determination No.</b>	01
<b>Normal consistency</b>	0.28
<b>A time when water is added to cement</b>	10:25 am
<b>Time at the initial setting</b>	12:17 pm
<b>Total time is taken for the Initial setting</b>	112 minutes
<b>Time at Final setting</b>	03:04 pm
<b>Total time is taken for the Final setting</b>	279 minutes

The properties of the cement utilized, as well as its fundamental amenities are determined by ASTM tests such as specific gravity and other tests.



## 2.2 Test

In this study, shear strength, strength properties, and permeability of cement grouted sand are investigated in depth. Grouting materials' physical characteristics are also investigated. The following are detailed descriptions of the various test techniques.

## 2.3 Sand

In this research, cement is mixed with sand as a grouting material. Research material sand is collected from the “Indus river, Layyah”, which is used in the present investigation. The grain size distribution curve is shown in Figure 1 below.

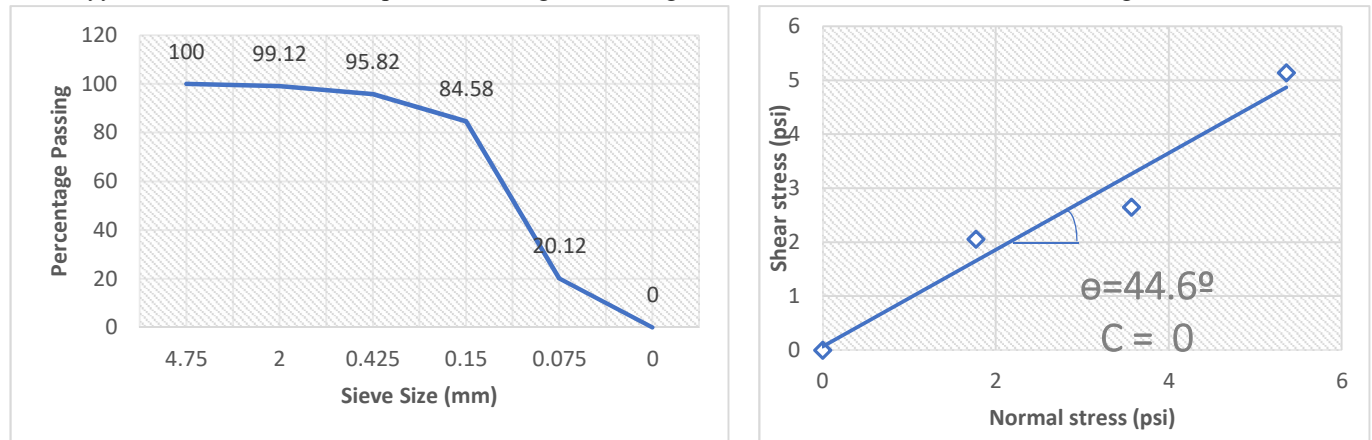


Figure 1 (a) Grain size distribution curve of sand

(b) Shear stress & Normal stress curve

## 2.4 Permeability test

The property of a permeable material that allows water or other fluids to travel through its interconnecting spaces is known as permeability. Gravel is extremely permeable, but stiff clay or due to plastic clay is not. A constant head test or a falling head test can be used in the lab to evaluate the coefficient of permeability. The permeability was determined in the current study using continuous head testing. The rigid wall specifications were 150 mm x 150 mm x 150 mm. The sand was put into the mould with a dry density of 14.5 kN/m<sup>3</sup> in mind. Water was allowed to flow through the sand's medium at a consistent rate. Once a constant condition was established, the discharge was measured.

## 3. Research Methodology

The dirt is poured into the tank without causing any damage to the four grout pipelines. Figure 2 depicts the inflow of cement and cement grouting into a 21 cm x 24 cm tank. The cement grout solution slurry is combined with the necessary percentage of water and poured evenly into all four grout pipes. There will be no pressure-induced flow of grout into the perforated pipes if the slurry solution is agitated constantly and completely.

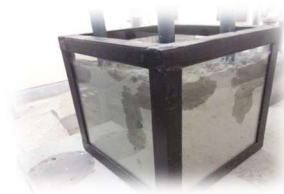


Figure 2: Permeation of grouting occur



A tank made of a poly-carbide sheet measuring 21cm x 24cm is used to prepare permeation grouted samples. The grouting sand is placed in the tank. For the grouting, four PVC pipes with a diameter of 20 mm are utilized, each with three-millimeter holes on the surface. The grout is dispersed circumferentially and the grouting is more effective by plugging the bottom of the PVC pipe. The grout is placed into the four PVC pipes similarly after being mixed in a cement solution with cement ratios of 7:1, 6:1, 5:1, and 4:1 and thoroughly agitated to provide a consistent grout solution. The shotcrete sample was maintained wet for 14 days during the curing process. When doing a plate load test, the mold is poured with the loosest sand possible. The sample is then placed in the Universal Testing Machine's two compression jaws (UTM). A 6-inch round plate distributes the load evenly. The sand is squeezed, and the results are used to calculate the load settling curve. The following is the load settling curve: On ungrouted soil, a shear strength test is performed, and the results of greater force and settlements are recorded. Graph 4 depicts a relationship between maximum load and settlements. Plate load tests are carried out for different grout ratios ranging from 7:1 to 4:1 water-cement ratio. After an efficient curing time of 7 days, grouted samples are tested to a plate load test, and the results are documented.

## 4. Results

Table. 2 Grouting proportions

Mixing the proportion of grout and their notations		
Notation	Water	Cement
G1	7	1
G2	6	1
G3	5	1
G4	4	1

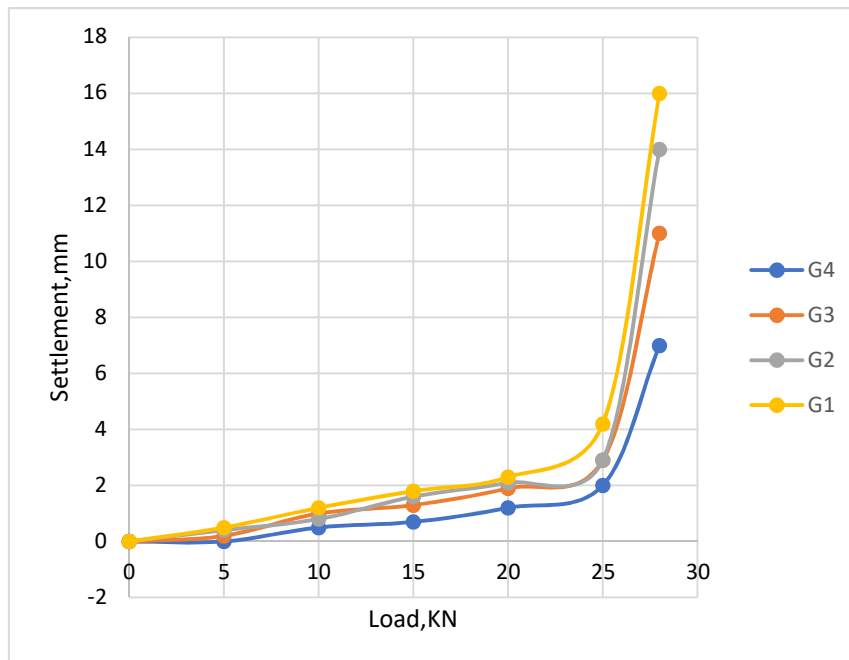


Figure 3:Combine load settlement graph



Figure 3 combine load settlement denotify relationship between load and settlement of sand and sample testing specimenes rename as G1,G2,G3,G4. From the result graph G4 curve is more effective than others three sample of group.Strength of cement grouting specimenes is more effectiveto bearing te load impact

## 5 Conclusion

The study looks at the strength of grouting materials in order to enhance sand bearing capacity. The efficiency of cement grouting is typically determined by the penetration of cementitious material through to the pores of sand. Various tests may be used to assess the influence of cement grouting on poor bearing capacity: The ultimate load reduces as the grouting ratio lowers.

- The strength of sand increases constantly by using grouted materials. So Loading conditions increase from 24 kN to 44 kN at 5:1 grouting.
- Due to curing and cement content increasing the cohesion ‘c’, shearing resistance steadily increased. Curing impact is more significant at the high value of content as compared to the low value of content. In the situation of values of c and,  $\phi$  the initial soil moisture of the cementitious material has a considerable impact. While the following equation decreases dramatically as the initial moisture contents of the grout increase, the value of increases as the initial liquid limit of the grout increases, except in the situation of fine sand. It is found that 4% cement grout is much more successful in medium and coarse sand than 2 percent and 6 percent.

Furthermore, when medium sand is grouted with 4% cement, the strength of the epoxy-coated sand is substantially higher than the strength of the sand in its loosest state. Because of the larger pore space available, coarse sand takes less cement than medium sand for grouting to be successful.

## Acknowledgment

The authors would like to thanks Engr.Hammad Raza who helped throughout the research work, particularly the Civil engineering department, Engr.Ghulam abbas. The careful review and constructive suggestions by the anonymous reviewers are gratefully acknowledged.

## References

- [1] M. U. Farooqi and M. Ali, "Effect of pre-treatment and content of wheat straw on energy absorption capability of concrete," *Construction and Building Materials*, vol. 224, pp. 572-583, 2019.
- [2] P. Dayakar, K. V. Raman, and K. Raju, "Study on permeation grouting using cement grout in sandy soil," *Journal of Mechanical and Civil Engineering*, vol. 4, no. 4, pp. 5-10, 2012.
- [3] T. Santhosh Kumar and A. Benny Mathews, "A Study on the Engineering Behaviour of Grouted Loose Soils," Cochin University of Science & Technology, 2010.
- [4] Q. Wang, S. Wang, S. W. Sloan, D. Sheng, and R. Pakzad, "Experimental investigation of pressure grouting in sand," *Soils and Foundations*, vol. 56, no. 2, pp. 161-173, 2016.
- [5] N. Borthakur and A. K. Dey, "Experimental investigation on load carrying capacity of micropiles in soft clay," *Arabian Journal for Science and Engineering*, vol. 43, no. 4, pp. 1969-1981, 2018.
- [6] W. Emad, A. Salih, and R. Kurda, "Experimental study using ASTM and BS standards and model evaluations to predict the compressive strength of the cement grouted sands modified with polymer," *Case Studies in Construction Materials*, vol. 15, p. e00600, 2021.
- [7] E. A. Miller and G. A. Roycroft, "Compaction grouting test program for liquefaction control," *Journal of Geotechnical and Geoenvironmental Engineering*, vol. 130, no. 4, pp. 355-361, 2004.



# SPATIO -TEMPORAL ANALYSIS OF PRECIPITATION IN PUNJAB PROVINCE, PAKISTAN

<sup>a</sup> Aarish Maqsood, <sup>b</sup> Muhammad Shoaib\* , <sup>c</sup> Muhammad Azhar Inam, <sup>d</sup> Mudasser M. Khan

a: Department of Agricultural Engineering, Bahauddin Zakariaya University, Multan, aarishmaqsood@gmail.com

b : Department of Agricultural Engineering, Bahauddin Zakariaya University, muhammadshoaib@bzu.edu.pk if any

c: Department of Agricultural Engineering, Bahauddin Zakariaya University, azharinam@bzu.edu.pk

d: Department of Civil Engineering, Bahauddin Zakariaya University, Multan, mudasserkhan@bzu.edu.pk

\* Corresponding author: Email ID: muhammadshoaib@bzu.edu.pk

**Abstract-** The monthly ground-based precipitation data from 39 stations were utilized to analyze the variation in Punjab Province from 1960-2019. The Mann–Kendall method was employed to evaluate precipitation spatial-temporal trends. There are also major periods, from 1974 to 1977 and 2009 to 2015, with rising yearly precipitation. The southern Punjab area noted a greater value of the coefficient of variation (CoV) for yearly precipitation. Summer & winter season showing increasing trend on overall stations. In contrast, autumn and spring show a decreasing trend for many stations. It can be found that the Punjab province has become wetter in summer and winter from the period of 1961 to 2019.

**Keywords-** Precipitation, Punjab, Spatio-temporal analysis, Stations data.

## 1 Introduction

The world climate seems to be varying at an exceptional rate. Punjab province of Pakistan is facing severe climatic catastrophes such as floods and droughts. It is extremely affected by the social, environmental and economic losses due to climate change [1]. It should be emphasized that 2005 and 2010 saw the majority of the catastrophic floods. It affects many people, land, crops, and property. Over 450 medical management centres, nearly a million homes, and nearly 90% of the regions used for food restoration were all destroyed [2]. According to a study, the 2010 flood in the Chenab and Jhelum was the worst since it caused more damage than the tidal wave disasters of 2004, 2005, and 2009, the earthquake catastrophes in Pakistan, and the earthquakes in the Caribbean countries combined [3]. Drought is also frequent in Pakistan, influencing social, economic, and environmental society [4]. Droughts have become more common and intense over the past 20 years. It has the worst effect on Punjab province's economy the most from 1998 to 2001 [5]. The drought from 2000 to 2002 is considered the worst since it caused many fatalities, widespread migrations, agricultural failures, and a water crisis. 2.2 million persons were impacted nationwide [6].

Precipitation is an essential factor that significantly affects the likelihood of severe climatic occurrences. Therefore, it is essential to comprehend precipitation properties properly as it forms the foundation of analyses of drought and flooding. Numerous research on precipitation trends has been conducted [7], [8]. Precipitation trends throughout the long or short term are mostly identified utilizing two approaches, i.e., Mann Kendall test and Sen's slope [9], [10]. Additionally, few articles on the study of precipitation, flooding, and drought in this area have been published [1]. Few studies have concentrated on this basin's long- and short-term precipitation study [11]. Therefore, a long term and thorough examination of precipitation variability for the Punjab province, Pakistan, is required.

This research examines the precipitation series' spatial and temporal variation. This study aims to: (1) get the fundamental properties of precipitation at various time scales; (2) get the trend and variations in precipitation, and (3) analyze extreme precipitation occurrences from 1961 to 2019.





## 2 Study Area

Punjab Province (Figure 1) is located at 31°79'48'' Latitude and 74°12'36'' Longitude with a total area of about 205,344 square kilometers and covers almost 26% of Pakistan. Punjab is the second largest province of Pakistan. This province's climate consists of tropical and costal climates, with annual mean precipitation of less than 400 mm [12]. In the cool zone, the yearly average temperature ranges from less than 7 to 12 degrees centigrade to more than 25 degrees centigrade in the scorching lowlands. The wet season, known as the monsoon, lasts from July -September. The sub-mountain area averages 960 mm of annual rainfall, whereas the plains receive 460 mm [13]. The ratio of rainfall fluctuates by around 50 mm/month in the rest of the months. Thus, irrigation water from canals is utilized to grow crops during this period. The monthly climatic data for all stations is extracted from spatial data and downloaded from the **NASA Earth science data** website. Table 1 shows the statistics from 1961 to 2019 of 39 ground stations in Punjab. These stations were chosen depending on their past temporal analysis, consistency, and totality of data; their locations are shown in Figure 1.

Table 1 Overview of 39 ground-based observation data in terms of annual and monthly mean precipitation

Cities	Maximum [mm]	Minimum [mm]	Monthly Mean Precipitation [mm]	Annually Mean precipitation [mm]	Standard Deviation [mm]	Cv
Islamabad	621.87	0.88	80.55	966.57	82.17	1.02
Bahawalnagar	137.64	0.75	16.71	200.47	21.82	1.31
Bahawalpur	154.84	0.60	13.27	159.23	17.89	1.35
Rahimyar Khan	149.25	0.74	13.22	158.66	17.45	1.32
Dera Ghazi Kha	173.66	0.71	18.78	225.39	23.84	1.27
Layyah	119.52	0.48	15.54	186.53	19.04	1.22
Muzaffargarh	135.20	0.59	14.43	173.15	19.30	1.34
Rajan Pur	173.35	0.91	16.16	193.97	21.91	1.35
Faisalabad	195.42	0.74	29.68	356.22	37.15	1.25
Jhang	133.58	0.65	22.14	265.74	26.15	1.18
Toba Tek Singh	144.60	0.67	22.12	265.44	27.04	1.22
Gujarat	329.50	0.57	43.56	522.77	50.66	1.16
Gujranwala 1	307.94	0.58	45.06	540.71	54.09	1.20
Gujranwala 2	354.63	0.57	48.27	579.22	57.13	1.18
Gujrat	563.93	0.72	69.17	830.08	84.12	1.22
Hafizabad	266.92	0.55	36.85	442.21	43.38	1.18
Narowal 1	547.96	0.79	76.28	915.37	96.34	1.26
Narowal 2	402.14	0.74	57.78	693.36	72.68	1.26
Sialkot	524.90	0.76	69.25	831.03	86.67	1.25
Kasur	196.60	0.59	32.03	384.30	40.30	1.26
Lahore	240.22	0.68	40.82	489.78	50.64	1.24
Nankana Sahib	212.93	0.59	32.39	388.63	39.74	1.23
Okara 1	153.64	0.63	25.00	300.03	32.26	1.29
Okara	179.86	0.62	26.58	318.91	33.68	1.27
Sheikhupura	258.98	0.61	40.27	483.26	49.11	1.22
Khanewal	99.37	0.44	14.05	168.61	17.63	1.25
Lodhran	109.94	0.40	10.97	131.63	14.07	1.28
Multan	117.05	0.38	11.87	142.48	15.74	1.32
Pakpattan	137.09	0.58	19.15	229.79	23.73	1.24



Sahiwal	144.56	0.61	21.30	255.58	26.87	1.26
Vehari	98.89	0.60	13.98	167.71	17.40	1.24
Attok	278.79	0.55	45.00	540.05	40.78	0.91
Chakwal	284.49	0.56	41.12	493.47	40.86	0.99
Jhelum	411.55	0.57	53.46	641.50	59.50	1.11
Rawalpindi	511.13	0.74	68.07	816.89	67.00	0.98
Bhakkar	116.24	0.47	19.42	233.07	21.64	1.11
Khushab	179.53	0.65	29.03	348.32	31.03	1.07
Mianwali	196.10	0.48	32.11	385.31	32.90	1.02
Sargodha	226.45	0.66	31.93	383.22	36.94	1.16

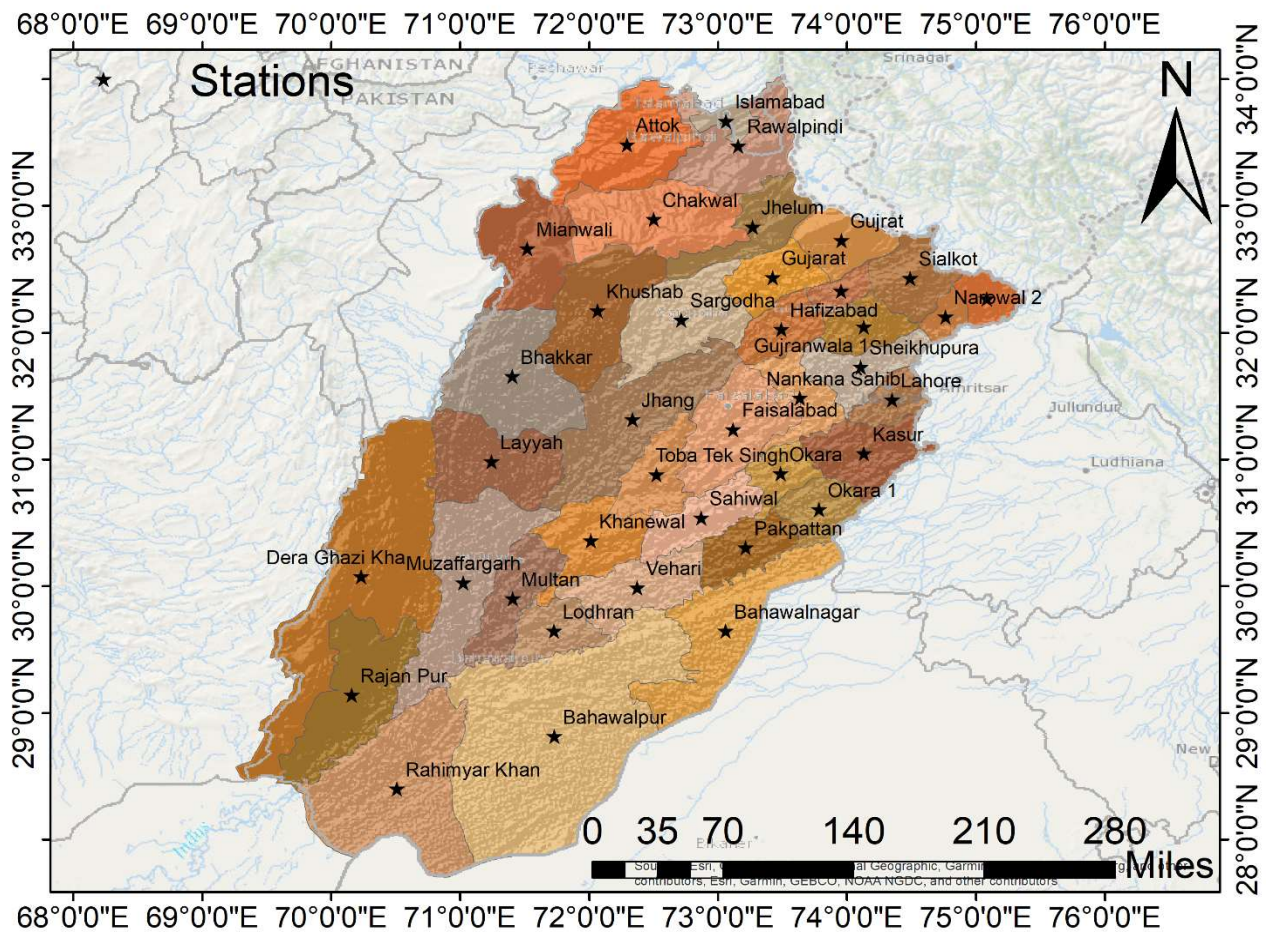


Figure 1: Study area of Punjab province, Pakistan, with the network of 39 ground-based observations

### 3 Methods

#### 3.1 Mann-Kendal test (MK Test)

In the current investigation, the non-parametric trend diagnosis MK test was employed. Trends in metrological temporal data series have been extensively detected using the MK test [14], [15]. The approach is resilient against outliers and



missing numbers and is less susceptible to abrupt breakpoints [16]. The test is susceptible to a serial correlation which might impact the test outcomes [17], [18]. The sequential correlation strategy was used in the present study to assess the statistical significance of trends in the climatic data set before the MK test was run. The MK test whole process is described by [19], [20]. The standardized MK statistic “S” is calculated as:

$$S = \sum_{z=i+1}^m \text{sgn}(y_z - y_m) \quad (1)$$

$$\text{sgn}(y_z - y_m) = \begin{cases} +1 & y_z > y_m \\ 0 & y_z = y_m \\ -1 & y_z < y_m \end{cases} \quad (2)$$

where  $m$  is the series length, and  $y_z, y_m$  is the sequential values of data. If  $n$  is greater or equal to 10, then the  $S$  statistic is typically dispersed, and the variance is given by

$$E(S) = 0$$

$$\text{Variance}(S) = m(m-1)(2m+5) - \sum_{i=1}^n s_i(s_i-1)(2s_i+5)/18 \quad (3)$$

where  $n$  is the number of tied groups, and  $s_i$  is the size of the  $i$ th sth group. The test statistic  $Z$  is computed by:

$$Z = \begin{cases} \frac{(S-1)}{\sqrt{\text{var}(S)}} & S > 0 \\ 0 & S = 0 \\ \frac{(S+1)}{\sqrt{\text{var}(S)}} & S < 0 \end{cases} \quad (4)$$

The MK test  $Z$  statistics have a null hypothesis of no trend and follow the normal distribution with an average of 0 and a variation of 1[21]. The statistics  $Z$  positive and negative values indicate rising and falling tendencies.

## 4 Results

### 4.1 Features of average annual precipitation of all ground-based stations

The average annual precipitation is 131.63 to 966.57 mm for 39 ground-based stations from 1961 to 2019 (Table 1). The Bahawalpur and Rajan pur stations, situated in the province's southern region, had the largest coefficient of variation (CoV) of the average annual precipitation. In contrast, Attock station had the lowest CoV, measuring 0.91 (north of the Punjab province). The yearly mean precipitation for 39 meteorological stations is shown in **Figure 2**.

As **Figure 2** demonstrates, there are significant fluctuations in the yearly precipitation between 1961 and 2019. In Southern Punjab, the year with the most precipitation, 404 mm, was recorded at the Dera ghazi khan station, and the year with the least 69 mm, was recorded at the Lodhran station. While in central and northern Punjab, the maximum & minimum precipitation were recorded at Narowal (with at least 1390) & Pakpattan (with at least 141) and Islamabad (with at least 1390) & Bhakkar (with at least 149).

In Northern Punjab, like Islamabad (1976, 2006, 2010, 2015), and Central Punjab, like Sialkot (2006) and Narowal (1988, 1990, 1995, 1997, 2006) are stations with annual precipitation above 1200 mm. There are also two major periods, from 1974 to 1977 and 2009 to 2015, in which most station's yearly precipitation is mostly rising. These finding are in line with the outcomes of [22].

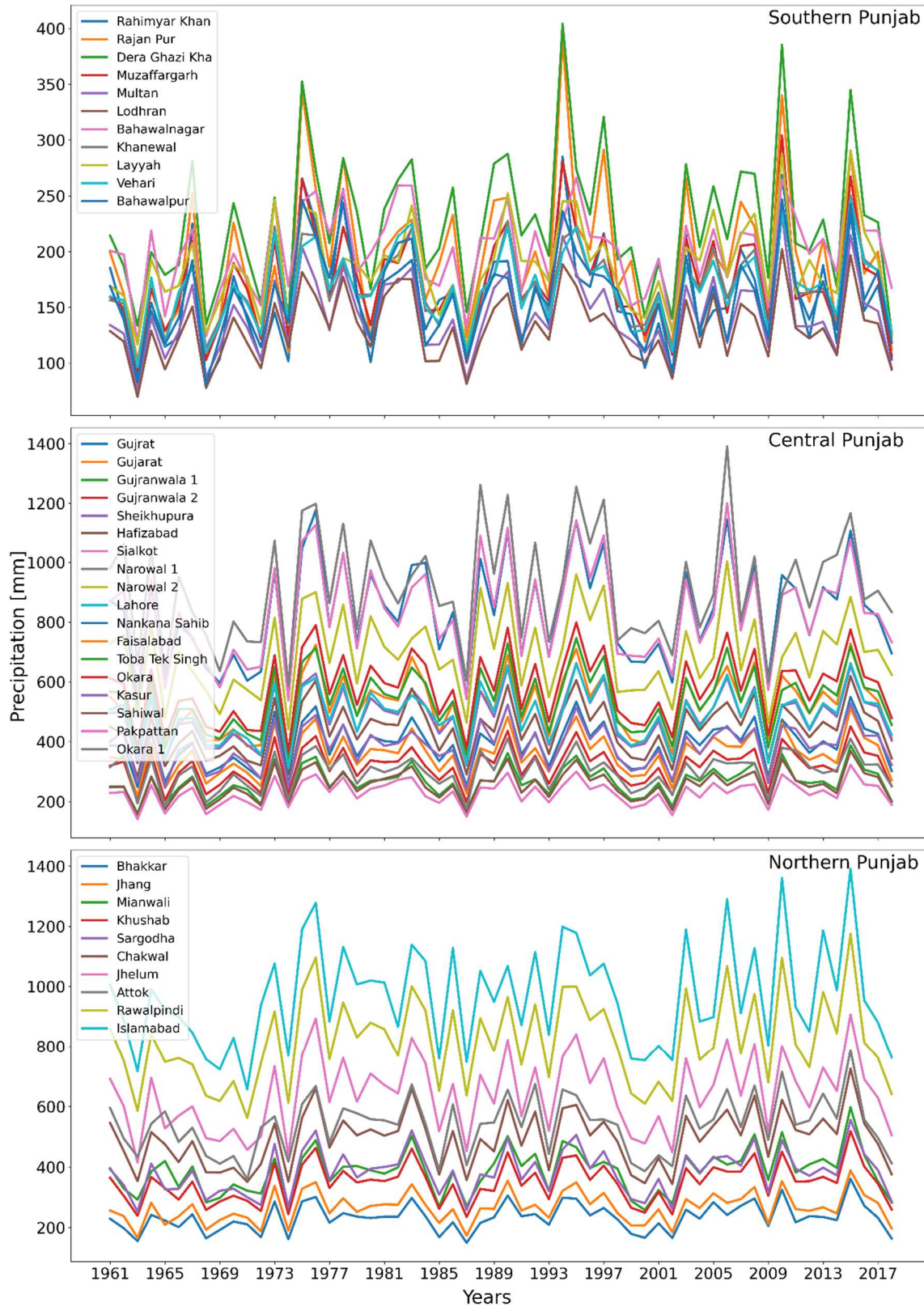


Figure 2: Annual averaged precipitation series for 39 ground-based stations



#### 4.2 Statistical characteristics of monthly precipitation for all ground-based stations

Some statistical details of the monthly precipitation series at 39 ground-station stations are reported in Table 1. The average annual precipitation is 10.97 to 80.55 mm for 39 ground-based stations from 1961 to 2019. The maximum mean monthly precipitation is found in Dera Ghazi Khan (Located in southern Punjab), Narowal (Central Punjab), and Islamabad (Northern Punjab). The minimum mean monthly precipitation is found in Multan (Located in southern Punjab), Hafizabad (Central Punjab), and Bhakkar (Northern Punjab). The Bahawalpur and Rajanpur station, situated in the southern province region, had the largest coefficient of variation (CoV), 135% of the average annual precipitation, while the Attack station had the lowest CoV, measuring 91 % (in the north of the Punjab province). The percentage is greater than 100% because the data points are very distant from the mean.

The statistical information on average monthly precipitation for every station from 1961 to 2019 is presented in Table 2. The station in north Punjab (Islamabad) had the highest average monthly precipitation in August, and the minimum average monthly precipitation was observed in November. Similarly, the station in central Punjab (Narowal station) also had the highest maximum monthly precipitation in August, while the lowest precipitation is found in November, respectively. On the contrary, the station in the south (Multan station) had the lowest average monthly precipitation in April and maximum in July. The results are consistent with the outcomes of [22].

Figure 3 depicts the temporal distribution of this basin's average monthly precipitation (as determined by the Thiessen Polygon technique). More precipitation is observed in July and August and less from October to December, which is intense in spring and summer.

Table 2 Monthly mean precipitation of all ground-based stations data from 1960 to 2019

Stations	Jan	Feb	Mar	Apr	May	Jun	Jul	Aug	Sep	Oct	Nov	Dec
Islamabad	56.3	72.9	73.1	60.8	36.5	58.6	210.6	236.1	91.8	22.5	14.9	32.4
Bahawalnagar	6.7	9.9	9.7	6.4	6.2	16.2	62.4	47.6	25.4	2.2	2.4	5.2
Bahawalpur	5.3	8.3	8.1	6.4	6.5	15.1	51.4	32.6	18.1	1.3	2.4	3.8
Rahimyar Khan	5.4	8.1	11.5	8.7	6.7	13.5	40.9	40.1	16.9	1.3	1.8	3.8
Dera Ghazi Kha	10.7	12.4	16.9	13.9	9.6	18.7	55.4	58.2	16.9	3.3	2.2	7.2
Layyah	8.1	10.6	12.6	10.2	6.7	13.0	49.5	47.5	18.1	2.0	1.9	6.2
Muzaffargarh	7.4	10.6	9.0	7.2	6.0	12.8	49.4	45.1	16.1	2.1	1.4	6.0
Rajan Pur	8.9	11.2	11.6	9.0	7.8	17.7	46.4	51.8	19.8	2.5	1.7	5.5
Faisalabad	15.7	17.2	18.4	12.3	10.8	30.7	95.0	98.4	41.7	4.9	3.0	8.2
Jhang	10.6	14.3	16.4	12.6	10.3	22.5	70.9	67.3	26.9	3.9	2.6	7.3
Toba Tek Singh	10.5	13.1	13.9	10.8	7.9	25.1	69.1	71.0	30.4	3.6	2.5	7.5
Gujarat	27.6	31.8	31.0	22.8	19.0	38.7	129.2	140.3	55.7	7.8	5.9	13.0
Gujranwala 1	26.8	29.1	26.6	18.6	18.0	46.8	140.0	145.5	63.7	7.7	5.4	12.4
Gujranwala 2	31.0	33.3	30.4	20.6	18.5	45.9	144.2	155.9	70.6	8.1	6.1	14.5
Gujrat	42.5	47.9	46.6	28.7	23.8	57.3	217.7	223.3	99.5	13.1	9.0	20.6
Hafizabad	22.3	25.4	24.2	19.4	16.9	35.4	108.3	120.6	48.3	6.5	4.5	10.3
Narowal 1	55.6	46.5	42.4	20.4	19.1	67.9	246.4	250.4	120.8	17.0	7.5	21.3
Narowal 2	35.4	36.1	31.9	18.5	18.1	61.4	189.4	192.8	77.0	10.4	6.6	15.7
Sialkot	43.4	42.9	39.7	23.5	21.4	64.0	223.5	227.5	105.1	11.9	7.6	20.4
Kasur	16.9	15.6	16.8	9.5	10.3	32.8	102.5	101.2	60.5	7.2	3.2	7.8
Lahore	20.1	22.4	24.2	16.1	15.1	44.4	141.1	125.4	58.1	9.4	4.5	8.9
Nankana Sahib	18.2	19.8	19.2	14.1	13.3	33.6	99.6	107.8	45.4	5.9	3.5	8.1
Okara 1	12.4	11.2	12.2	5.8	7.7	23.3	79.5	72.6	61.1	4.1	2.9	7.3
Okara	14.9	14.1	14.7	7.8	8.9	27.4	84.9	86.1	46.0	3.9	3.0	7.2



Sheikhupura	21.8	24.7	24.0	17.2	16.4	43.0	130.7	129.2	54.4	7.7	4.6	9.6
Khanewal	6.5	10.9	8.1	5.3	6.7	14.8	47.4	42.9	15.4	2.1	2.0	6.3
Lodhran	5.2	10.1	7.2	4.1	6.2	9.3	41.7	26.1	13.4	1.4	2.0	5.0
Multan	6.0	10.3	7.2	4.5	5.8	9.9	44.9	32.7	12.0	1.9	1.6	5.8
Pakpattan	9.5	11.9	12.3	7.0	6.8	20.1	68.1	54.7	27.7	2.1	3.0	6.5
Sahiwal	11.0	12.7	13.6	7.4	7.2	22.5	70.9	68.1	29.7	2.6	2.7	7.2
Vehari	6.4	10.8	8.2	5.7	6.9	14.6	45.1	44.1	16.2	2.0	2.1	5.9
Attok	37.8	46.5	51.8	39.5	23.9	25.9	96.2	124.1	54.1	12.8	7.7	19.7
Chakwal	29.2	34.7	38.6	30.4	23.8	31.7	99.7	121.7	52.6	10.4	6.1	14.6
Jhelum	35.5	42.1	41.4	30.7	23.9	44.4	154.9	165.0	66.6	11.3	7.9	17.8
Rawalpindi	49.9	62.5	62.6	51.0	33.7	52.2	172.2	192.8	80.5	19.8	12.7	27.0
Bhakkar	10.0	14.2	20.1	13.6	9.4	17.7	57.9	54.7	23.8	3.0	2.3	6.1
Khushab	15.9	21.4	28.1	19.5	17.2	25.1	82.4	84.8	34.9	6.1	3.9	9.1
Mianwali	17.7	25.2	38.6	26.8	19.1	22.0	76.0	97.6	40.9	8.3	3.5	9.7
Sargodha	16.9	22.2	25.9	20.4	19.0	26.4	95.3	103.6	33.6	6.2	4.0	9.7

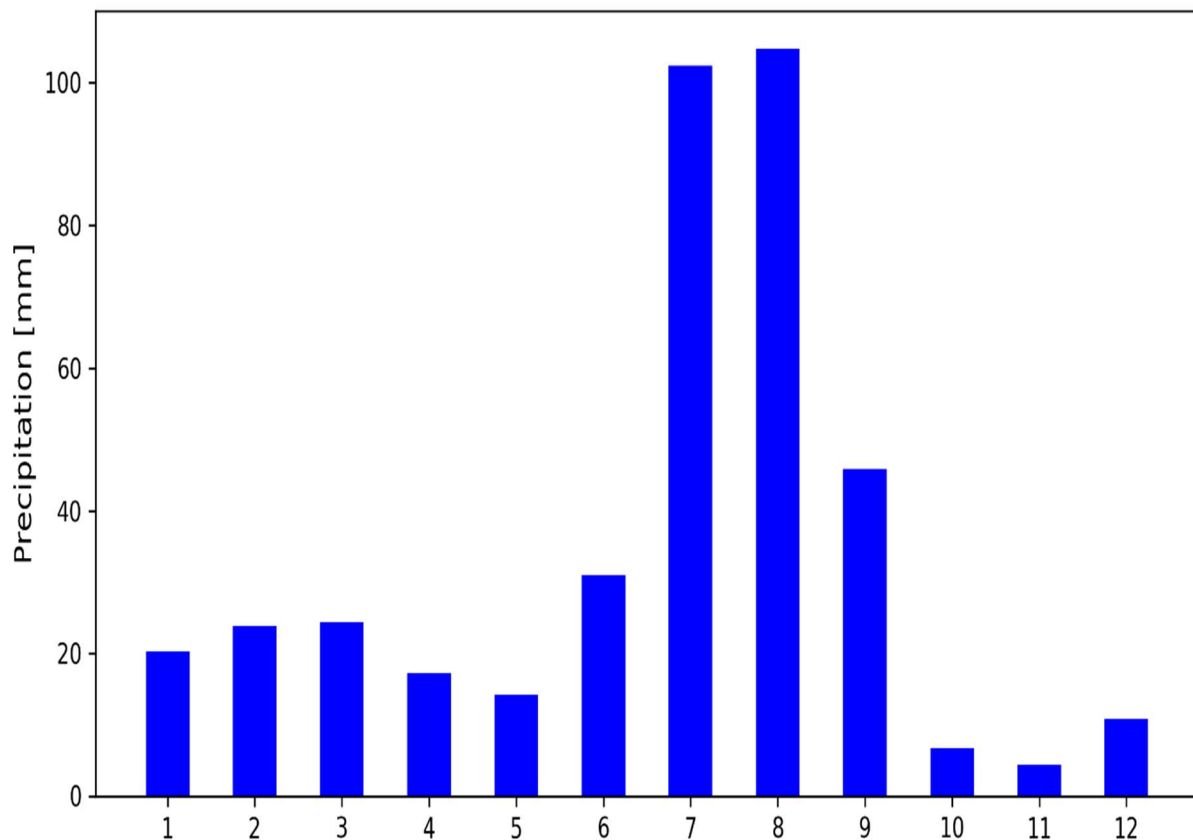


Figure 3 Temporal trend analysis of ground-based precipitation year data from 1961 to 2019

#### 4.3 Trends analysis of precipitation for all ground-based stations

Precipitation spatial trends for different seasons and the whole year from 1961 to 2019 are exhibited in **Figure 4**, where 0.05, showing the significant level.

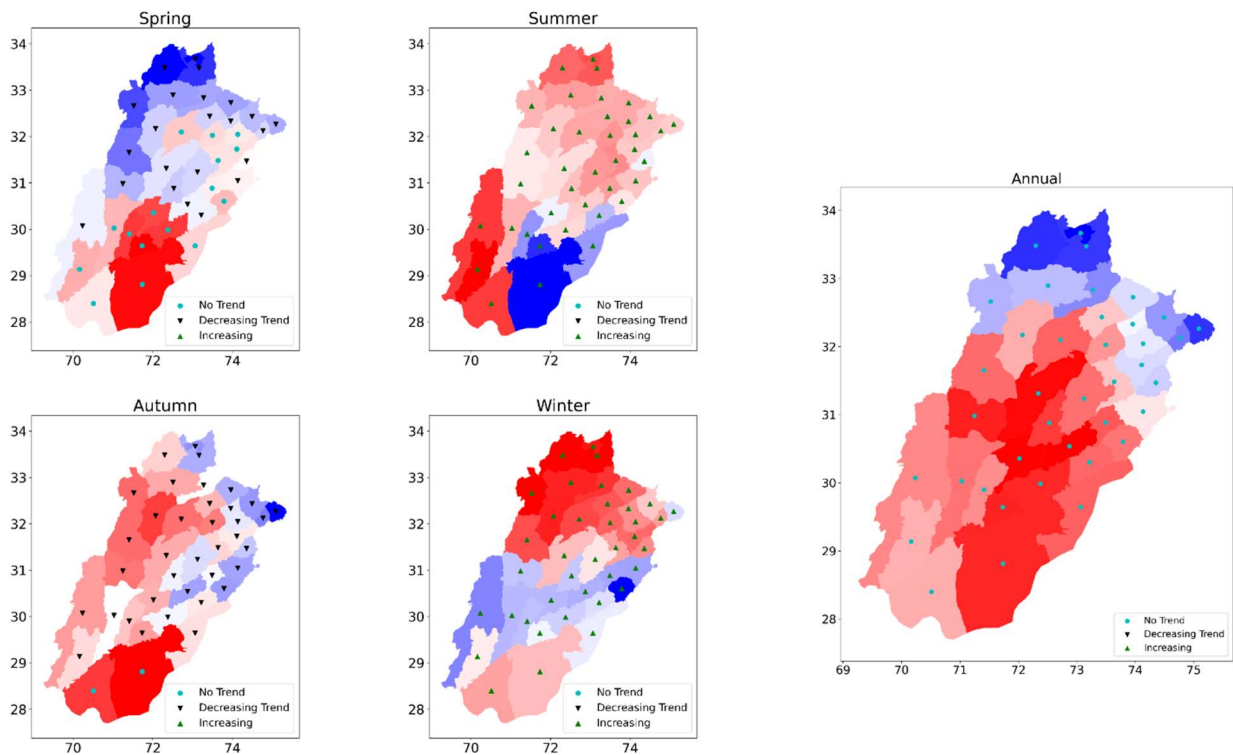


Figure 4 Spatial trends of precipitation for different seasons and a whole year

If  $|Z|$  is greater than 1.96, then the precipitation distribution is significant. When  $Z > 1.96$ , it shows an increasing trend; when  $Z < -1.96$ , it shows a decreasing trend. If the  $Z$  is less than 95 percent confidence level, it will be exhibited in terms of increasing or decreasing trends.

As in figure 4, the summer & winter seasons show an increasing trend in overall stations. In comparison, autumn and spring exhibit a decreasing trend for many stations. It is also noted that 37 stations show a significant decrease in autumn while 2 have no significant trend. Twenty-three stations noted a significant decrease in spring, while 26 have no significant trend. Moreover, no significant trend was found on an annual scale. These trends are consistent with the outcomes of [23], which showed that India's rainfall trend decreased between 1949 and 2012. Our findings concur with [24], who discovered negative trends in Iran's southeast and northwest between 1951 and 2009. This demonstrates that there has been a decline in precipitation in this South Asian region, which is also indicated as having "mostly decreased" in the Fifth Assessment Report of the Inter-Governmental Panel on Climate Variation [25]. The findings here demonstrate the need for good water resource management in the Punjab province, which have the biggest populations and make up the majority of Pakistan's overall agricultural output and the country's Gross Domestic Product.

## 5 Conclusion

In this study, the precipitation variations between 1961 and 2019 were evaluated. The annual precipitation decreased from south to north. Some stations like Islamabad, Sialkot, and Narowal have annual precipitation exceed from 1200 mm. The majority of occurrence falls from 1974 to 1977 and 2009 to 2015 with increasing precipitation. The higher variation is noted in south Punjab in contrast to northern Punjab. The monthly precipitation follows the same trend from south to north. High precipitation was observed from July to August, while low precipitation was noted from October to December. Seasonal precipitation shows the different trends in different regions of Punjab. Winter and summer exhibit an overall increasing trend, while a decreasing trend is noted in spring and autumn. Understanding these trends and adhering to the recommended adaption techniques is necessary. Therefore, a better understanding Pakistan's climate extreme (such as floods and droughts) will lessen their negative effects in the future.



## References

- [1] S. M. Ali, B. Khalid, A. Akhter, A. Islam, and S. Adnan, "Analyzing the occurrence of floods and droughts in connection with climate change in Punjab province, Pakistan," *Natural Hazards*, vol. 103, no. 2, pp. 2533–2559, Sep. 2020, doi: 10.1007/S11069-020-04095-5/TABLES/6.
- [2] R. Polastro, A. Nagrah, N. Steen, F. Z.-M. DARA, and undefined 2011, "Inter-agency real time evaluation of the humanitarian response to Pakistan's 2010 flood crisis," *humanitarianlibrary.org*, 2011, Accessed: Jul. 29, 2022. [Online]. Available: <https://humanitarianlibrary.org/sites/default/files/2014/02/1266.pdf>
- [3] B. Khalid *et al.*, "Riverine flood assessment in Jhang district in connection with ENSO and summer monsoon rainfall over Upper Indus Basin for 2010," *Natural Hazards*, vol. 92, no. 2, pp. 971–993, Jun. 2018, doi: 10.1007/S11069-018-3234-Y.
- [4] N. Mazhar, M. Nawaz, A. Mirza, K. K.-S. A. Studies, and undefined 2020, "Socio-political impacts of meteorological droughts and their spatial patterns in Pakistan," *journals.pu.edu.pk*, Accessed: Jul. 29, 2022. [Online]. Available: <http://journals.pu.edu.pk/journals/index.php/IJSAS/article/view/2989>
- [5] W. Adger, S. Huq, ... K. B.-P. in, and undefined 2003, "Adaptation to climate change in the developing world," *journals.sagepub.com*, vol. 3, no. 3, pp. 179–195, 2003, doi: 10.1191/1464993403ps0600a.
- [6] S. Anjum, L. Wang, J. Salhab, ... I. K.-J. of F., and undefined 2010, "An assessment of drought extent and impacts in agriculture sector in Pakistan.," *cabdirect.org*, Accessed: Jul. 29, 2022. [Online]. Available: <https://www.cabdirect.org/cabdirect/abstract/20113030681>
- [7] Z. Nawaz, X. Li, Y. Chen, Y. Guo, X. Wang, and N. Nawaz, "Temporal and spatial characteristics of precipitation and temperature in Punjab, Pakistan," *Water (Switzerland)*, vol. 11, no. 9, Sep. 2019, doi: 10.3390/W11091916.
- [8] S. Siddiqui and K. Javid, "Spatio-temporal Analysis of Aridity Over Punjab Province, Pakistan using Remote Sensing Techniques," *Int.J.Econ.Envirion.Geol*, vol. 9, no. 2, pp. 1–10, 2018, Accessed: Jul. 29, 2022. [Online]. Available: <https://www.researchgate.net/publication/337389183>
- [9] Fiaz Hussain, Ghulam Nabi, and Muhammad Waseem Boota, "RAINFALL TREND ANALYSIS BY USING THE MANN-KENDALL TEST & SEN'S SLOPE ESTIMATES: A CASE STUDY OF DISTRICT CHAKWAL RAIN GAUGE, BARANI AREA, NORTHERN PUNJAB PROVINCE, PAKISTAN," *Sci.Int.(Lahore)*, vol. 27(4), pp. 3159–3165, 2015, Accessed: Jul. 29, 2022. [Online]
- [10] Z. Nawaz, X. Li, Y. Chen, Y. Guo, X. Wang, and N. Nawaz, "Temporal and spatial characteristics of precipitation and temperature in Punjab, Pakistan," *Water (Switzerland)*, vol. 11, no. 9, Sep. 2019, doi: 10.3390/W11091916.
- [11] Z. Nawaz, X. Li, Y. Chen, Y. Guo, X. Wang, and N. Nawaz, "Temporal and Spatial Characteristics of Precipitation and Temperature in Punjab, Pakistan," *Water 2019, Vol. 11, Page 1916*, vol. 11, no. 9, p. 1916, Sep. 2019, doi: 10.3390/W11091916.
- [12] S. Siddiqui and K. Javid, "Spatio-temporal Analysis of Aridity Over Punjab Province, Pakistan using Remote Sensing Techniques," *Int.J.Econ.Envirion.Geol*, vol. 9, no. 2, pp. 1–10, 2018, Accessed: Jul. 29, 2022. [Online]. Available: <https://www.researchgate.net/publication/337389183>
- [13] S. M. Ali, B. Khalid, A. Akhter, A. Islam, and S. Adnan, "Analyzing the occurrence of floods and droughts in connection with climate change in Punjab province, Pakistan," *Natural Hazards 2020 103:2*, vol. 103, no. 2, pp. 2533–2559, Jun. 2020, doi: 10.1007/S11069-020-04095-5.
- [14] L. Hamlaoui-Moulai, M. Mesbah, D. Souag-Gamane, and A. Medjerab, "Detecting hydro-climatic change using spatiotemporal analysis of rainfall time series in Western Algeria," *Natural Hazards*, vol. 65, no. 3, pp. 1293–1311, Jan. 2013, doi: 10.1007/S11069-012-0411-2.
- [15] P. Yang, J. Xia, Y. Zhang, and S. Hong, "Temporal and spatial variations of precipitation in Northwest China during 1960–2013," *Atmospheric Research*, vol. 183, pp. 283–295, Jan. 2017, doi: 10.1016/J.ATMOSRES.2016.09.014.
- [16] R. Zamani, R. Mirabbasi, S. Abdollahi, and D. Jhajharia, "Streamflow trend analysis by considering autocorrelation structure, long-term persistence, and Hurst coefficient in a semi-arid region of Iran," *Theoretical and Applied Climatology*, vol. 129, no. 1–2, pp. 33–45, Jul. 2017, doi: 10.1007/S00704-016-1747-4.
- [17] Y. Chen, Y. Guan, G. Shao, D. Z.- Water, and undefined 2016, "Investigating trends in streamflow and precipitation in Huangfuchuan Basin with wavelet analysis and the Mann-Kendall test," *mdpi.com*, vol. 8, no. 3, Mar. 2016, doi: 10.3390/w8030077.





- [18] S. A. Salman, S. Shahid, T. Ismail, E. S. Chung, and A. M. Al-Abadi, “Long-term trends in daily temperature extremes in Iraq,” *Atmospheric Research*, vol. 198, pp. 97–107, Dec. 2017, doi: 10.1016/J.ATMOSRES.2017.08.011.
- [19] M. Kendall, “Rank correlation methods.,” 1948, Accessed: Jul. 29, 2022. [Online]. Available: <https://psycnet.apa.org/record/1948-15040-000>
- [20] H. B. Mann, “Nonparametric Tests Against Trend,” *Econometrica*, vol. 13, no. 3, p. 245, Jul. 1945, doi: 10.2307/1907187.
- [21] Y. Hu, S. Maskey, S. Uhlenbrook, and H. Zhao, “Streamflow trends and climate linkages in the source region of the Yellow River, China,” *Hydrological Processes*, vol. 25, no. 22, pp. 3399–3411, Oct. 2011, doi: 10.1002/HYP.8069.
- [22] S. Siddiqui and K. Javid, “Spatio-temporal Analysis of Aridity Over Punjab Province, Pakistan using Remote Sensing Techniques,” 2018. [Online]. Available: <https://www.researchgate.net/publication/337389183>
- [23] A. K. Taxak, A. R. Murumkar, and D. S. Arya, “Long term spatial and temporal rainfall trends and homogeneity analysis in Wainganga basin, Central India,” *Weather and Climate Extremes*, vol. 4, pp. 50–61, Aug. 2014, doi: 10.1016/J.WACE.2014.04.005.
- [24] S. H. Sadeghi, H. Nouri, and M. Faramarzi, “Assessing the Spatial Distribution of Rainfall and the Effect of Altitude in Iran (Hamadan Province):,” <https://doi.org/10.1177/1178622116686066>, vol. 10, Mar. 2017, doi: 10.1177/1178622116686066.
- [25] IPCC, “Climate change widespread, rapid, and intensifying,” 2021. <https://www.ipcc.ch/2021/08/09/ar6-wg1-20210809-pr/> (accessed Feb. 05, 2022).



# REMOVAL OF ARSENIC AND PHARMACEUTICAL COMPOUNDS FROM DRINKING WATER: A META-ANALYSIS

<sup>a</sup> Abaid Ullah\*, <sup>b</sup> Mubashira Sitarish, <sup>c</sup> Mustafa Haidar, <sup>d</sup> Qandeel Zahra

a: Department of Environmental Engineering, University of Engineering & Technology Taxila, Pakistan  
[abaid.ullah@uettaxila.edu.pk](mailto:abaid.ullah@uettaxila.edu.pk)

b: Department of Environmental Engineering, University of Engineering & Technology Taxila, Pakistan  
[18-env-25@students.uettaxila.edu.pk](mailto:18-env-25@students.uettaxila.edu.pk)

c: Department of Environmental Engineering, University of Engineering & Technology Taxila, Pakistan  
[18-env-34@students.uettaxila.edu.pk](mailto:18-env-34@students.uettaxila.edu.pk)

d: Department of Environmental Engineering, University of Engineering & Technology Taxila, Pakistan  
[18-env-01@students.uettaxila.edu.pk](mailto:18-env-01@students.uettaxila.edu.pk)

**Abstract-** Arsenic being a global contaminant and highly toxic metalloid has gained much attention for many years. Intending to provide potable water to millions of people around the globe, the research community has practiced intensive efforts to remove arsenic. This review is focused on the possible treatment methods which can be deployed to curb arsenic contamination. Apart from discussing arsenic, this review also explored the occurrence and removal strategies of pharmaceutical contaminants. Unlike conventional contaminants, the problem associated with pharmaceutical contaminants is not their presence in abundance but rather very minute concentrations. Nearly undetectable concentration of pharmaceutical compounds, and their unpredictable impacts on the environment and humans are fundamental concerns for the research community. It has been found that conventional treatment technologies are insufficient for the remediation of pharmaceutically contaminated environmental segments; therefore advanced oxidation processes, membrane technologies, adsorption processes, and various integrated approaches have been evaluated in this paper. This review provides an insight into the advances being made till now in removing such contaminants from water.

**Keywords-** Arsenic, Emerging contaminants, Meta-analysis, Pharmaceutical compounds, Water treatment.

## 1 Introduction

Arsenic (As) is a highly lethal and cancer-causing metalloid that creates approximately 0.00005% Earth's crust and distributes in an extensive range via groundwater and surface water systems[1]. Arsenic can be found in inorganic and organic forms, generally two forms of arsenic found in aqueous environment including arsenite "As(III)" and arsenate "As(V)" [2]. It has an atomic weight of 74.9 g.mol<sup>-1</sup> and a specific gravity of 5.73 g.cm<sup>-3</sup> with boiling and melting points of 614°C and 817°C, respectively. In terms of mobility, the As(III) is highly mobile (25–65 times) in the natural environment as compared to As(V), predominantly due to its electro neutrality[3]. It exists as a deformable crystal-like solid material with a silver grey color. Moreover, it is tasteless, transparent, odorless, and difficult to detect. Since arsenic occurs naturally in geologic environments, therefore, groundwater pollution may arise because of mining, agricultural, and industrial practices. It is also known for its toxicity to humans and marine species [4, 5]. Researchers identified arsenic pollution as a 21st century disaster. Before the year 1993, the World Health Organization (WHO) endorsed 0.05 mg/L as a threshold limit for arsenic in drinking water. Later, the Environmental Protection Agency (EPA) approved a new lower limit of 0.01mg/L in the year 2001. Keeping in view the immediate toxicity and long-term consequences of arsenic, ranging from mild skin disease to cancer, the World Health Organization (WHO) further decreased its nontoxic limit to 10µg/L due to its hazardous nature. For instance, consumption of inorganic arsenic-contaminated rice and prolonged exposure to water containing its high concentrations (i.e., >100 mg/L) cause lung, bladder cancer and other organ failure [6, 7].

Pakistan is at the 80th position out of 122 countries in the world, which are facing severe arsenic contamination in water. In Pakistan, 3% of the population of Punjab is exposed to a concentration of greater than 50 g/L of arsenic and 20% of



Punjab's population is exposed to greater than 10 g/L concentration of arsenic. Similar to Punjab, situation is worse in Sindh, where 16% of the population is said to be exposed to greater than 50 g/L and 36% to greater than 10 g/L concentration of arsenic [8].

Apart from Arsenic, the presence of emerging micro-pollutants (EMPs) found in water bodies is also a matter of rising concern at the global level [9]. Major sources of these pollutants include industrial chemicals, illicit drugs, pharmaceutical and personal care products (PPCPs), perfluorinated compounds, and flame retardants [10]. Their presence has been identified in various natural environments including surface and groundwater sources along with water and wastewater treatment facilities [11]. However, their monitoring is globally out of reach as there is a scarcity of data about the quantity and occurrence of EMPs in water [12].

Among various EMPs, pharmaceutical compounds are getting more attention due to their persistence and toxicity [13, 14]. Pharmaceuticals are a vast range of chemicals used in medicine for both humans and animals [15]. Although their presence in water bodies has been identified for decades, however, their concentration in the natural environment has just started to be recognized as potentially dangerous and unsafe for the ecosystems [16]. Even the small concentrations of pharmaceutical compounds in drinking water supplies can cause harmful effects on the health of humans. The existence of pharmaceuticals in water comes from hospital waste, therapeutic drugs, and pharmaceutical industry waste. Due to the increase in human pharmaceutical consumption, various pharmaceutically active compounds (PACs) are disposed into the environment each day [17]. This increasing usage has raised queries related to their harmful risks to the environment, quality of water, and human health [18]. The absence of discharge standards and relevant regulations is a major reason behind these issues. Even after the conventional treatment, many of the PACs remain in the effluent and be part of the environment [19].

Therefore, the focus of this review is on the potential treatment technologies that can be utilized to remove both arsenic and pharmaceutical contaminants from water. Contrary to ordinary pollutants, these micro-pollutants are problematic when they are present at extremely low levels. The research community has shown serious concerns about the nearly undetectable concentration of pharmaceutical contaminants and their unpredictable effects on the environment and human beings. Since conventional treatment methods are ineffective for the removal of such contaminants, therefore, an attempt has been made in this review to evaluate various advanced treatment methods (e.g., advanced oxidation processes, membrane technologies, adsorption processes, and their integrated schemes) for the effective treatment of such toxic contaminants.

## **2 Treatment Methods used for the Removal of Arsenic**

The status of arsenic as a global contaminant has not faded yet. According to the United States Geological Survey (USGS), developed and developing countries are exposed to the threat posed by arsenic and emerging contaminants [20]. Currently, their sustainable removal is a challenge for the scientific community. To overcome this issue, extensive research has been conducted on arsenic removal. The methods used for this purpose include adsorption, ion exchange, chemical precipitation, phytoremediation, electro-coagulation, phytobial remediation, and electro-kinetic method [21]. These methods along with their strengths and limitations have been described in the following sections.

### **2.1 Removal of Arsenic by using the adsorption method**

Adsorption is an efficient and cost-effective arsenic removal method, which is directly applicable in developing regions having a lack of qualified staff and fluctuations in electrical supply. Recently adsorption has provided more than 95% efficiency for the removal of arsenite and arsenate [22]. This process is primarily determined by the separation process using the Van der Waals concept and the electrostatic attraction forces. The efficiency of this method depends upon various process parameters including pH, exposure time, presence of other reactive species, adsorbent concentration, original arsenic absorption, and temperature. Various adsorbents used for arsenic removal include zero-valent iron, metal oxides coated in sand, iron oxide-based sorbents engineered biochar (80% removal), granular adsorbents (35% removal), clinoptilolite-rich zeolitic tuff, activated carbon (20-40% removal), and activated alumina (>85% removal) [23-25].

### **2.2 Removal of Arsenic by using the Ion-exchange method**

Ion exchange is a physicochemical treatment process. Ions electrostatically maintained on the hard surface of ion-exchange resin solution are swapped from solution with the ion of a similar charge [26]. The United States Environmental Protection Agency (USEPA) also suggested specific ion exchange resins for arsenic subtraction [27]. The process parameters influencing the efficiency of this method include the concentration of arsenic, type of resin, high sulfate salts, competing



ions, and total dissolved solids (TDS). Previously, Ortega, et al. [28] reported 18.9% arsenic removal efficiency by using the ion-exchange method.

### 2.3 Removal of Arsenic by using the chemical precipitation method

Chemical precipitation uses mixtures such as sulfides, calcium, magnesium, and ferric salts for treatment. These reagents aid in the removal of arsenic by reducing dissolved arsenic to molecules with limited solubility compounds [29]. Previously, two-stage nanofiltration and chemical precipitation were used to treat gold excavation wastewater for arsenic and calcium removal [30]. Similarly, removal efficiencies of 98.5%, 96.3%, and 26.5% were reported by using lead hydroxide, lead nitrate, and lead oxide, respectively. Since this process produces toxic sludge, therefore pre-oxidation is necessary which results in the production of hazardous disinfection byproducts. To overcome this issue, sequential oxidation, chemical treatment, sedimentation, and filtration all are required for treatment.

### 2.4 Removal of Arsenic by using the phytoremediation method

This process utilizes plants for the removal of contaminants with minimum fertilizer input, thereby making it socially acceptable and environmentally sustainable [31]. These plants generally have deep roots, high tolerance, fast development, and are capable to absorb arsenic from contaminated soil [31, 32]. For this purpose, some plant species use direct absorption for aerial metal buildup, whereas, other plant species transfer metals via transporter proteins [33]. Studies also suggest combining nanomaterial with plants and microbes to enhance conventional bioremediation methods [34]. For instance, Yang, et al. [35] reported an arsenic accumulation of up to 171% by inoculating the process with *Cupriavidus Basilensis* bacteria. However, the non-specific presence can harm the surrounding environment. Since the removal efficiency is dependent on the type of macrophyte, therefore, further research is required to better understand this process [34].

### 2.5 Removal of Arsenic by using the electrocoagulation method

It is one of the most prominent methods for the removal of arsenic from water. This process has a high removal efficiency of 93-99.9% for arsenic removal [36], however, its limitations include (i) complexity, (ii) the electrodes get passive during the removal process, (iii) high power consumption [37], (iv) high cost, and (v) sludge production. For instance, the cost of arsenic removal through this process is 1.8 times of a simple coagulation process due to high energy consumption [38]. Despite various attempts have been made to overcome the aforementioned limitations, however, further research is required for its optimization [39].

### 2.6 Removal of Arsenic by using the phytobial remediation method

It is an inexpensive and environmentally friendly method. The microbe-assisted plant remediation has been widely studied for the degradation of arsenic in rhizophores [40]. Although this process provides 99.9% arsenic removal efficiency [41], however, it is time-consuming due to slow plant growth and the sensitivity of plant species to arsenic concentration. The use of bacteria for the degradation of arsenic through genes is complex and is in the research phase for arsenic removal [42, 43].

### 2.7 Removal of Arsenic by using the electro-kinetic method

This method has been used to remove arsenic from soil and dissolved heavy metals from tainted groundwater [44]. Since this treatment method cannot remove arsenic in its dissolved phase, therefore, using an integrated treatment would be an environmentally friendly, technically efficient, and economically viable solution [45]. This aspect demands further research to investigate the integration of the electro-kinetic method with other treatment techniques. A summary of arsenic removal efficiencies achieved by using above mentioned methods has been provided in Table 1 [46].

Table 1: Arsenic removal efficiencies achieved by using different treatment methods.

Method	Arsenic Removal Efficiency
Adsorption	95%
Ion Exchange	18.9%
Chemical Precipitation	98.5% by using lead hydroxide 96.3% by using lead nitrate
Phytoremediation	88% by using <i>A. Pinnata</i> 83% by using <i>L. Minor</i> 78% by using <i>H. Verticillate</i>



Method	Arsenic Removal Efficiency
	85.5% by using their mixture
Electrocoagulation	93-99.9%
Phytobial remediation	99.9%

Table 1 is an illustration of different arsenic removal efficiencies that have been achieved by using various treatment methods. Among them, the adsorption process has been used extensively due to the easy availability of adsorbent materials, simple operation, and cost-effectiveness.

### 3 Treatment methods used for the removal of pharmaceutical compounds

The use of physical, chemical, and biological treatment processes in conventional treatment plants can eliminate a plethora of contaminants, however, they are not specially designed to eliminate new pollutants like antibiotics to safe permissible levels [47]. Therefore, relying solely on conventional treatment methods would not fulfill the task of removing emerging contaminants (ECs). Various researchers examined the possibility of removing emerging contaminants (ECs) using these methods, but overall results remained unsatisfactory [48-50]. For instance, Sun, et al. [51] claimed the inadequacy of conventional methods for the subtraction of polyfluoroalkyls and perfluoroalkyls. Similarly, He, et al. [52] described the incomplete elimination of tetracycline using the coagulation-flocculation method by utilizing polyferric sulfate, polyaluminium chloride, and polyaluminium sulfate as coagulants. Likewise, Petrovic, et al. [53] achieved only 7% removal efficiency of ECs by using the coagulation-flocculation followed by rapid sand filtration. To overcome these limitations, several advanced treatment methods have been developed by previous researchers including adsorption, membrane technologies, and advanced oxidation processes (e.g., Fenton/Fenton-like methods) as described below.

#### 3.1 Removal of pharmaceuticals by using adsorption

In this process, mass is transferred between the liquid-solid phase, gas-solid phase, liquid-liquid phase, or gas-liquid phase [54]. Contaminants adsorb on the surface of the adsorbent via intermolecular forces such as electrostatic attraction, hydrophobic interfaces and Van der Waals forces. Previously, different types of adsorbent materials have been used for the removal of ECs including activated carbon [55], graphene oxides [56], biochar [57], chitosan [58], and iron oxides [59]. The removal efficiency of these adsorbents depends on the type of targeted ECs. For instance, activated carbon gave complete removal of ciprofloxacin [60], however, the results were not satisfactory for the removal of paracetamol and tetracycline [61]. Similarly, biochar has also been used as an adsorbent for the removal of ECs [62], where thermochemical conditions maintained during the synthesis of biochar greatly affect the adsorption efficiency [63].

Likewise, Azqhandi, et al. [64] observed the complete removal of ciprofloxacin by using montmorillonite clay. Furthermore, alum-based adsorbents and zeolite have also been utilized for the removal of such compounds from an aqueous medium. The detail of ECs removed by various adsorbent materials has been provided in Table 2 [65].

Table 2: Adsorption capacities of different adsorbent materials for the removal of various emerging contaminants.

Emerging contaminants	Adsorbent type	Adsorption capacity (mg. g <sup>-1</sup> )
Perfluoro octane sulfonate	Polyaniline nanotubes	1651
Methyl paraben	Activated carbon chitosan composite	85.90
Propyl Paraben	Activated carbon chitosan composite	90.0
Perfluoro octane sulfonate	Bentonite	99.90
Phenanthrene	Bentonite	4.05
Perfluoro octanoate	Polyaniline nanotubes	1100
Estriol	Graphene	200
Imidacloprid	Peanut husk	6.53
17b-estradiol	Modified activated carbon cloths	12.66
17a-ethinylestradiol	Modified activated carbon cloths	11.11
P-chloro-m-xyleneol	Powder activated carbon	1.3
Bisphenol-a	Bagasse-b-cyclodextrin polymer	121
Atenolol	Oxidized activated carbon	100.6
Diazinon	Fe <sub>3</sub> O <sub>4</sub> -guar gum-montmorillonite	80.0



Emerging contaminants	Adsorbent type	Adsorption capacity (mg. g <sup>-1</sup> )
Diazinon	Fe <sub>3</sub> O <sub>4</sub> -guar gum	47.17
Paraquat	Modified zeolite	166.71
Triclosan	High-silica zeolites	378
Metalaxyl	Natural clay	0.09
Atrazine	Graphene nanosheets oxide	23.84
Tricyclazole	Natural clay	0.08
Tetracycline	Biochar	58.80
4-chlorophenoxyacetic acid	Activated carbon	0.002
Clofibric acid	Activated carbon	0.002
Acetaminophen	Double-oxidized graphene oxide	704
Carbamazepine	Powdered activated carbon	0.04
Diclofenac	Powdered activated carbon	0.04
Sulfamethazine	Biochar (tea waste)	33.81
Atenolol	Granular activated carbon	4.00
Bentazon	Calcined hydrotalcite	123.10

Table 2 shows a list of emerging contaminants removed by using different adsorbent materials having varying adsorption capacities. For instance, polyaniline nanotubes exhibited maximum adsorption capacity (i.e., 0.002 mg.g-1) for the removal of perfluoro octane sulfonate, whereas, activated carbon exhibited the least adsorption capacity (i.e., 1651 mg.g-1) for the removal of 4-chlorophenoxyacetic acid and clofibric acid.

### 3.2 Removal of pharmaceuticals by using membrane technologies

Among various physical treatment methods, membrane treatment stands out because of its remarkable efficiency in eliminating a range of contaminants from water [66]. Commonly microfiltration (MF), ultrafiltration (UF), nanofiltration (NF), and reverse osmosis (RO) membranes are used in water treatment [67]. This method is promising in terms of removal efficiency; however, high cost and energy consumption make it an out of reach option for developing countries. Various researchers studied the removal of pharmaceuticals using UF and MF but the results were not satisfactory [68, 69]. Apart from the membrane type, the nature of pharmaceuticals also dictates the contaminant-removing capacity. For instance, the UF membrane is effective in removing non-steroidal anti-inflammatory drugs (NSAIDs), however, results are underrated for polar phthalate esters [70]. NF membranes exhibit higher removal efficiency as compared to MF and UF due to their small pore size [71]. Taking into consideration different membrane characteristics and working conditions, NF and RO can remove 40% to 100% of emerging contaminants [72].

### 3.3 Removal of pharmaceuticals using Fenton or Fenton-like process

Fenton or Fenton-like processes are the types of advanced oxidation processes (AOPs) that use hydrogen peroxide to produce hydroxyl radical ( $\cdot\text{OH}$ ) for oxidation of the contaminants in an aqueous medium [73]. Previously, this process was applied for the removal of amoxicillin and a remarkable degradation rate was achieved, however, bioactive photoproducts of amoxicillin were formed [74]. Similarly, Sun, et al. [75] reported 100% degradation rates for norfloxacin, cephalexin, and ofloxacin via photolysis with hydrogen peroxide. Table 3 shows the efficiencies obtained by using Fenton/Fenton-like processes for the removal of ECs [76].

Table 3: Studies conducted on the removal of ECs by using Fenton/Fenton-like processes.

Emerging contaminants	Process	Removal efficiency (%)
Levofloxacin	Photo-Fenton	80
Tetracycline	Photo-Fenton	80
Carbamazepine	Electro-Fenton	100
Pymetrozine	Electro-Fenton	90
Dimethyl phthalate	Electro-Fenton	96
Bisphenol A	Photo-Fenton	75

Table 3 shows that reasonable efficiencies have been achieved for the removal of a range of ECs by using these processes.



Out of all processes, the Electro-Fenton process has shown promising efficiency i.e., 100%, 90%, and 96% removal of carbamazepine, pymetrozine, and dimethyl phthalate, respectively.

## 4 Practical Implication

The information provided in this review can be utilized in choosing appropriate treatment options under given circumstances. Furthermore, this review also holds its significance as a single-read source for upcoming researchers in the domain of arsenic and emerging contaminants removal. Comparative analysis of various treatment methods has disclosed the need for integrated treatment technologies to formulate a universal solution for treatment. This review is helpful for upcoming researchers, practitioners and water engineers striving for the effective removal of understudy emerging contaminants.

## 5 Conclusion

This review concludes that health impacts of arsenic contamination have been widely explored, however, a huge gap of obscurity exists when it comes to the health impacts of emerging contaminants. Further, it was found that both natural and anthropogenic sources trigger arsenic contamination; whereas, pharmaceuticals are mostly released into the environment by anthropogenic means. The drastic rise in arsenic and pharmaceutical load in the water has compelled the researchers to investigate various treatment methods. Outcomes disclosed that the selection of suitable treatment technologies depends on user constraints and prevailing conditions.

## Acknowledgment

The authors are thankful to the University of Engineering and Technology Taxila, Pakistan for providing a conducive learning environment and ample research opportunities. The careful review and constructive suggestions by the anonymous reviewers are gratefully acknowledged.

## References

- [1] H. Chen, J. Xu, H. Lin, Z. Wang, and Z. Liu, "Multi-cycle aqueous arsenic removal by novel magnetic N/S-doped hydrochars activated via one-pot and two-stage schemes," *Chemical Engineering Journal*, vol. 429, p. 132071, 2022/02/01/ 2022, doi: <https://doi.org/10.1016/j.cej.2021.132071>.
- [2] S. Phearom, M. K. Shahid, and Y. Choi, "Nature of surface interactions among Fe<sub>3</sub>O<sub>4</sub> particles and arsenic species during static and continuous adsorption processes," *Groundwater for Sustainable Development*, vol. 18, p. 100789, 2022/08/01/ 2022, doi: <https://doi.org/10.1016/j.gsd.2022.100789>.
- [3] R. Irunde *et al.*, "Arsenic in Africa: potential sources, spatial variability, and the state of the art for arsenic removal using locally available materials," *Groundwater for Sustainable Development*, vol. 18, p. 100746, 2022/08/01/ 2022, doi: <https://doi.org/10.1016/j.gsd.2022.100746>.
- [4] A. Sarkar and B. Paul, "The global menace of arsenic and its conventional remediation - A critical review," *Chemosphere*, vol. 158, pp. 37-49, 2016/09/01/ 2016, doi: <https://doi.org/10.1016/j.chemosphere.2016.05.043>.
- [5] L. N. Rodríguez-Cantú, M. A. Martínez-Cinco, J. J. Balderas-Cortés, I. Mondaca-Fernández, M. d. M. Navarro-Farfán, and M. M. Meza-Montenegro, "Arsenic-contaminated drinking water and associated health risks in children from communities located in a geothermal site of Michoacán, México: Monte Carlo probabilistic method," *Human and Ecological Risk Assessment: An International Journal*, vol. 28, no. 3-4, pp. 408-432, 2022.
- [6] Y. Zheng, "Global solutions to a silent poison," *Science*, vol. 368, no. 6493, pp. 818-819, 2020/05/22 2020, doi: [10.1126/science.abb9746](https://doi.org/10.1126/science.abb9746).
- [7] M. Rokonzaman, W. C. Li, C. Wu, and Z. Ye, "Human health impact due to arsenic contaminated rice and vegetables consumption in naturally arsenic endemic regions," *Environmental Pollution*, p. 119712, 2022.
- [8] K. Khosravi-Darani, Y. Rehman, I. A. Katsoyiannis, E. Kokkinos, and A. I. Zouboulis, "Arsenic Exposure via Contaminated Water and Food Sources," *Water*, vol. 14, no. 12, 2022, doi: [10.3390/w14121884](https://doi.org/10.3390/w14121884).
- [9] J.-O. Drangert and A. Cronin, "Use and abuse of the urban groundwater resource: Implications for a new management strategy," *Hydrogeology Journal*, vol. 12, pp. 94-102, 02/01 2004, doi: [10.1007/s10040-003-0307-z](https://doi.org/10.1007/s10040-003-0307-z).
- [10] K. Schirmer and M. Schirmer, "Who is chasing whom? A call for a more integrated approach to reduce the load of micro-pollutants in the environment," *Water Science and Technology*, vol. 57, no. 1, pp. 145-150, 2008, doi: [10.2166/wst.2008.826](https://doi.org/10.2166/wst.2008.826).
- [11] A. Musolff, S. Leschik, M. Möder, G. Strauch, F. Reinstorf, and M. Schirmer, "Temporal and spatial patterns of micropollutants in urban receiving waters," *Environmental Pollution*, vol. 157, no. 11, pp. 3069-3077, 2009/11/01/ 2009, doi: <https://doi.org/10.1016/j.envpol.2009.05.037>.
- [12] D. J. Lapworth, N. Baran, M. E. Stuart, and R. S. Ward, "Emerging organic contaminants in groundwater: A review of sources, fate and occurrence," *Environmental Pollution*, vol. 163, pp. 287-303, 2012/04/01/ 2012, doi: <https://doi.org/10.1016/j.envpol.2011.12.034>.



- [13] K. Kümmerer, "The presence of pharmaceuticals in the environment due to human use – present knowledge and future challenges," *Journal of Environmental Management*, vol. 90, no. 8, pp. 2354-2366, 2009/06/01/ 2009, doi: <https://doi.org/10.1016/j.jenvman.2009.01.023>.
- [14] D. Cerveny *et al.*, "Water temperature affects the biotransformation and accumulation of a psychoactive pharmaceutical and its metabolite in aquatic organisms," *Environment International*, vol. 155, p. 106705, 2021.
- [15] P. Vaudin, C. Augé, N. Just, S. Mhaouty-Kodja, S. Mortaud, and D. Pillon, "When pharmaceutical drugs become environmental pollutants: Potential neural effects and underlying mechanisms," *Environmental Research*, vol. 205, p. 112495, 2022.
- [16] M. Chen *et al.*, "Occurrence of Pharmaceuticals in Calgary's Wastewater and Related Surface Water," *Water Environment Research*, vol. 87, no. 5, pp. 414-424, 2015. [Online]. Available: <http://www.jstor.org/stable/24585987>.
- [17] C. G. Daughton and T. A. Ternes, "Pharmaceuticals and personal care products in the environment: agents of subtle change?," *Environmental Health Perspectives*, vol. 107, no. suppl 6, pp. 907-938, 1999/12/01 1999, doi: 10.1289/ehp.99107s6907.
- [18] A. J. Ebele, M. Abou-Elwafa Abdallah, and S. Harrad, "Pharmaceuticals and personal care products (PPCPs) in the freshwater aquatic environment," *Emerging Contaminants*, vol. 3, no. 1, pp. 1-16, 2017/03/01/ 2017, doi: <https://doi.org/10.1016/j.emcon.2016.12.004>.
- [19] N. Delgado, A. Capparelli, D. Marino, A. Navarro, G. Peñuela, and A. Ronco, "Adsorption of Pharmaceuticals and Personal Care Products on Granular Activated Carbon," *Journal of Surface Engineered Materials and Advanced Technology*, vol. 06, pp. 183-200, 01/01 2016, doi: 10.4236/jsemat.2016.64017.
- [20] J. U. Angai, C. J. Ptacek, E. Pakostova, J. G. Bain, B. R. Verbuyst, and D. W. Blowes, "Removal of arsenic and metals from groundwater impacted by mine waste using zero-valent iron and organic carbon: Laboratory column experiments," *Journal of Hazardous Materials*, vol. 424, p. 127295, 2022/02/15/ 2022, doi: <https://doi.org/10.1016/j.jhazmat.2021.127295>.
- [21] S. Alka, S. Shahir, N. Ibrahim, M. J. Ndejiko, D.-V. N. Vo, and F. A. Manan, "Arsenic removal technologies and future trends: A mini review," *Journal of Cleaner Production*, vol. 278, p. 123805, 2021/01/01/ 2021, doi: <https://doi.org/10.1016/j.jclepro.2020.123805>.
- [22] R. Kumar *et al.*, "Emerging technologies for arsenic removal from drinking water in rural and peri-urban areas: Methods, experience from, and options for Latin America," *Science of The Total Environment*, vol. 694, p. 133427, 2019/12/01/ 2019, doi: <https://doi.org/10.1016/j.scitotenv.2019.07.233>.
- [23] J.-B. Huo, K. Gupta, C. Lu, H. C. Bruun Hansen, and M.-L. Fu, "Recyclable high-affinity arsenate sorbents based on porous Fe<sub>2</sub>O<sub>3</sub>/La<sub>2</sub>O<sub>2</sub>CO<sub>3</sub> composites derived from Fe-La-C frameworks," *Colloids and Surfaces A: Physicochemical and Engineering Aspects*, vol. 585, p. 124018, 2020/01/20/ 2020, doi: <https://doi.org/10.1016/j.colsurfa.2019.124018>.
- [24] Q. L. Zhang, Y. C. Lin, X. Chen, and N. Y. Gao, "A method for preparing ferric activated carbon composites adsorbents to remove arsenic from drinking water," *Journal of Hazardous Materials*, vol. 148, no. 3, pp. 671-678, 2007/09/30/ 2007, doi: <https://doi.org/10.1016/j.jhazmat.2007.03.026>.
- [25] Y. Sun, T. Wang, L. Bai, C. Han, and X. Sun, "Application of biochar-based materials for remediation of arsenic contaminated soil and water: Preparation, modification, and mechanisms," *Journal of Environmental Chemical Engineering*, p. 108292, 2022.
- [26] K. a. Zouboulis, "comparitive evaluation of conventional and alternative methods for the removal of arsenic from contaminated groundwaters," *Rev.Environ.Health*, 2006.
- [27] S. V. Jadhav, E. Bringas, G. D. Yadav, V. K. Rathod, I. Ortiz, and K. V. Marathe, "Arsenic and fluoride contaminated groundwaters: A review of current technologies for contaminants removal," *Journal of Environmental Management*, vol. 162, pp. 306-325, 2015/10/01/ 2015, doi: <https://doi.org/10.1016/j.jenvman.2015.07.020>.
- [28] A. Ortega, I. Oliva, K. E. Contreras, I. González, M. R. Cruz-Díaz, and E. P. Rivero, "Arsenic removal from water by hybrid electro-regenerated anion exchange resin/electrodialysis process," *Separation and Purification Technology*, vol. 184, pp. 319-326, 2017/08/31/ 2017, doi: <https://doi.org/10.1016/j.seppur.2017.04.050>.
- [29] H. Long, Y.-j. Zheng, Y.-l. Peng, G.-z. Jin, W.-h. Deng, and S.-c. Zhang, "Comparison of arsenic(V) removal with different lead-containing substances and process optimization in aqueous chloride solution," *Hydrometallurgy*, vol. 183, pp. 199-206, 2019/01/01/ 2019, doi: <https://doi.org/10.1016/j.hydromet.2018.12.006>.
- [30] J. He *et al.*, "Comparative study of remediation of Cr(VI)-contaminated soil using electrokinetics combined with bioremediation," *Environmental Science and Pollution Research*, vol. 25, no. 18, pp. 17682-17689, 2018/06/01 2018, doi: 10.1007/s11356-018-1741-8.
- [31] S. R. Manoj *et al.*, "Understanding the molecular mechanisms for the enhanced phytoremediation of heavy metals through plant growth promoting rhizobacteria: A review," *Journal of Environmental Management*, vol. 254, p. 109779, 2020/01/15/ 2020, doi: <https://doi.org/10.1016/j.jenvman.2019.109779>.
- [32] N. K. Niazi *et al.*, "Phosphate-assisted phytoremediation of arsenic by Brassica napus and Brassica juncea: Morphological and physiological response," *International Journal of Phytoremediation*, vol. 19, no. 7, pp. 670-678, 2017/07/03 2017, doi: 10.1080/15226514.2016.1278427.
- [33] G. DalCorso, E. Fasani, A. Manara, G. Visioli, and A. Furini, "Heavy Metal Pollutions: State of the Art and Innovation in Phytoremediation," *International Journal of Molecular Sciences*, vol. 20, no. 14, 2019, doi: 10.3390/ijms20143412.
- [34] J. Hou, D. Lin, J. C. White, J. L. Gardea-Torresdey, and B. Xing, "Joint Nanotoxicology Assessment Provides a New Strategy for Developing Nanoenabled Bioremediation Technologies," *Environmental Science & Technology*, vol. 53, no. 14, pp. 7927-7929, 2019/07/16 2019, doi: 10.1021/acs.est.9b03593.





- [35] C. Yang, Y.-N. Ho, R. Makita, C. Inoue, and M.-F. Chien, "Cupriavidus basilensis strain r507, a toxic arsenic phytoextraction facilitator, potentiates the arsenic accumulation by *Pteris vittata*," *Ecotoxicology and Environmental Safety*, vol. 190, p. 110075, 2020/03/01/ 2020, doi: <https://doi.org/10.1016/j.ecoenv.2019.110075>.
- [36] E. Demirbas, M. Kobya, M. S. Oncel, E. Şik, and A. Y. Goren, "Arsenite removal from groundwater in a batch electrocoagulation process: Optimization through response surface methodology," *Separation Science and Technology*, vol. 54, no. 5, pp. 775-785, 2019/03/24 2019, doi: 10.1080/01496395.2018.1521834.
- [37] E. Mohora, S. Rončević, J. Agbaba, K. Zrnčić, A. Tubić, and B. Dalmacija, "Arsenic removal from groundwater by horizontal-flow continuous electrocoagulation (EC) as a standalone process," *Journal of Environmental Chemical Engineering*, vol. 6, no. 1, pp. 512-519, 2018/02/01/ 2018, doi: <https://doi.org/10.1016/j.jece.2017.12.042>.
- [38] C. Calderón Mólgora, A. Martin, M. Avila, P. Drogui, and G. Buelna, "Removal of arsenic from drinking water: A comparative study between electrocoagulation-microfiltration and chemical coagulation-microfiltration processes," *Separation and Purification Technology*, vol. 118, 10/01 2013, doi: 10.1016/j.seppur.2013.08.011.
- [39] M. Kobya, R. D. C. Soltani, P. I. Omwene, and A. Khataee, "A review on decontamination of arsenic-contained water by electrocoagulation: Reactor configurations and operating cost along with removal mechanisms," *Environmental Technology & Innovation*, vol. 17, p. 100519, 2020/02/01/ 2020, doi: <https://doi.org/10.1016/j.eti.2019.100519>.
- [40] S. Alka, S. Shahir, N. Ibrahim, T.-T. Chai, Z. Mohd Bahari, and F. Abd Manan, "The role of plant growth promoting bacteria on arsenic removal: A review of existing perspectives," *Environmental Technology & Innovation*, vol. 17, p. 100602, 2020/02/01/ 2020, doi: <https://doi.org/10.1016/j.eti.2020.100602>.
- [41] A. Shukla and S. Srivastava, "Chapter 8 - A Review of Phytoremediation Prospects for Arsenic Contaminated Water and Soil," in *Phytomanagement of Polluted Sites*, V. C. Pandey and K. Bauddh Eds.: Elsevier, 2019, pp. 243-254.
- [42] L. Liu, M. Bilal, X. Duan, and H. M. N. Iqbal, "Mitigation of environmental pollution by genetically engineered bacteria — Current challenges and future perspectives," *Science of The Total Environment*, vol. 667, pp. 444-454, 2019/06/01/ 2019, doi: <https://doi.org/10.1016/j.scitotenv.2019.02.390>.
- [43] C. Ke, C. Zhao, C. Rensing, S. Yang, and Y. Zhang, "Characterization of recombinant *E. coli* expressing *arsR* from *Rhodospseudomonas palustris* CGA009 that displays highly selective arsenic adsorption," *Applied Microbiology and Biotechnology*, vol. 102, no. 14, pp. 6247-6255, 2018/07/01 2018, doi: 10.1007/s00253-018-9080-8.
- [44] D. Leszczynska and H. Ahmad, "Toxic Elements in Soil and Groundwater: Short-Time Study on Electrokinetic Removal of Arsenic in the Presence of other Ions," *International Journal of Environmental Research and Public Health*, vol. 3, no. 2, 2006, doi: 10.3390/ijerph2006030023.
- [45] J. Li *et al.*, "Comparison of humic and fulvic acid on remediation of arsenic contaminated soil by electrokinetic technology," *Chemosphere*, vol. 241, p. 125038, 2020/02/01/ 2020, doi: <https://doi.org/10.1016/j.chemosphere.2019.125038>.
- [46] A. R. Karbassi, M. Fakhraee, S. Tajziehchi, T. Shahriari, and S. Maddah, "An Efficient Treatment System for Arsenic Removal from Groundwater," *Ambient Science*, vol. 5, 07/01 2018, doi: 10.21276/ambi.2018.05.2.ta01.
- [47] P. R. Rout, T. C. Zhang, P. Bhunia, and R. Y. Surampalli, "Treatment technologies for emerging contaminants in wastewater treatment plants: A review," *Science of The Total Environment*, vol. 753, p. 141990, 2021/01/20/ 2021, doi: <https://doi.org/10.1016/j.scitotenv.2020.141990>.
- [48] V. Naddeo, M. F. N. Secondes, L. Borea, S. W. Hasan, F. Ballesteros, Jr., and V. Belgiorno, "Removal of contaminants of emerging concern from real wastewater by an innovative hybrid membrane process - UltraSound, Adsorption, and Membrane ultrafiltration (USAME®)," (in eng), *Ultrason Sonochem*, vol. 68, p. 105237, Nov 2020, doi: 10.1016/j.ultsonch.2020.105237.
- [49] P. Westerhoff, Y. Yoon, S. Snyder, and E. Wert, "Fate of Endocrine-Disruptor, Pharmaceutical, and Personal Care Product Chemicals during Simulated Drinking Water Treatment Processes," *Environmental Science & Technology*, vol. 39, no. 17, pp. 6649-6663, 2005/09/01 2005, doi: 10.1021/es0484799.
- [50] M. Y. Alazaiza *et al.*, "Application of natural coagulants for pharmaceutical removal from water and wastewater: a review," *Water*, vol. 14, no. 2, p. 140, 2022.
- [51] M. Sun *et al.*, "Legacy and Emerging Perfluoroalkyl Substances Are Important Drinking Water Contaminants in the Cape Fear River Watershed of North Carolina," *Environmental Science & Technology Letters*, vol. 3, no. 12, pp. 415-419, 2016/12/13 2016, doi: 10.1021/acs.estlett.6b00398.
- [52] Z. He *et al.*, "Effects of suspended particulate matter from natural lakes in conjunction with coagulation to tetracycline removal from water," *Chemosphere*, vol. 277, p. 130327, 2021/08/01/ 2021, doi: <https://doi.org/10.1016/j.chemosphere.2021.130327>.
- [53] M. Petrovic, A. Diaz, F. Ventura, and D. Barceló, "Occurrence and Removal of Estrogenic Short-Chain Ethoxy Nonylphenolic Compounds and Their Halogenated Derivatives during Drinking Water Production," *Environmental Science & Technology*, vol. 37, no. 19, pp. 4442-4448, 2003/10/01 2003, doi: 10.1021/es034139w.
- [54] M. K. Shahid, M. Pyo, and Y.-G. Choi, "The operation of reverse osmosis system with CO<sub>2</sub> as a scale inhibitor: A study on operational behavior and membrane morphology," *Desalination*, vol. 426, pp. 11-20, 2018/01/15/ 2018, doi: <https://doi.org/10.1016/j.desal.2017.10.020>.
- [55] B. N. Bhadra and S. H. Jhung, "A remarkable adsorbent for removal of contaminants of emerging concern from water: Porous carbon derived from metal azolate framework-6," *Journal of Hazardous Materials*, vol. 340, pp. 179-188, 2017/10/15/ 2017, doi: <https://doi.org/10.1016/j.jhazmat.2017.07.011>.
- [56] Y.-L. Zhang, Y.-J. Liu, C.-M. Dai, X.-F. Zhou, and S.-G. Liu, "Adsorption of Clofibric Acid from Aqueous Solution by Graphene Oxide and the Effect of Environmental Factors," *Water, Air, & Soil Pollution*, vol. 225, no. 8, p. 2064, 2014/07/16 2014, doi: 10.1007/s11270-014-2064-0.



- [57] F. Tomul *et al.*, "Peanut shells-derived biochars prepared from different carbonization processes: Comparison of characterization and mechanism of naproxen adsorption in water," *Science of The Total Environment*, vol. 726, p. 137828, 2020/07/15/ 2020, doi: <https://doi.org/10.1016/j.scitotenv.2020.137828>.
- [58] W. Phasuphan, N. Praphairaksit, and A. Imyim, "Removal of ibuprofen, diclofenac, and naproxen from water using chitosan-modified waste tire crumb rubber," *Journal of Molecular Liquids*, vol. 294, p. 111554, 2019/11/15/ 2019, doi: <https://doi.org/10.1016/j.molliq.2019.111554>.
- [59] T. Ahamad, M. Naushad, T. Al-Shahrani, N. Al-hokbany, and S. M. Alshehri, "Preparation of chitosan based magnetic nanocomposite for tetracycline adsorption: Kinetic and thermodynamic studies," *International Journal of Biological Macromolecules*, vol. 147, pp. 258-267, 2020/03/15/ 2020, doi: <https://doi.org/10.1016/j.ijbiomac.2020.01.025>.
- [60] S. A. C. Carabineiro, T. Thavorn-Amornsri, M. F. R. Pereira, and J. L. Figueiredo, "Adsorption of ciprofloxacin on surface-modified carbon materials," *Water Research*, vol. 45, no. 15, pp. 4583-4591, 2011/10/01/ 2011, doi: <https://doi.org/10.1016/j.watres.2011.06.008>.
- [61] B. Ruiz *et al.*, "Surface heterogeneity effects of activated carbons on the kinetics of paracetamol removal from aqueous solution," *Applied Surface Science*, vol. 256, no. 17, pp. 5171-5175, 2010/06/15/ 2010, doi: <https://doi.org/10.1016/j.apsusc.2009.12.086>.
- [62] M. Ahmad *et al.*, "Effects of pyrolysis temperature on soybean stover- and peanut shell-derived biochar properties and TCE adsorption in water," *Bioresource Technology*, vol. 118, pp. 536-544, 2012/08/01/ 2012, doi: <https://doi.org/10.1016/j.biortech.2012.05.042>.
- [63] S. M. Mitchell, M. Subbiah, J. L. Ullman, C. Frear, and D. R. Call, "Evaluation of 27 different biochars for potential sequestration of antibiotic residues in food animal production environments," *Journal of Environmental Chemical Engineering*, vol. 3, no. 1, pp. 162-169, 2015/03/01/ 2015, doi: <https://doi.org/10.1016/j.jece.2014.11.012>.
- [64] M. H. A. Azghandi, M. Foroughi, and E. Yazdankish, "A highly effective, recyclable, and novel host-guest nanocomposite for Triclosan removal: A comprehensive modeling and optimization-based adsorption study," *Journal of Colloid and Interface Science*, vol. 551, pp. 195-207, 2019/09/01/ 2019, doi: <https://doi.org/10.1016/j.jcis.2019.05.007>.
- [65] J. Rivera-Utrilla, M. Sánchez-Polo, M. Á. Ferro-García, G. Prados-Joya, and R. Ocampo-Pérez, "Pharmaceuticals as emerging contaminants and their removal from water. A review," *Chemosphere*, vol. 93, no. 7, pp. 1268-1287, 2013/10/01/ 2013, doi: <https://doi.org/10.1016/j.chemosphere.2013.07.059>.
- [66] A. I. Schäfer, I. Akanyeti, and A. J. C. Semião, "Micropollutant sorption to membrane polymers: A review of mechanisms for estrogens," *Advances in Colloid and Interface Science*, vol. 164, no. 1, pp. 100-117, 2011/05/11/ 2011, doi: <https://doi.org/10.1016/j.cis.2010.09.006>.
- [67] S. Alipoori *et al.*, "Polymer-Based Devices and Remediation Strategies for Emerging Contaminants in Water," *ACS Applied Polymer Materials*, vol. 3, no. 2, pp. 549-577, 2021/02/12 2021, doi: 10.1021/acsapm.0c01171.
- [68] J. L. Acero, F. J. Benitez, F. Teva, and A. I. Leal, "Retention of emerging micropollutants from UP water and a municipal secondary effluent by ultrafiltration and nanofiltration," *Chemical Engineering Journal*, vol. 163, no. 3, pp. 264-272, 2010/10/01/ 2010, doi: <https://doi.org/10.1016/j.cej.2010.07.060>.
- [69] A. Lidén and K. M. Persson, "Comparison between ultrafiltration and nanofiltration hollow-fiber membranes for removal of natural organic matter: a pilot study," *Journal of Water Supply: Research and Technology-Aqua*, vol. 65, no. 1, pp. 43-53, 2015, doi: 10.2166/aqua.2015.065.
- [70] C. V. Faria, B. C. Ricci, A. F. R. Silva, M. C. S. Amaral, and F. V. Fonseca, "Removal of micropollutants in domestic wastewater by expanded granular sludge bed membrane bioreactor," *Process Safety and Environmental Protection*, vol. 136, pp. 223-233, 2020/04/01/ 2020, doi: <https://doi.org/10.1016/j.psep.2020.01.033>.
- [71] M. Riera-Torres, C. Gutiérrez-Bouzán, and M. Crespi, "Combination of coagulation–flocculation and nanofiltration techniques for dye removal and water reuse in textile effluents," *Desalination*, vol. 252, no. 1, pp. 53-59, 2010/03/01/ 2010, doi: <https://doi.org/10.1016/j.desal.2009.11.002>.
- [72] A. M. Urriaga, G. Pérez, R. Ibáñez, and I. Ortiz, "Removal of pharmaceuticals from a WWTP secondary effluent by ultrafiltration/reverse osmosis followed by electrochemical oxidation of the RO concentrate," *Desalination*, vol. 331, pp. 26-34, 2013/12/16/ 2013, doi: <https://doi.org/10.1016/j.desal.2013.10.010>.
- [73] J. L. Wang and L. J. Xu, "Advanced Oxidation Processes for Wastewater Treatment: Formation of Hydroxyl Radical and Application," *Critical Reviews in Environmental Science and Technology*, vol. 42, no. 3, pp. 251-325, 2012/02/01 2012, doi: 10.1080/10643389.2010.507698.
- [74] Y. J. Jung, W. G. Kim, Y. Yoon, J.-W. Kang, Y. M. Hong, and H. W. Kim, "Removal of amoxicillin by UV and UV/H<sub>2</sub>O<sub>2</sub> processes," *Science of The Total Environment*, vol. 420, pp. 160-167, 2012/03/15/ 2012, doi: <https://doi.org/10.1016/j.scitotenv.2011.12.011>.
- [75] Y. Sun *et al.*, "Degradation of antibiotics by modified vacuum-UV based processes: Mechanistic consequences of H<sub>2</sub>O(2) and K(2)S(2)O(8) in the presence of halide ions," (in eng), *Sci Total Environ*, vol. 664, pp. 312-321, May 10 2019, doi: 10.1016/j.scitotenv.2019.02.006.
- [76] E. Yamal Turbay, "Efficient operation of photo-Fenton process for the treatment of emerging contaminants in water solutions," 2021.



# IDENTIFICATION AND COUNTERMEASURES OF SPATIAL CONCENTRATION FACTORS FOR PARTICULATE MATTER 2.5

*Ibrahim\**

Department of Engineering Management, U.E.T, Taxila, [mibrahimbjr@gmail.com](mailto:mibrahimbjr@gmail.com)  
Corresponding author: Email ID: [mibrahimbjr@gmail.com](mailto:mibrahimbjr@gmail.com)

**Abstract**-As we know PM<sub>2.5</sub> has adverse effects on human health and decrease the progress of humanity. For this purpose, air quality monitoring departments try to find the composition of the PM<sub>2.5</sub> and their source of origin and identify the high polluted areas. Geographic information systems (GIS) provide useful tools, providing the spatial concentration of a region and by these spatial concentrations, an equation is made to predict the values of PM<sub>2.5</sub> concentration. The research's basic purpose is to identify the PM<sub>2.5</sub> concentration and create an Equation which is composed of main factors of meteorology, which are collected using an inverse distance raster analysis, results to carry out analysis at temporal resolution and finer spatial, and to identify the yearly and monthly PM<sub>2.5</sub> concentrations in Ohio Country. Factors of meteorology and concentration of PM<sub>2.5</sub> are studied and projected at a large scale in the Ohio state, by using measurements from 55 meteorological stations in the study region Ohio for annual and for three months (July, August, September). A GIS spatial interpolation procedure is used for them. An Ordinary least squares method was used for each of these three months' data, and in this way, models were created. The research results show the model performance was at this accuracy level (98, 99, and 97). To validate the results of these models, the predicted value of PM<sub>2.5</sub> data was compared with the value of PM<sub>2.5</sub> data observed, and the accuracy level for that is at (97, 98, and 96 percent, respectively). The show results of the models have a very strong fit of the Ordinary least Squares model to the data observed, which confirms, that the results of this work will examine and forecast PM<sub>2.5</sub> accurately.

**Keywords**- GIS, IDW, OLS, PM 2.5

## 1 Introduction

Because of the hazardous impacts on human health of PM<sub>2.5</sub> pollution, it is critical to identify the changing levels of PM<sub>2.5</sub> and to take future preventative steps to overcome the concentration level up to the standard level. PM<sub>2.5</sub> is now the leading environmental contributor to the global burden of disease. PM<sub>2.5</sub> rising from being the fifth leading contributor among environmental risk factors in 1990, in part driven by declines in household air pollution and unsafe water and sanitation [1]. Cities' PM<sub>2.5</sub> concentrations can be improved at various sectors (industrial, transportation, and residential, for example) and geographic levels. The US Environmental Protection Agency categorized and identified a comprehensive list of harmful air pollutants. These pollutants may go beyond the high risks in various metropolitan areas and harm people's health[2]. Nowadays, there is prevalent concern about that, the increasing number of vehicles on the road and their impact on public health. One of the health studies showed that a variation in cardiovascular mortality rates is associated with PM<sub>2.5</sub>, concerning the geographical distance from the central monitoring sites. Spatiotemporal variation has, therefore, become a matter of concern for environmental scientists, health researchers, public health officials, and the public[3]. It is thus important to spot regions where PM<sub>2.5</sub> levels exceed the standard



level to make a realistic PM<sub>2.5</sub> prediction method [4]. Given the severity of the air pollution problems in regional or national, measurement of PM<sub>2.5</sub> has recently attracted more consideration to identify spatial concentration.

A useful indicator to describe air quality is Air Quality Index (AQI). Which provides information on the recent air quality of an area and its health consequences [2]. Government air quality departments used these values to express the degree of air pollution in the atmosphere and their public relation, and its value can change according to the air emissions variation. To point out the harmfulness of air contamination, the United States Environmental Protection Agency ([www.epa.gov/aqi](http://www.epa.gov/aqi)) developed an AQI indicator. There are five foremost pollutants of air involved: CO<sub>2</sub>, PM<sub>2.5</sub>, O<sub>3</sub>, NO<sub>2</sub>, and SO<sub>2</sub> [5]. AQI is one of the best ways to continuously assess and explain air quality of an area. AQI aims to show the severity of ambient air pollution levels in an easy way to the public by showing the concentration of each pollutant on a common scale where health effects, occur at a value that is common to all pollutants. Such transformations presented air pollution in an easy accessible way with little knowledge of how the public uses the data [6]. The air quality index is reported as the combination of diverse pollutants and this combination is represented by a single value [7].

Geographic information systems (GIS) have the ability of strong data processing and modeling. It has analysis ways to support decision-makers and academics to enhance interpretation and explain data more precisely, hence advancing helpful and more significant data[8]. Where analysts and academics use the GIS results to conclude supportive arguments on harsh conditions [9]. In recent years different methods and data are presented for quantifying air pollution. In environmental research, Geographic Information Systems (GIS) and Remote sensing (RS) techniques have been widely used, because of their easy use and accessibility of temporal environmental satellite-driven data[10].

Various land base regression methods based are made to look at spatial patterns of PM<sub>2.5</sub> concentration in a specific region [11]. The two fundamental types of linear regression methods are non-parametric (such as Passing Bablok's Linear Regression) and parametric (such as Ordinary or Least-Square Linear Regression and Deming's Linear Regression) [12]. The accessibility of extensive tools for fitting linear regression models, fitting the linear mean function to geo statistical data is simple and easy [13]. Accurate and precise estimation is necessary for appropriate exposure assessments of PM<sub>2.5</sub> concentration. Land use regression (LUR) models have generally been used to prevent misclassification and biased risk evaluation in estimation [14].

In this paper, we construct an alternative way for measuring PM<sub>2.5</sub> based on data obtained from the GIS toolbox of geo statistical way analysis. Following that, the proposed method used the GIS-based OLS strategy to evaluate three individual equations of PM<sub>2.5</sub> estimation. The estimations are made for three months from July to September based on the data obtained from Ohio State. Using Ordinary linear regressions between the dependent variable (PM<sub>2.5</sub>) and the other independent Metrological factors to form the associations; for this reason, the predictable values will be used to represent PM<sub>2.5</sub> levels, and the predictor variables will correctly clarify the geographical variations of PM<sub>2.5</sub> concentration in a specific region.

## 2 Measuring Procedures

### *IDW*

In Arc GIS, the main method used for spatial patterns is inverse distance weighting (IDW). Because inverse distance weighting (IDW) is a precise interpolator, data is apprehensively taken into account in this method. The interpolation method's purpose is to use measurements  $z(s_i)$ ,  $i=1,2,3,\dots, n$ , placed at different point locations, for the reason to provide a possibility of the point value of the experienced possessions in the position  $s_0$  when observations of the point do not exist. The weights assigned to different elements are determined by the element's distance from the estimated location. Weights are commonly obtained using the inverse squared distance (represented by the exponent -2), and the interpolation approximation function can be specified as:

$$\hat{z}(s_0) = \frac{\sum_{i=1}^n z(s_i) d_{i0}^{-2}}{\sum_{i=1}^n d_{i0}^{-2}}$$



Here  $d_{i0}$  represented the path between  $s_0$  and  $s_i$

### **OLS model**

Ordinary linear squares are the most often used method for fitting a preliminary linear mean function to geo-statistical[13]. The formula for OLS regression with  $k$  independent parameters is:

$$z_i = \beta_0 + \beta_1 x_{1i} + \dots + \beta_k x_{ki} + \varepsilon$$

Here  $i$  represent locations, and  $x_{1i}, x_{2i}, x_{3i}, \dots, x_{ki}$  represents independent variables at location  $i$ ,  $\beta_0, \beta_1, \beta_2, \beta_3, \dots, \beta_k$  represents variables that will be predicted, and  $\varepsilon$  represents the term of error.

## **3 Research Methodology**

The essential capabilities like data management and mapping, Arc GIS includes logical approaches that have long been a basis for Arc GIS. The spatial data tools of Arc GIS are a collection of approaches for characterizing and modeling geographic data. They also examine the geographical pattern of a specific region, processing, trends, distributions, and linkages. The study's procedure was implemented in three steps for the prediction of PM<sub>2.5</sub>: inverse distance weighted (IDW) raster analysis interpolation method, regression models formation, and confirmation of the regression models. This study's analysis is based on two types of data: an Ohio climate record acquired from NASA satellite data using the RET Screen software, and yearly data of PM<sub>2.5</sub>, AQI data downloaded from the source <https://www.epa.gov/outdoor-air-quality-data/download-daily-data>. Arc GIS version 10.3 was used for Ordinary linear squares model development and interpolation procedure, as well as making final maps outputs, which were built in the legends and scale bar in the respective prediction maps.

## **4 Results**

To calculate values of PM<sub>2.5</sub> for any site in Ohio State, Inverse Distance Weighting (IDW) method was performed by utilizing the measured parameter data of the 55 stations in Ohio State. The resulting Inverse Distance Weighting (IDW) map includes AQI, PM<sub>2.5</sub>, TEMP, HUMIDITY, PRESSURE, and WIND SPEED values are grouped as classes with Different colors ranging from lowest value to highest value. The predicted values are limited to the interpolation range of the values. Because Inverse Distance

Weighting (IDW) is an average distance weighted, this average distance weighted cannot be more than the upper value or less than the lower value of the given values. As a result, ridges or valleys are not constructed if these limitations are not sampled previously. The Inverse Distance Weighting (IDW) was used to distinguish the values of the cell using a set of sample points of a site. In comparison to tools of the same function, the Inverse Distance Weighting (IDW) is easy to use and execute in the program because there is no need for pre-modeling or subjective assumptions like other tools. Figure 1, 2, and 7 shows the IDW resulting maps of the Ohio state for 2018 and from July to September 2018 respectively.

### **Annual IDW analysis of PM<sub>2.5</sub>**

To show the spread of PM<sub>2.5</sub> in Ohio State for yearly Inverse Distance Weighting (IDW) procedure has been used and the role of the higher and lower value map by colors range (Figure 1). The IDW results have shown the uppermost values of PM<sub>2.5</sub> at the Western Side stations and Southern stations of State Ohio with a value of 8.89 $\mu$ g/m<sup>3</sup> and 11 $\mu$ g/m<sup>3</sup> respectively. The lower PM<sub>2.5</sub> values at southern sites are 7 $\mu$ g/m<sup>3</sup> and 5 $\mu$ g/m<sup>3</sup>. The Northern sides of Ohio have an unhealthy value of 8 $\mu$ g/m<sup>3</sup>.

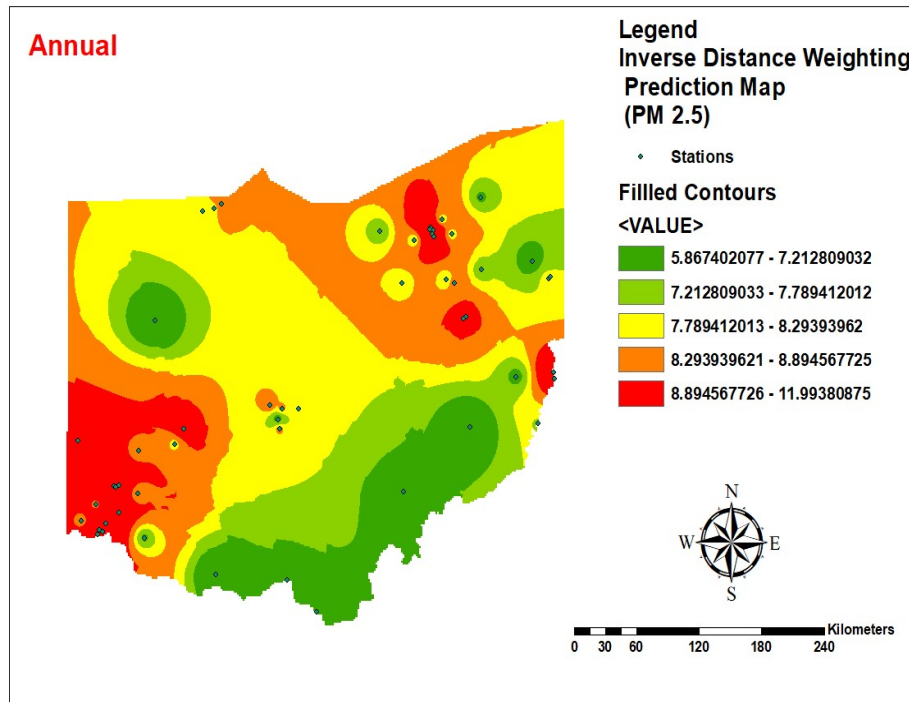


Fig. 1 PM 2.5 map of Ohio State.

### Annual IDW analysis of AQI

Air Quality index increases as the concentration of PM 2.5 increases in the respective regions (Figure 2). The IDW results of AQI have shown the higher values of AQI at the Western Side stations and Southern stations of State Ohio with a value of 35.48ug/m<sup>3</sup> and 46.30ug/m<sup>3</sup> respectively. The lower AQI values at southern sites are 24.4ug/m<sup>3</sup> and 29.4ug/m<sup>3</sup>. The Northern sides of Ohio have an unhealthy value of 33.33ug/m<sup>3</sup>.

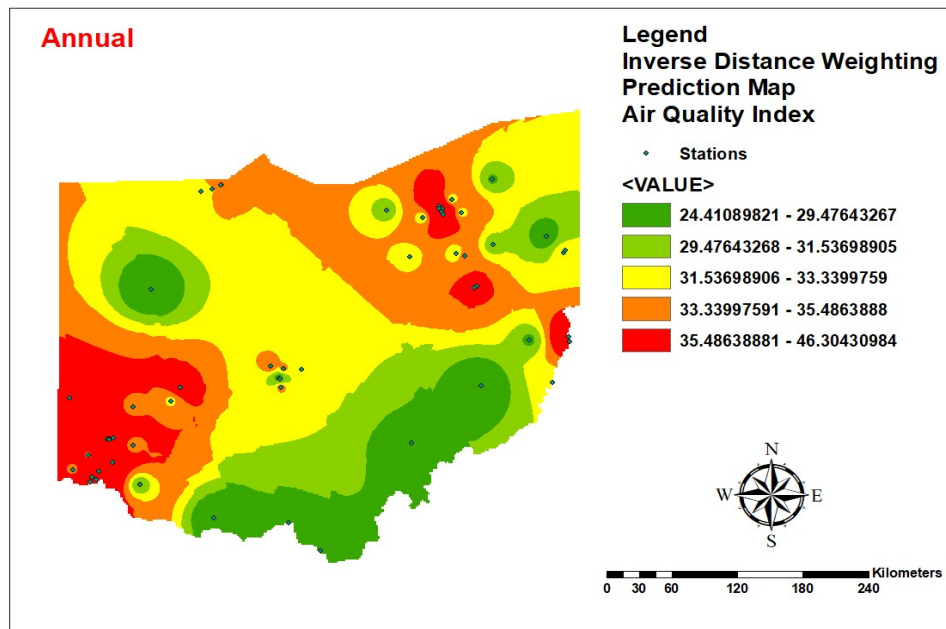


Fig. 2 AQI map of Ohio State.



### ***Correlation between PM<sub>2.5</sub> and Wind Speed***

The highest concentration regions have Wind speed that influences the parallel and perpendicular transport of air pollutants. As wind speed rises, the concentration of PM<sub>2.5</sub> decreases noticeably. When wind speed increases from 0-5 km/h to 5-10 km/h, the mean PM<sub>2.5</sub> concentration decreases from 55 g/m<sup>3</sup> to 33 g/m<sup>3</sup>. This is because strong wind speeds support the increase of PM<sub>2.5</sub>. Low wind speed, on the other hand, hinders PM<sub>2.5</sub> diffusion and causes air pollutants to build up at the surface. Next, wind direction has a considerable impact on PM<sub>2.5</sub> levels in different regions. PM<sub>2.5</sub> levels varied depending on the direction of the wind blowing. In this way, the west wind carried the maximum PM<sub>2.5</sub> throughout the spring. In the summer, the South East wind, North West wind, and West wind conveyed additional PM<sub>2.5</sub> than other directions of the wind. In this way, in fall, the West wind, and South East wind bring more PM<sub>2.5</sub> than any other wind direction. In the winter, the South West wind, East South wind, North Wind, and West wind transport more PM<sub>2.5</sub> concentration than the other winds. In every season, the west wind brings more PM<sub>2.5</sub> than the other winds. Thus, one reason may be air pollutants in Ohio State come mostly from Indiana State.

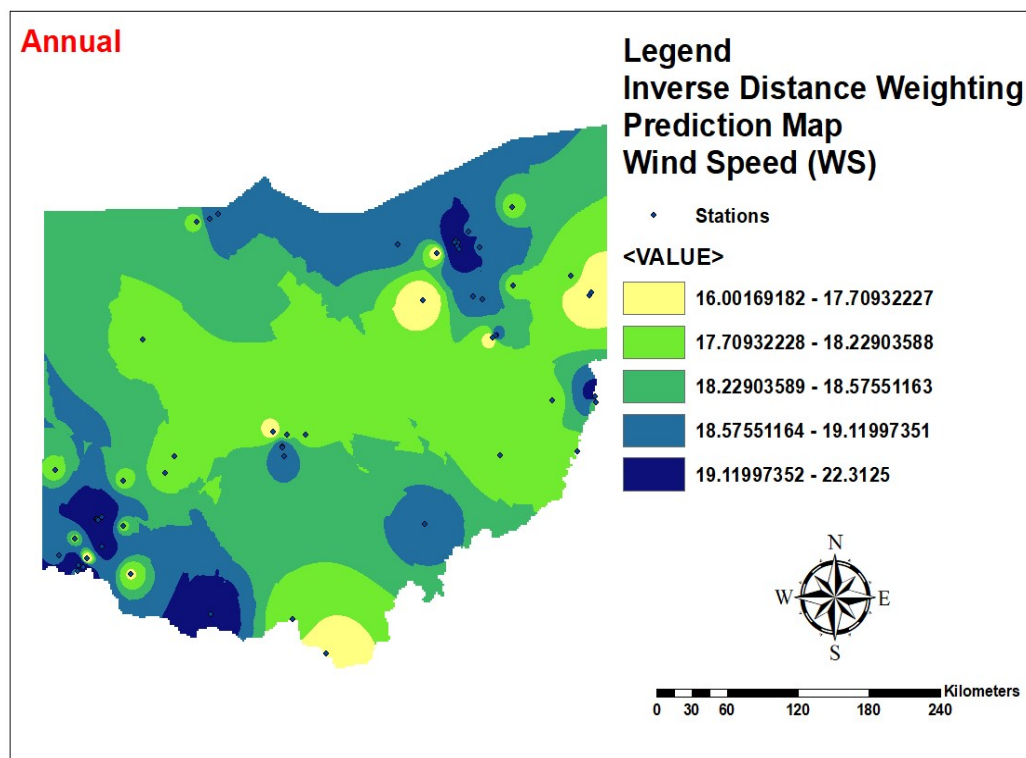


Fig. 3 Wind speed map of Ohio State.

### ***Correlation between PM<sub>2.5</sub> and Temperature***

The Temperature values in 2018 are divided into five ranges which are: 10-15, 15-20, 20-25, 25-30, and 30-35. Due to the subtropical monsoon climate in Ohio State temperature variation is smaller than in other high latitude areas. PM<sub>2.5</sub> concentrations mean values decrease with the increase of temperature up to some level. PM<sub>2.5</sub> mean value is highest (11 µg/m<sup>3</sup>) in the temperature range of 10.1-10.5°C. When the temperature value is equal to 10.5°C or greater than 10.5°C, the air convection at the lower surface is strong enough to reduce the PM<sub>2.5</sub> concentration up to 10µg/m<sup>3</sup> by upward transportation. Some months of Ohio State show a positive correlation of PM<sub>2.5</sub> with temperature. One of the reasons for the positive correlation is high temperature contribute to the formation of particulate matter due to the Photochemical process between the particles.

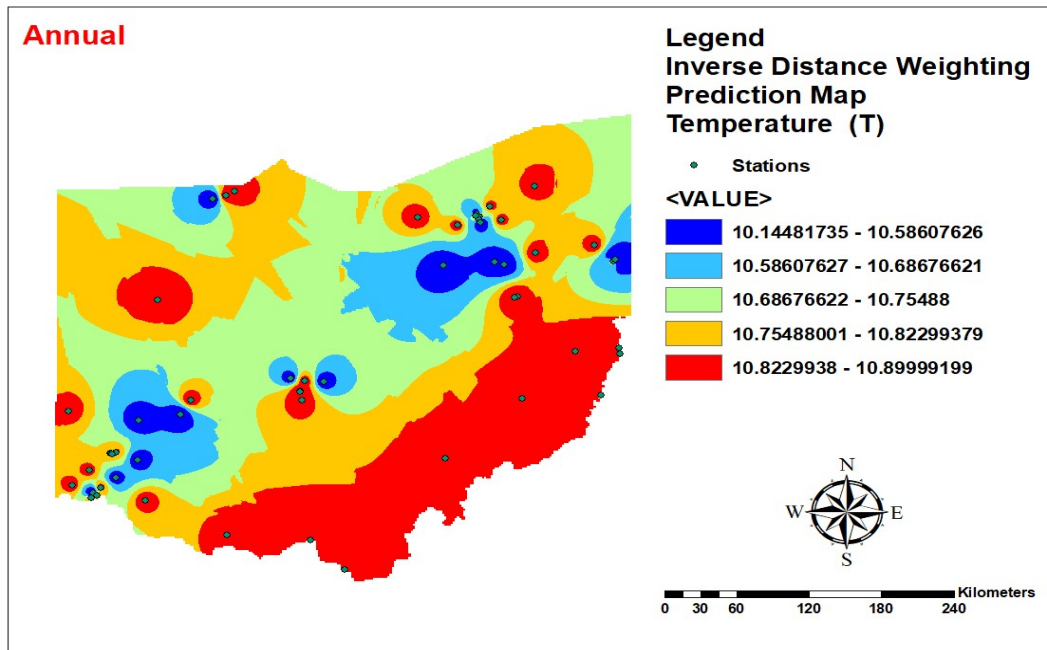


Fig. 4 Temperature map of Ohio State.

### Correlation between PM<sub>2.5</sub> and Precipitation

The rainfall in 2018 was divided into six ranges: 80-90, 90-100, 100-110, 110-120, 120-130, >150. PM<sub>2.5</sub> values were calculated for each interval of RH values. About 60% of days in 2018 have rainfall less than 115 mm. The frequency in 110-115 is 15%. The rainfall >120 mm has a low frequency of 2%. PM<sub>2.5</sub> concentrations mean values reduce with rainfall for different RH intervals. Especially when the rainfall changes from <110 to 115, PM<sub>2.5</sub> concentration has reduced from 8 µg/m<sup>3</sup> to 7 µg/m<sup>3</sup>. Therefore, precipitation can improve air quality by wet deposition, and PM<sub>2.5</sub> concentration can be reduced significantly.

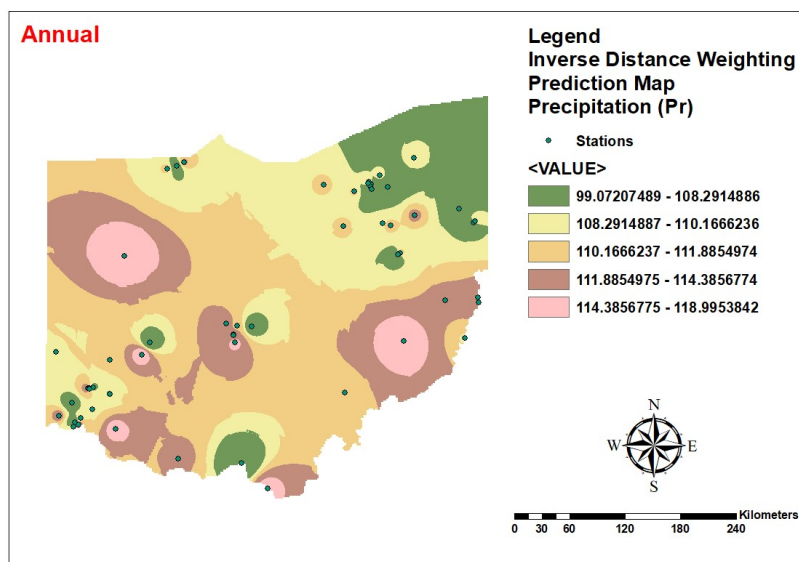


Fig. 5 Precipitation map of Ohio State.





### Correlation between PM2.5 and Relative Humidity

The relative humidity in 2018 ranging from 80% - 90% was classified into 3 intervals: 60-70, 70-80, 80-90. Ohio State has a humid climate and has a strong negative correlation between PM2.5 concentration and RH. The frequency of RH between 80% and 90% exceeds 60% in Ohio State. PM2.5 concentration means the value reduces in each interval with the increase of RH value. Some months show positive correlations in Ohio State but the correlation coefficient is very low. A negative correlation exists between PM2.5 and RH in summer in Ohio State because the humidity value is higher than 80%. When the humidity value is low in other months the concentration of PM2.5 increases due to hygroscopic growth present in the air. As a result of the heavy weight of dry deposition, the particles fall and the concentration of PM2.5 reduces.

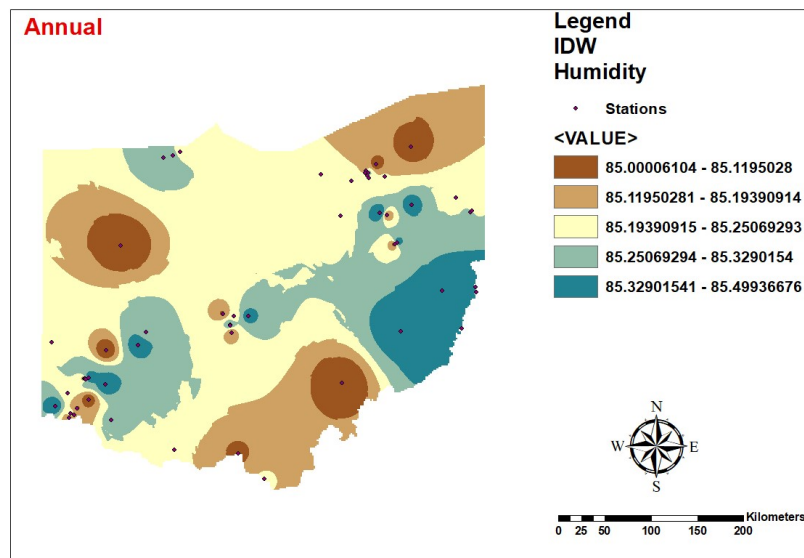


Fig. 6 Humidity map of Ohio State

### Three months IDW analyses (July-September)

The highest concentration region in August and September indicates Wind speed influences the horizontal and vertical transport of Air pollutants. Humidity and Precipitation also have a positive correlation with Air quality in these months, temperature has a negative correlation with PM2.5 in these months.

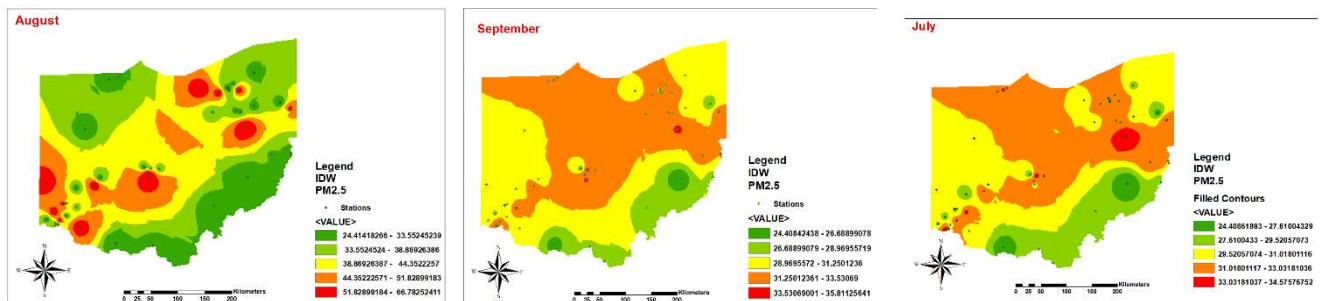


Fig. 7 PM2.5 maps of July to September 2018

### Ordinary linear squares models of PM2.5

By using Ordinary linear squares regression to develop equations for PM2.5 based on the use of independent variables with a typical accurateness of 97%. OLS results in summary for July, August, and September 2018 are shown in Tables 1, 2, and 3 respectively.



#### 4.8.1 OLS results in July 2018

Table 1 OLS results summary for July

Variable	Coefficient	Std Error	t_Statistic	Probability	Std Coefficient
Intercept	-8.9877	29.7821	-0.2976	0.8231	0
Precipitation	3.1334	0.1972	9.9832	4.2372E - 14	0.8824
Temperature	0.0828	0.4972	0.2011	0.9402	0.0207
Wind speed	2.9822	0.6973	3.9521	1.9721E - 06	0.0697
Humidity	0.2011	0.1894	0.7923	0.3922	0.0683

#### 4.8.2 OLS results in August 2018

Table 2 OLS results summary for August

Variable	Coefficient	Std Error	t_Statistic	Probability	Std Coefficient
Intercept	-396.8748	198.8743	-1.9824	0.0452	0
Precipitation	-0.6321	0.8734	-0.6021	0.6012	-0.3032
Temperature	-2.1021	0.5228	-1.7341	0.0424	-0.3141
Wind speed	22.4264	1.6731	6.7824	1.397E - 09	0.6972
Humidity	6.6374	1.9372	1.7866	0.0200	0.8774

#### 4.8.3 OLS results in September 2018

Table 3 OLS results summary for September

Variable	Coefficient	Std Error	t_Statistic	Probability	Std Coefficient
Intercept	-498.3970	206.5856	-2.5156	0.02175	0
Precipitation	9.6224	3.2465	3.9762	4.9747E - 06	0.9872
Temperature	-6.5832	1.9982	-2.1556	0.0357	-0.7797
Wind speed	16.1574	4.3215	3.2155	0.0029	0.3917
Humidity	8.2432	1.9858	3.9826	2.626E - 06	2.0022

When ordinary linear squares investigation was completed based on data, in this way three analytical models have been set to study Particulate Matter (PM<sub>2.5</sub>). The association and modeling among dependent and independent variables according to the circumstances mentioned have been experienced.

#### Equations

The obtained three modeling equations from regression analysis have been made for the measurement of Particulate Matter (PM<sub>2.5</sub>) from July to September represented by three Equations (1, 2, and 3) respectively.

$$\text{PM}_{2.5} \text{ July} = -8.9877 + 2.9822 W_s + 3.1334 P \quad (1)$$

$$\text{PM}_{2.5} \text{ August} = -396.8748 - 2.1021 T + 6.6374 H + 22.4264 W_s \quad (2)$$

$$\text{PM}_{2.5} \text{ September} = -498.3970 - 6.5832 T + 8.2432 H + 16.1574 W_s + 9.6224 P \quad (3)$$



Where, Particulate Matter value is represented by PM<sub>2.5</sub>, Relative Humidity is represented by H (%), Temperature is represented by T (°C), Wind speed is represented by Ws (m/sec), and Precipitation is represented by P (mm). The Parameters used as independent variables are; T, H, P, and Ws, with PM<sub>2.5</sub> as a dependent variable. Based on both of the results of IDW and NASA satellite data, which are combined through RET screen software and OLS PM<sub>2.5</sub> prediction equations were made to approximate the value of PM<sub>2.5</sub> at all the points recorded in the region. It's depending upon the multiple regressions formula.

In the first case to analyze the relationships between independent and dependent variables OLS regression method was used. Precipitation and wind speed are included in the first equation used in the modeling. In July temperature has no impact on PM<sub>2.5</sub>. Linear relationships between variables are limited by the correlation. Most of the variables have a high level of co-linearity with each other but the co-linearity of independent variables temperature and humidity, in this case, is low. The Temperature probability value as shown in Table 1 is 0.97 which is high than the 0.05 value, for this reason, it has not been included in the first equation. The studies consider a good correlation which is more than 0.70. But in this case, the goal is to find minimum relations between the variables to find the impacts of these variables. Therefore, based on the use of these two variables, a regression model was made represented in Equation (1).

In the second case, the model represented by Equation (2) included three independent variables: wind speed, humidity, and temperature. In this case, precipitation does not correlate so we excluded it from the equation and model construction. In the third case, the model that we have represented by Equation (3) included temperature, humidity, wind speed, and precipitation. In this case, all independent variables correlate.

These three equations find the values of the predicted variable for three months. It does not produce the predicted variable absolute values but represents the closed or near approximated to the real observed value. In these three equations, the coefficients' physical significance shows us a good optimization level, which represented the near value of the real observed value can be determined accurately. The three estimated mathematical equations have accuracy corresponding to  $R^2$  and the probability value obtained from the regression analysis. Forward computations were used to achieve the extra high  $R^2$  adjusted in estimated model equations. The correlation shown by the three equations, wind speed has the highest share in the increased concentration of PM<sub>2.5</sub> and next the precipitation. When the speed of the wind is strong it increases dust storms and resulting in increased particle sizes.

### ***OLS model justification***

In the below Figure, by using 40 points, the justification has been experienced. This justification uses the polynomial linear polynomial fitting to calculate PM<sub>2.5</sub> values by the OLS model and compare them to the observed values of PM<sub>2.5</sub>.

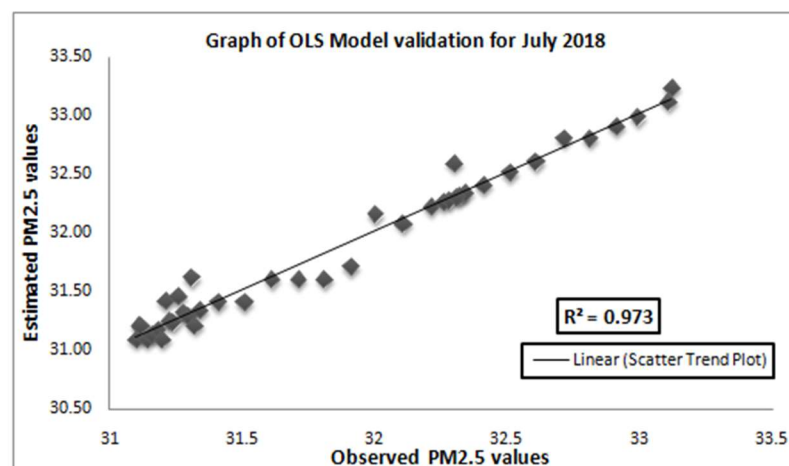


Fig.8 Graph of OLS Model validation for July 2018

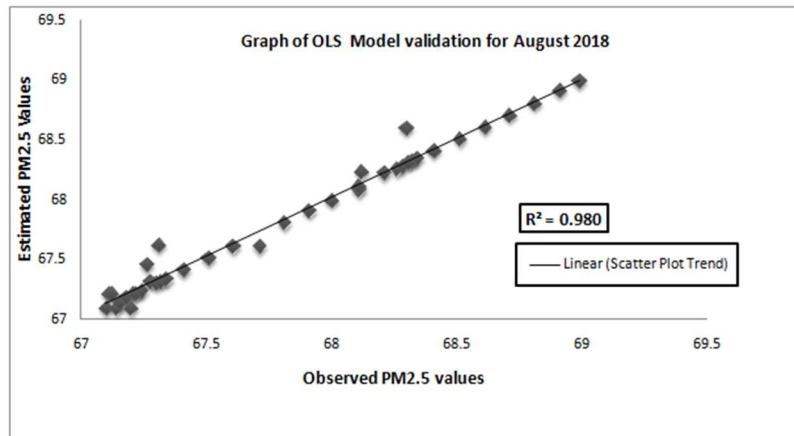


Fig.9 Graph of OLS Model validation for August 2018

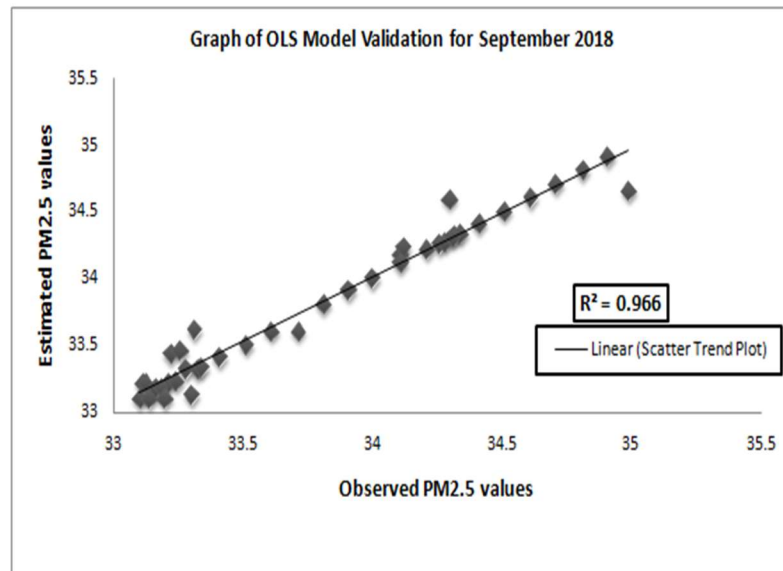


Fig 10 Graph of OLS Model validation for September 2018

The justification applied for the months (July, August, and September). The results with  $R^2$  up to 0.97 in July and  $R^2$  up to 0.98 in August, and 0.96 in September showed that the total records are within the boundary of confidence. Here the observed PM2.5 values refer to the values entered in the PM2.5 model and the estimated PM2.5 represents the values that are calculated from the result regression. The predicted method by putting the point's objective is to accuracy attainment and to test the concentration of PM2.5 at the position point.

### **Practical Relevance**

This study will contribute to air quality monitoring Agencies in the following ways. The IDW and OLS proposed in this study are important because it can support efficient future spatial PM2.5 monitoring. Next, various other hazardous pollutants which increase the air quality index can be estimated by adopting these proposed methods. Engineers will be able to develop Air quality monitoring systems and mapping systems based on including meteorological factors. This study will also help in regulatory or policy assessments to reduce the impacts of PM2.5 by estimating the concentration of pollutants.



## 5 Conclusion

- 1 The Inverse Distance Weighting (IDW) method is valuable for measuring the consequence of particular meteorological factors on PM<sub>2.5</sub> concentrations.
- 2 The Ordinary least squares (OLS) method is valuable for investigating the general influence on PM<sub>2.5</sub> concentrations by meteorological factors.
- 3 PM<sub>2.5</sub> concentrations are interrelated to meteorological factors: wind speed, temperature, wind direction, precipitation, relative humidity, and air pressure in several ways, including spreading, expansion, chemical creation, photolysis, and deposition.
- 4 To enhance the perception of PM<sub>2.5</sub> meteorological relations, further field tests (e.g., smog chambers and sounding) should be conducted to confirm model results. Second, the accuracy of CTM methods should be increased. Third, quantitative data should be extracted for forecasting and regulating PM<sub>2.5</sub> concentrations.
- 5 To mitigate PM<sub>2.5</sub> pollution in a specific area, wind corridors and artificial precipitation can be used according to the geographical circumstances.

## Acknowledgment

The authors would like to thank every person/department who helped thorough out the research work, particularly the EM department, and IE department. The careful review and constructive suggestions by the anonymous reviewers are gratefully acknowledged.

## Reference

- [1] V. A. Southerland *et al.*, "Global urban temporal trends in fine particulate matter (PM<sub>2.5</sub>) and attributable health burdens: estimates from global datasets," vol. 6, no. 2, pp. e139-e146, 2022.
- [2] C.-M. J. E. M. Liu and Software, "Effect of PM<sub>2.5</sub> on AQI in Taiwan," vol. 17, no. 1, pp. 29-37, 2002.
- [3] M. Roy, C. Brokamp, and S. J. A. Balachandran, "Clustering and Regression-Based Analysis of PM<sub>2.5</sub> Sensitivity to Meteorology in Cincinnati, Ohio," vol. 13, no. 4, p. 545, 2022.
- [4] A. Gattrell and M. Loytonen, *GIS and Health*. Houghton Mifflin Harcourt, 1998.
- [5] P. Poursafa, M. Mansourian, M.-E. Motlagh, G. Ardalán, and R. J. E. r. Kelishadi, "Is air quality index associated with cardiometabolic risk factors in adolescents? The CASPIAN-III Study," vol. 134, pp. 105-109, 2014.
- [6] P. L. Fung *et al.*, "Improving the current air quality index with new particulate indicators using a robust statistical approach," vol. 844, p. 157099, 2022.
- [7] A. P. Dadhich, R. Goyal, P. N. J. T. E. J. o. R. S. Dadhich, and S. Science, "Assessment of spatio-temporal variations in air quality of Jaipur city, Rajasthan, India," vol. 21, no. 2, pp. 173-181, 2018.
- [8] Y. Murayama and R. B. J. T. G. L. Thapa, "Spatial analysis and modeling in geographical transformation process," vol. 100, 2011.
- [9] T. L. Nyerges and P. Jankowski, *Regional and urban GIS: a decision support approach*. Guilford Press, 2009.
- [10] D. Xu *et al.*, "PM<sub>2.5</sub> Exposure and Health Risk Assessment Using Remote Sensing Data and GIS," vol. 19, no. 10, p. 6154, 2022.
- [11] Y. Tian, X. Yao, L. J. C. Chen, Environment, and U. Systems, "Analysis of spatial and seasonal distributions of air pollutants by incorporating urban morphological characteristics," vol. 75, pp. 35-48, 2019.
- [12] P. Twomey and M. J. I. j. o. c. p. Kroll, "How to use linear regression and correlation in quantitative method comparison studies," vol. 62, no. 4, pp. 529-538, 2008.
- [13] A. E. Gelfand, P. Diggle, P. Guttorp, and M. Fuentes, *Handbook of spatial statistics*. CRC press, 2010.
- [14] T. Thongthammachart, S. Araki, H. Shimadera, T. Matsuo, A. J. E. M. Kondo, and Software, "Incorporating Light Gradient Boosting Machine to land use regression model for estimating NO<sub>2</sub> and PM<sub>2.5</sub> levels in Kansai region, Japan," vol. 155, p. 105447, 2022.